Geometrical Growth Models for Computational Anatomy

Irène Kaltenmark

Université Paris-Saclay
École doctorale de mathématiques Hadamard (EDMH, ED 574)

Établissement d'inscription : École normale supérieure de Cachan

Laboratoire d'accueil : Centre de mathématiques et de leurs applications, UMR 8536 CNRS

THÈSE DE DOCTORAT

Spécialité : Mathématiques appliquées

Irène KALTENMARK

Geometrical Growth Models for Computational Anatomy

Date de soutenance : 10 Octobre 2016

Après avis des rapporteurs : Peter Michor (Université de Vienne)
Gabriel Peyré (Université Paris-Dauphine)

Jury de soutenance :

Mohamed Daoudi (Institut Mines-Télécom Lille)	Président du jury
Joan Glaunès (Université Paris Descartes)	Examinateur
Jean-François Mangin (CEA Neurospin)	Examinateur
Peter Michor (Université de Vienne)	Rapporteur
Gabriel Peyré (Université Paris Dauphine)	Rapporteur
Alain Trouvé (ENS Cachan)	Directeur de thèse

NNT : 2016SACLN049

Remerciements

Je remercie très chaleureusement mon directeur de thèse, Alain Trouvé, de m'avoir confié un sujet de thèse aussi passionnant et d'avoir dirigé mon travail de recherche avec une curiosité et un enthousiasme communicatifs et stimulants, un souci de rigueur constant et une grande patience.

Je remercie mes deux rapporteurs, Peter Michor et Gabriel Peyré, pour leur lecture attentive de mon manuscrit et pour leur appui. Je remercie Mohamed Daoudi, Joan Glaunès, Jean-François Mangin, Peter Michor et Gabriel Peyré pour l'intérêt qu'ils ont porté à mon travail et d'avoir accepté de faire partie du jury.

Je suis très reconnaissante à Michael Miller, à Laurent Younes et à toute l'équipe du CIS de l'Université Johns Hopkins de m'avoir invitée à Baltimore et accueillie si chaleureusement.

Les conférences annuelles (Shape Meeting), dont je remercie les différents organisateurs, ont été une belle source d'enrichissement, de motivation et d'intégration au sein d'une communauté dynamique et conviviale pour laquelle j'ai la plus grande estime.

La sympathie et l'enthousiasme des chercheurs du CMLA ont rendu ce cadre de travail agréable et je pense également à Micheline, à Véronique et à Virginie toujours disponibles.

Du plus loin que je me souvienne, de l'École primaire à l'Université, j'ai suivi l'enseignement de professeurs passionnés et dévoués à leur mission. J'adresse, en particulier, mes remerciements et j'exprime toute mon estime à M. Malric, professeur de Mathématiques au Lycée Charlemagne.

Quand un certain camarade d'école me décrivit son sujet de thèse, nous ignorions tous deux qu'il semait les graines de cette nouvelle aventure. Fortement intriguée, je commençais la lecture de la thèse de Joan Glaunès et avide d'en apprendre d'avantage, je m'orientais vers le cours de Master d'Alain Trouvé sur les espaces de formes. Je remercie donc tout naturellement Nicolas de m'avoir menée vers ce thème captivant et pour toutes les discussions qui s'en sont suivies jusqu'au pied des murs d'escalade. Je remercie également Barbara d'avoir pris le relais, pour toutes nos conférences ensemble et d'avoir partagé les derniers mois de labeur de rédaction du manuscrit.

Du labo, je me remémorerai avec nostalgie, les sandwichs au jambon de pays du jeudi, les pauses piscine, le tennis et l'escalade, la confidente toujours joyeuse et le compère des pauses toxiques les premières années, les rituels méticuleux, le féminisme et le criticisme (dans son plus noble sens), les risottos dont je ne maîtrise toujours pas la recette de base, à ma plus grande consternation, etc.

Il y a des événements que l'on retient plus que d'autres : voir ses amis revenir sur le campus pour vous soutenir en jouant au tarot les veilles d'écrits d'agreg en fait partie. Un petit merci tout particulier à Popoff et à Gaëlle pour leur aide précieuse pour ce concours.

Et puis, il y a tous les non-matheux, les Grimanciens du QG Belleville ou ceux avec qui l'aventure a pu commencer dès le début des années 2000 et qui se demandent encore comment on peut finir une thèse sans savoir dissocier sa gauche de sa droite. Je vous remercie pour les innombrables fous rires.

Je remercie tous mes partenaires de tarots ou de coinches !

Mes derniers remerciements vont à Yohann et Ba Ky toujours présents surtout dans les moments de doute et qui m'ont encore témoigné leur amitié en cette matinée du 10 octobre. Et enfin, à ma famille mais bien sûr à ma petite sœurette je ne peux dire qu'un *joyeux non-merci* !

À mes parents,

À ma mamie,

Abstract

In the field of computational anatomy, the Large Deformation Diffeomorphic Metric Mapping (LDDMM) framework has proved to be highly efficient for addressing the problem of modeling and analysis of the variability of populations of shapes, allowing for the direct comparison and quantization of diffeomorphic morphometric changes. However, the analysis of medical imaging data also requires the processing of more complex changes, which especially appear during growth or aging phenomena. The observed organisms are subject to transformations over time that are no longer diffeomorphic, at least in a biological sense. One reason might be a gradual creation of new material uncorrelated to the preexisting one. The evolution of the shape can then be described by the joint action of a deformation process and a creation process.

For this purpose, we offer to extend the LDDMM framework to address the problem of non diffeomorphic structural variations in longitudinal data. We keep the geometric central concept of a group of deformations acting on embedded shapes. The necessity for partial mappings leads to a time-varying dynamic that modifies the action of the group of deformations. Ultimately, growth priors are integrated into a new optimal control problem for assimilation of time-varying surface data, leading to an interesting problem in the field of the calculus of variations where the choice of the attachment term on the data, current or varifold, plays an unexpected role. The underlying minimization problem requires an adapted framework to consider a new set of cost functions (penalization term on the deformation). This new model is inspired by the deployment of animal horns and will be applied to it.

Keywords : computation anatomy, shape spaces, group of diffeomorphisms, large deformation, growth model, variational method, optimal control, Riemannian metric.

Résumé en français

Dans le domaine de l'anatomie, à l'investissement massif dans la constitution de base de données collectant des données d'imagerie médicale, doit répondre le développement de techniques numériques modernes pour une quantification de la façon dont les pathologies affectent et modifient les structures biologiques. Le développement d'approches géométriques via les espaces homogènes et la géométrie riemannienne en dimension infinie, initialisé il y a une quinzaine d'années par U. Grenander, M.I. Miller et A. Trouvé, et mettant en œuvre des idées originales de d'Arcy Thompson, a permis de construire un cadre conceptuel extrêmement efficace pour attaquer le problème de la modélisation et de l'analyse de la variabilité de populations de formes.

Néanmoins, à l'intégration de l'analyse longitudinale des données, ont émergé des phénomènes biologiques de croissance ou de dégénérescence se manifestant via des déformations spécifiques de nature non difféomorphique. On peut en effet observer lors de la croissance d'un composant organique, une apparition progressive de matière qui ne s'apparente pas à un simple étirement du tissu initial. Face à cette observation, nous proposons de garder l'esprit géométrique qui fait la puissance des approches difféomorphiques dans les espaces de formes mais en introduisant un concept assez général de déploiement où l'on modélise les phénomènes de croissance comme le déploiement optimal progressif d'un modèle préalablement replié dans une région de l'espace. Nous présentons donc une généralisation des méthodes difféomorphiques classiques pour modéliser plus fidèlement l'évolution de chaque individu d'une population et saisir l'ensemble de la dynamique de croissance.

Nous nous appuyons sur l'exemple concret de la croissance des cornes animales. La considération d'un a priori sur la dynamique de croissance de la corne, nous permet de construire un chemin continu dans un espace de formes, modélisant l'évolution de la corne de sa naissance, d'un état réduit à un point (comme l'état d'embryon pour un humain ou de graine pour une plante) à un âge adulte quelconque de corne bien déployée. Au lieu d'étirer la corne, nous anticipons l'arrivée de matière nouvelle en des endroits prédéfinis. Pour cela, nous définissons une forme mère indépendante du temps dans un espace virtuel, qui est progressivement plongée dans l'espace ambiant en fonction d'un marqueur temporel prédéfini sur la forme mère.

Finalement, nous aboutissons à un nouveau problème de contrôle optimal pour l'assimilation de données de surfaces évoluant dans le temps, conduisant à un problème intéressant dans le domaine du calcul des variations où le choix pour la représentation des données, courant ou varifold, joue un rôle inattendu. De plus, privilégier le mode de déploiement naturel amène à considérer de nouveaux termes de pénalisation.

Contents

Introduction et présentation des travaux

Cette partie en français sera reproduite dans le Chapitre 1.

1 Motivation

Dans le domaine de l'anatomie, à l'investissement massif dans la constitution de bases de données collectant des données d'imagerie médicale, doit répondre le développement de techniques numériques modernes pour une quantification de la façon dont les pathologies affectent et modifient les structures biologiques. Le développement d'approches géométriques à travers les espaces homogènes et la géométrie riemannienne en dimension infinie, initialisé il y a une vingtaine d'années par U. Grenander, M.I. Miller [30], A. Trouvé [50] et L. Younes [54], et mettant en oeuvre des idées originales de d'Arcy Thompson [47], a permis de construire un cadre conceptuel extrêmement efficace pour aborder le problème de la modélisation et de l'analyse de la variabilité de populations de formes [55], conduisant à la naissance d'une nouvelle discipline appelée *Anatomie computationnelle*. Ce concept d'*espace de formes*, reformalisé récemment par S. Arguillière [6, 7], exploite l'action sur une population de formes de groupes de difféomorphismes munis d'une distance invariante à droite pour induire une structure riemannienne sur cet ensemble.

Cette approche géométrique a produit des algorithmes efficaces (méthodes LDDMM [10], Deformetrica [17, 18], champs stationnaires [8], DARTEL [2]) ayant déjà fait leurs preuves sur des applications comme l'étude de l'hippocampe, en lien avec la maladie d'Alzheimer, ou du planum temporale pour la schizophrénie, l'étude d'IRM pour la trisomie 21, l'analyse de la connectivité neuronale basée sur l'imagerie par tenseur de diffusion (DTI), l'étude des malformations cardiaques, etc. Un bilan sur la recherche des géodésiques dans les espaces de formes, de l'approche par l'équation d'Euler-Lagrange à la reformulation Hamiltonienne, et mettant en avant les applications, est fait dans [48].

Données longitudinales et problématique

L'analyse longitudinale de données concerne le cas spécifique et plus complexe où un sujet est représenté par une série temporelle d'un même type de données. Cette analyse plus fine est motivée entre autres par l'étude clinique de maladies ou de traitements se manifestant dans la durée et entraînant des modifications progressives d'un organisme ciblé. La quantification de ces modifications au cours du temps est une piste d'exploration importante pour la compréhension d'une maladie ou pour l'optimisation des

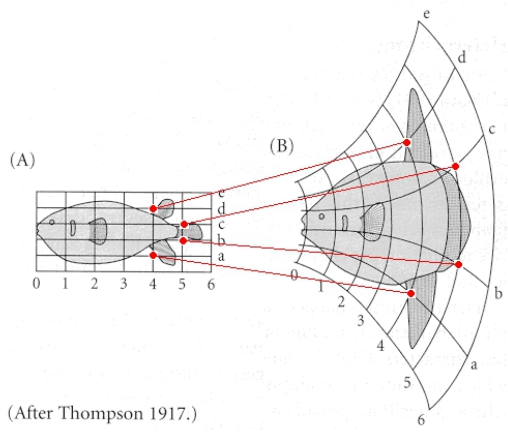

Figure 1 – Entre deux formes similaires, il existe une déformation simple qui transforme l'une en l'autre.

dosages de traitements lourds [41]. La méthode employée se déroule en deux temps. Une modélisation unifiée des données passe par la reconstitution, pour chaque sujet d'une population, de l'évolution continue partiellement observée par ses données longitudinales, ce qui permet par la suite une analyse transversale de la population. La notion d'espaces de formes vus comme des variétés riemanniennes est encore particulièrement adaptée à l'étude d'évolutions de formes donnant lieu à de nombreuses méthodes basées sur le transport parallèle [44], les splines riemanniennes [51] ou la régression géodésique [42, 53, 25], incluant l'inférence statistique et la variabilité spatio-temporelle d'une population de scénarios [19]. Relevons enfin que ces méthodes ne s'appliquent pas qu'au milieu médical, avec par example une étude comparative de l'ontogenèse du crâne entre les chimpanzés et les bonobos [22].

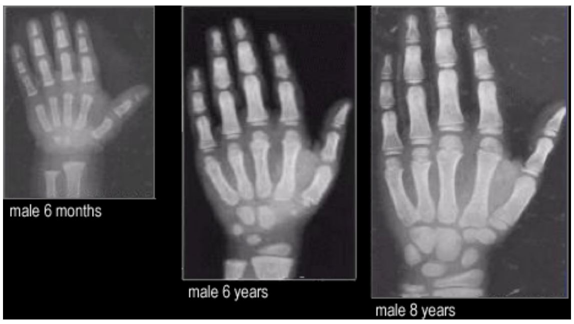

Figure 2 – L'apparition de petits os à la base de la main met en défaut les méthodes d'appariements difféomorphiques pour modéliser des processus de croissance qui impliquent de la création de nouvelle matière. Source: *Musée d'archéologie et d'ethnologie de l'Université Simon Fraser.*

Jusqu'à présent, l'étude longitudinale de données s'est appuyée sur une hypothèse d'homologie entre les observations qui ne permet pas néanmoins de décrire tous les phénomènes biologiques pouvant intervenir au cours d'une évolution temporelle, en particulier lors de processus de croissance ou de dégénérescence. Pour reconstruire, par exemple, la croissance d'une main à partir d'un échantillon de trois âges différents, illustrée sur la Figure 2, on pourrait chercher un flot de difféomorphismes qui produirait une solution globalement cohérente d'un point de vue biologique. Cependant, on peut observer au bas de la main la formation progressive de nouveaux os, disjoints de leurs voisins. Dans cette zone, il n'existe alors pas de bijection naturelle entre deux âges t_1 et t_2, dès lors qu'un os présent à l'âge t_2 n'existe pas encore à l'âge t_1. Cet exemple illustre parfaitement deux types de processus de croissance: un processus de déformation élastique qui peut s'apparenter dans cet exemple à un étirement de la main dans son ensemble et un processus de création quand la croissance résulte de la formation de matière nouvelle comme de nouveaux os, une nouvelle couche de tissu organique, etc.

L'observation extérieure de la forme d'un organisme ne permet pas toujours de distinguer ces deux processus. Le développement d'une corne animale est alors un cas d'étude idéal. Une corne est en effet un objet rigide qui se développe par extension à partir de sa base. La nouvelle matière progressivement créée pousse en continu le reste de la corne vers l'extérieur de la tête de l'animal. On peut donc supposer que globalement la corne est seulement déplacée par des rotations et des translations. Le processus de création dans cet exemple est donc dégagé de toute interaction avec d'autres phénomènes biologiques pouvant obscurcir sa compréhension. Un difféomorphisme, entre deux âges d'une corne donnée au cours de sa croissance, ne peut que produire un étirement de la petite corne sur la plus grande. Ce type de déformation ne reproduit donc pas processus de croissance réel. On aimerait au contraire avoir un plongement de la petite corne dans la grande et être capable de modéliser la nouvelle tranche créée à la base de la corne (voir la Figure 3). En conclusion, un processus de création fait appel à des appariements partiels, ce qui soulève la question de pouvoir délimiter l'image d'un tel appariement et de pouvoir intégrer à l'évolution le complémentaire de cet image à savoir les parties de l'organisme progressivement créées.

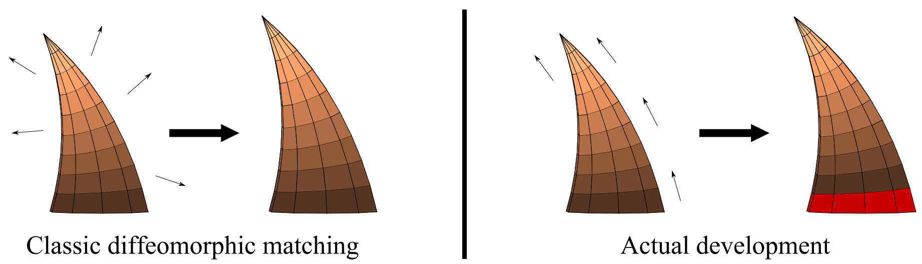

Figure 3 – Un difféomorphisme ne peut que produire un étirement d'une petite corne sur une plus grande. On aimerait au contraire avoir un plongement de la petite corne dans la grande pour pouvoir reproduire fidèlement le processus biologique qui génère le développement d'une corne.

2 Présentation des travaux

2.1 Résumé

Cette thèse ouvre la voie sur les appariements par des déformations de nature non difféomorphiques. L'hypothèse de départ pour compenser la perte d'homologie entre deux formes, est de supposer que les évolutions liées à chaque individu, mais d'un même objet

d'étude, partagent un processus de croissance commun. Le thème central de cette thèse est alors de définir de nouveaux outils qui permettent l'étude statistique d'une population de tels scénarios, en s'attachant à reproduire le plus fidèlement possible ce processus biologique. Tout en gardant l'approche géométrique d'un groupe de déformations agissant sur un ensemble de formes, qui fait la puissance des approches difféomorphiques dans les espaces de formes, le Chapitre 2 explore d'un point de vue ensembliste la recherche de nouveaux modèles génératifs capables d'intégrer l'apparition de nouvelle matière au cours d'un développement. Une seconde étape réalisée dans le Chapitre 3 est d'étudier la reconstruction d'un scénario soumis à un processus de croissance donné. La réécriture d'un des modèles présentés au Chapitre 2 permet de conditionner par rapport à ce processus un nouveau problème de contrôle optimal pour l'assimilation d'évolutions de formes. Ce dernier conduit à un problème intéressant du domaine du calcul des variations, où le choix du terme d'attache aux données, sur des courants ou sur des varifolds, joue un rôle inattendu comme on le verra au Chapitre 4. Le Chapitre 3 aboutit à un concept assez général de déploiement où l'on modélise les phénomènes de croissance comme le déploiement optimal progressif d'un modèle préalablement replié dans une région de l'espace. Sa mise en application au Chapitre 5 invite à moduler le problème central de contrôle optimal à travers de nouvelles fonctions de coût, qui pénalisent l'action du groupe de déformations, pour tendre vers une modélisation au plus proche du processus biologique.

Le processus de croissance qui nous intéresse principalement peut être décrit au moyen d'une *foliation*. Une foliation est une forme qui ressemble localement à une union de formes parallèles de dimension plus petite (par exemple, les droites horizontales d'un plan ou les cercles concentriques). Ces sous-formes sont appelées les feuilles de la foliation. Le processus de croissance d'une corne induit l'addition progressive d'extensions régulières à la base de la corne. Ces ensembles de nouveaux points forment les feuilles de la foliation sous-jacente. Ils sont similaires à des disques ou à des cercles selon que la corne est représentée par sa forme pleine ou par la surface qui délimite son bord. Avec ce point de vue, le processus de croissance se décrit très simplement par l'apparition continue de nouvelles feuilles.

L'introduction d'un système de coordonnées biologiques permet de modéliser et d'exploiter ce processus. Ce système est la donnée d'un espace X, appelé espace des coordonnées, et d'une fonction scalaire $\tau : X \to \mathbb{R}$, appelée marqueur du temps de naissance et dont les lignes de niveau forment les feuilles de la foliation sous-jacente. Cette fonction définit une collection de sous-ensembles $X_t = \{x \in X \mid \tau(x) \leq t\}$ de X, de l'ensemble des feuilles apparues au plus tard au temps t. Le scénario d'un individu peut alors être paramétré par cette collection de sous-ensembles du système de coordonnées biologiques. Ce dernier définit un invariant de la population étudiée permettant d'anticiper tout processus de création. La Figure 4 illustre ce modèle sur le développement d'une corne.

Un objectif pratique de la thèse est, étant données quelques observations $(S_i^{\mathrm{tar}})_i$ d'une corne à différents âges $(t_i)_i$, de produire des algorithmes numériques capables de reconstruire le déploiement continu de cette corne de son plus jeune âge jusqu'au dernier. En d'autres termes, il s'agit de générer un scénario de formes $t \mapsto S_t$ tel que $S_{t_i} \approx S_i^{\mathrm{tar}}$ à tout temps t_i initialement donné. Nous verrons que la rigidité du développement d'une corne permet à notre modèle de proposer un scénario à partir de la seule donnée d'un

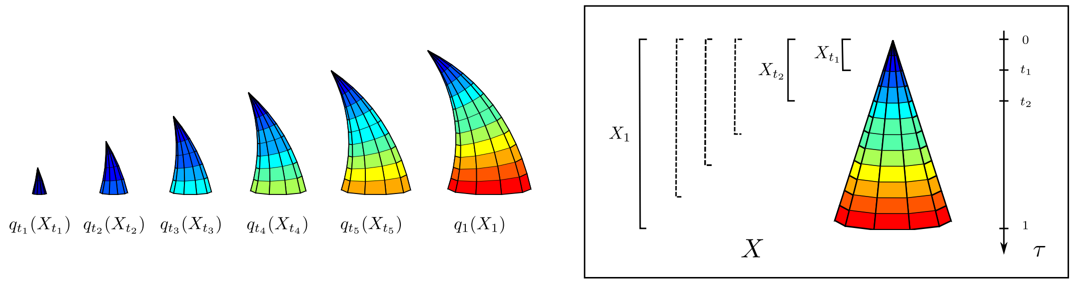

Figure 4 – A gauche, échantillon de six âges différents $\{t_1, t_2, \dots, 1\} \in [0,1]$ du déploiement d'une corne représentée par une forme dans un espace ambiant fixé. A droite, représentation du système de coordonnées biologiques (X, τ). Toute corne à droite est une image d'un sous-ensemble X_t de X. Les couleurs correspondent aux lignes de niveau du marqueur temporel τ.

âge final. Si on imagine que la corne à sa naissance est réduite à un point, on peut reconstruire un chemin continu de formes initialisée par ce point et se terminant sur la forme non dégénérée représentant l'âge final observé. Enfin, pour chaque application, le scénario obtenu est codé par une variable de faible dimension qui peut être vue comme une condition initiale anticipée et qui ouvre la voie sur une analyse statistique.

2.2 Organisation des chapitres :

Les Chapitres 2, 3, et 4 sont relativement indépendants. Le Chapitre 5 s'appuie sur le problème d'appariement détaillé dans le Chapitre 3 et présente les expériences numériques validant le modèle et ses variantes. Le contenu de chaque chapitre peut être résumé comme suit (nous ferons référence aux sections du Chapitre 1 qui présentent le cadre mathématique dans lequel se place cette thèse) :

Chapitre 2 : Appariements partiels et évolutions de croissance appariées dans un espace de formes

Ce chapitre étudie les modèles génératifs en amont des problèmes d'appariement. Les premières idées à l'origine de ce travail de thèse ont rapidement conduit au modèle présenté dans le Chapitre 3. La remise en question des choix de modélisation nous a alors poussés à rechercher l'objet atomique irréductible à la source des modèles de scénarios de croissance. De la volonté de garder l'approche géométrique d'un ensemble de formes évoluant dans un espace ambiant fixe E à travers un flot difféomorphique exercé sur cet espace, a alors émergé ce que nous avons appelé des *évolutions de croissance appariées (GMEs)*. Il s'agit de la donnée d'un ensemble de formes $(S_t)_{t \in T}$ indexé par un ensemble de temps $T \subset \mathbb{R}$ et évoluant dans E à travers un flot $(\phi_{s,t})_{s \leq t \in T}$ décrivant la déformation de l'espace E entre les paires d'instants (s,t). Pour s'affranchir de la contrainte d'homologie totale entre deux états quelconques S_s et S_t, on impose alors uniquement une condition de plongement : pour toute paire $s \leq t$ dans T,

$$\phi_{s,t}(S_s) \subset S_t \,.$$

On a donc un emboîtement successif à travers le flot de tous les âges de la forme induisant un système de datation du scénario. La forme S_t est en effet composée d'une

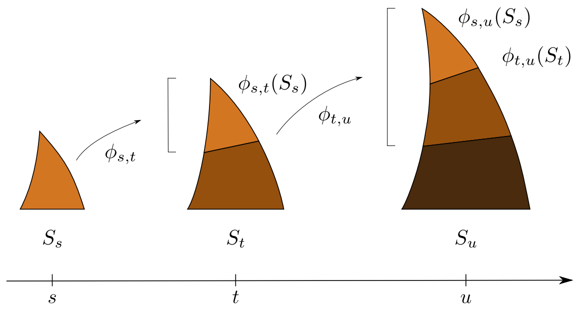

Figure 5 – Appariements partiels sous des contraintes illustrées par les différentes couleurs qui délimitent les images cibles de chaque appariements.

part par l'image $\phi_{s,t}(S_s)$ d'un état antérieur, d'autre part par la création de nouveaux points entre les temps s et t appelant à considérer le temps de naissance de chaque point. Pour comprendre ce phénomène, l'objet atomique d'évolution de croissance appariée est enrichie d'un jeu de fonctions attribuant un label à chaque point du scénario

$$\tau_t : S_t \to L, \qquad \forall t \in T\,.$$

Ces fonctions appelées marqueurs sont invariantes sous l'action du flot de sorte que chaque point évoluant à l'intérieur du scénario conserve son label au cours du temps. Nous dégagerons en particulier un marqueur du temps de naissance (*birth tag*) de chaque point du scénario.

De cette brique élémentaire, on en revient alors à ce qui a fait la puissance des espaces de formes. Les scénarios sont comparés les uns aux autres via des morphismes. En particulier, on peut regarder l'action d'un groupe G de déformations spatio-temporelles agissant sur l'espace-temps $E \times T$ pour définir une structure Riemanienne sur nos espaces de scénarios. Des scénarios élémentaires dits *centrés* mettent en évidence une décomposition naturelle des orbites sous l'action de G pointant un motif de croissance commun à l'orbite qui mènera à l'introduction du *système de coordonnées biologiques* dans les prochains chapitres. Tout scénario est alors vu comme l'image d'un scénario centré.

Enfin, nous nous attachons tout au long du chapitre à identifier les paramètres minimaux permettant de reconstruire un scénario à partir du flot qui lui est associé. Le choix de ces paramètres dépend des informations disponibles pour anticiper la position des nouveaux points dans les problèmes de reconstruction de scénarios. Nous retrouvons en particulier la fonction d'emplacement à la naissance (*birth place function*) qui apparaît naturellement pour les déploiements de corne où la zone de création des nouveaux points est connue.

Transition vers le Chapitre 3

Nous fixons pour les chapitres suivants un intervalle de temps $T = [0, 1]$. Nous nous intéressons à une population de formes dont le processus de croissance s'identifie à un *système de coordonnées biologiques* (X, τ) où X est une sous-variété compacte à coins de dimension $k \leq d$ et $\tau : X \to [0, 1]$ joue le rôle de marqueur temporel qui induit un scénario centré dont la forme au temps t notée X_t est donnée par

$$X_t = \{x \in X \mid \tau(x) \leq t\} \,. \tag{1}$$

Nous appellons points actifs au temps t ce sous-ensemble de l'espace des coordonnées X. Ce système de coordonnées biologiques permet alors de paramétrer toute la population par des morphismes de scénarios. Chaque morphisme s'assimile à une collection de cartes $(q_t : X_t \to \mathbb{R}^d)_{t\in[0,1]}$ qui peut être reconstruite par une fonction d'emplacement à la naissance $\tilde{q} : X \to \mathbb{R}^d$ combinée à flot $(\phi_{s,t})_{s<t\in[0,1]}$ sur l'espace ambiant par

$$q_t(x) = \phi_{\tau(x),t}(\tilde{q}(x)) \qquad\qquad \text{pour tout } x \in X_t \tag{2}$$

et définissant la forme du nouveau scénario à tout instant t par

$$S_t = q_t(X_t) \,.$$

Chapitre 3 : Reconstruction du déploiement d'une forme soumise à un processus de croissance

Création de scénarios

Par définition, l'approche la plus naturelle pour générer un flot consiste à intégrer des champs de vecteurs dépendant du temps v (cf Section 2.1.3). L'équation (2) se réécrit alors pour tout $x \in X$ et tout $t \in]\tau(x), 1]$,

$$q_t(x) = \tilde{q}(x) + \int_{\tau(x)}^{t} v_s(q_s(x))\, ds \,. \tag{3}$$

Pour unifier les cartes $q_t : X_t \to \mathbb{R}^d$, où l'on rappelle que $X_t \subset X$ est défini par (1), dans un seul espace de fonctions, il convient de déterminer une extension à X. Cette extension dépend des informations connues. Dans notre cas, cette information initialisant le plongement dans l'espace ambiant $\mathbb{R}^d$ est donnée par la fonction d'emplacement à la naissance $\tilde{q}$ et on définit donc

$$q_t(x) = \begin{cases} \phi_{\tau(x),t}(\tilde{q}(x)) & \text{if } \tau(x) \leq t \,, \\ \\ \tilde{q}(x) & \text{sinon,} \end{cases} \tag{4}$$

conduisant à ce que l'on appelle la dynamique de croissance (*growth dynamic*)

$$\dot{q}_t(x) = \mathbb{1}_{\tau(x)\leq t} v_t(q_t(x)) = \begin{cases} v_t(q_t(x) & \text{if } x \in X_t \,, \\ \\ 0 & \text{sinon.} \end{cases} \tag{5}$$

Retrouver la collection de cartes $(q_t : X \to \mathbb{R}^d)_{t\in[0,1]}$ générée par un champ de vecteur v amène ainsi à résoudre une équation intégrale où la condition initiale est donnée par

$$q_0 = \tilde{q} \,. \tag{6}$$

Ce choix d'extension implique que $\dot{q}_t$ est rarement continue spatialement et cette équation ne peut donc pas être définie dans $\mathcal{C}(X, \mathbb{R}^d)$. L'étude de la régularité spatiale des cartes s'effectue alors dans un second temps. Nous montrons entre autres que la régularité spatiale des cartes q_t dépend de la régularité en temps du flot (et donc du champ de vecteur générateur). Cette nouveauté induite par la dynamique de croissance est due au fait que la forme à son état final ne peut pas s'exprimer en fonction de la seule valeur finale du flot : $q_1 \neq \phi_{0,1} \circ q_0$. L'action partielle du flot sur la restriction au sous-espace X_t laisse une trace sur la jonction entre X_t et son complémentaire. Nous montrons alors que les cartes sont continues mais seulement différentiables presque partout. Néanmoins, si le flot est continu en temps, i.e. $v \in \mathcal{C}([0,1], V)$, alors toutes les restrictions $q_{t|X_t}$ sont de classe $\mathcal{C}^1$.

Plus généralement, on propose un cadre théorique plus large où les évolutions de formes sont générées via une action infinitésimale dépendante du temps

$$\xi : B \times [0,1] \to \mathcal{L}(V, B)\,, \tag{7}$$

où B est un espace de Banach contenant l'ensemble des cartes possibles entre X et l'espace ambiant $\mathbb{R}^d$. Nous généralisons ainsi l'approche d'espaces de formes présentée en Section 2.1.2. La théorie de l'intégration dans un espace de Banach par S. Bochner [46], étendant celle de l'intégrale de Lebesgue, permet de garantir l'existence d'un scénario $q \in \mathcal{C}([0,1], B)$ solution du problème de Cauchy

$$\dot{q}_t = \xi_{(q_t,t)}(v_t) \qquad\qquad \text{pour presque tout } t \in [0,1]\,, \tag{8}$$

défini pour toute condition initiale $q_0 \in B$ et tout champ de vecteurs dépendant du temps et de carré intégrable $v \in L^2([0,1], V)$. Pour retrouver la dynamique de croissance (équation (5)), ξ est définie par

$$\xi_{(q,t)}(v) = \mathbb{1}_{\tau \leq t} v \circ q\,.$$

Le choix de l'espace de Banach a priori $B = L^\infty(X, \mathbb{R}^d)$ à défaut d'un espace plus régulier de type $\mathcal{C}^n(X, \mathbb{R}^d)$ s'avère plus délicat que prévu (cf Chapitre 3).

Problème de contrôle optimal

La reconstruction d'un scénario à partir de la donnée d'un état final $q^{\text{tar}}(X)$ et d'une fonction d'emplacement à la naissance $\tilde{q} : X \to \mathbb{R}^d$ consiste à trouver le flot $(\phi_{s,t})_{s<t\in[0,1]}$ *le plus simple possible* tel que le morphisme généré (cf équation (2)) vérifie $q_1 = q^{\text{tar}}$. Nous nous appuyons sur la recherche de flots géodésiques, présentée dans la Section 2.1.3, générés par des champs de vecteurs d'un espace de Hilbert V. La recherche d'un flot optimal paramétré par un champ de vecteurs dépendant du temps $v \in L^2([0,1], V)$ peut alors être vu comme un problème de minimisation d'une énergie de type

$$E(v) = \frac{1}{2}\int_0^1 C(v_t, t)\, dt + \mathcal{A}(v)\,, \tag{9}$$

où C est appelée fonction de coût et où la condition $q_1 = q^{\text{tar}}$ est relaxée par un terme d'attache aux données $\mathcal{A} : L^2([0,1], V) \to \mathbb{R}$ (cf Section 2.3 et Chapitre 4).

En suivant l'approche classique des méthodes LDDMM présentée dans la Section 2.2.1, le gradient de cette énergie s'exprime au moyen d'une variable moment $p \in \mathcal{C}([0,1], B^*)$ vérifiant

$$p_1 = -d\mathcal{A}(q_1) \in B^*\,, \qquad \dot{p}_t = -\partial_q \xi(q_t, t)(v_t)^* \cdot p_t\,, \tag{10}$$

et de l'application moment définie par

$$\begin{array}{rcl} \mathcal{J}_\xi : B \times B^* \times [0,1] & \longrightarrow & V^* \\ (q, p, t) & \longmapsto & \xi^*_{(q,t)} \cdot p\,. \end{array}$$

Cette notation abusive $d\mathcal{A}(q_1)$ n'est proprement définie que dans le cas d'un espace de coordonnées X discret où l'on peut définir directement le terme d'attache aux données $\mathcal{A}$ sur l'espace des cartes B. Plus généralement, montrer l'existence et expliciter la nature du multiplicateur de Lagrange p_1 est un problème à part entière étudié au Chapitre 4 (cf équation (17)).

Le gradient de l'énergie à tout instant $t \in [0,1]$ s'obtient alors par

$$\nabla_v E(v)_t = \nabla_v C(v_t, t) - K_V \mathcal{J}_\xi(q_t, p_t, t)\,, \tag{11}$$

où $K_V : V^* \to V$ est l'isomorphisme canonique pour l'espace de Hilbert V, menant directement à un algorithme de descente de gradient pour minimiser l'énergie E.

Nous utilisons alors l'élégance de l'approche hamiltonienne pour passer à un problème d'optimisation sur le moment initial p_0. Néanmoins, le système hamiltonien réduit englobant les solutions minimisantes dépend du temps. Il est défini par

$$\begin{array}{rcl} H_r : B \times B^* \times [0,1] & \longrightarrow & \mathbb{R} \\ (q, p, t) & \longmapsto & \max_{v \in V} \left(p \,|\, \xi_{(q,t)}(v)\right) - C(v, t)\,, \end{array}$$

de sorte que les solutions minimisantes satisfont le système

$$\begin{pmatrix} \dot{q}_t \\ \\ \dot{p}_t \end{pmatrix} = \begin{pmatrix} \frac{\partial H_r}{\partial p}(q_t, p_t, t) \\ \\ -\frac{\partial H_r}{\partial q}(q_t, p_t, t) \end{pmatrix}.$$

Montrer l'existence de solutions définies sur l'intervalle complet $[0,1]$ demande quelques observations préliminaires énoncées dans le paragraphe suivant. Une fois ce résultat établi, on étudie la régularité au second ordre de l'hamiltonien pour mettre au point un algorithme de descente de gradient optimisant le moment initial p_0. L'énergie à minimiser s'écrit sous la forme

$$E(q_0, p_0) = \int_0^1 C(q_t, p_t, t)\, dt + \mathcal{A}(q_1)\,, \tag{12}$$

où l'on fait encore, pour simplifier, un abus de notation sur le terme d'attache aux données $\mathcal{A}$ qui n'est défini que sur les cartes générées par les champs de vecteurs de $L^2([0,1], V)$.

Spécificités liées à la dynamique de croissance

L'action infinitésimale liée à la dynamique de croissance n'est pas continue en temps. Ce manque de régularité se répercute directement sur l'application moment associée, notée ici $\mathcal{J}$. Montrer sa continuité et dégager une borne fine de sa norme demande de réduire l'espace des moments.

Un résultat classique de l'approche hamiltonienne dans le cadre LDDMM est la conservation de l'énergie d'un champ de vecteur optimal. Ici le système hamiltonien soumis à la dynamique dépend donc du temps et nous perdons la conservation de l'énergie. Nous montrons typiquement pour la dynamique de croissance que la norme de l'application moment est bornée par une fonction affine du temps, voire linéaire dans le cas de la corne. On peut construire des exemples simples où cette majoration est optimale illustrant que la norme de l'application moment est croissante. C'est la prise en compte, à chaque instant, de l'ensemble des nouveaux points s'ajoutant à la forme préexistente qui explique cette propriété. Elle s'exprime très simplement pour des trajectoires $t \mapsto (q_t, p_t)$ homogènes en espace et en temps, c'est-à-dire telles que $(x,t) \mapsto (|q_t(x)|_{\mathbb{R}^d}, |p_t(x)|_{\mathbb{R}^d})$ soit à peu près constante. Il existe alors en effet des constantes $a \geq 0$ et $b \geq 0$ telles que pour tout $t \in [0,1]$,

$$|\mathcal{J}(q_t, p_t, t)|_{V^*} \approx at + b \tag{13}$$

ou encore plus radicalement dans le cas des cornes

$$|\mathcal{J}(q_t, p_t, t)|_{V^*} \approx at\,. \tag{14}$$

Cette propriété semble satisfaisante à première vue. En effet, il paraît naturel qu'un scénario ayant une forme grandissante au cours du temps ait un flot de plus en plus coûteux, agissant sur une plus grande partie de l'espace ambiant. Néanmoins, pour la modélisation de déploiements de cornes au moyen de déformations rigides, nous verrons au Chapitre 5 qu'un flot optimal devrait être généré par un champ de vecteurs de norme constante. Pour corriger le modèle, nous jouons sur la fonction de coût C, initialement fixée à

$$C(v,t) = \frac{1}{2}|v|_V^2\,.. \tag{15}$$

Le cas le plus simple proposé est l'ajout d'une fonction scalaire $\nu : [0,1] \to \mathbb{R}_+^*$, croissante, produisant une nouvelle fonction de coût

$$C(v,t) = \frac{\nu_t}{2}|v|_V^2. \tag{16}$$

Nous y faisons référence sous le nom de *norme adaptée*. Dans le cas des cornes, où la norme de l'application moment peut être majorée par une fonction linéaire, nous sommes amenés à autoriser cette fonction ν à s'annuler en 0.

Nous revenons alors à l'existence de solutions au système hamiltonien. L'existence globale demande un contrôle de l'application moment. Ce contrôle ne peut s'obtenir que sur des sous-espaces de l'espace initial des moments B^*, dépendant eux-mêmes du type de cartes considéré. Moins la fonction de coût est pénalisante, plus la démonstration est contraignante sur le choix de ces espaces. L'exemple le plus important étant celui des cornes où les cartes changent la topologie de l'espace des coordonnées X pour former la pointe de la corne. Nous mettons alors au point un cadre de résolution assez général où l'on peut choisir des couples de sous-espaces $B_0 \subset B$ et $B_1^* \subset B^*$ pour assurer l'existence globale des solutions. Cette construction nécessaire à l'utilisation de fonctions de coût dégénérées (lorsque $\nu(0) = 0$) sera validée dans le Chapitre 4 où l'on montrera que les solutions du problème de minimisation s'obtiennent bien à partir des sous-espaces choisis. Sous ces conditions, on montre alors que l'application moment définie le long d'une trajectoire $t \mapsto (q_t, p_t)$ peut être contrôlée en tout temps par les conditions initiales q_0 et p_0.

Chapitre 4 : Existence et continuité des minimiseurs globaux pour la dynamique de croissance

Ce chapitre regarde l'existence de minimiseurs globaux continus pour le problème d'optimisation étudié au chapitre précédent, lorsque l'action infinitésimale ξ reproduit la dynamique de croissance définie par l'équation (5). Les problèmes classiques d'appariement de formes s'identifient généralement à la recherche d'une géodésique dans un espace choisi G_V de difféomorphismes avec conditions aux extrémités. La reconstruction d'un déploiement à travers la dynamique de croissance ne contraint pas seulement les extrémités du flot de difféomorphismes. En effet, l'état final q_1 de la solution ne peut pas s'écrire comme une image de l'état initial q_0 par l'état final du flot ϕ_1^v mais dépend de toute l'évolution du flot au cours du temps. L'énergie ne peut donc pas s'écrire sous la forme

$$E(\phi_1) = C(\phi_1) + \mathcal{A}(\phi_1)\,.$$

Le flot optimal permettant d'approcher la cible n'est donc pas, a priori, une géodésique de G_V.

L'existence de solutions continues au problème de contrôle optimal étudié au chapitre précédent ne peut donc pas se déduire de résultats généraux existant dans la littérature. Le premier résultat du chapitre a été néanmoins plutôt inattendu. Nous montrons à travers un contre-exemple que pour un terme d'attache aux données construit sur la représentation de nos formes géométriques par des varifolds, l'existence de solutions continues peut être mise en défaut. La différence entre les représentations courants et varifolds vis-à-vis du modèle associé à la dynamique de croissance s'explique par le fait que des oscillations en temps du champ de vecteurs v génèrent des oscillations en espace des formes $q_t(X_t)$. Les courants par leur effet d'annulation sur ces oscillations spatiales permettent de bloquer ce type de comportement.

La démonstration de l'existence de solutions continues dans le cadre défini par la dynamique de croissance pour un terme d'attache aux données $\mathcal{A}$ de type courant, en toute généralité, demande en premier lieu de s'assurer que les formes sont suffisamment régulières pour être représentées par des courants. Rappelons en effet que les cartes q_t générées par des champs de vecteurs $v \in L^2([0,1], V)$ ne sont a priori ni $\mathcal{C}^1$ ni rectifiables. Il est néanmoins possible de définir $\mathcal{A}$ sur $L^2([0,1], V)$ par densité de $\mathcal{C}([0,1], V)$, dont les champs v génèrent des cartes appartenant à $\mathcal{C}^1(X, \mathbb{R}^d)$.

L'étape suivante consiste à montrer l'existence de solutions dans $L^2([0,1], V)$. La preuve s'appuie sur la linéarité envers la composante tangentielle décrivant une forme et permettant de déduire la semi-continuité inférieure de ce terme d'attache. La continuité d'un champ de vecteur v optimal n'en découle pas immédiatement. En effet, on a certes montré précédemment la continuité de l'application moment, mais dans un cas restreint où l'espace des moments peut s'identifier à un espace de fonctions sur $X \times \partial X$ où ∂X est le bord de X. Nous obtenons dans ce chapitre la continuité de tous les minimiseurs globaux sans condition sur l'espace des moments permettant en retour de légitimer la restriction de cet espace pour des scénarios générés par des champs de vecteurs continus en temps. Plus précisément, considérons v et une variation δv tous deux dans $\mathcal{C}([0,1], V)$ et $q^{v+\epsilon\delta v}$ le scénario généré par $v + \epsilon\delta v$ pour $\epsilon \in \mathbb{R}$. Nous montrons au Chapitre 3 qu'il existe $\delta q \in \mathcal{C}([0,1], B)$ tel qu'au premier ordre, $q^{v+\epsilon\delta v} \approx q^v + \epsilon\delta q$. Il existe alors $p_1^X \in \mathcal{C}(X, \mathbb{R}^n)$ et $p_1^{\partial X} \in \mathcal{C}(\partial X, \mathbb{R}^d)$ tels que

$$\mathcal{A}'(v; \delta v) = (p_1 \mid \delta q_1) \tag{17}$$

$$= \int_X \langle p_1^X(x), \delta q_1(x) \rangle_{\mathbb{R}^n} d\mathcal{H}^k(x) + \int_{\partial X} \langle p_1^{\partial X}(x), \delta q_1(x) \rangle_{\mathbb{R}^n} d\mathcal{H}^{k-1}(x)\,, \tag{18}$$

définissant le moment final p_1 comme une fonction sur X et son bord ∂X. On note l'apparition du rôle joué par ce bord ∂X qui donnera son impulsion initiale à l'application moment (existence de la constante $b > 0$ dans l'équation (13), cf Chapitre 3).

Notons enfin qu'on profite de ce chapitre pour justifier la structure canonique retenue pour décrire le système de coordonnées biologiques (X, τ) comme un produit direct $X = [0,1] \times X_0$ où la fonction de marquage τ s'identifie à la projection sur la première coordonnée. En adaptant le point de vue de la théorie de Morse, nous montrons que de nombreuses situations peuvent se ramener à ce cas canonique par l'action d'une déformation spatiale de l'espace X transportant le marqueur τ. Une conséquence importante de cette réécriture est la possibilité de s'affranchir des reparamétrisations en temps des scénarios générés par une fonction d'emplacement à la naissance (voir également Chapitre 2).

Chapitre 5 : Applications numériques et résultats

Le Chapitre 5 met en pratique le modèle de croissance étudié au long de cette thèse. Etant donnée une corne à un âge arbitrairement fixé à $t = 1$, nous nous concentrons sur la reconstruction de son déploiement de sa naissance à $t = 0$ (état où la corne est supposée réduite à un point) jusqu'à l'état final donné à $t = 1$. Toutes les expériences sont effectuées avec des données synthétiques, construites à partir du modèle génératif présenté aux Chapitres 2 et 3.

Pour mettre en avant le processus de création pure, nous modélisons les flots par des rotations et des translations. Le modèle de base où la fonction de coût classique C est donnée par l'équation (15) est alors inadapté parce qu'il ne permet pas d'initier correctement le processus de croissance quand la forme est trop petite à la naissance. Nous utilisons par conséquent de nouvelles fonctions de coût correspondant soit à une pondération en temps de la pénalisation sur le flot (*cadre de la norme adaptée*) soit à l'ajout d'une contrainte sur la norme du champ de vecteurs (*cadre de la norme contrainte*). Le terme d'attache aux données est déduit d'une représentation des surfaces par des varifolds orientés. Ces objets, présentés dans la Section 2.3, ne semblent pas avoir été déjà utilisés pour des applications numériques et trouvent tout leur intérêt face à des surfaces facilement orientables mais ayant des extrémités pointues ou similaires à des tubes effilés. Pour sortir du cadre assez spécifique des déformations affines, le chapitre se termine sur quelques expériences où les champs de vecteurs sont modélisés avec un espace à noyau reproduisant (RKHS) à noyau gaussien.

Cette thèse a été motivée par le besoin de nouveaux modèles permettant de dépasser des observations pour décrire un phénomène biologique demandant de sortir du cadre classique proposé par les méthodes LDDMM, afin de pouvoir intégrer des informations complétant les données observées. Dans notre cas, il s'agit non seulement du processus de création mais également de la quantification de ce processus. La validation des expériences numériques s'attache donc tout particulièrement à ce dernier critère. Les différentes fonctions de coût sont comparées par rapport aux normes des champs de vecteurs de la cible et de la solution (Exemple 1). La souplesse du modèle est testée dans le but de pouvoir identifier un comportement anormal comme un retard de croissance. Par opposition au LDDMM classique, la construction de l'application moment, avec la dynamique de croissance, s'effectue par un apport progressif de nouveaux moments initiaux qui donne cette flexibilité et rend inutile l'appel à des reparamétrisations en temps pour détecter ce type d'anomalies (Exemple 2). Enfin, le modèle intègre sans difficulté l'ajout de données à des temps intermédiaires connus pour reconstruire un scénario par interpolation, ce qui améliore les résultats d'une des expériences qui aurait pu approcher les limites du modèle par la finesse et la courbure élevée de la corne étudiée (Exemple 3).

Quelques expériences supplémentaires sont effectuées pour observer l'optimisation possible de la position initial q_0 (Exemple 5) ou encore l'effet de bord initial (Exemple 4).

Comme dans le cadre LDDMM classique, chaque scénario reconstruit est complètement paramétré par les variables de faible dimension position initiale q_0 et moment initial p_0, ouvrant la voix vers une analyse statistique de la population de scénarios étudiée.

Chapter 1

Introduction

Contents

1 Motivation

In the field of anatomy, the massive investment in the acquisition of medical imaging calls for the development of new numerical techniques. The emergence of large databases demands efficient tools to model and analyze their variability. Already a few decades ago, the willingness to help neuroscientists and diagnosticians in the analysis of the substructures of the human brain led to a new discipline named *Computational Anatomy* by Grenander and Miller in [30], Trouvé [50] and Younes [54]. The developed theory and methods have been successfully applied in, as some examples among many others, the study of the shape of Hippocampus in relation to the evolution of Alzheimer disease, similar works on the planum temporale for schizophrenia, Down syndrome, the analysis of brain connectivity based on DTI imaging, studies of heart shapes and malformations.

Instead of analyzing an object individually, the underlying philosophy in computational anatomy is to study its relative position inside a set of related objects. To analyze the relationships of an individual with the rest of the population, this set is modeled as a mathematical space that can be equipped with a distance. With this point of view, the distance allows then to estimate the mean, usually called a template or an atlas [21], and the variance of a given population (or subset of the space) and to achieve a statistical analysis of the population. The core of this framework is the construction of this distance. It relies on the very simple idea, introduced by d'Arcy Thompson [47] in the beginning of the 20^{th} century, that the differences between related shapes, eventually highly complex shapes, can be explained by simple diffeomorphic deformations as displayed in Figure 1.1. From that, the first layer of the concept of shape spaces is a consistent collection of shapes and diffeomorphic mappings between them. The structure of the mapping is somewhat simple since it coincides with a group action of diffeomorphisms given by transport on shapes and this induces the *differential layer* of most shape spaces as recently formalized by Arguillière [6, 7]. The second layer is *a metric layer* inherited from the introduction of a metric structure on the mappings satisfying the triangle inequality and coming from a right invariant metric on the acting group of diffeomorphisms. This extra structure allows the development of various shape population analysis [55]. A review on the characterization of the geodesics in shape spaces from the Euler-Lagrange equation to the Hamiltonian approach is conducted in [48], highlighting several applications.

In fine, this geometric approach of shape spaces has already afforded effective algorithms for images or geometrical meshes as the Large Deformation Diffeomorphic Metric Mapping (LDDMM) methods [10] (see Deformetrica [17, 18]), stationary LDDMM [8] or DARTEL [2].

Longitudinal data set and problematic

Besides the cross-sectional variability analysis emerges the study of longitudinal data sets. Each subject of a population is represented by a sequence of measurements at different times. Among many other examples, the interest for these more complex data is motivated by the clinical studies of diseases or treatments that have a progressive impact over time and therefore entail changes on these evolution scenarios [41]. Scientists want thus to quantify these effects. For this purpose, given a population of longitudinal data sets, a first step consists in retrieving the continuous evolution for each subject interpolat-

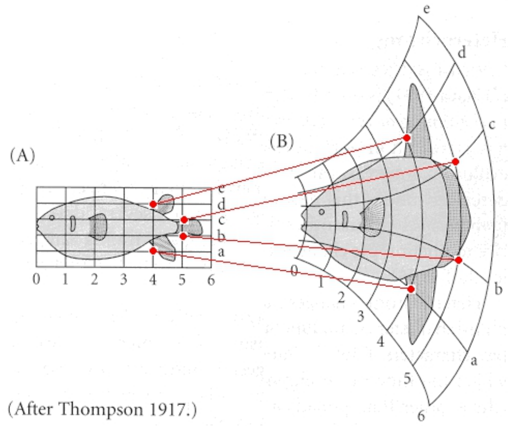

Figure 1.1 – Given two similar shapes, there exists a simple deformation that matches them.

ing his different measurements, then in performing a cross-sectional variability analysis on these evolution scenarios. Shape spaces as Riemannian manifolds are also well adapted to the study of shape evolutions and longitudinal analysis by various methods ranging from parallel transport [44], Riemannian splines [51], geodesic regression [42, 53, 25] including the inference from a population of a prototype scenario of evolution and its spatio-temporal variability [19]. Although modeling evolution scenarios and analyzing their variations appear as two different processes, in a lot of situations they can both be achieved with the diffeomorphic approach of the LDDMM framework. An example of application in an original theme was the comparison of the endocranial ontogenies between chimpanzees and bonobos [22].

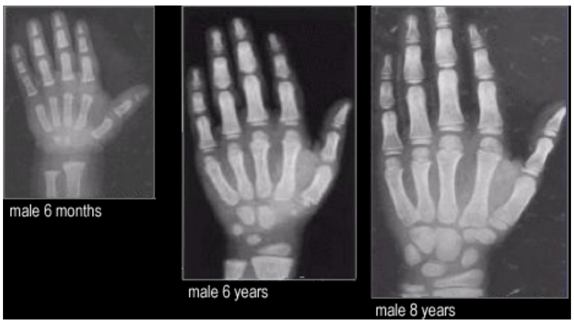

Figure 1.2 – Inadequacy of diffeomorphic matching to model a growth process involving creation of new material. Source: *Simon Fraser University Museum of Archaeology and Ethnology.*

Up to now, the longitudinal analysis has been limited to the study of data sets with homologous observations. Yet, in some situations this assumption seems inappropriate. During the growth or the degeneration of an organism, the changes occurring over time cannot always be modeled by diffeomorphic transformations, at least in a biological sense. This situation happens for example when new material is created over time in specific areas distinguishing this new material from the pre-existing shape. If one wants to retrieve the continuous evolution of the hand displayed in Figure 1.2, one can consider a flow of diffeomorphisms that would globally give a biologically coherent explanation of the growth. However, small bones are progressively emerging at the bottom of the hand and one cannot explain by one-to-one correspondences between two ages the changes occurring in these areas. This example illustrates two types of growth processes: a deformation process when a living organism is deforming through time and an expansion process when the growth results from the creation of new material. The observation of the shape without more information may not always allow to distinguish these two processes. The development of an animal horn is thus an interesting case study. Indeed, we assume that the base of the horn plays the role of an active area where new material is progressively created pushing outwards the rest of the horn. The horn is assumed to be rigid and is thus only subjected to rotations and translations due to physical constraints. This example isolates the creation process from the general deformation and reduces to its minimum any kind of distortions of the shape due to other biological phenomena. As displayed in Figure 1.3, a diffeomorphic matching of two horns can only provide a global stretching of the small to the large horn. Yet, a gradual stretching of the horn does not reflect the biological evolution described hereinabove. A creation process calls instead for partial inner matchings. It raises issues as how to delimit the image of a partial mapping and how to anticipate the creation of new material.

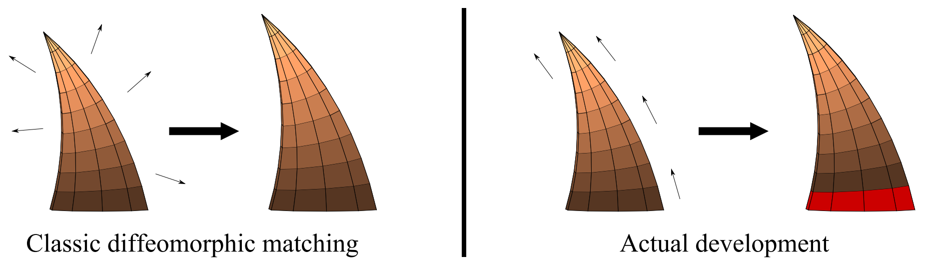

Figure 1.3 – A classic diffeomorphic matching would stretch the small horn to the large one and would thus not reflect the actual development of the horn. Instead, we would like to see an embedding of the small horn inside the target as much as a creation of new material at the base.

2 Introduction to Computational Anatomy

2.1 Shape space

2.1.1 Group action

The central idea, introduced by d'Arcy Thompson, to compare shapes via deformations requires to assume that given a population of shapes, any pair of them can be linked by a deformation. It leads to the introduction of homogeneous spaces.

Definition 2.1. *Given a group G acting on a set $\mathcal{S}$, we say that $\mathcal{S}$ is a homogeneous space if G acts transitively on $\mathcal{S}$, i.e. for any pair (S_1, S_2) of $\mathcal{S}$, there exists $g \in G$ such that $g \cdot S_1 = S_2$.*

In other words, $\mathcal{S}$ has only one orbit under the action of G which can be written by $\mathcal{S} = G \cdot S_0 \doteq \{g \cdot S_0 \,|\, g \in G\}$ for any $S_0 \in \mathcal{S}$. Thus, if $\mathcal{S}$ is a set of shapes and if we fix a shape S_0 called for example a template, any other shape $S \in \mathcal{S}$ can be reconstructed by a deformation of G applied to S_0. Moreover, a classic result of group theory implies that the set $\mathcal{S}$ is in bijection with G/G_0 where $G_0 \doteq \{g \in G \,|\, g \cdot S_0 = S_0\}$ is the stabilizer of S_0. Hence, the set $\mathcal{S}$ can inherit the structure of G/G_0.

Since biological shapes are embedded in an ambient space, denoted E and usually equal to $\mathbb{R}^d$, one can consider a group of deformations on the ambient space. G is usually a subgroup of the group $\mathrm{Diff}^\ell(\mathbb{R}^d)$ of $\mathcal{C}^\ell$-diffeomorphisms on $\mathbb{R}^d$. The natural action in most cases is then the evaluation of the deformation $g \in G$ on the shape $S \in \mathcal{S}$:

$$g \cdot S = g(S)\,.$$

In front of the wide variety of databases of shapes, as images, landmarks, curves, surfaces, fiber sets, etc., this approach to compare embedded shapes through the deformations on the ambient space offers a unified framework for registering this plethora of data types.

Example 2.1. *Assume that we want to register a population of connected surfaces with smooth boundary in the euclidean plan. These shapes can be represented by their boundaries as smooth curves of the plan. This last set can be seen as the homogeneous space generated by the orbit of the unit circle $\mathbb{S}^1$ under the action of the group of diffeomorphisms of the plan* $\mathrm{Diff}(\mathbb{R}^2)$.

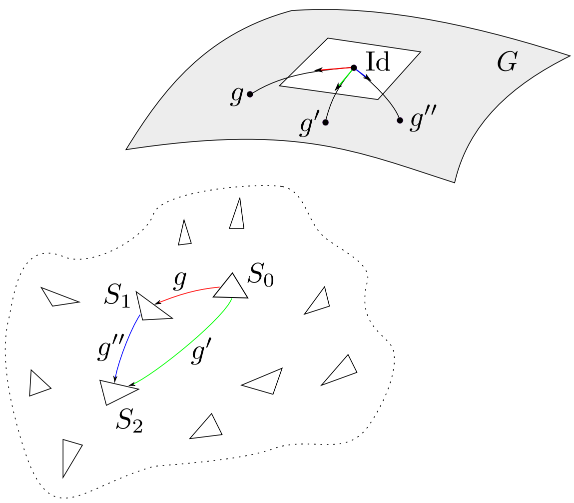

Figure 1.4 – The action of a group G on a homogeneous set of shapes induces a complete graph on the unstructured set. The equality $S_1 = g \cdot S_0$ creates an oriented edge from S_0 to S_1. If G is equipped with a distance d_G, one can assign the weight $d_G(\mathrm{Id}, g)$ to this edge. One can then deduce a distance on the set of shapes by considering the minimal paths in the graph.

The next step towards a shape space is to quantify the deformation induced by an element $g \in G$. Indeed, if G is equipped with a distance d_G, we can define for any pair (S_1, S_2) in $\mathcal{S}$

$$d(S_1, S_2) = \inf_{g \in G} \{d_G(Id, g) \,|\, S_1 = g(S_2)\}\,. \tag{1.1}$$

If d_G is right-equivariant (i.e. $d(g_1 h, g_2 h) = d(g_1, g_2)$ for any $g_1, g_2, h \in G$), then d satisfies the triangle inequality and we have

Theorem 2.1. *d is a pseudo-distance on $\mathcal{S}$.*

Proof. See [38]. $\square$

2.1.2 Infinitesimal action

The notion of shape spaces generalizes the previous results. It has been recently unified by Arguillière [6, 7]. For any $\ell \geq 1$, we denote $\mathcal{C}_0^\ell(\mathbb{R}^d)$ the Banach space of $\mathcal{C}^\ell$-mappings $v : \mathbb{R}^d \to \mathbb{R}^d$ vanishing at the infinity, equipped with the usual sup norm $|v| \doteq \sum_{\alpha \leq \ell} |\partial_\alpha v|_\infty$ and $\mathrm{Diff}_0^\ell(\mathbb{R}^d)$ the affine smooth manifold $(\mathrm{Id} + \mathcal{C}_0^\ell(\mathbb{R}^d)) \cap \mathrm{Diff}_0^\ell(\mathbb{R}^d)$ of the $\mathcal{C}^\ell$-diffeomorphisms modeled on the Banach space $\mathcal{C}_0^\ell(\mathbb{R}^d)$.

Definition 2.2. *Let $\mathcal{S}$ be a Banach manifold equipped with a compatible complete distance $d_\mathcal{S}$ and $\ell \in \mathbb{N}^*$. Assume that the group $\mathrm{Diff}_0^\ell(\mathbb{R}^d)$ continuously acts on $\mathcal{S}$, according to the action*

$$\begin{array}{ccc} \mathrm{Diff}_0^\ell(\mathbb{R}^d) \times \mathcal{S} & \longrightarrow & \mathcal{S} \\ (\phi, q) & \longmapsto & \phi \cdot q\,. \end{array} \tag{1.2}$$

We say that $\mathcal{S}$ is a shape space of order ℓ on $\mathbb{R}^d$ if the following conditions are satisfied:

1. *The action is semi-Lipschitz, that is, for any $q \in \mathcal{S}$, there exists $k_q > 0$ such that $d_\mathcal{S}(\phi_1 \cdot q, \phi_2 \cdot q) \leq k_q d_{\mathrm{Diff}_0^\ell(\mathbb{R}^d)}(\phi_1, \phi_2)$ for any $\phi_1, \phi_2 \in \mathrm{Diff}_0^\ell(\mathbb{R}^d)$.*
2. *For any $q \in \mathcal{S}$, the function $R_q : \phi \mapsto \phi \cdot q$ is smooth with respect to the usual norm on $\mathrm{Diff}_0^\ell(\mathbb{R}^d)$. Its differential at $\mathrm{Id} \in \mathrm{Diff}_0^\ell(\mathbb{R}^d)$ is denoted ξ_q and called the **infinitesimal action** of $\mathcal{C}_0^\ell(\mathbb{R}^d)$.*
3. *For any $k \in \mathbb{N}$, the following mappings are of class $\mathcal{C}^k$:*

$$\begin{array}{cccc} \xi : & \mathcal{S} \times \mathcal{C}_0^{\ell+k}(\mathbb{R}^d) & \longrightarrow & T\mathcal{S} \\ & (q, v) & \longmapsto & \xi_q(v)\,. \end{array} \tag{1.3}$$

An element $q \in \mathcal{S}$ is called a shape*, and $\mathbb{R}^d$ the* ambient space*.*

The most usual shape spaces are the manifolds of all differentiable (or even topological) embedding $q : X \to \mathbb{R}^d$ of a compact Riemannian manifold X into $\mathbb{R}^d$. The action is the usual composition: $\phi \cdot q = \phi \circ q$.

This definition of shape space gives thus a general setting where a set $\mathcal{S}$ can inherit the Riemannian structure of the group $\mathrm{Diff}_0^\ell(\mathbb{R}^d)$. It actually induces a sub-Riemannian distance on $\mathcal{S}$ for which the metric and geodesic completeness is guaranteed under some compactness condition satisfied by the previous examples of embeddings $q : X \to \mathbb{R}^d$ of a compact Riemannian manifold X into $\mathbb{R}^d$.

2.1.3 Groups of diffeormophisms with right invariant metric

A general approach to define a group action on a set of shapes embedded in an ambient space is to consider the diffeomorphisms obtained by integrating time-varying vector fields. The group generated depends then on the choice of the space V of vector fields. Two ways are classically considered in the existing literature. The first is based on $\mathcal{C}^\infty$ vector fields with compact support and weak Sobolev norms (see [12, 11, 37]). The second, that we will present here, consists in considering a Hilbert space V that satisfies some regularity conditions, so called *admissibility conditions* as introduced in [50]:

$$(H^V) \quad \left| \begin{array}{l} V \subset \mathcal{C}^2(\mathbb{R}^d, \mathbb{R}^d). \\ \exists c > 0, \forall x \in \mathbb{R}^d, \forall v \in V, \\ |v(x)|_{\mathbb{R}^d} + |dv(x)|_\infty + |d^2 v(x)|_\infty \leq c|v|_V. \end{array} \right. \tag{1.4}$$

This last approach led to the successful **Large Deformation Diffeomorphic Metric Mapping** (LDDMM) framework [10, 9, 33, 39, 40] that offers a practical and efficient possibility to construct such groups G with a right-invariant distance. The time-varying vector fields are then modeled by $L^2([0,1], V)$ (denoted L^2_V). The flow ϕ^v generated by any $v \in L^2_V$ is the unique solution of the integral equation:

$$\phi^v_t = \mathrm{Id} + \int_0^t v_s \circ \phi^v_s \, ds \,. \tag{1.5}$$

The group of diffeomorphisms generated by V is then defined by

$$G_V \doteq \left\{ \phi^v_1 \,|\, v \in L^2([0,1], V) \right\} \,. \tag{1.6}$$

With the point of view of Section 2.1.2, G_V is the orbit of the identity for the restriction of the infinitesimal action to the subspace V :

$$\begin{array}{rccc} \xi : & G_V \times V & \longrightarrow & T_\phi G_V \\ & (\phi, v) & \longmapsto & \xi_\phi(v) = v \circ \phi \,. \end{array} \tag{1.7}$$

The group G_V is then equipped a right invariant distance.

Proposition 2.1. *Under the* (H^V) *conditions,* G_V *is a group and is complete for the metric given by*

$$d_{G_V}(\mathrm{Id}, \varphi) \doteq \inf \left\{ |v|_{L^2_V} \,\middle|\, v \in L^2([0,1], V), \varphi = \phi^v_1 \right\} \,.$$

and extended by right invariance to $d_{G_V}(\varphi, \psi) = d_{G_V}(\mathrm{Id}, \psi \circ \varphi^{-1})$*.*

Theorem 2.2 (Existence of geodesics in G_V)**.** *For any* $\varphi \in G_V$*, there exists* $v \in L^2_V$ *such that* $\varphi = \phi^v_1$ *and*

$$d_{G_V}(\mathrm{Id}, \varphi) = |v|_{L^1_V} = |v|_{L^2_V} \,.$$

Remark 2.1. *The equality* $|v|_{L^1_V} = |v|_{L^2_V}$ *implies that* $t \mapsto |v_t|_V$ *is a constant. This geodesic path in* G_V *has a thus constant speed.*

These results are proved in [55] or [26] where more details can also be found.

One can now consider the action of G_V on a set of shapes $\mathcal{S}$. The distance previously defined on shapes in equation (1.1) becomes

$$d(S_1, S_2) = \inf \left\{ |v|_{L^2_V} \,\middle|\, v \in L^2([0,1], V), S_1 = \phi^v_1(S_2) \right\} \,. \tag{1.8}$$

With this metric, the geodesics of G_V become (locally) geodesics of $\mathcal{S}$ and give optimal continuous paths of shapes between any pair of shapes in $\mathcal{S}$. A path of diffeormorphisms

$t \in [0,1] \mapsto \phi_t^v \in G_V$ gives the path of shapes $t \in [0,1] \mapsto S_t \in \mathcal{S}$ defined by

$$S_t \doteq \phi_t^v(S_0) = \phi_0^v(S_0) + \int_0^t v_s \circ \phi_s(S_0)\, ds = S_0 + \int_0^t v_s(S_s)\, ds\,. \tag{1.9}$$

When shapes are modeled by mappings $q : X \to \mathbb{R}^d$, equation (1.9) can be rewritten for any $x \in X$ by:

$$q_t(x) \doteq \phi_t^v(q_t(x)) = q_0(x) + \int_0^t v_s(q_s(x))\, ds\,.$$

Again, with the point of view of Section 2.1.2 and when the infinitesimal action is defined by equation (1.7), this last equation can be induced by

$$q_t(x) = q_0(x) + \int_0^t \xi_{q_s}(v_s)(x)\, ds\,. \tag{1.10}$$

Note that at the end, the group of deformations G_V is hidden and its role is completely filled by V.

2.2 Inexact registration

We present now the resolution of a matching problem between two shapes by an optimal deformation. This thesis and especially Chapter 3 will extend the method developed in this section.

2.2.1 Optimal control problem

The inexact matching problem of a source shape S_0 to a target shape S^{tar} consists in finding a geodesic in G_V that deforms S_0 to an approximation of S^{tar}. This geodesic is obtained by an optimal time-varying vector field $v \in L^2_V$ that minimizes an energy of the type

$$E(\phi) = d_{G_V}(\text{Id}, \phi) + \mathcal{A}(\phi \cdot S_0)\,, \tag{1.11}$$

where $\mathcal{A}$, called the *data attachment term*, measures the discrepancy between two shapes $\phi \cdot S_0$ and S^{tar}. The existence of geodesics in G_V ensures then that the energy can be rewritten

$$E(v) = |v|^2_{L^2_V} + \mathcal{A}(\phi_1^v \cdot S_0)\,, \tag{1.12}$$

where ϕ_1^v is the final point of the flow generated by v (see equation (1.5)).

We consider, here, that the shapes are represented by a Banach space B whose elements are denoted $q \in B$. We will be indeed interested in this thesis by a space of mappings of the type $B = L^\infty(X, \mathbb{R}^d)$. The data attachment term is then defined as a functional $\mathcal{A} : B \to \mathbb{R}$ and we assume to simplify that $\mathcal{A}$ is of class $\mathcal{C}^1$. We also intend to keep the general framework of an unknown infinitesimal action

$$\xi : B \times [0,1] \to \mathcal{L}(V, B)\,. \tag{1.13}$$

With this setting, the energy to minimize is defined by

$$E(q_0, v) = \int_0^1 C(v_t)\, dt + \mathcal{A}(q_1)\,, \tag{1.14}$$

where we integrate the initial shape as a variable and we also generalize the penalization on the vector field v by a function C called the *cost function.* At last, we assume, in addition of the (H^V) conditions (defined by equation (1.4)), that ξ and C satisfy

$$(H^\xi) \quad \left| \begin{array}{l} \textit{(i)}\ \xi \in \mathcal{C}^1(B, \mathcal{L}(V, B))\,. \\ \textit{(i)}\ \text{There exists } c > 0, \text{ such that for any } q \in B\,, \\ \qquad\qquad |\partial_q \xi_q|_{op} \leq c\,. \end{array} \right. \tag{1.15}$$

$$(H^C) \quad \left| \begin{array}{l} \textit{(i)}\ C \in \mathcal{C}^1(V, \mathbb{R})\,. \\ \textit{(ii)}\ \text{There exists } c > 0, \text{ such that for any } v \in V\,, \\ \qquad |C(v)| + |\nabla_v C(v)|_V^2 \leq c|v|_V^2\,. \end{array} \right. \tag{1.16}$$

Proposition 2.2. *Under the (H^V) and (H^ξ) conditions, for any $(q_0, v) \in B \times L_V^2$, there exists a unique solution $q \in \mathcal{C}([0,1], B)$ to the integral equation*

$$q_t = q_0 + \int_0^t \xi_{q_s}(v_s)\, ds\,. \tag{1.17}$$

We define then

$$\begin{array}{rccc} \Phi: & B \times L_V^2 & \longrightarrow & B \\ & (q_0, v) & \longmapsto & q_1\,. \end{array} \tag{1.18}$$

Φ is continuous.

Proof. See Chapter 3. $\square$

The energy (1.14) is thus defined for any $(q_0, v) \in B \times L_V^2$. A fundamental question is the existence of a minimizer. Since the condition to exactly match the target is relaxed, it does not result from the existence of geodesics in G_V, even when ξ and C lead to the initial setting.

Theorem 2.3. *If for any $q_0 \in B$, the functional $v \mapsto \mathcal{A}(\Phi(q_0, v))$ is weakly continuous from L_V^2 to $\mathbb{R}$ and if $C(v)$ tends to $+\infty$ when $|v|_V$ tends to $+\infty$, then the minimization of the energy E given by equation* (1.14) *admits a solution.*

Proof. See for example [26]. $\square$

To explicit the gradient of E, let us introduce $\mathcal{J}_\xi$, called the **momentum map** [36], that depends on the infinitesimal action ξ. It is defined as follows:

Definition 2.3. *The momentum map is the application associated to ξ*

$$\begin{array}{rccc} \mathcal{J}_\xi: & B \times B^* & \longrightarrow & V^* \\ & (q, p) & \longmapsto & \xi_q^* \cdot p\,, \end{array}$$

so that we have for any $v \in V$

$$\big(\mathcal{J}_\xi(q,p)\,|\,v\big) = \big(p\,|\,\xi_q(v)\big)\,,$$

*where $(\,.\,|\,.\,)$ denotes the dual bracket, here, between B^* and B. The variable p is called the **momentum**.*

We can now describe the local minimizers of the energy.

Theorem 2.4. *Assume the (H^V), (H^C) and (H^ξ) conditions. For any $(q_0, v) \in B \times L^2_V$, the energy E and the function $\Phi(q_0, v) \mapsto q_1$ are Gâteaux-derivable and the Gâteaux-derivative of the energy at (q_0, v) in any direction $(\delta q_0, \delta v) \in B \times L^2_V$ is given by*

$$E'\big((q_0,v);(\delta q_0,\delta v)\big) = (p_0\,|\,\delta q_0) + \int_0^1 \big(dC(v_t) - \mathcal{J}_\xi(q_t,p_t)\,\big|\,\delta v_t\big)\,dt\,,$$

where $p \in \mathcal{C}([0,1], B^*)$ satisfies for almost any $t \in [0,1]$,

$$p_1 = -d\mathcal{A}(q_1) \in B^* \qquad\qquad \dot{p}_t = -\partial_q \xi_{q_t}(v_t)^* \cdot p_t\,. \tag{1.19}$$

Hence, the gradient of the energy with respect to the vector field is given at almost any time $t \in [0,1]$ by

$$\nabla_v E(q_0,v)_t = \nabla_v C(v_t) - K_V \mathcal{J}_\xi(q_t,p_t)\,, \tag{1.20}$$

where $K_V : V^* \to V$ is the canonical isomorphism of the Hilbert space V.

Proof. See Theorems 2.2 and 4.4 in Chapter 3. □

When equation (1.20) admits a unique explicit solution, the theorem leads thus to a first resolution method by a gradient descent on v.

Example 2.2. *To retrieve the distance d_{G_V}, the cost function is usually given by*

$$C(v) = \frac{1}{2}|v|^2_V\,.$$

Therefore, $\nabla_v C(v) = v$ and given $q_0 \in B$, any minimizer $v^* \in L^2_V$ of E satisfies at any time $t \in [0,1]$,

$$v^*_t = K_V \mathcal{J}_\xi(q_t,p_t)\,.$$

where $(q,p) \in \mathcal{C}([0,1], B \times B^*)$ is defined by (1.17) and (1.19).

2.2.2 Hamiltonian approach and shooting

Interestingly, the set of coupled differential equations on q and p can be interpreted as a Hamiltonian system of equations. Let us introduce the following Hamiltonian function

$$\begin{array}{rccc} H: & B \times B^* \times V & \longrightarrow & \mathbb{R} \\ & (q,p,v) & \longmapsto & (p\,|\,\xi_q(v)) - C(v) \end{array} \tag{1.21}$$

or equivalently $H(q,p,v) = (\mathcal{J}_\xi(q,p)\,|\,v) - C(v)$.

By construction, a minimizer v of the energy E is at any time a local extrema of the functional $V \ni v \mapsto H(q,p,v)$. Moreover, the cost function is usually a quadratic function on the norm of v. We will thus assume in the following that the derivative of this functional admits a unique zero denoted $v^*(q,p)$ or v^* to simplify. This assumption allows to define the reduced Hamiltonian as follows:

$$\begin{array}{rccc} H_r: & B \times B^* & \longrightarrow & \mathbb{R} \\ & (q,p) & \longmapsto & \max_{v \in V} H(q,p,v)\,. \end{array} \tag{1.22}$$

If $v \in V$ maximizes the Hamiltonian, we have $\partial_v H(q,p,v) = 0$ and therefore the partial derivatives of H_r are given for any $(q,p) \in B \times B^*$ by:

$$\begin{aligned} \partial_q H_r(q,p) &= \partial_q H(q,p,v^*) = \partial_q \xi_q(v^*)^* \cdot p\,, \\ \partial_p H_r(q,p) &= \partial_p H(q,p,v^*) = \xi_q(v^*)\,. \end{aligned}$$

We can now state the central theorem that characterizes the solution of a matching problem by the reduced Hamiltonian system:

Theorem 2.5. *Assume the (H^V), (H^C) and (H^ξ) conditions. Consider $(q_0, v) \in B \times L^2_V$ and $q = \Phi(q_0, v)$ be the unique trajectory generated by v from the initial condition q_0. Let p be the retrograde solution of $p_1 = -d\mathcal{A}(q_1)$ and $\dot{p}_t = -\partial_q \xi_{q_t}(v_t)^* \cdot p_t$. Then for any $\delta v \in L^2_V$,*

$$\frac{\partial E}{\partial v}(q_0, v) \cdot \delta v = \int_0^1 \left(-\frac{\partial H}{\partial v}(q_t, p_t, v_t) \,|\, \delta v_t \right) dt\,, \tag{1.23}$$

where for almost any $t \in [0,1]$,

$$H(q_t, p_t, v_t) = (p_t \,|\, \xi_{q_t}(v_t)) - C(v_t)\,.$$

Moreover, if we assume that for any $(x,y) \in B \times B^*$ the equation $\partial_v H(x,y,v) = 0$ admits a unique solution, then if v locally minimizes E, the trajectory (q,p) satisfies at almost any time the following Hamiltonian system

$$\left\{ \begin{array}{rl} \dot{q}_t & = \frac{\partial H_r}{\partial p}(q_t, p_t) \\ \\ \dot{p}_t & = -\frac{\partial H_r}{\partial q}(q_t, p_t)\,, \end{array} \right. \tag{1.24}$$

where $H_r(q_t, p_t) = H(q_t, p_t, v_t)$.

Proof. See Theorem 2.3 in Chapter 3. □

This characterization of the solutions by the reduced Hamiltonian system (1.24) is a weak form of the Pontryagin Maximum Principle [43].

Example 2.3 (Conservation property of the energy)**.** *We saw in Example 2.2 that when C is the classic cost function given by $C(v) = \frac{1}{2}|v|^2_V$, any optimal vector field $v^* \in L^2_V$ of E satisfies at almost any time $t \in [0,1]$ the equation*

$$v^*_t = K_V \mathcal{J}_\xi(q_t, p_t)\,.$$

It results that

$$H_r(q_t, p_t) = \frac{1}{2}|\mathcal{J}_\xi(q_t, p_t)|^2_{V^*} = \frac{1}{2}|v_t^*|^2_V\,.$$

Moreover, the Hamiltonian is always conserved during the evolution of (q,p) *which implies that at any time*

$$H_r(q_t, p_t) = H_r(q_0, p_0) = \frac{1}{2}|v_t^*|^2_V\,.$$

The norm of the optimal vector field is thus constant.

At last, this parameterization of any solution (q,p) by its initial position q_0 and initial momentum p_0 enables to solve the inexact matching problem by an optimization of the initial momentum. The new energy to minimize is of the type

$$E(q_0, p_0) = \int_0^1 C(q_t, p_t)\,dt + \mathcal{A}(q_1)\,, \tag{1.25}$$

where (q,p) is generated by the reduced Hamiltonian system. It requires to prove the existence and uniqueness of the solution (q,p) for any initial condition (q_0,p_0). We will prove it in chapter 3 in a more general framework. The gradient of this energy can be obtained with a method similar to the one described in Section 2.2.1. Namely, one introduces the auxiliary variable $(\mathcal{Q},\mathcal{P})$ of (q,p) that satisfies

$$\begin{cases} \dot{\mathcal{Q}}_t = \partial_q C(q_t,p_t) - \partial_p\partial_q H_r(q_t,p_t)\cdot\mathcal{Q}_t + \partial_q^2 H_r(q_t,p_t)\cdot\mathcal{P}_t \\ \dot{\mathcal{P}}_t = \partial_p C(q_t,p_t) - \partial_p^2 H_r(q_t,p_t)\cdot\mathcal{Q}_t + \partial_q\partial_p H_r(q_t,p_t)\cdot\mathcal{P}_t \\ \mathcal{Q}_1 = -d\mathcal{A}(q_1), \quad \mathcal{P}_1 = 0\,. \end{cases} \tag{1.26}$$

In practice, the derivatives of H_r appearing in these equations can be efficiently approximated using finite differences [5].

The Gateaux-derivative of the energy has then a particularly simple expression:

$$E'\big((q_0,p_0);(\delta q_0,\delta q_0)\big) = -(\mathcal{Q}_0\,|\,\delta q_0) - (\mathcal{P}_0\,|\,\delta p_0)\,. \tag{1.27}$$

leading to a new algorithm of gradient descent. An interest of this approach is to parameterize the solution with variables of smaller dimension paving the way for a statistical analysis. Moreover, since a gradient descent's algorithm usually returns an approximation of a local minimizer, the gradient descent on the vector field does not provide a geodesic. Conversely, the initial momentum extracted from this last optimization problem always represents a geodesic.

2.2.3 Towards numerical applications

The deformations involved in the model are determined by the choice of the space of vector fields V. Since V is continuously embedded in $\mathcal{C}_0^\ell(\mathbb{R}^d)$ (see the (H^V) conditions (1.4)), V is a Reproducing Kernel Hilbert Space (RKHS). Such spaces can be defined from the choice of a kernel and in many practical situations, all the computations only depends on the explicit expression of such kernel. We will now explicit the previous results in the case of a discrete shape given as a set of points with a mesh. The space B is then of the type $(\mathbb{R}^d)^m$ and its elements are identified to mappings $q : X \to \mathbb{R}^d$ where X is a finite set. By the Riesz representation theorem, p can also be identified to such a mapping. Then, with the notation of the previous sections, the momentum map is given by

$$\big(\mathcal{J}(q,p)\,|\,v\big) = \sum_{x\in X} p(x)^T v(q(x))\,.$$

Consider now a solution $(q,p) \in \mathcal{C}([0,1], B^2)$ generated by an optimal vector field v^*. With the classic cost function given by $C(v,t) = \frac{1}{2}|v|_V^2$ as presented in Example 2.2, v^* must satisfies the equation $v_t^* = K_V \mathcal{J}_\xi(q_t, p_t)$ at almost all time $t \in [0,1]$. With V an RKHS, this leads for any $y \in \mathbb{R}^d$ to

$$v_t^*(y) = \sum_{x\in X} k(y, q_t(x)) p_t(x)\,,$$

where $k : \mathbb{R}^d \times \mathbb{R}^d \to \mathcal{L}(\mathbb{R}^d)$ is the kernel of the RKHS. With a scalar Gaussian kernel, this expression becomes

$$v_t^*(y) = \sum_{x\in X} e^{-\frac{|y-q_t(x)|^2}{2\sigma^2}} p_t(x)\,.$$

This optimal vector field is thus a linear combination of Gaussian blobs centered on the points of the discrete shape.

Specific case of rigid deformations

To model rigid deformations, one can use the group of rotations and translations. This group is the semidirect product $\mathbb{R}^d \rtimes SO_d(\mathbb{R})$, for which $V = \mathrm{Skew}_d \times \mathbb{R}^d$ where Skew_d is the space of skew-symmetric $d \times d$ matrices. Any optimal vector field $v_t^* = (A_t^*, N_t^*)$ is then given by

$$A_t^* = \mathrm{proj}_{\mathrm{Skew}_d} \sum_{x\in X} p_t(x) q_t(x)^T \qquad \text{and} \qquad N_t^* = \sum_{x\in X} p_t(x)\,.$$

Algorithms

Given q_0, we usually do not have an explicit expression of the critical points of the energy. However, we can perform a standard gradient descent as described in Algorithm 1 and Algorithm 2 (remind that $B = (\mathbb{R}^d)^m = B^*$).

Algorithm 1 Gradient descent on v

1 - Given $q_0^0 \in B$, initialize $v^0 \in L_V^2$ at zero.
Then for any $n \in \mathbb{N}$, given q_0^n and v^n :
2 - Integrate forward with equation (1.17) to get $q^n \in \mathcal{C}([0,1], B)$ the path generated by $v^n \in L_V^2$.
3 - Compute $p_1^n = -d\mathcal{A}(q_1^n)$.
4 - Integrate backward with equation (1.19) to get $p^n \in \mathcal{C}([0,1], B)$.
5 - Compute the gradient at v^n : $\delta v^n = \nabla_v C(v_t^n) - K_V \mathcal{J}_\xi(q_t^n, p_t^n)$.
6 - Update the vector field by $v^{n+1} = v^n + \epsilon \delta v^n$ for a small $\epsilon > 0$.
7 - (Optional) Update q_0^n by $q_0^{n+1} = q_0^n + \epsilon p_0^n$ for a small $\epsilon > 0$.

Algorithm 2 Gradient descent on p_0

1 - Given $q_0^0 \in B$, initialize $p_0^0 \in B$ at zero.
Then for any $n \in \mathbb{N}$, given q_0^n and p_0^n :
2 - Integrate forward with the Hamiltonian system (1.24) to get $(q^n, p^n) \in \mathcal{C}([0,1], B^2)$.

3 - Compute $\mathcal{Q}_1^n = -d\mathcal{A}(q_1^n)$, defined $\mathcal{P}_1^n = 0$.
4 - Integrate backward with the second order Hamiltonian system (1.26) to get $(\mathcal{Q}^n, \mathcal{P}^n) \in \mathcal{C}([0,1], B^2)$.
4 - Update p_0^n by $p_0^{n+1} = p_0^n + \epsilon \mathcal{P}_0^n$ for a small $\epsilon > 0$.
5 - (Optional) Update q_0^n by $q_0^{n+1} = q_0^n + \epsilon \mathcal{Q}_0^n$ for a small $\epsilon > 0$.

Additionally, the expressions of the gradient with respect to v (1.20) or to the initial momentum p_0 (1.27), also say how to optimize the initial condition q_0. Typically, if q_0 is partially known and a reconstruction has been guessed, we can optimize it under some constraints (for example, inside a subset of the ambient space). This optimization should of course be controlled, otherwise the initial condition would just tend straightforwardly to the target.

At last, note that despite the existence of a solution, we do not have the uniqueness of a global minimizer of E. We do not have much more information about the local minimizers. The convergence speed of the gradient descent can quickly decrease in a rather large neighborhood of a local minimizer.

2.3 Overview of currents and varifolds

The inexact matching setting with the presence of an attachment term is justified by the fact that the homogeneous space M is not intended to accurately describe the real data but is instead a set of (smooth) representatives sampling the data. Indeed, we do not want to capture too small differences that could result from very specific characteristics of an individual or from noise. The flexibility given by the group of deformations and the precision of the attachment term (mostly the typical scale of these two elements) will determine the level of details of the model and the independence with respect to local noises. The aim of the data attachment term $\mathcal{A}$ is then to measure the shape dissimilarities at close range. For shapes like curves or surfaces $\mathcal{A}$ can be chosen as the distance on currents presented in [26, 27] or the distance on varifolds, more recently introduced in [15]. Both of these choices enable to measure the discrepancy between shapes regardless of the parameterization.

Throughout the text, we will adopt the following notation and definitions:

— X is a k-dimensional compact smooth submanifold of $\mathbb{R}^d$, eventually orientable and with boundary (X could also be only rectifiable).

— $\bigwedge^k \mathbb{R}^d$, $(0 \leq k \leq d)$: k-times exterior product of $\mathbb{R}^d$, which is a vector space of dimension $\binom{n}{k}$ spanned by the set of simple k-vectors $\xi_1 \wedge \ldots \wedge \xi_k$.

— $\bigwedge^k \mathbb{R}^d$ is equipped with the usual euclidean metric given for two simple k-vectors $\xi = \xi_1 \wedge \ldots \wedge \xi_k$ and $\zeta = \zeta_1 \wedge \ldots \wedge \zeta_k$ by the determinant of their Gram matrix: $\langle \xi, \zeta \rangle = \det(\langle \xi_i, \zeta_j \rangle_{i,j})$. In particular, $|\xi|$ gives the volume of the corresponding parallelotope.

— $\mathcal{C}_0(\mathbb{R}^d, (\bigwedge^k \mathbb{R}^d)^*)$: the set of continuous k-dimensional differential forms on $\mathbb{R}^d$ vanishing at infinity. This space equipped with the infinite norm is thus a Banach space.

— $\mathcal{H}^n$ is the n-dimensional Hausdorff measure on $\mathbb{R}^d$. We remind that $\mathcal{H}^n$ is defined as an outer measure on $\mathbb{R}^d$ that basically measures the n-dimensional volume of a subset of $\mathbb{R}^d$. In particular, when $n = d$, we have $\mathcal{H}^d = \lambda^d$ the Lebesgue measure. $\mathcal{H}^n(X)$ is the k-volume of X if $n = k$, vanishes if $n > k$ and equals $+\infty$ when $n < k$.

— K_H is the canonical isomorphism $H^* \to H$ for any Hilbert space H.

The idea of currents or varifolds is similar to the notion of distributions. In both cases, a shape is considered as a linear form on a space of test functions. These test functions are evaluated and integrated on the shape. However, in order to capture the geometry of the shape, these functions also depend at each point of the shape on the tangent space at this point. The differences between currents and varifolds lies on the properties of these test functions with respect to the tangent space.

We will call tangential data an object coding the tangent space at any point $x \in X$ with eventually its orientation (for example a normal vector). Let us denote formally $\mathcal{T}$ the set of all possible tangent data. A test function is then a real function $\omega : \mathbb{R}^d \times \mathcal{T} \to \mathbb{R}$ and the linear form μ_X associated to X is formally defined by

$$\mu_X(\omega) = \int_X \omega(x, T(x)) d\mathcal{H}^k(x) \,, \tag{1.28}$$

where $T(x) \in \mathcal{T}$ is the tangential data at the point $x \in X$.

2.3.1 Currents

We follow here the definition of currents as introduced by Vaillant and Glaunes in [28] as the topological dual of $\mathcal{C}_0(\mathbb{R}^d, (\bigwedge^k \mathbb{R}^d)^*)$.

Definition 2.4 (Current)**.** *A k-dimensional current on $\mathbb{R}^d$ is a continuous linear form on $\mathcal{C}_0(\mathbb{R}^d, (\bigwedge^k \mathbb{R}^d)^*)$.*

In the case of currents, the tangential data at $x \in X$ is given by an orthonormal oriented basis $(T_1(x), \dots, T_k(x))$ of the tangent space T_xX. The test function at any point x, $\omega_x \doteq \omega(x, \cdot)$ is a alternating multilinear form on $(T_xX)^k$ and consequently does not depend on the choice of the basis. X is thus *oriented* and considering the alternating linear mapping $(\zeta_1, \dots, \zeta_k) \mapsto \zeta_1 \wedge \dots \wedge \zeta_k$, one can consider that $\omega_x \in (\bigwedge^k \mathbb{R}^d)^*$. *In fine*, X is then identified to the current $\mu_X \in \mathcal{C}_0(\mathbb{R}^d, (\bigwedge^k \mathbb{R}^d)^*)'$ defined for any $\omega \in \mathcal{C}_0(\mathbb{R}^d, (\bigwedge^k \mathbb{R}^d)^*)$ by equation (1.28) or more precisely

$$\mu_X(\omega) = \int_X \omega_x(T_1(x) \wedge \dots \wedge T_k(x)) d\mathcal{H}^k(x) \,. \tag{1.29}$$

Example 2.4. *Let X be a close curve parameterized by a smooth immersion $\gamma : \mathbb{S}^1 \to \mathbb{R}^d$, then*

$$\mu_X(\omega) = \int_{\mathbb{S}^1} \omega_{\gamma(\theta)}(\gamma'(\theta)) d\theta = \int_{\mathbb{S}^1} \langle K_{\mathbb{R}^d} \omega_{\gamma(\theta)}, \gamma'(\theta) \rangle_{\mathbb{R}^d} d\theta \,.$$

The change of variables formula ensures that this expression is independent of any positive parameterization.

When $k = 1$ or $k = d-1$, $\bigwedge^k \mathbb{R}^d = \mathbb{R}^d$ and as described in the previous example, the set of test functions can be identified to $\mathcal{C}_0(\mathbb{R}^d, \mathbb{R}^d)$:

Example 2.5. *Let X be an oriented surface embedded in $\mathbb{R}^3$, then $\bigwedge^2 \mathbb{R}^3 = \mathbb{R}^3$, $\omega \in \mathcal{C}_0(\mathbb{R}^3, \mathbb{R}^3)$ and*

$$\mu_X(\omega) = \int_X \langle \omega(x), N(x) \rangle_{\mathbb{R}^d} d\mathcal{H}^2(x)\,,$$

where $N(x)$ is the unit normal vector at x given by the orientation of X.

2.3.2 Varifolds and oriented varifolds

The concept of varifolds is more general and we will even see in the end that for a non trivial set of test functions oriented varifolds can be equivalent to currents.

Definition 2.5. *The* Grassmann manifold *or* Grassmannian *of dimension k in $\mathbb{R}^d$, denoted $G_k(\mathbb{R}^d)$, is the set of all k-dimensional linear subspaces of $\mathbb{R}^d$.*

The oriented Grassmann manifold *of dimension k in $\mathbb{R}^d$, denoted $\tilde{G}_k(\mathbb{R}^d)$, is the set of all oriented k-dimensional linear subspaces of $\mathbb{R}^d$.*

It is well-known that $G_k(\mathbb{R}^d)$ is a homogeneous space under the action of the orthogonal group $O(\mathbb{R}^d)$. The stabilizer group of a k-dimensional subspace V of $\mathbb{R}^d$ is the product space $O(V) \times O(V^\perp)$ and it results that

$$G_k(\mathbb{R}^d) = O(\mathbb{R}^d)/(O(\mathbb{R}^k) \times O(\mathbb{R}^{d-k}))\,.$$

If V is oriented, we have likewise

$$\tilde{G}_k(\mathbb{R}^d) = SO(\mathbb{R}^d)/(SO(\mathbb{R}^k) \times SO(\mathbb{R}^{d-k}))\,,$$

where $SO(\mathbb{R}^d)$ is the special orthogonal group of $\mathbb{R}^d$.

Example 2.6. *The application $G_k(\mathbb{R}^d) \to G_{d-k}(\mathbb{R}^d)$, $V \mapsto V^\perp$ identifies $G_k(\mathbb{R}^d)$ to $G_{d-k}(\mathbb{R}^d)$. When X is a curve or a shape of codimension 1, $G_1(\mathbb{R}^d) = G_{d-1}(\mathbb{R}^d)$ is the set of lines through the origin, i.e. the real projective space $\mathbb{P}(\mathbb{R}^d)$. Likewise, if the orientation of $\mathbb{R}^d$ is fixed, $\tilde{G}_k(\mathbb{R}^d)$ can be identified to $\tilde{G}_{d-k}(\mathbb{R}^d)$ and $\tilde{G}_1(\mathbb{R}^d) = \tilde{G}_{d-1}(\mathbb{R}^d)$ to the sphere $\mathbb{S}^{d-1}$.*

The definition of a varifold is then given in [15] by:

Definition 2.6 (Varifold)**.** *A k-dimensional varifold on $\mathbb{R}^d$ is a Borel finite measure on the product space $\mathbb{R}^d \times G_k(\mathbb{R}^d)$. A non-oriented rectifiable set X of $\mathbb{R}^d$ of dimension k is identified to the varifold $\mu_X \in \mathcal{C}_0(\mathbb{R}^d \times G_k(\mathbb{R}^d))'$ defined for any $\omega \in \mathcal{C}_0(\mathbb{R}^d \times G_k(\mathbb{R}^d))$ by equation (1.28) or more precisely*

$$\mu_X(\omega) = \int_X \omega(x, T_x X) d\mathcal{H}^k(x)\,. \tag{1.30}$$

Definition 2.7 (Oriented varifold)**.** *A k-dimensional oriented varifold on $\mathbb{R}^d$ is a Borel finite measure on the product space $\mathbb{R}^d \times \tilde{G}_k(\mathbb{R}^d)$. An oriented rectifiable set X of $\mathbb{R}^d$ of dimension k is identified to the oriented varifold $\mu_X \in \mathcal{C}_0(\mathbb{R}^d \times \tilde{G}_k(\mathbb{R}^d))'$ defined for any $\omega \in \mathcal{C}_0(\mathbb{R}^d \times \tilde{G}_k(\mathbb{R}^d))$ by equation (1.28).*

Example 2.7. *With the assumptions of Example 2.6, the set of test functions can be identified respectively to $\mathcal{C}_0(\mathbb{R}^d \times \mathbb{P}(\mathbb{R}^d))$ for the varifolds or $\mathcal{C}_0(\mathbb{R}^d \times \mathbb{S}^{d-1})$ for the oriented varifolds. In this last case, when X is an oriented surface in $\mathbb{R}^3$ we get*

$$\mu_X(\omega) = \int_X \omega(x, N(x)) d\mathcal{H}^2(x)\,,$$

where $N(x)$ is the unit normal vector at x given by the orientation of X.

A fundamental example of current or varifold is the Dirac associated to a point $x \in \mathbb{R}^d$ and a tangential data $T \in \mathcal{T}$ defined for any test function $\omega : \mathbb{R}^d \times \mathcal{T} \to \mathbb{R}$ by

$$\delta_x^T(\omega) = \omega(x, T)\,.$$

Indeed, for any smooth shape X, its representation μ_X can locally be approximated by a Dirac. Let $U \ni x_0$ be a neighborhood of a point $x_0 \in X$. Then

$$\mu_U(\omega) = \int_U \omega(x, T(x)) d\mathcal{H}^k(x) \approx \int_U \omega(x_0, T(x_0)) d\mathcal{H}^k(x) = \delta_{x_0}^{T(x_0)}(\omega)\mathcal{H}^k(U)\,. \qquad (1.31)$$

Therefore, a discrete shape given as a set of points with a mesh can be modeled by a sum of weighted Diracs. Each cell of the mesh is approximated by the Dirac $\ell\delta_x^{T(x)}$ where x is the center of the cell, $T(x)$ is the tangential data at x and ℓ is the k-volume of the cell. *In fine*, a discrete shape with n cells is modeled by a current or a varifold of the type

$$\mu_X \approx \sum_{i=1}^n \ell_i \delta_{x_i}^{T(x_i)}\,.$$

2.3.3 Introduction of RKHSs

The Reproducing Kernel Hilbert Spaces (RKHS) are a very efficient tool to construct a scalar product on currents or varifolds. They are particularly well-fitted to compute distances between discretized shapes because of the simple expression of the scalar product between two Diracs. The concept of RKHS allows to create Hilbert spaces W, each one being continuously embedded in one of the different spaces of test functions previously introduced. By duality, the respective set of currents or varifolds is then naturally embedded in the dual spaces W'.

A test function is defined on $\mathbb{R}^d \times \mathcal{T}$. A RKHS W should thus be generated by a positive kernel $k_W : (\mathbb{R}^d \times \mathcal{T})^2 \to \mathbb{R}$. The new space of test functions W is then given by the completion of the vector space spanned by the fundamental functions $k_W((x, T), \cdot)$:

$$(x', T') \in \mathbb{R}^d \times \mathcal{T} \mapsto k_W((x, T), (x', T'))$$

for any $(x,T) \in \mathbb{R}^d \times \mathcal{T}$. Moreover, by definition of a RKHS,

$$K_W \delta_x^T = k_W((x,T),\cdot)\,,$$

where we recall that $K_W : W' \to W$ is the canonical isomorphism of Hilbert spaces. It results then that

$$\delta_{x'}^{T'}\left(k_W((x,T),\cdot)\right) = \langle \delta_x^T, \delta_{x'}^{T'} \rangle_{W'} = k_W((x,T),(x',T'))\,. \tag{1.32}$$

The construction of metrics via RKHSs becomes from there rather simple in practice and can be induced by the choice of two real positive kernels on the ambient space $E = \mathbb{R}^n$ and $\mathcal{T}$ (general situation). A kernel k_E measures the distance between the positions of two infinitesimal shapes and a kernel k_T measures the distance between their respective tangential data (the tangent space with eventually the orientation). The kernel k_W is finally given by the tensor product $k_E \otimes k_T$ defined for any $(x,T),(x',T') \in \mathbb{R}^d \times \mathcal{T}$ by

$$k_W\left((x,T),(x',T')\right) = k_E(x,x')k_T(T,T')\,. \tag{1.33}$$

At last, we can formally state the following proposition:

Proposition 2.3. *Given an RKHS W generated by a kernel $k_W = k_E \otimes k_T$ and two shapes X and Y of dimension k modeled by $\mu_X, \mu_Y \in W'$*

$$\langle \mu_X, \mu_Y \rangle_{W'} = \int_X \int_Y k_E(x,y)k_T\left(T(x),T(y)\right) d\mathcal{H}^k(y) d\mathcal{H}^k(x)\,. \tag{1.34}$$

When X and Y are discretised and respectively modeled by the finite sums $\mu_X = \sum_i \ell_i^X \delta_{x_i}^{T(x_i)}$ and $\mu_Y = \sum_j \ell_j^Y \delta_{y_j}^{T(y_j)}$, equation (1.34) becomes

$$\langle \mu_X, \mu_Y \rangle_{W'} = \sum_i \sum_j \ell_i^X \ell_j^Y k_E(x_i,y_j)k_T\left(T(x_i),T(y_j)\right)\,. \tag{1.35}$$

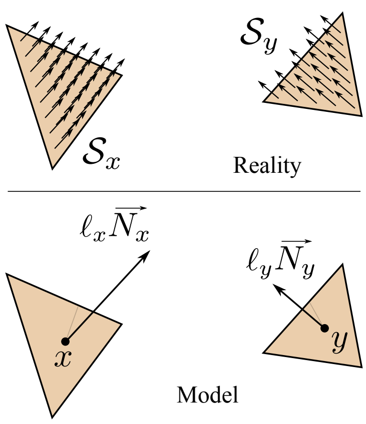

Figure 1.5 – Modeling of a triangle. A triangle is approximated by the position of its center x, its normal unit vector $\overrightarrow{N_x}$ and its area ℓ_x that can also be coded as the length of its normal vector $(\ell_x \overrightarrow{N_x})$. The first triangle is modeled by the linear form $\mu_{\mathcal{S}_x} = \ell_x \delta_x^{\overrightarrow{N_x}}$ and the second by $\mu_{\mathcal{S}_y} = \ell_y \delta_y^{\overrightarrow{N_y}}$. The scalar product between these two Diracs is given by equation (1.32) and compares simultaneously the position of the centers $(k_E(x,y))$ and the normal vectors $(k_T(T(x),T(y)) = k_T(\overrightarrow{N_x},\overrightarrow{N_y}))$.

Remark 2.2. *Note that for the currents, the tangential kernel k_T is necessarily given by the usual scalar product on $\bigwedge^k \mathbb{R}^d$.*

Example 2.8 (Currents as oriented varifolds)**.** *$\tilde{G}_1(\mathbb{R}^d)$ is set of lines through the origin of $\mathbb{R}^d$ and can be identified to the unit sphere $\mathbb{S}^{d-1}$. The Plücker embedding generalizes* *this idea and embeds $\tilde{G}_k(\mathbb{R}^d)$ into the unit sphere of $\bigwedge^k \mathbb{R}^d$. When the tangential kernel is then given by the usual scalar product on $\bigwedge^k \mathbb{R}^d$, currents are naturally embedded in the associated RKHS W'.*

Example 2.9. *With surfaces embedded in $\mathbb{R}^3$, the tangential data is given as the normal vector. The Gaussian kernel leads then to the following scalar products*

$$\begin{aligned}
&\textit{with currents:} && \langle \delta_x^{N_x}, \delta_y^{N_y} \rangle_{W'} &&= \exp\left(-\frac{|x-y|^2_{\mathbb{R}^d}}{2\sigma^2}\right) \langle N_x, N_y \rangle_{\mathbb{R}^d}\,,\\
&\textit{with oriented varifolds:} && \langle \delta_x^{N_x}, \delta_y^{N_y} \rangle_{W'} &&= \exp\left(-\frac{|x-y|^2_{\mathbb{R}^d}}{2\sigma^2}\right) \exp\left(-\frac{|N_x-N_y|^2_{\mathbb{R}^d}}{2\sigma_N^2}\right)\,.
\end{aligned}$$

With varifolds, one can randomly orientate the normal vectors and define for any RKHW W_{OV} designed to model oriented varifolds

$$\begin{aligned}
\langle \delta_x^{T(x)}, \delta_y^{T(y)} \rangle_{W'} =& \langle \frac{1}{2}(\delta_x^{N_x} + \delta_x^{-N_x}), \frac{1}{2}(\delta_y^{N_y} + \delta_y^{-N_y}) \rangle_{W'_{OV}}\\
=& \frac{1}{4}\langle \delta_x^{N_x}, \delta_y^{N_y} \rangle_{W'_{OV}} + \frac{1}{4}\langle \delta_x^{N_x}, \delta_y^{-N_y} \rangle_{W'_{OV}}\\
&+ \frac{1}{4}\langle \delta_x^{-N_x}, \delta_y^{N_y} \rangle_{W'_{OV}} + \frac{1}{4}\langle \delta_x^{-N_x}, \delta_y^{-N_y} \rangle_{W'_{OV}}\,.
\end{aligned}$$

This leads for a Gaussian kernel to the scalar product

$$\begin{aligned}
&\langle \delta_x^{T(x)}, \delta_y^{T(y)} \rangle_{W'} =\\
&\qquad \exp\left(-\frac{|x-y|^2_{\mathbb{R}^3}}{2\sigma^2}\right)\left(\frac{1}{2}\exp\left(-\frac{|N_x-N_y|^2_{\mathbb{R}^3}}{2\sigma_N^2}\right) + \frac{1}{2}\exp\left(-\frac{|N_x+N_y|^2_{\mathbb{R}^3}}{2\sigma_N^2}\right)\right)\,.
\end{aligned}$$

The common parameter σ gives the global scale of these two norms. For the varifolds, σ_N is attached to the comparison of the normal vectors. Since these last ones are unit vectors, σ_N can be fixed independently of the data.

Finally, once we fixed a RKHS W, we note $\mu^{\text{tar}} \in W'$ the identification of the target shape and μ^v the identification of the final state of the solution generated by a vector field $v \in L^2([0,1], V)$. The attachment term is then given by

$$\mathcal{A}(v) \doteq \frac{1}{2}\left|\mu^v - \mu^{\text{tar}}\right|^2_{W'}\,. \tag{1.36}$$

2.3.4 Differences between currents and varifolds

In the case of currents, the test functions are linear with respect to the tangential data. Hence, the integration of two close tangent spaces with opposite orientations will cancel their respective contributions. Indeed, for any test function ω and any couple $(x,T) \in \mathbb{R}^d \times \mathcal{T}$, $\omega(x,-T) = -\omega(x,T)$ so that $\delta_x^{-T} + \delta_x^{T} = 0$. This property makes the currents resistant to the noise. However, as a downside, this linearity also prevents the capture of structures like sharp spines or tails. See figures 1.6 and 1.7.

Remark 2.3. *[15] is focused on varifolds with the aim to model non orientable shapes or shapes with no rational orientation as fiber bundles (see Figure 1.8). So far, no research has been found on the application of oriented varifolds in computer vision and the concept remains rare in geometric measure theory.*

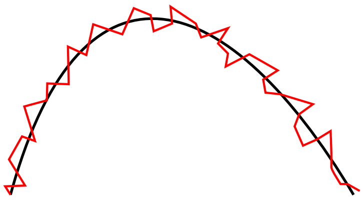

Figure 1.6 – Denote X the noisy red curve and Y the smooth one. From a current point of view, $\mu_X \approx \mu_Y$. Conversely, with varifolds, the length of X is about twice the length of Y and this approximation no longer holds.

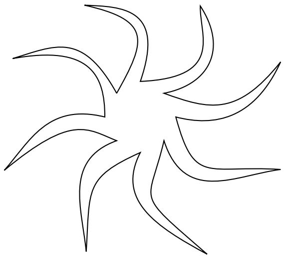

Figure 1.7 – Example of shape for which currents would be inadequate and that would rather call for oriented varifolds.

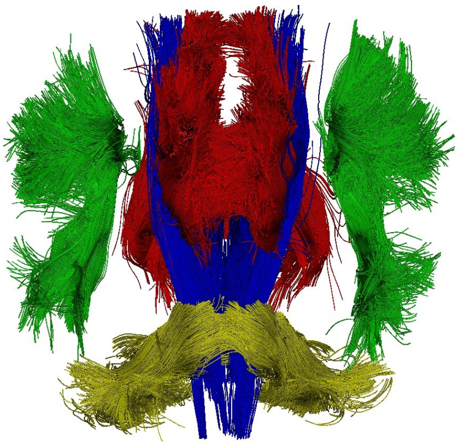

Figure 1.8 – Example of white matter fiber bundle estimated from Diffusion Tensor Imaging (DTI) illustrating the potential difficulty of consistent orientation of all differents fibers. This figure is extracted from [20]. In this article prior to the work of Charon and Trouvé on varifolds [15], the authors study the registration of such shapes modeled as currents.

Remark 2.4. *All numerical experiments in this thesis have been achieved with the oriented varifold model. This choice will be explained in chapter 5. However, we will see in chapter 4 that unlike currents the existence of a solution to the problem of matching growth scenarios is conserved neither with varifolds nor with oriented varifolds.*

The discussion on currents and varifolds will be shortly extended in chapter 5. More details on the Grassmann manifold can be found in [1] or on varifold from a more theoretical point of view in [3, 4].

3 Presentation of the work

3.1 Short summary

In this thesis, we open the door to non diffeomorphic deformations. The starting hypothesis to compensate the loss of homology is to assume that a population of related scenarios shares a common growth pattern. The central thread is to faithfully reproduce the biological evolution of an organism. A first step achieved in Chapter 2 is to explore new models able to integrate the creation of matter over time from a set theory point of view while keeping the geometric central concept making the essence and the strength of shape spaces of a group of deformations acting on a set of shapes. A second step conducted in Chapter 3 is to investigate the reconstruction of a scenario that satisfies growth priors. These priors are integrated into a new optimal control problem for the assimilation of time-varying shapes, leading to an interesting problem in the field of the calculus of variations where the choice of the attachment term on the data, current or varifold, plays an unexpected role as we will see in Chapter 4. At last, this underlying minimization problem requires to consider new cost functions to penalize the action of the group of deformations in order to favor the natural biological development as initiated in Chapter 3 and applied in Chapter 5.

The typical evolution of the shapes we are interested in can be described by a *foliation*. A foliation [24, 35] looks locally like a union of parallel shapes of smaller dimension called the leaves of the foliation. As described for the horns, the creation process induces a progressive addition of regular extensions at one boundary of the shape. To model the regularity of this process, we assume that the set of new points extending at each time the horn have usually the same shape and are locally parallel. They form therefore the leaves of the foliation. When the horn is represented by a surface, the leaves are similar to circles. For a full horn, the leaves are similar to disks. The introduction of a biological coordinate system will model and allow to exploit this growth pattern. This system consists in a space X called the coordinate space and a function $\tau : X \to \mathbb{R}$ called the birth tag whose lower sets induce a collection of subset $X_t = \{x \in X \mid \tau(x) \leq t\}$ of X. The evolution of an individual can then be parameterized by this time-varying ordered collection of subsets of the biological coordinate system. It allows thereby to anticipate the appearance of every new point involved in the evolution of the shape. Figure 1.9 illustrates this model on the development of a horn.

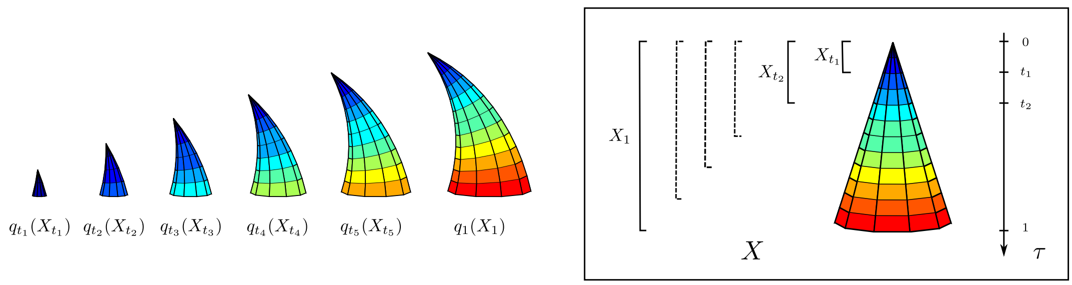

Figure 1.9 – Development of a horn. On the left, the horn is represented at six different ages $\{t_1, t_2, \ldots, 1\} \in [0, 1]$, in the ambient space. On the right, an arbitrary representation of the coordinate space X. Any horn on the left is an image of a subset of X. The colors correspond to the level sets of the birth tag function τ and indicate when a leaf appears.

A practical goal of this thesis is, given few observations $(S_i^{\text{tar}})_i$ of a horn at different times $(t_i)_i$, to provide numerical algorithms able to retrieve its continuous development from its youngest state to its oldest one. This means to generate a scenario $t \mapsto S_t$ such that $S_{t_i} \approx S_i^{\text{tar}}$ for all the times $(t_i)_i$. We will see that our model can also produce a path modeling the complete development of a horn from only one final observation.

If we imagine the horn at its birth as reduced to a single point, we can construct a continuous path from this point to a nontrivial shape at the final time matching the given observation. In each application, the complete development of a horn produced by the algorithm is encoded in a low-dimensional forecast initial condition, providing the support to a statistical analysis.

3.2 Organization of the chapters :

Chapters 2, 3, and 4 are somewhat independent. Chapter 5 illustrates the matching problem detailed in Chapter 3 by some numerical experiments to validate the model and its variations. The contents of each chapter can be summarized as follows:

Chapter 2 : Partial Matchings and Growth Mapped Evolutions in Shape Spaces

This chapter explores the generative models underlying the matching problems. The first ideas behind this thesis quickly led to the model presented in Chapter 3. The questioning of modeling choices then pushed us to seek the irreducible atomic object at the source of growth scenarios' models. From the willingness to keep the geometric approach of a set of shapes moving in a fixed ambient space E through a diffeomorphic flow applied to this space, emerges what we called the *growth mapped evolutions (GMEs)*. It consists in a set of shapes $(S_t)_{t\in T}$ indexed by a time interval $T \subset \mathbb{R}$ and evolving in E through a flow $(\phi_{s,t})_{s\leq t\in T}$ that describes the deformation of the space E between any pairs of times (s,t). To replace the constraint of exhaustive homology between any two shapes S_s and S_t, we only impose an inclusion condition: for any pair $s \leq t$ in T,

$$\phi_{s,t}(S_s) \subset S_t\,.$$

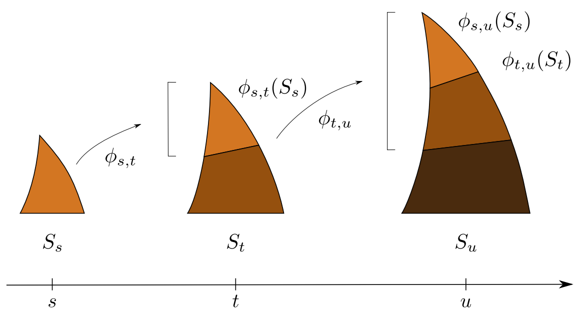

Figure 1.10 – Inner partial matchings under constraints delimiting their image illustrated by the different colors.

A growth mapped evolution is therefore a nested sequence of all ages of the shape through the flow inducing dating system as the history of the creation process. The shape S_t is indeed composed partly by the image $\phi_{s,t}(S_s)$ of a previous state and by the new points that appeared between the time s and t calling to consider the time of birth of each point. To understand this phenomenon, the atomic object of growth mapped evolution is enriched with a set of functions assigning a label to each point of the scenario

$$\tau_t : S_t \to L, \qquad \forall t \in T\,.$$

These functions called markers are invariant under the action of the flow, meaning that each point within the scenario retains its label over time. We will exhibit in particular a marker of the time of birth of each point of the scenario called the *birth tag*.

Once our objects are defined, we return to what made the power shape spaces. The scenarios are compared with each other via morphisms. In particular, one can consider the action of a group G of space-time deformation acting on the space-time $E \times T$ to define a Riemannian structure on our scenarios spaces. Elementary scenarios said *centered*, whose associated flow is reduced to the identity at all time, enlighten a natural decomposition of the orbits under the action of G exhibiting a common growth pattern in orbit that will lead to the introduction of the *biological coordinate system* in the following chapters. Any scenario is then seen as the image of a centered scenario.

Finally, we focus throughout the chapter to identify the minimal set of parameters to represent a scenario. The choice of these parameters depends on the available information to anticipate the position of the new points in the matching problems. In particular, we retrieve the *birth place function* that emerges naturally for the horn developments where the creation area of the new points is known.

Transition to Chapter 3

The time interval $T = [0, 1]$ is fixed for the following chapters. We are interested in a population of time-varying shapes whose growth process is described by a *biological coordinate system* (X, τ) where X is a compact k-dimensional submanifold with corners and $\tau : X \to [0, 1]$ plays the role of the birth tag. The lower sets of τ induce a centered scenario whose shape at time t is denoted X_t and given by

$$X_t = \{x \in X \mid \tau(x) \leq t\}\,. \tag{1.37}$$

The points of X_t are called active points at time t of the coordinate space X. This biological coordinate system allows then to parameterize the entire population via morphisms of scenarios. Each morphism consists in a collection of mappings $(q_t : X_t \to \mathbb{R}^d)_{t\in[0,1]}$ that can be generated by a *birth place function* $\tilde{q} : X \to \mathbb{R}^d$ and a flow $(\phi_{s,t})_{s<t\in[0,1]}$ on the ambient space. More precisely, we have for any $t \in [0, 1]$ and for any $x \in X_t$,

$$q_t(x) = \phi_{\tau(x),t}(\tilde{q}(x))\,. \tag{1.38}$$

The shape at any time t of the new scenario is then given by

$$S_t = q_t(X_t)\,.$$

Chapter 3 : Reconstruction of a Shape Development

Creation of scenarios

By definition, the most natural approach to generate a flow is to integrate a time-varying vector field v (see Section 2.1.3). Equation (1.38) can then be rewritten for any $x \in X$ and any $t \in]\tau(x), 1]$,

$$q_t(x) = \tilde{q}(x) + \int_{\tau(x)}^{t} v_s(q_s(x))\, ds\,. \tag{1.39}$$

To unify the mappings $q_t : X_t \to \mathbb{R}^d$ in a unique space of functions, where we recall that $X_t \subset X$ is defined by (1.37), one needs to extend them to the whole coordinate space X. This extension depends on the prior information, given in our case by the birth place function $\tilde{q}$. Hence, the simplest extension is the following one

$$q_t(x) = \begin{cases} \phi_{\tau(x),t}(\tilde{q}(x)) & \text{if } \tau(x) \leq t\,, \\ \\ \tilde{q}(x) & \text{otherwise,} \end{cases} \tag{1.40}$$

leading to what we call the *growth dynamic*

$$\dot{q}_t(x) = \mathbb{1}_{\tau(x) \leq t} v_t(q_t(x)) = \begin{cases} v_t(q_t(x) & \text{if } x \in X_t\,, \\ \\ 0 & \text{otherwise.} \end{cases} \tag{1.41}$$

The retrieval of the collection of mappings $(q_t : X \to \mathbb{R}^d)_{t\in[0,1]}$ generated by a time-varying vector field v leads to solve an integral equation where the initial condition is given by

$$q_0 = \tilde{q}. \tag{1.42}$$

This choice of extension implies that $\dot{q}_t$ is rarely spatially continuous and therefore this equation cannot be set in $\mathcal{C}(X, \mathbb{R}^d)$. The study of the spatial regularity of the mappings is thus performed afterwards. We show among other things that the spatial regularity mappings q_t depends on the temporal regularity of the flow (and thus of the generator vector field). This novelty induced by the growth dynamic is due to the fact that the shape at its final state cannot be expressed via the only final value of the flow: $q_1 \neq \phi_{0,1} \circ q_0$. The partial action of the flow on the restriction $q_{t|X_t}$ leaves a mark on the junction between X_t and its complementary. One can then only show that the mappings are continuous but only differentiable almost everywhere. However, if the flow is continuous in time, i.e. $v \in \mathcal{C}([0,1], V)$, then all the restrictions $q_{t|X_t}$ are of class $\mathcal{C}^1$.

More generally, we offer a broader theoretical framework where the evolution of a shape is generated via a time-dependent infinitesimal action

$$\xi : B \times [0,1] \to \mathcal{L}(V, B)\,, \tag{1.43}$$

where B is a Banach space that contains all the possible mappings between X and the ambient space $\mathbb{R}^d$. It generalizes the approach of shape spaces presented in Section 2.1.2. The theory of integration in a Banach space by S. Bochner [46], extending the Lebesgue integral, ensures the existence and uniqueness of a scenario $q \in \mathcal{C}([0,1], B)$ solution of the Cauchy problem

$$\dot{q}_t = \xi_{(q_t,t)}(v_t) \qquad \text{for almost any } t \in [0,1] \tag{1.44}$$

defined for any initial condition $q_0 \in B$ and any square integrable time-varying vector field $v \in L^2([0,1], V)$. To retrieve the growth dynamic (equation (1.41)), ξ is then defined by

$$\xi_{(q,t)}(v) = \mathbb{1}_{\tau \le t} v \circ q \,.$$

The choice of the Banach space to represent the mappings, most naturally $B = L^\infty(X, \mathbb{R}^d)$, is more delicate than expected (see Chapter 4).

Problem of optimal control

Building a scenario ending on a target final state $q^{\text{tar}}(X)$ given a birth place function $\tilde{q} : X \to \mathbb{R}^d$ consists in finding the flow $(\phi_{s,t})_{s<t \in [0,1]}$ *as simple as possible* such that the generated morphism (see equation (1.38)) satisfies $q_1 = q^{\text{tar}}$. This is done using the construction of geodesic flows as presented in Section 2.1.3 generated by vector fields of a Hilbert space V. The search for an optimal flow by a time-varying vector field $v \in L^2([0,1], V)$ can then be seen as a minimization problem on an energy of the type

$$E(v) = \frac{1}{2} \int_0^1 C(v_t, t)\, dt + \mathcal{A}(v) \,, \tag{1.45}$$

where C is called the cost function and where the constraint $q_1 = q^{\text{tar}}$ is relaxed by a data attachment term $\mathcal{A} : L^2([0,1], V) \to \mathbb{R}$ (see Section 2.3 and Chapter 4).

Following the standard approach presented in Section 2.2.1, the gradient of this energy can be expressed via a momentum $p \in \mathcal{C}([0,1], B^*)$ that satisfies

$$p_1 = -d\mathcal{A}(q_1) \in B^* \qquad \dot{p}_t = -\partial_q \xi(q_t, t)(v_t)^* \cdot p_t \tag{1.46}$$

and via the momentum map defined by

$$\begin{array}{rccc} \mathcal{J}_\xi : & B \times B^* \times [0,1] & \longrightarrow & V^* \\ & (q, p, t) & \longmapsto & \xi^*_{(q,t)} \cdot p \,. \end{array}$$

The abusive notation $d\mathcal{A}(q_1)$ is only properly defined when the coordinate space X is a discrete set. Otherwise, the data attachment term is actually not directly defined on the space B and the existence and explicit formula of the Lagrange multiplier p_1 is a significant problem addressed in Chapter 4 (see equation (1.53)).

The gradient of the energy at any time $t \in [0,1]$ is then written

$$\nabla_v E(v)_t = \nabla_v C(v_t, t) - K_V \mathcal{J}_\xi(q_t, p_t, t) \,, \tag{1.47}$$

where $K_V : V^* \to V$ is the canonical isomorphism for the Hilbert space V. It leads to a straightforward algorithm of gradient descent to minimize the energy E.

The elegance of the Hamiltonian approach is used again to move towards an optimization problem on the initial momentum p_0. However, the reduced Hamiltonian system defining the minimizing solutions depends on the time. It is defined by

$$\begin{array}{rcl} H_r : B \times B^* \times [0,1] & \longrightarrow & \mathbb{R} \\ (q,p,t) & \longmapsto & \max_{v\in V} (p \,|\, \xi_{(q,t)}(v)) - C(v,t) \,. \end{array}$$

Hence, the solutions generated by minimizers of E satisfy the system

$$\begin{pmatrix} \dot{q}_t \\ \\ \dot{p}_t \end{pmatrix} = \begin{pmatrix} \frac{\partial H_r}{\partial p}(q_t,p_t,t) \\ \\ -\frac{\partial H_r}{\partial q}(q_t,p_t,t) \end{pmatrix} .$$

The existence of solutions defined on the entire interval $[0,1]$ requires some preliminary observations outlined in the next paragraph. Once this result is established, we study the regularity of the Hamiltonian system to develop an algorithm that optimizes the initial momentum p_0. It relies on minimizing an energy of the type

$$E(q_0,p_0) = \int_0^1 C(q_t,p_t,t)\, dt + \mathcal{A}(q_1)\,, \tag{1.48}$$

with again an abuse of notation on the data attachment term that is only defined on the final mappings generated by the vector fields of $L^2([0,1],V)$.

Specific properties induced by the growth dynamic

The infinitesimal action related to the growth dynamic is not continuous in time. This lack of regularity directly impacts the associated momentum map, denoted here by $\mathcal{J}$. A solution to guarantee the continuity and to exhibit a pertinent upper bound of its norm is to reduce the space of momenta p.

A strength of the Hamiltonian approach for the LDDMM methods is to ensure that the norm of an optimal vector field is conserved over time. Here, the Hamiltonian system induced by a time-varying dynamic depends therefore on the time and we lose energy conservation. With the growth dynamic, we typically show that the norm of the momentum map is bounded by an affine function of time, even linear in the case of horns. Simple examples can be constructed where this upper bound is optimal, meaning that the norm of the momentum map over a trajectory (q_t,p_t) is increasing. This results from the additional contribution at each time of the new points extending the shape. To highlight this property, one can consider any trajectory $t \mapsto (q_t,p_t)$ that is homogeneous in space and time, meaning that $(x,t) \mapsto (|q_t(x)|_{\mathbb{R}^d}, |p_t(x)|_{\mathbb{R}^d})$ is approximately constant. There exist then indeed two constants $a \geq 0$ and $b \geq 0$ such that for any $t \in [0,1]$,

$$|\mathcal{J}(q_t,p_t,t)|_{V^*} \approx at + b \tag{1.49}$$

or even more drastically in the case of horns

$$|\mathcal{J}(q_t,p_t,t)|_{V^*} \approx at\,. \tag{1.50}$$

This property appears satisfactory at first. Indeed, it seems natural that the flow associated to the scenario of a growing shape over time is increasingly expensive as it progressively acts on a larger part of the ambient space. However, when modeling growth scenarios for the horns via rigid deformations, we will see in Chapter 5 that optimal flow should be generated by a vector field of constant norm. To correct the model, we play with the cost function C initially set at

$$C(v,t) = \frac{1}{2}|v|_V^2 \,. \tag{1.51}$$

The simplest example among a set of cost functions referred to as *adapted norm setup* is to weight the previous classic cost function with an increasing scalar function $\nu : [0,1] \to \mathbb{R}_+^*$ as follows

$$C(v,t) = \frac{\nu_t}{2}|v|_V^2 \,. \tag{1.52}$$

In the case of horns, the norm of the momentum map is controlled by linear function of the time. It leads to additionally allow the possibility to have $\nu(0) = 0$. We say then that the setup is *degenerated*.

We finally return to the existence of the solutions to the Hamiltonian system. The global existence requires a control on the momentum map. This control can only be guaranteed on subspaces of B^* for the initial momentum. Moreover, the choice of these subspaces depends on the space of the mappings. For the main example of the horns, the mappings change the topology of the coordinate space X to form the tip of the horn (not without consequences). Hence, we develop a general resolution framework where we can choose a pair of *compatible* subspaces $B_0 \subset B$ and $B_1^* \subset B^*$ to ensure the existence of global solutions. This construction is required to use cost functions of the *degenerate adapted norm setup* (where $\nu(0) = 0$) and will be validated in Chapter 4 where we will show that the solutions of the minimization problem are indeed obtained with the selected subspaces. Under these conditions, we can then show that the momentum map defined along a trajectory $t \mapsto (q_t, p_t)$ can be controlled at all times by the initial conditions q_0 and p_0.

Chapter 4 : Existence and Continuity of the Global Minimizers for the Growth Dynamic

This chapter examines the existence of continuous global minimizers v to the optimization problem discussed in the previous chapter when the infinitesimal action ξ reproduces the growth dynamic defined by equation (1.41). In the usual approach of shape spaces, the problem of matchings two shapes is to search a geodesic in a chosen space G_V of diffeomorphisms with constraints on the ends. Retrieving an optimal growth scenario via the growth dynamic does not only constrain the ends of the flow of diffeomorphisms. Indeed, the final status q_1 of a solution cannot be written as an image of the initial mapping q_0 by the final state of the flow ϕ_1^v. It depends instead on the whole evolution of the flow over time. In other words, the energy cannot be written as

$$E(\phi_1) = C(\phi_1) + \mathcal{A}(\phi_1) \,.$$

Thus, the optimal flow to reach a final target is usually not a geodesic of G_V.

Hence, the soughtafter existence of continuous global minimizers v cannot be deduced from existing general results in the literature. The first result of the chapter was rather unexpected. We exhibit a setting with a data attachment term built on the representation by varifolds where no global minimizers is continuous. The difference between representations by currents or varifolds, regarding the models associated to the growth dynamic, is explained by the fact that oscillations in time of the vector field v generate oscillations in space for the shapes $q_t(X_t)$. The currents through their cancellation effect on these spatial oscillations can prevent this behavior.

Proving the existence of continuous minimizers within the framework defined by the growth dynamic for a current data term attachment $\mathcal{A}$ first requires to ensure that the shapes are sufficiently regular to be represented by currents. Let us recall that the mappings q_t generated by vector fields $v \in L^2([0,1], V)$ are a priori neither $\mathcal{C}^1$ nor rectifiable. It is yet possible to define $\mathcal{A}$ on $L^2([0,1], V)$ by density of $\mathcal{C}([0,1], V)$ whose vector fields v generate mappings of $\mathcal{C}^1(X, \mathbb{R}^d)$.

The next step is to show the existence of solutions in $L^2([0,1], V)$. The proof is based on the linearity to the tangential component of the current representation that allows to deduce the lower semi-continuity of $\mathcal{A}$. The continuity of an optimal vector field v does not follow immediately. Indeed, we did show previously the continuity of the momentum map but the momentum space was restricted to be identified with a space of functions on $X \times \partial X$ where ∂X is the boundary of X. However, we show that this restriction is well-grounded if the scenarios are generated by continuous vector fields in time. Moreover, the central result of this chapter is the continuity of any global minimizer unconditionally on the momentum space. Therefore, these two results validate the functional representation of the momentum announced in the previous chapter. More precisely, consider v and a variation δv both in $\mathcal{C}([0,1], V)$ and $q^{v+\epsilon\delta v}$ the scenario generated by $v+\epsilon\delta v$ for any $\epsilon \in \mathbb{R}$. We show in Chapter 3 that there exists $\delta q \in \mathcal{C}([0,1], B)$ such that $q^{v+\epsilon\delta v} = q^v + \epsilon\delta q + o(\epsilon)$. There exist then $p_1^X \in \mathcal{C}(X, \mathbb{R}^n)$ and $p_1^{\partial X} \in \mathcal{C}(\partial X, \mathbb{R}^d)$ such that

$$\begin{aligned} \mathcal{A}'(v;\delta v) &= (p_1 \,|\, \delta q_1) && (1.53) \\ &= \int_X \langle p_1^X(x), \delta q_1(x)\rangle_{\mathbb{R}^n} d\mathcal{H}^k(x) + \int_{\partial X} \langle p_1^{\partial X}(x), \delta q_1(x)\rangle_{\mathbb{R}^n} d\mathcal{H}^{k-1}(x)\,, && (1.54) \end{aligned}$$

ensuring the existence of the final momentum p_1 and providing a pointwise expression as a function on X and its boundary ∂X. Note the appearance of the role played ∂X that gives the initial impulse to the momentum map, i.e. the existence of a constant $b > 0$ in equation (1.49) (see Chapter 3).

At last, we detail in this chapter the foliated structure induced by the birth tag τ on the coordinate space X when the creation process is regular meaning that the amount of newly created points at each time, i.e. the level sets of τ, evolves smoothly. After a brief presentation of submanifold with corners, we justify the canonical description of the biological coordinate system (X, τ) via a direct product $X = [0,1] \times X_0$ where τ is identified with the projection on the first coordinate. Indeed, with the point of view of the Morse theory, we show that many situations can be reduced to this canonical case by the action of spatial deformation of the space X carrying the tagging function τ. Note that the study of the growth dynamic achieved in Chapter 3 and all the experiments conducted in Chapter 5 are based on this specific system. The choice of the cost functions relies on it as it provides a first estimation to quantify the creation process over time. Another important consequence of this rewriting is the ability to overcome the reparameterizations in time of the scenarios generated by a birth place function (see also Chapter 2).

Chapter 5 : Numerical Applications and Results

This chapter examines the algorithm to optimize the initial momentum p_0 and applies it to illustrate the matching problem detailed in Chapter 3. Given a horn at a final age arbitrarily set at $t = 1$, the aim is to model its development from its birth at time $t = 0$ (state where the horn is reduced to a point) to the given final state $t = 1$. All experiments are performed with synthetic data built from the generative model presented in Chapters 2 and 3.

To highlight the pure creation process, the flows are reduced to rotations and translations. The basic model where the classic cost function C is given by equation (1.51) is unsuitable since it does not correctly initiate the growth process when the shape is too small at its birth. We use therefore new cost functions corresponding either to a time-varying weighting of the penalization on the flow (*adapted norm setup*) or to the addition of a constraint on the norm of the vector field (*constrained norm setup*). The data attachment term is derived from a representation of surfaces by oriented varifolds. It seems that these objects, presented in Section 2.3, have not yet been used for numerical applications. They find yet all their interest with easily orientable surfaces having structures like sharp spines or tails. Since the model should not be limited to affine deformations, the chapter concludes with some experiments with a Gaussian kernel RKHS to model vector fields.

This thesis was motivated by the need for new models to faithfully reproduce a biological phenomenon. It raises the issue to integrate additional prior information into the traditional framework proposed by the LDDMM methods. In the case of growth scenarios, the aim is to model the creation process but also to quantify it. The validation of the numerical experiments focuses specifically on the latter criterion. The different cost functions are compared regarding the goal to retrieve the norm of the vector field used to generate the target (Example 1). The flexibility of the model is tested in order to evaluate its ability to identify abnormal behavior such as growth delay. In contrast to the classic LDDMM, building the momentum map with the growth dynamic through a gradual influx of new initial momenta gives this flexibility and eliminates the need of reparametrizations in time to detect such anomalies (Example 2). At last, the model integrates without difficulty the addition of input data at known intermediate times to reconstruct a scenario by interpolation. It can improve the results of an experiment that could have approached the limits of the model by the high sharpness and curvature of the studied horn (Example 3).

Some other experiments are performed to observe the optimization of the initial position q_0 (Example 5) or the initial boundary effect (Example 4).

At last, as in the classic LDDMM framework, each scenario is completely characterized by the low dimensional variables initial position q_0 and initial momentum p_0, paving the way to a statistical analysis of the scenarios' population.

3.3 Glossary and notation

Throughout this thesis, shapes are modeled by mappings $q_t : X \to \mathbb{R}^d$ parameterized by a space X called the coordinate space. $\mathbb{R}^d$ is called the ambient space. The subscript t means that q_t describes the shape at time $t \in [0, 1]$. A scenario is typically a continuous set of mappings $t \in [0, 1] \mapsto q_t$. V is be a Hilbert space of vector fields on the ambient space $\mathbb{R}^d$ and $L^2([0, 1], V)$, eventually denoted L^2_V, is the space of square integrable time-varying vector fields.

Specific vocabulary:

- *Biological coordinate system* (X, τ) : indexation of the points of an time-varying shape. The function $\tau : X \to \mathbb{R}$ is called the *birth tag*.
- Biological coordinate space or *coordinate space* X : set of all the coordinates used to parameterize the shape over the time interval T of observation (fixed after Chapter 2 to $T = [0, 1]$).
- $X_t = \{x \in X \,|\, \tau(x) \le t\}$: subset of the so called *active points* at time t. A point in the complementary subset is called *inactive*.
- $X_{\{t\}} = \{x \in X \,|\, \tau(x) = t\}$: subset of the so called *new points* at time t, points that appear exactly at time t. These subsets are called the *leaves*.

Basic notation:

- If t is a real variable and g is a derivable function of t, we denote $g_t = g(t)$ and $\dot{g}_t = \frac{dg}{dt}(t)$.
- If $g : E \times [0, 1] \to F$ is a function with a time parameter, we note for any $t \in [0, 1]$, $g_t \doteq g(\cdot, t) : E \to F$.
- $L_V : V \to V^*$ and $K_V : V^* \to V$, $K_V = L_V^{-1}$, are the canonical isomorphisms between a Hilbert space and its dual.
- Given a Hilbert space H, if $f : H \to \mathbb{R}$ is a differentiable at $x \in H$, we denote $df(x)$ this differential and $\nabla_x f(x)$ its gradient. Likewise, we denote $\frac{\partial f}{\partial x_1}$ or $\partial_{x_1} f(x)$ a partial differential and $\nabla_{x_1} f(x)$ the associated gradient.
- We denote $\mathcal{B}(b, r)$ the close ball of center b and radius r.
- $\mathcal{AC}$ denotes the class of absolutely continuous functions.
- Given two Banach spaces E and F, $\mathcal{L}(E, F)$ denotes the set of continuous linear operators between E and F. We also denote $\mathcal{L}(E)$ for $\mathcal{L}(E, E)$.

Chapter 2

Partial Matchings and Growth Mapped Evolutions in Shape Spaces

Contents

1 Introduction

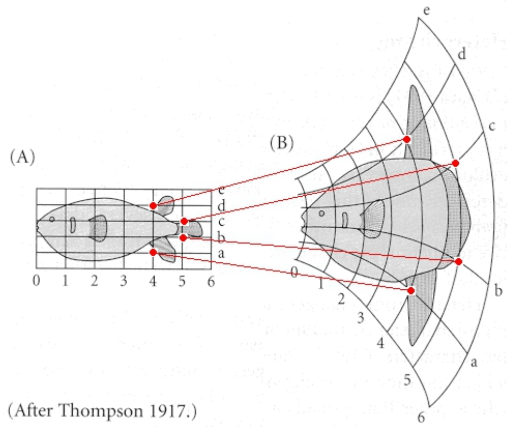

Figure 2.1 – Illustration after D'Arcy Thompson's works (1917). Given two similar shapes, there exists a simple deformation that matches them.

In order to introduce the idea of *foliated shapes*, we return to the reference work of D'Arcy Thompson. He illustrated through several examples that the differences between related species could be explained by simple geometrical deformations. The Figure 2.1 gives the implicit matching of two different fishes. The deformation provides a coherent mapping between the characteristic points of the fishes (head on head, eye on eye, fin on fin, etc.). The position in the ambient space of a characteristic point is variable from one fish to another, but the relative position of each point compared to the others is preserved and is thereby a descriptor of the species. The deformation of the grid highlights this consistence through a coordinate system common to the two fishes. Any point of the shape has a label that depends on the species and not on its position. We call these labels the **biological coordinate system**. It gives a general description of any individual of a population of related shapes independently of "simple" deformations that can be applied to them.

From a biological point of view, the matching of two fishes is not a geometrical matching of shapes but a set of one-to-one correspondences between *homologous points*, including in particular all the characteristic points. In Figure 2.1, these two processes coincide. The geometry of the shapes gives enough information to obtain a meaningful mapping. However, during a growth evolution, two shapes at different ages do not necessarily share the same set of homologous points. In Figure 2.2, we extrapolate the drawings of D'Arcy Thompson to examine growth or degeneration processes on some examples. On the left on top, we compare two ages of an animal horn. Below, we represent an organism with a *foliated* structure like an onion or the cross section of a tree trunk. Finally on the right, an other representation of a *foliated* membrane, such as the human skin where the double arrow indicates that we can read this example in both directions, as the growth or the degeneration of an organic tissue.

In each case, we assume that new material is progressively created during the growth at the boundary of the shape. The subsets of the new points created at each time, induce a natural decomposition of the complete set of all the coordinates. These subsets have all the

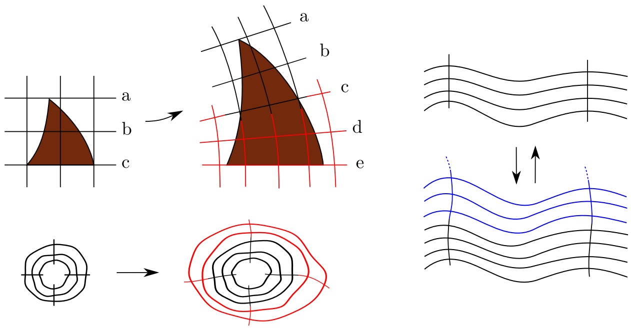

Figure 2.2 – The creation of new material during a growth process is linked to the appearance of new coordinates.

same shape: similar to lines for the horns or circles for the onion. They induce a collection of *foliated leaves* meaning that the shape is locally similar to a connected disjoint union of parallel lines. The creation of new material is thus linked to the appearance of new coordinates. Consequently, the grids are either extended or shortened with the red or blue lines. The biological coordinate system can thus code the pointwise homology between two ages of a shape. The matching should thus be achieved via a **partial mapping** delimited by the restriction to the black grids. Moreover, the biological coordinate system can help us to anticipate the creation of new material.

Note that the example of the fishes could also illustrate the growth of a fish. Yet in this case the growth process is similar to a scaling deformation and *although one could consider that we have a creation of new material stricto sensus, the homology structure remains stable*. The biological coordinates have already been introduced by Grenander et al. in [31] where they study their diffeomorphic evolution in homogeneous situations through elementary local deformations.

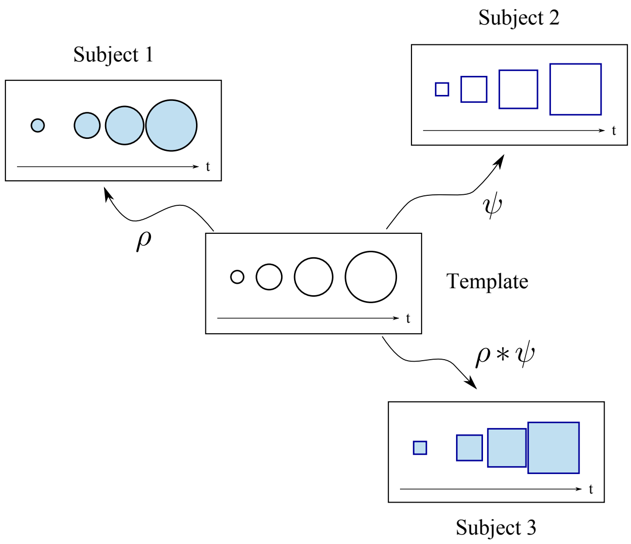

Figure 2.3 – Shape space point of view on growth scenarios. What deformations between scenarios ? A time warping ρ delays the growth of subject 1 with respect to the template. A spatial mapping ψ generates subject 2 and to be as general as possible, one need to allow at all time a new deformation so that ψ can be time dependent.

To deal with some of the core issues about the processing of shape evolutions in the context of growth, we propose in this chapter to follow a somewhat axiomatic point of view that can be parallel to the development of the shape space point of view (see Figure 2.3). In section 2, we first introduce a proper definition of the *objects* that are the atoms for the study of partial mappings and growth evolutions $(S_t)_{t\in T}$ with the notion of *growth mapped evolutions* incorporating the addition of a flow of mappings $(\phi_{s,t})_{s\leq t\in T}$ providing the homology correspondences between points within the evolution sequence. Then we define a web of morphisms between the objects organizing the relationship between the atoms. A core result will be to show in section 3 that part of this web can be interpreted as coming from space-time group actions from which we can derive a metric on appropriate orbits of growth mapped evolutions. We analyse further these orbits by showing the role of the centered evolutions corresponding to pure expansion scenarios for which the homology correspondences are trivial and on which a simple subgroup of space-time mappings can act. In section 4, we show that under reasonable regularity assumptions, any growth mapped evolution can be equipped with a tagging function, called the *birth function*, that provides a consistent stratification of the evolving shapes generalizing the idea of tree-ring dating to growth mapped evolutions. Finally, in section 5, we introduce a new parameter, called the *birth place function*, to initialize a growth mapped evolution. This new parameter will play a key role in the problem to retrieve the growth scenario of a shape as studied in the next chapters of this thesis.

2 Growth mapped evolutions (GMEs)

2.1 Embedded shapes

We aim to model partial relations inside a collection of shapes with diffeomorphisms. To compose and then compare these mappings require to consider shapes embedded in an ambient space.

Definition 2.1 (Embedded shapes (ES))**.** — *An embedded shape is a pair (E, S) where E is a set called the* embedding space *or the* ambient space *and $S \subset E$.*

- *Inner partial matching: For any two embedded shapes $A = (E^A, S^A)$ and $B = (E^B, S^B)$ the set* $\mathrm{Hom}(A, B)$ *of morphisms between A and B is given as the set of* invertible *mappings $\phi^{AB} : E^A \to E^B$ such that $\phi^{AB}(S^A) \subset S^B$. We check easily that if $\phi^{AB} \in \mathrm{Hom}(A, B)$ and $\phi^{BC} \in \mathrm{Hom}(B, C)$ then $\phi^{AC} \doteq \phi^{BC} \circ \phi^{AB} \in \mathrm{Hom}(A, C)$.* $\mathrm{Hom}(A, B)$ *will be denoted* $\mathrm{Hom}_{\mathrm{ES}}(A, B)$*. The morphisms will be called* ***inner partial matchings*** *between embedded shapes.*
- *Define* $\mathrm{Hom}^*(A, B)$ *as the set of* ***outer partial matchings*** *$\psi^{AB} : E^A \to E^B$ such that its inverse $\psi^{AB,-1} \in \mathrm{Hom}(B, A)$ i.e. the set of invertible mappings ψ^{AB} such that $\psi^{AB}(S^A) \supset S^B$. Obviously, if $\psi^{AB} \in \mathrm{Hom}^*(A, B)$ and $\psi^{BC} \in \mathrm{Hom}^*(B, C)$ then $\psi^{AC} = \psi^{BC} \circ \psi^{AB} \in \mathrm{Hom}^*(A, C)$.*
- *Define the* ***symmetric matchings*** *between two embedded shapes A and B as the set of $\phi^{AB} \in \mathrm{Hom}(A, B)$ such that $\phi^{AB,-1} \in \mathrm{Hom}(B, A)$ i.e. $\phi^{AB} \in \mathrm{Sym}(A, B) \doteq \mathrm{Hom}(A, B) \cap \mathrm{Hom}^*(A, B)$.*

Remark 2.1. *The LDDMM point of view is deeply associated with the idea of homogeneous spaces and diffeomorphic transformations of a shape S^A into an other shape S^B. This corresponds to the notion of symmetric matching defined just above. Indeed, if $\phi^{AB} \in \mathrm{Sym}(A,B)$, then since $\phi^{AB} \in \mathrm{Hom}(A,B)$, we have $\phi^{AB}(S^A) \subset S^B$ and since $\phi^{AB} \in \mathrm{Hom}^*(A,B)$ we have $\phi^{AB,-1}(S^B) \subset S^A$ i.e. $S^B \subset \phi^{AB}(S^A)$. Hence, $\phi^{AB}(S^A) = S^B$ and ϕ^{AB} is an invertible mapping matching exactly S^A to S^B. Moreover, when the shapes are embedded in a common ambient space E and if G is a group of invertible mappings on E, we can associate to any $\phi \in G$ and any template object $A_0 = (E, S_0)$ a transformed object $B = \phi \cdot A_0 \doteq (E, \phi(S_0))$ so that ϕ can be seen as an element in $\mathrm{Sym}(A_0, \phi \cdot A_0)$.*

Growth naturally induces inner partial mappings but the relations between homologous points when they exist should be preserved through time. This leads to the introduction of a set $\mathcal{L}$ of tags and of tagging functions. They will allow to add constraints to a matching between two shapes S^A and S^B. Mainly, assume that S^A and S^B are partitioned and given with predetermined correspondences between the parts of S^A and S^B. A tagging function on both shapes can therefore encode these sought-after correspondences.

Definition 2.2 (Tagged embedded shapes (TES))**.** — *A tagged shape over a set of tags $\mathcal{L}$ is defined as $A = (E, S, \tau)$ where (E, S) is an embedded shape and $\tau : S \to \mathcal{L}$.*

— $\mathrm{Hom}(A,B)$ *is given as the set of* invertible *mappings $\phi^{AB} : E^A \to E^B$ such that*

1. $\phi^{AB}(S^A) \subset S^B$,
2. $\tau^B \circ \phi^{AB} = \tau^A$ *on* S^A,
3. $\phi^{AB}(S^A) = \tau^{B,-1}(\tau^A(S^A))$.

The elements of $\mathrm{Hom}(A,B)$ *are* ***tag consistent inner partial matchings*** *between embedded shapes and* $\mathrm{Hom}(A,B)$ *is denoted* $\mathrm{Hom}_{\mathrm{TES}}(A,B)$

See Figure 2.4 for an illustration. We will denote $L^A = \tau^A(S^A)$, $L^B = \tau^B(S^B)$, etc. the set of tags involved on S^A, S^B, etc.

Remark 2.2. — *If L^A and L^B are both reduced to a singleton and $L^A = L^B$, then the inner partial mapping is actually a standard LDDMM matching. Note that the condition $L^A = L^B$ alone does not provide a standard matching (see the mapping between C and D in Figure 2.4).*

— *If $\mathrm{Hom}(A,B) \neq \emptyset$ then $L^A \subset L^B$. Indeed, if $\phi^{AB} \in \mathrm{Hom}(A,B)$, then* (1) *and* (2) *imply that $\tau^A(S^A) = \tau^B(\phi^{AB}(S^A)) \subset \tau^B(S^B)$. A strict inclusion corresponds from the biological point of view to a creation of new points.*

— *The point* (3) *of the definition enforces every point of S^B with a common tag of S^A to be reached by ϕ^{AB}. In other words, for any tag $l \in L^A \cap L^B$, ϕ^{AB} induces an invertible mapping between the level sets $\tau^{A,-1}(l) \subset S^A$ and $\tau^{B,-1}(l) \subset S^B$.*

— *There is no constraint on the matching inside the respective level sets of τ^A and τ^B. For example, if $L^A = \{0\}$ and $L^B = \{0,1\}$, then the tags only demarcates the subset of S^B to be matched with S^A.*

Remark 2.3 (Extension of ES into TES)**.** *From the opposite point of view, an inner partial morphism ϕ^{AB} between two general embedded shapes $A = (E^A, S^A)$ and $B = (E^B, S^B)$ induces a natural minimal pair of tagging functions given by τ^A constant equal to* 0 *and*

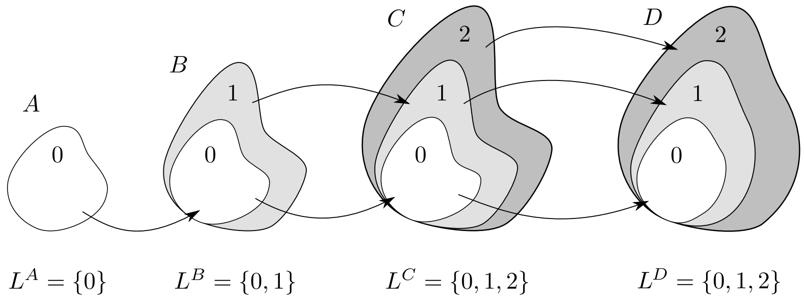

Figure 2.4 – A morphism $\phi^{A,B} \in \mathrm{Hom}_{\mathrm{TES}}(A, B)$ must match S^A on the subset of S^B demarcated by the tag 0. The tag only defines the image set of the source shape inside the target shape. Between B and C, the tag also imposes a constraint inside the image of S^B. The points of S^B tagged by 0 are sent to the points of S^C tagged by 0 and likewise for the points tagged by 1. The arrows represent invertible mappings between the level sets of the tagging functions, given by the restrictions of ϕ^{AB}, ϕ^{BC} and ϕ^{CD}. The appearance of a new tag corresponds therefore to the creation of matter uncorrelated to the previous shape. Otherwise, as between C and D, the shape is only deformed by ϕ^{CD}. We will say that the evolution is given by **pure deformation**. Even without creation ϕ^{CD} is still constrained by the tags.

τ^B equal to 0 on the image of S^A and equal to 1 on the complement. By construction, ϕ^{AB} is then tag consistent with τ^A and τ^B. Any tagging function τ^A on S^A could also be imported and extended to a tagging function on S^B with respect to ϕ^{AB}. Indeed, we can define $\tau^B \doteq \tau^A \circ \phi^{AB,-1}$ on $\phi^{AB}(S^A)$ and $\tau^B = l^B$ on the complement, with any $l^B \notin L^A$ so that $L^B = L^A \sqcup \{l^B\}$. Then again ϕ^{AB} becomes tag consistent with τ^A and τ^B.

These tag consistent inner partial mappings can be composed.

Proposition 2.1. *If $\phi^{AB} \in \mathrm{Hom}_{\mathrm{TES}}(A, B)$ and $\phi^{BC} \in \mathrm{Hom}_{\mathrm{TES}}(B, C)$ then $\phi^{AC} \doteq \phi^{BC} \circ \phi^{AB} \in \mathrm{Hom}_{\mathrm{TES}}(A, C)$.*

Proof. Indeed, $\phi^{AC}(S^A) = \phi^{BC}(\phi^{AB}(S^A)) \subset \phi^{BC}(S^B) \subset S_C$, $\tau_C \circ \phi^{AC} = \tau_C \circ \phi^{BC} \circ \phi^{AB} = \tau^B \circ \phi^{AB} = \tau^A$ and $\phi^{AC}(S^A) = \phi^{BC}(\phi^{AB}(S^A)) = \phi^{BC}(\tau^{B,-1}(\tau^A(S^A))$. However, if $L_0 \subset \tau^B(S^B)$ then

$$\phi^{BC}(\tau^{B,-1}(L_0)) = \tau^{C,-1}(L_0)\,. \tag{2.1}$$

Indeed $\phi^{BC}(\tau^{B,-1}(L_0)) \subset \tau_C^{-1}(L_0)$. Conversely, if $y \in \tau_C^{-1}(L_0)$, since we have $\tau_C^{-1}(L_0) \subset \tau_C^{-1}(\tau^B(S^B))$ we get $y \in \phi^{BC}(S^B)$ so that there exists $x \in S^B$ such that $\phi^{BC}(x) = y$. Now, using (2), we get $\tau_C(y) = \tau^B(x)$ so that $\tau^B(x) \in L_0$, $x \in \tau^{B,-1}(L_0)$ and $y \in \phi^{BC}(\tau^{B,-1}(L_0))$.

Using (2.1) for $L_0 = \tau^A(S^A)$, we get $\phi^{BC}(\tau^{B,-1}(\tau^A(S^A)) = \tau^{C,-1}(\tau^A(S^A)) = \phi^{AC}(S^A)$. □

Definition 2.3 (Outer and symmetric tag consistent matchings)**.** *As we did previously, we can define the set of outer tag consistent matchings $\mathrm{Hom}^*_{\mathrm{TES}}(A, B)$ and the set of symmetric tag consistent matchings as $\mathrm{Sym}_{\mathrm{TES}}(A, B) = \mathrm{Hom}_{\mathrm{TES}}(A, B) \cap \mathrm{Hom}^*_{\mathrm{TES}}(A, B)$.*

Remark 2.4. *If two tagged embedded shapes share the same set of tags $L^A = L^B$, then for any $\phi \in \mathrm{Hom}_{\mathrm{TES}}(A, B)$, Definition 2.2 says that $\phi^{AB}(S^A) = \tau^{B,-1}(\tau^A(S^A)) =$*

$\tau^{B,-1}(L^B) = S^B$, *and* $\phi \in \mathrm{Sym}_{\mathrm{TES}}(A, B)$. *Conversely, if there exists* $\phi \in \mathrm{Sym}_{\mathrm{TES}}(A, B)$, *then* $\phi^{AB}(S^A) = S^B$, $L^A = L^B$ *and again* $\mathrm{Hom}_{\mathrm{TES}}(A, B) = \mathrm{Sym}_{\mathrm{TES}}(A, B)$.

2.2 Growth mapped evolutions (GMEs)

A growth mapped evolution aims to model the growth scenario of an individual. The different ages of the object are represented by a collection of shapes $(S_t)_{t\in T}$ in a fixed ambient space E.

Definition 2.4 (Growth mapped evolution of embedded shapes)**.** *A growth mapped evolution of embedded shapes (GME) in* E *indexed by* $T \subset \mathbb{R}$ *is given as*

$$g = (T, (A_t)_{t\in T}, (\phi_{s,t})_{s\leq t\in T})$$

such that

1. $A_t = (E, S_t)$ *is an embedded shape for any* $t \in T$,
2. $\phi_{s,t} \in \mathrm{Hom}_{\mathrm{ES}}(A_s, A_t)$ *for any* $s \leq t \in T$,
3. $\phi_{s,t} \circ \phi_{r,s} = \phi_{r,t}$ *for any* $r \leq s \leq t \in T$.

We denote $\mathrm{GME}(T, E)$ *the set of all such growth mapped evolutions.*

Property (3) says that applying successively the deformations between time r and s and between time s and t gives the deformation between r and t. Note that $\phi_{t,t} = \mathrm{Id}$. We will also note $\phi_{t,s} = \phi_{s,t}^{-1}$ when $s \leq t$. $(\phi_{s,t})_{s\leq t\in T}$ will be called the *flow* of g.

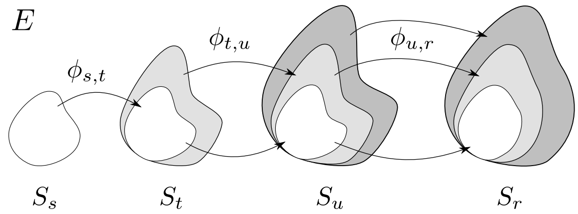

Figure 2.5 – Illustration of a GME in an ambient space E.

At all time, the growing shape is formed by new points that just appeared and old points.

Definition 2.5 (**New points** and **old points**)**.** *Let* $g = (T, (A_t)_{t\in T}, (\phi_{s,t})_{s\leq t\in T})$ *be a GME. For any time* $s \in T$ *and any point* $x \in S_s$, *we consider the evolution of* x *backwards and forwards through the deformation* ϕ. *It defines a path* $t \mapsto x_t = \phi_{s,t}(x)$ *in the embedding space* E. *Now for any* $t \in T$ *such that* $x_t \in S_t$, x_t *is called a new point at time* t *or a new point of* S_t *if for any previous time* $r \in T$, $r < t$, $x_r \notin S_r$, *and called an old point otherwise. Note at last that if* $x_t \in S_t$ *is a new point, for any following time* $r > t$, $x_r \in S_r$.

The growth scenarios under tag constraints are defined likewise.

Definition 2.6 (Growth mapped evolution of tagged embedded shapes)**.** *A growth mapped evolution of tagged embedded shapes (TGME) in* E *indexed by* $T \subset \mathbb{R}$ *is given as*

$$g = (T, (A_t)_{t\in T}, (\phi_{s,t})_{s\leq t\in T})$$

such that

1. $A_t = (E, S_t, \tau_t)$ *is a tagged embedded shape in* E *for any* $t \in T$,
2. $\phi_{s,t} \in \mathrm{Hom}_{\mathrm{TES}}(A_s, A_t)$ *for any* $s \leq t \in T$,
3. $\phi_{s,t} \circ \phi_{r,s} = \phi_{r,t}$ *for any* $r \leq s \leq t \in T$.

Remark 2.5 (Decomposition of the growth process)**.** *The evolution of a growing shape can be described by the combination of two different processes. A **pure deformation** process when there is no creation of new points and a **pure expansion** process when the inner partial matching between two ages is reduced to the identity. In the first case, the sets of tags, denoted* $L_t = \tau_t(S_t)$*, are constant. In the second case, the flow of the scenario is trivial i.e.* $\phi_{s,t} = \mathrm{Id}$ *for any* $s, t \in T$.

New points correspond to the growth by expansion of the shape. A set of new points comes necessarily with a new tag (or eventually several new tags).

Remark 2.6. *Following Remark 2.2, the sets of tags* $(L_t)_{t\in T}$ *form a non decreasing sequence in the sense of set inclusion. This means, regarding the homology, that a shape can only be expanding (the shape could yet shrink via a deformation similar to a scaling). When two sets* L_s *and* L_t *are equal, the shape evolves only through a pure deformation. It can be written for* $s < t \in T$ *by*

$$L_s \subsetneq L_t \quad \Leftrightarrow \quad \phi_{s,t}(S_s) \subsetneq S_t\,.$$

Moreover, if there is no creation of points between times s *and* t*, then there is no creation between any intermediate times:*

$$L_s = L_t \quad \Leftrightarrow \quad \forall r \in [s,t] \cap T, \quad L_r = L_s \quad \Leftrightarrow \quad \forall r \in [s,t] \cap T, \quad \phi_{r,t}(S_r) = S_t\,.$$

Example 2.1 (Generation of a circle)**.** *Let us show how two growth mapped evolutions can give two different explanations of the development of a circle. Let* $T = [0, 2\pi]$ *be the time interval of observations,* $E = \mathbb{R}^2$*, and* $S_t = \{(cos(\theta), sin(\theta)) | \theta \in [0,t]\}$ *a collection of arcs of the unit circle, growing from a point* $S_0 = \{(1,0)\}$ *to the unit circle* $S_{2\pi} = \mathbb{S}^1$*. Let us define two GMEs* g^A *and* g^B *sharing* E*,* T *and* $(S_t)_{t\in T}$ *as previously introduced (see Figure 2.6).*

1. *First scenario:*
   Complete g^A *with* $\phi^A_{s,t} = \mathrm{Id}$*. The arcs are static. A new point appears at every time* t *at the extremity* $(cos(t), sin(t)) \in E$*. The shape is only evolving by **pure expansion**.*
2. *Second scenario:*
   Complete g^B *with* $\phi^B_{s,t} = R_t \circ R_s^{-1}$ *where* R_θ *is the rotation of angle* θ*. Here the arcs are gradually rotated and a new point appears at every time at the extremity* $(1,0) \in E$*. The speed of the rotation canceled exactly the speed of the creation of new points so that the point at the extremity* $(1,0)$ *seems static.*

In both cases, we have an expansion of the shape on its boundary, but in the second scenario, new points are all created at the same location. The creation is constrained to a specific area. This last case is similar to the development of an animal horn.

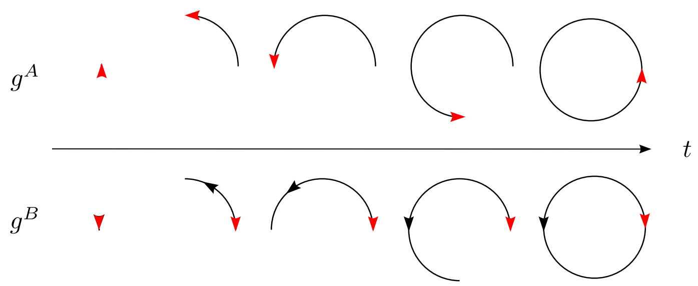

Figure 2.6 – Illustration of Example 2.1. On the first row, the first scenario. Below, the second scenario. The red arrows show where the shape is expanding and therefore point to the direction in which the shape should be extending without any deformation. During the second scenario, the ambient space is rotated as implied by the black arrows.

The tagging functions allow to encode a wide range of information to guide the reconstruction of a coherent scenario. However, throughout this chapter, we will be interested in one particular tagging function. As introduced in Remark 2.3, in some cases a canonical temporal tag can extend a general GME to a TGME.

Example 2.2 (Minimal extension of a GME : Finite case.)**.** *For a GME defined on a finite time set $T = \{t_{\min}, \ldots, t_i, \ldots, t_{\max}\}$, we can construct by recurrence for any $t \in T$, the tagging functions $\tau_t : S_t \to T$ by*

— $\tau_{t_{\min}} = t_{\min}$,

— $\tau_{t_{i+1}}(x) = \begin{cases} \tau_{t_i} \circ \phi^{-1}_{t_i,t_{i+1}}(x) & \textit{if } x \in \phi_{t_i,t_{i+1}}(S_{t_i}) \,, \\ t_{i+1} & \textit{otherwise.} \end{cases}$

Then the flow $(\phi_{s,t})_{s<t\in T}$ of the GME is consistent with this tag.

*To enlighten this tag, consider a point $x \in S_s$ and follow its evolution through the flow backwards and forwards. The path $t \mapsto x_t = \phi_{s,t}(x)$ is defined in the embedding space E since x_t does not necessarily belong to S_t at the beginning of the evolution. Since the flow is consistent with τ, $t \mapsto \tau_t(x_t)$ gives a constant value t_{birth} of T that is exactly the first time $t \in T$ such that $x_t \in S_t$. According to Definition 2.5, $x_{t_{\text{birth}}}$ is a new point of $S_{t_{\text{birth}}}$. Then for any $t \geq t_{\text{birth}}$, $x_t \in S_t$. This tag is consequently called the **birth tag** of the GME. Note that since T is finite, t_{birth} always exists.*

In the next sections, we will see how to define rigorously the **birth tag** of any GME on a compact set T. It will require some regularity conditions on the set of shapes to ensure the existence of t_{birth}. We can yet already give an example on the circles where T is a closed interval and exactly one point appears at each time.

Example 2.3 (Generation of a circle)**.** *Consider g^A and g^B as defined in Example 2.1. As we saw previously, g^A is expanding anticlockwise and g^B is expanding clockwise. In both cases, the shapes at any time $t \in [0, 2\pi[$ are the arc image of $[0, t] \subset [0, 2\pi[$ by the function $s \mapsto (cos(s), sin(s))$. Exactly one point appears at any time $t \in T$ except for the last time $t = 2\pi$ (see the red arrows in Figure 2.6). In g^A, this new point appears at the position $(cos(t), sin(t))$ such that we define $\tau^A_t(cos(t), sin(t)) = t$. All the other points are old points, so we import their tag from their older position. In g^B, this new point appears always at position $(1, 0)$ such that we define $\tau^B_t(1, 0) = t$. Then again, all the other tags* *are determined to be consistent with the deformation. In fine, for any $t \in T$, we define $\tau_t^A : S_t^A \to T$ and $\tau_t^B : S_t^B \to T$ displayed in Figure 2.7 and defined by*

$$\tau_t^A(cos(\theta), sin(\theta)) = \theta \qquad \textit{for any } \theta \in [0, t], \theta \neq 2\pi\,,$$
$$\tau_t^B(cos(\theta), sin(\theta)) = t - \theta[2\pi] \qquad \textit{for any } \theta \in [0, t], \theta \neq 2\pi\,.$$

Hence, $(\phi_{s,t}^A)_{s<t\in T}$ and $(\phi_{s,t}^B)_{s<t\in T}$ are respectively consistent with τ^A and τ^B so that g^A and g^B can be extended to growth mapped evolutions of tagged shapes (TGMEs) and these tagging functions are the ***birth tags*** *as defined in Example 2.2 of g^A and g^B. See Figure 2.7.*

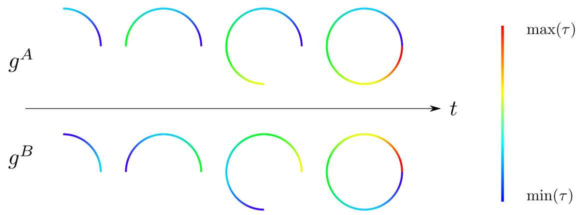

Figure 2.7 – The shapes S_t (for $t \in \{\pi/2, \pi, 3\pi/4, 2\pi\}$) are colored in function of τ_t, on top for g^A and below for g^B. The red indicates the points that just appeared at the end of the growth process and the blue the first points.

Remark 2.7. *The example of the circles illustrate the role of the flow to retrieve the evolution of a growing shape. Note that $(\phi_{s,t}^B)_{s<t\in T}$ is not consistent with τ^A and likewise $(\phi_{s,t}^A)_{s<t\in T}$ is not consistent with τ^B. The tagging functions allow to discriminate the hypothetical scenarios.*

2.3 Morphisms between GMEs

Morphisms between GMEs are the core of this framework. They allow us to generate a set of GMEs sharing a common growth pattern and therefore to organize them. Following the ideas illustrated in Figure 2.3, a morphism between two GMEs g^A and g^B requires a time warping ρ between T^A and T^B. Then at any time t, a spatial mapping matches the two "shapes" A and B at age t and $\rho(t)$ respectively. Moreover, these mappings must be consistent with the respective flows of each GME. This means that (assume to simplify that there is no time warping here) if we consider two points $x \in S_s^A$ and $y \in S_s^B$ at any aligned ages $s \in T$, then the spatial mappings between the two GMEs send the evolution of x in g^A, $t \mapsto x_t = \phi_{s,t}^A(x)$, to the evolution of y in g^B, $t \mapsto y_t = \phi_{s,t}^B(y)$. Finally if the GMEs are tagged, the spatial mappings must also be consistent with the tags (modulo again a mapping between the tag sets of g^A and g^B).

Definition 2.7. (i) *For any two GMEs g^A and g^B, the set* $\mathrm{Hom}_{\mathrm{GME}}(g^A, g^B)$ *of morphisms between g^A and g^B is given by a time warping $\rho^{AB} : T^A \to T^B$ (non decreasing function) and a set of spatial mappings $(q_t^{AB} : S_t^A \to S_{\rho^{AB}(t)}^B)_{t\in T^A}$, such that for any $s \leq t \in T^A$*

$$(1)\; q_t^{AB}(S_t^A) = S_{\rho^{AB}(t)}^B \qquad (2)\; \phi_{\rho^{AB}(s),\rho^{AB}(t)}^B \circ q_s^{AB} = q_t^{AB} \circ \phi_{s,t}^A\big|_{S_s^A}\,.$$

(ii) For any two TGMEs g^A and g^B, the set $\mathrm{Hom}_{\mathrm{TGME}}(g^A, g^B)$ *of morphisms bewteen g^A and g^B is given by a time warping $\rho^{AB} : T^A \to T^B$, a label mapping $\eta^{AB} : L^A \to L^B$ and a set of spatial mappings $(q_t^{AB} : S_t^A \to S^B_{\rho^{AB}(t)})_{t\in T^A}$, such that for any $s \le t \in T^A$*

$$(1)\ q_t^{AB}(S_t^A) = S^B_{\rho^{AB}(t)} \qquad\qquad (2)\ \phi^B_{\rho^{AB}(s),\rho^{AB}(t)} \circ q_s^{AB} = q_t^{AB} \circ \phi^A_{s,t}|_{S_s^A}\ .$$

Moreover, for any $t \in T^A$ and any $y \in S^B_{\rho^{AB}(t)}$, there exists $x \in S_t^A$ such that $q_t^{AB}(x) = y$ and

$$(3)\ \tau^B_{\rho^{AB}(t)}(y) = \eta^{AB}(\tau_t^A(x))\,.$$

When q_t^{AB} is one-to-one, this means that $\tau^B_{\rho^{AB}(t)} \circ q_t^{AB} = \eta^{AB} \circ \tau_t^A$ but this is not equivalent to (3) *if q_t^{AB} is not one-to-one.*

This definition can be illustrated by the following commutative diagram. On the top row, a scenario g^A, on the bottom row, its image g^B.

$$\begin{tikzcd}
S_s^A \arrow[r, hook, "\phi^A_{s,t}"] \arrow[d, "q_s"'] & S_t^A \arrow[r, hook, "\phi^A_{t,u}"] \arrow[d, "q_t"] & S_u^A \arrow[d, "q_u"] \\
S^B_{\rho(s)} \arrow[r, hook, "\phi^B_{\rho(s),\rho(t)}"'] & S^B_{\rho(t)} \arrow[r, hook, "\phi^B_{\rho(t),\rho(u)}"'] & S^B_{\rho(u)}
\end{tikzcd}$$

Remark 2.8. *If q_s^{AB} is invertible and $\eta^{AB} = \mathrm{Id}$, point* (3) *in Definition 2.7 implies that the mapping preserve the tags. If $(L_t^A)_{t\in T^A}$ is moreover strictly increasing then any time warping ρ^{AB} of* $\mathrm{Hom}_{\mathrm{TGME}}(g^A, g^B)$ *is necessarily strictly increasing. Indeed, for any $s < t \in T^A$, $L_s^A \subsetneq L_t^A$ implies that $L^B_{\rho^{AB}(s)} = L_s^A \subsetneq L_t^A = L^B_{\rho^{AB}(t)}$. Then since $(L_t^B)_{t\in T^B}$ is at least increasing, $\rho^{AB}(s) < \rho^{AB}(t)$. Actually, the equalities $(L_t^A = L^B_{\rho^{AB}(t)})_{t\in T^A}$ define here completely ρ^{AB}.*

The next examples intend to illustrate some properties and issues of growth scenarios generated as the images of a template scenario. It brings indeed the possibility for a shape to enter in collision with itself and self-intersect during the evolution. This phenomena happens when the spatial mapping q^{AB} is not injective. Indeed, even if a flow induces a diffeomorphic deformation of the ambient space, a new point of the shape can meet an old one (see when the arcs of the circle are closing in the next example). We will see at the end of this chapter, from our choice of modeling that we cannot distinguish shapes with a collision point and shapes without collision point (to separate for example curves with or without intersections). In practice, we aim for one-to-one mappings but with a possible localized exception when the first state of a shape is degenerated. For example, at the beginning of its growth, a horn is reduced to a point that will form its tip (see Chapter 4).

The different biological interpretations of a collision are linked to the complexity of the third condition in Definition 2.7.

Example 2.4 (Collision and overlapping I)**.** *The development of the unit circle presented in Example 4.1 can be seen as the image of a simpler TGME g^I defined by a collection of intervals*

— $I_t = [0, t]$, $t \in T^I = [0, 1]$,

— $\phi^I_{s,t} = \mathrm{Id}$,

— $\tau^I_t : I_t \to T, x \mapsto x$.

g^I is a static segment, extending on its right side. To retrieve the TGMEs g^A and g^B of Example 2.3, the morphisms $m^{IA} : g^I \mapsto g^A$ and $m^{IB} : g^I \mapsto g^B$ can be defined by

— $\rho^{IA}, \rho^{IB} : T^I \to T, t \mapsto 2\pi t$,

— $\eta^{IA}, \eta^{IB} : T^I \to T, t \mapsto 2\pi t$,

— $q^{IA}_t : I_t \to S_t, x \mapsto (cos(\theta), sin(\theta))$, *with* $\theta = 2\pi x$,

— $q^{IB}_t : I_t \to S_t, x \mapsto (cos(\theta), sin(\theta))$, *with* $\theta = 2\pi(t - x)$.

Indeed, all shapes are reduced to a singleton at time 0 so that necessarily in both cases $q^*_0(0) = (1, 0)$ (where $*$ denote simultaneously a property for A and B). Then, Definition 2.7 (2) implies that once two points are mapped by a morphism, their respective evolutions are also mapped together. Hence, since there is no deformation on g^I and g^A, the spatial mappings q^{IA}_t are constant in time ($x \mapsto q^{IA}_t(x)$ for any $x \in I_t$). For the other morphism, we get that $q^{IB}_t(0) = \phi^B_{0,2\pi t}(q^{IB}_0(0)) = (cos(2\pi t), sin(2\pi t))$.

As regards the tags, in both cases, for any $t \in T^I$ such that $t \neq 1$, the spatial mappings q^*_t are one to one and the morphisms are consistent with the tags. Indeed, we can easily check that

$$\tau^A_{2\pi t}(cos(\theta), sin(\theta)) = \eta^{IA}(x) = 2\pi x, \text{ with } \theta = 2\pi x,$$
$$\tau^B_{2\pi t}(cos(\theta), sin(\theta)) = \eta^{IB}(x) = 2\pi x, \text{ with } \theta = 2\pi(t - x)$$

coincide with the tags introduced in Example 2.3.

At the end of the evolution, the segment $[0, 1]$ is sent to the closed circle. The point $(1, 0)$ of the circle has two inverse images and only one of its inverses gives its label (adjusted by η). It can a priori be seen as both a new point of $S_{2\pi}$, as the image $q^*_1(1)$, and the initial point of S_0, as the image $q^*_1(0)$. Yet, when the inverse images have not been created at the same time, it is necessarily the oldest one that gives its tag. More precisely, Definition 2.2 (2) imposes $\tau^*_{2\pi}(1, 0) = \tau^*_{2\pi}(\phi^*_{0,2\pi}(1, 0)) = \tau^*_0(1, 0) = 0$.

Remark 2.9. *Note in this example that since $\phi^A_{s,t} = \mathrm{Id}$ for any $s, t \in T$, the flow does not play any role in the collision. It is the only consequence of the intrinsic expansion.*

Moreover, when the spatial mappings are not invertible the apparent choice of tags in the definition of the morphism is not as free as it could seem. We will progressively see that the tags have a natural ordered structure induced by Definition 2.2.

Example 2.5 (Collision and overlapping II)**.** *Figure 2.8 illustrates the possibility of an overlapping during the development of animal horns. When the deformations of the ambient space are given by diffeomorphisms, the evolution of the shape outside the areas of creation is diffeomorphic. Hence, an overlapping can only start at the neighborhood of a new point.*

We turn back to our presentation of morphism between growth mapped evolutions and describe now the composition laws.

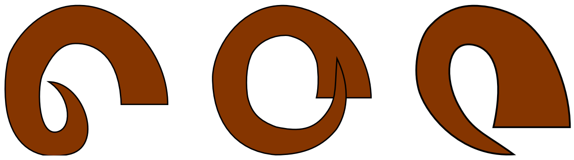

Figure 2.8 – Curved horns with and without overlapping. On these examples, we assume that the apparition of new points occur at the base of the horns so that a collision can only appear around this base. On the left, no collision should happen since the top of the horn is moving away from the base of the horn. On the middle, the top of the horn previously hit once the base, then the apparition of new points created the overlapping. On the right, likewise, a collision and an important overlapping may be about to occur.

Proposition 2.2. *i) If* $m^{AB} \in \mathrm{Hom}_{\mathrm{GME}}(g^A, g^B)$ *and* $m^{BC} \in \mathrm{Hom}_{\mathrm{GME}}(g^B, g^C)$ *are given by*

$$m^{AB} = (\rho^{AB}, (q_t^{AB})_{t\in T^A}) \quad \text{and} \quad m^{BC} = (\rho^{BC}, (q_t^{BC})_{t\in T^B}),$$

then $m^{AC} \doteq m^{AB} \circ m^{BC} = \big(\rho^{BC} \circ \rho^{AB}, (q^{BC}_{\rho^{AB}(t)} \circ q_t^{AB})_{t\in T}\big) \in \mathrm{Hom}_{\mathrm{GME}}(g^A, g^C)$.
Likewise,
ii) If $m^{AB} \in \mathrm{Hom}_{\mathrm{TGME}}(g^A, g^B)$ *and* $m^{BC} \in \mathrm{Hom}_{\mathrm{TGME}}(g^B, g^C)$ *are given by*

$$m^{AB} = (\rho^{AB}, \eta^{AB}, (q_t^{AB})_{t\in T^A}) \quad \text{and} \quad m^{BC} = (\rho^{BC}, \eta^{BC}, (q_t^{BC})_{t\in T^B}),$$

then $m^{AC} \doteq m^{AB} \circ m^{BC} = \big(\rho^{BC} \circ \rho^{AB}, \eta^{BC} \circ \eta^{AB}, (q^{BC}_{\rho^{AB}(t)} \circ q_t^{AB})_{t\in T}\big) \in \mathrm{Hom}_{\mathrm{TGME}}(g^A, g^C)$.

Proof. We only check the transitivity of the composition for the TGMEs since it implies immediately the same property for the GMEs. For any $t \in T^A$, m^{AC} is given by $q_t^{AC} = q^{BC}_{\rho^{AB}(t)} \circ q_t^{AB}$, $\rho^{AC} = \rho^{BC} \circ \rho^{AB}$ and $\eta^{AC} = \eta^{BC} \circ \eta^{AB}$. We verify the three properties of Definition 2.7 (ii). For property (1), we have

$$q_t^{AC}(S_t^A) = q^{BC}_{\rho^{AB}(t)}(S^B_{\rho^{AB}(t)}) = S^C_{\rho^{BC}(\rho^{AB}(t))} = S^C_{\rho^{AC}(t)}\,.$$

Then for property (2), we have for any $s \le t \in T^A$

$$\begin{aligned}
\phi^C_{\rho^{AC}(s),\rho^{AC}(t)} \circ q_s^{AC} &= \phi^C_{\rho^{BC}\circ\rho^{AB}(s),\rho^{BC}\circ\rho^{AB}(t)} \circ q^{BC}_{\rho^{AB}(s)} \circ q_s^{AB} \\
&= q^{BC}_{\rho^{AB}(t)} \circ \phi^B_{\rho^{AB}(s),\rho^{AB}(t)} \circ q_s^{AB} \\
&= q^{BC}_{\rho^{AB}(t)} \circ q_t^{AB} \circ \phi^A_{s,t} = q_t^{AC} \circ \phi^A_{s,t}\,.
\end{aligned}$$

Finally, for property (3) we see that for any $r \in T^A$ and for any $z \in S_t^C$ with $t = \rho^{AC}(r)$, since m^{BC} is a morphism, there exists $y \in S_s^B$ with $s = \rho^{AB}(r)$ such that $q_s^{BC}(y) = z$ and $\tau_t^C(z) = \eta^{BC}(\tau_s^B(y))$. Moreover, since m^{AB} is a morphism, there exists $x \in S_r^A$ such that $q_r^A(x) = y$ and $\tau_s^B(y) = \eta^{AB}(\tau_r^A(x))$. Thus, we have $z = q_s^{BC}(y) = q_s^{BC} \circ q_r^{AB}(x) = q_r^{AC}(x)$ and

$$\tau_t^C(z) = \eta^{BC}(\tau_s^B(y)) = \eta^{BC}(\eta^{AB}(\tau_r^A(x))) = \eta^{AC}(\tau_r^A(x))\,.$$

□

3 Space of GMEs

3.1 Spatio-temporal group action

The definition of a set of morphisms connecting GMEs can be parallel to the first layer of the construction of shape spaces. To go further, let us show that a large subset of morphisms can be identified to a natural group action. Consider now that $T = [t_{\min}, t_{\max}]$ and E is a smooth manifold. Denote $\mathrm{Diff}(T)^+$, $\mathrm{Diff}(L)$ and $\mathrm{Diff}(E)$ the groups of C^1 diffeomorphisms on T (increasing), L and E respectively. Denote $\mathrm{TGME}(T, L, E)$ the set of growth mapped evolutions of tagged embedded shapes in the space E sharing the same timeline T and the same set of tags L. Denote likewise $\mathrm{GME}(T, E)$ the set of GMEs on T and E.

Proposition 3.1. *Consider* $G(T, L, E) \doteq \mathrm{Diff}(T)^+ \times \mathrm{Diff}(L) \times \mathrm{Diff}(E)^T$ *and for any* $\Psi = (\rho, \eta, \psi = (\psi_t)_{t\in T})$, $\Psi' = (\rho', \eta', \psi' = (\psi'_t)_{t\in T}) \in G(T, L, E)$ *the composition law defined by*

$$\Psi * \Psi' \doteq (\rho \circ \rho', \eta \circ \eta', (\psi_{\rho'(t)} \circ \psi'_t)_{t\in T})) \in G(T, L, E)\,. \tag{2.2}$$

Then, we have

i) $(G(T, L, E), *)$ *is a group with neutral element* $\Psi_{\mathrm{Id}} = (\mathrm{Id}, \mathrm{Id}, \mathbf{Id} = (\mathrm{Id}_t)_{t\in T})$ *and* $\Psi^{-1} = (\rho^{-1}, \eta^{-1}, (\psi^{-1}_{\rho^{-1}(t)})_{t\in T})$.

ii) $G(T, L, E)$ *acts on* $\mathrm{TGME}(T, L, E)$. *For any* $g^A \in \mathrm{TGME}(T, L, E)$, *any* $\Psi = (\rho, \eta, \psi) \in G(T, L, E)$, *we define* $g^B \doteq \Psi \cdot g^A$ *by*

(1) $S^B_{\rho(t)} = \psi_t(S^A_t)$ (2) $\phi^B_{\rho(s),\rho(t)} = \psi_t \circ \phi^A_{s,t} \circ \psi_s^{-1}$

(3) $\tau^B_{\rho(t)} = \eta \circ \tau^A_t \circ \psi_t^{-1}$

Ψ *induces thus a morphism* $m = (\rho, \eta, (q^{AB}_t)_{t\in T}) \in \mathrm{Hom}_{\mathrm{TGME}}(g^A, g^B)$ *with* $q^{AB}_t = \psi_t{}_{|_{S^A_t}}$. *Likewise,* $G(T, E) \doteq \mathrm{Diff}(T)^+ \times \mathrm{Diff}(E)^T$ *acts on* $\mathrm{GME}(T, E)$.

Proof. The law in associative:

$$\begin{aligned}
\Big((\rho, \eta, (\psi_t)_{t\in T}) \circ (\rho', \eta', (\psi'_t)_{t\in T})\Big) &\circ (\rho'', \eta'', (\psi''_t)_{t\in T}) \\
&= \Big(\rho \circ \rho' \circ \rho'', \eta \circ \eta' \circ \eta'', (\psi_{\rho'\circ\rho''(t)} \circ \psi'_{\rho''(t)} \circ \psi''_t)_{t\in T}\Big) \\
&= (\rho, \eta, (\psi_t)_{t\in T}) \circ \Big(\rho' \circ \rho'', \eta' \circ \eta'', (\psi'_{\rho''(t)} \circ \psi''_t)_{t\in T}\Big) \\
&= (\rho, \eta, (\psi_t)_{t\in T}) \circ \Big((\rho', \eta', (\psi'_t)_{t\in T}) \circ (\rho'', \eta'', (\psi''_t)_{t\in T})\Big)\,.
\end{aligned}$$

The remaining part of *i)* is straightforward. Regarding *ii)*, if $g^C = (\rho', \eta', \psi') \cdot g^B$ then $S^C_{\rho'\circ\rho(t)} = \psi'_{\rho(t)}(S^B_{\rho(t)}) = \psi'_{\rho(t)} \circ \psi_t(S^A_t)$, $\phi^C_{\rho'\circ\rho(s),\rho'\circ\rho(t)} = \psi'_{\rho(t)} \circ \phi^B_{\rho(s),\rho(t)} \circ (\phi'_{\rho(s)})^{-1} = (\psi'_{\rho(t)} \circ \psi_t) \circ \phi^A_{s,t} \circ (\psi_s^{-1} \circ (\psi'_{\rho(s)})^{-1}) = (\psi'_{\rho(t)} \circ \psi_t) \circ \phi^A_{s,t} \circ (\psi'_{\rho(s)} \circ \psi_s)^{-1}$ and $\tau^C_{\rho'\circ\rho(t)} = \eta' \circ \tau^B_{\rho(t)} \circ (\psi'_{\rho(t)})^{-1} = (\eta' \circ \eta) \circ \tau^A_t \circ (\psi'_{\rho(t)} \circ \psi_t)^{-1}$. $\square$

Example 3.1 (Spatial and temporal reparameterizations)**.** *The restrictions of* $G(T, L, E)$ *to the subgroups* $\mathrm{Diff}(T)^+$ *and* $\mathrm{Diff}(E)$ *define the basic reparameterizations in time or in space of a growth evolution. For any* $\rho \in \mathrm{Diff}(T)$ *and any* $\psi \in \mathrm{Diff}(E)$, *any* $g \in$

TGME(T, L, T), *the new growth scenarios* $g^\rho \doteq (\rho, \mathrm{Id}, \mathbf{Id}) \cdot g$ *and* $g^\psi \doteq (\mathrm{Id}, \mathrm{Id}, \psi) \cdot g$ *are given respectively by*

$$g^\rho = (T, (E, S_{\rho^{-1}(t)}, \tau_{\rho^{-1}(t)})_{t\in T}, (\phi_{\rho^{-1}(s),\rho^{-1}(t)})_{s\leq t\in T}),$$
$$g^\psi = (T, (E, \psi(S_t), \tau_t \circ \psi^{-1})_{t\in T}, (\psi \circ \phi_{s,t} \circ \psi^{-1})_{s\leq t\in T}).$$

3.2 Centered growth mapped evolution and centering

Let us recall that we assume that $T = [t_{\min}, t_{\max}]$ and E is a smooth manifold. We also assume now that the flow $(\phi_{s,t})_{s\leq t\in T}$ of a GME is a set of diffeomorphisms on the ambient space (a subset of $\mathrm{Diff}(E)$).

We introduced previously the concepts of pure deformation and pure expansion to discriminate specific behaviors during a growth scenario. In the case of a **pure expansion** at all time, we will say that the GME is centered:

Definition 3.1. *We say that g is a centered growth mapped evolution of embedded shapes if $\phi_{s,t} = \mathrm{Id}$ for any $s \leq t \in T$. The same notion is immediately extended to tagged embedded shapes.*

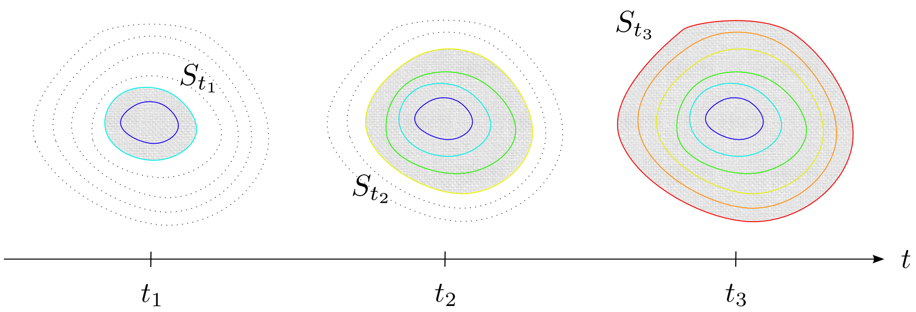

Figure 2.9 – Evolution of a centered scenario. The colors of the curves correspond to the different tags. (The dot curves are drawn by anticipation to highlight the absence of deformation.)

The first development of the unit circle (GME g^A) defined in Example 2.1 is centered. Another example is displayed in Figure 2.9.

Remark 3.1. *When a GME is centered, we get that for any $s \leq t \in T$, $S_s = \phi_{s,t}(S_s) \subset S_t$ so that the shapes form a sequence of nested sets. In particular, with $T = [t_{\min}, t_{\max}]$, any shape S_t can be seen as a subset of the end shape $S_{t_{\max}}$.*

If g is a centered TGME, then its tagging function is constant in time. We can write for any $t \in T$, $\tau_t = \tau_{|S_t}$.

We will see now that any GME g over an embedding space E can be transformed into a centered one. This will have a important consequence on how we can model the GME. Indeed, the set of these elementary scenarios in the orbit of g forms a small orbit for a subgroup of $G(T, E)$ much smaller. This new orbit highlights the growth process share by the original orbit. Informally, it means that we can attach to any scenario g a less complex scenario that still encodes how g is expanding independently of its shape.

Proposition 3.2 (Centering a GME or a TGME)**.** *If $g = (T, (E, S_t, \tau_t)_{t\in T}, (\phi_{s,t})_{s\leq t\in T})$ is a growth mapped evolution of tagged embedded shapes and $c \in T$, then $\Phi_c = (\mathrm{Id}, \mathrm{Id}, (\phi_{t,c})_t)$ belongs to $G(T, L, E)$ and defines a new element of* $\mathrm{TGME}(T, L, E)$

$$\overline{g}_c \doteq \Phi_c \cdot g\,.$$

$\overline{g}_c$ is centered and called the centered evolution of g at time c. The mapping Φ_c does not depend on the tagging function τ. The same construction can be applied to the GMEs.

Proof. Indeed, $\overline{g}_c = (\overline{T}, (\overline{E}, \overline{S}_t, \overline{\tau}_t)_{t\in T}, (\overline{\phi}_{s,t})_{s\leq t\in T})$ is given by $\overline{T} = T$, $\overline{E} = E$ and

$$(1)\ \overline{S}_t \doteq \phi_{t,c}(S_t)\,, \qquad (2)\ \overline{\phi}_{s,t} \doteq \phi_{t,c} \circ \phi_{s,t} \circ \phi_{c,s} = \mathrm{Id}\,,$$
$$(3)\ \overline{\tau}_t \doteq \tau_t \circ \phi_{c,t}\,.$$

□

The action of Φ_c consists in pushing forward and pulling backward through the the flow of the GME every shape S_t at time c. This gives for any time $t \in T$ prior to c the future image $\phi_{t,c}(S_t) \subset S_c$ of S_t at time c and gives a fictional inverse image $\phi^{-1}_{c,t}(S_t) \supset S_c$ at the earlier time c of the later shapes S_t when $t > c$. See an example on Figure 2.10.

Remark 3.2. *Note that if g is a centered GME, g is its own centered evolution at any time: for any $c \in T, \overline{g}_c = g$. Moreover, all centered evolutions of a general GME g are equal up to an invertible spatial mapping: for any pair $(c, c') \in T$, $\phi_{c,c'} \in \mathrm{Diff}(E)$ generates an element $\Phi_{c,c'} = (\mathrm{Id}, (\phi_{c,c'})_t) = \Phi_{c'} * \Phi_c^{-1}$ of $G(T, E)$ and $\overline{g}_{c'} = \Phi_{c,c'} \cdot \overline{g}_c$. The choice of c is thus meaningless and $t_{\min}$ will be the reference.*

Definition 3.2 (Initial centered evolution)**.** *For any GME g, when $c = t_{\min}$, we call $\overline{g}_c$ the initial centered evolution of g. In the following, it will simply be denoted $\overline{g}$ and we will denote $\Phi = (\mathrm{Id}, (\phi_{t,t_{\min}})_t)$ (respectively $\Phi = (\mathrm{Id}, \mathrm{Id}, (\phi_{t,t_{\min}})_t)$ if g is a TGME) so that*

$$\overline{g} \doteq \Phi \cdot g \qquad \text{and} \qquad g \doteq \Phi^{-1} \cdot \overline{g}\,. \tag{2.3}$$

Remark 3.3 (Invertibility of the centering)**.** *Since Φ belongs to $G(T, E)$ (respectively to $G(T, L, E)$), the orbit of any GME g is generated by its initial centered evolution $\overline{g}$ i.e.*

$$O_g = O_{\overline{g}}\,,$$

where $O_g = G(T, E) \cdot g$ (resp. $O_g = G(T, L, E) \cdot g$).

Any general GME can thus be retrieved from its initial centered evolution and its flow. This means that GMEs can be generated by centered evolutions and flows. Let us explicit it in the case of TGMEs. Consider any centered evolution $\overline{g}_*$ and any flow $(\phi_{s,t})_{s\leq t\in T}$ of $\mathrm{Diff}(E)$ that satisfies the transitive property (3) of Definition 2.4. Denote $(\overline{S}_t)_{t\in T}$ its set of shapes and $\overline{\tau}_*$ its tag (constant in time). Then $\Phi = (\mathrm{Id}, \mathrm{Id}, (\phi_{t,t_{\min}})_t)$ belongs to $G(T, L, E)$ so that $g \doteq \Phi^{-1} \cdot \overline{g}_*$ belongs to $\mathrm{TGME}(T, L, E)$. This new TGME is defined by

$$g = (T, (E, (S_t), \tau_t)_{t\in T}, (\phi_{s,t})_{s<t\in T})\,, \tag{2.4}$$

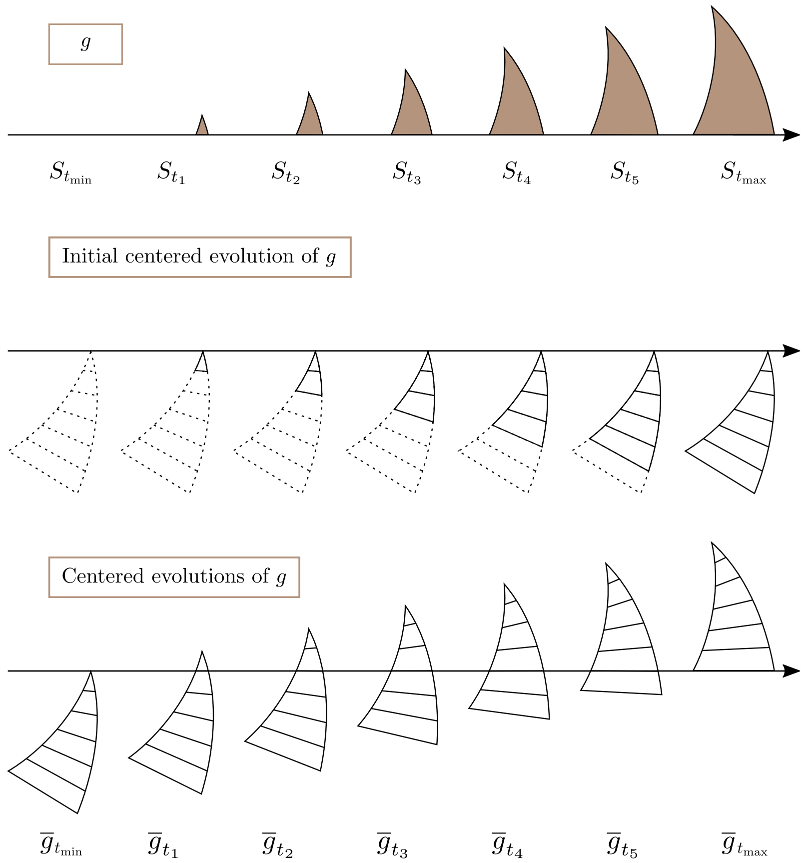

Figure 2.10 – On the first row, a general GME g. On the middle row, $\overline{g}_{t_{\min}}$ the initial centered evolution of g (see Definition 3.2). Below, the centered evolutions $\overline{g}_{t_i}$ of g for every times t_i. On this last row, we do not display the trivial evolution on a time line of each $\overline{g}_{t_i}$ but only their final age with a track of every younger ages. Note that the flow is similar to a rotation anticlockwise on the ambient space. Applying this flow to the initial centered scenario restores the original scenario g (see Remark 3.3).

with

$$S_t \doteq \phi_{t_{\min},t}(\overline{S}_t) \quad \text{and} \quad \tau_t \doteq \overline{\tau}_* \circ \phi_{t,t_{\min}}\big|_{S_t}. \tag{2.5}$$

Moreover, $\bar{g}_*$ is the initial centered evolution of g.

Proposition 3.3 (Stability of centered TGMEs)**.** *The image of a centered TGME by an element $\Psi = (\rho, \eta, (\psi_t)_{t\in T}) \in G(T, L, E)$ is centered if and only if $(\psi_t)_t$ is constant in time. Hence, it defines an action of the subgroup* $\mathrm{Diff}(T)^+ \times \mathrm{Diff}(L) \times \mathrm{Diff}(E)$ *of* $G(T, L, E)$ *on the subset of* $\mathrm{TGME}(T, L, E)$ *of centered evolutions.*

Proof. For any $g^A, g^B \in \mathrm{TGME}(E)$ such that $g^A = \Psi \cdot g^B$, g^A and g^B are centered if and only if $\phi^A_{s,t} = \phi^B_{\rho(s),\rho(t)} = \mathrm{Id}$ for any $s \leq t \in T^A$. Then *ii)* (2) in Proposition 3.1 gives that $\psi_s = \psi_t$ for any $s, t \in T^A$. □

Consequently, two TGMEs $g^A, g^B \in \mathrm{TGME}(T, E)$ are in the same $G(T, L, E)$-orbit if and only if $\bar{g}^A$ and $\bar{g}^B$ are in the same $\mathrm{Diff}(T)^+ \times \mathrm{Diff}(L) \times \mathrm{Diff}(E)$-orbit. On the diagram below, $\Psi \in G(T, L, E)$ exists if and only if $\bar{\Psi} \in \mathrm{Diff}(T)^+ \times \mathrm{Diff}(L) \times \mathrm{Diff}(E)$ exists.

$$\begin{tikzcd} g^A \arrow[r, "\Phi^A"] \arrow[d, "\Psi"] & \bar{g}^A \arrow[d, "\bar{\Psi}"] \\ g^B \arrow[r, "\Phi^B"] & \bar{g}^B \end{tikzcd} \tag{2.6}$$

We have explicitly for $\Psi = (\rho, \eta, (\psi_t)_{t\in T})$ (remind in the following derivations that $t_{\min} = \rho(t_{\min})$)

$$\begin{aligned} \bar{\Psi} &= \Phi^B \circ \Psi \circ (\Phi^A)^{-1} \\ &= \left(\rho, \eta, \phi^B_{\rho(t),\rho(t_{\min})} \circ \psi_t \circ \phi^A_{t_{\min},t}\right) \\ &= \left(\rho, \eta, \left(\psi_{t_{\min}} \circ \phi^A_{t,t_{\min}} \circ \psi_t^{-1}\right) \circ \psi_t \circ \phi^A_{t_{\min},t}\right) \\ &= \left(\rho, \eta, \psi_{t_{\min}} \circ \phi^A_{t_{\min},t_{\min}}\right) \\ &= \left(\rho, \eta, \psi_{t_{\min}}\right) . \end{aligned}$$

In conclusion, we can reconstruct the $G(T, L, E)$-orbit of g^A from $\bar{g}^A_{t_{\min}}$, the action of $\mathrm{Diff}(T)^+ \times \mathrm{Diff}(L) \times \mathrm{Diff}(E)$ to retrieve all the centered GMEs of the orbit and finally the set of all diffeomorphic flows $(\phi_{s,t})_{s\le t\in T}$ on the ambient space. Again, the GMEs share the same decomposition of their orbits. Figure 2.11 illustrates this structure.

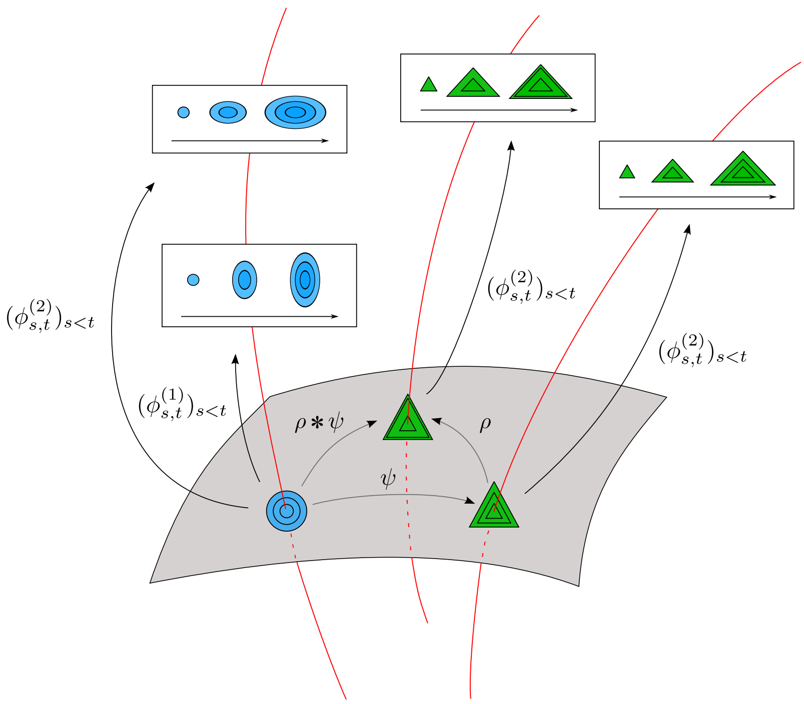

Figure 2.11 – *Growth Evolution Space.* The gray area represents an orbit of centered GMEs under the action of $\mathrm{Diff}(T)^+ \times \mathrm{Diff}(E)$. The trivial evolution of each centered GME is implicitly displayed by a unique shape. The action of the flows of the embedding space is then represented by the vertical fibers.

3.3 Metrics on GMEs

In this section, the ambient space is fixed to $E = \mathbb{R}^d$. The aim, here, is to reproduce the construction of a Riemannian structure on the spaces of growth mapped evolutions. The first step is to consider a Reproducible Kernel Hilbert Space (RKHS) to model a subspace of $T_{\mathrm{Id}}G(T,E)$ the tangent space at the Identity of the acting group of deformations (see Figure 2.12). This subspace has then a canonical image in any other tangent space $T_g G(T,E)$. These images allow then to build a subgroup of $G(T,E)$ with all the paths parallel to these subspaces (see Figure 2.13).

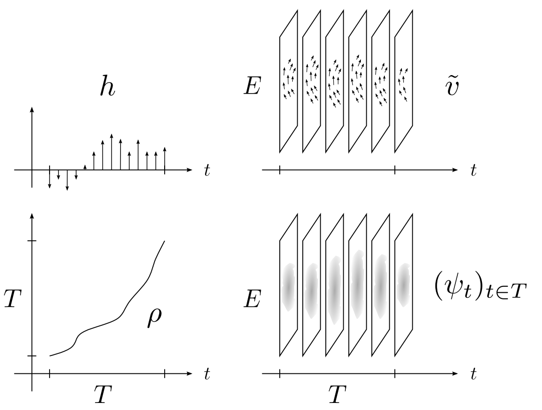

Figure 2.12 – Description of the tangent space at $\Psi = (\rho, (\psi_t)_{t\in T}) \in G(T,E)$. A small variation of ρ is an 1D vector field on T, denoted h, and a small variation of all the $(\psi_t)_t$ is a time-varying vector field on E, denoted $\tilde{v}$.

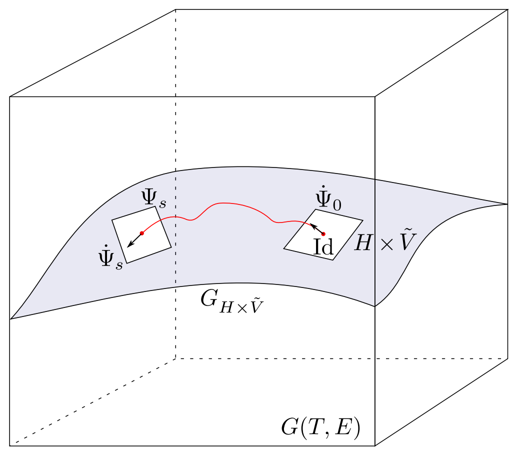

Figure 2.13 – We consider all paths in $G(T,E)$ such that the velocity vector always belongs to the image of $H \times \tilde{V}$. These images are deduced by the differential of the right translation in $G(T,E)$.

Let us consider $\tilde{V}$, a RKHS of space-time functions $\tilde{v} : T \times E \to E$, and H a RKHS of functions $h : T \to \mathbb{R}$ on T vanishing at the boundaries of T and satisfying the regularity assumptions

$$\begin{cases} \sup_{T\times E}(|\tilde{v}(t,x)| + |\partial_x \tilde{v}(t,x)|) \leq K|\tilde{v}|_{\tilde{V}}\,, \\ \sup_T(|h(t)| + |h'(t)|) \leq K|h|_H\,. \end{cases} \tag{2.7}$$

we have the following theorem:

Theorem 3.1. *For any* $(\boldsymbol{h} = (h_s)_{s\in[0,1]}, \tilde{\boldsymbol{v}} = (\tilde{v}_s)_{s\in[0,1]}) \in L^2([0,1], H \times \tilde{V})$*, we have existence and uniqueness of the flow*

$$\begin{cases} \partial_s \psi_s(t,x) = \tilde{v}_s(\rho_s(t), \psi_s(t,x))\,, \\ \partial_s \rho_s(t) = h_s(\rho_s(t))\,, \\ \rho_0 = \mathrm{Id},\ \ \psi_0 = \mathbf{Id}\,, \end{cases} \tag{2.8}$$

between $s = 0$ *and* $s = 1$*. If we note* $\Psi_1^{\boldsymbol{h},\tilde{\boldsymbol{v}}} = (\rho_1, \psi_1)$ *the solution at time* 1*, then*

$$G_{H\times\tilde{V}}(T,E) \doteq \{\ \Psi_1^{\boldsymbol{h},\tilde{\boldsymbol{v}}}\ |\ (\boldsymbol{h},\tilde{\boldsymbol{v}}) \in L^2([0,1], H\times\tilde{V})\} \tag{2.9}$$

is a subgroup of $G(T,E)$ *and*

$$D(\Psi,\Psi') = \inf\{\ \|(\boldsymbol{h},\tilde{\boldsymbol{v}})\|_2 \mid \Psi_1^{\boldsymbol{h},\tilde{\boldsymbol{v}}} * \Psi = \Psi'\} \tag{2.10}$$

is a right invariant distance on $G_{H\times\tilde{V}}(T,E)$.

Proof. The existence and uniqueness of the flow is an adaptation of a similar proof given in [52] where the condition (2.7) is an extension of the so called admissibility condition introduced in [50]. Indeed, the existence and uniqueness of ρ follows immediately. Then, one can consider separately the evolution of ψ at each time t. If $t \in T$ is fixed, one can introduce the control u defined for any $(s,x) \in T\times E$ by $u_s(x) = \tilde{v}_s(\rho_s(t),x)$. We retrieve thus the usual setting to build a group of spatial deformation and equation (2.7) ensures that u satisfies the admissibility condition. We deduce thus the existence and uniqueness of $\partial_s\varphi_s(x) = u_s(\varphi_s(x))$ and we have $\psi(t,\cdot) = \varphi$.

Consider then on $L^1([0,1],H\times\tilde{V})$ the operation $\big((\boldsymbol{h},\tilde{\boldsymbol{v}}),(\boldsymbol{g},\tilde{\boldsymbol{w}})\big) \to (\boldsymbol{h},\tilde{\boldsymbol{v}})\star(\boldsymbol{g},\tilde{\boldsymbol{w}})$ defined by $s \mapsto \big(2(h_{2s},\tilde{v}_{2s})\mathbb{1}_{s\le 1/2} + 2(g_{2s},\tilde{w}_{2s})\mathbb{1}_{s>1/2}\big)$. This operation is stable on $L^1([0,1],H\times\tilde{V})$ and we have $\Psi_1^{(\boldsymbol{h},\tilde{\boldsymbol{v}})\star(\boldsymbol{g},\tilde{\boldsymbol{w}})} = \Psi_1^{\boldsymbol{h},\tilde{\boldsymbol{v}}} \circ \Psi_1^{\boldsymbol{g},\tilde{\boldsymbol{w}}}$. Moreover, the equality $\|(\boldsymbol{h},\tilde{\boldsymbol{v}})\star(\boldsymbol{g},\tilde{\boldsymbol{w}})\|_1 = \|(\boldsymbol{h},\tilde{\boldsymbol{v}})\|_1 + \|(\boldsymbol{g},\tilde{\boldsymbol{w}})\|_1$ ensures that

$$d(\Psi,\Psi') \doteq \inf\{\ \|(\boldsymbol{h},\tilde{\boldsymbol{v}})\|_1 \mid \Psi_1^{\boldsymbol{h},\tilde{\boldsymbol{v}}} * \Psi = \Psi'\}$$

satisfies the triangle inequality and we deduce that it defines a right invariant distance on

$$G_{H\times\tilde{V}}(T,E) \doteq \{\ \Psi_1^{\boldsymbol{h},\tilde{\boldsymbol{v}}} \mid (\boldsymbol{h},\tilde{\boldsymbol{v}}) \in L^1([0,1],H\times\tilde{V})\}\,. \tag{2.11}$$

The last step is to show that we can retrieve the L^2 norm by time reparameterizations. Consider $(\boldsymbol{h},\tilde{\boldsymbol{v}}) \in L^1([0,1],H\times\tilde{V})$ and $\epsilon > 0$. Define the function $s_\epsilon : t \mapsto \big(\int_0^t |h_r,\tilde{v}_r|\,dr + \epsilon t\big)/(\|(\boldsymbol{h},\tilde{\boldsymbol{v}})\|_1 + \epsilon)$. Then s_ϵ is absolutely continuous and strictly increasing from $[0,1]$ to $[0,1]$. Its inverse $s \mapsto t_\epsilon(s)$ is also absolutely continuous and we have $t'_\epsilon(s) = (\|(\boldsymbol{h},\tilde{\boldsymbol{v}})\|_1 + \epsilon)/\big(|h_{t_\epsilon(s)},\tilde{v}_{t_\epsilon(s)}| + \epsilon\big)$ a.e. Finally, if we define $(\boldsymbol{g},\tilde{\boldsymbol{w}})$ by $(g_s,\tilde{w}_s) \doteq t'_\epsilon(s)(h_s,\tilde{v}_s)$, we have $|(g_s,\tilde{w}_s)| \le \|(\boldsymbol{h},\tilde{\boldsymbol{v}})\|_1 + \epsilon$ for any $s \in [0,1]$, so that $(\boldsymbol{g},\tilde{\boldsymbol{w}}) \in L^\infty([0,1],H\times\tilde{V}) \subset L^2([0,1],H\times\tilde{V})$ and $\|(\boldsymbol{g},\tilde{\boldsymbol{w}})\|_2 \le \|(\boldsymbol{g},\tilde{\boldsymbol{w}})\|_1 \le \|(\boldsymbol{h},\tilde{\boldsymbol{v}})\|_1 + \epsilon$. Moreover, we have $\Psi_1^{\boldsymbol{g},\tilde{\boldsymbol{w}}} = \Psi_1^{\boldsymbol{h},\tilde{\boldsymbol{v}}}$. Hence, we can define for any $(\boldsymbol{h},\tilde{\boldsymbol{v}}) \in L^1([0,1],H\times\tilde{V})$ a sequence $((\boldsymbol{g},\tilde{\boldsymbol{w}})_n)_{n\ge 0}$ in $L^2([0,1],H\times\tilde{V})$ such that $\Psi_1^{(\boldsymbol{g},\tilde{\boldsymbol{w}})_n} = \Psi_1^{\boldsymbol{h},\tilde{\boldsymbol{v}}}$ for any $n \ge 0$ and $\liminf \|(\boldsymbol{g},\tilde{\boldsymbol{w}})_n\|_2 \le \|(\boldsymbol{g},\tilde{\boldsymbol{w}})\|_1$. It follows that

$$G_{H\times\tilde{V}}(T,E) \doteq \{\ \Psi_1^{\boldsymbol{h},\tilde{\boldsymbol{v}}} \mid (\boldsymbol{h},\tilde{\boldsymbol{v}}) \in L^2([0,1],H\times\tilde{V})\} \tag{2.12}$$

and that $d \equiv D$. □

This right invariant distance can be seen as the Riemannian distance for the metric structure given at $(\mathrm{Id},\mathbf{Id}) \in G_{H\times\tilde{V}}(T,E)$ by the metric on $H\times\tilde{V}$. Now, we are ready to deduce a Riemannian structure induced by the action of the space-time deformation groups $G_{H\times\tilde{V}}(T,E)$ on any orbit $O_{g^0} \doteq \{\ \Phi\cdot g^0 \mid \Phi \in G_{H\times\tilde{V}}(T,E)\}$. The difference between two scenarios g and g' of the orbit O_{g^0} is evaluated by the energy required to generate the shortest path in $G_{H\times\tilde{V}}(T,E)$ that deforms g to g'.

$$d(g,g') \doteq \inf\{D((\mathrm{Id},\mathbf{Id}),\Psi) \mid g' = \Psi\cdot g\}\,. \tag{2.13}$$

At last we deduce from standard arguments on homogeneous spaces that

Theorem 3.2. *The function d defines a pseudometric on the orbit O_{g^0}.*

Proof. This follows from standard arguments when considering a right-invariant distance on a group acting on a homogeneous space (see [38]). □

4 Canonical temporal tag

A growth mapped evolution of tagged embedded shapes ($TGME$) is described by a sequence of tagged embedded shapes $(E, S_t, \tau_t)_{t\in T}$ and a flow $(\phi_{s,t})_{s\leq t\in T}$. The last remark says that the first object is equivalent to a centered evolution. The main aim of this framework is to exhibit a minimal set of parameters to describe an individual. We will see in the next section that a centered evolution can be reduced (with one regularity condition) to the set of points of one mega shape and a tag on this set. More precisely, the tag will extract the shape at any given time $t \in T$ from this mega shape.

4.1 Birth function and birth tag

Example 2.2 in Section 2 introduced a method to construct a temporal tag on any GME with an finite indexing set T. This construction was then extended on the developments of the unit circle in Example 2.3. In the two following sections, we will show that a large class of GME can be equipped with a canonical temporal tag.

Denote $\S = (S_t)_{t\in T}$ the time-varying shape as a single entity. A tagging function $(\tau_t)_{t\in T}$ allows to follow through the time a set of time-varying points inside $\S$ from their creation to the end of the time index. The birth tag we introduced in the examples cited above says exactly for any time-varying point when it appears in $\S$. We will first introduce an auxiliary function, the birth function, then formally define the birth tag and study some of their properties. In the next section, we will ensure that this tag can extend a GME to a GTME.

Consider a general GME $g = (T, (E, S_t)_{t\in T}, (\phi_{s,t})_{s\leq t\in T})$ on $T = [t_{\min}, t_{\max}]$. Recall that we denote $\overline{g} = (T, (E, \overline{S}_t)_{t\in T}, (\mathrm{Id})_{s\leq t\in T})$ its initial centered evolution. Define for any GME g

$$S_{\text{all}} \doteq \cup_{t\in T}\phi_{t,t_{\min}}(S_t)$$

reduced to $S_{\text{all}} = \cup_{s\in T} S_t = S_{t_{\max}}$ if g is centered. Let us start with centered GMEs. The growth process is given by pure expansion so that the shapes are simply nested and not deformed.

Definition 4.1 (Birth function of a centered GME)**.** *When a GME g is centered, one can introduce a function $b : S_{\text{all}} \to T$ called hereafter the **birth function** and defined by*

$$b(x) \doteq \inf\{t \in T \mid x \in S_t\}\,.$$

Note that since T is closed, $b(x) \in T$. This function determines the onset of a point x in the evolution of shapes $(S_t)_{t\in T}$.

The notion of birth function can be defined for any arbitrary GME as following:

Definition 4.2 (Birth function for a general GME)**.** *The **birth function** b of a GME g is defined as the birth function of its initial centered evolution $\overline{g}$ (see Definition 3.2). Hence, b is defined on $S_{\text{all}} = \cup_{t \in T} \overline{S}_t = \cup_{t \in T} \phi_{t,t_{\min}}(S_t)$ and for any $x \in S_{\text{all}}$ we have*

$$b(x) = \inf\{t \in T \mid \phi_{t_{\min},t}(x) \in S_t\} \,.$$

Note that this definition is coherent with the previous one since a centered GME is its own initial centered evolution. The birth function is thus defined on the projection S_{all} of all shapes at time $t_{\min}$. These birth dates can now be pushed forward to the original shapes $(S_t)_{t \in T}$ to define the birth tag.

Definition 4.3 (Birth tag)**.** *For any GME g, we define a canonical temporal tag called the **birth tag** and given by*

$$\tau_t^b : S_t \to T, \qquad \tau_t^b \doteq (b \circ \phi_{t,t_{\min}})_{|S_t} \,. \tag{2.14}$$

Note that for any $x \in S_t$, Definition 4.2 gives

$$\tau_t^b(x) = \inf\{s \in T \mid \phi_{t,s}(x) \in S_s\} \,. \tag{2.15}$$

Remark 4.1. *When the GME is centered, the birth function and the birth tag coincide i.e. $\tau_t^b = b$ for all $t \in T$.*

Example 4.1 (Birth tags of the circles)**.** *In examples 2.1 and 2.3, two GMEs g^A and g^B model the development of the unit circle. Let recall that $T = [0, 2\pi]$, $E = \mathbb{R}^2$, and $S_t = \{(cos(\theta), sin(\theta)) | \theta \in [0, t]\}$ are common to g^A and g^B, but $\phi_{s,t}^A = \mathrm{Id}$ and $\phi_{s,t}^B = R_t \circ R_s^{-1}$ where R_θ is the rotation of angle θ. Then, for any $t \in T$, any $\theta \in [0, 2\pi[$, we defined the tags*

$$\begin{aligned} &\tau_t^A(cos(\theta), sin(\theta)) = \theta \,, \\ &\tau_t^B(cos(\theta), sin(\theta)) = t - \theta[2\pi] \,. \end{aligned}$$

These tags are the birth tags as formalized in Definition 4.3. Note that $\tau_t^A = b^A$ for all $t \in [0, 2\pi]$. See Figure 2.7.

Remark 4.2 (Continuity of the birth function)**.** *One can see in Figure 2.7 that on both scenarios g^A and g^B, the collision happening at the end when the curve closes itself induces a discontinuity of the birth function and the birth tag.*

A natural question is to understand how the birth function characterizes a GME. In order to extract some condensed parameters of a GME, we would like for a centered GME that the birth function and the set of all points S_{all} allow to retrieve the evolution (and then extend it to the general GMEs). However, the birth function does not precise if a point x that appears at time $t = b(x)$ belongs to S_t (for a centered GME). In other words, is the infinium a minimum in Definition 4.1 ? For each label, the answer must be the same for all associated points. Indeed, let us recall that the flow of a TGME is a set of tag consistent partial matchings (see Definition 2.2 and Remark 2.2). This property enforces all points associated to one label to belong to the same subset of shapes of the complete evolution $(S_t)_{t \in T}$.

In fine, the answer requires some topological regularity on the set of shapes. Some examples will be presented in Remark 4.6 to illustrate this property.

Definition 4.4 (Right continuity (RC))**.** *We say that a GME g is **right continuous** if for any $t \in T$ and any decreasing sequence $(t_n)_{n\geq 0}$ of element of T converging to t we have*

$$S_t = \bigcap_{n\geq 0} \phi_{t_n,t}(S_{t_n}) .$$

Remark 4.3. *When g is centered the notion of right-continuity is reduced to the property*

$$S_t = \bigcap_{n\geq 0} S_{t_n} .$$

Proposition 4.1. *If g is a right continuous centered GME then for any $t \in T$*

$$x \in S_t \quad \textit{iff} \quad b(x) \leq t .$$

Proof. Indeed, if $x \in S_t$, then by definition of b, we have $b(x) \leq t$. Moreover, if $b(x) < t$, then there exists $s \in T$, such that $b(x) \leq s < t$ so that $x \in S_s \subset S_t$. Now if $b(x) = t$ and $x \notin S_t$, then there exists a decreasing sequence t_n of elements of T converging to t such that $x \in S_{t_n}$. Using the right continuity, we get $x \in S_t$ which is a contradiction. Hence, if $b(x) = t$, we have $x \in S_t$. □

The proposition can be extended to any GME.

Proposition 4.2. *If g is a right continuous GME then for any $t \in T$, any $x \in S_t$,*

$$x \in \phi_{s,t}(S_s) \textit{ iff } \tau_t^b(x) \leq s .$$

Proof. Indeed, if $x \in \phi_{s,t}(S_s)$, then by definition of τ_t^b, we have $\tau_t^b(x) \leq s$. Moreover,

$$\begin{aligned} \tau_t^b(x) \leq s &\Rightarrow b \circ \phi_{t,t_{\min}}(x) \leq s \\ &\Rightarrow \phi_{t,t_{\min}}(x) \in \overline{S}_s \\ &\Rightarrow \phi_{t_{\min},s} \circ \phi_{t,t_{\min}}(x) \in S_s \\ &\Rightarrow \phi_{s,t}(x) \in S_s . \end{aligned}$$

□

In conclusion, given any right continuous centered GME g, the single shape S_{all} and the birth function completely describe g. Explicitly, we have for any $t \in T$,

$$S_t = \{x \in S_{\text{all}} \,|\, b(x) \leq t\} .$$

Then, by Definition 3.2, any GME can be retrieved from its initial centered evolution and its flow $(\phi_{s,t})_{s<t\in T}$. It follows that

Corollary 4.1. *A right continuous GME is characterized by these three parameters:*

1. *an embedded shape (E, S_{all}),*

2. *a birth function* $b : S_{\text{all}} \to T$,

3. *a flow* $(\phi_{s,t})_{s<t\in T}$.

From a modeling point of view, these two last propositions say that under the right continuous condition, if g is a centered GME, for any $x \in S_{all}$ there exists a first shape S_t containing x. Likewise if g is a general GME, if we follow any point through the flow $x_t = \phi_t(x)$ (such that $\phi_{t_{\max}}(x) \in S_{t_{\max}}$), there exists a first shape S_t containing x_t. Formally, the definition of b and τ^b can be rewritten:

$$\begin{aligned} b(x) &= \min\{t \in T \mid \phi_{t_{\min},t}(x) \in S_t\}\,, \\ \tau_t^b(x) &= \min\{s \in T \mid \phi_{t,s}(x) \in S_s\}\,. \end{aligned}$$

At last, the last proposition says that the birth tag demarcates at all time t, each image of the previous shapes S_s in S_t : for any $s < t \in T$,

$$\phi_{s,t}(S_s) = \{x \in S_t \,|\, \tau_t^b(x) \leq s\}\,.$$

All these sets contain the old points of S_t (see Definition 2.5). The new points are exactly the points such that $\tau_t^b(x) = t$. This is the final ingredient to ensure that the birth function or the birth tag of a GME gives a consistent stratification coding the complete creation process during the evolution of the shape regardless of its spatial localization. This will allow to extend any right continuous GME to a TGME.

Before this important result, we finish this section with few more technical remarks.

Remark 4.4. *The right continuity is a necessary condition to Proposition 4.1 as soon as T is not a discrete set. Indeed, if there exist $t \in T$ and a decreasing sequence $t_n \to t^+$ such that $S_t \subsetneq \bigcap_{n\geq 0} S_{t_n}$. Then any $x \in \bigcap_{n\geq 0} S_{t_n} \setminus S_t$ verifies $x \notin S_t$ and $b(x) \leq t$.*

Remark 4.5 (Semi-continuity of the birth function)**.** *Under the right continuity condition, the shapes $(S_t)_{t\in T}$ are the lower level sets of the birth function. If the shapes are closed, the birth function is therefore lower semi-continuous.*

4.2 Minimal extension of a growth mapped evolution of shapes (GME)

As announced, an interesting fact is that when g is a right continuous GME then one can extend it to a TGME $\tilde{g}$ with the addition of the tagging sequence $(\tau_t^b)_{t\in T}$ *with values in* T. By construction, the birth tag τ^b is indeed consistent with the flow as proved in the next proposition.

Proposition 4.3. *If $g = (T, (E, (S_t)_{t\in T}), (\phi_{s,t})_{s<t\in T})$ is a right continous GME with birth function b and birth tag $(\tau_t)_{t\in T}$ as defined by* (2.14)*, then for any times $s < t \in T$*

— $\tau_t \leq t$,

— $\tau_t \circ \phi_{s,t|S_s} = \tau_s$,

— *if $x \in S_t$ and $\tau_t(x) \in \tau_s(S_s)$ then $x \in \phi_{s,t}(S_s)$.*

In particular, $(\tau_t)_{t\in T}$ is a consistent tagging with respect to the flow $(\phi_{s,t})_{s<t\in T}$ and

$$\tilde{g} \doteq (T, (E, (S_t)_{t\in T}), (\tau_t)_{t\in T}, (\phi_{s,t})_{s<t\in T})$$

is a TGME.

Proof. From (2.15), we get immediately that $\tau_t \leq t$ and from (2.14) we get that $\tau_t \circ \phi_{s,t} = b \circ \phi_{s,t_{\min}} = \tau_s$ on S_s. The last point is a direct consequence of Proposition 4.2. $\square$

Definition 4.5. *The extension $\tilde{g}$ of a right continuous GME g defined by the previous proposition will be called the **minimal extension** of g.*

Remark 4.6 (Examples about the right continuity)**.** *We present here two examples to understand the right continuous condition.*

— *Let be $T = [0,2]$ and g a centered GME defined by a collection of intervals*

$$I_t = \begin{cases} [0,t] & \text{if } t \leq 1\,, \\ [0,1+t] & \text{otherwise.} \end{cases}$$

The collection is strictly increasing by pure expansion from $I_0 = \{0\}$ to $I_2 = [0,3]$. At each time, one point is created, except after time $t = 1$ where there is a jump. We have $I_1 = [0,1]$, then $I_{1+\epsilon} = [0,2+\epsilon]$ (for $\epsilon > 0$). Consequently, for any time sequence $t_n \to 1^+$, $\bigcap_{n\geq 0} I_{t_n} = [0,2]$ so that g is not right continuous. The birth function is then equal to

$$b(x) = \begin{cases} x & \text{if } x \in [0,1]\,, \\ 1 & \text{if } x \in [1,2]\,, \\ x-1 & \text{if } x \in [2,3]\,. \end{cases}$$

In particular, for any $x \in]1,2]$, $b(x) = 1$, yet, $x \notin I_1$. Although the birth function can still be defined, it cannot be extended to a tag because of the third condition of Definition 2.2

$$\phi_{s,t}(S_s) = \tau_t^{-1}(\tau_s(S_s)).$$

Indeed, since for $x = 1$, $x \in I_1$ and $b(x) = 1$, the birth tag $s = 1$ belongs to $\tau_1^b(I_1)$. Yet, $I_1 = [0,1] \subsetneq \tau_t^{b,-1}([0,1]) = [0,2]$ for any $t > 1$.

— *If we just modify $I_1 = [0,1[$, g is still not right continuous but we can extend it to a TGME. If we assume that the shapes are closed, we can still generate an example. Take $T = [0,3]$ and*

$$I_t = \begin{cases} [0,t] & \text{if } 0 \leq t \leq 1\,, \\ [0,1] & \text{if } 1 \leq t \leq 2\,, \\ [0,1+t] & \text{if } 2 < t \leq 3\,. \end{cases}$$

Then $b(2) = 2$, yet $2 \notin I_2$. Hence, g is not right continuous but we can show that it can be extended to a TGME.

The (RC) condition is thus not necessary in general. Yet, it seems to be a reasonable sufficient condition and its most important justification is to allow the birth function to delimit the shapes $(S_t)_{t\in T}$.

We can now state the central theorem on morphisms between minimal extensions of GMEs.

Theorem 4.1. *Let $m^{AB} = (\rho^{AB}, (q_s^{AB})_{s\in T^A})$ be a morphism $m^{AB} : g^A \to g^B$ between two GMEs indexed by the closed intervals T^A and T^B such that*

1. *g^A is centered,* ***right continuous****, defined on a topological embedding space E^A and S_s^A is compact for any $s \in T^A$.*
2. *E^B is a topological space.*
3. *The time warping $\rho^{AB} : T^A \to T^B$ is a increasing homeomorphism.*
4. *For any $s \in T^A$, the spatial mapping $q_s^{AB} : S_s^A \to S_{\rho^{AB}(s)}^B$ is continuous.*

Then g^B is right continuous. Moreover, there exists a morphism $\tilde{m}^{AB} = (\rho^{AB}, \eta^{AB}, (q_s^{AB})_{s\in T^A})$ between the minimal extensions $\tilde{g}^A$ and $\tilde{g}^B$ of g^A and g^B into TGMEs. At last, we have necessarily $\eta^{AB}|_{\rho^{AB,-1}(\Im(\tau^B))} = \rho^{AB}$ and for any $s \in T^A$ and any $y \in S_t^B$, where $t = \rho^{AB}(s)$, that

$$\tau_{\rho^{AB}(s)}^B(y) = \rho^{AB}\left(\inf_{S_s^{A,y}} \tau_s^A(x)\right), \tag{2.16}$$

where $S_s^{A,y} \doteq \{\ x \in S_s^A \mid q_s^{AB}(x) = y\}$.

If $\rho^{AB}(\Im(\tau^A)) = \Im(\tau^B)$, $\tilde{m}^{AB}$ is unique.

Proof. In the sequel, we use the notation q_s for q_s^{AB}, η for η^{AB} and ρ for ρ^{AB}. Let $t_n \to t^+$ be a decreasing sequence of elements in T^B converging to $t \in T^B$. Consider $y \in \bigcap_{n\geq 0} \phi_{t_n,t}^B(S_{t_n}^B)$ and let us show that $y \in S_t^B$. Since ρ is an increasing homeomorphism, there exists a unique decreasing sequence (s_n) in T^A converging to $s \in T^A$ such that $\rho(s_n) = t_n$. Therefore, $y \in \bigcap_{n\geq 0} \phi_{t_n,t}^B \circ q_{s_n}(S_{s_n}^A)$ and there exists $x_n \in S_{s_n}^A$ such that $q_{s_n}(x_n) = \phi_{t,t_n}^B(y)$. Since g^A is centered and $S_{s_0}^A$ is compact, up to the extraction of a subsequence, we can assume that x_n converges to $x \in \cap_{n\geq 0} S_{s_n}^A$. We push forward every point x_n at time s_0 but since g^A is centered, we have $x_n = \phi_{s_n,s_0}^A(x_n)$. The image in g^B of this new sequence is a constant sequence equal to y. Indeed, since the flows and the spatial mapping q commute, we have $q_{s_0}(x_n) = q_{s_0}(\phi_{s_n,s_0}^A(x_n)) = \phi_{t_n,t_0}^B(q_{s_n}(x_n)) = \phi_{t_n,t_0}^B(\phi_{t,t_n}^B(y)) = \phi_{t,t_0}^B(y)$.

On the left-hand side, we have $q_{s_0}(x_n) \to q_{s_0}(x)$ (q_{s_0} is continous), so that $q_{s_0}(x) = \phi_{t,t_0}^B(y)$. Finally, we get $y = \phi_{t_0,t}^B(q_{s_0}(x)) = q_s(\phi_{s_0,s}^A(x)) = q_s(x)$. By right continuity of g^A, we have $x \in S_s^A$. Hence $y \in q_s(S_s^A) = S_t^B$ so that we have proved that $\bigcap_n \phi_{t_n,t}^B(S_{t_n}^B) \subset S_t^B$. Since the reverse inclusion is always true, we get that g^B is right continuous.

Since g^A is centered, note that for any $s \in T^A$, τ_s^A does not depend on s and is now denoted τ^A. Let us prove first that if $t = \rho(s)$, with $s \in T^A$, $y \in S_t^B$ and $S_s^{A,y} = \{\ x \in S_s^A \mid q_s(x) = y\}$ then we have for any $t' = \rho(s')$ with $s' \in T^A$, $s' < s$ that

$$\phi_{t,t'}^B(y) \in S_{t'}^B \quad \text{iff} \quad S_s^{A,y} \cap S_{s'}^A \neq \emptyset\,. \tag{2.17}$$

Indeed, $\phi_{t,t'}^B(y) \in S_{t'}^B$ iff there exists $x \in S_{s'}^A$ such that $y = \phi_{t',t}^B(q_{s'}(x)) = q_s(\phi_{s',s}^A(x)) = q_s(x)$ which is equivalent to $S_s^{A,y} \cap S_{s'}^A \neq \emptyset$.

The characterization of birth tags by Proposition 4.2 implies then that if $x \in S_s^{A,y}$, $\tau_t^B(y) \leq \rho(\tau^A(x))$ so that $\tau_t^B(y) \leq \inf_{x\in S_s^{A,y}} \rho(\tau^A(x))$. Now, if $s'_* = \inf\{\ s' \leq s \mid s' \in T^A,\ S_s^{A,y} \cap S_{s'}^A \neq \emptyset\ \}$ then since T^A is compact $s'_* \in T^A$ and $\tau_t^B(y) \geq \rho(s'_*)$. Moreover, by right continuity we have $S_{s'_*}^A = \cap_{u>s'_*, u\in T^A} S_u^A$ and since S_s^A is compact and

$S_s^{A,y}$ closed (we assume that q_s is continuous) there exists $x_* \in S^A_{s'_*} \cap S_s^{A,y}$ so that $\tau^A(x_*) \leq s'_*$ and $q_s(x_*) = y$. Hence $\tau_t^B(y) \geq \rho(\tau^A(x_*))$ and we have proved that $\tau_t^B(y) = \inf_{x\in S_s^{A,y}} \rho(\tau^A(x)) = \rho(\tau^A(x_*))$. In conclusion, for the particular choice $\eta = \rho$, $\tilde{m}^{AB}$ is a morphism between the minimal extensions $\tilde{g}^A$ and $\tilde{g}^B$.

Finally, let us prove that η is completely determined on $\rho^{-1}(\Im(\tau^B))$. With the same notation, let us introduce $t'_* = \rho(s'_*)$ and $y' = \phi^B_{t,t'_*}(y) = q_{s'_*}(x_*)$. Let us show that $\tau^A(S^{A,y'}_{s'_*}) = \{s'_*\}$. We have $S^{A,y'}_{s'_*} \subset S_s^{A,y}$ so that $\tau^A(S^{A,y'}_{s'_*}) \subset \tau^A(S_s^{A,y})$. Now, for any $x \in S^{A,y'}_{s'_*}$, since $x \in S^A_{s'_*}$ we have $\tau^A(x) \leq s'_*$. Hence, $\rho(s'_*) = t'_* = \tau^B_{t'}(y') = \tau^B_t(y) = \eta(s'_*)$. $\square$

Note that the definition of the image tag is here a bit more precise than in the general definition of morphisms between TGMEs (Definition 2.7). The uniqueness property above allows us to *transfer the birth tag of a GME on its images and to retrieve the birth tags of these images*:

Corollary 4.2. *Let g^A and g^B be two GMEs and m^{AB} a morphism such that*

$$g^B = m^{AB}(g^A)\,.$$

With the assumptions of the last proposition, if τ^A is the birth tag of g^A, then the image of this tag defined by equation (2.16) *is the birth tag of g^B.*

Example 4.2. *The birth tags of the two GMEs on the unit circle g^A and g^B are given in Example 4.1. In Example 2.4, we introduced a source GME g^I, the centered collection of segments $([0,t])_{t\in T^I}$, to generate g^A and g^B. The image of its birth tag gives indeed the birth tags of g^A and g^B.*

Remark 4.7 (Linked between time warpings and spatial mappings)**.** *For any centered GME g^A reparameterized by a time warping ρ into $g^B \doteq (\rho, \mathrm{Id}) \cdot g^A$, the birth function becomes $b^B = \rho \circ b^A$. In practice, if a centered GME is given by an encompassing embedded shape (E, S_{all}) and a birth function $b : S_{\text{all}} \to T$, a reparameterization in time is equivalent to compose on the left the birth function with an invertible mapping. A spatial mapping $\psi : S_{\text{all}} \to E$ acts on the birth function on the right. Yet, if ψ induces one-to-one correspondences between the level sets of the birth functions, it can be seen as the action of a time warping. Conversely, given ρ a time warping, the existence of a spatial mapping to reproduce the action of ρ is not immediate and will be deepened in Chapter 4.*

4.3 Factorisation of general tagging function

The next proposition says that the birth tag is always hidden under a general tag.

Proposition 4.4. *[Temporal factorisation of the tags] Let g be a right continuous TGME of tagged shapes over L and time indexed on T. Let $(\tau_t)_{t\in T}$ be the family of tagging functions in L and $(\tau^b_t)_{t\in T}$ the birth tag (Definition 4.3). Then there exists a function $b^L : L \to T$, such that for any $t \in T$ we have on S_t :*

$$\tau^b_t = b^L \circ \tau_t\,. \tag{2.18}$$

Proof. It is sufficient to prove that for any $s, t \in T$, any $x \in S_s$ and $y \in S_t$, if $\tau_s(x) = \tau_t(y)$ then $\tau_s^b(x) = \tau_t^b(x)$. Let us first consider the case where $s = t$ and assume that there exist $x, y \in S_t$ such that $\tau_t(x) = \tau_t(y)$ and $\tau_t^b(x) < \tau_t^b(y)$. Then there exists $\tau_t^b(x) \leq u < \tau_t^b(y)$ so that $\phi_{t,u}(y) \notin S_u$ since $\tau_t^b(y) = \inf\{\, s \in T \mid \phi_{t,s}(y) \in S_s \,\}$. However, by right continuity of g, $\tau_t^b(x) \leq u$ implies that $\phi_{t,u}(x) \in S_u$ and $\tau_t(y) = \tau_t(x) \in \tau_u(S_u)$. Hence, $y \in \phi_{u,t}(S_u)$ which is a contradiction.

Now assume that $s \leq t$ are arbitrary in T. If $\tau_s(x) = \tau_t(y)$ then $\tau_t(\phi_{s,t}(x)) = \tau_s(x) = \tau_t(y)$ so that $\tau_t^b(\phi_{s,t}(x)) = \tau_t^b(y)$. But $\tau_t^b(\phi_{s,t}(x)) = b(\phi_{t,t_{\min}}(\phi_{s,t}(x)) = b(\phi_{s,t_{\min}}(x)) = \tau_s^b(x)$. $\square$

Remark 4.8. *The function b^L defined a birth tagging of the label set L itself.*

5 Birth place functions

Corollary 4.1 says that any right continuous GME g can be retrieved from the encompassing embedded shape (E, S_{all}), the birth function $b : S_{\text{all}} \to T$ and the flow $(\phi_{s,t})_{s<t\in T}$. More precisely, the shapes $(S_t)_{t\in T}$ can be retrieved as follows

$$S_t = \{\phi_{t_{\min},t}(x) \,|\, x \in S_{\text{all}}, b(x) \leq t\}\,. \tag{2.19}$$

Indeed, the birth function b reconstructs with S_{all} the initial centered evolution $\overline{g}$ of g. Then one can retrieve g by $g = \Phi^{-1} \cdot \overline{g}$ where $\Phi^{-1} = (\text{Id}, (\phi_{t_{\min},t})_{t\in T}) \in G(T, E)$. This is to say that=

$$S_t = \phi_{t_{\min},t}(\overline{S}_t)\,.$$

where $(\overline{S}_t)_{t\in T}$ are the shapes of $\overline{g}$ (see Proposition 3.2).

We will see in this section that one can consider another approach. Moreover, we will extend it to more general morphisms eventually not invertible as introduced in Definition 2.7. We will see how to express a morphism $m^{AB} : g^A \to g^B$ between two GMEs as a function of the flow ϕ^B. Since $g^B = m^{AB}(\Phi^{-1} \cdot \overline{g}^A)$, one can naturally assume that g^A is a centered evolution.

Recall the diagram that illustrates a morphism between two GMEs:

$$\begin{tikzcd}
S_s^A \arrow[r, hook, "\phi^A_{s,t}"] \arrow[d, "q_s"'] & S_t^A \arrow[r, hook, "\phi^A_{t,u}"] \arrow[d, "q_t"] & S_u^A \arrow[d, "q_u"] \\
S^B_{\rho(s)} \arrow[r, hook, "\phi^B_{\rho(s),\rho(t)}"'] & S^B_{\rho(t)} \arrow[r, hook, "\phi^B_{\rho(t),\rho(u)}"'] & S^B_{\rho(u)}
\end{tikzcd}$$

Note that given a time-varying point x_t through the flow inside the scenario g^A or g^B, one can only follow it backwardly until its time of birth $\tau_t^b(x_t)$ (that does not depend on t). Inside the centered scenario g^A, $t \mapsto x_t$ is constant and $\tau_t^b(x_t) = b(x_t)$. This induces the next proposition.

Proposition 5.1. *Consider two GMEs g^A and g^B, and a morphism $m^{AB} = (\rho, (q_t^{AB})_{t\in T^A})$. Assume that g^A is right continuous and centered and denote b its birth function. Then* *there exists a unique function $\tilde{q}^{AB} : S^A_{all} \to E^B$, called the **birth place function**, such that for any $t \in T^A$, any $x \in S^A_t$,*

$$q^{AB}_t(x) = \phi^B_{\rho(b(x)),\rho(t)}(\tilde{q}^{AB}(x))\,.$$

This function is given by

$$\tilde{q}^{AB}(x) \doteq q^{AB}_{b(x)}(x)\,.$$

Proof. It is an immediate consequence of Definition 2.7 (2). Indeed, if $x \in S^A_t$ and $s = b(x)$, then assuming that g^A is right continuous, we have $x \in S^A_s$ and since m^{AB} is a morphism between two GMEs, we have $q^{AB}_t(x) = q^{AB}_t(\phi^A_{s,t}(x)) = \phi^B_{\rho(s),\rho(t)}(q^{AB}_s(x)) = \phi^B_{\rho(b(x)),\rho(t)}(q^{AB}_{b(x)}(x))$. □

The birth place function gives the location of the new points of g^B.

Remark 5.1. *The birth place function is independent of the time warping ρ. It only depends on the spatial mapping and the birth function of the source GME.*

Equation (2.19) makes explicit the image of a general scenario from its initial centered evolution. With the birth place function, the new scenario is described by

$$\begin{aligned} S^B_{\rho(t)} &= \{\phi^B_{\rho(b(x)),\rho(t)}(\tilde{q}^{AB}(x)) \,|\, x \in S^A_t\} \\ &= \{\phi^B_{\rho(b(x)),\rho(t)}(\tilde{q}^{AB}(x)) \,|\, x \in S^A_{\text{all}}, b(x) \le t\}\,. \end{aligned} \tag{2.20}$$

Conversely, we would like to understand if starting from an arbitrary function $\tilde{q} : S^A_{all} \to E^B$, an increasing function $\rho : T^A \to T^B$ and a flow $(\phi_{s,t})_{s \le t \in T^B}$ on E^B, then one can define a target g^B and a morphism $m^{AB} : \tilde{g}^A \to \tilde{g}^B$ between the minimal extensions as TGME.

Theorem 5.1. *Let g^A be a centered right continuous GME indexed by a (compact) time index set T^A with an associated **continuous** birth function b^A and such that $S^A_{t_{\max}}$ is **compact**. Now for any **continuous** $\tilde{q} : S^A_{all} \to E^B$, any homeomorphic increasing time warping $\rho^{AB} : T^A \to T^B$ and any flow $(\phi^B_{t,t'})_{t \le t' \in T^B}$ of invertible mappings on E^B such that $\phi^B_{t,t'}(y)$ is continous in t, t' and y, we have:*

1. *$g^B \doteq (T^B, (E^B, S^B_t)_{t \in T^B}, (\phi^B_{s,t})_{s \le t \in T^B})$ where $S^B_{\rho^{AB}(t)} \doteq \{\phi^B_{\rho^{AB}(b^A(x)),\rho^{AB}(t)}(\tilde{q}(x)) \mid x \in S^A_t\ \}$ is a right continous GME*
2. *if we defined for any $s \in T^A$, $q^{AB}_s : S^A_s \to S^B_{\rho(s)}$ by $q^{AB}_s(x) = \phi^B_{\rho(b^A(x)),\rho(s)}\tilde{q}(x)$ for $x \in S^A_s$ then $m^{AB} = (\rho^{AB}, (q^A_s)_{s \in T^A})$ is a morphism between g^A and g^B that can be extended to their minimal extension as TGME.*

Proof. The proof is mainly a consequence of Theorem 4.1. Denote ρ for ρ^{AB}. For any $t \in T^A$, $S^A_t = (b^A \le t)$ is closed since b^A is continuous and compact as a closed subset of the compact set $S^A_{t_{\max}}$. It is quite immediate that g^B is a GME. Consider indeed $s < t \in T^A$. For any $y \in S^B_{\rho(s)}$, there exists $x \in S^A_s$ such that $y = \phi^B_{\rho(b^A(x)),\rho(s)}(\tilde{q}(x))$. We have then

$$\phi^B_{\rho(s),\rho(t)}(y) = \phi^B_{\rho(s),\rho(t)} \circ \phi^B_{\rho(b^A(x)),\rho(s)}(\tilde{q}(x)) = \phi^B_{\rho(b^A(x)),\rho(t)}(\tilde{q}(x)) \tag{2.21}$$

so that $\phi^B_{\rho(s),\rho(t)}(y) \in S^B_{\rho(t)}$. Since ρ is a homeomorphism, it follows that for any $s < t \in T^B$, $\phi^B_{s,t}(S^B_s) \subset S^B_t$ so that $\phi^B_{s,t} \in \mathrm{Hom}_{\mathrm{ES}}((E, S^B_s), (E, S^B_t))$ and g^B is a GME.

Let us prove now that m^{AB} is a morphism between g^A and g^B as defined in Definition 2.7. By construction, for any $t \in T^A$, $S^B_{\rho(t)} = q^{AB}_t(S^A_t)$. Since g^A is centered, one then needs to show that $\phi^B_{\rho(s),\rho(t)} \circ q^{AB}_s = q^{AB}_t{}_{|S^A_s}$ which results directly from (2.21) where $y = q^{AB}_s(x)$.

At last, since $x \to \phi^B_{\rho(b^A(x)),\rho(s)}(\tilde{q}(x))$ is continuous we get that q_s is continous and Theorem 4.1 gives that g^B is right continuous and that m^{AB} can be extended as defined in Theorem 4.1. □

Remark 5.2. *Note that b^B is not necessarily continuous. Indeed, in Example 2.4, $b^I = \tau^I_{t_{\max}}$ is continuous, but we saw in Remark 4.2 that b^A and b^B are not continuous.*

The birth place function is a new descriptor of the spatial mapping between two GMEs. Note that since the birth place function is not always an embedding (see Example 5.4 where its image is reduced to a point), its image cannot replace the centered GME g^A.

Theorem 5.1 will be the core of the growth model studied in this thesis built on a centered evolution g^A of the type:

Example 5.1. *If $t_0 < t_1$ are two real numbers such that $S^A_{all} = [t_0, t_1] \times X_0$, where X_0 is a compact manifold with boundary and b^A is the projection on the first coordinate, then $T^A = [t_0, t_1]$, for any $t \in T^A$, $S_t = [t_0, t] \times X$, b^A is continuous, and g^A is right continuous.*

This centered evolution will play the role of the **biological coordinate system** presented in the introduction.

We end this section with few examples to highlight the birth place function.

Example 5.2. *Define for $t \in [0,1]$, $I_t = [0,t]$.*

a) Consider $E^A = \mathbb{R}$, $E^B = \mathbb{R}^2$ and $T^A = T^B = [0,1]$. Let g^A be a centered right continuous GME given by $S^A_t = I_t$ and g^B be given by $S^B_t = I_t \times \{t\}$ and $\phi^B_{s,t} = \mathrm{Id} + (0, t-s)$ the vertical translation. A morphism $m^{AB} : g^A \to g^B$ can be defined by $\rho^{AB} = \mathrm{Id}$ and

$$\begin{array}{rccc} q^{AB}_t : & I_t & \to & I_t \times \{t\}\,, \\ & x & \mapsto & (x,t) \end{array}$$

(we could actually show here with Definition 2.7 (2) that m^{AB} is unique up to the choice of ρ^{AB}). We also have $b^A(x) = x$, for any $x \in S^A_{all}$ (here $S^A_{all} = I_{t_{\max}} = [0,1]$). Then

$$\tilde{q}^{AB}(x) \doteq q^{AB}_{b^A(x)}(x) = (x,x)\,.$$

The image of the birth place function is thus the diagonal of the square $[0,1] \times [0,1]$. It gives the positions where appear all the new points of g^B over the time. We can parameterize the sets of g^B by $S^B_t = q^{AB}_t(S^A_t) = \{\phi^B_{x,t}(\tilde{q}^{AB}(x)) \mid x \in S^A_t\} = \{(x,t) \mid x \in S^A_t\}$.

b) An interesting fact is that the area of creation or the image of the birth place function can be reduced to a point and still generates a non trivial GME. Let keep g^A as introduced in the previous example and define g^B by $S^B_t = \{0\} \times I_t$ and $\phi^B_{s,t} = \mathrm{Id} + (0, t-s)$. A morphism $m^{AB} : g^A \to g^B$ can be defined by $\rho^{AB} = \mathrm{Id}$ and

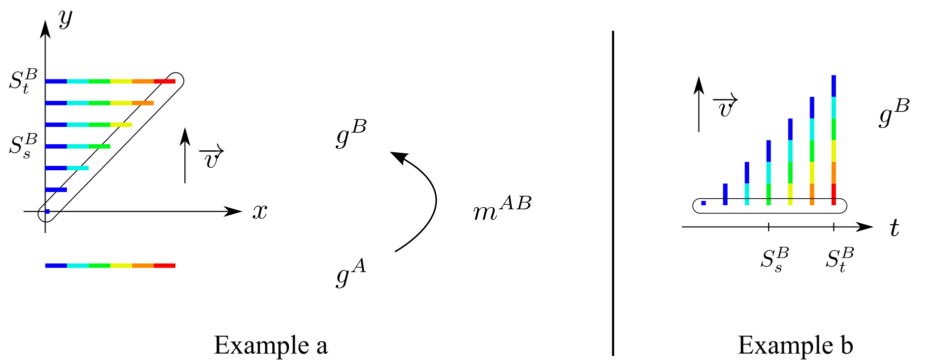

Figure 2.14 – Illustration of Example 5.2. *Example a:* Two GMEs represent the evolution of a segment. At the bottom is displayed g^A, a segment embedded in $\mathbb{R}$ that evolves by pure expansion on its right side. Above, g^B evolves in $\mathbb{R}^2$. The segment is expanding on its right side but also gradually translated upwards (with a constant velocity displayed by the vector v). We point the shapes S_s^B and S_t^B at times $s = 0.5$ and $t = 1$. We circle the image of the birth place function : the position of all new points of g^B. *Example b:* In this case, the evolution of g^B is displayed along a timeline. Note that this evolution is actually constrained in a straight line of the plan. It is now a vertical segment extending by creation of new points at the bottom and gradually displaced upwards. The circled image of the birth place function is displayed as a horizontal segment in $\mathbb{R} \times T^B$ and is thus spatially reduced to a point.

$$\begin{array}{rccl} q_t^{AB}: & I_t & \to & I_t \times \{t\}\,, \\ & x & \mapsto & (0, t-x)\,. \end{array}$$

Now, for any $x \in S_{all}^A$, we still have $b^A(x) = x$, and thus,

$$\tilde{q}^{AB}(x) \doteq q_{b^A(x)}^{AB}(x) = q_x^{AB}(x) = (0,0)\,.$$

Yet, we can fully reconstruct the sets $S_t^B = \{\phi_{x,t}^B(\tilde{q}^{AB}(x)) \mid x \in S_t^A\} = \{(0, t-x) \mid x \in S_t^A\}$.

Example 5.3. *For the horn as a surface, we assume that the creation of matter occurs at the base of the horn and that locally this base (or the head of the animal) is flat. Then the image of the birth place function is constrained to a plan and diffeomorphic to a disk. The level sets of the birth function are close to circles, the head of the horn is a point at the center of these level sets, and the boundary of the disk is the base of the final horn. See Figure 2.15. A natural centered source GME can be a cone or a cylinder. With a cone, note then that the birth place function is an embedding. However, if some collisions happen as seen in Figure 2.8, the spatial mapping q is not invertible.*

Example 5.4 (Degenerated BPF)**.** *Let refer again to the two GMEs g^A and g^B modeling two developments of the unit circle as the images of a centered GME g^I as presented in Example 2.4. Let recall that $T = [0, 2\pi]$, $E = \mathbb{R}^2$, and $S_t = \{(cos(\theta), sin(\theta)) | \theta \in [0,t]\}$ are common to g^A and g^B, but $\phi_{s,t}^A = \mathrm{Id}$ and $\phi_{s,t}^B = R_t \circ R_s^{-1}$ where R_θ is the anticlockwise rotation of angle θ. Then the images of their birth place function are*

$$\Im(\tilde{q}^{IA}) = \mathbb{S}^1 \qquad \textit{and} \qquad \Im(\tilde{q}^{IB}) = \{(1,0)\}\,.$$

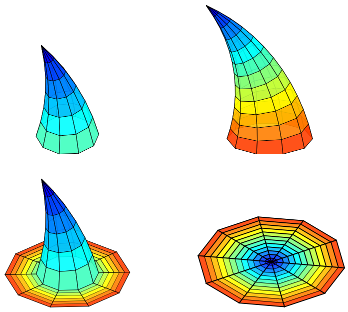

Figure 2.15 – *First row*: two ages of a horn given at an intermediate time $t_1 \in [0,1]$ and the final time 1. The small horn is modeled by $q_{t_1}(S_{t_1})$ and the large horn by $q_1(S_1) = q_1(S_{\text{all}})$. *Second row:* on the left, we can see the initial position of all the leaves that will gradually appear to form the large horn. This shape is the union of $q_{t_1}(S_{t_1})$ and $\tilde{q}(S_{\text{all}} \setminus S_{t_1})$. On the right, we display the virtual horn at time 0. It is a flat disc, set of initial positions of every points, given by $\tilde{q}(S_{\text{all}})$. The sizes and points of view have been adjusted for a better visibility but the colors give the pointwise correspondences between the figures.

Quantify the growth: note that for the centered GME g^A, the amount of creation can be measured by the spreading of its birth function. On the opposite for g^B, it is quantified by the flow. However, remark that we have an isometric transport by the flow. The creation of matter comes as for g^A by an intrinsic expansion but the phenomenon is hidden by the action of flow.

The birth place function can thus be highly non injective and yet generate a non trivial scenario. The flow $(\phi^B_{s,t})_{s<t}$ on the ambient space E^B is indeed able to separate the images by the BPF of the foliated leaves $(\{x \in S^A_{\text{all}} \,|\, b(x) = t\})_{t \in T^A}$. Note however that the flow cannot separate two points of the same leave that would appear at the same position in E^B (i.e. two points $x, y \in S^A_{\text{all}}$ such that $\tilde{q}^{AB}(x) = \tilde{q}^{AB}(y)$ and $b^A(x) = b^A(y)$).

6 Conclusion

6.1 Final parameters of a population

To end this chapter we recall and highlight the parameters fixed for a population of related time-varying shapes and the free parameters modeling each individual of the population. A population embedded in an ambient space E and evolving on a time interval T can be defined from a set of centered evolutions. Denote one of them g^X and (S^X_{all}, b^X) its minimal parameters.

Then one can generate a general individual g image of g^X by its flow $(\phi_{s,t})$ and one of the two following spatial mappings from S^X_{all} to E :

1. a spatial mapping $q_{\text{all}} : S^X_{\text{all}} \to E$ that defines $\overline{g}$ by $S_{\text{all}} \doteq q_{\text{all}}(S^X_{\text{all}})$ and by $b(x) \doteq \inf b^X(q^{-1}_{\text{all}}(x))$ for any $x \in S_{\text{all}}$. Then g is defined by

$$S_t \doteq \{\phi_{t_{\min},t}(x) \,|\, x \in S_{\text{all}}, b(x) \leq t\}. \tag{2.22}$$

or

2. a birth place function $\tilde{q} : S_{\text{all}}^X \to E$ that defines g by

$$S_t \doteq \{\phi_{\rho(b^X(x)),\rho(t)}(\tilde{q}(x)) \,|\, x \in S_{\text{all}}^X, b^X(x) \leq t\} \,. \tag{2.23}$$

Note here that $\tilde{q}$ is a mapping from location $x \in S_{\text{all}}^X$ at a given time $t_{\min}$ to location $\tilde{q}(x)$ at different time of birth $b(x)$. Hence, $\tilde{q}$ is a mapping across time in contrast with q_{all}. This last construction deviates from the approach of a group of spatio-temporal deformations acting on a set of scenarios, as presented in Section 3. As we will see in Chapter 3, an important consequence is that the spatial regularity of the generated scenarios will depends on the temporal regularity of the flows that generate them.

At last, to determine only one centered evolution of a population, one can easily see that a spatial deformation of the centered scenario g^X can be absorbed by the mappings q_{all} and $\tilde{q}$ (by composition). One then need to know to how rewrite the time warping. This question has been raised in Remark 4.7. One can easily notice that when g^X has the canonical type given is Example 5.1, it always exists a spatial mapping translating the foliated leaves $(\{t\} \times X_0)_{t \in T}$ to rewrite a time warping. Therefore, the time warping can again be absorbed by the individual functions q_{all} and $\tilde{q}$. Otherwise, we will see in Chapter 4 how a lot of general centered scenarios can be reduced to this canonical decomposition by a spatial mapping. This allow to conclude that one can fix the centered evolution g^X (inside the orbit generated by $\text{Diff}^+(T) \times \text{Diff}(E)$) of the population and retrieve all the individuals by one of the two previous methods. This scenario g^X will play the role of the **biological coordinate system** of the population.

In the next chapters, the second model will be exploited to reconstruct the scenario g^A of an individual from some observed times denoted (Obs^A). The problem leads to complete the following diagram with the individual input (Obs^A) and the population input g^X.

$$\begin{tikzcd} (g^X) \arrow[r, "\tilde{q}^A{,}\phi^A"] & (g^A) \arrow[d, "\pi"] \\ & (Obs^A) \end{tikzcd}$$

where π is the canonical projection.

6.2 Conclusion

As we have seen, the notions of growth mapped evolutions and tagged growth mapped evolutions are quite effective to build a mathematical framework to handle important issues on growth modeling and analysis from a mathematical point of view. Interestingly, a Riemannian point of view can be developed on a space of growth mapped evolutions leading to the idea of *growth evolution spaces* as infinite dimensional Riemannian manifolds. The properties of such spaces can be understood thanks to the analysis of the space-time group actions acting on them and the semi-direct structure of the interactions between space and time.

Many interesting facts are emerging from this point of view as the key role of centered growth mapped evolutions and canonical temporal tagging. These two parameters characterize the expansion process of a population of growth scenarios opening new directions for investigation on these processes. At last, the introduction of the birth place function defines a new construction to generate growth scenarios paving the way for new registration models able to integrate growth priors.

Chapter 3

Reconstruction of a Shape Development

Contents

1 Introduction to the generative model

Longitudinal data analysis is the study of a population of time-varying shapes. It requires to investigate a low-dimensional modeling of their evolution. The continuous evolution of a time-varying shape, called the scenario of the shape, is usually only given through a sample of data at a finite set of times. This chapter addresses the reconstruction of theses scenarios. A core hypothesis is that all the scenarios of the studied population follows a common growth process induced by a canonical centered growth mapped evolution as introduced in Chapter 2. It allows to generate these scenarios by time-varying vector fields leading a new optimal control problem for the assimilation of time-varying shapes. At last, we are invited to tune this problem with new cost functions in order to redefine an optimal development of the shapes.

1.1 Biological coordinate system

In order to model the evolution of a shape during a growth process, we developed in Chapter 2 the concept of *growth mapped evolution* (GME) . A GME is given as a path of shapes $[0, 1] \ni t \mapsto S_t$ and a flow of mappings $(\phi_{s,t})_{s\leq t}$ such that for any pair $s \leq t \in [0, 1]$, the flow deforms the older shape S_s into the younger one S_t: $\phi_{s,t}(S_s) \subset S_t$. The shape S_t is thus made of the image of S_s at time t and of a set of new points created in the time interval $]s, t]$. In this chapter, all the GMEs are defined on a global time interval fixed to $T = [0, 1]$.

When $\phi_{s,t}(S_s) = S_t$ for any s, t, the shape evolves through a pure deformation process and we retrieve the standard dynamic through the flow. On the contrary, in the absence of global deformation, $\phi_{s,t} = \mathrm{Id}$ for any s, t so that the shape evolves by pure expansion and we have $S_s \subset S_t$. This last type of scenario plays a central role and such GMEs are called centered. Following D'Arcy Thompson's ideas, these GMEs represent the biological coordinate system of a set of homologous scenarios.

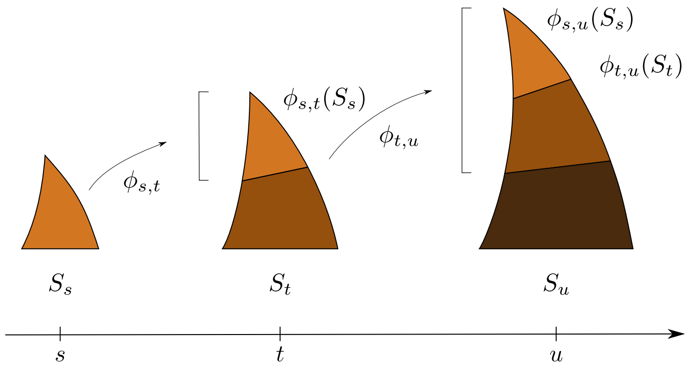

Figure 3.1 – Sequence of three discrete times to illustrate the development of a horn.

A **biological coordinate system** is a pair (X, τ) where X is a space called the coordinate space and $\tau : X \to [0, 1]$ the birth tag on X. It induces a set of shapes

$$X_t \doteq \{x \in X \,|\, \tau(x) \leq t\}\,, \tag{3.1}$$

of the so called active points of the coordinate space X at time t. The birth tag indicates when a point $x \in X$ starts to be active. The sets of points

$$X_{\{t\}} \doteq \{x \in X \,|\, \tau(x) = t\} \tag{3.2}$$

are called the *leaves* of the coordinate space. This sequence of nested shapes X_t forms a canonical scenario that describes the growth pattern of a population of related shapes. Figure 3.2 displays for example this scenario when the biological coordinate system is fixed to

$$\begin{cases} X \doteq [0,1] \times \mathbb{S}^1 \,, \\ \\ \tau(x) \doteq t \quad \text{ for any } x = (t, x_0) \in X \,. \end{cases} \tag{3.3}$$

At time 0, the shape is a circle. It growths into a cylinder under a pure expansion process by the progressive adjunction of the leaves. Here, each leave $X_{\{t\}} = \{t\} \times \mathbb{S}^1$ is a circle. Any shape X_t is a connected disjoint reunion of some of these leaves.

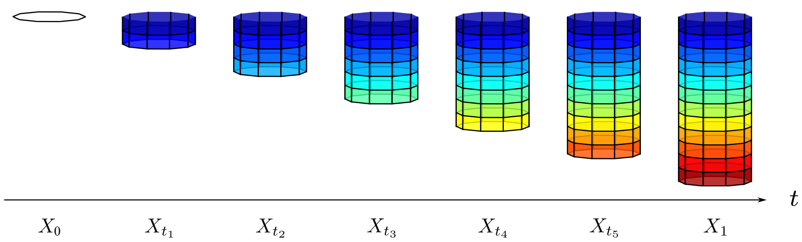

Figure 3.2 – Trivial scenario of the biological coordinate system.

The denomination of *leaves* emerges from this type of biological coordinate system where the creation process is particularly regular. Indeed, the set of new points are all diffeomorphic to a (k-1)-dimensional submanifold of X where k is the dimension of X. Moreover, they are all parallel. The coordinate space X is thus a disjoint reunion of these sets that induce a so called **foliation** on X. A foliation can be simply described as a decomposition of a manifold into path-connected submanifolds, called leaves, such that the manifold looks locally like a parallel union of these leaves. Each X_t inherits this foliated structure. We refer to [24, 35] for more details. For a general biological coordinate system, the existence of this foliation relies on the regularity of the birth tag τ as it will be deepened in Chapter 4. We will yet retain the denomination of leaves in the general case.

1.2 A new dynamic : evolution equations of a growing system

A general scenario $(t \mapsto S_t)_{t\in[0,1]}$ is modeled on the biological coordinate space by a sequence of spatial mappings $t \mapsto (q_t : X \to \mathbb{R}^d)$. The shape S_t is given by the image $q_t(X_t)$ of the active points of X. Depending on the injectivity of the mappings $(q_t)_t$, the generated scenario follows the same expansion process as the biological coordinate system. At each time $t \in]0,1]$, a new leaf $q_t(X_{\{t\}})$ appears whose points have no biological correspondence with the points of the younger shapes $S_s, s < t$.

Figure 3.3 illustrates two such types of scenario built on the coordinate system (X, τ) given by equation (3.3). The only difference between these two types is the behavior of the spatial mapping on the first leaf $X_{\{0\}}$. For the first scenario, the spatial mapping is an embedding at all time. For the second one, q_t is an embedding of all leaves but the first one and $q_t(X_{\{0\}})$ is reduced to a point.

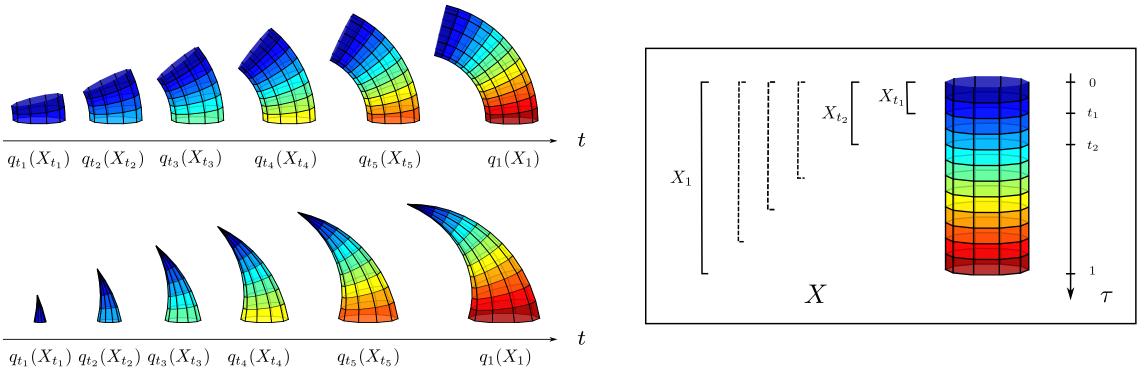

Figure 3.3 – Two examples of scenarios built on a given biological coordinate system (X, τ). Each image scenario inherits the foliation of the biological coordinate system, enlightened by the color gradient.

In these two examples, the last leaf is always included in the horizontal plane. The **birth place function** introduced in Chapter 2 allows to express this constraint. This constraint will be central to initiate the reconstruction of a scenario from a final state of the shape. The birth place function $\tilde{q} : X \to \mathbb{R}^d$ of a scenario associated to a mapping q is defined by

$$\tilde{q}(x) = q_{\tau(x)}(x) = \phi^{-1}_{\tau(x),1}(q_1(x))\,.$$

It can be seen as the pull backward through the flow of each leaf $q_1(X_{\{t\}})$ of the final shape to its initial position $q_t(X_{\{t\}})$ at time $t = \tau(x)$ when it appeared. The evolution of this leaf can then be completely retrieved by the flow $(\phi_{s,t})_{s\leq t}$ of the scenario: for any $x \in X$ and any $t \in [\tau(x), 1]$

$$q_t(x) = \phi_{\tau(x),t}(q_{\tau(x)}(x)) = \phi_{\tau(x),t}(\tilde{q}(x))\,. \tag{3.4}$$

To extend the mappings $q_t : X_t \to \mathbb{R}^d$ into homologous mappings on X, we then say that

$$q_t(x) = \begin{cases} \phi_{\tau(x),t}(\tilde{q}(x)) & \text{if } \tau(x) \leq t\,, \\ \\ \tilde{q}(x) & \text{otherwise.} \end{cases} \tag{3.5}$$

If a point $x \in X$ does not exist yet at time t, $q_t(x)$ returns its future place of birth. Hence, we have

$$q_0 = \tilde{q}. \tag{3.6}$$

This mapping q_0 is called the initial condition and the planar constraint can then easily be written as a constraint on the image of q_0. The shapes are then retrieved by the restriction of these new mappings:

$$S_t = q_{t|X_t}(X_t)\,.$$

A flow $(\phi_{s,t})_{s\leq t\in[0,1]}$ can be generated by a time-varying vector field on the ambient space $\mathbb{R}^d$. As for the construction of a group of diffeomorphisms (see Chapter 1), let us therefore consider V a Hilbert space of diffeomorphisms on the ambient space $\mathbb{R}^d$. Any time-varying vector field $v \in L^2([0,1], V)$ induces a diffeomorphic flow on the ambient space. The derivation of (3.5) invites us to consider the continuous time-varying mappings q solutions of

$$\dot{q}_t(x) = \begin{cases} v_t(q_t(x)) & \text{if } \tau(x) \leq t\,. \\ \\ 0 & \text{otherwise} \end{cases}$$

$$= \mathbb{1}_{\tau(x)\leq t}\; v_t(q_t(x))\,, \tag{3.7}$$

for a given initial condition $q_0 : X \to \mathbb{R}^d$ and a given $v \in L^2([0,1], V)$.

An important part of this chapter will consist in studying this approach to generate continuous paths in a space B of mappings from X to $\mathbb{R}^d$, by the set $L^2([0,1], V)$ of time-varying vector fields of V. Equation (3.7) will be referred as the **growth dynamic** and it will sometimes be rewritten

$$\dot{q}_t = \mathbb{1}_{\tau\leq t}\; v_t \circ q_t\,. \tag{3.8}$$

1.3 Illustration of the generative model

We propose here few examples to illustrate the dynamic of the model. We consider again the biological coordinate system given by $X = [0,1] \times \mathbb{S}^1 \subset \mathbb{R}^3$ and τ the projection on the first coordinate. We recall that Figure 3.2 highlights the trivial scenario induced by this system and Figure 3.3 offers two examples of image scenario.

For the first example, the initial position q_0 is given by the projection of X on the horizontal plane so that each leaf is sent on the unit circle of $\{0\} \times \mathbb{R}^2$. This localizes the area where occurs all the creation of the growth process. The time-varying vector fields acting on the ambient space are simple vertical translations ($v \in L^2([0,1], \mathbb{R})$) . Finally, we present in Figure 3.4 one example of this setting where the scenario is generated by a constant upward translation. In this example, one can see that the initial position of the shape, given by q_0, is not an embedding in the ambient space. This initial shape can be seen as a compressed accordion that will be progressively unfolded. Since the flow, although it is diffeomorphic, sees only gradually the shape, these mingled leaves can indeed be separated over time. The flow will yet never be able to separate two points that appear at the same time and at the same position.

In order to produce horns, the initial position covers now the complete unit disk. In the next examples, we will play with a parameter ρ to generate different initial positions

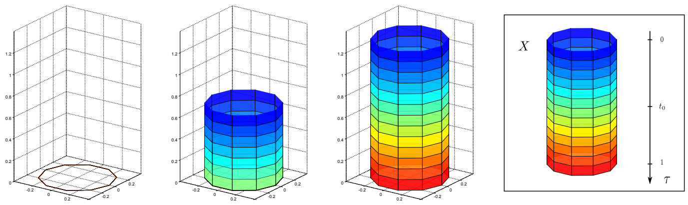

Figure 3.4 – Generation of a cylinder. From left to right, the initial position $q_0(X)$, an intermediate position $q_{t_0}(X)$ at time $t_0 \in]0,1[$, the final position $q_1(X)$ and the biological coordinate system (X, τ). This example shows a situation where q_0 is not an embedding and yet q_1 is one. The cylinder at time 0 is completely folded flat on itself and it unfolds gradually until the time 1 when it is fully grown. All the creation process occurs at the base of the cylinder. Each newly created leaf pushes upwards the rest of the cylinder.

as follows:

$$\begin{array}{rccc} q_0 : & [0,1] \times [0, 2\pi[& \to & \{0\} \times \mathbb{R}^2 \\ & (t, \theta) & \mapsto & \big(0, \rho(t)\cos(\theta), \rho(t)\sin(\theta)\big)\,, \end{array} \tag{3.9}$$

where $\rho : [0,1] \to [0,1]$ is an increasing homeomorphism. The deformations are still modeled by vertical translations and we consider three particular $v \in L^2([0,1], \mathbb{R})$. One is constant, one is increasing, and the last one is decreasing. Figure 3.5 gives then the generated scenarios with also three different ρ where ρ' is either constant, increasing or decreasing. This figure only displays the final state of the scenarios. However, since their flow are built with rigid deformations, the initial position and the foliation, induced by the disjoint images of the leaves $X_{\{t\}}$, allow to retrieve each scenario. These sets are enlightened by the meshes of the shapes and the color gradient. One can thus compare each result with a reference shape, fixed here as the cone. When the shape induces a convex 3D shape, one can see that the growth of the scenario is delayed with respect to the cone. Otherwise, this growth is accelerated. The middle column illustrates therefore that the choice of the initial position can have the effect of a time warping on a scenario. This justifies the decision to fix the biological coordinate system. They will therefore not be submitted to optimization in the problem addressed in Section 2. Note that this question has already been deepened in Chapter 2 but we will also return to it in Chapter 4. Note at last, that even with a fixed system (X, τ), two distinct pairs (q_0, v) can generate the same final shape. In this last sentence, the word distinct implies that the images $(q_0(X_{\{t\}}))_{t \in [0,1]}$ of the leaves by the two initial positions q_0 are different from a set point of view. However, the two evolutions $t \mapsto (S_t = q_t(X_t))$ are not equal (consider for example the evolution of the base).

Remark 1.1. *Note, in Figure 3.5, that the spatial regularity at the top of the final shape varies depending on the example.*

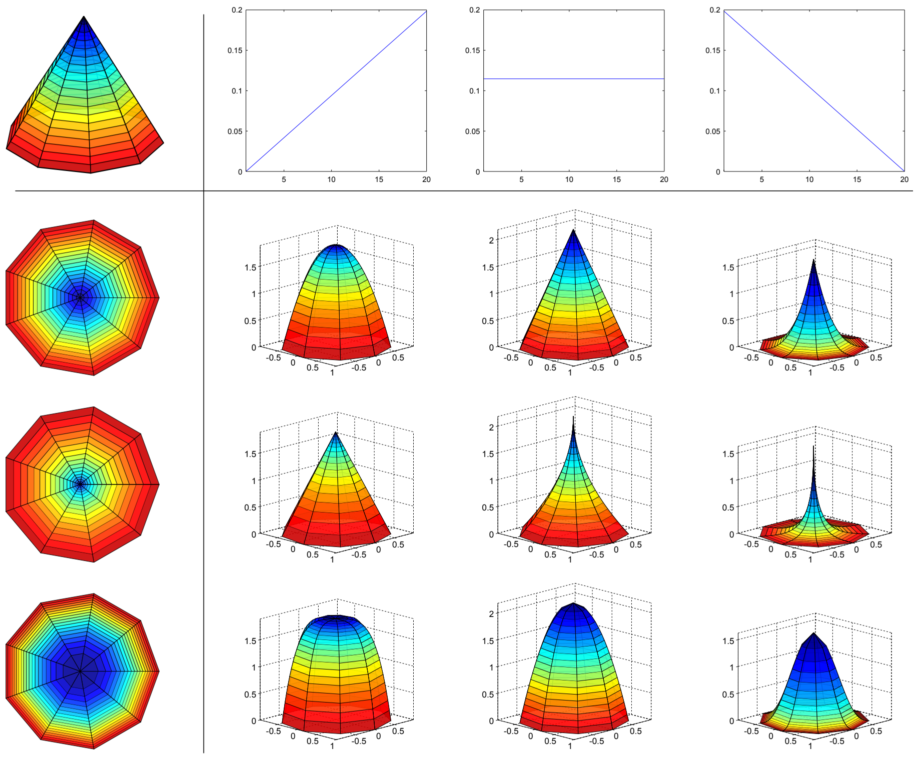

Figure 3.5 – “Horns” generated with different initial positions and vector fields. The deformations are restrained to vertical upward translations whose amplitudes are displayed in the first row. The first column shows the initial positions $q_0(X)$. We display in the center of the table the final cones $q_1(X)$ resulting from this nine configurations. The aim is to compare, regarding to the growth process, the variations of the solutions with respect to the cone on the top left corner.

1.4 Presentation of the generative model properties

The previous introduction invites to study general integral equations of the type

$$q_t^v = q_0 + \int_0^t f(q_s^v, v_s, s)\, ds\,, \tag{3.10}$$

where f is an application from $B \times V \times [0,1]$ to B with B and V two Banach spaces. We will denote only q instead of q^v to simplify the notation. V can be more generally seen as a space of control. In our situation, it will be a space of vector fields on the ambient space and more precisely a subspace of $\mathcal{C}^2(\mathbb{R}^d, \mathbb{R}^d)$. The specificity of this model lies on the fact that f depends on time in addition to the control v. A detailed study will be achieved in Section 4. We will summarize here the main properties.

Remark 1.2. *Equation* (3.10) *is the integral version of the standard equation*

$$\dot{q}_t = f(q_t, v_t, t)\,, \tag{3.11}$$

with a given initial condition q_0 at time 0. *However, we will see that the function $t \mapsto f(q_t, v_t, t)$ is not regular enough to imply the existence of a derivative at all time. In Proposition 4.2, we will prove that a solution q of the integral equation* (3.10) *admits* *a time derivative $\dot{q}_t$ at almost all time and that this derivative is integrable. This is a property shared by any absolutely continuous function (definition recalled below).*

Definition 1.1. *A function $F : [0,1] \to B$ with values in a Banach space B is said* absolutely continuous *if there exists a function $f \in L^1([0,1], B)$ such that for any $t \in [0,1]$, $F_t = \int_0^t f_s\, ds$. The space of absolutely continuous functions with values in B will be denoted $\mathcal{AC}([0,1], B)$.*

We will denote by (H^f) and (H^V) few sets of regularity conditions on f and V that will be introduced in Section 4. Mostly, it consists in the existence of time integrable controls on f and v and their derivatives. Throughout this chapter, these conditions will be progressively supplemented. They are gathered in Appendix B. Consider for now

$$
(H_1^f) \quad \left|
\begin{array}{l}
\textit{(i)} \text{ For any } t \in [0,1], f_t \in \mathcal{C}^1(B \times V, B)\,. \\
\textit{(ii)} \text{ There exists } c > 0, \text{ such that for any } (q,v,t) \in B \times V \times [0,1], \\
\begin{cases}
\left| \dfrac{\partial f}{\partial q}(q,v,t) \right|_{op} \leq c\,|v|_V\,, \\
\left| \dfrac{\partial f}{\partial v}(q,v,t) \right|_{op} \leq c\,(|q|_B + 1)\,.
\end{cases}
\end{array}
\right.
$$

$$
(H_1^V) \quad \left|
\begin{array}{l}
\textit{(i)}\ V \subset \mathcal{C}^2(\mathbb{R}^d, \mathbb{R}^d)\,. \\
\textit{(ii)} \text{ There exists } c > 0 \text{ such that} \\
\text{for any } (x,v) \in \mathbb{R}^d \times V, \text{ we have} \\
\begin{cases}
|v(x)|_{\mathbb{R}^d} \leq c|v|_V(|x|_{\mathbb{R}^d} + 1), \\
|dv(x)|_{\mathcal{L}(\mathbb{R}^d,\mathbb{R}^d)} + |d^2v(x)|_{\mathcal{L}(\mathbb{R}^d \otimes \mathbb{R}^d, \mathbb{R}^d)} \leq c|v|_V\,.
\end{cases}
\end{array}
\right.
$$

Proposition 1.1. *Let $f : B \times V \times [0,1] \to B$ be a function that satisfies the (H_1^f) conditions. Then one can define the function Φ_f that returns, for any initial condition $q_0 \in B$ and any control $v \in L^2([0,1], V)$, the unique solution $q \in \mathcal{AC}([0,1], B)$ of the integral equation* (3.10)*.*

$$
\begin{array}{rccc}
\Phi_f : & B \times L^2([0,1], V) & \longrightarrow & \mathcal{AC}([0,1], B) \\
& (q_0, v) & \longmapsto & q : t \mapsto q_0 + \int_0^t f(q_s, v_s, s) ds\,.
\end{array}
$$

Proof. See Theorem 4.2 and Proposition 4.2 and note (H_1^f) is actually reduced to (H_0^f). □

Definition 1.2. *When a space X is equipped with a temporal marker $\tau : X \to [0,1]$ and B is a space of mappings $q : X \to \mathbb{R}^d$, we define the **growth dynamic** by the specific function $f : B \times V \times [0,1] \to B$*

$$
f(q,v,t) = (x \mapsto \mathbb{1}_{\tau(x) \leq t}\, v(q(x)))\,. \tag{3.12}
$$

We retrieve the setting introduced in the previous sections as well as the evolution given by equation (3.7). We will progressively verify that under the (H^V) conditions, this function f satisfies all the sets of conditions (H^f).

Remark 1.3 (Spatial regularity of the mappings)**.** *Although the vector fields are spatially smooth, the indicator given by the temporal marker implies that f does not take values in a space of continuous mappings. The reference space to model the shapes will thus be $L^\infty(X, \mathbb{R}^d)$. The spatial regularity of q_t thus demands a special attention. Nevertheless, we will show that for an initial position $q_0 \in \mathcal{C}(X, \mathbb{R}^d)$, the continuity is preserved. That is to say that the development q belongs to $\mathcal{C}([0,1], \mathcal{C}(X, \mathbb{R}^d))$. Moreover, unlike the standard dynamic, a new characteristic appears here. The spatial regularity of q_t depends on the temporal regularity of the vector field. We will see that without more assumption on v, q_t is only differentiable almost everywhere.*

Remark 1.4. *The choice of the space B will play an unexpected role and we will see in Section 3.5 that we will have to browse through more than one space.*

Progressively the function f will be replaced by a more natural operator

$$\xi : B \times [0,1] \to \mathcal{L}(V, B)\,,$$

induced by the differentiation of the action of a group of diffeomorphisms, and therefore called *infinitesimal action*, as presented in Chapter 1. The introduction of this new notation highlights the linearity with respect to the control v.

Definition 1.3. *The operator $\xi : B \times [0,1] \to \mathcal{L}(V, B)$ induced by the* ***growth dynamic*** *is formally given by*

$$\xi_{(q,t)}(v) = (x \mapsto \mathbb{1}_{\tau(x) \leq t}\, v(q(x)))\,. \tag{3.13}$$

Proposition 1.2. *If $B = L^\infty(X, \mathbb{R}^d)$, the (H_1^V) conditions ensure that the operator ξ induced by the growth dynamic, given by equation (3.13), takes indeed values in $\mathcal{L}(V, B)$.*

At last, Section 4.3 studies how a solution $q = \Phi_f(q_0, v)$ reacts to some variations of the initial condition and of the vector field. More precisely, consider two small variations $\delta q_0 \in B$ and $\delta v \in L^2([0,1], V)$ that define for $\epsilon > 0$ a new set of parameters $q_0^\epsilon = q_0 + \epsilon \delta q_0$ and $v^\epsilon = v + \epsilon \delta v$. The question is to study the link between the two solutions $q = \Phi_f(q_0, v)$ and $q^\epsilon = \Phi_f(q_0^\epsilon, v^\epsilon)$.

Let us recall the definition of directional derivative in Banach spaces.

Definition 1.4 (Gâteaux-derivative)**.** *Let $f : E \to F$ be an application between two Banach spaces E and F. Let be $x_0, \delta x_0 \in E$. Define the application $g : \mathbb{R} \to F$ given by $g(h) = f(x_0 + h\delta x_0)$. If g is derivable at 0, we say that f is Gâteaux-differentiable at x_0 in the direction δx_0 and in this case, we note and define the Gâteaux-derivative $f'(x_0; \delta x_0) \doteq g'(0)$.*

This definition leads to consider the function $g : \mathbb{R} \to B$ defined with the previous notation by $g(\epsilon) = q^\epsilon$. Then Theorem 4.2 says that g is derivable at 0 and $g'(0)$ is the Gâteaux-derivative of Φ_f at point (q_0, v) in the direction $(\delta q_0, \delta v)$. The expression of this derivative is given in the next proposition.

Proposition 1.3. *Consider f and Φ_f as defined in Proposition 1.1 and such that f satisfies the (H_1^f) conditions. For any $(q_0, v) \in B \times L_V^2$ and any $(\delta q_0, \delta v) \in B \times L_V^2$, the*

Gâteaux-derivative $\Phi'_f(q_0, v; \delta q_0, \delta v) \in \mathcal{AC}([0,1], B)$ *of* Φ_f *is defined by the unique solution of the linearized equation*

$$\delta q_t = \delta q_0 + \int_0^t \frac{\partial f}{\partial q}(q_s, v_s, s) \cdot \delta q_s + \frac{\partial f}{\partial v}(q_s, v_s, s) \cdot \delta v_s \, ds \,.$$

In conclusion, if we denote $\delta q = \Phi'_f(q_0, v; \delta q_0, \delta v)$, we have for any small ϵ and at any time $t \in [0,1]$

$$q_t^\epsilon \approx q_t + \epsilon \delta q_t \,.$$

Note at last again that δq is not derivable at all time but absolutely continuous.

2 Optimal matching with a time dependent dynamic

2.1 Reconstitution of a growth scenario

We consider from now a longitudinal data set. Each individual of a given population is represented by a sample of its evolution at a finite number of times. The main problem addressed in this chapter is to retrieve, for any individual, its complete evolution on the time interval $[0,1]$. Consider thus a target scenario given by a collection of shapes $(S_i^{\text{tar}})_i$ at a finite number of intermediate times $(t_i)_i \subset [0,1]$ (with $\max\{t_i, i\} = 1$). The aim is to generate a continuous path $(t \mapsto S_t)_{t\in[0,1]}$ such that $S_{t_i} \approx S_i^{\text{tar}}$. Additionally, we assume that the population shares a common growth pattern. Each evolution can thus be represented by a growth scenario parameterized by a common biological coordinate system (X, τ). With the notation of Proposition 1.1, we aim thus to find a good approximation $q \in \mathcal{C}([0,1], B)$ in the image of the generating function Φ_f.

The discrepancy between the data and a solution $q \in \mathcal{C}([0,1], B)$ is estimated at the different times t_i with a **data attachment term** $\mathcal{A}$ of the form

$$\sum_{i=1}^n d(S_{t_i}, S_i^{\text{tar}})^2 \,,$$

where the shape S_{t_i} is induced by q_{t_i} and d is a distance that depends on the type of the data. To simplify the problem, we will assume throughout this chapter that $n = 1$. The quality of a matching with respect to the data is measured by $\mathcal{A}(q_1)$ for a general functional

$$\mathcal{A} : B \to \mathbb{R}^+ \,.$$

An inexact registration problem between the trivial scenario of a biological coordinate system and a final target shape can thus be generalized as a minimization problem on an energy

$$E(q_0, v) = \int_0^1 C(v_t, t) \, dt + \mathcal{A}(q_1) \,, \tag{3.14}$$

where v is a time-varying vector field that belongs to $L^2([0,1], V)$, $q_0 \in B$ is the initial condition and $q = \Phi_f(q_0, v) \in \mathcal{C}([0,1], B)$ is the development generated by v as previously introduced (see Proposition 1.1). At last, this energy penalizes the deformation through a **cost function** $C : V \times [0,1] \to \mathbb{R}$. We assume that

$$(H^C) \quad \left| \begin{array}{l} \textit{(i)}\ C \in \mathcal{C}^1(V \times [0,1], \mathbb{R})\,. \\ \textit{(ii)}\ \text{There exists } c > 0, \text{ such that for any } (v,t) \in V \times [0,1], \\ |C(v,t)| + |\nabla_v C(v,t)|_V^2 \le c|v|_V^2. \end{array} \right.$$

C is generally the square norm of V but we will have to explore other possibilities. We also assume that $\mathcal{A} : B \to \mathbb{R}$ is of class $\mathcal{C}^1$. In our experiments, $\mathcal{A}$ will measure the difference of the image of q_1 and $\mathcal{S}^{\text{tar}}$ with the square norm of an Reproducing Kernel Hilbert Space (RKHS) modeling a current space or a varifold space. In practice, this target $\mathcal{S}^{\text{tar}}$ will usually induce a good estimation of the initial position q_0 thanks to a biological prior that restricts the area where the new points of the scenario can appear (see Chapter 5) .

2.2 Expression of the gradient via the momentum

The minimization of E is achieved by a gradient descent. A prerequisite to establish the gradient of E is the introduction of the momentum.

2.2.1 The momentum

In order to compute an explicit formulation of the gradient, we define as in the classical LDDMM framework a new variable p called the **momentum**.

Proposition 2.1 (Existence of the Momentum)**.** *If f satisfies the (H_1^f) conditions (defined in the previous section), the **momentum** $p \in \mathcal{AC}([0,1], B^*)$ associated to $q = \Phi_f(q_0, v)$ is the unique solution of the equation*

$$\dot{p}_t = -\frac{\partial f}{\partial q}(q_t, v_t, t)^* \cdot p_t\,, \tag{3.15}$$

with the final condition

$$p_1 = -d\mathcal{A}(q_1) \in B^*. \tag{3.16}$$

Proof. Under the (H_1^f) conditions, $t \mapsto \frac{\partial f}{\partial q}(q_t, v_t, t)$ belongs to $L^2([0,1], \mathcal{L}(B))$. The time-varying adjoint operator $t \mapsto \frac{\partial f}{\partial q}(q_t, v_t, t)^*$ belongs thus to $L^2([0,1], \mathcal{L}(B^*))$. The existence and uniqueness of p are given by the linear Cauchy-Lipschitz formulation given in Corollary 4.2. $\square$

Remark 2.1. *As in the LDDMM framework (with the standard dynamic), the momentum is a central element of the theory developed here. We will see in Example 2.1 that the optimal vector field is parameterized by the trajectory q, its momentum p and the time variable. With the Hamiltonian approach and via the shooting method, we will rewrite the optimization problem with respect to the initial position q_0 and the initial momentum p_0.*

2.2.2 Expression of the gradient

Theorem 2.1 (Expression of the gradient)**.** *Assume the (H_1^f), (H_1^V) and (H^C) conditions and consider $\mathcal{A} : B \to \mathbb{R}$ of class $\mathcal{C}^1$. Let be $(q_0, v) \in B \times L_V^2$ and $q = \Phi_f(q_0, v)$ the solution* *to the integral equation*

$$q_t = q_0 + \int_0^1 f(q_s, v_s, s)\, ds\,.$$

Define the ***momentum*** $p \in \mathcal{AC}([0,1], B^*)$ *associated to* q *as the solution of*

$$p_1 = -d\mathcal{A}(q_1) \in B^* \qquad\qquad \dot{p}_t = -\frac{\partial f}{\partial q}(q_t, v_t, t)^* \cdot p_t\,. \tag{3.17}$$

Consider the energy

$$E(q_0, v) = \int_0^1 C(v_t, t)\, dt + \mathcal{A}(q_1)\,.$$

Then the Gâteaux-derivative of the energy at the point (q_0, v) *is given in any direction* $(\delta q_0, \delta v) \in B \times L^2_V$ *by*

$$E'\big((q_0, v); (\delta q_0, \delta v)\big) = (p_0 \,|\, \delta q_0) + \int_0^1 \left(\frac{\partial C}{\partial v}(v_t, t) - \frac{\partial f}{\partial v}(q_t, v_t, t)^* \cdot p_t \,\middle|\, \delta v_t \right) dt\,.$$

Hence, the gradient of the energy with respect to the vector field is given at any time $t \in [0,1]$ *by*

$$\nabla_v E(q_0, v)_t = K_V \left(\frac{\partial C}{\partial v}(v_t, t) - \frac{\partial f}{\partial v}(q_t, v_t, t)^* \cdot p_t \right), \tag{3.18}$$

where $K_V : V^* \to V$ *is the canonical isomorphism.*

Proof. Consider and denote $\delta q = \Phi'_f(q_0, v; \delta q_0, \delta v)$ the Gateaux-derivative of Φ_f given in Proposition 1.3. Since δq and p are absolutely continuous, $t \mapsto (p_t \,|\, \delta q_t)$ is also absolutely continuous and we have then

$$\begin{aligned}
(p_1 \,|\, \delta q_1) &= (p_0 \,|\, \delta q_0) + \int_0^1 \frac{d}{dt}(p_t \,|\, \delta q_t)\, dt = (p_0 \,|\, \delta q_0) + \int_0^1 (p_t \,|\, \delta \dot{q}_t) + (\dot{p}_t \,|\, \delta q_t)\, dt \\
&= (p_0 \,|\, \delta q_0) + \int_0^1 \left(p_t \,\middle|\, \frac{\partial f}{\partial q}(q_t, v_t, t) \cdot \delta q_t + \frac{\partial f}{\partial v}(q_t, v_t, t) \cdot \delta v_t \right) \\
&\qquad\qquad - \left(\frac{\partial f}{\partial q}(q_t, v_t, t)^* \cdot p_t \,\middle|\, \delta q_t \right) dt \\
&= (p_0 \,|\, \delta q_0) + \int_0^1 \left(p_t \,\middle|\, \frac{\partial f}{\partial q}(q_t, v_t, t) \cdot \delta q_t + \frac{\partial f}{\partial v}(q_t, v_t, t) \cdot \delta v_t \right) \\
&\qquad\qquad - \left(p_t \,\middle|\, \frac{\partial f}{\partial q}(q_t, v_t, t) \cdot \delta q_t \right) dt \\
&= (p_0 \,|\, \delta q_0) + \int_0^1 \left(\frac{\partial f}{\partial v}(q_t, v_t, t)^* \cdot p_t \,\middle|\, \delta v_t \right) dt\,.
\end{aligned}$$

This expression is well defined since under the (H_1^f) assumption, there exists $c > 0$ such that for any $t \in [0,1]$

$$\left| \frac{\partial f}{\partial v}(q_t, v_t, t)^* \cdot p_t \right| \leq c(|q_t|_B + 1)|p_t|_{B^*} \leq c(|q|_\infty + 1)|p|_\infty.$$

Therefore, define

$$\delta E = \int_0^1 \left(\frac{\partial C}{\partial v}(v_t, t) \,\middle|\, \delta v_t \right) dt + (d\mathcal{A}(q_1) \,|\, \delta q_1) \tag{3.19}$$

$$= \int_0^1 \left(\frac{\partial C}{\partial v}(v_t, t) \,\middle|\, \delta v_t \right) dt - (p_1 \,|\, \delta q_1) \tag{3.20}$$

$$= (p_0 \,|\, \delta q_0) + \int_0^1 \left(\frac{\partial C}{\partial v}(v_t, t) - \frac{\partial f}{\partial v}(q_t, v_t, t)^* \cdot p_t \,\middle|\, \delta v_t \right) dt\,. \tag{3.21}$$

The existence of a gradient $\nabla_v C(v_t, t) \in V$ at any time $t \in [0, 1]$ is given by the Riesz representation theorem. The (H^C) conditions ensures that this gradient is L^2-integrable so that the gradient of E is well defined. Note that (H^C) conditions are satisfied when C returns the square norm of v.

In fine, δE is finite and if $e(\epsilon) = E(q_0^\epsilon, v^\epsilon)$, the Gâteaux-derivative of E is then equal to

$$E'\big((q_0, v); (\delta q_0, \delta v)\big) = e'(0) = \delta E\,.$$

$\square$

Note that this theorem implies neither the existence of local minimizers of the energy E nor the uniqueness. The existence of solutions is a problem studied in Chapter 4.

2.3 Momentum map

The function f is intended to model the infinitesimal action of v on q and should thus always be linear with respect to v. We can thus rewrite it through an operator defined as follows

$$\xi : B \times [0, 1] \to \mathcal{L}(V, B)\,,$$

with for any $(q, v, t) \in B \times L^2_V \times [0, 1]$

$$f(q, v, t) = \xi(q, t)(v)\,.$$

In the next sections, the dynamic will be fixed by ξ. If $q = \Phi_f(q_0, v)$ is the solution generated by $v \in L^2_V$, at almost any time $\dot{q}_t$ is given by

$$\dot{q}_t = \xi(q_t, t)(v_t)\,.$$

We will eventually denote $\xi_t(q)$ for $\xi(q, t)$. As we have introduced the (H^f) conditions, we will usually assume that ξ is of class $\mathcal{C}^1$ with respect to q and satisfies then

(H_1^ξ)

(i) $\xi_t \in \mathcal{C}^1(B, \mathcal{L}(V, B)$ for any $t \in [0, 1]$.

(ii) There exists $c > 0$ such that
$|\xi(q, t)|_{\mathcal{L}(V,B)} \leq c(|q|_B + 1)$ and $|\partial_q \xi(q, t)|_{\mathcal{L}(B,\mathcal{L}(V,B))} \leq c$,
for any $(q, t) \in B \times [0, 1]$.

We can now introduce $\mathcal{J}_\xi$, usually called the **momentum map** and implicitly associated to ξ in this general study. Its definition is based on the linearity of ξ with respect to v. $\mathcal{J}_\xi$ will be the key to describe optimal vector fields.

Proposition 2.2 (Definition of the Momentum Map)**.** *The momentum map is the application $\mathcal{J}_\xi$ associated to ξ defined under the (H_1^ξ) conditions by*

$$\begin{array}{rcl}\mathcal{J}_\xi : B \times B^* \times [0,1] & \longrightarrow & V^* \\ (q,p,t) & \longmapsto & \xi^*_{(q,t)} \cdot p\,.\end{array}$$

We have for any $(q,p,t) \in B \times B^* \times [0,1]$ and any $v \in V$

$$(\mathcal{J}_\xi(q,p,t) \,|\, v) = \big(p \,\big|\, \xi_{(q,t)}(v)\big)\ .$$

Proof. Let us verify that $\mathcal{J}_\xi$ is well defined. Under the (H^ξ) conditions, there exists $c > 0$ such that for any $(q,p,t) \in B \times B^* \times [0,1]$, $|\xi(q,t)|_{\mathcal{L}(V,B)} \leq c(|q|_B + 1)$. Hence,

$$|\mathcal{J}_\xi(q,p,t)|_{V^*} \leq c(|q|_B + 1)|p|_{B^*} \tag{3.22}$$

and $\mathcal{J}_\xi$ takes indeed its values in V^*. □

The regularity with respect to time of this momentum map will play an important role in the next sections. At this stage, we start with the following proposition.

Proposition 2.3. *Under the (H_1^ξ) conditions, the momentum map is $\mathcal{C}^1$ with respect to its two first variables.*

Proof. Since under (H_1^ξ), $q \mapsto \xi_t(q)$ is of class $\mathcal{C}^1$ for any $t \in [0,1]$, and $p \mapsto (p \,|\, \delta q)$ is smooth for any $\delta q \in B$, we get immediately the result. □

Theorem 2.1 can be rewritten with these new variables.

Theorem 2.2 (Expression of the Gradient via the Momentum Map)**.** *Assume the (H_1^ξ), (H_1^V) and (H^C) conditions and consider $\mathcal{A} : B \to \mathbb{R}$ of class $\mathcal{C}^1$. Let be $(q_0, v) \in B \times L^2_V$ and $q = \Phi_\xi(q_0, v)$ the solution to the integral equation*

$$q_t = q_0 + \int_0^1 \xi_{(q_s,s)}(v_s)\, ds\,.$$

With the previously introduced momentum $p \in \mathcal{C}([0,1], B^*)$ associated to q and momentum map $\mathcal{J}_\xi : B \times B^* \times [0,1] \to V^*$, the Gâteaux-derivative at point (q_0, v) of the energy

$$E(q_0, v) = \int_0^1 C(v_t, t)\, dt + \mathcal{A}(q_1)$$

is given in any direction $(\delta q_0, \delta v) \in B \times L^2_V$ by

$$E'\big((q_0, v); (\delta q_0, \delta v)\big) = (p_0 \,|\, \delta q_0) + \int_0^1 \left(\frac{\partial C}{\partial v}(v_t, t) - \mathcal{J}_\xi(q_t, p_t, t) \middle|\, \delta v_t \right) dt\,.$$

Hence, the gradient of the energy with respect to the vector field is given at any time $t \in [0,1]$ by

$$\nabla_v E(q_0, v)_t = \nabla_v C(v_t, t) - K_V \mathcal{J}_\xi(q_t, p_t, t)\,. \tag{3.23}$$

Proof. It results from Theorem 2.1. We have

$$
\begin{aligned}
E'\big((q_0, v); (\delta q_0, \delta v)\big) &= (p_0 \,|\, \delta q_0) + \int_0^1 \left(\frac{\partial C}{\partial v}(v_t, t) - \frac{\partial f}{\partial v}(q_t, v_t, t)^* \cdot p_t \,\middle|\, \delta v_t \right) dt \\
&= (p_0 \,|\, \delta q_0) + \int_0^1 \left(\frac{\partial C}{\partial v}(v_t, t) - \mathcal{J}_\xi(q_t, p_t, t) \,\middle|\, \delta v_t \right) dt \\
&= (p_0 \,|\, \delta q_0) + \int_0^1 \langle \nabla_v C(v_t, t) - K_V \mathcal{J}_\xi(q_t, p_t, t), \delta v_t \rangle_V dt \,.
\end{aligned}
$$

□

Remark 2.2. *Note that equation* (3.22) *implies that for any pair* $(q, p) \in \mathcal{C}([0, 1], B \times B^*)$, *the associated momentum map is a* L^2*-function of time interval* $[0, 1]$, *i.e.*

$$
\big(t \mapsto K_V \mathcal{J}_\xi(q_t, p_t, t)\big) \in L^2_V \,.
$$

Example 2.1. *When* C *is given by the* classic cost function

$$
C(v, t) = \frac{1}{2} |v|^2_V \,,
$$

we have $\nabla_v C(v, t) = v$. *Hence, given* $q_0 \in B$, *any minimizer* $v^* \in L^2_V$ *of* E *satisfies at any time* $t \in [0, 1]$ *the equation*

$$
v^*_t = K_V \mathcal{J}_\xi(q_t, p_t, t) \,.
$$

We will consider other cost functions, but for all of them, an optimal vector field is always build on $K_V \mathcal{J}_\xi(q_t, p_t, t)$ *up to some weighting. The momentum map is thus in all cases the main ingredient of an optimal vector field. Section 3.4 will present an important class of cost functions. See Chapter 5 for another class of cost functions that we will use in our numerical experiments.*

Remark 2.3 (Time regularity of an optimal vector field)**.** *An important issue with time-varying dynamics is that* $t \mapsto \xi_t$ *has no reason to be continuous. Consider for example* $X = [0, 1]$, $\tau = \mathrm{Id}$ *and* $v \equiv y$ *with* $y \in \mathbb{R}^d$ *a constant vector field. Then we have with the growth dynamic for any* $q \in B = L^\infty([0, 1], \mathbb{R}^d)$ *and any* $t < t' \in [0, 1]$

$$
|\xi(q, t)(v) - \xi(q, t')(v)|_\infty = \big|\big(x \mapsto \mathbb{1}_{t < x \le t'} y\big)\big|_\infty = |y|_{\mathbb{R}^d} \,,
$$

so that $\xi_{t'}$ *does not tend to* ξ_t *when* t' *tends to* t. *Consequently and as mentioned before, we have no control on the time regularity of the momentum map and thus on the continuity of an optimal vector field.*

2.4 Hamiltonian framework

The central Theorem 2.1 that gives the expression of the gradient to the energy, says that given an initial condition q_0 in B, any local minimizer $v^* \in L^2_V$ of $E(q_0, \cdot)$ must satisfy at any time $t \in [0, 1]$ the equation

$$
\frac{\partial C}{\partial v}(v^*_t, t) - \frac{\partial f}{\partial v}(q_t, v_t, t)^* \cdot p_t = 0 \,, \tag{3.24}
$$

where q and p are the spatial mapping and the momentum associated to q_0 and v^*.

This leads to the introduction of the following Hamiltonian function

$$\begin{array}{rcl} H : B \times B^* \times V \times [0,1] & \longrightarrow & \mathbb{R} \\ (q,p,v,t) & \longmapsto & (p \mid f(q,v,t)) - C(v,t)\,. \end{array}$$

Then, an optimal trajectory (q,p) associated to a local minimizer v^* is at any time a local extrema of this Hamiltonian. Indeed, the partial derivatives of H are given for any $(q,p,v,t) \in B \times B^* \times V \times [0,1]$ by

$$\begin{aligned} \frac{\partial H}{\partial q}(q,p,v,t) &= -\frac{\partial f}{\partial q}(q,v,t)^* \cdot p\,, \\ \frac{\partial H}{\partial p}(q,p,v,t) &= f(q,v,t)\,, \\ \frac{\partial H}{\partial v}(q,p,v,t) &= \frac{\partial f}{\partial v}(q,v,t)^* \cdot p - \frac{\partial C}{\partial v}(v,t)\,, \\ \frac{\partial H}{\partial t}(q,p,v,t) &= \frac{\partial}{\partial t}(p \mid f(q,v,t)) - \frac{\partial C}{\partial t}(v,t)\,, \end{aligned}$$

and in particular, equation (3.24) is equivalent to $\frac{\partial H}{\partial v}(q_t,p_t,v_t^*,t) = 0$ which is nothing but a weak form of the Pontryagin Maximum Principle [43].

Usually, the cost function is a quadratic function on the norm of v. Hence, we will assume in the following that the derivative of the application $V \ni v \mapsto H(q,p,v,t)$ admits a unique zero that is the maximum of this application and we will note it $v^*(q,p,t)$ or v^* to simplify. This assumption allows to define the reduced Hamiltonian as follows:

$$\begin{array}{rcl} H_r : B \times B^* \times [0,1] & \longrightarrow & \mathbb{R} \\ (q,p,t) & \longmapsto & \max_{v \in V} H(q,p,v,t)\,. \end{array}$$

If $v \in V$ maximizes the Hamiltonian, we have $\frac{\partial H}{\partial v}(q,p,v,t) = 0$ and therefore, assuming that $v^*(q,p,t)$ is derivable with respect to q and p, the partial derivatives of H_r are given for any $(q,p,t) \in B \times B^* \times [0,1]$ by :

$$\begin{aligned} \frac{\partial H_r}{\partial q}(q,p,t) &= \frac{\partial H}{\partial q}(q,p,v^*,t) + \frac{\partial H}{\partial v}(q,p,v^*,t) \cdot \frac{\partial v^*}{\partial q}(q,p,t) = \frac{\partial H}{\partial q}(q,p,v^*,t) \\ \frac{\partial H_r}{\partial p}(q,p,t) &= \frac{\partial H}{\partial p}(q,p,v^*,t) + \frac{\partial H}{\partial v}(q,p,v^*,t) \cdot \frac{\partial v^*}{\partial p}(q,p,t) = \frac{\partial H}{\partial p}(q,p,v^*,t) \\ \frac{\partial H_r}{\partial t}(q,p,t) &= \frac{\partial H}{\partial t}(q,p,v^*,t) + \frac{\partial H}{\partial v}(q,p,v^*,t) \cdot \frac{\partial v^*}{\partial t}(q,p,t) = \frac{\partial H}{\partial t}(q,p,v^*,t)\,. \end{aligned}$$

We can now derive the characterization of the Gâteaux-derivative of the functional E as well as the critical paths in term of the Hamiltonian.

Theorem 2.3. *Assume the (H_1^f), (H_1^V) and (H^C) conditions and consider $\mathcal{A} : B \to \mathbb{R}$ of class $\mathcal{C}^1$. Let be $v \in L^2([0,1],V)$, let $q = \Phi_f(q_0,v)$ be the unique solution associated to an initial condition $q_0 \in B$ and let p be the retrograde solution of $p_1 = -d\mathcal{A}(q_1)$ and $\dot{p}_t = -\frac{\partial f}{\partial q}(q_t,v_t,t)^* \cdot p_t$. Then for any $\delta v \in L^2_V$,*

$$\frac{\partial E}{\partial v}(q_0,v) \cdot \delta v = \int_0^1 \left(-\frac{\partial H}{\partial v}(q_t,p_t,v_t,t) \mid \delta v_t \right) dt\,,$$

where for any $t \in [0,1]$,

$$H(q_t, p_t, v_t, t) = (p_t \,|\, f(q_t, v_t, t)) - C(v_t, t)\,.$$

Moreover, if for any $(x, y, t) \in B \times B^* \times [0,1]$ the equation $\partial_v H(x, y, v, t) = 0$ admits a unique solution $v^*(q, p, t)$ that is derivable with respect to q and p, then if $t \mapsto v_t$ locally minimizes E, the trajectory $(q, p) \in \mathcal{AC}([0,1], B \times B^*)$ satisfies at almost any time the following Hamiltonian system

$$\begin{cases} \dot{q}_t &= \frac{\partial H_r}{\partial p}(q_t, p_t, t)\,, \\ \\ \dot{p}_t &= -\frac{\partial H_r}{\partial q}(q_t, p_t, t)\,. \end{cases}$$

where

$$H_r(q_t, p_t, t) = H(q_t, p_t, v_t, t)\,.$$

Proof. We saw in Theorem 2.1 that

$$\nabla_v E(q_0, v)_t = K_V \left(\frac{\partial C}{\partial v}(v_t, t) - \frac{\partial f}{\partial v}(q_t, v_t, t)^* \cdot p_t \right) = -K_V \left(\frac{\partial H}{\partial v}(q_t, p_t, v_t, t) \right)\,.$$

Therefore, if v locally minimizes E, for almost any $t \in [0,1]$, v_t is the unique solution to $\frac{\partial H}{\partial v}(q, p, v, t) = 0$, i.e. $v_t = v^*(q_t, p_t, t)$ as previously defined. Then we retrieve with the partial derivatives of the reduced Hamiltonian $\frac{\partial H_r}{\partial p}(q_t, p_t, t) = \dot{q}_t$ and $\frac{\partial H_r}{\partial q}(q_t, p_t, t) = -\dot{p}_t$. □

Remark 2.4. *This theorem is an immediate application of the Pontryagin's maximum principle. When $C(v,t) = \frac{1}{2}|v|_V^2$, the application $V \ni v \mapsto H(q, p, v, t)$ admits a unique local extremum that is its maximum. However, with some other interesting cost functions, this application might have several local extrema. There exist yet Pontryagin's maximum principle theorems (in more specific configurations, for example, when V has a finite dimension) to prove that an optimal vector field v^* is then the global maximum of the Hamiltonian [49].*

This Hamiltonian can again be written with the operator ξ.

$$H(q, p, v, t) = (\xi^*_{(q,t)} \cdot p \,|\, v) - C(v, t) \tag{3.25}$$

$$= (\mathcal{J}_\xi(q, p, t) \,|\, v) - C(v, t)\,. \tag{3.26}$$

Example 2.2. *We saw in Example 2.1 that when C is the* classic cost function *given by $C(v,t) = \frac{1}{2}|v|_V^2$, any optimal vector field $v^* \in L_V^2$ of E satisfies at any time $t \in [0,1]$ the equation*

$$v_t^* = K_V \mathcal{J}_\xi(q_t, p_t, t)\,.$$

It results that

$$H_r(q_t, p_t, t) = \frac{1}{2}|\mathcal{J}_\xi(q_t, p_t, t)|_{V^*}^2 = \frac{1}{2}|v_t^*|_V^2\,.$$

Remark 2.5. *An important novelty appears here. This Hamiltonian is not constant in time. Its derivative with respect to t equals*

$$\begin{aligned}\frac{dH_r}{dt}(q_t,p_t,t) &= \frac{\partial H_r}{\partial q}(q_t,p_t,t)\cdot\dot q_t + \frac{\partial H_r}{\partial p}(q_t,p_t,t)\cdot\dot p_t + \frac{\partial H_r}{\partial t}(q_t,p_t,t)\\ &= -\dot p_t\cdot\dot q_t + \dot p_t\cdot\dot q_t + \frac{\partial H_r}{\partial t}(q_t,p_t,t)\\ &= \frac{\partial}{\partial t}\big(p_t\,|\,f(q_t,v_t^*,t)\big) - \frac{\partial C}{\partial t}(v_t^*,t)\,.\end{aligned}$$

In the situation of the Example 2.2, if the reduced Hamiltonian is not constant in time, the norm of the optimal vector field also varies in time and we have more precisely

$$\frac{dH_r}{dt}(q_t,p_t,t) = \left(\frac{\partial \mathcal{J}_\xi}{\partial t}(q_t,p_t,t)\middle|\, v_t^*\right)\,.$$

We will see in Section 3 that with the ***growth dynamic*** *this partial derivative of the momentum map measures the appearance of new points. Hence, when there is no creation at time t, we retrieve the classic LDDMM case and the norm of the vector field is constant. Otherwise, when there is appearance of new points, this norm should increase.*

Moreover, since the norm of v^* varies, this new model on time-varying dynamics does no longer generate geodesics on the group of deformations. This results from the fact that with the growth dynamic for example, the final shape q_1 does not depend anymore only on the final deformation generated by v^* but on the complete path or at least at every time when new points are created.

2.5 Shooting method

This section presents a formal approach of the shooting method. The following results will be proved in Sections 5.5 and 5.6.

We saw in the previous section that an optimal vector field or equivalently an optimal path $q \in \mathcal{C}([0,1],B)$ can be generated as a solution of the reduced Hamiltonian system. These solutions are parameterized by an initial position q_0 and an initial momentum p_0. Instead of playing with the vector field as the control in the set of paths, we can thus define the initial momentum as the new control that can be optimized.

Denote $y = \Psi(q_0,p_0)$ the unique solution of the reduced Hamiltonian system associated to the initial condition $(q_0,p_0) \in B\times B^*$. We have thus $y \in \mathcal{C}([0,1],B\times B^*)$ and at any time $t\in[0,1]$,

$$y_t = (q_t,p_t)$$

and

$$y_t = y_0 + \int_0^t h(y_s,s)\,ds\,,$$

where h is the symplectic gradient of H_r with respect to (q,p) defined as follows

$$\begin{array}{rcccc} h & : & (B \times B^*) \times [0,1] & \longrightarrow & B \times B^* \\ & & ((q,p),t) & \longmapsto & \begin{pmatrix} \frac{\partial H_r}{\partial p}(q,p,t) \\ \\ -\frac{\partial H_r}{\partial q}(q,p,t) \end{pmatrix} \end{array} \tag{3.27}$$

With this notation, we introduce a new expression of the energy

$$\hat{E}(y_0) = \int_0^1 \hat{C}(y_t, t)\, dt + \hat{\mathcal{A}}(y_1)\,,$$

where $\hat{C}(y_t, t) = C(v_t^*, t)$ is equivalent to the old cost function and $\hat{\mathcal{A}}(y_1) = \mathcal{A}(q_1)$ is equivalent to the old attachment term. Therefore, if an initial momentum p_0 and a time-varying vector field v generate the same solution $(q,p) \in \mathcal{C}([0,1], B \times B^*)$ then the two respective energies are equal

$$\hat{E}(y_0) = \hat{E}(q_0, p_0) = E(q_0, v)\,. \tag{3.28}$$

In the following, we will not distinguish $\hat{E}$, $\hat{C}$ and $\hat{\mathcal{A}}$ from E, C and $\mathcal{A}$.

The method to explicit the gradient of the energy is the same as before, reduced to two main steps and its conclusion as follows:

— The first step is to define the covariable of y as the momentum p is the covariable of q. We introduce thus $z_1 = -d\mathcal{A}(y_1) \in (B \times B^*)^*$ and we integrate it backward through the equation

$$\dot{z}_t = \frac{\partial C}{\partial y}(y_t, t) - \frac{\partial h}{\partial y}(y_t, t)^* \cdot z_t\,. \tag{3.29}$$

— The second step is to establish that the Gâteaux-derivative $\Psi'(y_0; \delta y_0)$ is given by

$$\delta y_t = \delta y_0 + \int_0^t \frac{\partial h}{\partial y}(y_s, s) \cdot \delta y_s\, ds\,.$$

— Then we can write

$$\begin{aligned} E'(y_0; \delta y_0) &= \int_0^1 \left(\frac{\partial C}{\partial y}(y_t, t) \,\middle|\, \delta y_t \right) dt + (d\mathcal{A}(y_1) \,|\, \delta y_1) \\ &= \int_0^1 \left(\frac{\partial C}{\partial y}(y_t, t) \,\middle|\, \delta y_t \right) dt - (z_1 \,|\, \delta y_1) \\ &= \int_0^1 \left(\frac{\partial C}{\partial y}(y_t, t) \,\middle|\, \delta y_t \right) dt - (z_0 \,|\, \delta y_0) + \int_0^1 (\dot{z}_t \,|\, \delta y_t) - (z_t \,|\, \dot{\delta y_t})\, dt \\ &= -(z_0 \,|\, \delta y_0) + \int_0^1 \left(\frac{\partial C}{\partial y}(y_t, t) - \dot{z}_t - \frac{\partial h}{\partial y}(y_t, t)^* \cdot z_t \,\middle|\, \delta y_t \right) dt \\ &= -(z_0 \,|\, \delta y_0)\,. \end{aligned}$$

At last, if we write at any time t the covariable z_t as $(\mathcal{Q}_t, \mathcal{P}_t) \in B^* \times B^{**}$, we get more explicitly

$$E'\big((q_0, p_0); (\delta q_0, \delta q_0)\big) = -(\mathcal{Q}_0 \,|\, \delta q_0) - (\mathcal{P}_0 \,|\, \delta p_0)\,. \tag{3.30}$$

The Gâteaux-derivative of the energy has thus a particularly simple expression leading to a new algorithm of gradient descent. An interest of this approach is to parameterize the solution with variables of smaller dimension paving the way for a statistical analysis.

Algorithm 3 Gradient descent on p_0

1 - Given $q_0^0 \in B$, initialize $p_0^0 \in B$ at zero.
Then for any $n \in \mathbb{N}$, given q_0^n and p_0^n :
2 - Integrate forward with the Hamiltonian system (3.27) to get $(q^n, p^n) \in \mathcal{C}([0,1], B^2)$.

3 - Compute $\mathcal{Q}_1^n = -d\mathcal{A}(q_1^n)$, defined $\mathcal{P}_1^n = 0$.
4 - Integrate backward with the second order Hamiltonian system (3.29) to get $(\mathcal{Q}^n, \mathcal{P}^n) \in \mathcal{C}([0,1], B^2)$.
4 - Update p_0^n by $p_0^{n+1} = p_0^n + \epsilon \mathcal{P}_0^n$ for a small $\epsilon > 0$.
5 - (Optional) Update q_0^n by $q_0^{n+1} = q_0^n + \epsilon \mathcal{Q}_0^n$ for a small $\epsilon > 0$.

3 Applications with the growth dynamic

We will now apply the previous results in the setting of mappings from a biological coordinate system (X, τ). We give the explicit expression of previous variables with the **growth dynamic** given by the operator $\xi : B \times [0,1] \to \mathcal{L}(V, B)$ defined by

$$\xi_{(q,t)}(v) = f(q, v, t) = \left(x \mapsto \mathbb{1}_{\tau(x) \leq t} v(q(x))\right).$$

In order to remember that ξ is now fixed throughout this section, the momentum map will be denoted $\mathcal{J}$ instead of $\mathcal{J}_\xi$, likewise with Φ.
The sets $X_{\{t\}}$ and X_t of new points and active points at time t, defined by (3.2) and (3.1), will play an important role to understand the construction of an optimal scenario.

3.1 Discrete coordinate space

We assume that X is given as finite set of k points with a mesh. At any time $t \in [0,1]$, q_t is an element of $B = (\mathbb{R}^d)^k$ with a mesh. Under the (H_1^V) conditions, the (H_1^ξ) conditions are satisfied (see Proposition 4.3).

3.1.1 The momentum

The general definition of the momentum and its evolution are given in Proposition 2.1. Here, with the Riez representation theorem, the momentum p can be seen as an element of $\mathcal{C}([0,1], (\mathbb{R}^d)^k)$. At time $t = 1$, p_1 is given by definition as the gradient of the attachment term $\mathcal{A}$

$$d\mathcal{A}(q_1) \cdot \delta q_1 = \sum_{x \in X} \langle \nabla_{q_1(x)} \mathcal{A}(q_1), \delta q_1(x) \rangle_{\mathbb{R}^d}$$

and p_1 can thus be parameterized by X as follows

$$p_1(x) = \nabla_{q_1(x)} \mathcal{A}(q_1),$$

so that $(p_1 \,|\, \delta q_1) = \langle p_1, \delta q_1 \rangle_{(\mathbb{R}^d)^k}$. This pointwise expression is conserved by the backward integration and we have at any time $t \in [0,1]$ for any $y \in B = (\mathbb{R}^d)^k$

$$(p_t \,|\, y) = \sum_{x \in X} \langle p_t(x), y(x) \rangle_{\mathbb{R}^d}.$$

In this configuration, the behaviors of q and p over time share a common pattern. For any x in X, $q_t(x)$ and $p_t(x)$ are both static when x does not exist, i.e. t is smaller than $\tau(x)$, and jointly active once x has appeared. Indeed, their dynamics are explicitly given for any $x \in X$ and at any time $t \in [0,1]$ by

$$\dot{q}_t(x) = \mathbb{1}_{\tau(x) \leq t}\, v_t(q_t(x)) \qquad \dot{p}_t(x) = -\mathbb{1}_{\tau(x) \leq t}\, dv_t(q_t(x))^T \cdot p_t(x)\,. \tag{3.31}$$

3.1.2 Expression of the momentum map

As we said in Example 2.1, the momentum map is the main ingredient to define optimal vector fields for all of the cost functions that we will consider. For any $(q,p,t) \in (\mathbb{R}^d)^k \times (\mathbb{R}^d)^k \times [0,1]$ and any $v \in V$, we have

$$\begin{aligned}\big(\mathcal{J}(q,p,t) \,|\, v\big) &= \langle p, \mathbb{1}_{\tau \leq t}\, v \circ q \rangle_{(\mathbb{R}^d)^k} \\ &= \sum_{x \in X, \tau(x) \leq t} \langle p(x), v(q(x)) \rangle_{\mathbb{R}^d}\,.\end{aligned}$$

Equivalently, $\mathcal{J}$ can be written

$$\mathcal{J}(q,p,t) = \sum_{x \in X, \tau(x) \leq t} \delta_{q(x)}^{p(x)}\,,$$

where for any $(x,y) \in (\mathbb{R}^d)^2$ and any $v \in V$, the functional $\delta_x^y \in V^*$ is defined by

$$\delta_x^y(v) = \langle y, v(x) \rangle_{\mathbb{R}^d}\,.$$

The vector field associated to $\mathcal{J}$ via the canonical isomorphism K_V has then an explicit expression in both Gaussian RKHS and affine situations.

- When V is a RKHS with a kernel denoted k_V, we have

$$K_V \mathcal{J}(q,p,t) = \sum_{x \in X, \tau(x) \leq t} k_V(q(x), \cdot) p(x)\,.$$

- In the specific case of rotations and translations, where V is the direct product $\mathrm{Skew}_d \times \mathbb{R}^d$ equipped with the usual norm, we have

$$K_V \mathcal{J}(q,p,t) = \left(\mathrm{proj}_{\mathrm{Skew}_d} \left(\sum_{x \in X, \tau(x) \leq t} p(x) q(x)^T \right), \sum_{x \in X, \tau(x) \leq t} p(x) \right).$$

Remark 3.1. *The reader familiar with the LDDMM framework will recognize all these equations. The difference with the classical model only resides in the addition of the indicator function. Each point $x \in X$ eventually contributes to v_t^* with a combination* *of its position $q_t(x)$ and its momentum $p_t(x)$. However, here, the set of points involved at each time or in other words the effective support of the vector field varies over time. At every time t, the coordinate space X and likewise the shape $q_t(X)$ are divided in two parts:*

1. *the active part composed of all the points already appeared*

$$X_t = \{x \in X \,|\, \tau(x) \leq t\},$$

2. *the inactive part (its complementary).*

At time t, the vector field v_t carries only the active part. Therefore, it is natural to obtain an optimal vector field v_t^* constructed only with the points of the active area and likewise, as noticed before, the active points have their position and momentum moving whereas the inactive points have a static position and momentum. See Figure 3.6.

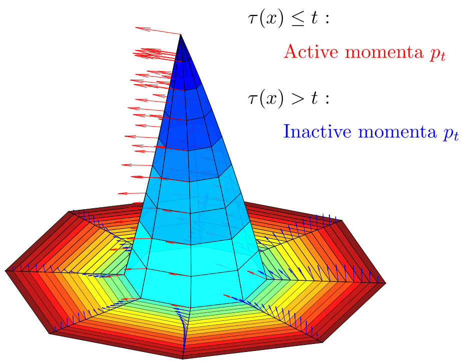

Figure 3.6 – The active part of the shape modeling the horn is blue. The inactive part of anticipated points goes from green to red. The arrows are the respective momenta $p_t(x)$ at points $q_t(x)$.

Remark 3.2 (Continuity of the momentum map)**.** *We stated already that the momentum map is of class $\mathcal{C}^1$ with respect to its two first variables. Since X is a finite set, the image of τ is also a finite subset of $[0,1]$ and given $q, p \in (\mathbb{R}^d)^k$, the function*

$$t \mapsto \mathcal{J}(q,p,t) = \sum_{X_t} \delta_{q(x)}^{p(x)}$$

is therefore piecewise constant. Given now a trajectory $q \in \mathcal{C}([0,1], (\mathbb{R}^d)^k)$ and its associated momentum $p \in \mathcal{C}([0,1], (\mathbb{R}^d)^k)$, thanks to Proposition 2.3,

$$t \mapsto \mathcal{J}(q_t, p_t, t)$$

is piecewise continuous as well as $t \mapsto K_V \mathcal{J}(q_t, p_t, t)$. More precisely, it is continuous on any interval $[t_i, t_{i+1}[$ where t_i and t_{i+1} are two consecutive values of $\tau(X)$. The jump at time t_{i+1} is given by

$$\sum_{x \in X, \tau(x) = t_{i+1}} \delta_{q_{t_{i+1}}(x)}^{p_{t_{i+1}}(x)} .$$

This jump is thus due to the contribution of the new points that appear at time t_{i+1}. An important remark here is that at any time t, for any $x \in X$ such that $\tau(x) = t$, we have

$q_t(x) = q_0(x)$ and $p_t(x) = p_0(x)$. The jump at time t_{i+1} is thus equal to

$$\sum_{x \in X, \tau(x) = t_{i+1}} \delta_{q_0(x)}^{p_0(x)} .$$

Therefore, all jumps depend only on q_0, p_0 and τ.

Inside these intervals $[t_i, t_{i+1}[$, the evolution of $K_V \mathcal{J}$ is the same as in the LDDMM framework. Otherwise, the jumps result from the extension of the support of $K_V \mathcal{J}$ with the set of points that progressively appear (the new points that contribute in the sum). We will see however in the next section in a non discrete case, that if the creation of points is smooth over time, the support of $K_V \mathcal{J}$ increases continuously and this last one is then also continuous.

3.1.3 Algorithm for the gradient descent

In fine, Algorithm 1 explicits an algorithm very similar to the LDDMM model to construct a minimizer v^*. The main difference in practice is to trace at each discrete time

Algorithm 4 Gradient descent on v

1 - Initiate $v^0 \in L^2_V$ at zero
Then for any $n \in \mathbb{N}$, given q_0 and v^n,
2 - Compute $q^n \in \mathcal{C}([0,1], (\mathbb{R}^d)^k)$ the path generated by $v^n \in L^2_V$
3 - Compute $p^n_1 = -\nabla \mathcal{A}(q^n_1)$ and integrate it backward to construct $p^n \in \mathcal{C}([0,1], (\mathbb{R}^d)^k)$

4 - Compute at any time the gradient at v^n_t : $\delta v^n_t = \nabla_v C(v^n_t, t) - K_V \mathcal{J}(q^n_t, p^n_t, t)$
5 - Update the vector field by $v^{n+1} = v^n + \epsilon \delta v^n$ for a small $\epsilon > 0$

$t_i \in [0,1]$ the set of active points.

Additionally, Theorem 2.1 also allows to optimize the initial condition q_0 if necessary. Typically, if q_0 is partially known and a reconstruction has been guessed, we can optimize it under some constraints (for example, inside a subset of the ambient space). This optimization should of course be controlled, otherwise the initial condition would just tend straightforward to the target. See an example in Chapter 5.

3.2 Continuous coordinate space

In this section, X is a compact submanifold eventually with corners. The evolution of the shape is still given by the operator $\xi : B \times [0,1] \to \mathcal{L}(V, B)$ defined by

$$\xi(q,t)(v) = \left(x \mapsto \mathbb{1}_{\tau(x) \leq t} v(q(x))\right) .$$

The definition of B needs to be slightly refined to involve the boundary of X. We will see indeed that ∂X will play an important role to explicit the momentum and the momentum map.

Definition 3.1 (The B space)**.** *For any Borel set $A \subset X$, we define the measure μ on X as follows*

$$\mu(A) \doteq \mathcal{H}^k(A) + \mathcal{H}^{k-1}(A \cap \partial X) .$$

We introduce then

$$B = L^{\infty}_{\mu}(X, \mathbb{R}^d) \tag{3.32}$$

the space of measurable functions from X to $\mathbb{R}^d$ defined μ-almost everywhere that are essentially bounded. We note $|q|_{\infty,\mu}$ the essential supremum with respect to μ and define $|q|_B \doteq |q|_{\infty,\mu}$.

One can easily verify that under the (H_1^V) conditions, ξ is well defined for $B = L^{\infty}_{\mu}(X, \mathbb{R}^d)$ and satisfies the (H_1^{ξ}) conditions.

Remark 3.3 (Spatial regularity of the solution)**.** *Consider a smooth initial position $q_0 \in \mathcal{C}^{\infty}(X, \mathbb{R}^d)$. We will show in Section 4, that even if $v \in \mathcal{C}([0,1], V)$, the final shape q_1 of the solution $q = \Phi(v, q_0)$ belongs to $\mathcal{C}^1(X, \mathbb{R}^d)$. However, if v is only square-integrable, q_1 is a priori only differentiable almost everywhere (see Proposition 4.8).*

Remark 3.4 (Definition of the attachment term)**.** *We recalled in Chapter 1 how to build a distance on shapes based on their current representations. The currents are yet generally used to model shapes that are at least rectifiable sets. The final shape q_1 is thus not enough regular when v is only integrable. We will show however in Chapter 4 that $\mathcal{A}$ can be extended from its standard definition on*

$$\{q_1 \,|\, q_0 \in \mathcal{C}^{\infty}(X, \mathbb{R}^d), v \in \mathcal{C}([0,1], V), q = \Phi(q_0, v)\} \subset \mathcal{C}^1(X, \mathbb{R}^d)$$

to

$$\{q_1 \,|\, q_0 \in \mathcal{C}^{\infty}(X, \mathbb{R}^d), v \in L^2_V, q = \Phi(q_0, v)\} \,,$$

the sets of all the shapes generated with the growth dynamic from smooth initial conditions. Hence, we will define the attachment term $\mathcal{A}$ on this set only (subset of B) as a function of q_0 and v. In other words, the previous energy is not modified but is now written

$$E(q_0, v) = \int_0^1 C(v_t, t)\, dt + \mathcal{A}(q_0, v)\,.$$

At last, let us announce a central result of the next chapter.

Remark 3.5 (Continuity of an optimal vector field v^*)**.** *Following the previous remark, we will also show in Chapter 4 that for any $v \in L^2_V$, $\mathcal{A}$ is Gâteaux-differentiable with respect to v and that E admits a minimizer. Moreover, any minimizer v^* is continuous with respect to time, i.e. $v^* \in \mathcal{C}([0,1], V)$.*

3.2.1 The momentum

In this general configuration, the nature of the momentum p strongly depends on the attachment term $\mathcal{A}$. As noted in Remark 2.3, the momentum map $\mathcal{J}$ is a priori not continuous with respect to time. However, if the momentum belongs to an adequate subspace of B^*, this continuity can be guaranteed. We will see that for a continuous vector field, p can be identified to an element of such a space denoted hereafter B_1^*. The last result of Chapter 4 says indeed that under the (H_1^V) conditions, the evaluation of the Gâteaux-derivative of $\mathcal{A}$ on δv can be rewritten as a linear form evaluated on δq_1 and define a pointwise momentum as follows:

For any $(q_0, v) \in \mathcal{C}^\infty(X, \mathbb{R}^d) \times \mathcal{C}([0,1], V)$, there exists $p_1 \in \mathcal{C}(X, \mathbb{R}^d) \times \mathcal{C}(\partial X, \mathbb{R}^d)$ such that for any $(\delta q_0, \delta v) \in \mathcal{C}^\infty(X, \mathbb{R}^d) \times \mathcal{C}([0,1], V)$,

$$\mathcal{A}'(q_0, v; \delta q_0, \delta v) = \int_X \langle p_1^X(x), \delta q_1(x) \rangle_{\mathbb{R}^d} \, d\mathcal{H}^k(x) + \int_{\partial X} \langle p_1^{\partial X}(x), \delta q_1(x) \rangle_{\mathbb{R}^d} \, d\mathcal{H}^{k-1}(x) \,. \tag{3.33}$$

Remark 3.6. *The fact that p_1 is not an arbitrary distribution in $\mathcal{C}^\infty(X, \mathbb{R}^d)'$ but can be represented by two simple continuous functions on X and ∂X will allow us to extend important properties of optimal vector fields from the discrete case to the continuous case for X. In the following, $\mathcal{A}$ does not have to be an attachment term built on currents but only to satisfy this previous property (equation* (3.33)*).*

To go further, one needs to show that the integration backward of p_1 preserves its simple pointwise representation as a pair of two continuous functions. It requires to introduce a new space smaller than B^*. As for q, a space of continuous functions is not admissible since the expression of $\dot{p}_t$ under the growth dynamic involves the indicator $\mathbb{1}_{\tau \le t}$. It leads then naturally to choose $B_1^* = L^\infty(X, \mathbb{R}^d) \times L^\infty(\partial X, \mathbb{R}^d)$. The choice of B_1^* is here validated by the two next propositions.

Proposition 3.1. *If $B = L^\infty_\mu(X, \mathbb{R}^d)$ and $B_1^* = L^\infty(X, \mathbb{R}^d) \times L^\infty(\partial X, \mathbb{R}^d)$, there exists a continuous linear embedding of B_1^* into B^*.*

Proof. One can show it directly or see Proposition 5.5 and Proposition 5.1. □

Proposition 3.2. *Assume the (H_1^V) conditions. For any $p_1 \in B_1^* = L^\infty(X, \mathbb{R}^d) \times L^\infty(\partial X, \mathbb{R}^d)$ and any $v \in L^2([0,1], V)$, there exists a unique solution $p \in \mathcal{AC}([0,1], B_1^*)$ that satisfies at almost all time*

$$\dot{p}_t^X(x) = \mathbb{1}_{\tau(x) \le t} dv_t(q_t(x))^T \cdot p_t^X(x) \qquad \dot{p}_t^{\partial X}(x) = -\mathbb{1}_{\tau(x) \le t} dv_t(q_t(x))^T \cdot p_t^{\partial X}(x) \,. \tag{3.34}$$

Proof. These equations are linear with respect to p_t and B_1^* is a Banach space. In both cases, (H_1^V) allows to control the operators with the norm of v_t so that they are both square-integrable. The linear Cauchy-Lipschitz Corollary 4.2 ensures thus the existence, uniqueness and stability of the momentum in this space on the time interval $[0,1]$. □

3.2.2 Expression of the momentum map

The expression of the momentum map (see Definition 2.2) on the two previously introduced spaces B and B_1^* is given by

$$\big(\mathcal{J}(q,p,t) \,|\, v\big) = \big(p \,|\, \mathbb{1}_{\tau(x) \le t} v(q(x))\big) \tag{3.35}$$

$$= \int_X \mathbb{1}_{\tau(x) \le t} \langle p^X(x), v(q(x)) \rangle_{\mathbb{R}^d} \, d\mathcal{H}^k(x) \tag{3.36}$$

$$+ \int_{\partial X} \mathbb{1}_{\tau(x) \le t} \langle p^{\partial X}(x), v(q(x)) \rangle_{\mathbb{R}^d} \, d\mathcal{H}^{k-1}(x) \,. \tag{3.37}$$

As for the discrete shapes (see Remark 3.1), the momentum map is at any time $t \in [0,1]$ built as an integral on the active part $X_t = \{x \in X \,|\, \tau(x) \le t\} \subset X$. We have yet an additional term built with the active points of the boundary of X.

To highlight the role played by the time marker τ via the indicator function in this equation, we assume now to simplify that $X = [0,1] \times X_0$ with $\partial X_0 = \emptyset$ and that τ is the projection on the first coordinate. In this configuration, the boundary of X is given by

$$\partial X = \big(\{0\} \times X_0\big) \cup \big(\{1\} \times X_0\big) .$$

This is exactly the set of points that appear at times $t = 0$ and $t = 1$. The previous equation becomes

$$\begin{aligned}
\big(\mathcal{J}(q,p,t) \,|\, v\big) = & \int_0^t \int_{X_0} \langle p^X(s,x_0), v(q(s,x_0))\rangle_{\mathbb{R}^d} \, d\mathcal{H}^{k-1}(x_0) ds && (3.38)\\
& + \int_{X_0} \langle p^{\partial X}(0,x_0), v(q(0,x_0))\rangle_{\mathbb{R}^d} \, d\mathcal{H}^{k-1}(x_0) && (3.39)\\
& + \mathbb{1}_{t=1} \int_{X_0} \langle p^{\partial X}(1,x_0), v(q(1,x_0))\rangle_{\mathbb{R}^d} \, d\mathcal{H}^{k-1}(x_0) . && (3.40)
\end{aligned}$$

This general example shows that when the new points appear regularly over time **the momentum map is continuous with respect to time** (for t in $[0,1[$) . The jump at time $t = 1$ is here meaningless since the evolution stops at this time.

Remark 3.7 (Pointwise expression of p to continuity of $\mathcal{J}$)**.** *The existence of a pointwise expression of the momentum implies thus the continuity of the momentum map with respect to time and thus the continuity of an optimal vector field (see Example 2.1). The continuity of an optimal vector field is yet not systematic with any attachment term. We will show indeed that with an attachment term built on varifolds, the optimal vector fields are not always continuous. However, note that with discrete shapes the attachment term does not play any specific role in the pointwise expression of the momentum as long as it is differentiable.*

Remark 3.8. *As we did in the previous section with a discrete coordinate space X, we can explicit the momentum map and its image in the vector field space V. From equations* (3.36) *and* (3.37)*, $\mathcal{J}$ can be rewritten*

$$\mathcal{J}(q,p,t) = \int_X \mathbb{1}_{\tau \leq t} \delta_q^{p^X} + \int_{\partial X} \mathbb{1}_{\tau \leq t} \delta_q^{p^{\partial X}} ,$$

where we recall that $p = (p^X, p^{\partial X})$. Then if V is a RKHS with a kernel k_V

$$K_V \mathcal{J}(q,p,t) = \\ \int_X \mathbb{1}_{\tau(x) \leq t} k_V(\cdot, q(x)) p^X(x) \, d\mathcal{H}^k(x) + \int_{\partial X} \mathbb{1}_{\tau(x) \leq t} k_V(\cdot, q(x)) p^{\partial X}(x) \, d\mathcal{H}^{k-1}(x)$$

and when we specify $X = [0,1] \times X_0$ and τ the projection on the first coordinate, this *expression becomes*

$$
\begin{aligned}
K_V \mathcal{J}(q,p,t) = & \int_0^t \int_{X_0} k_V(\cdot, q(s,x_0)) p^X(s,x_0)\, d\mathcal{H}^{k-1}(x_0) ds \\
& + \int_{X_0} k_V(\cdot, q(0,x_0)) p^{\partial X}(0,x_0)\, d\mathcal{H}^{k-1}(x_0) \\
& + \mathbb{1}_{t=1} \int_{X_0} k_V(\cdot, q(1,x_0)) p^{\partial X}(1,x_0)\, d\mathcal{H}^{k-1}(x_0)\,.
\end{aligned}
$$

Remark 3.9 (Time derivative and control on this derivative)**.** *We will prove in Section 5.4 (see Proposition 5.8) that the momentum map is derivable with respect to t almost everywhere:*

$$
\left(\frac{\partial \mathcal{J}}{\partial t}(q,p,t) \,\middle|\, \tilde{v} \right) = \int_{X_0} \langle p^X(t,x_0), \tilde{v}(q(t,x_0)) \rangle_{\mathbb{R}^d}\, d\mathcal{H}^{k-1}(x_0)\,. \tag{3.41}
$$

When X is a discrete set, the jumps of the momentum map result from the appearance of new points at the discrete times $(t_i)_{i=1:n} \subset [0,1]$. Likewise here, at each time, the support of the integral increases with the new layer $X_{\{t\}} = \{t\} \times X_0$. If we use as before the fact that the points and the momenta of a new layer have not been displaced, i.e. that at any time t, for any $x \in X$ such that $\tau(x) = t$ we have $q_t(x) = q_0(x)$ and $p_t(x) = p_0(x)$, we get for any trajectory $q \in \mathcal{C}([0,1], B)$ with its momentum $p \in \mathcal{C}([0,1], B_1^*)$ that for any $\tilde{v} \in L_V^2$

$$
\begin{aligned}
\left(\frac{\partial \mathcal{J}}{\partial t}(q_t,p_t,t) \,\middle|\, \tilde{v} \right) &= \int_{X_0} \langle p_t^X(t,x_0), \tilde{v}(q_t(t,x_0)) \rangle_{\mathbb{R}^d}\, d\mathcal{H}^{k-1}(x_0) && (3.42) \\
&= \int_{X_0} \langle p_0^X(t,x_0), \tilde{v}(q_0(t,x_0)) \rangle_{\mathbb{R}^d}\, d\mathcal{H}^{k-1}(x_0)\,. && (3.43)
\end{aligned}
$$

This last equation shows that the partial derivative with respect to time of the momentum map only depends on the initial condition q_0 and the initial momentum p_0. This will play an important role in the existence of solutions by shooting (Section 3.5).

3.3 Specific behavior of the momentum map with the growth dynamic

The previous pointwise decomposition of the momentum allow to suppose that the norm of an optimal vector field increase with the apparition of new points. Although we cannot explicitly show it, we can yet propose an upper bound of this norm by an increasing function of time.

3.3.1 Discrete setup

With a discrete coordinate space, we saw that the momentum map is given for any $(q,p,t) \in B \times B^* \times [0,1]$ and any $v \in V$ by

$$
\big(\mathcal{J}(q,p,t) \,|\, v \big) = \sum_{x \in X, \tau(x) \le t} \langle p(x), v(q(x)) \rangle_{\mathbb{R}^d} \tag{3.44}
$$

(note that $B^* = B = (\mathbb{R}^d)^k$) . For any couple $(q,p) \in \mathcal{C}([0,1], B \times B^*)$, there exists under the (H_1^V) conditions a constant $c > 0$ such that for any $t \in [0,1]$,

$$|K_V \mathcal{J}(q_t, p_t, t)|_V \leq c|p|_\infty (1 + |q|_\infty) \sum_{x \in X, \tau(x) \leq t} 1 \,.$$

Hence, n points periodically appear at each time $\frac{i}{m}$ for $i = 0, 1, \ldots, m$ and $m \in \mathbb{N}^*$, we get

$$|K_V \mathcal{J}(q_t, p_t, t)|_V \leq nc|p|_\infty (1 + |q|_\infty)\big(1 + \text{floor}(mt)\big) \,. \tag{3.45}$$

3.3.2 General current setup

Let us recall the configuration presented in Section 3.2. X is a compact submanifold given as $X = [0,1] \times X_0$ with $\partial X_0 = \emptyset$ and τ is the projection on the first coordinate. The object space is given by $B = L^\infty_\mu(X, \mathbb{R}^d)$ and the momentum space by $B_1^* = L^\infty(X, \mathbb{R}^d) \times L^\infty(\partial X, \mathbb{R}^d) \hookrightarrow B^*$.

Proposition 3.3. *There exists a real valued function $m(r)$ defined for $r \geq 0$ such that for any $(q,p) \in \mathcal{C}([0,1], B \times B_1^*)$ and any time $t \in [0,1]$, we have*

$$|K_V \mathcal{J}(q_t, p_t, t) - K_V \mathcal{J}(q_0, p_0, 0)|_V \leq m(|q|_B + |p|_{B^*})t \,. \tag{3.46}$$

Proof. We saw that the momentum map is given for any couple $\big(q, (p^X, p^{\partial X})\big) \in \mathcal{C}([0,1], B \times B_1^*)$, any time $t \in [0,1]$ and any $v \in V$ by

$$\big(\mathcal{J}(q_t, p_t, t) \,|\, v\big) = \int_0^t \int_{X_0} \langle p_t^X(s, x_0), v(q_t(s, x_0)) \rangle_{\mathbb{R}^d} \, d\mathcal{H}^{k-1}(x_0) ds \tag{3.47}$$

$$+ \int_{X_0} \langle p_t^{\partial X}(0, x_0), v(q_t(0, x_0)) \rangle_{\mathbb{R}^d} \, d\mathcal{H}^{k-1}(x_0) \tag{3.48}$$

$$+ \mathbb{1}_{t=1} \int_{X_0} \langle p_t^{\partial X}(1, x_0), v(q_t(1, x_0)) \rangle_{\mathbb{R}^d} \, d\mathcal{H}^{k-1}(x_0) \,. \tag{3.49}$$

There exists then under the (H_1^V) conditions a constant $c > 0$ such that for any $t \in [0,1]$,

$$\begin{aligned} |K_V \mathcal{J}(q_t, p_t, t) - K_V \mathcal{J}(q_0, p_0, 0)|_V \leq\; & t\Big(c|p|_\infty (|q|_{\infty,\mu} + 1)\mathcal{H}^{k-1}(X_0)\Big) \\ & + \mathbb{1}_{t=1} c|p^{\partial X}|_\infty (|q|_{\infty,\mu} + 1)\mathcal{H}^{k-1}(X_0) \,. \end{aligned}$$

□

3.3.3 Current setup: case of horns

In the current setup, the example of horns presents an additional interesting aspect. A horn is not diffeomorphic to a product $[0,1] \times X_0$ because of the tip of the horn. Yet, we chose to keep this general configuration on X and allow the spatial mapping between X and $\mathbb{R}^d$ to be not invertible. This characteristic leads to the introduction of a new space $B_0 \subset B$.

Definition 3.2 (The B_0 Space for the Horns). *A class of function of $L^\infty_\mu(X,\mathbb{R}^d)$ is defined $\mathcal{H}^{k-1}$-almost everywhere on $\{0\}\times X_0$. This allows to consider the subspace of functions whose image of $\{0\}\times X_0$ is reduced to a singleton. With $B = L^\infty_\mu(X,\mathbb{R}^d)$, we define*

$$B_0 = \{q \in B \,|\, \exists y \in \mathbb{R}^d, q(0,\cdot) = y \ \mathcal{H}^{k-1}\text{-a.e. on } X_0\}\,. \tag{3.50}$$

This space will reveal the role of the singularity induced by the tip of the horn and hidden by the choice of X. The initial boundary formed by the first layer $\{0\}\times X_0$ actually does not contribute to the support of the momentum map. We will see indeed in the next chapter that if $q_1 \in B_0$ then for any $x_0 \in X_0$, we have $p_1^{\partial X}(0,x_0) = 0$ so that at any time $t \in [0,1]$, we have $p_t^{\partial X}(0,x_0) = 0$. Since the momentum on the last layer $\{1\}\times X_0$ is not significant, when $\partial X_0 = \emptyset$ so that $\partial X = \{0,1\}\times X_0$, we can do the approximation

$$\forall t \in [0,1], \qquad p_t^{\partial X} = 0\,.$$

That is to say that the momentum lives in a new space $\widetilde{B_1^*} = L^\infty(X,\mathbb{R}^d) \subset B_1^*$.

Remark 3.10. *Note that we introduced on both sides, for the shape q and its momentum p, new spaces smaller than B and B^*.*

These spaces refine even further the control on the momentum map.

Proposition 3.4. *There exists a real valued function $m(r)$ defined for $r \geq 0$ such that for any $(q,p) \in \mathcal{C}([0,1], B_0 \times \widetilde{B_1^*})$ and any time $t \in [0,1]$, we have*

$$|K_V \mathcal{J}(q_t,p_t,t)|_V \leq m(|q|_B + |p|_{B^*})t\,. \tag{3.51}$$

where B_0 is given by Definition 3.2 and $\widetilde{B_1^*} = L^\infty(X,\mathbb{R}^d)$.

Proof. See Proposition 3.3. □

Remark 3.11. *As presented in Example 2.1, with the classic cost function $C(v,t) = \frac{1}{2}|v|_V^2$, the optimal vector field is equal to the momentum map :*

$$v_t^* = K_V \mathcal{J}(q_t,p_t,t)\,.$$

Equation (3.51) gives thus a strong information on the behavior of an optimal vector field. ***Its norm increases no more than linearly and starts from 0.*** *This phenomenon can be explained quite naturally. When the horn starts to appear, the shape is reduced to a single point which is the tip of the horn. The cost function prevents to pay for a deformation that would have an insignificant impact. The vector field is therefore null at time 0. Such vector fields are yet unable to create a sharp peak as required to model the top of the horn. One can then deduce that the classic cost function is not adapted to the growth dynamic, especially with horns. A new cost function is thus presented in the next section. At last, note that the example of horns only highlights and amplifies a phenomenon that will also appear with a tube or when the coordinate space X is discrete (see Chapter 5).*

3.4 New cost functions: Adapted norm setup

The previous study on the norm of the momentum map calls for new cost functions.

Definition 3.3 (Adapted norm setup)**.** *We call the **adapted norm setup** the configuration where the cost function C is given for any $(v,t) \in V \times [0,1]$ by*

$$C(v,t) = \frac{1}{2}\langle v, \ell_t v\rangle_V \,,$$

where $\ell_t \in \mathcal{L}(V)$ is a self-adjoint operator on V. We assume that $t \to |\ell_t|_{op}$ is bounded on $[0,1]$ and that there exists a strictly increasing function $\alpha : [0,1] \to \mathbb{R}_+$ such that $\alpha(0) = 0$ and

$$\alpha(t)|v|_V^2 \leq \langle v, \ell_t v\rangle_V \,. \tag{3.52}$$

Proposition 3.5. *In the adapted norm setup, for any $t > 0$, ℓ_t is invertible and $|\ell_t^{-1}|_{op} \leq \alpha(t)^{-1}$. If $\alpha(0) \neq 0$, this inequality is satisfied for any $t \in [0,1]$.*

Proof. For any $t \in [0,1]$ such that $\alpha(t) \neq 0$, ℓ_t is coercive. The invertibility results from the Lax-Milgram theorem (see for example [14]). We deduce then from equation (3.52) that for any $v \in V$

$$\alpha(t)|\ell_t^{-1}v|_V^2 \leq \langle v, \ell_t^{-1}v\rangle_V \leq |\ell_t^{-1}v|_V |v|_V \,,$$

so that $|\ell_t^{-1}v|_V \leq \frac{1}{\alpha(t)}|v|_V$. ☐

Definition 3.4 (Nondegenerate Adapted Norm Setup)**.** *We call the **nondegenerate adapted norm setup** the adapted norm setup with the following additional assumption. There exists $\alpha > 0$ such that for any $v \in V$ and any $t \in [0,1]$*

$$\alpha|v|_V^2 \leq \langle v, \ell_t v\rangle_V \,.$$

Remark 3.12. *The nondegenerate adapted norm setup is a subcase of the adapted norm setup. Hence any results satisfied in the adapted norm setup holds in nondegenerate adapted norm setup. The classic cost function $C(v,t) = |v|_V^2$ is a specific case of the nondegenerate adapted norm setup (take $\ell_t = Id$ for any $t \in [0,1]$).*

Proposition 3.6. *In the **adapted norm setup**, the function giving the optimal vector field is defined when ℓ_t is invertible by*

$$v_t^* = v^*(q,p,t) = \ell_t^{-1}K_V\mathcal{J}_\xi(q,p,t) \,. \tag{3.53}$$

Proof. The optimal vector field must satisfy at any time the equation

$$\frac{\partial C}{\partial v}(v_t,t) - \mathcal{J}_\xi(q_t,p_t,t) = 0$$

or equivalently in V

$$\nabla_v C(v_t,t) = \ell_t v_t = K_V\mathcal{J}_\xi(q_t,p_t,t)$$

and the optimal vector field is given by

$$v_t^* = v^*(q_t,p_t,t) = \ell_t^{-1}K_V\mathcal{J}_\xi(q_t,p_t,t) \,. \tag{3.54}$$

☐

Example 3.1. *When $\ell_t = \mathrm{Id}$ at all time, we find the usual cost function $C(v,t) = \frac{1}{2}|v|_V^2$. In practice, ℓ_t will be either scalar in general or blockwise scalar when V admits a canonical decomposition as in the rotations-translation case where $V = \mathbb{A}_d \times \mathbb{R}^d$.*

Example 3.2. *When the coordinate space X is discrete, the momentum map $\mathcal{J}$ is piecewise constant with respect to time (see Remark 3.2). It results from Remark 2.5 that the time derivative of the reduced Hamiltonian is reduced for almost all time to*

$$\frac{dH_r}{dt}(q_t, p_t, t) = \left(\frac{\partial \mathcal{J}_\xi}{\partial t}(q_t, p_t, t) \middle| \, v_t^* \right) - \frac{\partial C}{\partial t}(v_t^*, t) \tag{3.55}$$

$$= -\langle v_t^*, \dot{\ell}_t v_t^* \rangle_V \,. \tag{3.56}$$

If $\ell > 0$ is then a scalar function that is also constant between each appearance of new layers, it comes that $\frac{dH_r}{dt}(q_t, p_t, t) = 0$ and

$$H_r(q_t, p_t, t) = (\mathcal{J}_\xi(q_t, p_t, t) \,|\, v_t^*) - C(v_t^*, t) \tag{3.57}$$

$$= \frac{\ell_t}{2} |v_t^*|_V^2 \,. \tag{3.58}$$

Therefore, the norm of the optimal vector field is constant between each appearance of new layers.

3.5 Existence and uniqueness of the solutions by shooting

Among the solutions of the Hamiltonian system generated from any initial condition $(q_0, p_0) \in B \times B^*$ is the sought-after trajectory $(q,p) \in \mathcal{C}([0,1], B) \times \mathcal{C}([0,1], B^*)$ associated to an optimal time-varying vector field v^*. Therefore, the optimization problem on v can be replaced by an optimization problem on p_0 as presented in Section 2.5 (*Shooting Method*). This new point of view requires to guarantee the existence and uniqueness of a solution (q,p) for any initial condition (q_0, p_0). We will prove it in Section 5 when f is linear and for a reduced Hamiltonian system associated to the cost functions introduced in Section 3.4. We summarize here the results.

We already saw that we are interested in smaller spaces than B and B^*. Smaller than B if we add constraints on the shapes. Smaller than B^* when the attachment term to the data implies specific properties of the momentum that provides additional information on the momentum map and therefore on the optimal vector field. One could also see this as a possibility to add some constraints on the momentum and therefore on the vector fields generated by the shooting. For this purpose, we introduce the notion of **compatible** spaces with the initial setup (B, V, ξ) (see Section 5.2 for more details) . It allows to provide one general theorem (Theorem 5.1) for the local existence of the solution and apply it to the different configurations (Section 5.3). We will then prove the global existence of the solutions for each situation (always with the growth dynamic) in Section 5.4.

When the coordinate space X is not discrete, we will assume to simplify that $X = [0,1] \times X_0$ with $\partial X_0 = \emptyset$ and that τ is the projection on the first coordinate (we will refer to this setup as *tube case*).

Theorem 3.1 (Global Solutions of the Reduced Hamiltonian System : Tube Case)**.** *Assume the (H_1^V) conditions. Consider the* ***nondegenerate adapted norm setup*** *and* *assume that* $\ell \in \mathcal{C}^1([0,1], \mathcal{L}(V))$*. Consider the Banach spaces*

$$\begin{aligned} B_0 &= B = L^\infty_\mu(X, \mathbb{R}^d) \\ B_1^* &= L^\infty_\mu(X, \mathbb{R}^d)\,. \end{aligned}$$

Then for any initial condition $(q_0, p_0) \in B_0 \times B_1^*$*, the reduced Hamiltonian system associated to the* ***growth dynamic***

$$\xi_{(q,t)}(v) = \mathbb{1}_{\tau \le t} v \circ q$$

admits a unique solution $(q, p) \in \mathcal{C}([0,1], B_0 \times B_1^*)$*.*

Moreover, there exists an increasing function $\varphi^Y : \mathbb{R}^+ \to \mathbb{R}^+$ *such that for any* $(q_0, p_0) \in B_0 \times B_1^*$ *and any* $t \in [0,1]$*, we have*

$$|q_t|_{B_0} + |p_t|_{B_1^*} \le \varphi^Y(|q_0|_{B_0} + |p_0|_{B_1^*})\,.$$

Proof. See Theorem 5.3. Note that we identified $L^\infty_{\mathcal{H}^k}(X, \mathbb{R}^d) \times L^\infty_{\mathcal{H}^{k-1}}(\partial X, \mathbb{R}^d)$ to $L^\infty_\mu(X, \mathbb{R}^d)$. □

Remark 3.13. *The theorem gives an interesting property of the solutions of the reduced Hamiltonian in the nondegenerate adapted norm setup. They are locally bounded with respect to the initial condition.*

We will also give a similar theorem in the case of a **discrete coordinate space** X with the same results (including the existence of φ^Y).

The case of the horn in the continuous current setup

The study of the momentum map in Section 3.3 led us to the introduction of the adapted norm setup to compensate the growth of the shape. In this setup, the cost functions are given by

$$C(v,t) = \frac{1}{2}\langle v, \ell_t v\rangle_V\,.$$

We saw in the different applications with the growth dynamic that the support of the momentum map at any time is made of the active part of the shape (see Remark 3.1 and Figure 3.6). This part at any time $t \in [0,1]$ is the set of points that actually exist in the ambient space at this time

$$\{q_t(x) \in X \mid \tau(x) \le t\}.$$

The case of the horns is extreme because at the initial time, the shape is reduced to a single point: the tip of the horn. When X is discrete, the counting measure gives a non-zero weight to this point. Otherwise, with the Hausdorff measure, the momentum map is then reduced to 0. In this last case and in order to get an optimal vector field with a constant norm over time, we would like to make ℓ_t tends to 0 when t tends to 0. This specificity requires a special care to prove the local existence. We impose then a control inversely proportional to the speed of creation of new points. As we assume to simplify that τ is the projection on the first coordinate of $X = [0,1] \times X_0$, the appearance of new points is thus linear ($d\tau = 1$) which explains the factor $\frac{1}{t}$ in equation (3.59).

Theorem 3.2 (Global Solutions of the Reduced Hamiltonian System : Horn Case)**.** *Assume the* (H_1^V) *conditions. Consider the* ***adapted norm setup****. Assume that* $\ell \in \mathcal{C}^1([0,1], \mathcal{L}(V))$ *and that there exist* $M > 0$ *and* $s \in [0,1[$ *two constants such that for any* $t \in]0,1]$

$$|\ell_t^{-1}|_{op} \leq \frac{M}{t^s} \cdot \frac{1}{t}\,. \tag{3.59}$$

Consider the Banach spaces

$$B = L^\infty_\mu(X, \mathbb{R}^d)\,,$$
$$B_0 = \{q \in B \,|\, \exists y \in \mathbb{R}^d, q(0,\cdot) = y \ \mathcal{H}^{k-1}\text{-a.e. on } X_0\}\,,$$
$$\widetilde{B_1^*} = \{\ p \in L^\infty_\mu(X, \mathbb{R}^d) \mid p(x) = 0 \ \mathcal{H}^{k-1}\text{-a.e. on } \partial X\ \} \text{ and } B_1^* = L^\infty_\mu(X, \mathbb{R}^d)\,.$$

Then for any initial condition $(q_0, p_0) \in B_0 \times B_1^*$*, the reduced Hamiltonian system associated to the* ***growth dynamic***

$$\xi_{(q,t)}(v) = \mathbb{1}_{\tau \leq t} v \circ q$$

admits a unique solution $(q,p) \in \mathcal{C}([0,1], B_0 \times B_1^*)$*.*

Proof. See Theorem 5.2. □

Remark 3.14. *Note that we lost the control by the initial condition that we had in the theorem for the tube case.*

4 Theoretical study of the generative model

The generative model, presented in Section 1, involves integral equations of the type

$$q_t = q_0 + \int_0^t f(q_s, v_s, s)\, ds\,, \tag{3.60}$$

where q evolves in a Banach space B, the flow is given by a function

$$f : B \times V \times [0,1] \to B\,,$$

and V is also a Banach space, often called the space of controls.

Remark 4.1. *The theory of integration in a Banach space has been studied by Bochner (1899-1982) and bears now its name. A brief overview of the main results needed hereafter is given in Appendix A.*

We will start to summarize few conditions satisfied by the space V that will be satisfied in our applications.

$$
(H_1^V) \quad \left|\begin{array}{l}
\textit{(i)}\ V \subset \mathcal{C}^2(\mathbb{R}^d, \mathbb{R}^d)\,. \\
\textit{(ii)}\ \text{There exists } c > 0 \text{ such that} \\
\text{for any } (x, v) \in \mathbb{R}^d \times V, \text{ we have} \\
\begin{cases} |v(x)|_{\mathbb{R}^d} \leq c|v|_V(|x|_{\mathbb{R}^d} + 1), \\ |dv(x)|_{\mathcal{L}(\mathbb{R}^d,\mathbb{R}^d)} + |d^2v(x)|_{\mathcal{L}(\mathbb{R}^d \otimes \mathbb{R}^d, \mathbb{R}^d)} \leq c|v|_V. \end{cases}
\end{array}\right.
$$

These conditions will be satisfied in our applications:

Lemma 4.1. *i) If V is embedded in $\mathcal{C}_0^2(\mathbb{R}^d, \mathbb{R}^d)$ (which we shall denote $V \hookrightarrow \mathcal{C}_0^2(\mathbb{R}^d, \mathbb{R}^d)$), then V satisfies the (H_1^V) conditions.*

ii) Let be $V = \mathbb{A}_d \times \mathbb{R}^d$ the direct product of antisymmetric matrices and translations on $\mathbb{R}^d$, equipped with the following norm depending on a parameter $\alpha > 0$

$$
|(A, N)|_{V,\alpha}^2 \doteq \alpha |A|_{\mathbb{A}_d}^2 + |N|_{\mathbb{R}^d}^2 \doteq \alpha\, tr(A^T A) + |N|_{\mathbb{R}^d}^2\,.
$$

Then V satisfies the (H_1^V) conditions.

iii) Under the (H^V) conditions, there exists $c > 0$ such that for any $v \in V$, any $x, y \in \mathbb{R}^d$

$$
|v(x) - v(y)|_{\mathbb{R}^d} + |dv(x) - dv(y)|_\infty \leq c|v|_V |x - y|_{\mathbb{R}^d}\,.
$$

Proof. The last inequality results directly from the (H_1^V) conditions.

If $V \hookrightarrow \mathcal{C}_0^2(\mathbb{R}^d, \mathbb{R}^d)$, then there is $c_1 \in \mathbb{R}_+$, such that for all $v \in V$, $|v|_\infty + |dv|_\infty + |d^2v|_\infty \leq c_1\, |v|_V$. This constant c_1 satisfies the inequalities of (H_1^V).

If $V = \mathbb{A}_d \times \mathbb{R}^d$, since all norms on $\mathbb{A}_d$ are equivalent, there exists $c_2 \in \mathbb{R}_+$ a constant such that for any $A \in \mathbb{A}_d$ the operator norm $|A|_{op}$ is lower than $c_2|(A, 0)|_{V,\alpha}$. We have thus for any $v = (A, N) \in V$ and any $x \in \mathbb{R}^d$:

$$
\begin{aligned}
|v(x)|_{\mathbb{R}^d} = |Ax + N|_{\mathbb{R}^d} &\leq |A|_{op}|x|_{\mathbb{R}^d} + |N|_{\mathbb{R}^d} \leq c_2\alpha|A|_{\mathbb{A}_d}|x|_{\mathbb{R}^d} + |N|_{\mathbb{R}^d} \\
&\leq (c_2 + 1)(\alpha|A| + |N|)(|x|_{\mathbb{R}^d} + 1) \leq (c_2 + 1)|(A, N)|_V(|x|_{\mathbb{R}^d} + 1)\,.
\end{aligned}
$$

So we obtain the first inequality of (H_1^V) with the constant $c_2 + 1$. And finally, $|dv(x)|_\infty = |A|_{op} \leq c_2|v|_V$ and $d^2v \equiv 0$ such that $c_2 + 1$ also leads to the second inequality. □

Let us also recall the Grönwalll's lemma.

Lemma 4.2 (Grönwalll's lemma)**.** *Let f and g be two positive measurable functions defined on the interval $[0, 1]$ and let $c > 0$ be a constant. Assume that f is bounded and that for any $t \in [0, 1]$,*

$$
f(t) \leq c + \int_0^t f(s)g(s)\,ds\,.
$$

Then for any $t \in [0, 1]$,

$$
f(t) \leq c \exp\left(\int_0^t g(s)\,ds\right)\,.
$$

4.1 Existence and uniqueness

For any metric space, $\mathcal{B}(b, r)$ will denote the close ball of center b and radius r.

Definition 4.1 (Locally Lipschitz Continuity)**.** *Let E and F be two Banach spaces. We say that a function $g : E \to F$ is locally Lipschitz continuous if for any $r > 0$, the restriction of g to the ball $\mathcal{B}(0, r)$ is Lipschitz continuous.*

Definition 4.2. *We define $\mathcal{L}ip^{\,loc}_{\,int}(E \times [0,1], F)$ the set of applications g such that*

- *for almost every $t \in [0,1]$, $g_t := g(\cdot, t)$ is locally Lipschitz continuous,*
- *for any $r > 0$, if we note k^r_t the Lipschitz constant of g_t on the ball $\mathcal{B}(0, r)$ (defined a.e.), then $t \mapsto k^r_t$ is integrable on $[0,1]$.*

4.1.1 Local existence

In order to prove the local existence and uniqueness of solutions, we need the following variant of the Cauchy-Lipschitz theorem.

Theorem 4.1 (A Cauchy-Lipschitz theorem)**.** *Let B be a Banach space, b_0 be a point of B and $f : B \times [0,1] \to B$ be a measurable function such that*

- *$f \in \mathcal{L}ip^{\,loc}_{\,int}(B \times [0,1], B)$*
- *there exists $b \in B$, such that $\int_0^1 |f(b,t)|_B \, dt < \infty$.*

Then for any $r > 0$, there exists $\epsilon > 0$ such that the Cauchy problem associated to f and any initial condition (b_0, t_0) with $|b_0|_B \leq r$ and $t_0 \in [0, 1[$ has a unique solution on the interval $[t_0, t_0 + \epsilon] \cap [0, 1]$.

Proof. The proof is based, as usual, on a fixed point method. Denote $c_b = \int_0^1 |f(b,t)|_B \, dt$ and consider $r > |b|_B$. Let us first show that there exists $m > 0$ such that for any $b_0 \in \mathcal{B}(0, r)$

$$\int_0^1 |f(b_0, t)|_B \, dt \leq \frac{m}{2} \, . \tag{3.61}$$

We have indeed

$$\begin{aligned} \int_0^1 |f(b_0,t)|_B \, dt &\leq \int_0^1 |f(b,t)|_B \, dt + \int_0^1 |f(b,t) - f(b_0,t)|_B \, dt \\ &\leq c_b + \int_0^1 k^r_t |b - b_0|_B \, dt \leq c_b + 2r \int_0^1 k^r_t \, dt < +\infty \, , \end{aligned}$$

where k^r_t is the Lipschitz constant of $f(\cdot, t)$ on $\mathcal{B}(0, r)$ defined a.e.

Define then $r' = r + m$ so that for any $b_0 \in \mathcal{B}(0, r)$, $\mathcal{B}(b_0, m) \subset \mathcal{B}(0, r')$. Let $k^{r'}_t$ be the Lipschitz constant of $f(\cdot, t)$ on $\mathcal{B}(0, r')$ defined a.e. Since $t \mapsto k^{r'}_t$ is integrable on the compact interval $[0,1]$, there exists $\epsilon > 0$ such that for any $t_0 \in [0, 1[$, $\int_{t_0}^{t_\epsilon} k^{r'}_t \, dt \leq 1/2$ where $t_\epsilon = \min(t_\epsilon, 1)$.

We can now prove the existence of a solution to the Cauchy problem for any initial condition $(t_0, b_0) \in [0, 1[\times \mathcal{B}(0, r)$ on the interval $[t_0, t_\epsilon]$. Consider thus $(t_0, b_0) \in [0, 1[\times \mathcal{B}(0, r)$

and define the set of continuous functions $E = \mathcal{C}([t_0, t_\epsilon], \mathcal{B}(b_0, m))$. E equipped with the uniform norm is complete. Introduce finally the operator $T_{b_0} : E \to E$ given for any $y \in E$ and any $t \in [t_0, t_\epsilon]$ by

$$T_{b_0} y(t) = b_0 + \int_0^t f(y(s), s)\, ds\,.$$

Let us show that T_{b_0} is well defined. We have for any $y \in E$

$$\begin{aligned}\int_{t_0}^t |f(y(s), s)|_B\, ds &\leq \int_{t_0}^t |f(b_0, s)|_B\, ds + \int_{t_0}^t |f(y(s), s) - f(b_0, s)|_B\, ds \\ &\leq \frac{m}{2} + \int_{t_0}^{t_\epsilon} k_s^{r'}\, |y(s) - b_0|_B\, ds \leq \frac{r}{2} + m \int_{t_0}^{t_\epsilon} k_s^{r'}\, ds \\ &\leq m\,.\end{aligned}$$

In particular, $|T_{b_0} y(t) - b_0|_B \leq m$ and thus $T_{b_0} y(t) \in \mathcal{B}(b_0, m)$. Moreover, $T_{b_0} y$ is continuous. Indeed, for any $t_1 \leq t_2$ in $[t_0, t_\epsilon]$,

$$\begin{aligned}|T_{b_0} y(t_1) - T_{b_0} y(t_2)|_B &\leq \int_{t_1}^{t_2} |f(y(s), s)|_B\, ds \\ &\leq \int_{t_1}^{t_2} |f(b_0, s)|_B + |f(y(s), s) - f(b_0, s)|_B\, ds \\ &\leq \int_{t_1}^{t_2} |f(b_0, s)|_B\, ds + m \int_{t_1}^{t_2} k_s^{r'}\, ds\end{aligned}$$

and since $t \mapsto f(b_0, t)$ and $t \mapsto k_t^{r'}$ are integrable, these integrals tend to 0 when $t_2 - t_1$ tends to 0. Therefore, T_{b_0} takes values in E. Let us show now that T_{b_0} is a contraction. For any $y, z \in E$, we have

$$\begin{aligned}|T_{b_0} y - T_{b_0} z|_\infty &\leq \int_0^{t_\epsilon} |f(y(t), t) - f(z(t), t)|_B\, dt \\ &\leq \int_0^{t_\epsilon} k_t^{r'}\, dt\, |y - z|_\infty \leq \frac{1}{2}\, |y - z|_\infty\,.\end{aligned}$$

Consequently, T_{b_0} is a contraction and admits thus a unique fixed point in the complete space E. This fixed point is the solution of the Cauchy problem. The uniqueness results from the Grönwalll's lemma. Let y and z be two solutions defined on any common time interval $[t_0, t_\epsilon]$ and both bounded by $r_\epsilon > 0$. For any $t \in [t_0, t_\epsilon]$, we have

$$\begin{aligned}|y(t) - z(t)|_B &\leq \int_{t_0}^t |f(y(s), s) - f(z(s), s)|_B\, ds \\ &\leq \int_{t_0}^t k_s^{r_\epsilon} |y(s) - z(s)|_B\, ds\,.\end{aligned}$$

The Grönwalll's lemma implies that for any $t \in [t_0, t_\epsilon]$, $|y(t) - z(t)|_B = 0$. Therefore, one of the two solutions is an extension of the other one. $\square$

In order to apply the theorem in our situation and satisfy its assumptions in a general case, we define in the following corollary a set of conditions on the function f denoted by (H_0^f).

Corollary 4.1. *Let be $f : B \times V \times [0,1] \to B$ a function that satisfies the conditions*

$$(H_0^f) \quad \left| \begin{array}{l} \text{(i) } \textit{There exists } c > 0, \textit{ such that for any } (q, q', v, t) \in B^2 \times V \times [0,1], \\ \begin{cases} |f(q,v,t)|_B \leq c|v|_V(|q|_B + 1), \\ |f(q,v,t) - f(q',v,t)|_B \leq c|v|_V|q - q'|_B. \end{cases} \end{array} \right.$$

then for any initial condition $q_0 \in B$ and any control $v \in L^2([0,1],V)$, the Cauchy problem associated to f

$$q_t = q_0 + \int_0^t f(q_s, v_s, s)\, ds$$

admits a unique maximal solution on an interval $I \subset [0,1]$ containing 0.

4.1.2 Global existence

Following a standard method to ensure global existence, we will show that a solution never explodes in finite time. Without a global Lipschitz continuity, we need the control offered by the (H_0^f) conditions. Assume thus that f verifies the (H_0^f) conditions. For any initial condition $q_0 \in B$ and any control $v \in L^2([0,1],V) (\subset L^1([0,1],V))$, if $q \in \mathcal{C}(I,B)$ is the maximal solution associated to (q_0, v), we have for all $t \in I$:

$$\begin{aligned} |q_t|_B &\leq |q_0|_B + \int_0^t |f(q_s, v_s, s)|_B\, ds \\ &\leq |q_0|_B + \int_0^t c|v_s|_V(|q_s|_B + 1)\, ds \end{aligned}$$

and the Growall's lemma applied to $t \mapsto |q_t|_B + 1$ gives

$$\begin{aligned} |q_t|_B + 1 &\leq (|q_0|_B + 1)\exp(\int_0^t c|v_s|_V\, ds) && (3.62)\\ &\leq (|q_0|_B + 1)\exp(c|v|_1)\,. && (3.63) \end{aligned}$$

Thus any partial solution is bounded and can be extended to $[0,1]$.

We can therefore summarize and define a function Φ_f that returns the solution associated to an initial condition q_0 and a control v.

Theorem 4.2. *Let $f : B \times V \times [0,1] \to B$ be a function that satisfies the (H_0^f) conditions. Let Φ_f be defined as follows*

$$\begin{array}{rccc} \Phi_f : & B \times L^2([0,1],V) & \longrightarrow & \mathcal{C}([0,1],B) \\ & (q_0, v) & \longmapsto & q\,, \end{array}$$

where q is the unique solution of the integral equation

$$q_t = q_0 + \int_0^t f(q_s, v_s, s)\, ds\,.$$

Φ_f is well defined.

Another important application of the Cauchy-Lipschitz theorem concerns the linearized integral equations.

Corollary 4.2. *Let B be a Banach space and $\mathcal{L}(B)$ be the space of continuous linear operators on B. Let $A_1 \in L^2([0,1], \mathcal{L}(B))$ and $A_2 \in L^2([0,1], B)$ be two square-integrable applications. Then for any $b_0 \in B$, there exists a unique solution $b \in \mathcal{C}([0,1], B)$ to the integral equation*

$$b(t) = b_0 + \int_0^t A_1(s) \cdot b(s) + A_2(s)\, ds\,.$$

Proof. This is a direct consequence of the previous theorem. With the notation of the theorem, we define for any $b \in B$, any $t \in [0,1]$, $f(b,t) = A_1(t) \cdot b + A_2(t)$. Then $f(\cdot, t)$ is Lipschitz continuous with the constant $|A_1(t)|$ and $t \mapsto |A_1(t)|$ is integrable on $[0,1]$. Moreover, $f(0,t) = A_2(t)$ is also integrable. The global existence is a direct consequence of the Grönwalll's lemma and the global Lipschitz continuity of f. $\square$

4.2 Temporal regularity

As discussed in Remark 1.2, we will see hereafter that the solutions given by Φ_f may not admit a time derivative at all time. Proving the existence of this derivative at least almost everywhere requires the notion of Bochner-Lebesgue points. The following definition and results are presented in more details in the Appendix.

Definition 4.3. *Let B be a Banach space and let be $f \in L^1([0,1], B)$. A point $t \in [0,1]$ is called* Bochner-Lebesgue point *if*

$$\lim_{r \to 0} \frac{1}{\lambda(\mathcal{B}(t,r))} \int_{\mathcal{B}(t,r)} |f(t) - f(s)|_B\, ds = 0\,,$$

where $\mathcal{B}(t,r) = [t-r, t+r] \cap [0,1]$ and λ is the Lebesgue measure.

Proposition 4.1. *Let be $f \in L^1([0,1], B)$, $t \in [0,1]$ a Bochner-Lebesgue point of f and $(A_r)_{r>0}$ a collection of measurable non negligible sets containing t (i.e. for any $r > 0$, $t \in A_r$ and $\lambda(A_r) > 0$). If there exists $c \in \mathbb{R}$ such that for any $r > 0$ we have:*

$$A_r \subset \mathcal{B}(t,r) \qquad \text{and} \qquad \lambda(\mathcal{B}(t,r)) \leq c\lambda(A_r)\,,$$

then

$$\lim_{r \to 0} \frac{1}{\lambda(A_r)} \int_{A_r} |f(t) - f(s)|_B\, ds = 0\,.$$

Example 4.1. *If $f \in L^1([0,1], B)$ is continuous, one can show easily by uniform continuity that any point of $[0,1]$ is a Bochner-Lebesgue point of f.*

Theorem 4.3. *If $f \in L^1([0,1], B)$, then almost every point $t \in [0,1]$ is a Bochner-Lebesgue point.*

This theorem implies some regularity on the time varying vector fields of $L^1([0,1], V)$ that we will use hereafter.

Proposition 4.2. *Consider for any initial condition $q_0 \in B$ and any control $v \in L^2_V$, the solution solution $q = \Phi_f(q_0, v)$. Under the (H_0^f) conditions, we have for almost any $t \in [0,1]$*

$$\dot{q}_t = f(q_t, v_t, t)$$

and this derivative is integrable.

Proof. Consider $g : [0,1] \to B$ defined by $g(t) = f(q_t, v_t, t)$. The (H_0^f) conditions imply that there exists $c > 0$ such that at any time $t \in [0,1]$

$$|g(t)|_B \leq c|v_t|_V(|q_t|_B + 1) \leq c|v_t|_V(|q|_\infty + 1)\,,$$

so that g is integrable. Therefore, almost any $t \in [0,1]$ is a Bochner-Lesbesgue point of g and Proposition 4.1 ensures that for any $\epsilon \neq 0$

$$\frac{q_{t+\epsilon} - q_t}{\epsilon} = \frac{1}{\epsilon}\int_t^{t+\epsilon} f(q_s, v_s, s)\, ds = \frac{1}{\epsilon}\int_t^{t+\epsilon} g(s)\, ds$$

tends to $g(t)$ when ϵ tends to 0. $\square$

4.3 Directional derivative of the solution with respect to its parameters

We are now interested in the variations of the solution $q = \Phi_f(q_0, v)$ with respect to its parameters q_0 and v. Recall that q is given at any time $t \in [0,1]$ by

$$q_t = q_0 + \int_0^t f(q_s, v_s, s)\, ds\,, \tag{3.64}$$

where we have $f : B \times V \times [0,1] \to B$ and where B and V are two Banach spaces. In other words, we want to explicit the Gâteaux-derivative of Φ_f.

Let us fix $(\delta q_0, \delta v) \in B \times L^2([0,1], V)$ and define the application $g : [0,1] \to \mathcal{C}([0,1], B)$ by

$$g(\epsilon) = \Phi_f(q_0 + \epsilon\delta q_0, v + \epsilon \delta v)\,.$$

If g is derivable at 0, then the Gâteaux-derivative of Φ_f in the direction $(\delta q_0, \delta v)$, denoted $\Phi'_f(q_0, v\,; \delta q_0, \delta v)$, is $g'(0)$.

Definition 4.4 (Linearized Equation)**.** *Let B and V be two Banach spaces and let $f : B \times V \times [0,1] \to B$ be a function of class $\mathcal{C}^1$ with respect to its two first variables. Assume that there exists $c > 0$ a constant such that for any $q \in B$, any $v \in V$, and any $t \in [0,1]$, we have*

$$(H_1^f) \qquad \begin{cases} \left|\dfrac{\partial f}{\partial q}(q, v, t)\right|_{op} \leq c\,|v|_V\,, \\ \left|\dfrac{\partial f}{\partial v}(q, v, t)\right|_{op} \leq c\,(|q|_B + 1)\,. \end{cases}$$

Then for any $(\delta q_0, \delta v) \in B \times L^2([0,1], V)$, there exists a unique solution $\delta q \in \mathcal{AC}([0,1], B)$ to the linear equation

$$\delta q_t = \delta q_0 + \int_0^t \frac{\partial f}{\partial q}(q_s, v_s, s) \cdot \delta q_s + \frac{\partial f}{\partial v}(q_s, v_s, s) \cdot \delta v_s \, ds \,. \tag{3.65}$$

This equation is called the linearized equation of $\dot{q}_t = f(q_t, v_t, t)$.

Proof. Since the applications $t \mapsto |\frac{\partial f}{\partial q}(q_t, v_t, t)|$ and $t \mapsto |\frac{\partial f}{\partial v}(q_t, v_t, t)|$ are integrable on $[0,1]$, it results directly from the Corollary 4.2 (the linear Cauchy-Lipschitz theorem). The absolute continuity is also immediate as in Proposition 4.2. $\square$

Theorem 4.4. *Consider f and Φ_f as defined in Theorem 4.2. Under the (H_1^f) conditions, the Gâteaux-derivative of Φ_f in the direction $(\delta q_0, \delta v) \in B \times L^2([0,1], V)$ exists and is given by the unique solution of the linearized equation*

$$\delta q_t = \delta q_0 + \int_0^t \frac{\partial f}{\partial q}(q_s, v_s, s) \cdot \delta q_s + \frac{\partial f}{\partial v}(q_s, v_s, s) \cdot \delta v_s \, ds \,.$$

Proof. Note that the (H_1^f) conditions imply (H_0^f). Let us fix the following notation: $q = \Phi_f(q_0, v)$, for any $\epsilon \in [-1,1]$, $v^\epsilon = v + \epsilon \delta v$, $q_0^\epsilon = q_0 + \epsilon \delta q_0$, $q^\epsilon = \Phi_f(q_0^\epsilon, v^\epsilon)$. Finally, for any $\epsilon \neq 0$ and any $t \in [0,1]$, we introduce $M_t^\epsilon = \left| \frac{q_t^\epsilon - q_t}{\epsilon} - \delta q_t \right|_B$. The proof consists thus to show that this quantity $t \mapsto M_t^\epsilon$ tends uniformly to 0 when ϵ tends to 0. Let us start with the following lemma.

Lemma 4.3. $|q^\epsilon - q|_\infty = O(|\epsilon|)$

Proof. Under (H_1^f), we can write

$$\begin{aligned}
|q_t^\epsilon - q_t|_B &\leq |\epsilon \delta q_0|_B + \int_0^t |f(q_s^\epsilon, v_s^\epsilon, s) - f(q_s, v_s, s)|_B \, ds \\
&\leq |\epsilon||\delta q_0|_B + \int_0^t |f(q_s^\epsilon, v_s^\epsilon, s) - f(q_s, v_s^\epsilon, s)|_B + |f(q_s, v_s^\epsilon, s) - f(q_s, v_s, s)|_B \, ds \\
&\leq |\epsilon||\delta q_0|_B + \int_0^t \sup_{r_s \in [0,1]} \left| \frac{\partial f}{\partial q}(q_s + r_s(q_s^\epsilon - q_s), v_s^\epsilon, s) \right|_{op} |q_s^\epsilon - q_s|_B \, \dots \\
&\qquad\qquad + \sup_{r_s \in [0,1]} \left| \frac{\partial f}{\partial v}(q_s, v_s + r_s(v_s^\epsilon - v_s), s) \right|_{op} |v_s^\epsilon - v_s|_V \, ds \\
&\leq |\epsilon||\delta q_0|_B + \int_0^t c|v_s^\epsilon|_V |q_s^\epsilon - q_s|_B + c(|q_s|_B + 1)|v_s^\epsilon - v_s|_V \, ds \\
&\leq |\epsilon|\big(|\delta q_0|_B + c(|q|_\infty + 1)|\delta v|_1\big) + \int_0^t c|v_s^\epsilon|_V |q_s^\epsilon - q_s|_B \, ds \quad (q \in \mathcal{C}([0,1], B)) \\
&\leq |\epsilon|\big(|\delta q_0|_B + c(|q|_\infty + 1)|\delta v|_1\big) \exp(c|v^\epsilon|_1) \quad \text{(Grönwalll's lemma)}\,.
\end{aligned}$$

Finally, since for any $|\epsilon| < 1$ we have $|v^\epsilon|_1 \leq |v|_1 + |\delta v|_1$, we deduce that $|q^\epsilon - q|_\infty = O(|\epsilon|)$. $\square$

We will now use the Grönwalll's lemma to show the uniform convergence of $M_t^\epsilon =$

$\left|\frac{q_t^\epsilon - q_t}{\epsilon} - \delta q_t\right|_B$.

$$\begin{aligned} M_t^\epsilon &\leq \int_0^t \left| \frac{f(q_s^\epsilon, v_s^\epsilon, s) - f(q_s, v_s, s)}{\epsilon} - \frac{\partial f}{\partial q}(q_s, v_s, s) \cdot \delta q_s - \frac{\partial f}{\partial v}(q_s, v_s, s) \cdot \delta v_s \right|_B ds \\ &\leq \int_0^t \left| \frac{\partial f}{\partial q}(q_s, v_s, s) \right|_{op} M_s^\epsilon + \frac{1}{|\epsilon|} R_s^\epsilon \, ds \,, \end{aligned}$$

where R_s^ϵ is defined for any $s \in [0,1]$ by

$$R_s^\epsilon = \left| f(q_s^\epsilon, v_s^\epsilon, s) - f(q_s, v_s, s) - \frac{\partial f}{\partial q}(q_s, v_s, s) \cdot (q_s^\epsilon - q_s) - \frac{\partial f}{\partial v}(q_s, v_s, s) \cdot (\epsilon \delta v_s) \right|_B \,.$$

In order to bound R_s^ϵ, we introduce the application $g_s : [0,1] \to B$ defined by

$$g_s(r) = f(q_s + r(q_s^\epsilon - q_s), v + r(v_s^\epsilon - v_s), s) - f(q_s, v_s, s) \,.$$

Thus, $g_s(0) = 0$, $g_s(1) = f(q_s^\epsilon, v_s^\epsilon, s) - f(q_s, v_s, s)$ and if we note $q_s^{r,\epsilon} = q_s + r(q_s^\epsilon - q_s)$ and $v_s^{r,\epsilon} = v + r(v_s^\epsilon - v_s)$, we have

$$g_s(1) = \int_0^1 g_s'(r) \, dr = \int_0^1 \frac{\partial f}{\partial q}(q_s^{r,\epsilon}, v_s^{r,\epsilon}, s)(q_s^\epsilon - q_s) + \frac{\partial f}{\partial v}(q_s^{r,\epsilon}, v_s^{r,\epsilon}, s)(v_s^\epsilon - v_s) \, dr \,.$$

Therefore,

$$\begin{aligned} R_s^\epsilon = \Bigg| \int_0^1 &\left(\frac{\partial f}{\partial q}(q_s^{r,\epsilon}, v_s^{r,\epsilon}, s) - \frac{\partial f}{\partial q}(q_s, v_s, s) \right) (q_s^\epsilon - q_s) \\ &+ \left(\frac{\partial f}{\partial v}(q_s^{r,\epsilon}, v_s^{r,\epsilon}, s) - \frac{\partial f}{\partial v}(q_s, v_s, s) \right) (\epsilon \delta v_s) \, dr \Bigg|_B \\ \leq \int_0^1 &\left| \frac{\partial f}{\partial q}(q_s^{r,\epsilon}, v_s^{r,\epsilon}, s) - \frac{\partial f}{\partial q}(q_s, v_s, s) \right| dr |q_s^\epsilon - q_s| \\ &+ \int_0^1 \left| \frac{\partial f}{\partial v}(q_s^{r,\epsilon}, v_s^{r,\epsilon}, s) - \frac{\partial f}{\partial v}(q_s, v_s, s) \right| dr |\epsilon \delta v_s| \,. \end{aligned}$$

Let us note

$$\alpha_s^\epsilon = \int_0^1 \left| \frac{\partial f}{\partial q}(q_s^{r,\epsilon}, v_s^{r,\epsilon}, s) - \frac{\partial f}{\partial q}(q_s, v_s, s) \right|_{op} + \left| \frac{\partial f}{\partial v}(q_s^{r,\epsilon}, v_s^{r,\epsilon}, s) - \frac{\partial f}{\partial v}(q_s, v_s, s) \right|_{op} dr \,,$$

so that

$$R_s^\epsilon \leq \alpha_s^\epsilon (|q^\epsilon - q|_\infty + |\epsilon \delta v_s|_V) \,.$$

Then, if we note

$$B^\epsilon = \frac{1}{|\epsilon|} \int_0^1 R_s^\epsilon \, ds \,,$$

we get with the Grönwall's lemma

$$\begin{aligned}M_t^\epsilon &\leq B^\epsilon \exp\Big(\int_0^1 \Big|\frac{\partial f}{\partial q}(q_s, v_s, s)\Big|\, ds\\ &\leq B^\epsilon \exp(c|v|_1)\,,\end{aligned}$$

where the constant $c > 0$ is given by (H_1^f). The final step is to prove that B^ϵ tends to 0 when ϵ tends to 0.

Note that for any $\epsilon \in [-1, 1]$, $s \mapsto \alpha_s^\epsilon$ is a square-integrable function on $[0, 1]$. Indeed, it can roughly be bounded as follows

$$\begin{aligned}\alpha_s^\epsilon \leq &\sup_{r_s\in[0,1]} \left|\frac{\partial f}{\partial q}(q_s + r_s(q_s^\epsilon - q_s), v_s^\epsilon, s)\right|_{op} + \left|\frac{\partial f}{\partial q}(q_s, v_s, s)\right| \dots\\ &+ \sup_{r_s\in[0,1]} \left|\frac{\partial f}{\partial v}(q_s, v_s + r_s(v_s^\epsilon - v_s), s)\right|_{op} + \left|\frac{\partial f}{\partial v}(q_s, v_s, s)\right|\\ \leq\ & c\big(|v_s^\epsilon|_V + |v_s|_V + 2(|q_s|_B + 1)\big)\\ \leq\ & c\big(|v_s^\epsilon|_V + |v_s|_V + 2(|q|_\infty + 1)\big)\,.\end{aligned}$$

Moreover, the previous lemma says that $|q^\epsilon - q|_\infty = O(|\epsilon|)$. There exists thus $c' > 0$ a constant such that for any $\epsilon \in [-1, 1]$, $|\frac{q^\epsilon - q}{\epsilon}|_\infty \leq c'$. Hence,

$$\begin{aligned}B^\epsilon &= \frac{1}{|\epsilon|}\int_0^1 R_s^\epsilon\, ds\\ &\leq \int_0^1 \alpha_s^\epsilon\Big(\frac{|q^\epsilon - q|_\infty}{|\epsilon|} + |\delta v_s|\Big)\, ds\\ &\leq \left(\int_0^1 (\alpha_s^\epsilon)^2\, ds\right)^{\frac{1}{2}} \left(\int_0^1 (c' + |\delta v_s|)^2\, ds\right)^{\frac{1}{2}}\,.\end{aligned}$$

Finally, since $\frac{\partial f}{\partial q}$ and $\frac{\partial f}{\partial v}$ are continuous, for any sequence $\epsilon_n \to 0$, $s \mapsto \alpha_s^{\epsilon_n}$ tends to 0 almost everywhere. Thus, the Lebesgue's dominated convergence theorem ensures that $|\alpha^{\epsilon_n}|_{L^2}$ tends to 0. Hence, M^ϵ converges uniformly to 0. $\square$

4.4 Application to the growth dynamic

In our model, the shapes are parameterized by the coordinate space X so that the object space can be given by $B = L^\infty(X, \mathbb{R}^d)$ where X is given as a submanifold of $\mathbb{R}^d$. According to the *growth dynamic*, f is defined by

$$f(q, v, t) = \mathbb{1}_{\tau\leq t} v \circ q\,,$$

where $v \circ q : x \mapsto v(q(x))$.

We assume as before that the space of controls V satisfies the (H_1^V) conditions (introduced at the beginning of Section 4).

4.4.1 Existence of the solution and dependence with respect to the parameters

Lemma 4.4. *If $B = L^\infty(X, \mathbb{R}^d)$ and $f(q, v, t) = \mathbb{1}_{\tau \le t} v \circ q$, then the (H_0^f) conditions are satisfied.*

Proof. For any $q, \delta q \in L^\infty(X, \mathbb{R}^d)$ and any $v \in V$, (H_1^V) ensures that there exists $c > 0$ such that

$$|v \circ q|_\infty \le c|v|_V(|q|_\infty + 1) \text{ and } \qquad |(dv \circ q) \cdot \delta q|_\infty \le c|v|_V|\delta q|_\infty \,.$$

□

Consequently, Theorem 4.2 ensures that for any initial condition $q_0 \in L^\infty(X, \mathbb{R}^d)$ and any time-varying vector field $v \in L^2([0,1], V)$, there exists a unique $q = \Phi(q_0, v) \in \mathcal{C}([0,1], L^\infty(X, \mathbb{R}^d))$ such that for any $t \in [0,1]$,

$$q_t = q_0 + \int_0^t \mathbb{1}_{\tau \le t}\, v_s \circ q_s \, ds \,. \tag{3.66}$$

More precisely, for any $x \in X$,

$$q_t(x) = \begin{cases} q_0(x) & \text{if } t \le \tau(x)\,, \\ q_0(x) + \int_{\tau(x)}^t v_s(q_s(x))\, ds & \text{otherwise.} \end{cases} \tag{3.67}$$

The existence of directional derivatives of the solution with respect to initial position q_0 and the control v lies on the (H_1^f) conditions given in Definition 4.4. Let us verify that the function f associated to the *growth dynamic* satisfies these conditions. Consider F defined by:

$$\begin{array}{rccc} F: & L^\infty(X, \mathbb{R}^d) \times V & \longrightarrow & L^\infty(X, \mathbb{R}^d) \\ & (q, v) & \longmapsto & v \circ q : x \mapsto v(q(x))\,. \end{array}$$

F generates the standard infinitesimal action of the LDDMM setting. Under the (H_1^V) conditions, F takes its values in L^∞. Our model corresponds thus to the case $f(q, v, t) = \mathbb{1}_{\tau \le t} F(q, v)$.

Proposition 4.3. *Under the (H_1^V) conditions, F is of class $\mathcal{C}^1$. More explicitly, we have for any $\big((q, v), (\delta q, \delta v)\big) \in \big(L^\infty(X, \mathbb{R}^d) \times V\big)^2$*

$$\frac{\partial F}{\partial v}(q, v) \cdot \delta v = \delta v \circ q \qquad\qquad \frac{\partial F}{\partial q}(q, v) \cdot \delta q = (dv \circ q) \cdot \delta q \,.$$

In fine, *if f is given by the* growth dynamic, *i.e.* $f(q, v, t) = \mathbb{1}_{\tau \le t} F(q, v)$, *then f satisfies (H_1^f).*

Proof. The pointwise expressions of these derivatives are given by

$$\frac{\partial F}{\partial v}(q, v) \cdot \delta v : x \mapsto \delta v(q(x))$$

and

$$\frac{\partial F}{\partial q}(q,v)\cdot\delta q : x \mapsto dv(q(x))\cdot\delta q(x)\,.$$

Indeed, F is linear with respect to v and under the (H_1^V) conditions there exists $c > 0$ such that

$$\left|\frac{\partial F}{\partial v}(q,v)\cdot\delta v\right|_\infty \leq c|\delta v|_V(|q|_\infty + 1)$$

and thus

$$\left|\frac{\partial F}{\partial v}(q,v)\right|_{op} \leq c(|q|_\infty + 1)\,.$$

Regarding the first variable, we have

$$\begin{aligned}|F(q+\delta q,v) - F(q,v) - (dv\circ q)\cdot\delta q|_\infty &= \sup_{x\in X}|v(q(x)+\delta q(x)) - v(q(x)) - dv(q(x))\cdot\delta q(x)|\\ &\leq \frac{c}{4}|v|_V|\delta q|_\infty^2\,,\end{aligned}$$

where the last inequality results from the Taylor's theorem with integral remainder applied on the application $g(r) = v(q(x) + r\delta(x))$ between 0 and 1. At last we have

$$\left|\frac{\partial F}{\partial q}(q,v)\right|_{op} \leq c|v|_V\,.$$

We deduce that F is of class $\mathcal{C}^1$ and that f satisfies (H_1^f). Note that if $v = (A,N) \in \mathbb{A}_d\times\mathbb{R}^d$, we have

$$\frac{\partial F}{\partial q}(q,v)\cdot\delta q = A\cdot\delta q\,.$$

□

Consequently, the Gâteaux-derivative of Φ at a point $(q_0,v) \in L^\infty(X,\mathbb{R}^d)\times L^2([0,1],V)$ in the direction $(\delta q_0,\delta v) \in L^\infty(X,\mathbb{R}^d)\times L^2([0,1],V)$ exists and is equal to the unique solution, denoted δq, of the integral equation:

$$\delta q_t = \delta q_0 + \int_0^t \mathbb{1}_{\tau\leq t}\left((dv_s\circ q_s)\cdot\delta q_s + \delta v_s\cdot q_s\right)\,ds\,. \tag{3.68}$$

4.4.2 Spatial regularity of the solution

We investigate in this section the spatial regularity of a solution $q = \Phi(q_0,v)$ generated with the *growth dynamic* by a time-varying vector field $v \in L_V^2$ from an initial condition $q_0 \in L^\infty(X,\mathbb{R}^d)$.

We assume hereafter that X is a smooth k-dimensional Riemannian submanifold of $\mathbb{R}^d$ (eventually with corners: for example, a convex or concave polygon is a submanifold with corners - see Chapter 4 for more details). We denote d_X its associated Riemannian distance. Let us also introduce:

Definition 4.5. *For any* $(x_0, \delta x_0) \in X \times TX$ *such that* $\delta x_0 \in T_{x_0}X$, $\mathcal{C}(x_0; \delta x_0)$ *denotes the set of smooth paths* $x : [-1, 1] \ni t \mapsto x(t)$ *in* X *such that* $x(0) = x_0$ *and* $\dot{x}(0) = \delta x_0$. *At any* $t \in [-1, 1]$, $x(t)$ *will be denoted* x_t.

Since the time derivative of q_t is usually not continuous on X because of the indicator function, we cannot solve the integral equation directly in a space of continuous functions like $(\mathcal{C}_b(X, \mathbb{R}^d), |\cdot|_\infty)$ (the Banach space of the bounded continuous functions). This indicator function divides at each time $t \in [0, 1]$ the coordinate space X into two parts: the set of active points

$$X_t \doteq \{x \in X \mid \tau(x) \leq t\} \tag{3.69}$$

and its complement $X_t^c = X \backslash X_t$. Likewise, the shape $q_t(X)$ is divided in two parts. Hence, since these two blocks have their own dynamic, it can induce some irregularity at the boundary between the two parts. This boundary is the image of $X_{\{t\}} = \{x \in X \mid \tau(x) = t\}$. Figure 3.7 illustrates the typical division of the shape modeling the development of a horn.

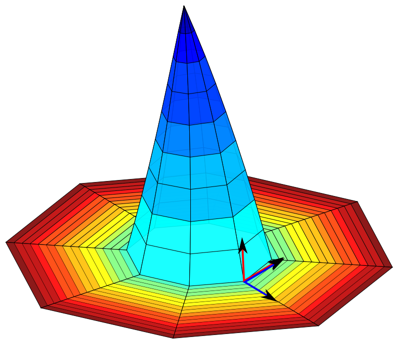

Figure 3.7 – Horn in the middle of its development. The colors correspond to the level lines of the birth tag τ. The shape $q_t(X)$ is divided in two parts. The active part (in blue) of real points and the inactive part (from green to red) of fictional points that will progressively appear. At the boundary between these two parts, the shape admits two half tangent planes.

Unlike the classic LDDMM framework, the spatial regularity of q is here strongly linked to the temporal regularity of v. With the growth dynamic, when v is continuous with respect to time, the shape admits two regular parts as described above. However, the boundary layer $X_{\{t\}}$ plays a central role in the global regularity of the shape throughout its evolution. When v has an irregularity at a time t_0, the shape captures it and keeps it at its layer $q_t(X_{\{t_0\}})$ from time t_0 to time 1. Figure 3.8 illustrates the impact of the discontinuity of v on the generated shape.

The integrability of v maintains yet some regularity of the solution. A solution defined on $\mathcal{C}([0, 1], L^\infty(X, \mathbb{R}^d))$ with a bounded continuous initial condition q_0 will actually stay in $\mathcal{C}_b(X, \mathbb{R}^d)$. Indeed, the application of the Grönwall's lemma (Lemma 4.2) specified at any point $x \in X$ (see equation (3.63)) gives

$$|q_t(x)|_{\mathbb{R}^d} + 1 \leq (|q_0(x)|_{\mathbb{R}^d} + 1) \exp(c|v|_1) \leq (|q_0|_\infty + 1) \exp(c|v|_1) . \tag{3.70}$$

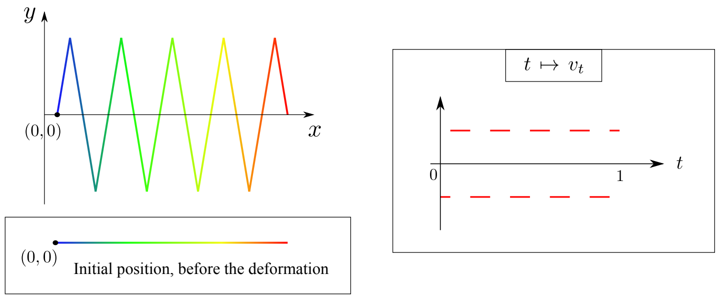

Figure 3.8 – The final state $q_1(X)$ displayed on the top left is a serrated curve with as many discontinuities as its associated vector field v given on the right as real-valued function modeling piecewise constant vertical translations upwards and downwards. The initial position $q_0(X)$ is a segment. At the beginning of the scenario, the vector field is directed downwards and the blue part of the segment is progressively displaced downwards while the rest of the segment remains fixed. It creates the first slope of the final polygonal curve. Once v becomes positive, the active part of the curve is displaced upwards and the second slope is created. The final polygonal line has as many irregularities as v has discontinuities.

Hence,

$$\sup_{t,x} |q_t(x)|_{\mathbb{R}^d} < \infty \,. \tag{3.71}$$

Moreover, we have

Proposition 4.4 (Spatial continuity of the solution)**.** *If $q_0 \in \mathcal{C}_b(X, \mathbb{R}^d)$ and $\tau \in \mathcal{C}(X, \mathbb{R}^+)$ then q belongs to $\mathcal{C}([0,1], \mathcal{C}_b(X, \mathbb{R}^d))$.*

Proof. For any $s, t \in \mathbb{R}$, we denote $s \wedge t = \min(s,t)$. We have

$$\begin{aligned} q_t(y) - q_t(x) &= q_0(y) - q_0(x) + \int_{\tau(y)\wedge t}^{t} v_s(q_s(y))\, ds - \int_{\tau(x)\wedge t}^{t} v_s(q_s(x))\, ds \\ &= q_0(y) - q_0(x) - \int_{\tau(x)\wedge t}^{\tau(y)\wedge t} v_s(q_s(x))\, ds + \int_{\tau(y)\wedge t}^{t} v_s(q_s(y)) - v_s(q_s(x))\, ds \,. \end{aligned}$$

Finally,

$$\begin{aligned} |q_t(y) - q_t(x)|_{\mathbb{R}^d} \leq |q_0(y) - q_0(x)|_{\mathbb{R}^d} &+ \int_{\tau(x)\wedge t}^{\tau(y)\wedge t} |v_s(q_s(x)|_{\mathbb{R}^d}\, ds \\ &+ \int_{\tau(y)\wedge t}^{t} |v_s(q_s(y)) - v_s(q_s(x))|_{\mathbb{R}^d}\, ds \,. \end{aligned}$$

The second term of the right hand side can be bounded with a Cauchy-Schwartz inequality. The third one can be bounded with the mean value theorem. Then, the (H_1^V) conditions and the lemma 4.1 can be applied to both upper bounds to give a constant $c > 0$ such that:

$$\int_{\tau(x)\wedge t}^{\tau(y)\wedge t} |v_s(q_s(x))|_{\mathbb{R}^d}\, ds \leq \int_{\tau(x)}^{\tau(y)} c|v_s|_V(|q_s|_\infty + 1)\, ds \tag{3.72}$$

$$\leq c(|q|_\infty + 1)|\tau(x) - \tau(y)|^{1/2}|v|_2 \tag{3.73}$$

and

$$\int_{\tau(y)\wedge t}^{t} |v_s(q_s(x)) - v_s(q_s(y))|_{\mathbb{R}^d}\, ds \leq \int_0^t c|v_s|_V|q_s(x) - q_s(y)|_{\mathbb{R}^d}\, ds\,,$$

where the uniform bound for q is given by equations (3.70) and (3.71). We can thus conclude with the Grönwall's lemma and the continuity of q_0 and τ :

$$|q_t(y) - q_t(x)|_{\mathbb{R}^d} \leq \Big(|q_0(y) - q_0(x)|_{\mathbb{R}^d} + c(|q|_\infty + 1)|\tau(x) - \tau(y)|^{1/2}|v|_2\Big) \exp\left(c|v|_1\right)\,.$$

Therefore, q_t is continuous on X. □

This result can easily be improved when v is bounded as follows:

Proposition 4.5 (Control on the vector field)**.** *Assume that q_0 and τ are Lipschitz continuous and that $t \mapsto v_t$ is uniformly bounded. Then for any $x \in X$, we have*

$$\sup_{t\in[0,1]} \big|q_t(x) - q_t(y)\big|_{\mathbb{R}^d} = O(d_X(x,y))\,.$$

Proof. Consider the previous proof. Equation (3.73) becomes here

$$\int_{\tau(x)}^{\tau(y)} |v_s(q_s(x))|_{\mathbb{R}^d}\, ds \leq \int_{\tau(x)}^{\tau(y)} c|v_s|_V(|q|_\infty + 1)\, ds$$

$$\leq c(|q|_\infty + 1)|v|_\infty|\tau(x) - \tau(y)|_{\mathbb{R}}\,,$$

leading to

$$|q_t(y) - q_t(x)|_{\mathbb{R}^d} \leq (|q_0(y) - q_0(x)|_{\mathbb{R}^d} + c(|q|_\infty + 1)|v|_\infty|\tau(x) - \tau(y)|_{\mathbb{R}}) \exp\left(c|v|_1\right)\,.$$

This upper bound does not depend on t and is a $O(d_X(x,y))$. □

We can be more precise on the spatial regularity of q without additional condition on v. Further exploiting the integrability of v requires again the notion of Bochner-Lebesgue point (see Definition 4.3). Theorem 4.3 says that almost any point of an integrable function is a Bochner-Lesbesgue point. This implies some regularity on the time-varying vector fields of $L^1([0,1],V)$. The next proposition enlightens the role of v:

Proposition 4.6. *Consider $v \in L^2_V$ and $q = \Phi(q_0, v)$ where $q_0 \in \mathcal{C}_b(X,\mathbb{R}^d)$. Any Bochner-Lebesgue points of v is a Bochner-Lebesgue point of $(s \mapsto v_s \circ q_s) \in L^1([0,1],\mathcal{C}_b(X,\mathbb{R}^d)$.*

Proof. Consider $t \in [0,1]$. Since q is continuous, t is a Bochner-Lebesgue point of q. Now, under the (H_1^V) conditions, there exists $c > 0$ such that

$$\int |v_s \circ q_s - v_t \circ q_t|_\infty \, ds \leq \int |(v_s - v_t) \circ q_s + (v_t \circ q_s - v_t \circ q_t)|_\infty \, ds$$
$$\leq c \int |v_s - v_t|_V (|q|_\infty + 1) + |v_t|_V |q_s - q_t|_\infty \, ds \, .$$

Therefore, if t is also a Bochner-Lebesgue point of v, then t is a Bochner-Lebesgue point of $s \mapsto v_s \circ q_s$. $\square$

Consequently, the set of non Bochner-Lebesgue points of $s \mapsto v_s \circ q_s$ is included in the set of non Bochner-Lebesgue points of v.

Definition 4.6. *Given $v \in L_V^2$, define $N \subset [0,1]$ the subset of non Bochner-Lebesgue points of v and*

$$\mathcal{N} = \{x \in X \mid \tau(x) \in N\} \, , \tag{3.74}$$

the associated level lines of τ. Then if τ is a submersion, $\mathcal{N}$ is a null subset of X.

Proposition 4.7. *Assume that $q_0 \in \mathcal{C}_b(X, \mathbb{R}^d)$ is k_0-Lipschitz continuous and that $\tau \in \mathcal{C}^1(X, [0,1])$ is a submersion (meaning that $d\tau(x)$ is surjective for any $x \in X$). For any $x \in X \setminus \mathcal{N}$, we have under the (H_1^V) conditions*

$$\sup_{t \in [0,1]} \big|q_t(x) - q_t(y)\big|_{\mathbb{R}^d} = O(d_X(x,y)) \, .$$

This property holds thus for the points x of almost any level lines of τ and these level lines correspond to the Bochner-Lebesgue points of v.

Proof. Consider any $x \in X \setminus \mathcal{N}$ and any $t \in [0,1]$. For any $y \in X$, denote $\Delta(y) = -\int_{\tau(x)\wedge t}^{\tau(y)\wedge t} v_s(q_s(x)) \, ds$. We have as before

$$|q_t(y) - q_t(x)|_{\mathbb{R}^d} \leq |q_0(y) - q_0(x)|_{\mathbb{R}^d} + |\Delta(y)|_{\mathbb{R}^d} + \int_{\tau(y)\wedge t}^{t} |v_s(q_s(y)) - v_s(q_s(x))|_{\mathbb{R}^d} \, ds$$
$$\leq k_0 d_X(y,x) + |\Delta(y)|_{\mathbb{R}^d} + \int_{\tau(y)\wedge t}^{t} |v_s(q_s(y)) - v_s(q_s(x))|_{\mathbb{R}^d} \, ds \, . \tag{3.75}$$

We still intend to apply the Grönwall's lemma but this time we need to be more accurate on the upper bound on $\Delta(y)$. Moreover, the next lemma will actually be useful in the next proposition.

Lemma 4.5. *If $x \in X \setminus \mathcal{N}$*

$$\Delta(y) = -(\tau(y) - \tau(x)) v_{\tau(x)}(q_{\tau(x)}(x)) + o(\tau(y) - \tau(x)) \, .$$

Proof. We have

$$\big|\Delta(y) + (\tau(y) - \tau(x)) v_{\tau(x)}(q_{\tau(x)}(x))\big|_{\mathbb{R}^d} \leq \left| \int_{\tau(x)}^{\tau(y)} (v_s \circ q_s - v_{\tau(x)} \circ q_{\tau(x)}) ds \right| (x) \, .$$

Since $x \in X \setminus \mathcal{N}$, $\tau(x)$ is a Bochner-Lebesque point for $(s \to v_s \circ q_s) \in L^1([0,1], \mathcal{C}_b(X, \mathbb{R}^d))$ and since $h \to h(x)$ is a smooth mapping from $\mathcal{C}_b(X, \mathbb{R})$ to $\mathbb{R}$ we get the result.

□

From this lemma, we deduce that since τ is $\mathcal{C}^1$

$$|\Delta(y)| = O(\tau(y) - \tau(x)) = O(d_X(x, y)) .$$

Now, using Grönwall's lemma on equation (3.75) we get

$$|q_t(y) - q_t(x)|_{\mathbb{R}^d} \leq (k_0 d_X(y, x) + |\Delta(y)|_{\mathbb{R}^d}) \exp(c|v|_1) .$$

At last, note that the rate of convergence of $|\Delta(y)|$ depends only on the regularity of τ and $s \mapsto v_s \circ q_s$ at the point x. Hence, it does not depend on t and

$$\sup_{t\in[0,1]} |q_t(y) - q_t(x)|_{\mathbb{R}^d} = O(d_X(x, y)) .$$

□

Proposition 4.8 (Differentiability of the solution)**.** *Assume that* $q_0 \in \mathcal{C}^1_b(X, \mathbb{R}^d)$ *and* $\tau \in \mathcal{C}^1(X, [0,1])$ *is a submersion. Assume the* (H^V_1) *conditions.*
(i) For any $t \in [0,1]$,

- *the restriction of* q_t *to the subset* $X^c_t = \{x \in X \mid \tau(x) > t\}$ *is of class* $\mathcal{C}^1$ *and we have there* $dq_t(x) = dq_0(x)$
- *for any* $x \in X \setminus \mathcal{N}$ *such that* $\tau(x) < t$, $q_t : X \to \mathbb{R}^d$ *is differentiable at* x *and* $dq_t(x)$ *is the solution at time* t *of the integral equation*

$$L_t(x) = dq_0(x) - v_{\tau(x)}(q_{\tau(x)}(x))d\tau(x) + \int_{\tau(x)}^{t} dv_s(q_s(x)) \circ L_s(x)\, ds \tag{3.76}$$

defined on $[0,1]$.

(ii) Moreover, if v *is continuous, i.e.* $v \in \mathcal{C}([0,1], V)$, *then for any* $t \in [0,1[$, q_t *is of class* $\mathcal{C}^1$ *on the two level sets* $\{x \in X \mid \tau(x) > t\}$ *and* $\{x \in X \mid \tau(x) < t\}$. *At last,* q_1 *belongs to* $\mathcal{C}^1(X, \mathbb{R}^d)$.

Proof. (i) Recall that for any $t \in [0,1]$, the restriction of q_t to the subset $\{x \in X \mid \tau(x) > t\}$ is equal to q_0, which gives the first point.

For any $x \in X$ and any $s \in [0,1]$, we have $dq_0(x) \in \mathcal{L}(T_xX, \mathbb{R}^d)$, $d\tau(x) \in \mathcal{L}(T_xX, \mathbb{R})$ so that $v_{\tau(x)}(q_{\tau(x)}(x))d\tau(x) \in \mathcal{L}(T_xX, \mathbb{R}^d)$ and $dv_s(q_s(x)) \in \mathcal{L}(\mathbb{R}^d, \mathbb{R}^d)$. The integral equation (3.76) is therefore well defined. Under the (H^V_1) conditions, the existence and uniqueness of a solution $L(x) \in \mathcal{C}\big([0,1], \mathcal{L}(T_xX, \mathbb{R}^d)\big)$ results from the linear Cauchy-Lipschitz theorem given in Corollary 4.2.

Now, for any smooth path $x \in \mathcal{C}(x_0; \delta x_0)$ centered on $x_0 \in X$ and of direction $\delta x_0 \in T_{x_0}X$ (see Definition 4.5), there exist $\tilde{x_0}, \delta\tilde{x_0} \in \mathbb{R}^k$ and a parameterization $\varphi : U \subset \mathbb{R}^k \to X$ such that $x = \varphi(\tilde{x})$ where for any $\epsilon \in [-1,1]$, $\tilde{x}_\epsilon = \tilde{x_0} + \epsilon\delta\tilde{x_0}$ and thus $\delta x_0 = d\varphi(x_0) \cdot \delta\tilde{x}_0$.

Define for any $\epsilon \neq 0$, $M_t^\epsilon = \left|\frac{q_t(x_\epsilon)-q_t(x_0)}{\epsilon} - L_t(x_0)\cdot\delta x_0\right|_{\mathbb{R}^d}$. The aim is thus to show that if $x_0 \in X\setminus\mathcal{N}$ then for any $t > \tau(x)$, M_t^ϵ tends to 0 when ϵ tends to 0. We have

$$\begin{aligned} M_t^\epsilon \leq \;& \left|\frac{q_0(x_\epsilon)-q_0(x_0)}{\epsilon} - L_0(x_0)\cdot\delta x_0\right|_{\mathbb{R}^d} \\ &+ \left|\int_{\tau(x_0)}^{\tau(x_\epsilon)} \frac{v_s(q_s(x_0))}{\epsilon}\,ds - d\tau(x_0)\cdot\delta x_0 v_{\tau(x_0)}(q_{\tau(x)}(x_0))\right|_{\mathbb{R}^d} \\ &+ \left|\int_{\tau(x_0)}^{\tau(x_\epsilon)} dv_s(q_s(x_0))\cdot L_s(x_0)\cdot\delta x_0\,ds\right|_{\mathbb{R}^d} \\ &+ \left|\int_{\tau(x_\epsilon)}^{t} \frac{v_s(q_s(x_\epsilon))-v_s(q_s(x_0))}{\epsilon} - dv_s(q_s(x_0))\cdot L_s(x_0)\cdot\delta x_0\,ds\right|_{\mathbb{R}^d}. \end{aligned}$$

Let us note T_1^ϵ, T_2^ϵ, T_3^ϵ, and T_4^ϵ these four terms. We have then

$$T_1^\epsilon = \left|\frac{q_0(x_\epsilon)-q_0(x_0)}{\epsilon} - dq_0(x_0)\right|_{\mathbb{R}^d} = o(1)\,.$$

Since $x_0 \notin \mathcal{N}$, Lemma 4.5 says that $T_2^\epsilon = o(1)$. Moreover, under the (H_1^V) conditions, there exists $c > 0$ such that

$$T_3^\epsilon \leq c\int_0^1 \mathbb{1}_{[\tau(x_0),\tau(x_\epsilon)]}|v_s|_V|L|_\infty\,ds\,.$$

The dominated convergence theorem ensures that for any sequence $(\epsilon_n)_{n\in\mathbb{N}}$ converging to 0, $T_3^{\epsilon_n}$ tends also to 0 and thus T_3^ϵ tends to 0 when ϵ tends to 0. At last, we will bound the last term in order to apply the Grönwall's lemma to the whole expression.

$$T_4^\epsilon \leq \int_{\tau(x_\epsilon)}^t \left|d_s v_s(q_s(x_0))\right|_{op} M_s^\epsilon\,ds + \int_{\tau(x_\epsilon)}^t \frac{1}{|\epsilon|}R_s^\epsilon\,ds$$

where

$$R_s^\epsilon = \left|v_s(q_s(x_\epsilon)) - v_s(q_s(x_0)) - dv_s(q_s(x_0))\cdot(q_s(x_\epsilon)-q_s(x_0))\right|_{\mathbb{R}^d}.$$

Denote for any $r, s \in [0,1]$, $y_s^{r,\epsilon} = q_s(x_0) + r(q_s(x_\epsilon) - q_s(x_0))$ and consider the function $g_s : [0,1] \to \mathbb{R}^d$ defined by $g_s(r) = v_s(y_s^{r,\epsilon}) - v_s(q_s(x_0))$. One can then write that

$$v_s(q_s(x^\epsilon)) - v_s(q_s(x_0)) = g_s(1) - g_s(0) = \int_0^1 g_s'(r)\,dr = \int_0^1 dv_s(y_s^{r,\epsilon})\cdot\big(q_s(x_\epsilon)-q_s(x_0)\big)\,dr$$

and

$$\begin{aligned} R_s^\epsilon &= \left|\int_0^1 \big(dv_s(y_s^{r,\epsilon}) - dv_s(q_s(x_0))\big)\cdot\big(q_s(x_\epsilon)-q_s(x_0)\big)\,dr\right|_B \\ &\leq \int_0^1 \left|dv_s(y_s^{r,\epsilon}) - dv_s(q_s(x_0))\right|_{op}\left|q_s(x_\epsilon)-q_s(x_0)\right|_{\mathbb{R}^d}dr\,. \end{aligned}$$

Since for any $r \in [0,1]$ and any $s \in [0,1]$, $y_s^{r,\epsilon}$ tends to $q_s(x_0)$ when ϵ tends to 0 and since dv_s is continuous, the integrand tends to 0. Moreover, according to Proposition 4.7, there exists $m > 0$ such that $\frac{|q_s(x_\epsilon)-q_s(x_0)|}{|\epsilon|} \leq m$ is bounded. Then under the (H_1^V) conditions,

$$\left|dv_s(y^{r,\epsilon}) - dv_s(q_s(x_0))\right|_{op} \frac{|q_s(x_\epsilon) - q_s(x_0)|}{|\epsilon|} \leq 2cm|v_s|_V\,.$$

Hence, the dominated convergence theorem ensures that for any $s \in [0,1]$, $\frac{R_s}{|\epsilon|}$ tends to 0 when ϵ tends to 0. Note also that since m does not depend on s, the same theorem ensures that

$$\int_0^1 \frac{R_s^\epsilon}{|\epsilon|}\, ds \underset{\epsilon\to 0}{\longrightarrow} 0\,.$$

In fine, the Grönwall's lemma allows to write

$$\begin{aligned}
M_t^\epsilon &\leq o(1) + \int_{\tau(x_\epsilon)}^t \frac{1}{|\epsilon|} R_s^\epsilon\, ds + \int_{\tau(x_\epsilon)}^t |d_s v_s(q_s(x))| M_s^\epsilon\, ds \\
&\leq o(1) + \int_0^1 \frac{1}{|\epsilon|} R_s^\epsilon\, ds + \int_0^t |d_s v_s(q_s(x))| M_s^\epsilon\, ds \\
&\leq \left(o(1) + \int_0^1 \frac{1}{|\epsilon|} R_s^\epsilon\, ds\right) \exp(c|v|_1)\,.
\end{aligned}$$

This proves the second point of (i).

(ii) If v is continuous, $\mathcal{N}$ is empty, and $q_t\big|_{\tau<t}$ is differentiable every where. At last, we can show that for any $t \in [0,1]$, L_t is continuous on X_t. Note that by construction, for any $x \in X$, $t \mapsto L_t(x)$ is continuous so that

$$|L(x)|_\infty \doteq \sup_{t\in[0,1]} |L_t(x)|_{\mathbb{R}^d} < \infty\,.$$

The two first terms of L_t are continuous in space. Let be $x \in X_t$ and y in a neighborhood $U \subset X_t$ of x. We have

$$\begin{aligned}
|L_t(y) - L_t(x)|_{op} \leq |dq_0(y) - dq_0(x)|_{op} &+ |v_{\tau(y)}(q_{\tau(y)}(y))d\tau(y) - v_{\tau(x)}(q_{\tau(x)}(x))d\tau(x)|_{op} \\
&+ \int_{\tau(x)}^{\tau(y)} |dv_s(q_s(x)) \circ L_s(x)|_{op}\, ds \\
&+ \int_{\tau(y)}^t |dv_s(q_s(x)) \circ L_s(x) - dv_s(q_s(y)) \circ L_s(y)|_{op}\, ds\,.
\end{aligned}$$

By continuity in space of dq_0, τ and $d\tau$, and continuity in space and time of q and v, $\epsilon_1(y) = |dq_0(y) - dq_0(x)|_{op} + |v_{\tau(y)}(q_{\tau(y)}(y))d\tau(y) - v_{\tau(x)}(q_{\tau(x)}(x))d\tau(x)|_{op}$ tends to 0 when y tends to x.

Under the (H_1^V) conditions there exists thus $c > 0$ such that

$$\epsilon_2(y) = \int_{\tau(x)}^{\tau(y)} |dv_s(q_s(x)) \circ L_s(x)|_{op}\, ds \leq \int_{\tau(x)}^{\tau(y)} c|v_s|_V |L_s(x)|_{op}\, ds \leq \int_{\tau(x)}^{\tau(y)} c|v_s|_V |L(x)|_\infty\, ds\,,$$

so that $\epsilon_2(y)$ tends to 0 when y tends to x. Likewise, the constant c also satisfies for any

$y \in U$

$$
\begin{aligned}
\int_{\tau(y)}^{t} &|dv_s(q_s(x)) \circ L_s(x) - dv_s(q_s(y)) \circ L_s(y)|_{op}\, ds \\
&\leq \int_{\tau(y)}^{t} |dv_s(q_s(x)) \circ \big(L_s(x) - L_s(y)\big)|_{op}\, ds \\
&\quad + \int_{\tau(y)}^{t} |dv_s(q_s(x)) \circ L_s(y) - dv_s(q_s(y)) \circ L_s(y)|_{op}\, ds \\
&\leq \int_{\tau(y)}^{t} c|v_s|_V |L_s(x) - L_s(y)|_{op}\, ds + \int_{\tau(y)}^{t} c|v_s|_V |q_s(y) - q_s(x)|_{\mathbb{R}^d} |L(y)|_\infty\, ds\,.
\end{aligned}
$$

Using the Cauchy-Schwartz inequality and Proposition 4.7, we deduce that

$$
\epsilon_3(y) = \int_{\tau(y)}^{t} c|v_s|_V |q_s(y) - q_s(x)|_{\mathbb{R}^d} |L(y)|_\infty\, ds
$$

tends to 0 when y tends to x. Putting every piece together, the Grönwall's lemma says that

$$
|L_t(y) - L_t(x)|_{op} \leq \epsilon(y) \exp(c|v|_1)\,,
$$

where $\epsilon(y) = \epsilon_1(y) + \epsilon_2(y) + \epsilon_3(y)$ which ends the proof. □

Remark 4.2. *For any $t \in]0,1]$, the level line $X_{\{t\}} = \{x \in X \mid \tau(x) = t\}$ is the critical boundary of points starting to move at time t. The previous proof could be adapted to show that the shape has there two tangent spaces given by:*

1. *$dq_0(x)$ for the set of stationary points (when $X_{\{t\}}$ is seen as the extension of $\{x \in X \mid \tau(x) > t\}$)*
2. *$dq_0(x) - v_{\tau(x)}(q_{\tau(x)}(x)) \nabla d\tau(x)$ for the active points (when $X_{\{t\}}$ is seen as the extension of $\{x \in X \mid \tau(x) < t\}$ and when t is a Bochner-Lebesgue point of v).*

See Figure 3.7.

Remark 4.3. *If $x \in \mathcal{C}(x_0; \delta x_0)$ is a path included in a level line of τ, ie. for any $\epsilon \in [-1,1]$, $\tau(x_\epsilon) = \tau(x_0)$, then $d\tau(x_0) \cdot \delta x_0 = 0$ and we retrieve a standard behavior of the LDDMM setting:*

$$
\begin{aligned}
q_t(x_\epsilon) - q_t(x_0) &= dq_t(x) \cdot \delta x_0 + O(|\epsilon|) \\
&= \left(dq_0(x) + \int_{\tau(x)}^{t} dv_s(q_s(x)) \circ dq_s(x)\, ds \right) \cdot \delta x_0 + O(|\epsilon|)\,.
\end{aligned}
$$

In conclusion, we saw that the spatial regularity of the solution results from the temporal regularity of the vector field. If v has a discontinuity at time $t_0 \in]0,1[$, the regularity of the shape will suffer on the whole level line $X_{\{t_0\}}$ from time t_0 and this accident will remain throughout the end of the evolution (on the time interval $]t_0, 1]$).

Remark 4.4 (Non injective mapping)**.** *The injectivity of q has never been requested. Note that we saw in the proof of Proposition 4.4, that there exists $M > 0$ such that*

$$
|q_t(y) - q_t(x)|_{\mathbb{R}^d} \leq M \left(|q_0(y) - q_0(x)|_{\mathbb{R}^d} + |\tau(x) - \tau(y)|^{1/2} \right)\,.
$$

Therefore, if two points x and y appear at the same time (i.e. belong to the same layer $X_{\{t_0\}}$) and at the same place, then $\tau(x) = \tau(y)$ and $q_0(x) = q_0(y)$ and at all time $t \in [0,1]$, $q_t(x) = q_t(y)$.

However, if they appear at the same place but at different times $\tau(x) \neq \tau(y)$, they can evolve independently. If $\tau(x) < \tau(y)$, then at time $\tau(x)$, $q_t(x)$ starts to leave the birth place $q_0(x) = q_0(y)$ but $q_t(y)$ remains still. Hence, at time $\tau(y)$ when $q_t(y)$ starts to move, $q_t(x)$ and $q_t(y)$ have no reason to be equal and from this time they are carried by the flow together and will never meet again.

5 Reduced Hamiltonian system properties

We assume hereafter that the dynamic of the model is given by an operator

$$\xi : B \times [0,1] \to \mathcal{L}(V, B)$$

instead of a more general function f (see Section 1.4), i.e. we have formally

$$\dot{q}_t = \xi_{q_t,t}(v_t)\,.$$

The Hamiltonian function is then given by

$$\begin{array}{rcl} H : B \times B^* \times V \times [0,1] & \longrightarrow & \mathbb{R} \\ (q,p,v,t) & \longmapsto & (p \,|\, \xi_{(q,t)}(v)) - C(v,t)\,. \end{array}$$

Let us recall that we defined in Section 3.4, under the names of **adapted norm setup** and **nondegenerate adapted norm setup**, two sets of cost functions of the common type

$$C(v,t) = \frac{1}{2}\langle v, \ell_t v\rangle_V\,.$$

5.1 Compatible spaces

In the next section, we will prove the local existence and uniqueness of solutions to the reduced Hamiltonian system introduced in Section 2.4. This system is defined on the product space $B \times B^*$ by

$$\begin{pmatrix} \dot{q}_t \\ \\ \dot{p}_t \end{pmatrix} = \begin{pmatrix} \frac{\partial H_r}{\partial p}(q_t, p_t, t) \\ \\ -\frac{\partial H_r}{\partial q}(q_t, p_t, t) \end{pmatrix}.$$

However, we would like to establish the existence and the uniqueness of its solutions on a smaller space product that we will note $B_0 \times B_1^*$.

Example 5.1. *When we consider $B = L^\infty(X, \mathbb{R}^d)$, we would like to constrain the momenta in a space smaller than B^*. For example, we would like to keep $B_0 = B = L^\infty(X, \mathbb{R}^d)$ but to define a new space $B_1 = L^1(X, \mathbb{R}^d)$ and study the solutions of the reduced Hamiltonian system in the subspace*

$$B_0 \times B_1^* = L^\infty(X, \mathbb{R}^d) \times L^\infty(X, \mathbb{R}^d)$$

of $B \times B^*$.

In order to ensure that the system is well defined and stable on the smaller space $B_0 \times B_1^*$, we introduce a notion of compatibility.

Definition 5.1. *Let B, B_0 and B_1 be three Banach spaces. We say that (B_0, B_1) is* ***compatible*** *with B if*

$$B_0 \overset{i_0}{\hookrightarrow} B \overset{i_1}{\hookrightarrow} B_1$$

with i_0 and i_1 two continuous linear embeddings such that the image $i_1(B)$ is dense in B_1. Moreover, we say that (B_0, B_1) is ***compatible with the system*** *(B, V, ξ) if (B_0, B_1) is compatible with B and if there exist two functions*

$$\xi^0 : B_0 \times [0,1] \to \mathcal{L}(V, B_0)\,,$$

$$\xi^1 : B_1 \times [0,1] \to \mathcal{L}(V, B_1)\,,$$

such that at any time $t \in [0,1]$, $\xi_t \circ i_0 = i_0 \circ \xi_t^0$ and $\xi_t^1 \circ i_1 = i_1 \circ \xi_t$.

Proposition 5.1. *Let be B, B_0 and B_1 three Banach spaces such that (B_0, B_1) is compatible with B. Then there exists a continuous linear embedding*

$$B_1^* \overset{i_1^*}{\hookrightarrow} B^*\,.$$

Proof. This is a consequence of a well known result. Let E and F be two Banach spaces and $i : E \to F$ a continuous linear mapping. Let us introduce $i^* : F^* \to E^*, f \mapsto f \circ i$. For any $f \in F^*$, $i^*(f) = f \circ i$ is continuous and $|i^*(f)|_{E^*} \leq |f|_{F^*} |i|_{\mathcal{L}(E,F)}$ so that i^* is also a continuous linear map. Assume now that $i(E)$ is dense in F. Let be $f \in F^*$, if $i^*(f) = f \circ i \equiv 0$, then $\tilde{f} = f_{|i(E)}$ is null on the dense subset $i(E)$ of F. Since f is continuous on F, we get that $f = 0$. $\square$

In the following, up to the embedding i_0 and i_1 we will consider that $B_0 \subset B \subset B_1$ and consider ξ^1 as an extension of ξ on B^1 and ξ^0 as the restriction of ξ to B_0. Likewise, up to the embedding i_1^* we will consider B_1^* as a subset of B^*.

We will consider throughout this section the previously introduced conditions

$$(H_1^\xi) \quad \left| \begin{array}{l} \textit{(i)}\ \xi_t \in \mathcal{C}^1(B, \mathcal{L}(V, B) \text{ for any } t \in [0,1]\,. \\ \textit{(ii)} \text{ There exists } c > 0 \text{ such that} \\ |\xi(q,t)|_{\mathcal{L}(V,B)} \leq c(|q|_B + 1) \text{ and } |\partial_q \xi(q,t)|_{\mathcal{L}(B, \mathcal{L}(V,B))} \leq c, \\ \text{for any } (q,t) \in B \times [0,1]\,. \end{array} \right.$$

The introduction of compatible spaces (B_0, B_1) calls yet for an additional set of conditions defined as follows:

$$(H^{\xi}_{B_0,B_1}) \quad \left| \begin{array}{l} \textit{(i)}\ q \to \xi^1(q,t) \text{ is Gâteaux-differentiable at any location } (q,t) \in B_0 \times [0,1] \\ \text{ and its differential denoted } \partial_q \xi^1(q,t) \text{ belongs to } \mathcal{L}(B_1, \mathcal{L}(V, B_1)). \\ \\ \textit{(ii)} \text{ There exists } q_0 \in B_0 \text{ such that} \\ \sup_t(|\xi^0(q_0,t)|_{\mathcal{L}(V,B_0)} + |\partial_q \xi^1(q_0,t)|_{\mathcal{L}(B_1,\mathcal{L}(V,B_1))} < \infty\,. \\ \\ \textit{(iii)} \text{ There exists } c > 0 \text{ such that} \\ \begin{cases} |\xi^0(q,t) - \xi^0(q',t)|_{\mathcal{L}(V,B_0)} \le c|q-q'|_{B_0}, \\ |\partial_q \xi^1(q,t) - \partial_q \xi^1(q',t)|_{\mathcal{L}(B_1,\mathcal{L}(V,B_1))} \le c|q-q'|_{B_0}\,, \end{cases} \\ \text{for any } q, q' \in B_0 \text{ and } t \in [0,1]\,. \end{array} \right.$$

Lemma 5.1. *The (H^{ξ}_1) and $(H^{\xi}_{B_0,B_1})$ conditions imply the following properties. There exists $c > 0$ such that for any $q, \delta q \in B_0$, any $p \in B_1^*$, any $(t,v) \in [0,1] \times V$, we have*

$$\begin{array}{ll} (P_1) & |\xi^0(q,t)|_{\mathcal{L}(V,B_0)} \le c(|q|_{B_0} + 1)\,, \\ (P_2) & |\xi^0(q,t)^* \cdot p|_{V^*} \le c(|q|_{B_0} + 1)|p|_{B_1^*}\,, \\ (P_3) & |\partial_q \xi^1(q,t)|_{\mathcal{L}(B_1,\mathcal{L}(V,B_1))} \le c(|q|_{B_0} + 1)\,, \\ (P_4) & |\partial_q \xi^1(q,t) \cdot \delta q|_{\mathcal{L}(V,B_1)} \le c|\delta q|_{B_0}(|q|_{B_0} + 1)\,, \\ (P_5) & (\partial_q \xi_{(q,t)}(v))^* \cdot p = (\partial_q \xi^1(q,t)(v))^* \cdot p \in B_1^*\,, \\ (P_6) & |(\xi^0(q,t) - \xi^0(q',t))^* \cdot p|_{V^*} \le c|p|_{B_1^*}|q-q'|_{B_0}\,, \\ (P_7) & |(\partial_q \xi^1(q,t) - \partial_q \xi^1(q',t)) \cdot \delta q|_{\mathcal{L}(V,B_1)} \le c|\delta q|_{B_0}|q-q'|_{B_0}\,. \end{array}$$

Proof. These properties will be used in the proof of Proposition 5.3 and 5.4. (P_1) and (P_3) result directly from $(H^{\xi}_{B_0,B_1})$. Then, for any $q \in B_0$, $\xi^0(q,t) \in \mathcal{L}(V, B_0)$ so that $\xi^0(q,t)^* \in \mathcal{L}(B_0^*, V^*)$ and since B_1^* is continuously embedded in B_0^*, we deduce (P_2) from (P_1). Since B is continuously embedded in B_1, we deduce likewise (P_4) from (P_3).

Since B is continuously embedded in B_1, for any $t \in [0,1]$, ξ_t and ξ^1_t have the same Gâteaux-derivatives at any location $q \in B_0 \subset B$ in any direction $\delta q \in B \subset B_1$, i.e.

$$\partial_q \xi_{(q,t)} \cdot \delta q = \partial_q \xi^1(q,t) \cdot \delta q\,. \tag{3.77}$$

It follows that $\partial_q \xi_{(q,t)} : B \to \mathcal{L}(V, B_1)$ is continuous when B is equipped with the norm of B_1 and since B is dense in B_1, it can be continuously extended and by uniqueness, this extension is equal to $\partial_q \xi^1(q,t)$. Hence, for any $v \in V$, since $\partial_q \xi^1(q,t)(v)^* \in \mathcal{L}(B_1^*)$ and we have for any $p \in B_1^*$,

$$(\partial_q \xi_{(q,t)}(v))^* \cdot p = (\partial_q \xi^1(q,t)(v))^* \cdot p \in B_1^*\,.$$

At last, we have with $(H^{\xi}_{B_0,B_1})$ *(iii)*, $B_1^* \hookrightarrow B_0^*$ that induces (P_6) and $B_0 \hookrightarrow B_1$ that induces (P_7). $\square$

5.2 Local analysis of the reduced Hamiltonian system

In order to apply the Cauchy-Lipchitz Theorem 4.1, we need to establish some regularity of the reduced Hamiltonian.

Proposition 5.2. *Let E, F and G be three Banach spaces. Let be $r > 0$, we note $\mathcal{B}(0,r)$ the ball of E of radius r. Let be $f : \mathcal{B}(0,r) \to F$ and $g : \mathcal{B}(0,r) \to G$ two functions. Let $b : F \times G \to H$ be a continuous bilinear function. Assume that f and g are both bounded and Lipschitz continuous and note m_f, m_g, k_f and k_g four respective upper bounds of f, g and of their Lipschitz constants.*

Then there exists $c_b > 0$ such that $\mathcal{B}(0,r) \ni x \mapsto b(f(x), g(x))$ is Lipschitz continous and the Lipschitz constant is bounded by $c_b(m_f k_g + m_g k_f)$.

Proof. Since b is continuous, there exists $c_b > 0$ such that for any $(X,Y) \in F \times G$

$$|b(X,Y)|_H \leq c_b |X|_F |Y|_G \,.$$

Then for any $x, x' \in \mathcal{B}(0,r)$, we have

$$\begin{aligned} |b(f(x), g(x)) - b(f(x'), g(x'))| &\leq |b(f(x), g(x) - g(x')) + b(f(x) - f(x'), g(x'))| \\ &\leq c_b |f(x)||g(x) - g(x')| + c_b |f(x) - f(x')||g(x')| \\ &\leq c_b (m_f k_g + m_g k_f)|x - x'|_E \,. \end{aligned}$$

□

Let us introduce a new class of functions.

Definition 5.2. *We define $\mathcal{L}ip^{loc}_{unif}(E \times [0,1], F)$ the set of applications g such that*

- *for almost every $t \in [0,1]$, $g_t := g(\cdot, t)$ is locally Lipschitz continuous,*
- *for any $r > 0$, if we note k^r_t the Lipschitz constant of g_t on the ball $\mathcal{B}(0,r)$ (defined a.e.), then $t \mapsto k^r_t$ is bounded on $[0,1]$.*

We recall that we introduced the class $\mathcal{L}ip^{loc}_{int}$ in Definition 4.1. The only difference between these two classes lies on the properties of the Lipschitz constant k^r_t (integrable or uniformly bounded) .

Proposition 5.3. *Let (B_0, B_1) be two Banach spaces* ***compatible with the system*** *(B, V, ξ). Assume that $w : B_0 \times B_1^* \times [0,1] \to V$ is a function of class $\mathcal{L}ip^{loc}_{int}$. For any $r > 0$ and almost any $t \in [0,1]$, assume that w_t is locally bounded and note m^r_t its supremum on the ball $\mathcal{B}(0,r)$. Then under the $(H^{\xi}_{B_0,B_1})$ and (H^{ξ}_1) conditions, if $t \mapsto m^r_t$ is integrable, the function*

$$\begin{aligned} h^w : B_0 \times B_1^* \times [0,1] &\longrightarrow B_0 \times B_1^* \\ (q,p,t) &\longmapsto \begin{pmatrix} \xi_{(q,t)}(w(q,p,t)) \\ \\ -(\partial_q \xi_{(q,t)})(w(q,p,t))^* \cdot p \end{pmatrix} \end{aligned} \tag{3.78}$$

is of class $\mathcal{L}ip^{loc}_{int}(B_0 \times B_1^* \times [0,1], B_0 \times B_1^*)$ (with $|(q,p)|_{B_0 \times B_1^*} = |q|_{B_0} + |p|_{B_1^*}$) .

Proof. The proof results from the regulariy of ξ and Proposition 5.2.

We start our proof by checking that $h^w(q,p,t) \in B_0 \times B_1^*$ for any $(q,p,t) \in B_0 \times B_1^* \times [0,1]$. Since B_0 and B_1 are compatible with (B,V,ξ), we have for any $(q,t,v) \in B_0 \times [0,1] \times V$,

$$\xi(q,t)(v) = \xi^0(q,t) \in B_0$$

and the first component of h^w is in B_0. Lemma 5.1 (P_5) ensures then that for any $(q,p) \in B_0 \times B_1^*$ and any $v \in V$, we have $(\partial_q \xi(q,t)(v))^* \cdot p = (\partial_q \xi^1(q,t)(v))^* \cdot p \in B_1^*$ so that h^w is thus well defined.

Note $c > 0$ the constant given by the $(H^{\xi}_{B_0,B_1})$ conditions and k_t^r the Lipschitz constant of w_t on the ball $\mathcal{B}(0,r)$. Now, let E and F be two Banach spaces. The bilinear function $b : \mathcal{L}(E,F) \times E \to F$, $(L,x) \mapsto L(x)$ is continuous and satisfies for any $L \in \mathcal{L}(E,F)$ and any $x \in E$,

$$|b(L,x)|_F \leq |L|_{op}|x|_E \,.$$

The bilinear function $b^* : \mathcal{L}(E,F) \times F^* \to E^*$, $(L,x) \mapsto L^*(x)$ is continuous and satisfies for any $L \in \mathcal{L}(E,F)$ and any $x \in F^*$, any $y \in E$,

$$|(b^*(L,x) \,|\, y)| = |(L^*(x) \,|\, y)| = |(x \,|\, L(y))| \leq |L|_{op}|y|_E|x|_{F^*} \,,$$

so that

$$|b^*(L,x)|_{E^*} \leq |L|_{op}|x|_{F^*} \,.$$

To prove the proposition, we will use repeatedly the previous result.

Let us first consider the regularity of the first component of h^w. For any $t \in [0,1]$ and any $r > 0$, define the functions $f_t(q,p) = \xi^0(q,t)$ and $g_t(q,p) = w(q,p,t)$ on $\mathcal{B}(0,r)$ the ball of $B_0 \times B_1^*$. Then g_t takes values in V and f_t takes values in $\mathcal{L}(V,B_0)$. Moreover, we deduce from Lemma 5.1 (P_1) that f_t and g_t satisfy the conditions of Proposition 5.2 and with the notation of the proposition we have $m_f \leq c(r+1)$, $k_f \leq c$, $m_g \leq m_t^r$ and $k_g \leq k_t^r$. Therefore, the first component of h_t^w is equal to $b(f_t(q,p), g_t(q,p))$, is Lipschitz continuous on $\mathcal{B}(0,r)$ and the Lipschitz constant satisfies

$$k^r_{h^w_{1,t}} \leq m_f k_g + m_g k_f \leq c(r+1)k_t^r + m_t^r c \,.$$

We turn now to the regularity of the second component of h^w. For any $t \in [0,1]$ and any $r > 0$, define the functions $f_t(q,p) = \partial_q \xi^1(q,t)$ and $g_t(q,p) = w(q,p,t)$ on $\mathcal{B}(0,r)$ the ball of $B_0 \times B_1^*$. Then g_t takes values in V and f_t takes values in $\mathcal{L}(V, \mathcal{L}(B_1))$. Moreover, we deduce from Lemma 5.1 (P_3) that f_t and g_t satisfy the conditions of Proposition 5.2 and with the notation of the proposition we have $m_f \leq c(r+1)$, $k_f \leq c$, $m_g \leq m_t^r$ and $k_g \leq k_t^r$. Therefore, the function $(q,p) \mapsto (\partial_q \xi^1(q,t))(w(q,p,t)) = b(f_t(q,p), g_t(q,p))$ is Lipschitz continuous on $\mathcal{B}(0,r)$ and the Lipschitz constant satisfies

$$k^r_{\text{halfway}} \leq m_f k_g + m_g k_f \leq c(r+1)k_t^r + m_t^r c \,.$$

To end the proof, let us define, for any $t \in [0,1]$ and any $r > 0$, the functions $f_t(q,p) = \partial_q \xi^1(q,t)(w(q,p,t))$ and $g_t(q,p) = p$ on $\mathcal{B}(0,r)$ the ball of $B_0 \times B_1^*$. Then g_t takes values in B_1^* and f_t takes values in $\mathcal{L}(B_1)$. Moreover, from the previous point, f_t and g_t satisfy the conditions of Proposition 5.2 and with the notation of the proposition we have $m_f \leq c(r+1)m_t^r$, $k_f \leq c(r+1)k_t^r + m_t^r c$, $m_g \leq r$ and $k_g \leq 1$. Therefore, the second component of h_t^w is equal to $b^*(f_t(q,p), g_t(q,p))$, is Lipschitz continuous on $\mathcal{B}(0,r)$ and the Lipschitz constant satisfies

$$\begin{aligned} k^r_{h^w_{2,t}} &\leq m_f k_g + m_g k_f \leq c(r+1)m_t^r + r(c(r+1)k_t^r + m_t^r c) \\ &\leq c(2r+1)m_t^r + cr(r+1)k_t^r \,. \end{aligned}$$

Recall at last that $t \mapsto m_t^r + k_t^r$ is integrable. Hence, h_t^w is of class $\mathcal{L}ip^{\,loc}_{int}(B_0 \times B_1^* \times [0,1] \to V)$. Indeed, on any ball of radius $r > 0$, its Lipschitz constant is bounded by $2c(r+1)m_t^r + c(r+1)^2 k_t^r$ and is thus integrable on $[0,1]$. □

In the previous proposition, w plays the role of the optimal vector field v^*. This last one is built on the momentum map. Its regularity depends thus on the regularity of the momentum map. In the following, we will note the momentum map $\mathcal{J}$ instead of $\mathcal{J}_\xi$. Let us recall that it is defined for any $(q,p,t) \in B \times B^* \times [0,1]$ by

$$\mathcal{J}(q,p,t) = \xi^*_{(q,t)} \cdot p \,.$$

We note now $\mathcal{J}_t \doteq \mathcal{J}(\cdot,\cdot,t)$. The next proposition gives some regularity properties of the momentum map and will allow to use hereafter Proposition 5.3.

Proposition 5.4. *Let (B_0, B_1) be two Banach spaces compatible with the system (B, V, ξ). The momentum map can be defined on $B_0 \times B_1^* \times [0,1]$. Then under the (H_1^ξ) and $(H^\xi_{B_0,B_1})$ conditions, for any $t \in [0,1]$, $\mathcal{J}_t$ belongs to $\mathcal{C}^1(B_0 \times B_1^*, V^*)$. Moreover, $\mathcal{J}_t$ and $d\mathcal{J}_t$ are locally bounded on $B_0 \times B_1^*$, uniformly with respect to t. Therefore, $\mathcal{J}$ belongs to $\mathcal{L}ip^{\,loc}_{unif}(B_0 \times B_1^* \times [0,1], V^*)$.*

Proof. Under the condition H_1^ξ, the momentum map is defined on $B \times B^*$ so that we can consider its restriction on $B_0 \times B_1^* \subset B \times B^*$. The most challenging part is to check that this restriction is $\mathcal{C}^1$ for the topology induced by associated norm on $B_0 \times B_1^*$. The proof lies on the properties established in Lemma 5.1.

To prove this, it is sufficient to check that there exists $A_t \in \mathcal{C}(B_0 \times B_1, \mathcal{L}(B_0 \times B_1^*, V^*))$ such that for any direction $(\delta q, \delta p) \in B_0 \times B_1^*$ we have in V^*

$$(\mathcal{J}_t(q + \epsilon\delta q, p + \epsilon\delta p) - \mathcal{J}_t(q,p))/\epsilon \underset{\epsilon \to 0}{\longrightarrow} A_t(q,p) \cdot (\delta q, \delta p) \,. \tag{3.79}$$

Consider

$$A_t(q,p) \cdot (\delta q, \delta p) = (\partial_q \xi(q,t) \cdot \delta q)^* \cdot p + \xi(q,t)^* \cdot \delta p \,.$$

Property (P_2) and (P_4) of Lemma 5.1 ensure that there exists $c > 0$ such that we have for any $(q,p,t) \in B_0 \times B_1^* \times [0,1]$ and any $(\delta q, \delta p) \in B_0 \times B_1^*$,

$$|A_t(q,p) \cdot (\delta q, \delta p)|_{V^*} \leq c|p|_{B_1^*}|\delta q|_{B_0}(|q|_{B_0} + 1) + c|\delta p|_{B_1^*}(|q|_{B_0} + 1) \,. \tag{3.80}$$

We have therefore $A_t(q,p) \in \mathcal{L}(B_0 \times B_1, V)$.

Let us check now that $(q,p) \to A_t(q,p)$ is continuous on $B_0 \times B_1^*$. For any $(q',p') \in$

$B_0 \times B_1^*$, and any $(\delta q, \delta p) \in B_0 \times B_1^*$ we have

$$\begin{aligned}
|(A_t(q',p') - & A_t(q,p)) \cdot (\delta q, \delta p)|_{V^*} \\
&= |(\partial_q \xi(q',t) \cdot \delta q)^* \cdot p' - (\partial_q \xi(q,t) \cdot \delta q)^* \cdot p + (\xi(q',t) - \xi(q,t))^* \cdot \delta p|_{V^*} \\
&\leq |(\partial_q \xi^1(q',t) - \partial_q \xi^1(q,t)) \cdot \delta q|_{\mathcal{L}(V,B_1)} |p'|_{B_1^*} \\
&\quad + |\partial_q \xi^1(q,t) \cdot \delta q|_{\mathcal{L}(V,B_1)} |p' - p|_{B_1^*} + |(\xi(q',t) - \xi(q,t))^* \cdot \delta p|_{V^*} .
\end{aligned}$$

We have thus from (P_7), (P_4) and (P_6) that there exists a constant $c > 0$, that does not depend on the variables, such that

$$\begin{aligned}
|(A_t(q',p') - & A_t(q,p)) \cdot (\delta q, \delta p)|_{V^*} \\
&\leq c(|p'|_{B_1^*} |q' - q|_{B_0} |\delta q|_{B_0} + |p' - p|_{B_1^*} |\delta q|_{B_0} (|q_0|_{B_0} + 1) + |\delta p|_{B_1^*} |q' - q|_{B_0}) .
\end{aligned}$$

This upper bound tends to 0 when (q',p') tends to (q,p) so that we get $A_t \in \mathcal{C}(B_0 \times B_1^*, \mathcal{L}(B_0 \times B_1^*, V^*))$.

The last thing to prove is equation (3.79). We have

$$\begin{aligned}
\big|(\mathcal{J}(q + \epsilon \delta q, p + \epsilon \delta p, t) - & \mathcal{J}(q,p,t))/\epsilon - A(q,p) \cdot (\delta q, \delta p)\big|_{V_*} \\
&\leq |p|_{B_1^*} \big|\big(\xi^1(q + \epsilon \delta q, t) - \xi^1(q,t)\big)/\epsilon - \partial_q \xi^1(q,t) \cdot \delta q\big|_{\mathcal{L}(V,B_1)} \\
&\quad + \big|\big(\xi(q + \epsilon \delta q, t) - \xi_{(q,t)}\big)^* \cdot \delta p\big|_{V^*} .
\end{aligned}$$

From (P_6) we deduce that the last term tends to 0 when ϵ tends to 0 and since from $(H^{\xi}_{B_0,B_1})$ we know that $q \to \xi^1(q,t)$ is Gâteaux differentiable at any location $q \in B_0$ we get the result.

At this point, we have proved that $\mathcal{J}_t : ((q,p) \to \mathcal{J}(q,p,t)) \in \mathcal{C}^1(B_0 \times B_1^*, V^*)$ and that for any $(q,p,t) \in B_0 \times B_1^* \times [0,1]$ and any $(\delta q, \delta p) \in B_0 \times B_1^*$

$$d\mathcal{J}_t(q,p) \cdot (\delta q, \delta p) = \xi^*_{(q,t)} \cdot \delta p + \big(\partial_q \xi_{(q,t)} \cdot \delta q\big)^* \cdot p .$$

Moreover, we get from (P_2) and (3.80) that there exists $c > 0$ such that for any $(q,p,t) \in B_0 \times B_1^* \times [0,1]$,

$$|\mathcal{J}_t(q,p)|_{V^*} = |\xi^*_{(q,t)} \cdot p|_{V^*} \leq c(|q|_{B_0} + 1)|p|_{B_1^*}$$

and

$$|d\mathcal{J}_t(q,p)|_{\mathcal{L}(B_0 \times B_1^*, V^*)} \leq c(|q|_{B_0} + 1)(|p|_{B_1^*} + 1) .$$

□

The next theorem finally proves the local existence and uniqueness of the solutions when the Hamiltonian is defined with the cost function of the adapted norm setup

$$C(v,t) = \frac{1}{2} \langle v, \ell_t v \rangle_V .$$

The core of the proof lies on the more general Proposition 5.3.

Theorem 5.1 (Local existence and uniqueness of the solutions to the reduced Hamiltonian system)**.** *Let us consider the* ***adapted norm setup****. Let (B_0, B_1) be two Banach spaces* ***compatible*** *with the system (B, V, ξ). Assume the (H_1^ξ) and (H_{B_0,B_1}^ξ) conditions. Then we have:*

1. *The momentum map $\mathcal{J}$ belongs to $\mathcal{L}ip_{unif}^{loc}(B_0 \times B_1^* \times [0,1], V^*)$ and $\mathcal{J}_t$ is locally bounded on $B_0 \times B_1^*$. Note m_t^r its supremum and k_t^r its Lipschitz constant on the ball $\mathcal{B}(0,r)$ of $B_0 \times B_1^*$.*
2. *Assume that for any $r > 0$, the function $t \mapsto |\ell_t^{-1}|(m_t^r + k_t^r)$ belongs to $L^1([0,1], \mathbb{R})$.*

   Then for any $r > 0$, there exists $\epsilon > 0$ such that the Cauchy problem associated to the reduced Hamiltonian system for any initial condition $(q_0, p_0) \in \mathcal{B}(0,r)$ in $B_0 \times B_1^*$ and $t_0 \in [0,1[$ has a unique solution on the interval $[t_0, t_0+\epsilon] \cap [0,1]$. Moreover, this solution stays in $B_0 \times B_1^*$.

Proof. In the adapted norm setup, the optimal vector field is given by the function

$$v^*(q,p,t) = \ell_t^{-1} K \mathcal{J}(q,p,t)\,.$$

The assumption of 2) allows to verify that v^* satisfies the conditions of Proposition 5.3 in order to apply the Cauchy-Lipschitz Theorem 4.1. Note h the reduced Hamiltonian system:

$$h(q_t,p_t,t) = \begin{pmatrix} \dot{q}_t \\ \\ \dot{p}_t \end{pmatrix} = \begin{pmatrix} \frac{\partial H_r}{\partial p}(q_t,p_t,t) \\ \\ -\frac{\partial H_r}{\partial q}(q_t,p_t,t) \end{pmatrix} = \begin{pmatrix} \xi_{(q_t,t)}(v_t^*) \\ \\ -\left(\partial_q \xi_t(q_t)(v_t^*)\right)^* \cdot p_t \end{pmatrix}.$$

The compatibility assumption and Proposition 5.1 ensure that there exists a continuous linear embedding

$$B_0 \times B_1^* \hookrightarrow B \times B^* \tag{3.81}$$

and implies that the system can be defined on $B_0 \times B_1^*$ and is stable. We have thus $B_0 \times B_1^*$ a Banach space and $h : B_0 \times B_1^* \times [0,1] \to B_0 \times B_1^*$ a measurable function.

The second condition of the Cauchy-Lipschitz Theorem 4.1 is satisfied for the point $(q,p) = (0,0)$. We have indeed for almost any $t \in [0,1]$, $\frac{\partial H_r}{\partial q}(0,0,t) = 0$ and since $\mathcal{J}$ is linear with respect to p, $v^*(0,0,t) = 0$ so that $\frac{\partial H_r}{\partial p}(0,0,t) = 0$.

Now, Proposition 5.4 says that $\mathcal{J} \in \mathcal{L}ip_{unif}^{loc}(B_0 \times B_1^* \times [0,1], V^*)$ and that $\mathcal{J}_t$ is locally bounded. Therefore, since for any $t \in]0,1]$, ℓ_t^{-1} is linear and continuous, v_t^* is also locally bounded and locally Lipschitz continuous. Indeed, for any $r > 0$, the supremum and the Lipschitz constant of v_t^* restricted to the ball $\mathcal{B}(0,r)$ are respectively bounded by $|\ell_t^{-1}| m_t^r$ and $|\ell_t^{-1}| k_t^r$. The assumption $t \mapsto |\ell_t^{-1}|(m_t^r + k_t^r) \in L^1([0,1], \mathbb{R})$ implies thus that v^* is at least of class $\mathcal{L}ip_{int}^{loc}$. Proposition 5.3 says then that h belongs to $\mathcal{L}ip_{int}^{loc}(B_0 \times B_1^* \times [0,1], B_0 \times B_1^*)$. The Cauchy-Lipschitz theorem can thus be applied. $\square$

Corollary 5.1. *Let us consider the* ***nondegenerate adapted norm setup****. Then for any set (B_0, B_1) compatible with the system (B, V, ξ) and that satisfies the (H_1^ξ) and(H_{B_0,B_1}^ξ)*

conditions, there exists a unique maximal solution to the Cauchy problem associated to the reduced Hamiltonian system for any initial condition $(q_0, p_0) \in B_0 \times B_1^*$. This solutions stays in $B_0 \times B_1^*$.

Proof. The assumption of point 2) of the previous theorem is always satisfied in the **nondegenerate adapted norm setup**. Indeed, $t \mapsto \ell_t^{-1}$ is bounded on $[0,1]$ (see Proposition 3.5). Moreover, with the notation of the theorem, Proposition 5.4 says that for any $t \in [0,1]$ and any $r > 0$, m_t^r and k_t^r are bounded uniformly with respect to time. Hence, for any $r > 0$, $t \mapsto |\ell_t^{-1}|(m_t^r + k_t^r)$ belongs to $L^1([0,1], \mathbb{R})$. □

5.3 Applications with the growth dynamic

Let us recall that the operator $\xi : B \times [0,1] \to \mathcal{L}(V, B)$ induced by the **growth dynamic** is formally given by

$$\xi_{(q,t)}(v) = (x \mapsto \mathbb{1}_{\tau(x) \leq t}\, v(q(x)))\,. \tag{3.82}$$

The next three configurations are defined with the growth dynamic and under the (H_1^V) conditions. Theorem 5.1 and its Corollary 5.1 will allow us to show in each case the local existence and uniqueness of solutions to the reduced Hamiltonian system.

Discrete coordinate space

The case of discrete shapes calls for the nondegenerate adapted norm setup and is thus cover by Corollary 5.1. We have $B = B^* = (\mathbb{R}^d)^k$ and there is in general no reason to work with any particular subspaces B_0 or B_1^*.

Shapes with initial boundary

Consider the situation where X is a compact submanifold and $q : X \to \mathbb{R}^d$. The choice of B_1^* depends then on the attachment term. For example, if the derivation of the attachment term leads to a momentum that can be represented by an element of $L^\infty(X, \mathbb{R}^d)$, the natural configuration is to define

$$\begin{aligned} B_0 &= B = L^\infty(X, \mathbb{R}^d)\,, \\ B_1 &= L^1(X, \mathbb{R}^d)\,. \end{aligned}$$

We saw in Section 3.2 that the current attachment term leads to a situation a bit more complex. Let us recall the B space introduced in Definition 3.1.

Example 5.2 (Tube Case)**.** *We defined a measure μ on X and we recall that for any Borel set $A \subset X$, we have*

$$\mu(A) = \mathcal{H}^k(A) + \mathcal{H}^{k-1}(A \cap \partial X)\,.$$

$L_\mu^\infty(X, \mathbb{R}^d)$ is the space of functions from X to $\mathbb{R}^d$ defined μ-almost everywhere and bounded, quotiented by the space of null functions.

To avoid any confusion, we will note here $L_{\mathcal{H}^k}^\infty(X, \mathbb{R}^d)$ the usual $L^\infty(X, \mathbb{R}^d)$ associated to the Hausdorff measure. When a class of function of $L_{\mathcal{H}^k}^\infty(X, \mathbb{R}^d)$ is defined $\mathcal{H}^k$-almost *everywhere on X, a class of function of $L^\infty_\mu(X,\mathbb{R}^d)$ is defined $\mathcal{H}^k$-almost everywhere on $\overset{\circ}{X}$ and $\mathcal{H}^{k-1}$-almost everywhere on ∂X. We introduce then*

$$\begin{aligned} B &= L^\infty_\mu(X,\mathbb{R}^d)\,, \\ B_0 &= B\,, \\ B_1 &= L^1_\mu(X,\mathbb{R}^d)\,. \end{aligned}$$

Proposition 5.5. *Let be $B = L^\infty_\mu(X,\mathbb{R}^d)$. If ξ is given by the* ***growth dynamic*** *then under the (H^V_1) conditions, the couple (B_0,B_1) introduced in the Example 5.2 with*

$$\begin{aligned} B_0 &= B\,, \\ B_1 &= L^1_\mu(X,\mathbb{R}^d)\,, \end{aligned}$$

is ***compatible with the system*** *(B,V,ξ) and the $(H^\xi_{B_0,B_1})$ conditions are satisfied.*

Proof. We note $|q|_{\infty,\mu}$ the essential supremum with respect to μ. $(L^\infty_\mu(X,\mathbb{R}^d),|\cdot|_{\infty,\mu})$ is a Banach space. Let us show now that (B_0,B_1) is compatible with B. We have trivially $B_0 = B \hookrightarrow B_1$ with B dense in B_1. Therefore, (B_0,B_1) is compatible with B.

Under the (H^V_1) conditions, there exists $c>0$ such that for any $q\in B$, any $t\in[0,1]$ and any $v\in V$

$$|\xi_t(q)(v)|_B \le c|v|_V(|q|_{\infty,\mu}+1) \le c|v|_V(|q|_B+1)\,.$$

Consequently, $\xi : B\times[0,1]\to\mathcal{L}(V,B)$.

Moreover, we can extend ξ to B_1. For any $q\in B^1$, any $t\in[0,1]$ and any $v\in V$ by

$$\xi^1_t(q)(v) = \mathbb{1}_{\tau\le t}\, v\circ q\,. \tag{3.83}$$

We have then likely with the same constant $c>0$ that for any $q\in B_1$, any $t\in[0,1]$ and any $v\in V$

$$|\xi_t(q)(v)|_{B_1} \le c|v|_V(|q|_{B_1}+\mu(X))\,.$$

Consequently, $\xi^1 : B_1\times[0,1]\to\mathcal{L}(V,B_1)$ and (B_0,B_1) is compatible with the system (B,V,ξ).

Let us check now that ξ^1 is Gâteaux differentiable as a function with values in $\mathcal{L}(V,B_1)$ at any location $q\in B_1$ (and not only at location $q\in B_0$). Indeed, we have for any $q\in B_1$, $\delta q\in B_1$ and $v\in V$

$$\begin{aligned} |(\xi^1(q+\epsilon\delta q,t)(v)-\xi^1(q,t)(v))/\epsilon - \mathbb{1}_{\tau\le t}\, dv(q)\cdot\delta q|_{B_1} &\le \int_0^1 |dv(q+s\epsilon\delta q)-dv(q))\cdot\delta q|_{B_1} ds \\ &\le \int_X c|v|_V(2\wedge\epsilon|\delta q(x)|_{\mathbb{R}^d})|\delta q(x)|_{\mathbb{R}^d} d\mu(x)\,, \end{aligned}$$

where we denote $a\wedge b=\min(a,b)$. We get indeed from H^V_1 that $|dv(x)-dv(y)|\le c|v|_V|x-y|$ and $|dv(x)-dv(y)|\le|dv(x)|+|dv(y)|\le 2c|v|_V$. Using the dominated convergence theorem, we get that $\int_X c(2\wedge\epsilon|\delta q(x)|)|\delta q(x)|d\mu(x)\to 0$ as $\epsilon\to 0$ and $\partial_q\xi^1(q,t)(v)\cdot\delta q =$

$\mathbb{1}_{\tau\le t}\, dv(q)\cdot\delta q$ for which we have

$$|\mathbb{1}_{\tau\le t}\, dv(q)\cdot\delta q|_{B_1}\le c|v|_V|\delta q|_{B_1}\,,$$

so that

$$\partial_q\xi^1(q,t)\in\mathcal{L}(B_1,\mathcal{L}(V,B_1)) \text{ with } |\partial_q\xi^1(q,t)|_{\mathcal{L}(B_1,\mathcal{L}(V,B_1))}\le c\,.$$

At last, for any $q,q'\in B_0$, any $\delta q\in B_1$, any $t\in[0,1]$ and any $v\in V$

$$\begin{aligned}&|(\xi_{(q,t)}-\xi_{(q',t)})(v)|_{B_0}\le c|v|_V|q-q'|_{B_0}\\ &\left|\big(\partial_q\xi^1_t(q)-\partial_q\xi^1_t(q')\big)(v)\cdot\delta q\right|_{B_1}\le c|v|_V|q-q'|_{B_0}|\delta q|_{B_1}\,.\end{aligned}$$

Therefore, the $(H^\xi_{B_0,B_1})$ conditions are satisfied. □

Remark 5.1. *An important point to note here is that even if $\partial_q\xi^1(q,t)$ is defined for any $q\in B_1$ as an element of $\mathcal{L}(B_1,\mathcal{L}(V,B_1))$ from directional derivative, the continuity is only on B_0 for the topology of B_0. In particular, $\xi^1(.,t)$ is **not** C^1 on B_1 so that H^ξ_1 cannot be verified for $B=B_1$.*

In fine, since B_1 can be identified with $L^1_{\mathcal{H}^k}(X,\mathbb{R}^d)\times L^1_{\mathcal{H}^{k-1}}(\partial X,\mathbb{R}^d)$, we get that $B_1^*=L^\infty_\mu(X,\mathbb{R}^d)\simeq L^\infty_{\mathcal{H}^k}(X,\mathbb{R}^d)\times L^\infty_{\mathcal{H}^{k-1}}(\partial X,\mathbb{R}^d)$ and we have as wanted

$$B_0=L^\infty_\mu(X,\mathbb{R}^d)=B_1^*\,,$$

and for any $\delta q\in B_0$ and any $p\in B_1^*$, the action of p on δq is given by

$$(p\,|\,\delta q)=\int_X\langle p(x),\delta q(x)\rangle_{\mathbb{R}^d}\,d\mu(x)$$

and is well defined.

This configuration calls again for the nondegenerate adapted norm setup and the local existence and uniqueness of the solutions of the reduced Hamiltonian system in $B_0\times B_1^*$ are given by Corollary 5.1.

Horns represented by currents

The horns with the current attachment term are a specific case of the previous configuration. As we said in Section 3.3, the image of the first layer $\{0\}\times X_0$ is reduced to a point. This implies that the boundary component of the momentum (of an optimal solution) is null on this set. A class of function of $L^\infty_\mu(X,\mathbb{R}^d)$ is defined $\mathcal{H}^{k-1}$-almost everywhere on $\{0\}\times X_0$. This allows to consider the following setup.

Definition 5.3 (Horn setup)**.** *We call the **horn setup** the following configuration.*

*Consider $B=L^\infty_\mu(X,\mathbb{R}^d)$ where $X=[0,1]\times X_0$, $\partial X_0=\emptyset$, τ is the projection on the first coordinate and ξ given by the **growth dynamic**. The shapes are actually modeled by the elements of*

$$B_0=\{q\in B\,|\,\exists y\in\mathbb{R}^d, q(0,\cdot)=y\ \mathcal{H}^{k-1}\text{-a.e. on } X_0\}\,. \tag{3.84}$$

We consider $B_1 = L^1_\mu(X, \mathbb{R}^d)$ *and the following subspace*

$$\widetilde{B_1^*} = \{\ p \in L^\infty_\mu(X, \mathbb{R}^d) \mid p(x) = 0\ \mathcal{H}^{k-1}\text{-a.e. on } \partial X\ \} \simeq L^\infty_{\mathcal{H}^k}(X, \mathbb{R}^d) \tag{3.85}$$

of $B_1^* = L^\infty_\mu(X, \mathbb{R}^d)$.

Remark 5.2. *Note that the more natural condition on the momenta would be* $p(x) = 0\ \mathcal{H}^{k-1}$*-a.e. on* X_0 *but since* $\partial X = X_0 \cup X_1$ *and since the momenta associated to* X_1 *play no role in the evolution of the shape, we consider this subspace* $\widetilde{B_1^*}$ *to simplify the notation.*

Proposition 5.6. *Consider the **horn setup**. Under the* (H_1^V) *conditions,* (B_0, B_1) *is **compatible with the system*** (B, V, ξ) *and the* $(H^\xi_{B_0,B_1})$ *conditions are satisfied.*

Proof. We note $|q|_{\infty,\mu}$ the essential supremum with respect to μ. $(B, |\cdot|_{\infty,\mu})$ is a Banach space. Let us show that $(B_0, |\cdot|_{\infty,\mu})$ is a Banach space. Let $(q_n)_{n\geq 0}$ be a Cauchy sequence in B_0. The sequence converges to a function q in B. By definition, for any $n \geq 0$, there exists $y_n \in \mathbb{R}^d$ such that for μ-almost every $x_0 \in X_0$, $q_n(0, x_0) = y_n$. The sequence $(y_n)_{n\geq 0}$ is a Cauchy sequence in $\mathbb{R}^d$ and converges thus to $y \in \mathbb{R}^d$. We have finally

$$\begin{aligned} |q_{|\{0\}\times X_0} - y|_{\infty,\mathcal{H}^{k-1}} &\leq |q_{|\{0\}\times X_0} - y_n|_{\infty,\mathcal{H}^{k-1}} + |y_n - y|_{\mathbb{R}^d} \\ &\leq |q_{|\{0\}\times X_0} - q_{n|\{0\}\times X_0}|_{\infty,\mathcal{H}^{k-1}} + |y_n - y|_{\mathbb{R}^d} \underset{n\to\infty}{\longrightarrow} 0\,. \end{aligned}$$

Therefore, $\mathcal{H}^{k-1}(\{x_0 \in X_0 \,|\, q(0, x_0) \neq y\}) = 0$ so that $q \in B_0$.

Since B_0 is a closed subspace of $B = L^\infty_\mu(X, \mathbb{R}^d)$, stable for the growth dynamic, we deduce immediately from Proposition 5.5 that $(H^\xi_{B_0,B_1})$ conditions hold.

□

Remark 5.3. *Note in this last example that* B_0 *is a strict closed subspace of* B *and* $B \not\subseteq B_1$*. Moreover, as mentioned previously, when consider the current data attachment term, the momentum will be an element of* $\widetilde{B_1^*}$ *with is also a strict closed subspace of* B^1_*.

The interest of these specific momenta is to give a more explicit expression of the momentum map. Its restriction to $B_0 \times \widetilde{B_1^*} \times [0, 1]$ is indeed given by

$$\begin{aligned} (\mathcal{J}_\xi(q, p, t) \,|\, v) &= (p \,|\, \xi_{(q,t)}(v)) &(3.86)\\ &= \int_X \langle p(x), \xi_{(q,t)}(v)(x)\rangle_{\mathbb{R}^d}\, d\mathcal{H}^k(x)\,. &(3.87) \end{aligned}$$

As seen in Section 3.3, this integral expression of the momentum map implies a degenerate behavior at time 0 : the norm of the momentum map tends to 0 when t tends to 0. To counter this phenomenon, we use the cost function of the adapted norm setup with an operator ℓ that also tends to 0 when t tends to 0. The function giving the optimal vector field

$$v^*(q, p, t) = \ell_t^{-1} K_V \mathcal{J}(q, p, t) \tag{3.88}$$

is not defined at time 0 and the norm of ℓ_t^{-1} tends to $+\infty$ when t tends to 0. We will thus need to verify that v^* still satisfies the conditions of Theorem 5.1.

Proposition 5.7. *Let us consider the combined* ***adapted norm setup*** *and* ***horn setup****. Assume the (H_1^V) conditions. Assume that there exist $M > 0$ and $s \in [0, 2[$ two constants such that for any $t \in]0, 1]$*

$$|\ell_t^{-1}|_{op} \leq \frac{M}{t^s}\,. \tag{3.89}$$

Then there exists a unique maximal solution to the Cauchy problem associated to the reduced Hamiltonian system for any initial condition $(q_0, p_0) \in B_0 \times \widetilde{B_1^*}$. This solutions stays in $B_0 \times \widetilde{B_1^*}$.

Proof. Proposition 5.6 says that (B_0, B_1) is **compatible with the system** (B, V, ξ) and the $(H^{\xi}_{B_0,B_1})$ conditions are satisfied.

Note also that for $(q, p) \in B_0 \times \widetilde{B_1^*}$, if $\overline{p} = (\partial_q \xi(q, t)(v))^* \cdot p$ then $\overline{p} \in \widetilde{B_1^*}$. Indeed, we have $\overline{p} \in B_*^1$ and $\overline{p}(x) = \mathbb{1}_{\tau(x)\leq t} dv(q(x))^* \cdot p(x)$ μ-a.e. so that $\overline{p}(x) = 0$ $\mathcal{H}^{k-1}$-a.e. on ∂X and $\overline{p} \in \widetilde{B_1^*}$. This implies that the reduced hamiltonian h^{v^*} (see equation (3.78)) can be restricted to $h^{v^*} : B_0 \times \widetilde{B_1^*} \times [0, 1] \to B_0 \times \widetilde{B_1^*}$. To complete the proof, we need to show that this restriction belongs to $\mathcal{L}ip^{loc}_{int}((B_0 \times \widetilde{B_1^*} \times [0, 1], B_0 \times \widetilde{B_1^*})$ and use our Cauchy-Lipschitz Theorem 4.1.

Proceeding as in the proof Theorem 5.1 it is sufficient to check that $v^* : B_0 \times \widetilde{B_1^*} \times [0, 1] \to V$ is a function of class $\mathcal{L}ip^{loc}_{int}$. We need to show for m_t^r the supremum and k_t^r the Lipschitz constant on the ball $\mathcal{B}(0, r)$ of $B_0 \times \widetilde{B_1^*}$ of $\mathcal{J}_t$ that the function $t \mapsto |\ell_t^{-1}|(m_t^r + k_t^r)$ belongs to $L^1([0, 1], \mathbb{R})$ for any $r > 0$. The idea is to use the pointwise expression of the momentum map to refine the results of Proposition 5.4. We deduce from equation (3.87) and the decomposition of X that for any $(q, p, t) \in B_0 \times \widetilde{B_1^*} \times [0, 1]$ and any $v \in V$, the momentum map is given by

$$\big(\mathcal{J}(q, p, t)\,|\, v\big) = \int_0^t \int_{X_0} \langle p(s, x_0), v(q(s, x_0))\rangle_{\mathbb{R}^d}\, d\mathcal{H}^{k-1}(x_0) ds\,. \tag{3.90}$$

Let $c > 0$ be the constant given by (H_1^V). We have then

$$\begin{aligned}\big|(\mathcal{J}_t(q, p)\,|\, v)\big| &\leq tc|p|_\infty |v|_V (|q|_\infty + 1)\mathcal{H}^{k-1}(X_0)\\ &\leq tc|p|_{B_1^*} |v|_V (|q|_{B_0} + 1)\mathcal{H}^{k-1}(X_0)\,,\end{aligned}$$

so that $m_t^r \leq tcr(r + 1)\mathcal{H}^{k-1}(X_0)$. Moreover, we have for any $(\delta q, \delta p) \in B_0 \times \widetilde{B_1^*}$

$$\begin{aligned}&\big|(d\mathcal{J}_t(q, p) \cdot (\delta q, \delta p)\,|\, v)\big|\\ &\quad= \left|\int_0^t \int_{X_0} \langle \delta p(s, x_0), v(q(s, x_0))\rangle_{\mathbb{R}^d} + \langle p(s, x_0), dv(q(s, x_0)) \cdot \delta q(s, x_0)\rangle_{\mathbb{R}^d}\, d\mathcal{H}^{k-1}(x_0) ds\right|\\ &\quad\leq \int_0^t c|\delta p|_\infty |v|_V (|q|_\infty + 1) + c|p|_\infty |v|_V |\delta q|_\infty \mathcal{H}^{k-1}(X_0) ds\\ &\quad\leq tc|v|_V (|q|_\infty + |p|_\infty + 1)(|\delta q|_\infty + |\delta p|_\infty)\mathcal{H}^{k-1}(X_0)\\ &\quad\leq tc|v|_V (|q|_{B_0} + |p|_{B_1^*} + 1)(|\delta q|_{B_0} + |\delta p|_{B_1^*})\mathcal{H}^{k-1}(X_0)\,,\end{aligned}$$

so that $k_t^r \leq tc(2r + 1)\mathcal{H}^{k-1}(X_0)$.

Consequently, there exists for any $r > 0$ a constant $c^r > 0$ such that for any $t \in [0, 1]$, we have

$$m_t^r + k_t^r \leq tc^r$$

and we deduce with equation (3.89) that the function $t \mapsto |\ell_t^{-1}|(m_t^r + k_t^r)$ belongs to $L^1([0,1],\mathbb{R})$ for any $r > 0$. So we can applied a localized version of Theorem 5.1 to $B_0 \times \widetilde{B_1^*}$ that gives the local existence and uniqueness of the solutions to the reduced Hamiltonian system and the stability with respect to $B_0 \times \widetilde{B_1^*}$. □

5.4 Specific theorems of global existence

We will now show that, in the previous configurations, the solutions do not explode. The idea is for any solution (q,p) defined on a maximal interval $I \subset [0,1]$, to control the reduced Hamiltonian $I \ni t \mapsto H_r(q_t, p_t, t)$ then deduce that neither q or p can explode. The solution could thus be extended.

General coordinate space with the current norm

Given an initial condition $(q_0, p_0) \in B_0 \times \widetilde{B_1^*}$, we just proved previously the existence and uniqueness of a maximal solution $(q,p) = \Psi(q_0,p_0) \in \mathcal{C}(I, B_0 \times \widetilde{B_1^*})$ with the growth dynamic (i.e. $\xi_{(q,t)}(v) = \mathbb{1}_{\tau \leq t} v \circ q$) in two configurations.

1. In the tube case, with the non degenerate adapted norm setup and with

$$\begin{aligned} B_0 &= B = L_\mu^\infty(X, \mathbb{R}^d)\,, \\ \widetilde{B_1^*} &= B_1^* = L_\mu^\infty(X, \mathbb{R}^d)\,. \end{aligned}$$

2. In the horn case, with the adapted norm setup and with

$$\begin{aligned} B &= L_\mu^\infty(X, \mathbb{R}^d)\,, \\ B_0 &= \{q \in B \,|\, \exists y \in \mathbb{R}^d, q(0,\cdot) = y \ \mathcal{H}^{k-1}\text{-a.e. on } X_0\}\,, \\ B_1^* &= L_\mu^\infty(X, \mathbb{R}^d)\,, \\ \widetilde{B_1^*} &= \{\ p \in L_\mu^\infty(X, \mathbb{R}^d) \mid p(x) = 0 \ \mathcal{H}^{k-1}\text{-a.e. on } \partial X\ \} \simeq L^\infty_{\mathcal{H}^k}(X, \mathbb{R}^d)\,. \end{aligned}$$

Note that the non degenerate adapted norm setup is a subcase of the adapted norm setup. Consider now a maximal solution $(q,p) = \Psi(q_0,p_0) \in \mathcal{C}(I, B_0 \times \widetilde{B_1^*})$ such that $I = [0, t_{\max}[\subset [0,1]$. We will show that this solution does not explode under the following assumptions common to both cases

— the cost function satisfies the adapted norm setup ($C(v,t) = \frac{1}{2}\langle v, \ell_t v\rangle_V$ (see Definition 3.3)),

— $\ell \in \mathcal{C}^1([0,1], \mathcal{L}(V))$,

— $B = L_\mu^\infty(X, \mathbb{R}^d)$ and $B_1^* = L_\mu^\infty(X, \mathbb{R}^d)$.

The three propositions following the next lemma aim to give a control independent of time on the momentum map and then on the reduced Hamiltonian. With this last control, we will prove in one theorem for each of the above cases that the solution cannot explode i.e. $I = [0,1]$.

Lemma 5.2. *The cost function is derivable with respect to time. Moreover, let $\alpha : [0,1] \to \mathbb{R}_+$ be a lower bound function associated with ℓ_t (see Definition 3.3). There exists $c > 0$ such that for any $(q,p,t) \in B \times B^* \times [0,1]$ and any $v \in V$ we have*

1. $H_r(q,p,t) = C(v^*(q,p,t),t) = \frac{1}{2}\langle v^*(q,p,t), \ell_t v^*(q,p,t)\rangle_V \geq 0\,,$
2. $|\mathcal{J}_\xi(q,p,t)|^2_{V^*} \leq \frac{c}{\alpha(t)} H_r(q,p,t)\,,$
3. $|v^*(q,p,t)|_V \leq \sqrt{\frac{c}{\alpha^3(t)}}\,|\mathcal{J}_\xi(q,p,t)|_{V^*}\,,$

where we recall that $v^*_t = \ell_t^{-1} K_V \mathcal{J}_\xi(q_t,p_t,t)$.

Proof. 1) We assume in the definition of the adapted norm setup that for any $t \in [0,1]$ and any $v \in V$, $C(v,t) = \frac{1}{2}\langle v, \ell_t v\rangle_V \geq \alpha(t)|v|^2_V \geq 0$. Moreover, we have the explicit expression of the reduced Hamiltonian

$$\begin{aligned} H_r(q,p,t) &= H(q,p,v^*_t,t) = (\mathcal{J}_\xi(q,p,t)\,|\,v^*_t) - C(v^*_t,t) \\ &= \langle K_V\mathcal{J}_\xi(q,p,t), v^*_t\rangle_V - \frac{1}{2}\langle v^*_t, \ell_t v^*_t\rangle_V = \frac{1}{2}\langle v^*_t, \ell_t v^*_t\rangle_V = C(v^*_t,t)\,. \end{aligned}$$

2) Let us consider $v \in V$, $t \in]0,1]$ and $w = \ell_t^{-1}v$. We have then

$$\langle v, \ell_t^{-1}v\rangle_V = \langle w, \ell_t w\rangle_V \geq \alpha(t)|w|^2_V = \alpha(t)|\ell_t^{-1}v|^2_V\,.$$

Since $|v|_V = |\ell_t \circ \ell_t^{-1}v|_V \leq |\ell_t|_{op}|\ell_t^{-1}v|_V$, we get $|\ell_t^{-1}v|_V \geq \frac{1}{|\ell_t|_{op}}|v|_V$ and thus

$$\langle v, \ell_t^{-1}v\rangle_V \geq \frac{\alpha(t)}{|\ell_t|^2_{op}}|v|^2_V\,.$$

Finally, since $H_r(q,p,t) = \frac{1}{2}\langle K_V\mathcal{J}_\xi(q,p,t), \ell_t^{-1}K_V\mathcal{J}_\xi(q,p,t)\rangle_V$, we have for $t \in [0,1]$

$$H_r(q,p,t) \geq \frac{\alpha(t)}{2|\ell_t|^2_{op}}|\mathcal{J}_\xi(q,p,t)|^2_{V^*}$$

and we get the result since $t \to |\ell|_{op}$ is continuous and so bounded.

3) At last, we have $v^*_t = \ell_t^{-1}K_V\mathcal{J}_\xi(q_t,p_t,t)$, so that $|v^*(q,p,t)|_V \leq |\ell_t^{-1}|_{op}\,|\mathcal{J}_\xi(q,p,t)|_{V^*}$. Since we get from Proposition 3.5 that $|\ell_t^{-1}|_{op} \leq \frac{1}{\alpha(t)}$, we get the result. □

The time derivative of the reduced Hamiltonian depends on the partial derivative with respect to time of the cost function C and the momentum map $\mathcal{J}_\xi$. The first one does not depends on the variable (q,p). The main issue is thus to control the evolution of the momentum map. The next proposition shows that this evolution actually only depends on the initial state of the variable.

Proposition 5.8 (Control on the Momentum Map)**.** *Under the (H_1^V) conditions, the momentum map admits a partial derivative with respect to time at almost every time. Moreover, there exists a constant $c > 0$ such that for any $t \in [0, t_{\max}[$*

$$\int_0^t \left|\frac{\partial \mathcal{J}_\xi}{\partial t}(q_s,p_s,s)\right|_{V^*} ds \leq c|p_0|_{B^*}(|q_0|_B + 1)\,. \tag{3.91}$$

Proof. Let recall that $\mathcal{J}_\xi(q,p,t) = \xi^*_{(q,t)} \cdot p$ and that

$$\xi_{(q,t)}(v) = \big(x \mapsto \mathbb{1}_{\tau(x)\leq t} v(q(x))\big)\,.$$

The function ξ is not derivable with respect to time in $B = L^\infty_\mu(X,\mathbb{R}^d)$. The pointwise expression of the momentum allows yet to avoid this problem. When τ is written as a projection in $X = [0,1] \times X_0$, the expression of the momentum map is given (see Section 3.2) for any $q \in B$, any $p \in B_1^*$, any $t \in [0,1[$ and any $\tilde{v} \in V$ by

$$\begin{aligned}(\mathcal{J}_\xi(q,p,t)\,|\,\tilde{v}) &= (\mathcal{J}_\xi(q,p,0)\,|\,\tilde{v}) + \int_0^t \int_{X_0} \langle p(s,x_0), \tilde{v}(q(s,x_0))\rangle_{\mathbb{R}^d}\, d\mathcal{H}^{k-1}(x_0) ds \\ &= (\mathcal{J}_\xi(q,p,0)\,|\,\tilde{v}) + \int_0^t \int_{X_0} \delta^{p(s,x_0)}_{q(s,x_0)}(\tilde{v})\, d\mathcal{H}^{k-1}(x_0) ds\,.\end{aligned}$$

Consider here $g : [0,1] \to V^*$ defined for almost all t by

$$g(t) = \int_{X_0} \delta^{p(t,x_0)}_{q(t,x_0)}\, d\mathcal{H}^{k-1}(x_0)\,.$$

The continuity of this function depends on the spatial regularity of q and p. However, there exists under the (H_1^V) conditions, a constant $c > 0$ such that for any $y_1, y_2 \in \mathbb{R}^d$

$$|\delta^{y_2}_{y_1}(\tilde{v})| \leq c|\tilde{v}|_V |y_2|_{\mathbb{R}^d}(|y_1|_{\mathbb{R}^d} + 1)\,,$$

so that

$$\begin{aligned}\int_0^1 |g(s)|_{V^*} ds &\leq c\int_0^1 \int_{X_0} |p(s,x_0)|_{\mathbb{R}^d}(|q(s,x_0)|_{\mathbb{R}^d} + 1)\, d\mathcal{H}^{k-1}(x_0) ds \\ &\leq c\int_X |p(x)|_{\mathbb{R}^d}(|q(x)|_{\mathbb{R}^d} + 1)\, d\mathcal{H}^k(x) \leq c|p|_{B^*}(|q|_B + 1) < \infty\,. \end{aligned} \tag{3.92}$$

Therefore, $g \in L^1([0,1], V^*)$ implies that $t \mapsto \mathcal{J}_\xi(q,p,t) = \mathcal{J}_\xi(q,p,0) + \int_0^t g(s)\, ds$ is absolutely continuous on $[0,1[$, derivable for almost every $t \in [0,1]$ and this derivative, when there exists, is

$$\frac{\partial \mathcal{J}_\xi}{\partial t}(q,p,t) = g(t) = \int_{X_0} \delta^{p(t,x_0)}_{q(t,x_0)}\, d\mathcal{H}^{k-1}(x_0)\,.$$

Moreover, if we consider again our solution $(q,p) = \Psi(q_0,p_0) \in \mathcal{C}([0,t_{\max}[, B \times B_1^*)$, we saw in Section 3.2 (equation (3.43)) that with the growth dynamic this partial derivative does not depend on q_t and p_t but on the initial conditions q_0 and p_0. We have more precisely at almost any time $t \in [0, t_{\max}[$ and for any $\tilde{v} \in V$

$$\begin{aligned}\left(\frac{\partial \mathcal{J}_\xi}{\partial t}(q_t,p_t,t)\,\middle|\,\tilde{v}\right) &= \int_{X_0} \langle p_t(t,x_0), \tilde{v}(q_t(t,x_0))\rangle_{\mathbb{R}^d}\, d\mathcal{H}^{k-1}(x_0) \\ &= \int_{X_0} \langle p_0(t,x_0), \tilde{v}(q_0(t,x_0))\rangle_{\mathbb{R}^d}\, d\mathcal{H}^{k-1}(x_0) \\ &= \left(\frac{\partial \mathcal{J}_\xi}{\partial t}(q_0,p_0,t)\,\middle|\,\tilde{v}\right)\,.\end{aligned}$$

We get then the final equation by (3.92). Note that we could prove this result with the coarea formula when X is a general submanifold and τ satisfies some simple regularity conditions (smooth and $d\tau(x) \neq 0$) . $\square$

Proposition 5.9 (Control on the Hamiltonian 1)**.** *Let $\epsilon \in]0, t_{\max}[$.*

1. *The function $t \to H_r(q_t, p_t, t)$ is absolutely continuous on $[\epsilon, t_{\max}[$.*
2. *There exists $M > 0$ such that for almost every time $t \in [\epsilon, t_{\max}[$,*

$$\left| \frac{d}{dt} \ln \big(1 + MH_r(q_t, p_t, t)\big) \right| \leq M^2 \left(\left| \frac{\partial \mathcal{J}_\xi}{\partial t}(q_t, p_t, t) \right|_{V^*} + 1 \right) .$$

Proof. We have $H_r(q_t, p_t, t) = \frac{1}{2} \langle K_V \mathcal{J}_\xi(q, p, t), \ell_t^{-1} K_V \mathcal{J}_\xi(q, p, t) \rangle_V$. Moreover, since $t \to \ell$ is $\mathcal{C}^1$ on $[0, 1]$ and ℓ_t invertible for $t > 0$, we deduce that $t \to \ell_t^{-1}$ is $\mathcal{C}^1$ on $]0, 1[$. Using the fact that $t \to \mathcal{J}(q_t, p_t, t)$ is absolutely continuous on $]0, t_{\max}[$ we deduce the first point.

Then with the previous lemma, since α is non decreasing and $\alpha(\epsilon) > 0$ there exists $M > 0$ such that a.e.

$$\begin{aligned}
\left| \frac{dH_r}{dt}(q_t, p_t, t) \right| &\leq M |\mathcal{J}_\xi(q_t, p_t, t)|_{V^*} \left| \frac{\partial \mathcal{J}_\xi}{\partial t}(q_t, p_t, t) \right|_{V^*} + M |\mathcal{J}_\xi(q_t, p_t, t)|_{V^*}^2 \\
&\leq M \left(1 + |\mathcal{J}_\xi(q_t, p_t, t)|_{V^*}^2\right) \left(\left| \frac{\partial \mathcal{J}_\xi}{\partial t}(q_t, p_t, t) \right|_{V^*} + 1 \right) \\
&\leq M \left(1 + MH_r(q_t, p_t, t)\right) \left(\left| \frac{\partial \mathcal{J}_\xi}{\partial t}(q_t, p_t, t) \right|_{V^*} + 1 \right) .
\end{aligned}$$

Hence,

$$\left| \frac{d}{dt} \ln \big(1 + MH_r(q_t, p_t, t)\big) \right| \leq \frac{M \left| \frac{dH_r}{dt}(q_t, p_t, t) \right|}{1 + MH_r(q_t, p_t, t)} \leq M^2 \left(\left| \frac{\partial \mathcal{J}_\xi}{\partial t}(q_t, p_t, t) \right|_{V^*} + 1 \right) .$$

$\square$

Proposition 5.10 (Control on the Hamiltonian 2)**.** *For any $\epsilon \in]0, t_{\max}[$, there exists an increasing function $\varphi^H : \mathbb{R}^+ \to \mathbb{R}^+$ such that for any $t \in [\epsilon, t_{\max}[$,*

$$H_r(q_t, p_t, t) \leq \frac{1}{2} \varphi^H(|q_\epsilon|_B + |p_\epsilon|_{B^*}) + \frac{1}{2} \varphi^H(|q_0|_B + |p_0|_{B^*})$$

and φ^H does not depend on (q, p).

Proof. We saw with the two previous propositions that the function $[\epsilon, t_{\max}[\ni t \mapsto \ln\big(1 + MH_r(q_t, p_t, t)\big) - \ln\big(1 + MH_r(q_\epsilon, p_\epsilon, \epsilon)\big)$ is bounded by $c_1 |p_0|_{B^*}(|q_0|_B + 1) + c_2$, where c_1 and c_2 are two positive constants independent of t, q and p. Therefore, there exists an increasing function $\varphi_1^H : \mathbb{R}^+ \to \mathbb{R}^+$ such that for any $t \in [\epsilon, t_{\max}[$,

$$H_r(q_t, p_t, t) \leq H_r(q_\epsilon, p_\epsilon, \epsilon) + \varphi_1^H(|q_0|_B + |p_0|_{B^*}) .$$

Likewise, we have for an $M > 0$ sufficiently large (but independent of q_ϵ and p_ϵ) that

$$H_r(q_\epsilon, p_\epsilon, \epsilon) = C(v_\epsilon^*, \epsilon) \leq |\ell_\epsilon|_{op} |v_\epsilon^*|_V^2 \leq M |\mathcal{J}_\xi(q_\epsilon, p_\epsilon, \epsilon)|_{V^*} \leq cM |p_\epsilon|_{B^*}(|q_\epsilon|_B + 1) ,$$

so that there exists therefore another increasing function $\varphi_2^H : \mathbb{R}^+ \to \mathbb{R}^+$ such that $H_r(q_\epsilon, p_\epsilon, \epsilon) \leq \varphi_2^H(|q_\epsilon|_B + |p_\epsilon|_{B^*})$. We get then the conclusion with $\varphi^H = 2(\varphi_1^H + \varphi_2^H)$. $\square$

We just prove that the reduced Hamiltonian system does not explode in finite time. The last step is to deduce that (q, p) is also bounded on $[0, t_{\max}[$ and leads to the next theorems where all the assumptions are recalled.

Theorem 5.2 (Global Solutions of the Reduced Hamiltonian System : Horn Case)**.** *Assume the (H_1^V) conditions. Consider the* ***adapted norm setup****. Assume that $\ell \in \mathcal{C}^1([0,1], \mathcal{L}(V))$ and that there exist $M > 0$ and $s \in [0, 2[$ two constants such that for any $t \in]0,1]$*

$$|\ell_t^{-1}|_{op} \leq \frac{M}{t^s} . \tag{3.93}$$

Consider the Banach spaces

$$\begin{aligned}
&B = L^\infty_\mu(X, \mathbb{R}^d) , \\
&B_0 = \{q \in B \,|\, \exists y \in \mathbb{R}^d, q(0, \cdot) = y \ \mathcal{H}^{k-1}\text{-a.e. on } X_0\} , \\
&\widetilde{B_1^*} = \{\ p \in L^\infty_\mu(X, \mathbb{R}^d) \mid p(x) = 0 \ \mathcal{H}^{k-1}\text{-a.e. on } \partial X\ \} \text{ and } B_1^* = L^\infty_\mu(X, \mathbb{R}^d) .
\end{aligned}$$

Then for any initial condition $(q_0, p_0) \in B_0 \times \widetilde{B_1^*}$, the reduced Hamiltonian system associated to the ***growth dynamic***

$$\xi_{(q,t)}(v) = \mathbb{1}_{\tau \leq t} v \circ q$$

admits a unique solution $(q, p) \in \mathcal{C}([0,1], B_0 \times \widetilde{B_1^*})$.

Proof. Let us show that our local solution (q, p) defined on $[0, t_{\max}[$ is bounded. The lemma gives us for any $\epsilon \in]0,1]$ a constant $M > 0$ such that for any $t \in [\epsilon, t_{\max}[$

$$|v^*(q_t, p_t, t)|_V^2 \leq M H_r(q_t, p_t, t)$$

and we have from the previous proposition

$$H_r(q_t, p_t, t) \leq \frac{1}{2}\varphi^H(|q_\epsilon|_B + |p_\epsilon|_{B^*}) + \frac{1}{2}\varphi^H(|q_0|_B + |p_0|_{B^*}) .$$

It follows that

$$|v^*(q_t, p_t, t)|_V \leq M^{\frac{1}{2}} \left(\frac{1}{2}\varphi^H(|q_\epsilon|_B + |p_\epsilon|_{B^*}) + \frac{1}{2}\varphi^H(|q_0|_B + |p_0|_{B^*})\right)^{\frac{1}{2}} . \tag{3.94}$$

Now, since $(H^\xi_{B_0,B_1})$ is satisfied, the properties (P_1) and (P_3) of Lemma 5.1 are true. If we apply the Grönwall's lemma and using (P_1), we deduce that there exists $c > 0$ such that for any $t \geq \epsilon$

$$
\begin{aligned}
|q_t|_{B_0} \leq |q_t|_{B_0} + 1 &\leq (|q_\epsilon|_{B_0} + 1) + \int_\epsilon^t \left|\xi_{(q_s,s)}(v_s^*)\right|_{B_0} ds \\
&\leq (|q_\epsilon|_{B_0} + 1) + \int_\epsilon^t c|v_s^*|_V(|q_s|_{B_0} + 1)\, ds \\
&\leq (|q_\epsilon|_{B_0} + 1)\exp(c\int_\epsilon^{t_{\max}} |v_s^*|_V\, ds)\,,
\end{aligned}
$$

Equation (3.94) shows that $\int_\epsilon^{t_{\max}} |v_s^*|_V\, ds$ is bounded and $m = \sup_{t\in[\epsilon,t_{\max}[} |q_t|_{B_0}$ is thus also bounded. Likewise, using (P_3), we have

$$
\begin{aligned}
|p_t|_{B_1^*} &\leq |p_\epsilon|_{B_1^*} + \int_\epsilon^t |\partial_q\xi_s(q_s)(v_s^*)|_{\mathcal{L}(B_1)}\, |p_s|_{B_1^*}\, ds \\
&\leq |p_\epsilon|_{B_1^*} + \int_\epsilon^t c|v_s^*|_V|p_s|_{B_1^*}(|q_s|_{B_0} + 1)\, ds \\
&\leq |p_\epsilon|_{B_1^*}\exp(c(m+1)\int_\epsilon^{t_{\max}} |v_s^*|_V\, ds)\,.
\end{aligned}
$$

We deduce that the solution is bounded (since it is continuous on $[0,\epsilon]$) and could thus be extended. Since we assume that the solution was maximal, this is a contradiction that proves the theorem. $\square$

Remark 5.4. *We explained that in the case of a horn, we are interested into cost functions such that ℓ_t tends to 0 when t tends to 0^+. Note however that this theorem obviously includes the simplest case where $|\ell_t^{-1}|_{op}$ is uniformly bounded on $[0,1]$.*

Theorem 5.3 (Global Solutions of the Reduced Hamiltonian System : Tube Case)**.** *Assume the (H_1^V) conditions. Consider the* ***nondegenerate adapted norm setup*** *and assume that $\ell \in \mathcal{C}^1([0,1],\mathcal{L}(V))$. Consider the Banach spaces*

$$
\begin{aligned}
B_0 &= B = L_\mu^\infty(X,\mathbb{R}^d) \\
B_1^* &= L_\mu^\infty(X,\mathbb{R}^d)\,.
\end{aligned}
$$

Then for any initial condition $(q_0,p_0) \in B_0 \times B_1^*$, the reduced Hamiltonian system associated to the ***growth dynamic***

$$\xi_{(q,t)}(v) = \mathbb{1}_{\tau\leq t} v \circ q$$

admits a unique solution $(q,p) \in \mathcal{C}([0,1], B_0 \times B_1^*)$.

Moreover, there exists an increasing function $\varphi^Y : \mathbb{R}^+ \to \mathbb{R}^+$ such that for any $(q_0,p_0) \in B_0 \times B_1^*$ and any $t \in [0,1]$, we have

$$|q_t|_{B_0} + |p_t|_{B_1^*} \leq \varphi^Y(|q_0|_{B_0} + |p_0|_{B_1^*})\,.$$

Proof. The proof is essentially the one of the previous theorem. All the properties satisfied for any $\epsilon > 0$ are now true for $\epsilon = 0$ and this ensures the existence of the solution on $[0,1]$. Replacing ϵ by 0 also leads to the existence of φ^Y. We have indeed with the previous notation

$$|v^*(q_t,p_t,t)|_V \leq M^{\frac{1}{2}} \left(\varphi^H(|q_0|_B + |p_0|_{B^*})\right)^{\frac{1}{2}} .$$

Since $|\cdot|_B = |\cdot|_{B_0}$ and $B_1^* \hookrightarrow B^*$, we can rewrite

$$|v^*(q_t,p_t,t)|_V \leq \psi(|q_0|_{B_0} + |p_0|_{B_1^*}) ,$$

where $\psi : \mathbb{R}^+ \to \mathbb{R}^+$ is an increasing function.

Finally, we have $m = \sup_{t\in[0,1]} |q_t|_{B_0} \leq (|q_0|_{B_0} + 1)\exp(c\psi(|q_0|_{B_0} + |p_0|_{B_1^*}))$ and then $\sup_{t\in[0,1]} |p_t|_{B_1^*} \leq |p_0|_{B^*} \exp(cm\psi(|q_0|_{B_0} + |p_0|_{B_1^*}))$. □

Discrete coordinate space

In this section, assume that X is a finite set of k points with a mesh. Denote $\{t_0, t_1, \ldots, t_n\}$ with $0 = t_0 \leq t_1 \leq \ldots \leq t_n = 1$ the image of the temporal marker $\tau : X \to [0,1]$. Consider $B = \mathbb{R}^{k\times d} = B^*$ and the **nondegenerate adapted norm setup** (see Section 3.4). Let us recall that $t \mapsto \ell_t^{-1}$ is thus defined at any time and uniformly bounded. Assume additionally that ℓ is of class $\mathcal{C}^1$ on each interval $[t_i, t_{i+1}[$.

Lemma 5.3. *There exists $M > 0$ such that for any $(q,p,t) \in B \times B^* \times [0,1]$ and any $v \in V$*

1. $H_r(q,p,t) \geq 0\,,$
2. $|\mathcal{J}_\xi(q,p,t)|^2_{V^*} \leq M H_r(q,p,t)\,,$
3. $|v^*(q,p,t)|_V \leq M\,|\mathcal{J}_\xi(q,p,t)|_{V^*}\,.$

Proof. The proof is essentially the one of the lemma 5.2 but here $t \mapsto \ell_t^{-1}$ is uniformly bounded. □

Proposition 5.11. *For any $(q,p) \in B \times B^*$, the function $t \mapsto H_r(q,p,t)$ is piecewise continuous and derivable on any interval $[t_i, t_{i+1}[$. There exists an increasing function $\varphi : \mathbb{R}^+ \to \mathbb{R}^+$ such that for any $i \in [\![0, n-1]\!]$, if $(q,p) \in \mathcal{C}([t_i, t_{\max}[, B \times B^*)$ is a local solution of the reduced Hamiltonian system with an initial condition given at time t_i, then for any $t \in [t_i, t_{\max}[\subset [t_i, t_{i+1}[$,*

$$H_r(q_t,p_t,t) \leq \varphi(H_r(q_{t_i}, p_{t_i}, t_i))\,.$$

Proof. We have for any $(q,p,t) \in B \times B^* \times [0,1]$ (see Example 3.2)

$$H_r(q,p,t) = \frac{1}{2}(\mathcal{J}(q,p,t)\,|\,v^*(q,p,t)) = \frac{1}{2}(\mathcal{J}(q,p,t)\,|\,\ell_t^{-1}K_V\mathcal{J}(q,p,t))\,.$$

We saw in Section 3.1 (Remark 3.2) that the momentum map is constant with respect to time with on each interval $[t_i, t_{i+1}[$. The reduced Hamiltonian evaluated on a solution is continuous and derivable with respect to time on any interval $[t_i, t_{i+1}[$. We have explicitly (see Example 3.2)

$$\frac{dH_r}{dt}(q_t,p_t,t) = -\frac{\partial C}{\partial t}(v_t^*, t) = -\langle v_t^*, \dot{\ell}_t v_t^* \rangle_V\,.$$

Therefore, with the previous lemma and since $t \mapsto \dot{\ell}_t$ is uniformly bounded on any interval $[t_i, t_{i+1}[$, there exist $M_1, M_2, M_3 > 0$ such that for any $i \in [\![0, n-1]\!]$ and any $t \in [t_i, t_{i+1}[$

$$\left|\frac{dH_r}{dt}(q_t, p_t, t)\right| \leq M_1 |v_t^*|_V^2 \leq M_2 |\mathcal{J}_\xi(q_t, p_t, t)|_{V^*}^2 \leq M_3 H_r(q_t, p_t, t)\,.$$

Finally, we deduce that $\left|\frac{d}{dt}\ln(1 + H_r(q_t, p_t, t))\right| \leq M_3$ and that there exists an increasing function $\varphi : \mathbb{R}^+ \to \mathbb{R}^+$ such that for any $i \in [\![0, n-1]\!]$, for any solution (q, p) defined on $[t_i, t_{\max}[$ and any $t \in [t_i, t_{\max}[$

$$H_r(q_t, p_t, t) \leq \varphi(H_r(q_{t_i}, p_{t_i}, t_i))\,.$$

□

Theorem 5.4 (Global Solutions of the Reduced Hamiltonian System : Discrete Case)**.** *Assume the (H_1^V) conditions. Assume that X is a finite set of k points with a mesh. Denote $\{t_0, t_1, \ldots, t_n\}$ with $0 = t_0 \leq t_1 \leq \ldots \leq t_n = 1$ the image of the temporal marker $\tau : X \to [0, 1]$. Consider $B = (\mathbb{R}^d)^k = \mathbb{R}^{k\times d}$ and the **nondegenerate adapted norm setup**. Assume that ℓ is of class $\mathcal{C}^1$ on each interval $[t_i, t_{i+1}[$.*

*Then for any initial condition $(q_0, p_0) \in B \times B$, the reduced Hamiltonian system associated to the **growth dynamic***

$$\xi_{(q,t)}(v) = \mathbb{1}_{\tau \leq t} v \circ q$$

admits a unique solution $(q, p) \in \mathcal{C}([0, 1], B \times B)$.

Moreover, there exists an increasing function $\varphi^Y : \mathbb{R}^+ \to \mathbb{R}^+$ such that

$$|q|_\infty + |p|_\infty \leq \varphi^Y(|q_0|_B + |p_0|_B)$$

and φ^Y does not depend on (q, p).

Proof. The previous proposition says that given a local solution defined on an interval $[t_i, t_{\max}[\subset [t_i, t_{i+1}[$, the reduced Hamiltonian $t \mapsto H_r(q_t, p_t, t)$ admits an upper bound on $[t_i, t_{\max}[$ that depends only on $H_r(q_{t_i}, p_{t_i}, t_i)$. We can show as before with the Grönwall's lemma (see the proof of Theorem 5.2 and 5.3) that $t \mapsto (q_t, p_t)$ admits also an upper bound on $[t_i, t_{\max}[$ that depends only on (q_{t_i}, p_{t_i}) and can thus be extended to the whole interval $[t_i, t_{i+1}]$. For any initial condition (q_0, p_0), there exists thus by induction a global solution defined on $[0, 1]$.

Now consider the function φ of the previous proposition. Under the (H_1^V) conditions, it exits $c > 0$ such that we have at any point of discontinuity of the reduced Hamiltonian system

$$
\begin{aligned}
H_r(q_{t_{i+1}},p_{t_{i+1}},t_{i+1}) &= H_r(q_{t_{i+1}},p_{t_{i+1}},t_{i+1}^-) + \sum_{\tau(x)=t_{i+1}} \langle p_{t_{i+1}}(x), v_{i+1}^*(q_{t_{i+1}}(x))\rangle_{\mathbb{R}^d} \\
&= H_r(q_{t_{i+1}},p_{t_{i+1}},t_{i+1}^-) + \sum_{\tau(x)=t_{i+1}} \langle p_0(x), v_{i+1}^*(q_0(x))\rangle_{\mathbb{R}^d} \\
&\leq \varphi(H_r(q_{t_i},p_{t_i},t_i)) + \sum_{\tau(x)=t_{i+1}} \langle p_0(x), v_{i+1}^*(q_0(x))\rangle_{\mathbb{R}^d} \\
&\leq \varphi(H_r(q_{t_i},p_{t_i},t_i)) + c|p_0|_B|v_{i+1}^*|_V(|q_0|_B+1) \\
&\leq \varphi(H_r(q_{t_i},p_{t_i},t_i)) + cM^{\frac{1}{2}}|p_0|_B(|q_0|_B+1)H_r(q_{i+1},p_{i+1},t_{i+1})^{\frac{1}{2}}\,.
\end{aligned}
$$

A basic study of the variations of the real valued function $g(x) = -x + a + b\sqrt{x}$ (with $a, b \in \mathbb{R}^+$) allows to conclude. Indeed, g is increasing (if $b > 0$) then strictly decreasing on $\mathbb{R}^+$. We have $g(0) = a = \varphi(H_r(q_{t_i},p_{t_i},t_i)) \geq 0$. There exists thus a unique point x_0 such that $g(x) \geq 0$ implies that $x \leq x_0$. Moreover, x_0 depends only on a and b and when a or b increases, x_0 increases. Hence, $H_r(q_{i+1},p_{i+1},t_{i+1})$ is bounded by an increasing function of $H_r(q_{t_i},p_{t_i},t_i)$ and $|p_0|_B(|q_0|_B+1)$. By induction, $H_r(q_{i+1},p_{i+1},t_{i+1})$ is bounded by an increasing function of $H_r(q_0,p_0,0)$ and $|p_0|_B(|q_0|_B+1)$. At last, we have $H_r(q_0,p_0,0) = O(|p_0|_B(|q_0|_B+1))$. Hence, there exists an increasing function $\varphi^H : \mathbb{R}^+ \to \mathbb{R}^+$ such that for any $t \in [0,1]$,

$$H_r(q_t,p_t,t) \leq \varphi^H(|q_0|_B + |p_0|_B)$$

and as before, we deduce from the Grönwall's lemma the existence of another increasing function $\varphi^Y : \mathbb{R}^+ \to \mathbb{R}^+$ such that for any solution $(q,p) = \Psi(q_0,p_0)$

$$|q|_\infty + |p|_\infty \leq \varphi^Y(|q_0|_B + |p_0|_B)\,.$$

□

5.5 Second order regularity of the reduced Hamiltonian system

We presented in section 2.5 the shooting method to perform a matching by an optimization of the initial momentum. We defined a new energy and expressed its gradient under some regularity assumption on the reduced Hamiltonian system that we will prove here. We will assume to simplify that the optimal vector field is directly given by the momentum map (it would be enough to assume that there exists $M > 0$ such that for any $(q,p,t) \in B \times B^* \times [0,1]$, $|v^*|_V \leq M|\mathcal{J}_\xi(q,p,t)|_{V^*})$.

Let us recall the reduced Hamiltonian system given by the function

$$
\begin{array}{rcccc}
h & : & (B\times B^*)\times[0,1] & \longrightarrow & B\times B^* \\
 & & (y,t) & \longmapsto & \begin{pmatrix} \frac{\partial H_r}{\partial p}(y,t) \\ \\ -\frac{\partial H_r}{\partial q}(y,t) \end{pmatrix}
\end{array},
$$

where a couple of variable (q,p) is now denoted y.

In this small section, we will show that $h_t : y \mapsto h(y,t)$ is of class $\mathcal{C}^1$ and that $t \mapsto \frac{\partial h}{\partial y}(y,t)$ is integrable. The regularity of h will result of the set of conditions (H_2^ξ) given by

$$(H_2^\xi) \quad \left| \begin{array}{l} \textit{(i)} \text{ For any } t \in [0,1], \xi_t \in \mathcal{C}^2(B, \mathcal{L}(V,B))\,. \\ \textit{(ii)} \text{ There exists } c > 0, \text{ such that for any } (q,t) \in B \times [0,1], \\ \left|\frac{\partial^2 \xi}{\partial q^2}(q,t)\right|_{op} \leq c\,. \end{array} \right.$$

Proposition 5.12. *If the optimal vector field is defined by $v^*(q,p,t) = K_V \mathcal{J}_\xi(q,p,t)$, then under the (H_1^ξ) and (H_2^ξ) conditions, h_t is of class $\mathcal{C}^1$. Moreover, there exists an increasing function $\varphi^h : \mathbb{R}^+ \to \mathbb{R}^+$ such that*

$$\left|\frac{\partial h}{\partial y}(y,t)\right| \leq \varphi^h(|y|_{B\times B^*})\,,$$

where $|y|_{B\times B^*} = |q|_B + |p|_{B^*}$. Hence, for any continuous curve $y \in \mathcal{C}([0,1], B \times B^*)$, the function $t \mapsto \frac{\partial h}{\partial y}(y_t,t)$ is integrable.

Proof. Let recall that $\mathcal{J}_\xi(q,p,t) = \xi^*_{(q,t)} \cdot p$ and (H_1^ξ) is

$$(H_1^\xi) \quad \left| \begin{array}{l} \textit{(i)}\ \xi_t \in \mathcal{C}^1(B, \mathcal{L}(V,B) \text{ for any } t \in [0,1]\,. \\ \textit{(ii)} \text{ There exists } c > 0 \text{ such that} \\ |\xi(q,t)|_{\mathcal{L}(V,B)} \leq c(|q|_B + 1) \text{ and } |\partial_q \xi(q,t)|_{\mathcal{L}(B,\mathcal{L}(V,B))} \leq c, \\ \text{for any } (q,t) \in B \times [0,1]\,. \end{array} \right.$$

Moreover, Proposition 5.4 in Section 5.2 says that

$$\mathcal{J}_\xi(q,p,t)| \leq c|p|_{B^*}(|q|_B + 1) \tag{3.95}$$

and

$$\left|\frac{\partial \mathcal{J}_\xi}{\partial q}(q,p,t)\right| + \left|\frac{\partial \mathcal{J}_\xi}{\partial p}(q,p,t)\right| \leq c(|q|_B + |p|_{B^*} + 1)\,.$$

If we denote h_1 and h_2 the two components of h, we have

$$h_1(q,p,t) = \xi_{(q,t)}(v^*) \quad \text{ and } \quad h_2(q,p,t) = \left(\partial_q \xi_{(q,t)}(v^*)\right)^* \cdot p\,.$$

Hence, since $\mathcal{J}_t$ is of class $\mathcal{C}^1$, $(q,p) \mapsto v^*(q,p,t)$ is of class $\mathcal{C}^1$, and since ξ_t is of class $\mathcal{C}^2$, h is of class $\mathcal{C}^1$ with respect to (q,p). Moreover, any term of both partial derivatives of h with respect to q or p are bounded by strictly increasing functions of $|q|_B$, $|p|_{B^*}$ and $|v^*|_V$. Therefore, with the addition of equation (3.95), there exists an increasing function $\varphi^h : \mathbb{R}^+ \to \mathbb{R}+$ such that

$$\left|\frac{\partial h}{\partial y}(y,t)\right| \leq \varphi^h(|y|_{B\times B^*})\,,$$

where $|y|_{B\times B^*} = |q|_B + |p|_{B^*}$. In particular, since φ^h does not depend on time, we have for any continuous curve $y \in \mathcal{C}([0,1], B \times B^*)$ that $\sup_t \left|\frac{\partial h}{\partial y}(y_t,t)\right| \leq \varphi^h(|y|_\infty)$ and that the function $t \mapsto \frac{\partial h}{\partial y}(y_t,t)$ is thus integrable on $[0,1]$. $\square$

Application

We extend the conditions on V as follows

$$(H_2^V)\quad\left|\begin{array}{l}\textit{(i)}\ V\subset\mathcal{C}^3(\mathbb{R}^d,\mathbb{R}^d)\,.\\ \textit{(ii)}\ \text{There exists } c>0, \text{ such that for any } (x,v)\in\mathbb{R}^d\times V, \text{ we have}\\ \begin{cases}|v(x)|_{\mathbb{R}^d}\le c|v|_V(|x|_{\mathbb{R}^d}+1),\\ |dv(x)|_\infty+|d^2v(x)|_\infty+|d^3v(x)|_\infty\le c|v|_V\,.\end{cases}\end{array}\right.$$

Proposition 5.13. *Consider $B=L^\infty(X,\mathbb{R}^d)$. If ξ is given by the growth dynamic the (H_2^V) conditions imply (H_2^ξ).*

Proof. We will show that the function

$$\begin{array}{rccc}F & : & L^\infty(X,\mathbb{R}^d)\times V & \longrightarrow & L^\infty(X,\mathbb{R}^d)\\ & & (q,v) & \longmapsto & v\circ q\end{array}$$

is of class $\mathcal{C}^2$. Proposition 4.3 says that $\frac{\partial F}{\partial q}(q,v)\cdot\delta q=(dv\circ q)\cdot\delta q$ and $\frac{\partial F}{\partial v}(q,v)\cdot\delta v=\delta v\circ q$ (note that F is not $\mathcal{C}^1$ for $L^1(X,\mathbb{R}^d)$). Therefore, we have

$$\frac{\partial^2F}{\partial q^2}(q,v)\cdot(\delta q,\delta q')=(d^2v\circ q)\cdot(\delta q,\delta q'),\qquad \frac{\partial^2F}{\partial v^2}(q,v)=0,$$
$$\frac{\partial^2F}{\partial q\partial v}(q,v)\cdot(\delta q,\delta v)=\frac{\partial^2F}{\partial v\partial q}(q,v)\cdot(\delta v,\delta q)=(d\delta v\circ q)\cdot\delta q\,.$$

Indeed, under the (H_2^V) assumption, there exists $c>0$ such that

$$\left|\frac{\partial F}{\partial q}(q+\delta q',v)\cdot\delta q-\frac{\partial F}{\partial q}(q,v)\cdot\delta q-(d^2v\circ q)\cdot(\delta q,\delta q')\right|_\infty \le |d^3v|_\infty|\delta q|_\infty|\delta q'|^2_\infty\le c|v|_V|\delta q|_\infty|\delta q'|^2_\infty$$

and

$$\left|\frac{\partial F}{\partial v}(q+\delta q,v)\cdot\delta v-\frac{\partial F}{\partial q}(q,v)\cdot\delta v-(d\delta v\circ q)\cdot\delta q\right|_\infty\le|d^2\delta v|_\infty|\delta q|^2_\infty\le c|\delta v|_V|\delta q|^2_\infty\,.$$

It follows that there exists $c>0$ such that for any $(q,v)\in L^\infty(X,\mathbb{R}^d)\times V$,

$$\left|\frac{\partial^2F}{\partial q^2}(q,v)\right|\le c|v|_V\qquad \frac{\partial^2F}{\partial v^2}(q,v)=0\qquad \left|\frac{\partial^2F}{\partial q\partial v}(q,v)\right|=\left|\frac{\partial^2F}{\partial v\partial q}(q,v)\right|\le c\,.$$

These partial derivatives are all continuous. Hence, F is of class $\mathcal{C}^2$ and also $\xi_t(q)(v)=\mathbb{1}_{\tau\le t}F(q,v)$. □

5.6 Directional derivative of the solution with respect to its parameters

The Gâteaux-derivative of the solutions to the shooting system is the last ingredient to give an expression of the gradient of the energy and allow an algorithm of gradient descent on the initial momentum p_0 (see Section 2.5). The proof presented here to ensure the existence of this Gâteaux-derivative requires that the solutions $y=\Psi(y_0)$ are locally bounded with respect to the initial condition. We will assume to simplify that X is a discrete set, i.e. $B = (\mathbb{R}^d)^k$.

As before we can define the linearized equation of the reduced Hamiltonian system

$$\delta y_t = \delta y_0 + \int_0^t \frac{\partial h}{\partial y}(y_s, s) \cdot \delta y_s \, ds \,. \tag{3.96}$$

Since the application $t \mapsto \left|\frac{\partial h}{\partial y}(y_t, t)\right|$ is integrable on $[0, 1]$, the Corollary 4.2 (linear Cauchy-Lipschitz) ensures the existence and the uniqueness of such functions for any $\delta y_0 \in B \times B^*$. The same corollary also guarantees the existence and uniqueness of the covariable z defined as introduced previously by $z_1 = -d\mathcal{A}(y_1) \in (B \times B^*)^*$ and

$$z_t = z_1 - \int_t^1 \frac{\partial C}{\partial y}(y_s, s) - \frac{\partial h}{\partial y}(y_s, s)^* \cdot z_s \, ds \,, \tag{3.97}$$

where the function $t \mapsto \left|\frac{\partial C}{\partial y}(y_t, t)\right|$ is integrable thanks to the (H^C) conditions.

Theorem 5.5. *We denoted $\Psi(q_0, p_0)$ the unique solution in $\mathcal{C}([0, 1], B \times B^*)$ to the reduced Hamiltonian system of initial conditions $y_0 = (q_0, p_0)$. The Gâteaux-derivative of Ψ in the direction $\delta y_0 = (\delta q_0, \delta p_0) \in B \times B^*$ exists and is given by the unique solution of the linearized equation*

$$\delta y_t = \delta y_0 + \int_0^t \frac{\partial h}{\partial y}(y_s, s) \cdot \delta y_s \, ds \,.$$

Proof. For any $\epsilon \in [-1, 1]$, denote $q_0^\epsilon = q_0 + \epsilon \delta q_0$, $p_0^\epsilon = p_0 + \epsilon \delta p_0$, and $y^\epsilon = \Phi(q_0^\epsilon, p_0^\epsilon)$. For any $\epsilon \neq 0$ and any $t \in [0, 1]$, consider $M_t^\epsilon = \left|\frac{y_t^\epsilon - y_t}{\epsilon} - \delta y_t\right|_{B \times B^*}$. The proof consists thus to show that this quantity $t \mapsto M_t^\epsilon$ tends uniformly to 0 when ϵ tends to 0. It starts with the following lemma.

Lemma 5.4. $|y^\epsilon - y|_\infty = O(|\epsilon|)\,.$

Proof. Let us show that for ϵ small enough, y^ϵ is bounded independently of ϵ. Theorem 5.4 says that the solutions $y = \Psi(y_0)$ are locally bounded with respect to the initial condition. More precisely, there exists an increasing function φ^Y such that for any $(q_0, p_0) \in B \times B^*$ if $(q, p) = \Psi(q_0, p_0)$ then $|q|_\infty + |p|_\infty \leq \varphi^Y(|q_0|_B + |p_0|_{B^*})$. Therefore, for any $|\epsilon| \leq 1$,

$$\begin{aligned}
|q^\epsilon|_\infty + |p^\epsilon|_\infty &\leq \varphi^Y(|q_0^\epsilon|_B + |p_0^\epsilon|_{B^*}) \\
&\leq \varphi^Y(|q_0 + \epsilon\delta q_0|_B + |p_0 + \epsilon\delta p_0|_{B^*}) \\
&\leq \varphi^Y(|q_0|_B + |\delta q_0|_B + |p_0|_{B^*} + |\delta p_0|_{B^*})\,.
\end{aligned}$$

With $|y|_{B \times B^*} = |q|_B + |p|_{B^*}$, it leads to

$$|y^\epsilon|_\infty \leq \varphi^Y(|y_0|_{B \times B^*} + |\delta y_0|_{B \times B^*})\,.$$

According to Proposition 5.12, there exists another increasing function $\varphi^h : \mathbb{R}^+ \to \mathbb{R}^+$

such that for any $(y,t) \in (B \times B^*) \times [0,1]$,

$$\left| \frac{\partial h}{\partial y}(y,t) \right| \leq \varphi^h(|y|_{B\times B^*}) \, .$$

For any $s, r \in [0,1]$, denote $y_s^{r,\epsilon} = y_s + r(y_s^\epsilon - y_s)$ and consider the application $g_s : [0,1] \to B$ defined by $g_s(r) = h(y_s^{r,\epsilon}, s) - h(y_s, s)$. Then, $g_s(0) = 0$, $g_s(1) = h(y_s^\epsilon, s) - h(y_s, s)$ and

$$h(y_s^\epsilon, s) - h(y_s, s) = \int_0^1 \dot{g}_s(r)\, dr = \int_0^1 \frac{\partial h}{\partial y}(y_s^{r,\epsilon}, s)(y_s^\epsilon - y_s)\, dr. \tag{3.98}$$

We have then

$$\begin{aligned}
|y_t^\epsilon - y_t|_{B\times B^*} &\leq |\epsilon \delta y_0|_{B\times B^*} + \int_0^t |h(y_s^\epsilon, s) - h(y_s, s)|_{B\times B^*}\, ds \\
&\leq |\epsilon||\delta y_0|_{B\times B^*} + \int_0^t \sup_{r\in[0,1]} \left| \frac{\partial h}{\partial y}(y_s^{r,\epsilon}, s) \right|_{op} |y_s^\epsilon - y_s|_{B\times B^*}\, ds \\
&\leq |\epsilon||\delta y_0|_{B\times B^*} + \int_0^t \sup_{r\in[0,1]} \varphi^h(|y_s^{r,\epsilon}|_{B\times B^*})|y_s^\epsilon - y_s|_{B\times B^*}\, ds \\
&\leq |\epsilon||\delta y_0|_{B\times B^*} + \int_0^t \varphi^h(2|y_s|_{B\times B^*} + |y_s^\epsilon|_{B\times B^*})|y_s^\epsilon - y_s|_{B\times B^*}\, ds \\
&\leq |\epsilon||\delta y_0|_{B\times B^*} + \int_0^t \varphi^h(3\varphi^Y(|y_0|_{B\times B^*} + |\delta y_0|_{B\times B^*}))|y_s^\epsilon - y_s|_{B\times B^*}\, ds \\
&\leq |\epsilon||\delta y_0|_{B\times B^*} \exp\left(\varphi^h(3\varphi^Y(|y_0|_{B\times B^*} + |\delta y_0|_{B\times B^*}))\right),
\end{aligned}$$

where the last inequality results from the Grönwall's lemma. Since this upper bound does not depend on time, we have thus $|y^\epsilon - y|_\infty = O(|\epsilon|)$. □

We will now use again the Grönwall's lemma to show the uniform convergence of $M_t^\epsilon = \left| \frac{y_t^\epsilon - y_t}{\epsilon} - \delta y_t \right|_{B\times B^*}$.

$$\begin{aligned}
M_t^\epsilon &\leq \int_0^t \left| \frac{h(y_s^\epsilon, s) - h(y_s, s)}{\epsilon} - \frac{\partial h}{\partial y}(y_s, s)\cdot \delta y_s \right|_{B\times B^*} ds \\
&\leq \int_0^t \left| \frac{\partial h}{\partial y}(y_s, s) \right|_{op} M_s^\epsilon + \frac{1}{|\epsilon|} R_s^\epsilon \, ds \, ,
\end{aligned}$$

where R_s^ϵ is defined for any $s \in [0,1]$ by

$$R_s^\epsilon = \left| h(y_s^\epsilon, s) - h(y_s, s) - \frac{\partial h}{\partial y}(y_s, s)\cdot (y_s^\epsilon - y_s) \right|_{B\times B^*} .$$

In order to control R^ϵ_s, consider again $y^{r,\epsilon}_s = y_s + r(y^\epsilon_s - y_s)$. Equation (3.98) leads to

$$\begin{aligned}
R^\epsilon_s &= \left| \int_0^1 \left(\frac{\partial h}{\partial y}(y^{r,\epsilon}_s, s) - \frac{\partial h}{\partial y}(y_s, s) \right) (y^\epsilon_s - y_s)\, dr \right|_{B\times B^*} \\
&\le \int_0^1 \left| \frac{\partial h}{\partial y}(y^{r,\epsilon}_s, s) - \frac{\partial h}{\partial y}(y_s, s) \right|_{op} dr |y^\epsilon_s - y_s|_{B\times B^*} \\
&\le \alpha^\epsilon_s |y^\epsilon - y|_\infty \,,
\end{aligned}$$

where

$$\alpha^\epsilon_s = \int_0^1 \left| \frac{\partial h}{\partial y}(y^{r,\epsilon}_s, s) - \frac{\partial h}{\partial y}(y_s, s) \right|_{op} dr \,.$$

Denote at last

$$B^\epsilon = \frac{1}{|\epsilon|} \int_0^1 R^\epsilon_s\, ds \,.$$

The Grönwall's lemma implies then that

$$M^\epsilon_t \le B^\epsilon \exp\left(\int_0^1 \left| \frac{\partial h}{\partial y}(y_s, s) \right| ds \right) \,.$$

and we saw previously that $t \mapsto \left| \frac{\partial h}{\partial y}(y_s, s) \right|$ is integrable. The final step is to prove that B^ϵ tends to 0 when ϵ tends to 0.

Note that for any $\epsilon \in [-1, 1]$, $s \mapsto \alpha^\epsilon_s$ is an integrable function on $[0, 1]$. Indeed, we have as in the proof of lemma 5.4

$$\begin{aligned}
\alpha^\epsilon_s &\le \sup_{r_s \in [0,1]} \left| \frac{\partial h}{\partial y}(y^{r_s,\epsilon}_s, s) \right|_{op} + \left| \frac{\partial h}{\partial y}(y_s, s) \right|_{op} \\
&\le \varphi^h(3\varphi^Y(|y_0|_{B\times B^*} + |\delta y_0|_{B\times B^*})) + \varphi^h(|y_s|_{B\times B^*}) \\
&\le \varphi^h(3\varphi^Y(|y_0|_{B\times B^*} + |\delta y_0|_{B\times B^*})) + \varphi^h(|y|_\infty)
\end{aligned}$$

and this bound does not depend on ϵ.

Moreover, the same lemma says that $|y^\epsilon - y|_\infty = O(|\epsilon|)$. There exists thus $c > 0$ a constant such that for any $\epsilon \in [-1, 1]$, $|\frac{y^\epsilon - y}{\epsilon}|_\infty \le c$. Hence,

$$\begin{aligned}
B^\epsilon &= \frac{1}{|\epsilon|} \int_0^1 R^\epsilon_s\, ds \\
&\le \int_0^1 \alpha^\epsilon_s \frac{|y^\epsilon - y|_\infty}{|\epsilon|}\, ds \\
&\le c \int_0^1 \alpha^\epsilon_s\, ds \,.
\end{aligned}$$

Finally, since $\frac{\partial h}{\partial y}$ is continuous, for any sequence $\epsilon_n \to 0$, $s \mapsto \alpha^{\epsilon_n}_s$ tends to 0 almost every where. The Lebesgue's dominated convergence theorem ensures that $|\alpha^{\epsilon_n}|_{L^1}$ tends to 0. Hence, M^ϵ converges uniformly to 0. $\square$

6 Conclusion

We have studied in this chapter a generative model to create growth scenarios by time-varying vector fields as used in the classic construction of a group of diffeomorphisms. This construction leads to effective numerical implementations thanks to the introduction of reproducing kernel of Hilbert spaces. The model required a specific theoretical analysis since unlike the standard approach, the infinitesimal action of the vector field depends on time. The main issue raised by this novelty lies in the spatial regularity of the generated mappings that represent a new scenario.

This generative model allowed us to address the problem to retrieve the continuous evolution of a time-varying shape from its final state. It led to a new optimal control problem where the time dependency played again an important role. We extended the Hamiltonian approach used to describe the optimal solutions. The main consequence was yet the lost of the conservation property of an optimal vector field. To balance this phenomenon, we introduced new cost functions that required yet to refine the analysis of the minimization problem. Given a time-dependent dynamic, we defined a flexible framework to ensure the existence of the solutions to the new Hamiltonian system. *In fine*, a soughtafter growth scenario is encoded in a forecast initial position and initial momentum (q_0, p_0), providing the support to a statistical analysis.

Note at last that our model is able to produce a continuous path from a degenerated shape reduced to a point to a completely grown shape as for example a compact submanifold of any finite dimension.

7 Appendix A: Bochner integral

7.1 Integration in Banach spaces

In this subsection, B is a Banach space over the field $\mathbb{R}$, I is a compact interval of $\mathbb{R}$ endowed with the Lebesgue measure denoted λ. We are interested in integrating functions $f : I \to B$. There is a theory of integration of such functions introduced by Bochner (see for example [46]).

Definition 7.1. *We define two sets of functions : $\mathcal{F}_{FV}$, the finite valued measurable functions, called as well simple functions, and $\mathcal{F}_{CV}$, the countable valued measurable functions.*

$$\mathcal{F}_{FV} := \left\{ g : I \to B, \quad g(t) = \sum_{j=1}^{k} b_j \mathbb{1}_{E_j}(t), \quad k \in \mathbb{N} \right\},$$

$$\mathcal{F}_{CV} := \left\{ g : I \to B, \quad g(t) = \sum_{j=1}^{\infty} b_j \mathbb{1}_{E_j}(t) \right\},$$

where the b_j are vectors of B and the $(E_j)_{j\in\mathbb{N}}$ are pairwise disjoint measurable subsets of I.

Definition 7.2 (Bochner measurable function)**.** *A function $f : I \to B$ is called measurable if there exists a sequence $(f_n)_{n\in\mathbb{N}}$ of finite valued measurable functions, $f_n \in \mathcal{F}_{FV}$, such that f is the limit almost everywhere of $(f_n)_n$.*

Proposition 7.1 (cf Schwabik-Ye : Corollary 1.1.8)**.** *A function $f : I \to B$ is measurable if and only if there exists a sequence $(f_n)_{n\in\mathbb{N}}$ of countable valued measurable functions, $f_n \in \mathcal{F}_{CV}$, such that f is the uniform limit almost everywhere of $(f_n)_n$.*

Definition 7.3 (Integrability)**.** *Assume that g is a simple function given for any $t \in I$ by $g(t) = \sum_{j=1}^{k} b_j \mathbb{1}_{E_j}(t)$, we define the integral of $g : I \to B$ as:*

$$\int_I g(t)\,dt := \sum_{j=1}^{k} b_j \lambda(E_j)\,.$$

We now say that a general function $f : I \to B$ is Bochner integrable *if there exists a sequence of simple functions $(f_n)_{n\in\mathbb{N}}$ such that (f_n) converges almost everywhere to f and if $\lim \int_I |f_n(t) - f(t)|_B\,dt = 0$. In this case, we define the integral of f as:*

$$\int_I f(t)\,dt := \lim_{n\to\infty} \int_I f_n(t)\,dt\,.$$

We let the reader look in Schwabik-Ye for more details on the Bochner theory. We will focus on the few following results :

Theorem 7.1 (Density of continuous functions)**.** *$\mathcal{C}^\infty(I, B)$ is dense in $L^p(I, B)$, $1 \le p \le \infty$.*

Proof. For any function $f : I \to B$, we will note $|f|_B$ the function $I \ni t \mapsto |f(x)|_B$. Let be $f \in L^p(I, B)$ for $p < \infty$ and let be $\epsilon > 0$. We will successively show that f can be approximated for the L^p-norm by a countable valued function, a finite valued function and a finite combination of smoothed indicator functions.

— By the previous proposition, there is a countable valued measurable function $h \in \mathcal{F}_{CV}$

$$h(t) = \sum_{j=1}^{\infty} b_j \mathbb{1}_{E_j}(t)$$

such that $|f-h|_\infty$ is arbitrarily small over a complement of a negligeable set. Because $\lambda(I) < \infty$, it follows that $|f-h|_p$ is also arbitrary small and since $|h|_p \le |f-h|_p + |f|_p$, h belongs to $L^p(I, B)$.

— Let $(h_n)_n \in \mathcal{F}_{FV}$ be the partial sums of h : $h_n = \sum_{j=1}^{n} b_j \mathbb{1}_{E_j}(t)$. Since the E_j are disjoint, for any $t \in I$, $|h_n(t)|_B = \sum_{j=1}^{n} |b_j|_B \mathbb{1}_{E_j}(t)$ and by the scalar monotone convergence theorem, we have $|h_n|_B \to |h|_B$ in $L^p(I, \mathbb{R}_+)$, as $n \to +\infty$. Moreover, we have

$$\begin{aligned}|h - h_n|_B^p &= \int_I |h(t) - h_n(t)|_B^p\,dt = \int_I |\sum_{j>n} b_j \mathbb{1}_{E_j}(t)|_B^p dt \\ &= \int_I \left(\sum_{j>n} |b_j|_B \mathbb{1}_{E_j}(t)\right)^p dt = ||h|_B - |h_n|_B|_p^p\,.\end{aligned}$$

Therefore $|f - h_n|_p \le |f - h|_p + |h - h_n|_p$ can be arbitrarily small.

— We approximated f with h_n a finite valued function, now we just have to smooth our finite number of indicator functions $\mathbb{1}_{E_j}$ but these functions are scalar, they belong to $L^1(I, \mathbb{R})$ (since $\lambda(E_j) < \lambda(I) < \infty$) and $\mathcal{C}^\infty(I, \mathbb{R})$ is dense in $L^1(I, \mathbb{R})$.

□

7.2 Bochner-Lebesgue points

The Lebesgue differentiation theorem states that for almost every point, the value of an integrable function is the limit of infinitesimal averages taken about the point. The proof relies on the density of smooth functions in $L^1(\mathbb{R})$. We can now extend this result of real analysis to the Bochner integrable functions. This section is adapted from [45]. We will denote for any $x \in I, r > 0$, $\mathcal{B}(x, r) = [x - r, x + r] \cap I$.

Definition 7.4. *For any $f \in L^1(I, B)$, a point $t \in I$ is called* Bochner-Lebesgue point *of f if*

$$\lim_{r \to 0} \frac{1}{\lambda(\mathcal{B}(x, r))} \int_{\mathcal{B}(x,r)} |f(x) - f(t)|_B \, dt = 0 \, .$$

The mean here achieved on $\mathcal{B}(x, r)$ can also be done on a more general collection of sets converging to $\{x\}$. We will for example need it on semi-intervals of the type $([x, r])_r$.

Proposition 7.2. *Let be $f \in L^1(I, B)$, $t \in I$ a Bochner-Lebesgue point of f and $(A_r)_{r>0}$ a collection of measurable non negligible sets containing x (i.e. for any $r > 0$, $x \in A_r$ and $\lambda(A_r) > 0$). If there exists $c \in \mathbb{R}$ such that for any $r > 0$ we have:*

$$A_r \subset \mathcal{B}(x, r) \qquad \text{and} \qquad \lambda(\mathcal{B}(x, r)) \leq c\lambda(A_r) \, ,$$

then

$$\lim_{r \to 0} \frac{1}{\lambda(A_r)} \int_{A_r} |f(x) - f(t)|_B \, dt = 0 \, .$$

Proof. We just have to notice that for every $r > 0$:

$$\frac{1}{\lambda(A_r)} \int_{A_r} |f(x) - f(t)|_B \, dt \leq \frac{c}{\lambda(\mathcal{B}(x, r))} \int_{\mathcal{B}(x,r)} |f(x) - f(t)|_B \, dt \, .$$

□

The Hardy-Littlewood maximal operator is a significant non-linear operator used in real analysis. We recall its definition on locally integrable functions :

Definition 7.5 (Hardy-Littlewood maximal operator)**.** *The Hardy-Littlewood maximal operator M applied to $f \in L^1_{loc}(\mathbb{R}, \mathbb{R})$ defines a function $(Mf) : \mathbb{R} \to \mathbb{R}$ given for any $x \in \mathbb{R}$ by :*

$$Mf(x) = \sup_{r>0} \frac{1}{\lambda(\mathcal{B}(x, r))} \int_{\mathcal{B}(x,r)} |f(t)|_B \, dt \, .$$

Proposition 7.3 (Inequality of Hardy-Littlewood)**.** *For any function $f \in L^1(\mathbb{R})$ and any $c > 0$, we have*

$$\lambda(\{Mf > c\}) \leq \frac{3}{c}|f|_1 \,.$$

Theorem 7.2. *If $f \in L^1(I, B)$, then almost every point $t \in I$ is a Bochner-Lebesgue point of f.*

Proof. This proof is the same of the real case ($B = \mathbb{R}^d$), only one specificity appears when we need to approximate f by a continuous function. Consider the family of operators $(T_r f)_{r>0}$ defined for any $x \in B$ by

$$(T_r f)(x) = \frac{1}{\lambda(\mathcal{B}(x,r))} \int_{\mathcal{B}(x,r)} |f(x) - f(t)|_B \, dt$$

and

$$(Tf)(x) = \overline{\lim}_{r \to 0} (T_r f)(x) \,.$$

Let us show that $Tf = 0$ almost everywhere. Let be $c > 0$ and $n \in \mathbb{N}^*$. The previous theorem gives us $g \in \mathcal{C}(I, B)$ such that $|f - g|_1 \leq \frac{1}{n}$. Let us note $h = f - g$. Since g is continuous, $Tg = 0$. Then we have :

$$(T_r h)(x) \leq \frac{1}{\lambda(\mathcal{B}(x,r))} \int_{\mathcal{B}(x,r)} |h(t)|_B \, dt + |h(x)|_B$$

and

$$Th \leq M|h|_B + |h(x)|_B \,.$$

Since $T_r f \leq T_r g + T_r h$, we have $Tf \leq Tg + Th \leq M|h|_B + |h|_B$. Hence, $\{Tf > 2c\} \subset \{M|h|_B > c\} \cup \{|h|_B > c\}$. As $|h|_1 \leq \frac{1}{n}$, we have on one side $\lambda(\{|h|_B > c\}) \leq \frac{|h|_1}{c} \leq \frac{1}{nc}$ and on the other side we have by the inequality of Hardy-Littlewood that $\lambda(\{M|h|_B > c\}) \leq \frac{3|h|_1}{c} \leq \frac{3}{nc}$. In conclusion, we have :

$$\forall c > 0, \forall n \in \mathbb{N}^*, \lambda(Tf > 2c) \leq \frac{4}{cn} \,.$$

So for all $c > 0$, $\lambda(Tf > c) = 0$ which proves that almost every point of I is a Bochner-Lebesgue point of f. $\square$

8 Appendix B: Regularity conditions

We summarize in the following table the regularity conditions used throughout this chapter.

(H_1^V)	$V \subset \mathcal{C}^2(\mathbb{R}^d, \mathbb{R}^d)$. $\exists c > 0, \forall (x, v) \in \mathbb{R}^d \times V$, $\begin{cases} \lvert v(x)\rvert_{\mathbb{R}^d} \leq c\lvert v\rvert_V(\lvert x\rvert_{\mathbb{R}^d} + 1) , \\ \lvert dv(x)\rvert_\infty + \lvert d^2v(x)\rvert_\infty \leq c\lvert v\rvert_V . \end{cases}$
(H_2^V)	$V \subset \mathcal{C}^3(\mathbb{R}^d, \mathbb{R}^d)$. $\exists c > 0, \forall (x, v) \in \mathbb{R}^d \times V$, $\begin{cases} \lvert v(x)\rvert_{\mathbb{R}^d} \leq c\lvert v\rvert_V(\lvert x\rvert_{\mathbb{R}^d} + 1) , \\ \lvert dv(x)\rvert_\infty + \lvert d^2v(x)\rvert_\infty + \lvert d^3v(x)\rvert_\infty \leq c\lvert v\rvert_V . \end{cases}$
(H^C)	$C \in \mathcal{C}^1(V \times [0, 1], \mathbb{R})$. $\exists c > 0, \forall (v, t) \in V \times [0, 1]$, $\lvert C(v, t)\rvert + \lvert\nabla_v C(v, t)\rvert_V^2 \leq c\lvert v\rvert_V^2$.
(H_0^f)	$\exists c > 0, \forall q, q' \in B, \forall v \in V, \forall t \in [0, 1]$, $\begin{cases} \lvert f(q, v, t)\rvert_B \leq c\lvert v\rvert_V(\lvert q\rvert_B + 1) , \\ \lvert f(q, v, t) - f(q', v, t)\rvert_B \leq c\lvert v\rvert_V\lvert q - q'\rvert_B . \end{cases}$
(H_1^f)	$\forall t \in [0, 1], f_t \in \mathcal{C}^1(B \times V, B)$. $\exists c > 0, \forall (q, v, t) \in B \times V \times [0, 1]$, $\begin{cases} \left\lvert \frac{\partial f}{\partial q}(q, v, t) \right\rvert_{op} \leq c\,\lvert v\rvert_V , \\ \left\lvert \frac{\partial f}{\partial v}(q, v, t) \right\rvert_{op} \leq c\,(\lvert q\rvert_B + 1) . \end{cases}$
(H_1^ξ)	$\forall t \in [0, 1], \xi_t \in \mathcal{C}^1(B, \mathcal{L}(V, B)$. $\exists c > 0, \forall (q, t) \in B \times [0, 1]$, $\lvert\partial_q \xi_t(q)\rvert_{op} \leq c$.
(H_2^ξ)	$\forall t \in [0, 1], \xi_t \in \mathcal{C}^2(B, \mathcal{L}(V, B))$. $\exists c > 0, \forall (q, t) \in B \times [0, 1]$, $\left\lvert \frac{\partial^2 \xi}{\partial q^2}(q, t) \right\rvert_{op} \leq c$.
(H_{B_0,B_1}^ξ)	$\forall t \in [0, 1], \xi_t \in \mathcal{C}^1\big(B_0, \mathcal{L}(V, B_1)\big)$. $\exists c > 0, \forall q, q' \in B_0, \forall t \in [0, 1]$, $\begin{cases} \lvert\xi_{(q,t)} - \xi_{(q',t)}\rvert_{\mathcal{L}(V,B_0)} \leq c\lvert q - q'\rvert_{B_0} , \\ \lvert\partial_q \xi_t(q) - \partial_q \xi_t(q')\rvert_{\mathcal{L}(B_1,\mathcal{L}(V,B_1))} \leq c\lvert q - q'\rvert_{B_0} . \end{cases}$

Chapter 4

Existence and Continuity of the Global Minimizers for the Growth Dynamic

Contents

1 Introduction

We presented in the previous chapters a general framework to model the growth of a horn by a continuous time-varying shape built on a biological coordinate system (X, τ) where X is a compact smooth manifold and $\tau : X \to [0,1]$ the birth tag. The shape is represented by a path of mappings $(q_t : X \to \mathbb{R}^d)_{t\in[0,1]} \subset B$ in a Banach space B. The deformation of the shape is partially modeled by a space of vector fields V on the ambient space $\mathbb{R}^d$. The birth tag τ indicates a creation process that completes the description of the shape's deformation. The evolution of $t \mapsto q_t$ is thus given by the action of a time-varying vector field v defined via the birth tag by

$$\dot{q}_t(x) = \mathbb{1}_{\tau(x)\leq t}\, v(q(x))\,.$$

This dynamic, called **growth dynamic**, is studied in Chapter 3. We defined a set of *admissibility* conditions on V to ensure the existence of a function

$$\Phi(v) : L^2([0,1], V) \to \mathcal{C}([0,1], B)$$

that returns, for any given initial condition $q_0 \in B$, the unique solution of the integral equation

$$q_t = q_0 + \int_0^t \mathbb{1}_{\tau\leq t}\, v_s \circ q_s\, ds\,.$$

We investigated the reconstitution of a development via the inexact matching of an initial condition q_0 to an implicit target $\mathcal{S}^{\text{tar}}$. This problem can be expressed as a **minimization problem** on an energy of the type

$$E(v) = \int_0^1 C(v_t, t)\, dt + \mathcal{A}(v)\,, \tag{4.1}$$

where v belongs to $L^2([0,1], V)$, the initial mapping $q_0 \in B$ is fixed and $q = \Phi(q_0, v) \in \mathcal{C}([0,1], B)$. Moreover, $C : V \times [0,1] \to \mathbb{R}$ and $\mathcal{A} : L^2_V \to \mathbb{R}$ are two applications usually called the cost function and the data attachment term. They respectively penalize the deformation induced by v and the discrepancy between the target and the final shape $q_1(X)$.

The model induced by the growth dynamic raises a new issue. The continuity of the global minimizers of the energy is no longer free. Indeed, the sought-after solution $q = \Phi(q_0, v)$ depends on the complete evolution of the time-varying vector field v even at its last state q_1. Let us recall that conversely, under the classic dynamic, the final shape q_1 only depends on the final diffeomorphism on the ambient space generated by v. Moreover, the spatial regularity of q_1 depends on the temporal regularity of v. The existence of continuous solutions $v^* \in \mathcal{C}([0,1], V)$ to the minimization problem is thus a crucial point. The choice of the data attachment term plays an unexpected role in this problem studied in the Section 2 and 4.

At last, we will see in Section 5 that the continuity of these optimal vector fields ensures the existence of a pointwise expression of the momentum. This allows to explicit the momentum map (as done in Chapter 3) in the general situation where X is a compact manifold.

2 Discontinuity for varifold data term

This section highlights a counterexample to the existence of continuous minimizers of the energy when the attachment term is build on a space of varifolds. We present a first counterexample in a 2D case that will then be adapted to a 3D case.

2.1 Setting of the counterexample

We aim for a particularly simple situation to produce a counterexample. The shape is a horn modeled by a curve in $\mathbb{R}^2$. The coordinate space should be defined by $X = [0,1] \times \{-1,1\}$ and the birth tag τ by the projection on the first coordinate. However, to simplify the notation, the curve will be parameterized by the interval $I = [-1,1]$ and the birth tag will be defined for any $r \in I$ by $\tau(r) \doteq |r|$. The initial condition is given by $q_0(r) = (r, 0)$. The horn is thus initially flattened on the horizontal segment $[-1,1] \times \{0\} \subset \mathbb{R}^2$. This means that as for the 3D case, all the creation occurs at the base of the horn. The tip of the horn is thus modeled by the point $0 \in I$ and appears at the origin of $\mathbb{R}^2$. The horn grows from the center and extends progressively towards the boundaries $\{-1\}$ and $\{1\}$ of its base. The deformations are reduced to vertical translations and the space of vector fields V is canonically identified to $\mathbb{R}$. For any $v \in L^2([0,1], \mathbb{R})$, the growth dynamic is given by

$$\dot{q}_t(r) = (0, v(t))\mathbf{1}_{|r| \leq t}$$

and $q_t(r) = (r, \mathbf{1}_{|r|\leq t} \int_{|r|}^{t} v(s)ds)$. The shape at its final age $t = 1$ is given by $q_1(r) = \gamma_v(r)$ where $\gamma_v : [-1,1] \to \mathbb{R}^2$ is defined by

$$\gamma_v(r) = (r, \int_{|r|}^{1} v(s)ds)\,. \tag{4.2}$$

Note that the curve γ_v is symmetric about the vertical axis $\{0\} \times \mathbb{R}$.

The underlying problem of calculus of variations is provided by a penalization term $\int_0^1 v^2(s)ds$ and a data attachment term modeled on varifolds that we will now introduce. As presented by Charon and Trouvé [15], and recalled in Chapter 1, the curves are modeled by the dual of a reproducing kernel Hilbert space (RKHS) W on $\mathcal{C}_0(\mathbb{R}^2 \times G_1(\mathbb{R}^2), \mathbb{R})$ where $G_1(\mathbb{R}^2)$ is the Grassmanniann of all lines through the origin of $\mathbb{R}^2$. W' represents then a space of varifolds. In all generality, a varifold $\mu \in W'$ evaluated on a function $\omega \in W$ is given by

$$\mu(\omega) = \int_{\mathbb{R}^2 \times G_1(\mathbb{R}^2)} \omega(x, V) d\mu(x, V)\,, \tag{4.3}$$

where for any Borel subset $A \subset \mathbb{R}^2 \times G_1(\mathbb{R}^2)$, $\mu(A) = \mathcal{H}^2(\{y \in \mathbb{R}^2 \,|\, (y, V) \in A\})$. For any $v \in L^2([0,1], \mathbb{R})$, the varifold associated to the curve γ_v is denoted $\mu_v \in W'$ and it is defined for any $\omega \in W$ by

$$\mu_v(\omega) = \int_{-1}^{1} \omega(\gamma_v(r), T_r\gamma_v)|\dot{\gamma}_v(r)|dr\,, \tag{4.4}$$

where $T_r\gamma_v$ is the line of $G_1(\mathbb{R}^2)$ generated by the vector $\dot{\gamma}_v(r) = (1, -v(r))$ (defined a.e.). With the symmetry of the curve, this expression can be rewritten

$$\mu_v(\omega) = \sum_{i=0}^{1} \int_{0}^{1} \omega(S^i(\gamma_v(r)), S^i(T_r\gamma_v))\sqrt{1+v^2(r)}dr\,, \tag{4.5}$$

where $S^1 = S$ is the symmetry with respect to the vertical axis through origin and $S^0 = \mathrm{Id}$.

The kernel of the RKHS W is denoted k_W and given by the tensor product $k_E \otimes k_T$ of a kernel $k_E(x,y)$ on the ambient space $\mathbb{R}^2$ and a kernel $k_T(u,v)$ on the Grassmannian $G_1(\mathbb{R}^2)$. We will assume that the target horn is also given by a parametric function $\gamma_{v^{\mathrm{tar}}} : [-1,1] \to \mathbb{R}^2$ produced by a "vector field" $v^{\mathrm{tar}} \in L^2([0,1],\mathbb{R})$. The comparison of the two curves γ_v and $\gamma_{v^{\mathrm{tar}}}$ is then achieved by the estimation of the distance between μ_v and $\mu_{v^{\mathrm{tar}}}$ in W', this is to say with the norm $|\mu_v - \mu_{v^{\mathrm{tar}}}|_{W'}$.

Finally, the problem consists in minimizing the energy given by the sum of the penalization term on v and this data attachment term

$$E_W^\lambda(v) \doteq \frac{1}{2}\int_0^1 v(r)^2 dr + \frac{\lambda}{2}|\mu_v - \mu_{v^{\mathrm{tar}}}|_{W'}^2\,. \tag{4.6}$$

Our aim is to know if the regularization L^2 on v and the data attachment term on varifolds ensure the continuity of global minimizers of E_W^λ. We will prove the following theorem:

Theorem 2.1. *There exist $v^{\mathrm{tar}} \in L^2([0,1],\mathbb{R})$, $\lambda > 0$ and W such that no global minizer v^* of E_W^λ given by (4.6) is a continuous function on $[0,1]$. Moreover, one can assume that $v^{\mathrm{tar}} \in \mathcal{C}^\infty([0,1],\mathbb{R})$.*

Remark 2.1 (RKHS properties)**.** *Denote $\omega = K_W(\mu_v - \mu_{v^{\mathrm{tar}}})$, where $K_W : W' \to W$ is the canonical isomophism of Hilbert spaces. By construction of a RKHS, ω is given at any $(x,V) \in \mathbb{R}^2 \times G_1(\mathbb{R}^2)$ by*

$$\omega(x,V) = \int_{\mathbb{R}^2 \times G_1(\mathbb{R}^2)} k_W\big((x,V),(y,V')\big) d(\mu_v - \mu_{v^{\mathrm{tar}}})(y,V')\,. \tag{4.7}$$

Let us recall then that $|\mu_v - \mu_{v^{\mathrm{tar}}}|_{W'}^2 = (\mu_v - \mu_{v^{\mathrm{tar}}})(\omega)$ and

$$\frac{\partial}{\partial v}\frac{1}{2}|\mu_v - \mu_{v^{\mathrm{tar}}}|_{W'}^2 = \left(\frac{\partial}{\partial v}\mu_v\right)(\omega)\,. \tag{4.8}$$

2.2 Proof of theorem 2.1

We will consider a perturbation parameterized by $\epsilon \geq 0$ of a degenerate constant kernel $k_W \equiv 1$. The solutions of the optimization problem associated to this kernel will be especially easy to explicit.

Definition 2.1. *We fix $k_T \equiv 1$ and k_E is given by a set of kernels $k_\epsilon(x,y) = \rho(\epsilon|x-y|^2_{\mathbb{R}^2})$ where ρ is a positive function such that $\rho(0) = 1$, $\dot\rho$ is bounded on $\mathbb{R}$ and $\dot\rho(0) < 0$. They generate a set of kernels $k_\epsilon \otimes k_T$ that do not see the tangential directions. Each kernel $k_\epsilon \otimes k_T$ for $\epsilon \geq 0$ produces a RKHS denoted W_ϵ. The test functions do thus not depend on the Grassmanniann component. We will write $\omega(x)$ instead of $\omega(x,V)$ and $d\mu(x)$ instead of $d\mu(x,V)$. Since W_ϵ depends on ϵ, the energy will be denoted $E^\lambda(\epsilon, v)$ to refer to $E^\lambda_{W_\epsilon}(v)$.*

This construction could probably be extended to a symmetric situation with a perturbation $k'_{\epsilon'}$ of k_T. Note yet that it would require to investigate the spatial regularity of the curve γ_v. Hence, we will only consider $k_T \equiv 1$.

The first step is to study the problem with the degenerate kernel. When $\epsilon = 0$, the kernel $k_{W_0} = k_0 \otimes k_T$ is constant and W_0 is a 1-dimensional space whose elements ω are all constant. In this case, the expression of the data attachment term is particularly simple:

$$\begin{aligned}
|\mu_v - \mu_{v^{\text{tar}}}|^2_{W_0'} &= \iint_{\mathbb{R}^2\times\mathbb{R}^2} k_0(x,y) d(\mu_v - \mu_{v^{\text{tar}}})(x) d(\mu_v - \mu_{v^{\text{tar}}})(y) \\
&= \left(\int_{\mathbb{R}^2} 1 d(\mu_v - \mu_{v^{\text{tar}}})(x) \right)^2 \\
&= \left(\int_{-1}^{1} |\dot\gamma_v(t)| - |\dot\gamma_{v^{\text{tar}}}(t)| dt \right)^2 \\
&= \left(\ell(v) - \ell(v^{\text{tar}})\right)^2 ,
\end{aligned}$$

where $\ell(v)$ measures the length of the curve generated by v

$$\ell(v) = 2\int_0^1 \sqrt{1 + v^2(t)} dt \,. \tag{4.9}$$

Finally, the energy in this case is given by

$$E^\lambda(0, v) = \frac{1}{2}\int_0^1 v(t)^2 dt + \frac{\lambda}{2}\left(\ell(v) - \ell(v^{\text{tar}})\right)^2 . \tag{4.10}$$

The global minimizers have then an explicit expression given by the following proposition.

Proposition 2.1. *Assume that $\ell_0 = \frac{4\lambda\ell(v^{\text{tar}})}{4\lambda+1} > 2$. Then $v^* \in L^2([0,1],\mathbb{R})$ is a global minimizer of $E^\lambda(0,\cdot)$ if and only if we have at almost all time $v^*(t)^2 = \ell_0^2/4 - 1$. In particular, if $v^* \in \mathcal{C}([0,1],\mathbb{R})$ then v^* is constant.*

Proof. We have the next elementary lemma:

Lemma 2.1. *If $\ell_0 = \frac{4\lambda\ell(v^{\text{tar}})}{4\lambda+1} > 2$, then ℓ_0 minimizes*

$$P(\ell) \doteq \frac{\ell^2/4 - 1}{2} + \frac{\lambda}{2}\left(\ell(v^{\text{tar}}) - \ell\right)^2$$

on $\mathbb{R}$. Moreover, if $v \in L^2([0,1],\mathbb{R})$ satisfies $v(t)^2 = \ell^2/4 - 1$ a.e. where $\ell \in \mathbb{R}$, then $E^\lambda(0,v) = P(\ell)$.

Define for $\ell \geq 2$, the function $\rho_\ell : \mathbb{R} \to \mathbb{R}$ by

$$\rho_\ell(z) \doteq \frac{z^2}{2} - \frac{\ell}{2}\sqrt{z^2+1}.$$

This function is even, tends to $+\infty$ when $|z|$ tends to $+\infty$ and $\dot{\rho}_\ell(z) = 0 \Leftrightarrow z - \frac{\ell}{2}\frac{z}{\sqrt{z^2+1}} = 0 \Leftrightarrow (z = 0 \text{ or } z^2 = \frac{\ell^2}{4} - 1)$. Therefore, ρ_ℓ admits two minimizers that satisfy

$$\begin{cases} z^2 = \ell^2/4 - 1 > 0 \\ \rho_\ell(z) = -(\ell^2/4+1)/2 \end{cases}.$$

It results that the minimum of

$$R_\ell(v) \doteq \int_0^1 \rho_\ell(v(t))dt$$

is reached at $v^* \in L^2([0,1],\mathbb{R})$ if and only if $v^*(t)^2 = \ell^2/4 - 1$ a.e.

By construction, these minimizers are exactly the solutions of the constrained optimization problem

$$\left| \begin{array}{l} \min_{L^2} \int v(t)^2 dt \\ \text{with } \ell(v) = \ell \end{array} \right. .$$

Indeed, $\ell(v^*) = 2\int_0^1 \sqrt{v^*(t)^2+1}dt = \ell$ and if there exists another $v \in L^2([0,1],\mathbb{R})$ such that $\ell(v) = \ell$ and $\int_0^1 v(t)^2 dt < \int_0^1 v^*(t)^2 dt$ then $R_\ell(v) < R_\ell(v^*)$ which is absurd.

Consequently, any minimizer $v^* \in L^2([0,1],\mathbb{R})$ of $E^\lambda(0,\cdot)$ satisfies $v^*(t)^2 = \ell_0^2/4 - 1$ a.e. where $\ell_0 = \ell(v^*)$ is defined on $[2,+\infty[$ and must minimize $\ell \mapsto E^\lambda(0,v^*) = \frac{\ell^2/4-1}{2} + \frac{\lambda}{2}(\ell(v^{\text{tar}}) - \ell)^2$, i.e. $\ell_0 = \frac{4\lambda\ell(v^{\text{tar}})}{1+4\lambda} > 2$. Moreover, there exist exactly two continuous minimizers in $L^2([0,1],\mathbb{R}) \cap \mathcal{C}([0,1],\mathbb{R})$ given by $v^+ \equiv \sqrt{\ell_0^2/4-1}$ and $v^- = -v^+$. $\square$

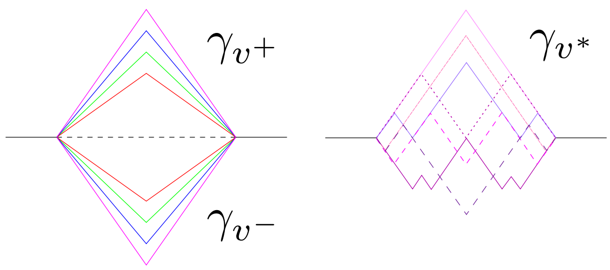

Figure 4.1 – On the left. Solutions generated by the continuous minimizers v^+ and v^-. Each color is associated to a length ℓ_0. The dot line is the image of the initial position, i.e. the base of the horn. On the right. Solutions generated by a set of discontinuous minimizers v^* at fixed ℓ_0 (and v^+ on the top).

Remark 2.2. *Note that with the degenerate kernel $k_W \equiv 1$, the energy has continuous global minimizers. However, they are only two of an infinite number of solutions. Figure 4.1 illustrates on its left the two curves generated by v^+ and v^- for four given lengths ℓ_0. Figure 4.1 illustrates on its right few examples where ℓ_0 is fixed. The condition to be a minimizer leads to a large set of different type of curves. Assume now that the target is* *some kind of sinusoidal curve. One can then easily see that from a spatial point of view, the two curves γ_{v^+} and γ_{v^-} are probably the less optimal solutions among the complete set of solutions γ_{v^*}. Hence, as soon as the kernel k_W is perturbed and allowed to capture some spatial position of the target, one can expect that the new energies associated to v^+ and v^- are higher than the energy of at least one other solution v^*.*

$$\begin{aligned} &\textit{Hypothesis: There exists } v^*, \textit{ such that for any } \epsilon > 0 \textit{ small enough,} \\ &\qquad E^\lambda(\epsilon, v^+) > E^\lambda(\epsilon, v^*) \quad \textit{and} \quad E^\lambda(\epsilon, v^-) > E^\lambda(\epsilon, v^*)\,. \end{aligned}$$

The next step to prove the theorem is to investigate the minimizers of $v \mapsto E^\lambda(\epsilon, v)$ where $\epsilon > 0$. The following proposition will establish that if some of these minimizers are continuous, they necessary lie in a neighborhood of v^+ or v^- (the two continuous global minimizers of $E^\lambda(0, v)$). Analyzing the variations of $\epsilon \to E^\lambda(\epsilon, v)$ will then indicate that in some situations these minimizers cannot be global minimizers.

Proposition 2.2. *Assume that $\ell_0 = \frac{4\lambda\ell(v^{\mathrm{tar}})}{4\lambda+1} > 2$. If for any $\epsilon > 0$ small enough, there exists a continuous global minimizer v_ϵ of $E^\lambda(\epsilon, \cdot)$, then*

$$\lim_{\epsilon\to 0} \big(\min(|v_\epsilon - v^+|_\infty, |v_\epsilon - v^-|_\infty) \big) = 0\,, \tag{4.11}$$

where $v^+ \equiv \sqrt{\ell_0^2/4 - 1}$ and $v^- = -v^+$ are the only continuous global minimizers of $E^\lambda(0, \cdot)$.

Proof. Denote $\omega_v(\epsilon, \cdot) = K_{W_\epsilon}(\mu_v - \mu_{v^{\mathrm{tar}}})$. Since k_W is reduced to k_E, the tangential component of the varifold $\mu_v - \mu_{v^{\mathrm{tar}}}$ can be ignored and we have (see Remark 2.1)

$$\omega_v(\epsilon, \cdot) = \int_{\mathbb{R}^2} k_\epsilon(\cdot, y) d(\mu_v - \mu_{v^{\mathrm{tar}}})(y)\,.$$

We then symmetrize ω_v as follows

$$\omega_v^S(\epsilon, x) \doteq \sum_{i=0}^{1} \omega_v(\epsilon, S^i(x)) = \sum_{i=0}^{1} \int_{\mathbb{R}^2} \rho(\epsilon|S^i(x) - y|^2) d(\mu_v - \mu_{v^{\mathrm{tar}}})(y)\,,$$

where S is the reflection across the vertical axis so that

$$\mu_v(K_{W_\epsilon}(\mu_v - \mu_{v^{\mathrm{tar}}})) = \int_0^1 \omega_v^S(\epsilon, \gamma_v(r))\sqrt{v(r)^2 + 1}dr\,.$$

Note that for any $v \in L^2$

$$\lim_{\epsilon\to 0} \omega_v^S(\epsilon, \cdot) \equiv 2(\ell(v) - \ell(v^{\mathrm{tar}}))\,. \tag{4.12}$$

One can easily prove that $v \mapsto E^\lambda(\epsilon, v)$ is differentiable with respect to v and we have for any $\delta v \in L^2$

$$\left(\frac{\partial E^\lambda}{\partial v}(\epsilon, v) \,\middle|\, \delta v\right) = \int_0^1 v(t)\delta v(t)dt + \lambda \left(\frac{\partial}{\partial v}\mu_v \,\middle|\, \delta v\right) (K_{W_\epsilon}(\mu_v - \mu_{v^{\mathrm{tar}}}))$$

$$\begin{aligned}\left(\frac{\partial E^\lambda}{\partial v}(\epsilon, v) \,\middle|\, \delta v\right) &= \int_0^1 v(t)\delta v(t)dt \\ &+ \lambda \int_0^1 \left(\left(\partial_2 \omega_v^S(\epsilon, \gamma_v(t)) \,\middle|\, (0, \int_t^1 \delta v(s)ds)\right)\sqrt{v^2(t)+1} + \omega_v^S(\epsilon, \gamma_v(t))\frac{v(t)\delta v}{\sqrt{v^2(t)+1}}\right) dt\,,\end{aligned}$$

where $\partial_2 \omega_v^S(\epsilon, x)$ is the derivative of ω_v^S with respect to x. Denote

$$\alpha_{\epsilon,v}(s) \doteq \int_0^s \left(\partial_2 \omega_v^S(\epsilon, \gamma_v(t)) \,\middle|\, (0,1)\right)\sqrt{v^2(t)+1}dt\,,$$

so that

$$\frac{\partial E^\lambda}{\partial v}(\epsilon, v) = \left(1 + \lambda \frac{\omega_v^S(\epsilon, \gamma_v)}{\sqrt{v^2+1}}\right) v + \alpha_{\epsilon,v}\,.$$

Note then that $|\alpha_{\epsilon,v}|_\infty = O(\epsilon)$. Indeed,

$$\partial_2 \omega_v^S(\epsilon, x) = \epsilon \sum_{i=0}^{1} S^i \left(\int_0^1 2(S^i(x) - y)\rho'(\epsilon|S^i(x) - y|^2)d(\mu_v - \mu_{v^{\mathrm{tar}}})(y)\right)$$

and since ρ' is bounded on $\mathbb{R}$ we deduce that for any bounded neighborhood of $(0,0)$ in $\mathbb{R}^+ \times L^2([0,1], \mathbb{R})$, we have $|\partial_2 \omega_v^S(\epsilon, \gamma_v)|_\infty = O(\epsilon)$ and

$$|\alpha_{\epsilon,v}|_\infty = O(\epsilon)\,. \tag{4.13}$$

Assume now that for any $\epsilon > 0$, there exists a continuous solution v_ϵ that minimizes $E^\lambda(\epsilon, \cdot)$. It must thus satisfy

$$\left(1 + \lambda \frac{\omega_{v_\epsilon}(\epsilon, \gamma_{v_\epsilon})}{\sqrt{v_\epsilon^2+1}}\right) v_\epsilon + \lambda \alpha_{\epsilon, v_\epsilon} = 0 \ a.e. \tag{4.14}$$

Hence, for ϵ small enough, equations (4.14) and (4.13) imply that there exist $M > 0$ and $\beta_\epsilon \geq 0$ such that at almost any time $t \in [0,1]$ we have either

$$|(\sqrt{v_\epsilon^2(t)+1} - \beta_\epsilon| \leq M\epsilon^{1/2}\sqrt{v_\epsilon^2(t)+1} \quad \text{or} \quad |v_\epsilon(t)| \leq M\epsilon^{1/2}\,. \tag{4.15}$$

According to equation (4.12), we have more precisely $\beta_\epsilon = 2\lambda(\ell(v^{\mathrm{tar}}) - \ell(v_\epsilon)) + o(1)$.

To go further let us first show that the length of the curves $(\gamma_\epsilon)_{\epsilon \geq 0}$ converge.

Lemma 2.2. *$\ell(v_\epsilon)$ tends to $\ell_0 = \ell(v_0)$.*

Proof. We have

$$E^\lambda(0, v_\epsilon) \leq E^\lambda(\epsilon, v_\epsilon) + o(1) \leq E^\lambda(\epsilon, v_0) + o(1) \leq E^\lambda(0, v_0) + o(1)\,. \tag{4.16}$$

Left and right inequalities result from the continuity of $E^\lambda(\cdot, v)$. Since v_ϵ minimizes $E^\lambda(\epsilon, \cdot)$, the central inequality is also true. Consider now $\ell_0 = \frac{4\lambda\ell(v^{\mathrm{tar}})}{4\lambda+1} > 2$ and the polynomial $P(\ell) = \frac{1}{2}(\ell^2/4 - 1) + \frac{\lambda}{2}(\ell(v^{\text{tar}}) - \ell)^2$ from Lemma 2.1. We have then $\ell(v_0) = \ell_0$ and $E^\lambda(0, v_0) = P(\ell(v_0)) = P(\ell_0)$. Moreover, if for any $\epsilon > 0$, we define $\delta v_\epsilon \equiv \sqrt{\ell(v_\epsilon)^2/4 - 1}$, then $\ell(\delta v_\epsilon) = \ell(v_\epsilon)$ and $E^\lambda(0, \delta v_\epsilon) \leq E^\lambda(0, v_\epsilon)$ (see proof of Proposition 2.1). It results from equation (4.16) and Lemma 2.1 that

$$P(\ell(v_\epsilon)) = E^\lambda(0, \delta v_\epsilon) \leq P(\ell_0) + o(1).$$

At last, since ℓ_0 minimizes P, we have

$$P(\ell_0) \leq P(\ell(v_\epsilon)) \leq P(\ell_0) + o(1)\,.$$

Hence, since P is continuous and $\lim_{\pm\infty} P = +\infty$, we have $\ell(v_\epsilon) = \ell_0 + o(1) = \ell(v_0) + o(1)$. $\square$

We will now prove that the first case of equation (4.15) is the only one true. Denote for any $\epsilon > 0$, $A_\epsilon \doteq \{t \in [0,1] \,|\, |\sqrt{v_\epsilon^2(t) + 1} - \beta_\epsilon| \leq O(\epsilon^{1/2})\sqrt{v_\epsilon^2(t) + 1}\}$ and $\ell_\epsilon \doteq 2(\lambda_{\mathbb{R}}(A_\epsilon)\beta_\epsilon + (1 - \lambda_{\mathbb{R}}(A_\epsilon))$ (where $\lambda_{\mathbb{R}}$ is the Lebesgue measure), then $\ell_\epsilon = \ell(v_\epsilon) + O(\epsilon^{1/2})$. Lemma 2.2 implies then that $\ell_\epsilon = \ell_0 + o(1)$. Moreover, $\beta_\epsilon = 2\lambda(\ell(v^{\text{tar}}) - \ell(v_\epsilon)) + o(1)$ and $\ell(v^{\text{tar}}) - \ell_0 = \ell_0/(4\lambda)$ so that the lemma also implies that $2\beta_\epsilon = \ell_0 + o(1)$. Finally, we deduce that $\lambda_{\mathbb{R}}(A_\epsilon) = 1 + o(1)$.

Therefore, there exists $M' > 0$ such that for almost any $t \in [0, 1]$,

$$|v_\epsilon(t)^2 - (\ell_0^2/4 - 1)| \leq M'\epsilon\,.$$

Since v_ϵ is continuous and $\ell_0 > 2$, it follows that v_ϵ satisfies either

$$|v_\epsilon - v^+|_\infty \leq M'\epsilon \quad \text{or} \quad |v_\epsilon - v^-|_\infty \leq M'\epsilon\,.$$

And finally,

$$\lim_{\epsilon \to 0} \big(\min(|v_\epsilon - v^+|_\infty, |v_\epsilon - v^-|_\infty)\big) = 0\,.$$

$\square$

The final step to prove the theorem is to study the variations of $E^\lambda(\cdot, v)$ with respect to ϵ at a global minimizer $v = v^*$. The aim is to show that the energy around v^+ and v^- increases too fast, with respect to ϵ, to allow any v in their neighborhood to be a global minimizer of $E^\lambda(\epsilon, \cdot)$. As announced in Remark 2.2, the idea is to compare the geometric properties of all the minimizers of $E^\lambda(0, \cdot)$. We will thus rewrite the gradient of this energy via some geometric descriptors.

Definition 2.2. *Denote x_v the* centroid *of the curve γ_v defined by*

$$x_v \doteq \frac{1}{\ell(v)} \int_{\mathbb{R}^2} x d\mu_v(x) \tag{4.17}$$

and $V(v)$ the associated variance *defined by*

$$V(v) \doteq \frac{1}{\ell(v)} \int_{\mathbb{R}^2} |x - x_v|^2 d\mu_v(x)\,. \tag{4.18}$$

Lemma 2.3. *The function $\epsilon \to E^\lambda(\epsilon, v)$ is derivable and for $\epsilon = 0$, we have*

$$\frac{\partial E^\lambda}{\partial \epsilon}(0, v) = \\ -\lambda\rho'(0)\Big(\Big(\ell(v^{\mathrm{tar}}) - \ell(v)\Big)\Big(\ell(v)V(v) - \ell(v^{\mathrm{tar}})V(v^{\mathrm{tar}})\Big) + \ell(v)\ell(v^{\mathrm{tar}})|x_{v^{\mathrm{tar}}} - x_v|^2\Big).$$

Proof. The proof depends neither on the dimension of the ambient space nor the dimension of the varifolds. Let assume that the ambient space is $\mathbb{R}^d$ and let us start to establish with varifolds the algebraic formulae for the variance ($V(X) = E[X^2] - E[X]^2$). For any $v \in L^2$, we have

$$\begin{aligned}
\ell(v)V(v) &= \int_{\mathbb{R}^d} |x - x_v|^2 d\mu_v(x) \\
&= \int_{\mathbb{R}^d} |x|^2 + |x_v|^2 - 2\langle x, x_v\rangle \, d\mu_v(x) \\
&= \int_{\mathbb{R}^d} |x|^2 \, d\mu_v(x) + |x_v|^2 - 2x_v \int_{\mathbb{R}^d} x \, d\mu_v(x) \\
&= \int_{\mathbb{R}^d} |x|^2 \, d\mu_v(x) - \ell(v)|x_v|^2 .
\end{aligned}$$

Then, one can easily show that $\epsilon \mapsto E^\lambda(\epsilon, v)$ is derivable and that

$$\begin{aligned}
\frac{\partial E^\lambda}{\partial \epsilon}(0, v) &= \frac{\partial}{\partial \epsilon}\frac{\lambda}{2}\big|\mu_v - \mu_{v^{\mathrm{tar}}}\big|_{W'_\epsilon}\Big|_{\epsilon=0} \\
&= \frac{\partial}{\partial \epsilon}\frac{\lambda}{2}\iint_{\mathbb{R}^d\times\mathbb{R}^d} \rho(\epsilon|x-y|^2)d(\mu_v - \mu_{v^{\mathrm{tar}}})(x)d(\mu_v - \mu_{v^{\mathrm{tar}}})(y)\Big|_{\epsilon=0} \\
&= \frac{\lambda}{2}\rho'(0)\iint_{\mathbb{R}^d\times\mathbb{R}^d} |x-y|^2 d(\mu_v - \mu_{v^{\mathrm{tar}}})(x)d(\mu_v - \mu_{v^{\mathrm{tar}}})(y) \\
&= \frac{\lambda}{2}\rho'(0)\iint_{\mathbb{R}^d\times\mathbb{R}^d} (|x|^2 + |y|^2 - 2\langle x, y\rangle) d(\mu_v - \mu_{v^{\mathrm{tar}}})(x)d(\mu_v - \mu_{v^{\mathrm{tar}}})(y) \\
&= \lambda\rho'(0)\Big(\underbrace{\big(\ell(v) - \ell(v^{\mathrm{tar}})\big)\int_{\mathbb{R}^d}|x|^2 d(\mu_v - \mu_{v^{\mathrm{tar}}})(x)}_{a} - \underbrace{\Big(\int_{\mathbb{R}^d} x d(\mu_v - \mu_{v^{\mathrm{tar}}})(x)\Big)^2}_{b}\Big).
\end{aligned}$$

The terms denoted by a and b can be rewritten as follows:

$$\begin{aligned}
a &= \big(\ell(v) - \ell(v^{\mathrm{tar}})\big)\int_{\mathbb{R}^d}|x|^2 d(\mu_v - \mu_{v^{\mathrm{tar}}})(x) \\
&= \big(\ell(v) - \ell(v^{\mathrm{tar}})\big)\left(\int_{\mathbb{R}^d}|x|^2 d\mu_v(x) - \int_{\mathbb{R}^d}|x|^2 d\mu_{v^{\mathrm{tar}}}(x)\right) \\
&= \big(\ell(v) - \ell(v^{\mathrm{tar}})\big)\big(\ell(v)V(v) - \ell(v^{\mathrm{tar}})V(v^{\mathrm{tar}})\big) \\
&\qquad + \ell(v)^2|x_v|^2 - \ell(v)\ell(v^{\mathrm{tar}})|x_v|^2 + \ell(v^{\mathrm{tar}})^2|x_{v^{\mathrm{tar}}}|^2 - \ell(v)\ell(v^{\mathrm{tar}})|x_{v^{\mathrm{tar}}}|^2
\end{aligned}$$

and

$$\begin{aligned}
b &= \Big| \int_{\mathbb{R}^d} x d(\mu_v - \mu_{v^{\mathrm{tar}}})(x) \Big|^2 \\
&= \Big| \int_{\mathbb{R}^d} x d\mu_v(x) - \int_{\mathbb{R}^d} x d\mu_{v^{\mathrm{tar}}}(x) \Big|^2 \\
&= \big| \ell(v) x_v - \ell(v^{\mathrm{tar}}) x_{v^{\mathrm{tar}}} \big|^2 \\
&= \ell(v)^2 |x_v|^2 + \ell(v^{\mathrm{tar}})^2 |x_{v^{\mathrm{tar}}}|^2 - 2\ell(v)\ell(v^{\mathrm{tar}}) \langle x_v, x_{v^{\mathrm{tar}}} \rangle \,.
\end{aligned}$$

Then $a - b$ is equal to

$$\begin{aligned}
a - b = &\big(\ell(v) - \ell(v^{\mathrm{tar}})\big)\big(\ell(v)V(v) - \ell(v^{\mathrm{tar}})V(v^{\mathrm{tar}})\big) \\
&- \ell(v)\ell(v^{\mathrm{tar}})\big(|x_v|^2 + |x_{v^{\mathrm{tar}}}|^2 - 2\langle x_v, x_{v^{\mathrm{tar}}} \rangle\big) \\
= &- \big(\ell(v^{\mathrm{tar}}) - \ell(v)\big)\big(\ell(v)V(v) - \ell(v^{\mathrm{tar}})V(v^{\mathrm{tar}})\big) - \ell(v)\ell(v^{\mathrm{tar}})\big|x_v - x_{v^{\mathrm{tar}}}\big|^2 \,.
\end{aligned}$$

We retrieve the announced formula. □

We exhibit now a condition to the existence of a sequence $(v_{\epsilon_n})_n \subset L^2$ such that $\epsilon_n \to 0$ and for any $n \geq 0$, v_{ϵ_n} is a continuous global minimizer of $E^\lambda(\epsilon_n, .)$.

Proposition 2.3. *Assume that* $\ell_0 = \frac{4\lambda\ell(v^{\mathrm{tar}})}{4\lambda+1} > 2$. *If there exists a decreasing sequence* $\epsilon_n \to 0$ *such that* v_{ϵ_n} *is a continuous global minimizer of* $E^\lambda(\epsilon_n, 0)$ *then for any global minimizer* v^* *of* $E^\lambda(0, \cdot)$*, we have*

$$\min\left(\frac{\partial E^\lambda}{\partial \epsilon}(0, v^+), \frac{\partial E^\lambda}{\partial \epsilon}(0, v^-)\right) \leq \frac{\partial E^\lambda}{\partial \epsilon}(0, v^*) \,, \tag{4.19}$$

where v^+ *and* v^- *are the only two continuous global minimizers of* $E^\lambda(0, \cdot)$ *(they are constant and defined by* $v^+ \equiv \sqrt{\ell_0^2/4 - 1}$ *and* $v^- = -v^+$*).*

Proof. Denote $v_n = v_{\epsilon_n}$. According to Proposition 2.2, either v^+ or v^- is an accumulation point of $(v_n)_n$. Assume that $(v_n)_n$ converges to v^+ (one can extract a subsequence if necessary) and consider v^* a global minimizer of $E^\lambda(0, \cdot)$. The continuity of $(\epsilon, v) \mapsto \partial_\epsilon E^\lambda(\epsilon, v)$ on a neighborhood of $(0, v^+)$ implies then that

$$\begin{aligned}
E^\lambda(\epsilon_n, v^*) \geq E^\lambda(\epsilon_n, v_n) &= E^\lambda(0, v_n) + \epsilon_n \partial_\epsilon E^\lambda(0, v_n) + o(\epsilon_n) \\
&= E^\lambda(0, v_n) + \epsilon_n \partial_\epsilon E^\lambda(0, v^+) + o(\epsilon_n) \\
&\geq E^\lambda(0, v^*) + \epsilon_n \partial_\epsilon E^\lambda(0, v^+) + o(\epsilon_n) \\
&\geq E^\lambda(\epsilon_n, v^*) - \epsilon_n \partial_\epsilon E^\lambda(0, v^*) + \epsilon_n \partial_\epsilon E^\lambda(0, v^+) + o(\epsilon_n) \,.
\end{aligned}$$

In fine, we have $\epsilon_n \big(\partial_\epsilon E^\lambda(0, v^+) - \partial_\epsilon E^\lambda(0, v^*) + o(1)\big) \leq 0$ and we deduced as wanted that $\partial_\epsilon E^\lambda(0, v^+) \leq \partial_\epsilon E^\lambda(0, v^*)$.

Likewise, if $(v_n)_n$ converges to v^-, we get that $\partial_\epsilon E^\lambda(0, v^-) \leq \partial_\epsilon E^\lambda(0, v^*)$. □

In conclusion, one needs to find a target, a well-chosen λ and v^* a global minimizer of $E^\lambda(0, \cdot)$ such that the inequality (4.19) is invalidated. It would consequently exist a deleted neighborhood of $\epsilon = 0$ (meaning a neighborhood of $\epsilon = 0$ without 0) for which there exists no continuous global minimizer of $E^\lambda(\epsilon, .)$. The sought-after vector fields v^{tar} and v^* must thus induce

$$\frac{\partial E^\lambda}{\partial \epsilon}(0, v^*) < \frac{\partial E^\lambda}{\partial \epsilon}(0, v^\alpha)\,, \tag{4.20}$$

where $v^\alpha \in \{v^+, v^-\}$. Let us recall that we chose a decreasing function ρ (which is the case of most usual kernels used to model varifolds) so that $\rho'(0) < 0$. Since all optimal curves have the same length, one can define $\ell_0 = \ell(v^*) = \ell(v^\alpha)$ and according to Proposition 2.3, this inequality (4.20) is equivalent to

$$\big(\ell(v^{\text{tar}}) - \ell_0\big)V(v^*) + \ell(v^{\text{tar}})|x_{v^{\text{tar}}} - x_{v^*}|^2 < \big(\ell(v^{\text{tar}}) - \ell_0\big)V(v^\alpha) + \ell(v^{\text{tar}})|x_{v^{\text{tar}}} - x_{v^\alpha}|^2\,.$$

Moreover, if we can have $\frac{4\lambda\ell(v^{\text{tar}})}{4\lambda+1} > 2$ then $\ell_0 = \frac{4\lambda\ell(v^{\text{tar}})}{4\lambda+1}$ and $\ell(v^{\text{tar}}) - \ell_0 = 1/(4\lambda+1)$. *In fine*, the counterexample must satisfy

$$\frac{V(v^*)}{4\lambda+1} + \ell(v^{\text{tar}})|x_{v^{\text{tar}}} - x_{v^*}|^2 < \frac{V(v^\alpha)}{4\lambda+1} + \ell(v^{\text{tar}})|x_{v^{\text{tar}}} - x_{v^\alpha}|^2\,. \tag{4.21}$$

Let us construct it explicitly. Consider for example $v^{\text{tar}}(t) = a\mathbf{1}_{t\le 1/2}$ with $a > 0$. The target curve $c_{v^{\text{tar}}}$ is then given by $t \to (t, a(1/2-t)^+)$ and we have $\ell(v^{\text{tar}}) = (1+\sqrt{a^2+1})$,

$$x_{v^{\text{tar}}} = \Big(0, \frac{\sqrt{a^2+1}}{1+\sqrt{a^2+1}}\frac{a}{4}\Big) \tag{4.22}$$

and

$$x_{v^\alpha} = \Big(0, \frac{\alpha}{2}\sqrt{\frac{\ell^2}{4} - 1}\Big)\,, \tag{4.23}$$

where we assume that λ is large enough so that $\ell = \frac{4\lambda\ell(v^{\text{tar}})}{4\lambda+1} > 2$.

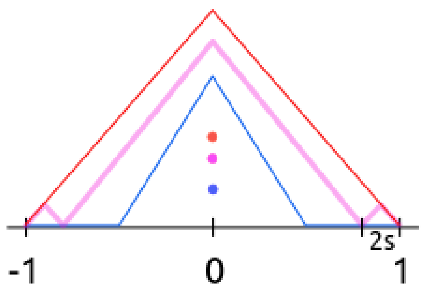

Figure 4.2 – The target c_{tar} is the blue curve. The red curve is c_{v^+} where v^+ is the positive unique global continuous minimizer of $E^\lambda(0, v)$. The pink curve belongs to the set of curves generated by the $v^{s,*}$. The three dots in the middle are the respective centroid of the curves. One can see on this figure that $x_s^2 - x_{v^{\text{tar}}}^2$ is strictly positive and it increases when s tends to 0 (the pink dot tends to the red dot when s tends to 0).

It results that the optimal continuous solution is $v^\alpha = v^+$. Let us introduce a set of vector fields $(v^{s,*})_{s\ge 0}$ defined by

$$v^{s,*}(t) = \sqrt{\ell^2/4 - 1}(\mathbf{1}_{t<1-2s} + \operatorname{sign}(t - (1-s))\mathbf{1}_{t\ge 1-2s})\,.$$

We have $v^+ = v^{0,*}$ and for any $s \geq 0$, $(v^{s,*})^2 + 1 \equiv \ell^2/4$ so that $v^{s,*}$ is a global minimizer of $E^\lambda(0,\cdot)$ that is not continuous when $s > 0$. In order to prove inequality (4.21), we just have to show that the derivative with respect to s of

$$s \mapsto \frac{V(v^{s,*})}{4\lambda + 1} + \ell(v^{\text{tar}})|x_{v^{\text{tar}}} - x_{v^{s,*}}|^2$$

is strictly negative on a neighborhood of $s = 0^+$.

Denote $x_s \doteq x_{v^{s,*}}$. We have

$$\begin{aligned} x_s &= \left(0, \left(s^2 + (1-2s)(1-2s)/2\right)\sqrt{\ell^2/4 - 1}\right) \\ &= \left(0, \left(3s^2 - 2s + \frac{1}{2}\right)\sqrt{\ell^2/4 - 1}\right). \end{aligned}$$

One can easily show that $\frac{d}{ds}(|x_{v^{\text{tar}}} - x_{v^{s,*}}|^2)_{|s=0} < 0$. It follows that $\frac{d}{ds}(V(v^{s,*}))_{|s=0} \leq 0$. If we denote $x_s = (x_s^1, x_s^2)$ then $s \mapsto x_s^1$ is constant and $\frac{dx_s^2}{ds}_{|s=0} < 0$. At last, we need to show that there exist a and λ such that $x_s^2 - x_{v^{\text{tar}}}^2 > 0$. Assume then that λ is close to $+\infty$ so that $\ell = \ell(v^{\text{tar}}) + o(1)$. Then since the sign of $g(a) = \sqrt{\ell^2/4 - 1}/2 - \frac{\sqrt{a^2+1}}{1+\sqrt{a^2+1}}a/4 = x_s^2 - x_{v^{\text{tar}}}^2 + o(1)$ where $\ell = (1 + \sqrt{a^2+1})$ is strictly positive when $a > 0$ (see Figure 4.2), we deduce the final result.

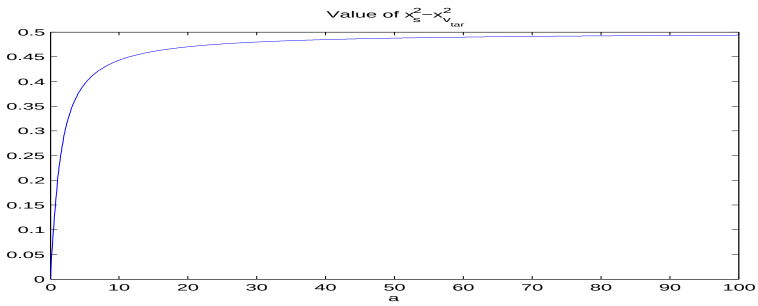

Figure 4.3 – Plot of the function g

In conclusion, we showed that for any $a > 0$, if λ is large enough and $\epsilon > 0$ small enough, the energy $E^\lambda(\epsilon, .)$ admits no global minimizer in $\mathcal{C}([0,1], \mathbb{R}) \cap L^2([0,1], \mathbb{R})$. Let us remark additionally that this is not a consequence of the discontinuity of v^{tar}. Indeed, one can easily replace v^{tar} by an approximation in $\mathcal{C}^\infty$ with respect to the L^2-norm and deduce the same result.

Remark 2.3. *Note that this counterexample could not be applied to the currents. Indeed, the choice of the kernel k_T is not open and the canceling effect of this kernel on opposite normal vectors would reduce the length of the set of curves generated by the $v^{s,*}$ (the pink curve displayed in Figure 4.2).*

2.3 Extension to the 3D case

As in the 2D case, we attempt now to show the following theorem for surfaces in $\mathbb{R}^3$.

Theorem 2.2. *There exist $v^{\text{tar}} \in L^2([0,1], \mathbb{R})$, $\lambda > 0$ and W such that E_W^λ has no time-continuous global minimizer.*

The main ideas of the proof remain the same. We consider as in Definition 2.1 a similar set of RKHS W_ϵ whose kernel is given by $k_\epsilon(x,y) = \rho(\epsilon|x-y|^2_{\mathbb{R}^3})$ where ρ is positive, $\rho(0) = 1$ and $\rho'(0) < 0$. Proposition 2.4 will establish that $E^\lambda_{W_0}$ admits again exactly two continuous global minimizers v^+ and v^- among an infinite number of global minimizers. Proposition 2.5 will then show that the continuous solutions relative to $\epsilon > 0$ lie necessary in a neighborhood of v^+ or v^-. At last, we will present a situation where the continuity is a constraint too restrictive as there exist global minimizers of $E^\lambda_{W_0}$ more stable with respect to ϵ than v^+ and v^-. In other words, if the energy increases more slowly around a discontinuous minimizer v^* than around v^+ and v^-, the existence of continuous global minimizers of $E^\lambda_{W_\epsilon}$ for ϵ in a deleted neighborhood of 0 is excluded. As before, this will require to compare the gradients of $E^\lambda_{W_0}$ with respect to ϵ at the minimizers of $v \mapsto E^\lambda_{W_0}(v)$. We will denote again $E^\lambda(\epsilon, \cdot) = E^\lambda_{W_\epsilon}$.

The coordinate space X is now the unit disc, equipped with the polar coordinate system. Points at their initial position are given by $q_0(\theta, r) = (r\cos\theta, r\sin\theta, 0)$. The birth tag τ is equal to the radius $\tau(\theta, r) = r$. The growth dynamic is as before limited to vertical translations:

$$v \in L^2([0,1],\mathbb{R}), \qquad\qquad \dot{q}_t(\theta, r) = (0,0,v_t)\mathbb{1}_{\tau \le t}\,.$$

The energy only refers to the final state of the shape. Thus, defining $\gamma_v(\theta, r) = q_1(\theta, r)$, it follows that any "vector field" $v \in L^2([0,1],\mathbb{R})$ generates a surface described by the parametric function

$$\gamma_v(\theta, r) = (r\cos\theta, r\sin\theta, \int_r^1 v_s\, ds)\,. \tag{4.24}$$

Let $\mathrm{J}\gamma_v$ be the Jacobian determinant of γ_v,

$$\begin{aligned} \partial_\theta\gamma_v(\theta,r) &= (-r\sin\theta, r\cos\theta, 0)\,, \qquad & \mathrm{J}\gamma_v(\theta,r) &= |\partial_\theta\gamma_v(\theta,r) \wedge \partial_r\gamma_v(\theta,r)| \\ \partial_r\gamma_v(\theta,r) &= (\cos\theta, \sin\theta, -v_r)\,, & \mathrm{J}\gamma_v(\theta,r) &= \mathrm{J}\gamma_v(r) = r\sqrt{1+v_r^2}\,. \end{aligned}$$

The linear form $\mu_v \in W'$ representing the horn γ_v is given for any $\omega \in W$ by

$$\mu_v(\omega) = \int_{\mathbb{R}^3 \times G_2(\mathbb{R}^3)} \omega(x,V)\, d\mu_v(x,V) = \int_0^{2\pi}\int_0^1 \omega(\gamma_v(\theta,r), T_{\gamma_v(\theta,r)}\gamma_v) r\sqrt{1+v_r^2}\, dr d\theta\,,$$

where $T_{\gamma_v(\theta,r)}\gamma_v$ is tangent plane at $\gamma_v(\theta, r)$. The energy functions to minimize, associated to the spaces W_ϵ, are unchanged

$$E^\lambda(\epsilon, v) = \frac{1}{2}\int_0^1 v_t^2\, dt + \frac{\lambda}{2}|\mu_{v^{\mathrm{tar}}} - \mu_v|^2_{W'_\epsilon}\,.$$

Consider now the case $\epsilon = 0$. The kernel of W_0 is the constant unit kernel. By analogy with the 2D case, the area of the surface γ_v is denoted $\ell(v)$ and we have

$$\ell(v) = |\mu_v|^2_{W'_0} = \int_0^{2\pi}\int_0^1 r\sqrt{1+v(r)^2}\, dr d\theta \tag{4.25}$$

$$= 2\pi\int_0^1 r\sqrt{1+v(r)^2}\, dr\,. \tag{4.26}$$

Remark 2.4. *Note that for any $v \in L^2([0,1], V)$, we have $\ell(v) \geq \pi$. The growth process can only expand the initial unit disc.*

In the degenerate situation (for $\epsilon = 0$ and $k_{W_0} \equiv 1$) the energy is thus given by

$$E^\lambda(0, v) = \frac{1}{2} \int_0^1 v(t)^2 \, dt + \frac{\lambda}{2} \left(\ell(v^{\text{tar}}) - \ell(v) \right)^2 .$$

The next proposition will establish the minimizers of this energy. For this purpose, given any constant $c \geq 1$, we will say that $v \in L^2([0,1], V)$ satisfies the (P_c) property if

$$(P_c) \left| \begin{array}{l} \text{for almost any time } t \in [0,1], \\ v^2(t) = \begin{cases} 0 & \text{if } t \leq \frac{1}{c} \\ (ct)^2 - 1 & \text{otherwise.} \end{cases} \end{array} \right.$$

Proposition 2.4. *For any $\lambda \geq 0$, there exists a unique constant $c_0 \geq 1$ such that: $v^* \in L^2([0,1], \mathbb{R})$ is a global minimizer of $E^\lambda(0, \cdot)$ if and only if it satisfies the (P_{c_0}) property.*

Additionally, $c_0 = 1$ if and only if $\ell(v^{\text{tar}}) \leq \pi + 1/(2\pi\lambda)$. In this last case, $v^* \equiv 0$ is the unique global minimizer of $E^\lambda(0, \cdot)$.

Proof. The proof is similar as the one of Proposition 2.1. Introduce for $c \geq 1$

$$\rho_c(z, t) = \frac{z^2}{2} - ct\sqrt{z^2 + 1} ,$$

defined on $\mathbb{R} \times [0,1]$. Given $t \in [0,1]$, the function $\rho_c(z,t)$ reaches its minimum at $z = 0$ if $t \leq \frac{1}{c}$ and at $z_c \doteq \pm \sqrt{(ct)^2 - 1}$ otherwise. Thus $v \in L^2([0,1], \mathbb{R})$ minimizes

$$\int_0^1 \rho_c(v(t), t) \, dt = \frac{1}{2} \int_0^1 v(t)^2 \, dt - \frac{c}{2\pi} \ell(v)$$

if and only if it satisfies the (P_c) property. Now, if v_c satisfies (P_c) then

$$\begin{aligned} \ell(v_c) &= 2\pi \int_0^1 t\sqrt{1 + v_c^2(t)} \, dt \\ &= 2\pi \left(\int_0^{\frac{1}{c}} t \, dt + \int_{\frac{1}{c}}^1 t\sqrt{(ct)^2} \, dt \right) \\ &= 2\pi \left(\frac{1}{2c^2} + c \left[\frac{t^3}{3} \right]_{\frac{1}{c}}^1 \right) \\ &= \frac{2\pi}{3} c + \frac{\pi}{3} \frac{1}{c^2} . \end{aligned}$$

Denote $\hat{\ell} : [1, +\infty[\to \mathbb{R}$ the function defined by

$$\hat{\ell}(c) = \frac{2\pi}{3} c + \frac{\pi}{3} \frac{1}{c^2} \tag{4.27}$$

and remark that $\hat{\ell}$ is a bijection from $[1, +\infty[$ to $[\pi, +\infty[$. (P_c) characterizes the minimizers of the constrained optimization problem

$$\left| \begin{array}{l} \min_{L^2} \int v_t^2 \, dt \\ \text{with } \ell(v) = \hat{\ell}(c) \end{array} \right. .$$

Therefore, (P_c) also determines exactly the minimizers of $E^\lambda(0,\cdot)$ when c minimizes

$$\begin{aligned}
g(c) = E^\lambda(0,v_c) &= \frac{1}{2}\int_{\frac{1}{c}}^{1} (ct)^2 - 1\, dt + \frac{\lambda}{2}(\hat{\ell}(c) - \ell(v^{\text{tar}}))^2 \\
&= \frac{1}{2}\left(c^2 \left[\frac{t^3}{3}\right]_{\frac{1}{c}}^{1} - (1 - \frac{1}{c}) \right) + \frac{\lambda}{2}\left(\frac{2\pi}{3}c + \frac{\pi}{3}\frac{1}{c^2} - \ell(v^{\text{tar}}) \right)^2 \\
&= \frac{c^2}{6} + \frac{1}{3c} - \frac{1}{2} + \frac{\lambda}{2}\left(\left(\frac{2\pi}{3}c + \pi\frac{1}{c^2} \right)^2 + \ell(v^{\text{tar}})^2 - 2\ell(v^{\text{tar}}) \left(\frac{2\pi}{3}c + \frac{\pi}{3}\frac{1}{c^2} \right) \right)^2 \\
&= \left(\frac{1}{6} + \frac{\lambda}{2}\left(\frac{2\pi}{3}\right)^2 \right) c^2 + C + \left(\frac{1}{3} + \frac{\lambda}{2}\left(\frac{2\pi}{3}\right)^2 \right) \frac{1}{c} + \frac{\lambda}{2}\left(\frac{\pi}{3}\right)^2 \frac{1}{c^4} \\
&\quad - \frac{\lambda}{2}\frac{2\pi}{3}\ell(v^{\text{tar}}) \left(2c + \frac{1}{c^2} \right),
\end{aligned}$$

where C is the constant $\frac{\lambda}{2}\ell(v^{\text{tar}})^2 - \frac{1}{2}$.
Since the uniqueness of c is required, let us study the variations of this function. We have

$$g'(c) = \left(\frac{1}{3} + \lambda\left(\frac{2\pi}{3}\right)^2 \right) c - \left(\frac{1}{3} + \frac{\lambda}{2}\left(\frac{2\pi}{3}\right)^2 \right) \frac{1}{c^2} - \frac{\lambda}{2}\left(\frac{2\pi}{3}\right)^2 \frac{1}{c^5}. + \lambda\frac{2\pi}{3}\ell(v^{\text{tar}}) \left(\frac{1}{c^3} - 1 \right)$$

and

$$g''(c) = \left(\frac{1}{3} + \lambda\left(\frac{2\pi}{3}\right)^2 \right) + 2\left(\frac{1}{3} + \frac{\lambda}{2}\left(\frac{2\pi}{3}\right)^2 \right) \frac{1}{c^3} + 5\frac{\lambda}{2}\left(\frac{2\pi}{3}\right)^2 \frac{1}{c^6} - 3\lambda\frac{2\pi}{3}\ell(v^{\text{tar}})\frac{1}{c^4}.$$

For $c \geq 1$, $g'' = 0$ is thus equivalent to $h(c) = 0$ where $h(c) = c^4 g''(c)$. The derivative of h is given by

$$\begin{aligned}
h'(c) &= 4\left(\frac{1}{3} + \lambda\left(\frac{2\pi}{3}\right)^2 \right) c^3 + 2\left(\frac{1}{3} + \frac{\lambda}{2}\left(\frac{2\pi}{3}\right)^2 \right) - 10\frac{\lambda}{2}\left(\frac{2\pi}{3}\right)^2 \frac{1}{c^3} \\
&= c^{-3} Q(c^3),
\end{aligned}$$

where $Q(X) = 4\left(\frac{1}{3} + \lambda\left(\frac{2\pi}{3}\right)^2\right) X^2 + 2\left(\frac{1}{3} + \frac{\lambda}{2}\left(\frac{2\pi}{3}\right)^2\right) X - 10\frac{\lambda}{2}\left(\frac{2\pi}{3}\right)^2$.

Therefore, since Q is strictly increasing on $[1,+\infty[$ and $Q(1) = 2$, $h' > 0$ and h is strictly increasing on $[1,+\infty[$. Moreover, $\ell(v^{\text{tar}}) \geq \pi$ so there exists $s \geq 1$ such that $\ell(v^{\text{tar}}) = s\pi$. Then $h(1) = 1 + 2\pi^2\lambda(1-s)$ and $h(1) < 0$ is equivalent to $s > 1 + 1/(2\pi^2\lambda)$. Under this condition, g'' has only one zero and g' is decreasing then increasing. Otherwise, g' is strictly increasing.

Finally, since $g'(1) = 0$, g has always only one global minimum on $[1,+\infty[$. Additionally, if $\ell(v^{\text{tar}}) \leq \pi + 1/(2\pi\lambda)$, the minimizer is $c_0 = 1$ and corresponds to the solution $v^* \equiv 0$. Otherwise, $c_0 > 1$. $\square$

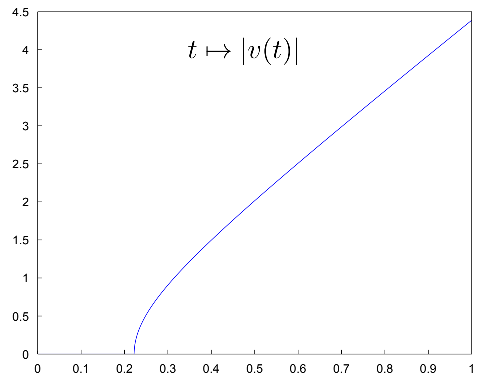

Figure 4.4 – Plot of the norm of any optimal vector field. The (P_c) condition on this example is defined with $c = 4.5$ so that $\ell(v) \approx 3\pi$. The area of the surface has tripled with respect to its initial position.

Remark 2.5. *As in the 2D case, the energy associated to the degenerate kernel admits two continuous global minimizers*

$$v^+(t) \doteq \mathbb{1}_{t > \frac{1}{c_0}} \sqrt{(c_0 t)^2 - 1} \qquad \text{and} \qquad v^- \doteq -v^+ \,. \tag{4.28}$$

They are again surrounded by an infinite number of discontinuous global minimizers. However, these two solutions are not constant anymore. Indeed, in the 2D case, a constant vertical translation creates at all time the same amount of new matter measured by the length of the curve just created above the base between two times t and $t + \delta t$. In the 3D case, the surface created by a constant vertical translation between two times t and $t + \delta t$ is similar to a cylinder whose radius increases with t. The penalization term on v tends thus to accelerate the creation over time (see the new cost functions in Chapter 2 and 5).

As before, we will now follow the continuous global minimizers of $v \mapsto E^\lambda(\epsilon, v)$ when ϵ tends to 0 and show that they belong to a neighborhood of v^+ or v^-.

Proposition 2.5. *Assume that $\lambda > 0$, $\ell(v^{\text{tar}}) > \pi + 1/(2\pi\lambda)$ and that for $\epsilon \geq 0$ small enough, there exists a global continuous minimum v_ϵ of $E^\lambda(\epsilon, \cdot)$. Then*

$$\lim_{\epsilon \to 0} \big(\min(|v_\epsilon - v^+|_\infty, |v_\epsilon - v^-|_\infty) \big) = 0 \tag{4.29}$$

where v^+ and v^- are the only continuous global minimizers of $E^\lambda(0, \cdot)$.

Proof. We first show the convergence of the areas.

Lemma 2.4. *Denote $\ell_0 = \hat{\ell}(c_0) = \ell(v_0)$, then $\ell(v_\epsilon)$ tends to ℓ_0.*

Proof. Consider the function $\hat{\ell}$ defined by equation (4.27). Recall that $\hat{\ell}$ is a bijection from $[1, +\infty[$ to $[\pi, +\infty[$ and as we said in Remark 2.4, that for any $v \in L^2_V$, $\ell(v) \geq \pi$. Therefore, for any $\epsilon \geq 0$, there exists a unique $c_\epsilon \geq 1$ such that $\ell(v_\epsilon) = \hat{\ell}(c_\epsilon)$. Let us show that

$$E^\lambda(0, v_\epsilon) \leq E^\lambda(\epsilon, v_\epsilon) + o(1) \leq E^\lambda(\epsilon, v_0) + o(1) \leq E^\lambda(0, v_0) + o(1) \,.$$

Left and right inequalities result from the continuity of $E^\lambda(\cdot, v)$. Since v_ϵ minimizes $E^\lambda(\epsilon, \cdot)$, the central inequality is also true. Moreover, Proposition 2.4 ensures that for any v_{c_ϵ} that satisfies (P_{c_ϵ}), we also have $E^\lambda(0, v_{c_\epsilon}) \leq E^\lambda(0, v_\epsilon)$. We introduced in the proof of Proposition 2.4 a function g that satisfies for any $\epsilon \geq 0$, $g(c_\epsilon) = E^\lambda(0, v_{c_\epsilon})$. Moreover, c_0 is the unique minimum of g. It results that

$$g(c_0) \leq g(c_\epsilon) \leq g(c_0) + o(1)\,.$$

Hence, $g(c_\epsilon)$ tends to $g(c_0)$ and since g is continuous and increases around $+\infty$, c_ϵ tends to c_0. The continuity of $\hat{\ell}$ ensures at last that $\hat{\ell}(c_\epsilon)$ tends to $\hat{\ell}(c_0)$ so that $\ell(v_\epsilon)$ converges as announced to $\ell_0 = \hat{\ell}(c_0) = \ell(v_0)$. $\square$

For any $\epsilon \geq 0$, v_ϵ is a zero of the gradient with respect to v of the energy

$$E^\lambda(\epsilon, v) = \frac{1}{2}\int_0^1 v_t^2\, dt + \frac{\lambda}{2}|\mu_v - \mu_{v^{\mathrm{tar}}}|^2_{W'_\epsilon}\,.$$

Consider $\omega_v(\epsilon, \cdot) = K_{W_\epsilon}(\mu_v - \mu_{v^{\mathrm{tar}}})$ given for any $x \in \mathbb{R}^3$ by

$$\omega_v(\epsilon, x) = K_{W_\epsilon}(\mu_v - \mu_{v^{\mathrm{tar}}})(x) = \int_{\mathbb{R}^3} \rho(\epsilon|x-y|^2)\, d(\mu_v - \mu_{v^{\mathrm{tar}}})(y)\,,$$

so that

$$\mu_v(K_{W_\epsilon}(\mu_v - \mu_{v^{\mathrm{tar}}})) = \int_0^{2\pi}\int_0^1 \omega(\epsilon, \gamma_v(\theta, r)) r\sqrt{1+v_r^2}\, dr d\theta\,.$$

We have then for any variation $\delta v \in L^2([0,1], \mathbb{R})$

$$\begin{aligned}
\Big(\partial_v E^\lambda(\epsilon, v)\,\big|\,\delta v\Big) &= \int_0^1 v_t\, \delta v_t\, dt + \lambda\big(\partial_v \mu_v\,|\,\delta v\big)(K_{W_\epsilon}(\mu_v - \mu_{v^{\mathrm{tar}}}))\\
&= \int_0^1 v_t\, \delta v_t\, dt
\end{aligned}$$
$$+\lambda\int_0^{2\pi}\int_0^1 \Big(\partial_2\omega_v(\epsilon, \gamma_v(\theta, r))\,|\,(0,0,\int_r^1 \delta v_s\, ds)\Big) r\sqrt{1+v_r^2} + \omega_v(\epsilon, \gamma_v(\theta, r))\frac{r v_r \delta v_r}{\sqrt{1+v_r^2}}\, dr d\theta\,,$$

with $\partial_2\omega_v(\epsilon, x) = 2\epsilon\int_{\mathbb{R}^3} \rho'(\epsilon|x-y|^2)(x-y)\, d(\mu_v - \mu_{v^{\mathrm{tar}}})(y)$. Denote at last

$$\begin{aligned}
z_{\epsilon,v}(r) &= \int_0^{2\pi} r\omega_v(\epsilon, \gamma_v(\theta, r))\, d\theta\\
\alpha_{\epsilon,v}(s) &= \lambda\int_0^{2\pi}\int_0^s \Big(\partial_2\omega_v(\epsilon, \gamma_v(\theta, r))\,|\,(0,0,1)\Big) r\sqrt{1+v_r^2}\, dr d\theta\,.
\end{aligned}$$

The gradient can thus be written

$$\nabla_v E^\lambda(\epsilon, v) = \left(1 + \lambda\frac{z_{\epsilon,v}}{\sqrt{1+v^2}}\right) v + \alpha_{\epsilon,v}\,.$$

We have as before $\lim_{\epsilon\to 0}\omega_v(\epsilon,\cdot)\equiv \ell(v)-\ell(v^{\mathrm{tar}})$ and therefore

$$\lim_{\epsilon\to 0} z_{\epsilon,v}(t) = -2\pi t(\ell(v^{\mathrm{tar}})-\ell(v))\,.$$

Moreover, on any bounded neighborhood of $(0,0)$ of $\mathbb{R}^+\times L^2([0,1],V)$, γ_v is bounded, $d\mu_v$ and $d\mu_{v^{\mathrm{tar}}}$ are finite, so that with ρ' bounded we have

$$|\partial_2\omega_v(\epsilon,\gamma_v)|_\infty = O(\epsilon) \qquad\text{and}\qquad |\alpha_{\epsilon,v}|_\infty = O(\epsilon)\,.$$

Now, a continuous minimizers of $E^\lambda(\epsilon,\cdot)$ must satisfy

$$\left(1+\lambda\frac{z_{\epsilon,v_\epsilon}}{\sqrt{1+v_\epsilon^2}}\right)v_\epsilon+\alpha_{\epsilon,v_\epsilon}=0\,. \tag{4.30}$$

Hence, there exist for $\epsilon>0$ small enough $M>0$ and $\beta_\epsilon\geq 0$ such that we have either

$$(i)\quad \left|\sqrt{1+v_\epsilon(t)^2}-t\beta_\epsilon\right|\leq M\epsilon^{\frac12}\sqrt{1+v_\epsilon(t)^2}\qquad\text{or}\qquad (ii)\quad |v_\epsilon(t)|\leq M\epsilon^{\frac12}\,.$$

More precisely, denote $\beta_0=2\pi\lambda(\ell(v^{\mathrm{tar}})-\ell_0)$ then Lemma 2.4 implies that $\beta_\epsilon=\beta_0+o(1)$. Note that if $\beta_0\leq 0$, then v_ϵ tends to 0 so that $\ell(v_\epsilon)$ tends to π and Lemma 2.4 implies that $\ell_0=\pi$. It results that if $\beta_0\leq 0$ then $\ell(v^{\mathrm{tar}})\leq\ell_0=\pi$. Hence, since $\ell(v^{\mathrm{tar}})>\pi+1/(2\pi\lambda)$, Proposition 2.4 ensures that $\ell_0>\pi$ so that v_ϵ does not tend to 0 and $\beta_0>0$.

Denote as before for any $\epsilon>0$, $A_\epsilon\doteq\{t\in[0,1]\,|\,|\sqrt{v_\epsilon^2(t)+1}-t\beta_\epsilon|\leq M\epsilon^{\frac12}\sqrt{v_\epsilon^2(t)+1}\}$. If $t\in A_\epsilon$, then

$$1-M\epsilon^{\frac12}\leq(1-M\epsilon^{\frac12})\sqrt{1+v_\epsilon^2(t)}\leq t\beta_\epsilon\leq\beta_\epsilon\,,$$

so that $A_\epsilon\subset[\frac{1-M\epsilon^{\frac12}}{\beta_\epsilon},1]$. Consequently, v_ϵ tends uniformly to 0 on $[0,\frac{1}{\beta_0}[$ and since v_ϵ is continuous, this is also true on $[0,\frac{1}{\beta_0}]$.

Now, if $t\in A_\epsilon$ is large enough, $v_\epsilon^2(t)$ admits a lower bound strictly positive. This will allow us to show that if $t\in A_\epsilon$, then $[t,1]\subset A_\epsilon$. For any $t\in A_\epsilon$

$$t\beta_\epsilon\leq(1+M\epsilon^{\frac12})\sqrt{1+v_\epsilon^2}\,. \tag{4.31}$$

Consider a small $\alpha>0$ and let us show that for $\epsilon>0$ small enough, $I_\alpha=]\frac{1}{\beta_0}(1+\alpha),1]\subset A_\epsilon$. There exists $\eta>0$ such that for any $\epsilon<\eta$, we have

1. for any $t\in I_\alpha$, $t\beta_\epsilon\geq 1+\alpha/2$,
2. $1+M\epsilon^{\frac12}\leq(1+\alpha/2)(1+\alpha/3)^{-\frac12}$ and $M\epsilon^{\frac12}\leq\alpha/4$.

Equation (4.31) ensures then that for any $\epsilon<\eta$, if $t\in I_\alpha\cap A_\epsilon$, then

$$v_\epsilon^2(t)\geq\frac{\alpha}{3}\,. \tag{4.32}$$

Conversely, if $t\in I_\alpha\cap A_\epsilon^c$ where $A_\epsilon^c=[0,1]\setminus A_\epsilon$, then

$$v_\epsilon^2(t)\leq\frac{\alpha}{4}\,. \tag{4.33}$$

Since v_ϵ is continuous, either $I_\alpha\cap A_\epsilon$ or $I_\alpha\cap A_\epsilon^c$ is empty. Since $\ell(v_\epsilon)$ tends to $\ell_0>\pi$, it results that for α and η small enough, for any $\epsilon < \eta$, $I_\alpha =]\frac{1}{\beta_0}(1+\alpha), 1] \subset A_\epsilon$.

Finally, v_ϵ converges uniformly to 0 on $[0, \frac{1}{\beta_0}]$ and $\sqrt{1+v_\epsilon^2}$ converges uniformly to $t \mapsto \beta_0 t$ on $[\frac{1}{\beta_0}, 1]$. In other words, this uniform limit satisfies the (P_c) property for $c = \beta_0$. Additionally, equation (4.30) says that any minimizer of $E^\lambda(0,\cdot)$ must also satisfy (P_c). Proposition 2.4 ensures the uniqueness of this constant c when (P_c) characterizes the minimizers of $E^\lambda(0,\cdot)$. Consider then v^+ and v^- the two continuous global minimizers of $E^\lambda(0,\cdot)$. Since v_ϵ is continuous, we just prove that there exists $M' > 0$ such that for any $\epsilon > 0$

$$|v_\epsilon - v^+|_\infty \leq M\epsilon \quad \text{or} \quad |v_\epsilon - v^+|_\infty \leq M\epsilon\,.$$

□

As before, we will now show that if such a sequence exists, then the energy, considered on a neighborhood of $\epsilon = 0^+$, must remain minimal on a neighborhood in L^2 of the limit v^+ or v^- of the sequence (or both if the sequence oscillates).

Proposition 2.6. *If there exists a decreasing sequence $\epsilon_n \to 0$ such that v_{ϵ_n} is a continuous global minimizers of $E^\lambda(\epsilon_n,\cdot)$ then for any global minimizers v^* of $E^\lambda(0,\cdot)$, we have*

$$\min\left(\partial_\epsilon E^\lambda(0,v^+), \partial_\epsilon E^\lambda(0,v^-)\right) \leq \partial_\epsilon E^\lambda(0,v^*)\,. \tag{4.34}$$

Proof. According to Proposition 2.5, there exists a subsquence of $(v_{\epsilon_n})_n$ which converges either to v^+ or v^-. The proof of Proposition 2.3 can then be applied here. □

The final step is to construct the counterexample for which inequality (4.34) does not occur. Recall the geometric expression of $\partial_\epsilon E^\lambda$ given by Lemma 2.3 :

$$\partial_\epsilon E^\lambda(0,v) = \lambda\rho'(0)\Big(\big(\ell(v^{\text{tar}}) - \ell(v)\big)\big(\ell(v^{\text{tar}})V(v^{\text{tar}}) - \ell(v)V(v)\big) - \ell(v)\ell(v^{\text{tar}})|x_{v^{\text{tar}}} - x_v|^2\Big)\,,$$

where

$$x_v = \frac{1}{\ell(v)}\int x\,d\mu_v(x) \qquad\qquad V(v) = \frac{1}{\ell(v)}\int |x - x_v|^2\,d\mu_v(x)\,.$$

Since all global minimizers of $E^\lambda(0,\cdot)$ have the same length, denote $\ell_0 = \ell(v^*) = \ell(v^+)$ and since $\rho'(0) < 0$, a counterexample should thus lead to a couple (v^*, v^+) satisfying:

$$V(v^*)\left[\ell(v^{\text{tar}}) - \ell_0\right] + \ell(v^{\text{tar}})|x_{v^{\text{tar}}} - x_{v^*}|^2 < V(v^+)\left[\ell(v^{\text{tar}}) - \ell_0\right] + \ell(v^{\text{tar}})|x_{v^{\text{tar}}} - x_{v^+}|^2\,. \tag{4.35}$$

We exclude the negative continuous solution v^- as it is easy to show that for a target above the plane $Z = 0$, this solution will not be approached by any global minimizer of E^λ_ϵ for $\epsilon > 0$. Moreover, we have explicitly $V(v^+) = V(v^-)$ and if $\gamma_{v^{\text{tar}}} \subset (Z \geq 0)$, $|x_{v^{\text{tar}}} - x_{v^+}| < |x_{v^{\text{tar}}} - x_{v^-}|$.

Proposition 2.7. *There exists a target such that for λ large enough inequality* (4.35) *occurs.*

As we saw earlier, the minimization of $E^\lambda(0,\cdot)$ admits either a unique solution (equal to 0) or an infinite number of solutions. In this last case, there are only two continuous solutions. One can observe that these solutions are those which, at a fixed area, produce the most widely deployed surface. We will show with the following example that this property can be very restrictive. The partial derivative of E^λ with respect to ϵ at $(0, v)$, where v is a minimum, measures the stability of this minimum with respect to small variations of ϵ. Intuitively, the best candidate among this infinite number of solutions, is the one which generates the surface that is geometrically the closest to the target. The previous expression gives an explicit description of this closeness according to the attachment term we chose. It requires a small variance and a centroid close the target's one. Here is then a possible example.

The idea is to create a compact accordion. It will allow to create a surface with a large area that yet remains close to the horizontal plane. Consider a target generated by one of the following vector fields

$$v_n^{\mathrm{tar}}(t) = nhs_n(t)\,, \qquad \text{with} \qquad \begin{array}{ccc} [0,1] & \xrightarrow{s_n} & \{-1,1\} \\ t & \mapsto & \mathbb{1}_{\lfloor nt \rfloor = 0[2]} - \mathbb{1}_{\lfloor nt \rfloor = 1[2]}\,, \end{array}$$

with $n \in \mathbb{N}$, $h \in]0,1]$ a scale constant. Figure 4.5 displays an example for $n = 21$ and $h = 0.1$.

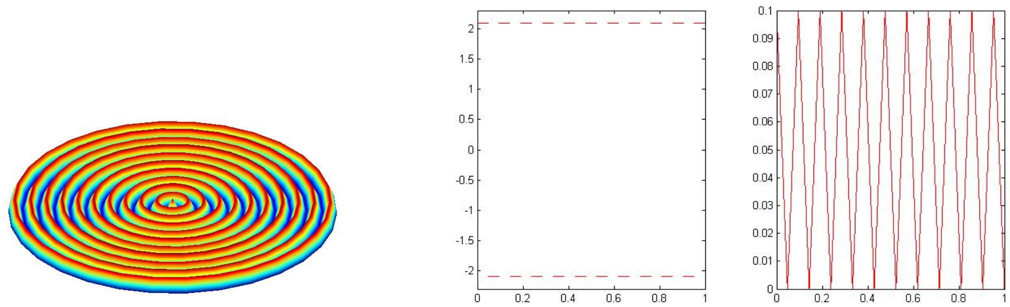

Figure 4.5 – From left to right: the target, the vector field which generates it from the unit disc with vertical translations, a radial cut of the surface (plot of the vertical component $z_{v^{\mathrm{tar}}}(r)$).

Let us recall that

$$\gamma_v(\theta, r) = (r\cos\theta, r\sin\theta, \int_r^1 v_s\, ds)\,.$$

Denote z_v the third component of γ_v. It satisfies for $v = v_n^{\mathrm{tar}}$, for any $r \in [0,1]$, $|z_{v_n^{\mathrm{tar}}}(r)| = |\int_r^1 v_n^{\mathrm{tar}}(s)\, ds| \leq h$. Moreover, $\ell(v_n^{\mathrm{tar}}) = 2\pi\sqrt{1 + (nh)^2}$. Therefore, no matter the choice of n, the target shape remains concentrated in $D \times [-h, +h]$ (where D is the unit disc). Yet, one can fix its area as large as necessary by increasing n.

The solutions v^* that minimize $E^\lambda(0, \cdot)$ are characterized by the (P_c) property with a optimal constant c to define and such that $\ell(v^*) = \hat{\ell}(c)$ denoted again ℓ_0. One can easily show that if λ tends to $+\infty$, ℓ_0 tends to $\ell(v^{\text{tar}})$. For λ large enough, we have thus

$$\ell_0 = \hat{\ell}(c) = \frac{2\pi}{3}c + \frac{\pi}{3c^2} \approx 2\pi\sqrt{1+(nh)^2} = \ell(v^{\text{tar}})\,.$$

If hn is large enough, one can do the approximation $c \approx 3hn$.

Let us compare v^+ and v_n^* defined for any $t \in [0,1]$ by

$$v^+(t) = \mathbb{1}_{t>\frac{1}{c}}\sqrt{(ct)^2-1} \qquad \text{and} \qquad v_n^*(t) = s_n(t)v^+(t)\,,$$

where n is given by the choice of the target. They both satisfy (P_c). These two vector fields are displayed in Figure 4.7 and the surfaces that they generate are presented in Figure 4.6. When n increases, the continuous solution grows in space when the other one remains concentrated since $|z_{v_n^*}(r)| \leq \frac{1}{n}\sqrt{c^2-1} \approx 3h$.

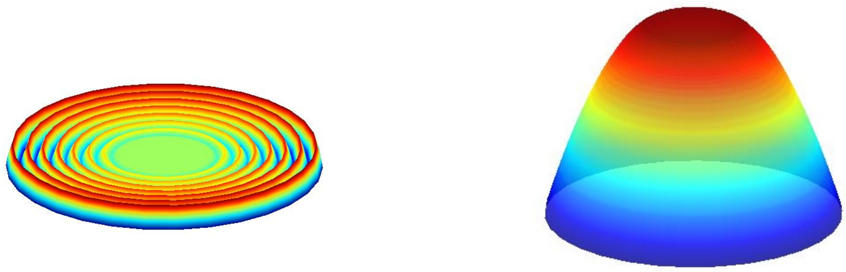

Figure 4.6 – Surfaces generated from two solutions for the matching of the surface displayed in Figure 4.5. On the left: with the discontinuous vector field $s_n v^+$, on the right: with the continuous vector field v^+

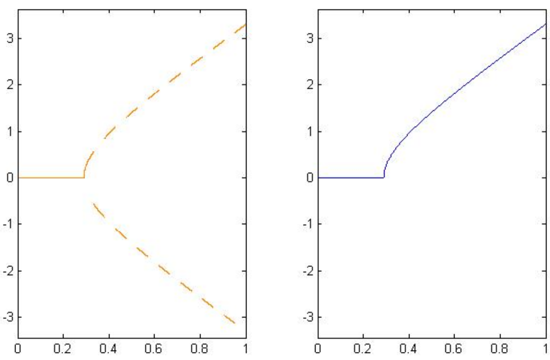

Figure 4.7 – On the left: $v_n^* = s_n v^+$, on the right: v^+.

More precisely, for any surface generated by $v \in L^2$, the centroid belongs to the vertical axis through the origin. When x_{v^+} will move upwards when n increase, we have conversely for any n

$$|x_{v_n^{\text{tar}}}| \leq \max_r |z_{v_n^{\text{tar}}}(r)| \leq h \quad \text{and} \quad |x_{v_n^*}| \leq \max_r |z_{v_n^*}(r)| \leq 3h\,.$$

Likewise, for any $v \in L^2$

$$
\begin{aligned}
V(v) &= \frac{1}{\ell(v)} \int_{\mathbb{R}^3} |x - x_v|^2 \, d\mu_v(x) \\
&= \frac{1}{\ell(v)} \int (r\cos\theta)^2 + (r\sin\theta)^2 + |z_v(r) - x_v|^2 \, d\mu_v(x) \\
&= \frac{1}{\ell(v)} \frac{2\pi}{3} + \frac{1}{\ell(v)} \int |z_v(r) - x_v|^2 \, d\mu_v(x) \, .
\end{aligned}
$$

It follows that

$$
V(v_n^*) \leq \frac{2\pi}{3\ell_0} + (6h)^2 \qquad \text{and} \qquad V(v^+) = \frac{2\pi}{3\ell_0} + \frac{1}{\ell_0} \int |z_{v^+}(r) - x_{v^+}|^2 \, d\mu_{v^+}(x) \, .
$$

In fine, if nh is fixed, $V(v^+)$ and $|x_{v_n^{\mathrm{tar}}} - x_{v^+}|^2$ are fixed and strictly positive. Yet in the same time, if h tends to 0, $V(v_n^*)$ can be reduced to the minimal variance over the vector fields that satisfy (P_c) and $|x_{v_n^{\mathrm{tar}}} - x_{v_n^*}|^2$ tends to 0. Therefore, the inequality

$$
V(v^*) \left[\ell(v^{\mathrm{tar}}) - \ell_0\right] + \ell(v^{\mathrm{tar}})|x_{v^{\mathrm{tar}}} - x_{v^*}|^2 < V(v^+) \left[\ell(v^{\mathrm{tar}}) - \ell_0\right] + \ell(v^{\mathrm{tar}})|x_{v^{\mathrm{tar}}} - x_{v^+}|^2
$$

can be satisfied.

In conclusion, note that $v^* = s_n v^+$ might not be the best candidate to minimize $\partial_\epsilon E^\lambda(\epsilon, \cdot)$ on a neighborhood of $\epsilon = 0$, but it was easy to demonstrate that it is strictly better than v^+ for n and λ large enough. As in the 2D case, one could generate similar surfaces with a smooth function s_n. This counterexample is not built on the discontinuity of v^{tar}.

At last, as pointed in Remark 2.5, this 3D example highlights a property of the optimal vector field that did not appear in the 2D case. With the growth dynamic, the norm of the optimal vector field tends to increase over time.

3 Foliation on the biological coordinate system

The development of a time-varying shape is modeled by a mapping between the biological coordinate system (X, τ) and the ambient space $\mathbb{R}^d$. In order to study the growth dynamic in Chapter 3, we assumed that the coordinate space X has a canonical decomposition in a direct product for which the birth tag τ is the projection on the first coordinate. This setting reflects a regularity of the birth tag that plays a role in the evolution of an optimal vector field in the registration problem.

The coordinate space X is then not a regular manifold. We have thus to investigate the boundary of X and the profile of the birth tag $\tau : X \to [0, 1]$ that will give to X a structure of *foliated* manifold.

We will assume that X is a k-dimensional **manifold with corners**. We start with some properties of manifolds with corners. For more details, we refer to [13, 35].

3.1 Manifolds with corners

An orthant of $\mathbb{R}^d$ is a subset $\{(x_1, \dots, x_d) \in \mathbb{R}^d \mid \epsilon_i x_i \geq 0 \text{ for any } i \in \{1, \dots, d\}\}$ where $\epsilon_i \in \{-1, 1\}$. A semi-orthant is a subset of $\mathbb{R}^d$ defined by specifying the signs of some of the coordinates. The simplest examples of **semi-orthant** are the sets $\mathbb{R}^{d-p} \times \mathbb{R}_+^p$ where $p \in \{0, \dots, d\}$.

A k-dimensional manifold with corners extends the definition of *regular* manifolds (in the usual sense) to allow the shape to locally resemble a semi-orthant of $\mathbb{R}^k$. At any $x_0 \in X$, there exists a chart (U, ψ)

$$\begin{array}{ccc} U & \longrightarrow & \mathbb{R}^{k-p} \times \mathbb{R}_+^p \\ x & \mapsto & (x_1, \dots, x_{k-p}, y_1, \dots, y_p)\,, \end{array} \tag{4.36}$$

centered at x_0, i.e. $\psi(x_0) = (0, \cdots, 0)$ between a open set $U \ni x_0$ and a semi-orthant $\mathbb{R}^{k-p} \times \mathbb{R}_+^p$ for an integer $p = p(x_0) \geq 0$ called the *depth* of x_0. For a regular manifold, p is always null. When $p(x) > 0$, x belongs to the boundary ∂X of X. This boundary is a (k-1)-dimensional manifold with corners. If p takes values only in $\{0, 1\}$ on X, then X is called a *manifold with boundary* and ∂X is a regular manifold. See Figure 4.8 for two examples of compact manifolds with corners. We will assume that the transition maps are of class $\mathcal{C}^\infty$. The depth can be seen as a function $p : X \to \{0, \dots, k\}$ that induces a natural stratification of X. Given any $x \in X$, there exists a maximal (k-$p(x)$)-dimensional connected regular manifold that contains x, denoted $\mathcal{M}_x$. These sets are the connected components of the inverse images of p. X is the disjoint union of these sets and ∂X is the disjoint union of all the sets of non maximal dimension.

Example 3.1. *Consider x a point of the full cube. If $p(x) = 0$, $\mathcal{M}_x = \overset{\circ}{X}$ is the interior of the cube. If $p(x) = 1$, respectively $p(x) = 2$, $\mathcal{M}_x$ is the face, respectively the edge, of the cube that contains x. At last, if $p(x) = 3$, $\mathcal{M}_x = \{x\}$ is a vertex.*

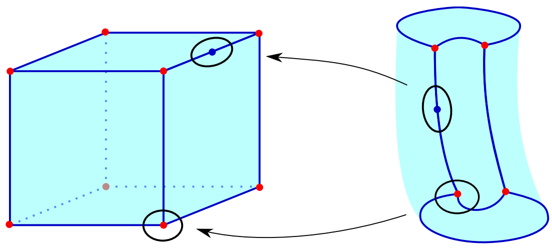

Figure 4.8 – Examples of manifolds with corners for $k = 3$. The colors of the points correspond to the value of the depth: cyan when $p = 1$, blue when $p = 2$, red when $p = 3$. The depth of any point in the interior of the shape is null. The full cube acts as the reference since for any manifold of dimension 3, there exists a local chart to map any of its point to a point of the cube with equal depth.

For any $x \in X$, the tangent space $T_x X$ is generated by $\left(\frac{\partial}{\partial x_1}, \cdots, \frac{\partial}{\partial x_{k-p}}, \frac{\partial}{\partial y_1}, \cdots, \frac{\partial}{\partial y_p}\right)$ for the local coordinates associated to ψ, with $p = p(x)$, and $T_x\mathcal{M}_x$ is the (k-p)-dimensional subspace of $T_x X$ generated by $\left(\frac{\partial}{\partial x_1}, \cdots, \frac{\partial}{\partial x_{k-p}}\right)$.

Example 3.2. *When $p(x) = 0$, $T_x\mathcal{M}_x = T_x X$. Consider now the manifolds X given in Figure 4.8. When $p(x) = 1$, x belongs locally to a regular surface painted in cyan and*

$T_x\mathcal{M}_x$ is the tangent plane to this surface. When $p(x) = 2$, x belongs locally to a regular curve painted in blue and $T_x\mathcal{M}_x$ is the tangent line to this curve. When $p(x) = 3$, the depth is maximal and $\dim T_x\mathcal{M}_x = 0$.

The tangent space at any point x of the cube is identified to $\mathbb{R}^3$. Yet, when x belongs to the boundary, one might want to reduced this space to the minimal semi-orthant through x that encompasses the cube. More precisely, when $p(x) > 0$, the tangent space T_xX is divided in two disjoint sets

$$T_x^+X = T_x\mathcal{M}_x \oplus \bigoplus_{j=1}^{p} \mathbb{R}_+ \frac{\partial}{\partial y_j} \qquad\qquad T_x^-X = -T_x^+X \setminus T_x\mathcal{M}_x\,. \tag{4.37}$$

$$= \bigoplus_{i=1}^{k-p} \mathbb{R}\frac{\partial}{\partial x_i} \oplus \bigoplus_{j=1}^{p} \mathbb{R}_+ \frac{\partial}{\partial y_j}\,, \tag{4.38}$$

The vectors of the first set are called *inward pointing tangent vectors*. Given a vector field u on X with values in T^+X, this definition allows to follow any path in X directed by u and be ensured that it does not end outside X (one could then extend the definition of the exponential map for Riemannian manifolds as a map between T_x^+X and X).

Proposition 3.1. *Consider u a $\mathcal{C}^\infty$ vector field on X. For any $x_0 \in X$, there exist $\epsilon > 0$ and a smooth curve $\gamma : I_\epsilon \to X$ such that $\gamma(0) = x_0$ and $\dot\gamma(t) = u(\gamma(t))$ where $I_\epsilon \ni 0$ is an interval defined as follows:*

1. *if $u(x_0) \in T_{x_0}\mathcal{M}_{x_0}$ and if there exists $U \subset X$ a neighborhood of x_0 such that for any $x \in U$, $u(x) \in T_x^+X$, then $I_\epsilon =]-\epsilon, \epsilon[$,*
2. *if $u(x_0) \in T_{x_0}^+X$, $I_\epsilon = [0, \epsilon[$,*
3. *if $u(x_0) \in T_{x_0}^-X$, $I_\epsilon =]-\epsilon, 0]$.*

Moreover, γ locally lies in $\mathcal{M}_{x_0}$ if and only if there exists $U \subset X$ a neighborhood of x_0 such that for any $x \in U \cap \mathcal{M}_{x_0}$, $u(x) \in T_x\mathcal{M}_{x_0}$.

Proof. Denote $p = p(x_0)$. The existence of γ in a local chart (U, ψ) is a standard Cauchy-Lipschitz problem in $\mathbb{R}^k$ but we need to verify the stability of the solution in $\mathbb{R}^{k-p} \times \mathbb{R}_+^p$. Denote $(x_1, \dots, x_{k-p}, y_1, \dots, y_k)$ the coordinates associated to (U, ψ). The local image $v : \psi(U) \subset \mathbb{R}^{k-p} \times \mathbb{R}_+^p \to \mathbb{R}^k$ of u is given by $v(x_1, \dots, x_{k-p}, y_1, \dots, y_k) = (\alpha_1, \dots, \alpha_{k-p}, \beta_1, \dots, \beta_p)$ where α and β are given by the unique decomposition $u(x) = \sum_{i=1}^{k-p} \alpha_i \frac{\partial}{\partial x_i} + \sum_{j=1}^{p} \beta_j \frac{\partial}{\partial y_j}$. One can extend v to a $\mathcal{C}^\infty$ vector field on $\mathbb{R}^k$ and deduce the existence of a solution γ that satisfies $\dot\gamma = v \circ \gamma$.

When $p = 0$, $T_{x_0}\mathcal{M}_{x_0} = T_{x_0}^+X = T_{x_0}X \simeq \mathbb{R}^k$ and 1. is immediate. Otherwise, denote $V = \psi(U) \subset \mathbb{R}^{k-p} \times \mathbb{R}_+^p$ and let us prove in each case that $\gamma(I_\epsilon) \subset V$.

1. The conditions of the first point imply that $\dot\gamma(0) = v(0) \in \mathbb{R}^{k-p}$ and that we have on $U \setminus \{0\}$ small enough, $\beta_j \geq 0$. There exists thus $\epsilon > 0$ such that $\gamma(]-\epsilon, \epsilon[) \subset V$.
2. $u(x_0) \in T_{x_0}^+X$ is equivalent to $\beta_j \geq 0$ and thus $\dot\gamma(0) = v(0) \in \mathbb{R}^{k-p} \times \mathbb{R}_+^p$. The integration forward is thus stable and there exists $\epsilon > 0$ such that $\gamma([0, \epsilon[) \subset V$.
3. Conversely, $u(x_0) \in T_{x_0}^-X$ is equivalent to $\beta_j < 0$. It follows that $-\dot\gamma(0) = -v(0) \in \mathbb{R}^{k-p} \times \mathbb{R}_+^p$. The integration backward is thus stable.

Regarding the last assertion the necessary condition is immediate. The sufficient condition is equivalent to the case $p = 0$. One can consider the restriction of the chart to $U \cap \mathcal{M}_x$. $\square$

As we saw previously, the boundary of X is a disjoint union of regular submanifolds of X of maximal dimension. A natural question is to know if the solutions generated by u are stable with respect to $\mathcal{M}_{x_0}$. For example, if x_0 belongs to an edge of the cube, one might want γ to be included in this edge. The last assertion of Proposition 3.1 gives the condition to this stability. Note that when $p(x_0) = k$, $\mathcal{M}_{x_0}$ is reduced to $\{x_0\}$ so that any path in $\mathcal{M}_{x_0}$ is constant equal to x_0. It brings conversely the question to move from a regular submanifold to another one. When $p(x) > 0$, $\mathcal{M}_x$ is the boundary of a larger manifold and any point $x \in \mathcal{M}_x$ can then jump into it so that its depth decreases. One can easily show by its definition that locally the depth along a path cannot increase. According to the proposition, as opposed to the necessary and sufficient condition for the stability, if $u(x_0) \in T^+_{x_0}X \setminus T_{x_0}\mathcal{M}_{x_0}$, the path γ exits $\mathcal{M}_{x_0}$ and for $\epsilon > 0$ small enough, we have for any $t \in]0, \epsilon[$, $p(\gamma(t)) < p(x_0)$. More precisely, with the notation of the proposition if $u(x) = \sum_{j=1}^{p} \beta_j \frac{\partial}{\partial y_j}$ where β admits exactly n non zero coordinates then $u(x)$ is a tangent vector pointing toward an adjacent (k-p+n)-dimensional submanifold $\mathcal{M}_y$.

Consider for example a corner x of the cube. This corner is at the intersection of $p = 3$ half hyperplanes. It can locally jump into one of the $\begin{pmatrix} p \\ n \end{pmatrix} = 3$ edges ($n = 1$), $\begin{pmatrix} p \\ n \end{pmatrix} = 3$ faces ($n = 2$) or the interior of the cube ($n = 3$).

We will be especially interesting in the case $n = 1$. It involves then the set of tangent vectors

$$(T_xX)^{(1)} = \bigcup_{j=1}^{p} \mathbb{R}^*_+ \frac{\partial}{\partial y_j} \,. \tag{4.39}$$

3.2 Regularity of the birth tag and foliation

In Chapter 3, we assumed that X could be written as a direct product space $X = [0, 1] \times X_0$ for which the birth tag $\tau : X \to [0, 1]$ would be given by the projection on the first coordinate. When a horn is modeled as a surface, the coordinate space is fixed to $X = [0, 1] \times \mathbb{S}^1$. All the level sets of τ are diffeomorphic to a circle. In this example, $X_0 = \mathbb{S}^1$ is a regular manifold but X is a manifold with boundary. Likewise, when the horn is full, $X = [0, 1] \times \mathbb{D}^1$, where $\mathbb{D}^1$ denotes the unit disc of $\mathbb{R}^2$ and the level sets are diffeomorphic to a disc. In this example $X_0 = \mathbb{D}^1$ is a manifold with boundary and X is a manifold with corners. The maximal depth is 2 and the respective points belong to the boundary of $X_{\{0\}} \doteq \tau^{-1}(\{0\}) = \{0\} \times \mathbb{D}^1$ and $X_{\{1\}} \doteq \tau^{-1}(\{1\})$. We highlight one last interesting example that could be pertinent to study the atrophy of subcortical structures in the brain due to degenerative diseases (see for example [56]). These shapes could be modeled by an onion structure $X = [0, 1] \times \mathbb{S}^2$ to analyze thickness data.

We will show, now, that this canonical decomposition of X as a direct product of manifolds is not reductive since more general situations can be reduced to this case. We assume that X is a k-dimensional **manifold with corners** and that τ is a surjective **submersion** of class $\mathcal{C}^\infty$, meaning that $d\tau(x)$ is surjective for any $x \in X$ or equivalently that τ has no critical points. We will see that, under some additional regularity conditions, this function induces a foliation on the manifold X. This means that it locally decomposes X as a union of parallel submanifolds of smaller dimension. These submanifolds are called the **leaves** of the foliation. For more details on foliated manifolds, see [35, 24].

We denote for any $t \in [0,1]$ the so-called **leaf**

$$X_{\{t\}} \doteq \tau^{-1}(\{t\}), \tag{4.40}$$

which is the subset of X whose points are called *new points* of X at time t. Since τ is surjective, X is the disjoint union of the leaves $X_{\{t\}}$ for $t \in [0,1]$. The sets $X_{\{t\}}$ for $t \in]0,1[$ are called *inner leaves*. We will call $X_{\{0\}}$ and $X_{\{1\}}$ *outer leaves* of X. They belong to the boundary of X.

Lemma 3.1. $(X_{\{0\}} \cup X_{\{1\}}) \subset \partial X$.

Proof. If $x \in X_1$ and $x \notin \partial X$ then there exists a chart (U, ψ) centered on x to an open set $V \ni 0$ of $\mathbb{R}^k$. Moreover, $\tau \circ \psi^{-1}$ is maximal at 0 so that x is a critical point of τ. Yet, τ is a submersion which leads to a contradiction. Likewise, $X_{\{0\}} \subset \partial X$. □

Remark 3.1. *The leaves $X_{\{t\}}$ are compact manifolds with corners. For any $t \in [0,1]$ and any $x \in X_{\{t\}}$, $T_x X_{\{t\}} \subset \ker(d\tau(x))$. Although τ is a submersion, the dimensions of these leaves can vary from 0 to $k-1$. Indeed, consider a chart (U,ψ) centered at $x \in \partial X$ to $\mathbb{R}^{k-p} \times \mathbb{R}^p_+$. The tangent space of a level set $\tau^{-1}(x)$ is included in an hyperplane of $\mathbb{R}^k$. Its intersection with $\mathbb{R}^{k-p} \times \mathbb{R}^p_+$ is then a n-dimensional semi-orthant where $n \in \{k-p, \ldots, k-1\}$. The most degenerated situation occurs when $p = k$ and for example $\ker(d(\tau \circ \psi^{-1})(0)) \subset (1, \ldots, 1)^{\perp}$. Conversely, if there exists $x \in X_{\{t\}}$ such that $p(x) = 0$, then $\dim X_{\{t\}} = k-1$.*

For example, consider X a square or a cube that lies on a corner at the origin so that one of its diagonal follows the vertical axis and consider τ the projection on this diagonal. Then $X_{\{0\}}$ and $X_{\{1\}}$ are the south corner and north corner.

We will then assume that:

$$(H^{\tau}) \quad \left| \begin{array}{l} i) \text{ if } x \in \partial X \setminus (X_{\{0\}} \cup X_{\{1\}}) \text{ then } T_x\mathcal{M}_x + \ker(d\tau(x)) = T_x X\,, \\ \\ ii) \text{ for } i = 0,1 \text{ if } x \in X_{\{i\}} \text{ then } \ker(d\tau(x)) = T_x X_i\,. \end{array} \right. \tag{4.41}$$

Remark 3.2. *Since τ is a submersion, $\ker(d\tau(x))$ is a (k-1)-dimensional space of T_xX. The first condition of (4.41) implies that for any $x \in X_{\{t\}}$ where $t \in]0,1[$, if $x \in \partial X$, then $T_x\mathcal{M}_x \not\subset \ker(d\tau(x))$ and there exists $u \in T_x\mathcal{M}_x$ such that $d\tau(x) \cdot u \neq 0$.*

The (H^{τ}) conditions is intended to ensure that all the leaves are diffeomorphic as it will be proved in the next proposition. The first point of (4.41) is a transversality condition. It implies that the intersection of an inner leaf $X_{\{t\}}$ and the boundary ∂X is a (k-2)-dimensional submanifold with corners. The second point partially answers to the issues raised by Remark 3.1. The ends $X_{\{0\}}$ and $X_{\{1\}}$ are (k-1)-dimensional manifolds.

We can investigate furthermore the decomposition of X in leaves with the ideas of the Morse theory. A Morse function is a smooth function $f : M \to \mathbb{R}$ on a compact manifold that admits no degenerate critical points. The time marker τ, that we assumed to be a submersion, will play the role of the Morse function. A fundamental theorem of the Morse theory says that

Theorem 3.1. *If f is a smooth real-valued function on a manifold M such that $f^{-1}([a,b])$, with $a < b$, is compact, and there are no critical values between a and b. Then $M_a = f^{-1}(\{a\})$ is diffeomorphic to $M_b = f^{-1}(\{b\})$.*

We will prove a similar result in the more general case of a manifold with corners:

Proposition 3.2. *Under the (H^τ) conditions given by (4.41), there exists a submersion $\pi : X \to X_{\{1\}}$ of class $\mathcal{C}^\infty$ such that for any $t \in [0,1]$, $\pi_{|X_{\{t\}}}$ is a $\mathcal{C}^\infty$ diffeomorphism between $X_{\{t\}}$ and $X_{\{1\}}$. Moreover, $x \mapsto (\tau(x), \pi(x))$ is a $\mathcal{C}^\infty$ diffeomorphism between X and the product manifold $[0,1] \times X_{\{1\}}$. The image of the time marker τ on this last manifold is the projection on the first coordinate.*

Our coordinate space admits thus a canonical decomposition as a product manifold $[0,1] \times X_{\{1\}}$ where $X_{\{1\}}$ is a compact manifold with corners. In our examples, $X_{\{1\}}$ is mostly a regular or with boundary. According to this proposition, all the leaves are diffeomorphic to $X_{\{1\}}$. This means that the topology of the leaves cannot change during the development of the shape. Such a change would induce a critical point for the time marker.

At last, note that we will choose the first leaf as reference, meaning that we will write $X = [0,1] \times X_{\{0\}}$ which is just a change of notation since all the leaves are diffeomorphic.

3.3 Proof of Proposition 3.2

The proof starts as in the Morse setup by providing a $\mathcal{C}^\infty$ vector field on X that will generate a flow similar to a gradient flow.

Lemma 3.2. *There exists u a $\mathcal{C}^\infty$ vector field on X such that for any $x \in X$, we have*

1. *$d\tau(x) \cdot u(x) = 1$,*
2. *(a) if $x \in \partial X \setminus (X_{\{0\}} \cup X_{\{1\}})$, then $u(x) \in T_x\mathcal{M}_x$,*

   (b) if $x \in X_i$ for $i = 0, 1$, then

$$(-1)^i u(x) \in (T_x\mathcal{M}_x)^{(1)} \doteq \bigcup_{j=1}^{p(x)} \left(T_x\mathcal{M}_x \oplus \mathbb{R}_+ \frac{\partial}{\partial y^j} \right)$$

where $(x_1, \dots, x_{k-p}, y_1, \dots, y_p)$ are local coordinates associated to a chart (U, ψ) centered at x to the semi-orthant $\mathbb{R}^{k-p} \times \mathbb{R}^p_+$ and $p = p(x)$ is the depth of x.

Remark 3.3. *Since we want the leaves to be diffeomorphic to each other, the flow generated by u needs to conserve the depth. The conditions (2a) ensures this property (see Proposition 3.1). The situation is yet different for the outer leaves $X_{\{0\}}$ and $X_{\{1\}}$ since they are embedded in the boundary of X. A point along a path from $X_{\{0\}}$ to $X_{\{1\}}$ will thus have its depth decrease when exiting $X_{\{0\}}$, remain constant while crossing all the inner leaves, and increase at the very end.*

Remark 3.4. *Note in condition (2b) that* $(T_x\mathcal{M}_x)^{(1)}$ *does not depend on the choice of the chart. Moreover, since* u *is of class* $\mathcal{C}^\infty$ *and* $T_xX_i = \ker(d\tau(x))$, *one could show that if (2b) is replaced by* $(-1)^i u(x) \in T_x^+X_i$ *then (2a) allows to retrieve the initial condition (2b).*

Proof. Recall that the transition maps are of class $\mathcal{C}^\infty$. We will establish for any $x \in X$ the existence of a neighborhood $U_x \subset X$ and a $\mathcal{C}^\infty$ vector field $u_x(\cdot)$ on U_x that satisfies the required conditions on U_x. By linearity of these conditions, one can then consider a partition of unity to prove the final result. Note that the first condition can be relaxed to $d\tau(x) \cdot u(x) > 0$ (consider $\alpha : X \to \mathbb{R}_+^*$ defined by $\alpha(x) = d\tau(x) \cdot u(x)$ then $\bar{u} = u/\alpha$). Consider for any $x \in X$ a chart (U_x, ψ) centered at x to the semi-orthant $\mathbb{R}^{k-p} \times \mathbb{R}_+^p$ where $p = p(x)$ and denote $(x_1, \dots, x_{k-p}, y_1, \dots, y_p)$ the associated coordinates. The idea of the proof is to select one coordinate x_i or y_j and define $u_x \doteq \frac{\partial}{\partial x_i}$ or $u_x \doteq \frac{\partial}{\partial y_j}$ on U_x.

- Let be $x \notin \partial X$ (i.e. $p(x) = 0$). Since $d\tau(x) \neq 0$, there exists necessarily one coordinate x_i such that $\frac{\partial \tau}{\partial x_i}(x) > 0$ and by continuity this inequality is conserved on a small neighborhood of x in U_x. We define thus $u_x \doteq \frac{\partial}{\partial x_i}$.
- Let be $x \in \partial X \setminus (X_{\{0\}} \cup X_{\{1\}})$ (so that $p(x) > 0$). Equation (4.41) implies that $T_x\mathcal{M}_x \not\subset \ker(d\tau(x))$ (see Remark 3.2). By definition $T_x\mathcal{M}_x$ is generated by the vectors $\left(\frac{\partial}{\partial x_i}\right)_{i\in\{1,\dots,k-p\}}$. There exists thus $i \in \{1, \dots, k-p\}$ such that $\frac{\partial \tau}{\partial x_i}(x) > 0$ and one can conclude as before.
- Let be $x \in X_{\{0\}}$. From Lemma 3.1, $p(x) > 0$. Equation (4.41) implies that $T_x\mathcal{M}_x \subset \ker(d\tau(x))$ and therefore for any $i \in \{1, \dots, k-p\}$, $\frac{\partial \tau}{\partial x_i}(x) = 0$. Since $d\tau(x) \neq 0$, there exists then $j \in \{1, \dots, p\}$ such that $\frac{\partial \tau}{\partial y_j}(x) > 0$.

□

We can now prove Proposition 3.2.

Proof. The sketch of the proof is standard and relies on the flow generated by u. Proposition 3.1 ensures that for any $t \in [0,1]$ and any $x_t \in X_{\{t\}}$, there exist $\epsilon > 0$ and a unique path $\gamma : s \mapsto x_s$ on $I =]t-\epsilon, t+\epsilon[\cap [0,1]$ that satisfies the equation $\dot{\gamma} = u \circ \gamma$. Moreover, since $\tau(x_t) = t$ and $\frac{\partial}{\partial s}\tau(x_s) = d\tau(x_s) \cdot u(x_s) = 1$, this solution satisfies at any time $s \in]t-\epsilon, t+\epsilon[$, $\tau(x_s) = s$. Since X is compact, the solution can be extended to $[0,1]$. Hence, for any $x \in X$, there exists a unique path $[0,1] \ni s \mapsto x_s$ such that $x_{\tau(x)} = x$.

One can then define $\pi : X \to X_{\{1\}}$ by $\pi(x) = x_1$. Let us show that π is of class $\mathcal{C}^\infty$. For any $x \in X \setminus X_{\{1\}}$, $u(x) \in T_x^+X$ and since u is of class $\mathcal{C}^\infty$, there exists for any $x \in X \setminus X_{\{1\}}$ a chart (U, ψ) centered at x such that $u_{|U} = \frac{\partial}{\partial x_1}$. Consider then $\varphi_h : U' \subset U \to U$ defined by $\varphi_h(x) = x_{t+h}$ for $t = \tau(x)$ and $h > 0$. Then $\psi \circ \varphi_h \circ \psi^{-1}$ is the translation by the vector $(h, 0_{\mathbb{R}^{k-1}})$ and for U' and h small enough, φ_h is well defined and is a $\mathcal{C}^\infty$ diffeomorphism between U' and $\varphi_h(U')$. Moreover, given $x_1 \in X_{\{1\}}$, there exists a path $[0,1] \ni s \mapsto x_s$ and therefore there also exist $x \in X \setminus X_{\{1\}}$ and a chart (U, ψ) centered at x such that $x_1 \in U$. One can then define $U' \ni x$ such that $x_1 \in \varphi_h(U' \cap X_{\tau(x)})$ and φ_h is thus a $\mathcal{C}^\infty$ diffeomorphism between $U' \cap X_{\tau(x)}$ and a neighborhood of x_1. For any path $[0,1] \ni s \mapsto x_s$, for any $s \in [0,1[$, there exists φ_h such that $x_{s+h} = \varphi_h(x_s)$ and for s large enough $x_{s+h} = x_1$. Since $[0,1]$ is compact, one can extract a finite number of functions φ_h such that for any $s \in [0,1]$, $x_s \mapsto x_1$ is given by composition of these functions. We deduce at last that π is a submersion of class $\mathcal{C}^\infty$. Moreover, for any $x \in X \setminus X_{\{1\}}$, $\tau(\varphi_h(x)) = \tau(x_{t+h}) = t + h$ i.e. $\varphi_h(x) \in X_{\{t+h\}}$ and φ_h can thus be extended to $X_{\{t\}}$. By uniqueness of the solutions of $\dot{x} = u(x)$, φ_h is one-to-one. It results that for any $t \in [0, 1[$, $\varphi_h : X_{\{t\}} \to X_{\{t+h\}}$ is a $\mathcal{C}^\infty$ diffeomorphism and by composition φ_h can be defined for any $h \in [0, 1-t]$.

In fine, π can be rewritten for any $x \in X$ by $\pi(x) = \varphi_{1-\tau(x)}(x)$ and we prove that $f : x \mapsto (\tau(x), \pi(x))$ is a bijective $\mathcal{C}^\infty$ submersion from X to $[0, 1] \times X_{\{1\}}$. Indeed, the surjectivity is immediate and for any $x, y \in X$, if $f(x) = f(y)$, denote $t = \tau(x) = \tau(y)$, then $f(x) = (t, \varphi_{1-t}(x)) = f(y) = (t, \varphi_{1-t}(y))$. Since φ_{1-t} is injective on $X_{\{t\}}$, f is injective. □

4 Existence of continuous minimizers in the current case

4.1 Reminder on differential geometry

We will assume from here that X is a k-dimensional submanifold with corners and we will use the classical notation $\mathcal{H}^k$ for the k-dimensional **Hausdorff measure** on $\mathbb{R}^d$. We remind that $\mathcal{H}^k$ is defined as an outer measure on $\mathbb{R}^d$ that basically measures the k-dimensional volume of a subset of $\mathbb{R}^d$. In particular, when $k = d$, we have $\mathcal{H}^d = \lambda^d$ the usual Lebesgue measure. If M is a p-dimensional submanifold of $\mathbb{R}^d$, then $\mathcal{H}^k(M)$ is the k-volume of M if $p = k$, vanishes if $p < k$ and equals $+\infty$ when $k < p$.

The interior product will highlight the linearity property of the currents with respect to the tangential data.

Definition 4.1. *The interior product is defined to be the contraction of a differential form with a vector field. Thus if v is a vector field on the manifold M, then*

$$\iota_v : (\Lambda^k M)^* \to (\Lambda^{k-1} M)^*$$

is the map which sends a (k-1)-form ω to the (k-1)-form $\iota_v\omega$ defined by the property that for any $m \in M$, (k-1)-vector $\xi_1 \wedge \cdots \wedge \xi_{k-1}$, $\xi_i \in T_m M$,

$$(\iota_v\omega)(m)\big(\xi_1 \wedge \cdots \wedge \xi_{k-1}\big) \doteq \omega(m)\big(v(m) \wedge \xi_1 \wedge \cdots \wedge \xi_{k-1}\big)\,.$$

Hence, ι is linear with respect to v.

The corollary 4.1, given hereafter, results from the Stokes' theorem and the Cartan's formula and will play a central role to exploit the linearity of the current representation with respect to the tangential data of a shape.

Theorem 4.1 (Stokes' theorem)**.** *Let M be an oriented compact k-dimensional differential manifold with corners. For any differential (k-1)-form ω of class $\mathcal{C}^1$*

$$\int_M d\omega = \int_{\partial M} \omega\,.$$

Proof. See [35]. □

The Lie derivative of differential forms with respect to vector fields in the direction of a vector field v expresses how a current associated to a shape X varies when X is deformed in the direction of v. More precisely, given a flow ϕ_t such that $\phi_0 = \mathrm{Id}$ and $\dot{\phi}_{t|_{t=0}} = v$

$$\mathcal{L}_v\omega = \lim_{t\to 0} \frac{\phi_t^*\omega - \omega}{t} = \frac{\partial}{\partial t}\phi_t^*\omega_{|t=0}\,. \tag{4.42}$$

It follows that

$$\frac{\partial}{\partial t}\mu_{\phi_t(X)}(\omega)_{|t=0} = \mu_X(\mathcal{L}_v\omega)\,. \tag{4.43}$$

Theorem 4.2 (Cartan's formula)**.** *Let ω be a differential form of class $\mathcal{C}^1$ and v a vector field then*

$$\mathcal{L}_v\omega = d\iota_v\omega + \iota_v d\omega\,.$$

Proof. See [34] (in french) Lemma 7.2.1 and 10.3.2. □

We will apply the Cartan's formula in a particularly simple case. The manifold M is embedded in $[0,1]\times M$ and the deformation is the translation among the first coordinate.

Corollary 4.1. *We denote $v = \partial_t$ the vector field defined at any point $(t,m) \in [0,1]\times M$ by $(1, 0_{T_mM})$ and $M_t = \{t\}\times M$ then*

$$\frac{\partial}{\partial t}\left(\int_{M_t}\omega\right)\Big|_{t=0} = \int_{\partial M}\iota_v\omega + \int_M \iota_v d\omega\,.$$

Proof. We deduce from the Cartan's formula that

$$\frac{\partial}{\partial t}\left(\int_{M_t}\omega\right)\Big|_{t=0} = \frac{\partial}{\partial t}\int_M \phi_t^*\omega_{|t=0} = \int_M \mathcal{L}_v\omega = \int_M d\iota_v\omega + \iota_v d\omega\,.$$

The Stokes' theorem allows then to conclude. □

4.2 Definition of the current representation with the growth dynamic

We return to the problem of the reconstitution of a scenario $t\mapsto S_t$ whose final state is known and given by a shape denoted S^{tar}. The scenario is modeled on a biological coordinate system (X,τ) and generated by a initial position $q_0 \in L^\infty(X,\mathbb{R}^d)$ and a time-varying vector field $v\in L^2_V$. More precisely, the development $q:[0,1]\times X\to\mathbb{R}^d$ is defined by the ODE in $L^\infty(X,\mathbb{R}^d)$

$$\dot{q}_t(x) = v(t, q_t(x))\mathbf{1}_{\tau(x)\le t}\,. \tag{4.44}$$

We will assume here that the initial position q_0 belongs to $\mathcal{C}^\infty(X,\mathbb{R}^d)$. Regarding the space of vector field V, we will assume the following conditions:

$$(H_1^V)\quad\left|\begin{array}{l} i)\, V\subset \mathcal{C}^2(\mathbb{R}^d,\mathbb{R}^d)\,.\\ ii)\,\text{There exists } c>0 \text{ such that for any } v\in V \text{ and any } x\in\mathbb{R}^d\,,\\ \qquad\qquad\begin{cases} |v(x)|_{\mathbb{R}^d}\le c|v|_V(|x|_{\mathbb{R}^d}+1)\,,\\ |dv(x)|_\infty + |d^2v(x)|_\infty \le c|v|_V\,.\end{cases}\end{array}\right. \tag{4.45}$$

It ensures the existence and uniqueness of a solution to the previous ODE (see Chapter 3).

We want to minimize an energy of the type:

$$E(v) \doteq \int_0^1 |v_t|_V^2 dt + \lambda \mathcal{A}(S^{\mathrm{tar}}, q_1(X)),$$

where S^{tar} is the target shape, $\mathcal{A}$ the data attachment term and $\lambda > 0$ a weight parameter. To consider a data attachment term built from a distance on a space of currents requires to investigate the regularity of the final shape $q_1(X)$. A current cannot be defined from an L^∞ mapping. So far, currents as varifolds have been applied to model shapes that are least rectifiable sets.

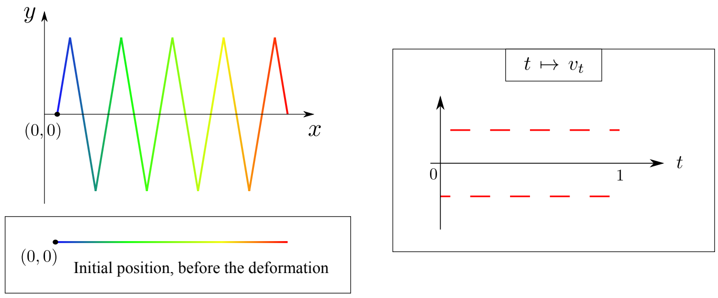

Figure 4.9 – The final state $q_1(X)$ displayed on the top left is a serrated curve with as many discontinuities as its associated vector field v given on the right as real-valued function modeling vertical translations upwards and downwards. The initial position $q_0(X)$ is a segment. This example is essentially the 2D analogue of the 3D shape illustrated in Figure 4.5

We saw in the previous chapter that the spatial regularity of q_t is related to the temporal regularity of v. Even when the initial condition q_0 is smooth, if v is any element of L^2_V, we can only show that q_1 is differentiable almost everywhere. In Figure 4.9, we illustrate the impact of the discontinuity of v on the generated shape (rectifiable yet on this basic example, but not $\mathcal{C}^1$).

However, we did show in Chapter 3 that if v is time continuous, q_1 is then of class $\mathcal{C}^1$. Its differential is given for any $x \in X$ by

$$dq_1(x) = d\phi_{\tau(x),1}(q_0(x)) \circ \big(dq_0(x) - v_{\tau(x)}(q_0(x))d\tau(x)\big), \tag{4.46}$$

where $\phi_{s,t}$ is the flow of v on the ambient space $\mathbb{R}^d$. It is well-known that under the (H_1^V) conditions, this flow is of class $\mathcal{C}^1$ and has a differential continuous in time and space [26, 55]. Note yet that when V is a general RKHS, it actually requires to assume that V is continuously embedded in $\mathcal{C}_0^2(\mathbb{R}^d)$ the space of $\mathcal{C}^2$ mappings $v : \mathbb{R}^d \to \mathbb{R}^d$ vanishing at the infinity, equipped with the usual sup norm. However, this assumption is not satisfied when the deformations belong to the group of rotations and translations on the ambient space for which the existence and the regularity of the differential of the flow are hopefully immediate. To encompass this last situation, we will thus only assume the less restrictive (H_1^V) conditions for the results presented hereafter.

Hence, to define properly a current associated to $q_1(X)$, we will extend a definition based on continuous trajectories $v \in \mathcal{C}([0,1],V)$ to all the solutions generated by L^2_V. Let us first recall how we can represent a shape by a current. Consider M is a smooth oriented k-dimensional submanifold and denote for any $x \in M$, $(T_1(x),\dots,T_k(x))$ an orthonormal oriented basis of the tangent space T_xM. Then M is then identified to the current $\mu_M \in \mathcal{C}_0(\mathbb{R}^d,(\bigwedge^k \mathbb{R}^d)^*)'$ defined for any $\omega \in \mathcal{C}_0(\mathbb{R}^d,(\bigwedge^k \mathbb{R}^d)^*)$ by

$$\mu_M(\omega) = \int_M \omega(x)(T_1(x)\wedge\ldots\wedge T_k(x))d\mathcal{H}^k(x)\,. \tag{4.47}$$

We can now define the current associated to the final mapping q_1 generated by a continuous vector field.

Definition 4.2. *For any $v \in \mathcal{C}([0,1],V)$, the current associated to the mapping $q_1 : X \to \mathbb{R}^d$ is defined for any $\omega \in \mathcal{C}_0(\mathbb{R}^d,(\bigwedge^k \mathbb{R}^d)^*)$ by*

$$\mu_v(\omega) = \int_X q_1^*\omega = \int_X \omega(q_1(x))\left(\frac{\partial q_1}{\partial x_1}(x)\wedge\ldots\wedge\frac{\partial q_1}{\partial x_k}(x)\right)dx_1\ldots dx_k\,. \tag{4.48}$$

The key of the next proposition is to use the density $\mathcal{C}([0,1],V)$ in $L^2([0,1],V)$ to extend by continuity the definition of μ_v to $L^2([0,1],V)$. For this purpose we rewrite equation (4.48) with the foliation of X given by its tagging function τ. With the result of the previous section, we can assume that $X = [0,1]\times B$ where B is an oriented compact manifold with corners so that τ is just the projection on the first coordinate (for any $(t,b)\in[0,1]\times B$, $\tau(t,b)=t$). In this case, we introduce the set of submanifolds $(Y_t)_{0<t<1}$ of $\mathbb{R}^d$ that are the images of $B_t \doteq \{t\}\times B$ by q_0. Moreover, we will assume that

(H^{q_0}) The restriction of q_0 to an inner leaf $X_{\{t\}}$ ($t\in]0,1[$) is a smooth immersion between $X_{\{t\}}$ and $\mathbb{R}^d$.

This condition ensures that for almost every $t\in[0,1]$ the restriction $q_0 : B_t \to Y_t$ is a $\mathcal{C}^1$ diffeomorphism.

Remark 4.1. *The initial condition q_0 has no reason to be an embedding of the whole coordinate space X. See for example the scenarios in Figure 4.10 where its image is reduced to a point. However, to ensure that a scenario generated by q globally corresponds to the trivial scenario induced by the coordinate system (see Chapter 2 and 3), we want each leaf $X_{\{t\}}$ to be embedded in $\mathbb{R}^d$. Some exceptions are yet allowed, typically for the outer leaves $X_{\{0\}}$ and $X_{\{1\}}$. It is for example necessary to model the tip of the horn.*

We can now extend for any L^2_V-scenario the definition of the current associated to its final age. The proof lies on the fact that almost all the restrictions of q_1 to the leaves $X_{\{t\}}$ are of class $\mathcal{C}^1$.

Proposition 4.1. *The function $v\mapsto\mu_v$ defined for $v\in\mathcal{C}([0,1],V)$ has a unique continuous extension*

$$\begin{array}{ccc} \left(L^2([0,1],V),|\cdot|_{L^2_V}\right) & \longrightarrow & \left(\mathcal{C}_0(\mathbb{R}^d,(\Lambda^k\mathbb{R}^d)^*),|\cdot|_\infty\right)^* \\ v & \longmapsto & \mu_v : \omega \mapsto \int_0^1\left[\int_{Y_t}\iota_{(h_t-v_t)}\phi^*_{t,1}\omega\right]dt\,, \end{array} \tag{4.49}$$

where $(\phi_{s,t})_{s\le t}$ is the flow of v, $\phi^*_{t,1}\omega$ is the pullback of ω by $\phi_{t,1}$, ι is the interior product *and h_t is the unique vector field on Y_t defined for almost any $t \in [0,1]$ and any $x \in B_t$ by $h_t(q_0(x)) = \frac{\partial q_0}{\partial t}(x)$.*

Proof. Let us call here φ the application $v \mapsto \mu_v$ given by Definition 4.2 when $v \in \mathcal{C}([0,1],V)$ and $\overline{\varphi}$ the application defined here by equation (4.49). We will first show that φ and $\overline{\varphi}$ coincides on $v \in \mathcal{C}([0,1],V)$. Then, we will show that $\overline{\varphi}$ is indeed a continuous linear application.

We decompose $X = [0,1] \times B$ with a partition of unity of B. Hence, we just have to consider the case of a support $[0,1] \times U$ where (U,ψ) is a coordinate chart around a point $b \in B$ (consistent with the orientation). We can thus define a local coordinate system $x = (t, b^1, \cdots, b^{k-1})$ on $[0,1] \times U$ and we have $\frac{\partial q_1}{\partial b^i}(x) = d\phi_{t,1}(q_0(x)) \circ \frac{\partial q_0}{\partial b^i}(x)$ and $\frac{\partial q_1}{\partial t}(x) = d\phi_{t,1}(q_0(x)) \circ \left(\frac{\partial q_0}{\partial t}(x) - v_t(q_0(x))\right) = d\phi_{t,1}(q_0(x)) \circ (h_t - v_t)(q_0(x))$. Therefore,

$$
\begin{aligned}
\int_{[0,1]\times U} q_1^*\omega &= \int_{[0,1]\times U} \omega(q_1(t,b)) \left(\frac{\partial q_1}{\partial t}(t,b) \bigwedge_{i=1}^{k-1} \frac{\partial q_0}{\partial b^i}(t,b) \right) db^1 \cdots db^{k-1} dt \\
&= \int_{[0,1]\times U} \omega(\phi_{t,1}(q_0(t,b))) \\
&\qquad \left(d\phi_{t,1}(q_0(t,b)) \circ \frac{\partial q_1}{\partial t}(t,b) \bigwedge_{i=1}^{k-1} d\phi_{t,1}(q_0(t,b)) \circ \frac{\partial q_0}{\partial b^i}(t,b) \right) db^1 \cdots db^{k-1} dt \\
&= \int_0^1 \left[\int_B (\phi_{t,1}^*\omega)(q_0(t,b)) \left((h_t - v_t)(q_0(t,b)) \bigwedge_{i=1}^{k-1} \frac{\partial q_0}{\partial b^i}(t,b) \right) db^1 \cdots db^{k-1} \right] dt \\
&= \int_0^1 \left[\int_{Y_t} \iota_{(h_t - v_t)} \phi_{t,1}^* \omega \right] dt \,.
\end{aligned}
$$

Now, we have $\sup_{t\in[0,1]} |d\phi_{t,1}| = \mathcal{C}_1(|v|^2_{L^2_V})$, dq_0 is also bounded X, so that h_t and v_t are bounded on $q_0(X)$ and therefore

$$
\left| \int_0^1 \left[\int_{Y_t} \iota_{(h_t - v_t)} \phi_{t,1}^* \omega \right] dt \right| \leq |\omega|_\infty \mathcal{C}_2(|v|^2_{L^2_V}) \,, \tag{4.50}
$$

where $\mathcal{C}_1$ and $\mathcal{C}_2$ are increasing functions independent of v and ω. Consequently, for any $v \in L^2_V$, $\overline{\varphi}(v) = \mu_v$ belongs to $\mathcal{C}_0(\mathbb{R}^d, (\Lambda^k \mathbb{R}^d)^*)^*$ and $\overline{\varphi}$ is continuous due to the regularity of the interior product and of $\phi_{t,1}$. Hence, since $\mathcal{C}([0,1],V)$ is dense in L^2_V and $(\mathcal{C}_0(\mathbb{R}^d, (\Lambda^k\mathbb{R}^d)^*), |\cdot|_\infty)^*$ is a Banach space, $\overline{\varphi}$ is the unique continuous extension of φ. $\square$

Remark 4.2. *Note that μ_v is not exactly the current associated to the image $q_1(X)$. Indeed, even if q_1 is differentiable, it might not be an embedding. Two counter-examples are presented in Figure 4.10. In the first case, the direction of the development is suddenly reversed twice so that the curve is folding on itself. Hence, if we refer to number of inverse images of each point of $q_1(X)$ as a thickness of the shape, then the thickness here is equal to* 1 *or* 3*. On the second case, the curve completely overwrites itself, so that the thickness is equal to* 2 *on each point.*

This phenomenon depends on q_0 and v and cannot be anticipated. The current associated to our shapes counts therefore these repetitions. However, in the first scenario, since

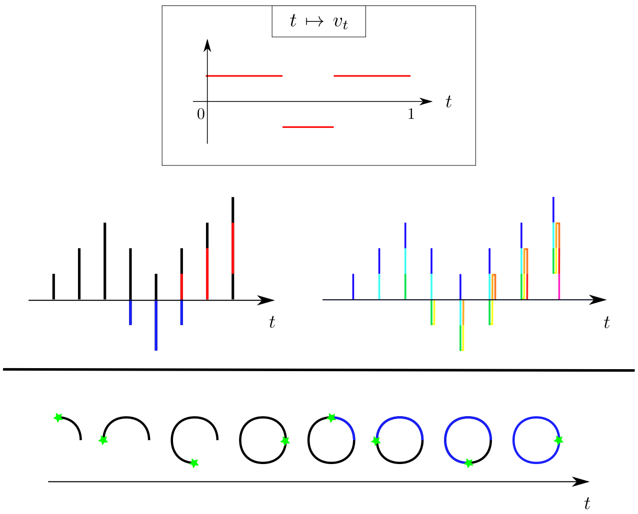

Figure 4.10 – Two examples of scenarios. In both situations, X is a segment but $q_0(X)$ is reduced to a point. On top, v is given by piecewise constant vertical translations upwards and downwards, modeled by real-valued function. The final image is a segment but when v changed its sign, the curve folded on itself. The scenario is displayed again on the left but we slightly separated the multiple fibers of the curve. One can think to a magic trick where colored attached strings are pulling out from the initial position point. On the bottom, the scenario is generated by a constant rotation anticlockwise. The ambient space is exactly rotated twice during the time interval $[0, 1]$. We display the development of the curves with three colors depending of the thickness : dark for 1, blue for 2 and red for 3. The green star on the bottom is just displayed to highlight the evolution of one specific point.

the orientation is reversed twice and by linearity of the currents with respect to the tangential data, the repetition is canceled and we have $\mu_v(\omega) = \int_{q_1(X)} \omega$. On the second example, the orientation is the same on each layer so that $\mu_v(\omega) = 2\int_{q_1(X)} \omega$. At last, note that in practice, these situations should not happen with optimal vector fields. The penalization of v should prevent these artifacts. Generating a cancel effect via an overlapping should induce an additional cost on v with yet no reduction of the data attachment term since the current would be the same without this overlapping. Likewise, the gain of thickness as in the second example is necessary taken from spatial correspondences with the target shape and should therefore not be profitable (at least for a metric with a reasonable scale so that the position of the points are enough discriminated).

4.3 Existence of global minimizers in $L^2([0, 1], V)$

We can now consider a target generated by a vector field v^{tar} and represent the solution and the target with currents. We denote as before μ_{tar} and μ_v the associated currents defined by equation (4.49). Unlike the varifolds, the currents provides a data attachment term that ensures the existence of continuous vector fields that minimizes the energy

$$E(v) \doteq \frac{1}{2}\int_0^1 |v|_V^2 dt + \frac{\lambda}{2}|\mu_{\text{tar}} - \mu_v|_{W'}^2 \,,$$

where W is now a RKHS embedded in the space of test functions $\mathcal{C}_0(\mathbb{R}^d, (\bigwedge^k \mathbb{R}^d)^*)$. However, this result is not immediate. In this section, we will first prove the existence of a solution in $L^2([0,1], V)$. The expression of the current μ_v given by Proposition 4.1 enlightens and isolates the specificity of our generated shapes. It also allows to show a central property of the current attachment terms that is not verified by the varifold attachment terms: the lower semi-continuity (l.s.c.) on L^2_V.

Proposition 4.2. *For any $\omega \in \mathcal{C}_0(\mathbb{R}^d, (\Lambda^k \mathbb{R}^d)^*)$, the application $v \to \mu_v(\omega)$ is continuous with respect to the weak topology of L^2_V. In particular, $v \to |\mu_{\mathrm{tar}} - \mu_v|^2_{W^*}$ is l.s.c. with respect to the weak topology.*

Proof. We recall partially the assumptions on the space of vector fields V

$$(H_1^V) \quad \left| \begin{array}{c} \text{There exists } c > 0 \text{ such that for any } v \in V \text{ and any } x \in \mathbb{R}^d\,, \\ |v(x)|_{\mathbb{R}^d} \leq c|v|_V(|x|_{\mathbb{R}^d} + 1)\,. \end{array} \right. \tag{4.51}$$

Consider a weakly convergent sequence $v_n \rightharpoonup v_\infty$ in L^2_V, we have for any $\omega \in \mathcal{C}_0(\mathbb{R}^d, (\Lambda^k \mathbb{R}^d)^*)$

$$\begin{aligned} &|\mu_{v^n}(\omega) - \mu_{v^\infty}(\omega)| \\ &\quad \leq \left| \int_0^1 \left[\int_{Y_t} \iota_{v_t^n - v_t^\infty} \phi_{t,1}^{v^\infty,*} \omega \right] dt \right| + \left| \int_0^1 \left[\int_{Y_t} \iota_{h_t - v_t^n} (\phi_{t,1}^{v^n,*}\omega - \phi_{t,1}^{v^\infty,*}\omega) \right] dt \right| . \end{aligned} \tag{4.52}$$

The first term of the right-hand side is a continuous linear form ℓ on L^2_V evaluated on $v^n - v^\infty$. *This is where the linearity of the currents attachment terms on the tangential data plays its role.* Indeed, we have for any $u \in L^2_V$

$$\begin{aligned} |\ell(u)| &= \left| \int_0^1 \left[\int_{Y_t} \iota_{u_t} \phi_{t,1}^{v^\infty,*}\omega \right] dt \right| \\ &\leq \sup_{t, y \in Y_t} |\phi_{t,1}^{v^\infty,*}\omega(y)|_\infty \left| \int_0^1 \left[\int_{Y_t} |u_t(y)|_{\mathbb{R}^d} \, d\mathcal{H}^{k-1}(y) \right] dt \right| \\ &\leq \sup_{t, y \in Y_t} |d\phi_{t,1}^{v^\infty}|_\infty^k |\omega(y)|_\infty \left| \int_0^1 \left[\int_{Y_t} c(|y|_{\mathbb{R}^d} + 1)|u_t|_V \, d\mathcal{H}^{k-1}(y) \right] dt \right| \\ &\leq c \sup_{t, y \in Y_t} |d\phi_{t,1}^{v^\infty}|_\infty^k |\omega(y)|_\infty \sup_{t, y \in Y_t} (|y|_{\mathbb{R}^d} + 1) \sup_t vol(Y_t) \int_0^1 |u_t|_V dt \\ &\leq c'|u|_{L^2_V}\,, \end{aligned}$$

where $vol(Y_t)$ is the volume of Y_t. Consequently, since $(v^n)_n$ weakly converges to v^∞, $\ell(v^n - v^\infty)$ converges to 0. The second term can be bounded as follows

$$\left| \int_0^1 \left[\int_{Y_t} \iota_{h_t - v_t^n} (\phi_{t,1}^{v^n,*}\omega - \phi_{t,1}^{v^\infty,*}\omega) \right] dt \right| \leq m_1 m_2\,,$$

where $m_1 = \sup_{t,y\in Y_t} |\phi_{t,1}^{v^\infty,*}\omega(y) - \phi_{t,1}^{v^n,*}\omega(y)|_\infty$ tends to 0 and

$$m_2 = \sup_t vol(Y_t)\big(\sup_X \left|\frac{\partial q_0}{\partial t}(x)\right| + c \sup_{t,y\in Y_t} (|y|_{\mathbb{R}^d} + 1) \underbrace{|v^n|_{L^2_V}}_{\leq \sup_n |v^n|_{L^2_V}} \big) .$$

We already know that if a sequence $(v_n)_n$ weakly converges to v_∞ then $(t,y) \to \phi_{t,1}^{v_n}(y)$ converges compactly to $(t,y) \to \phi_{t,1}^{v_\infty}(y)$. Moreover, since $(v_n)_n$ is weakly convergent, $(v_n)_n$ is bounded, so that finally this upper bound tends to 0. Therefore, the function $v \mapsto \mu_v$, with values in $\mathcal{C}_0(\mathbb{R}^d, (\Lambda^k\mathbb{R}^d)^*)^*$, is continuous with respect to the weak topology of L^2_V and the first result is proved.

Moreover, since W is continuously embedded into $\mathcal{C}_0(\mathbb{R}^d, (\Lambda^k\mathbb{R}^d)^*)$, there exists $c' > 0$ such that for any linear form $\ell \in \mathcal{C}_0(\mathbb{R}^d, (\Lambda^k\mathbb{R}^d)^*)^*$, $|\ell(\omega)| \leq |\ell|_\infty |\omega|_\infty \leq c'|\ell|_\infty|\omega|_W$ so that $|\ell|_{W^*} \leq c'|\ell|_\infty$. It follows that for any $\omega \in W$, $\mu_{v^n}(\omega)$ tends to $\mu_{v^\infty}(\omega)$, i.e. μ_{v^n} weakly converges to μ_{v^∞} in W^*. Hence, $\mu_{v^n}(\mu_{\text{tar}}) = \langle \mu_{v^n}, \mu_{\text{tar}}\rangle_{W^*}$ tends to $\langle \mu_{v^\infty}, \mu_{\text{tar}}\rangle_{W^*}$ and since the square norm of a Hilbert space is always lower semi-continuous with respect to the weak topology, we deduce that

$$\begin{aligned}
|\mu_{\text{tar}} - \mu_{v^\infty}|^2_{W^*} &= |\mu_{\text{tar}}|^2_{W^*} - 2\langle \mu_{v^\infty}, \mu_{\text{tar}}\rangle_{W^*} + |\mu_{v^\infty}|^2_{W^*} \\
&\leq |\mu_{\text{tar}}|^2_{W^*} - 2\lim\langle \mu_{v^\infty}, \mu_{\text{tar}}\rangle_{W^*} + \underline{\lim}\ |\mu_{v^n}|^2_{W^*} \\
&\leq \underline{\lim}\ \big(|\mu_{\text{tar}}|^2_{W^*} - 2\langle \mu_{v^n}, \mu_{\text{tar}}\rangle_{W^*} + |\mu_{v^n}|^2_{W^*}\big) \\
&\leq \underline{\lim}\ |\mu_{\text{tar}} - \mu_{v^n}|^2_{W^*} .
\end{aligned}$$

□

This proposition induces a first main result: the existence of a solution *in* $L^2([0,1], V)$ of the energy

$$E(v) = \frac{1}{2}|v|^2_{L^2_V} + \frac{\lambda}{2}|\mu_{\text{tar}} - \mu_v|^2_{W^*} .$$

Theorem 4.3. *Consider $X = [0,1] \times B$ where B is a compact oriented manifold with corners and τ the projection on the first coordinate of X. Assume that $q_0 \in \mathcal{C}^\infty(X, \mathbb{R}^d)$. Consider the standard cost function*

$$C(v) = \frac{1}{2}\int_0^1 |v_t|^2_V dt .$$

Under the (H^{q_0}) and (H_1^V) conditions, the energy defined for any v in $L^2([0,1], V)$ by

$$E(v) = C(v) + \frac{\lambda}{2}|\mu_v - \mu_{\text{tar}}|^2_{W^*}$$

admits a global minimizer.

Proof. Note that E is always positive. Let $(v^n)_n$ be a minimizing sequence of E. One can easily show that $(v^n)_n$ is bounded and we can then assume that v^n weakly converges in L^2_V. Denote v^∞ this limit. Proposition 4.2 says that E is lower semi-continuous with respect to the weak topology of L^2_V. It follows that $E(v^n)$ tends to $E(v^\infty)$ so that v^∞ minimizes E. □

Remark 4.3. *One can generalize the previous theorem with a cost function C that satisfies $C(v)$ tends to $+\infty$ when $|v|_{L^2_V}$ tends to $+\infty$. In Chapter 3, we presented a set of cost functions (in the so-called* adapted norm setup*) similar to*

$$C(v) = \frac{1}{2}\int_0^1 \alpha_t |v_t|_V^2 dt\,,$$

where $\alpha : [0,1] \to \mathbb{R}^+$. The theorem can thus be applied as soon as α admits a strictly positive lower bound, which will always be the case when the coordinate space X is a discrete set. However, we saw in the case of horns or more generally when $\mathcal{H}^{k-1}(q_0(X)) = 0$ that we are interested in functions α that tends to 0 at time 0. This could thus require deeper investigation.

4.4 Continuity of the global minimizers

At this point, the continuity of a minimizer v^* of E is not acquired. This continuity is yet necessary to provide an algorithm of shooting on the momentum (see Chapter 3). We will show now that all minimizers belong to $\mathcal{C}([0,1], V)$, which is not true when the attachment term is defined on varifolds. The outline of the proof is simple. We will show that E is differentiable with respect to v and study the critical points of E. We keep the assumptions of the previous theorem. We assume in this section that W is a RKHS embedded in the space of $\mathcal{C}^1$ differential forms $\mathcal{C}^1_0(\mathbb{R}^d, (\bigwedge^k \mathbb{R}^d)^*)$.

We recall a standard result on the flow of a vector field.

Proposition 4.3. *Assume the (H_1^V) conditions given by equation (4.45). Let be $v, \delta v \in L^2_V$ and introduce the variations $v^\epsilon_t = v_t + \epsilon\delta v_t$ of v in the direction δv where $\epsilon \in [0,1]$. Consider $\phi^\epsilon_{s,t}$ the flow of v^ϵ, meaning that $\phi^\epsilon_{s,t} = \phi^\epsilon_t \circ \phi^{\epsilon,-1}_s$ where ϕ^ϵ_t is the unique solution on $[0,1]$ of*

$$\phi^\epsilon_t = \mathrm{Id} + \int_0^1 v^\epsilon_s \circ \phi^\epsilon_s \, ds\,.$$

Then, the application $\epsilon \to \big(\phi^\epsilon_{s,t}(y), d\phi^\epsilon_{s,t}(y)\big)$ is of class $\mathcal{C}^1$. We have for any $y \in \mathbb{R}^d$,

$$\frac{\partial}{\partial\epsilon}\phi^\epsilon_{s,t}(y)\big|_{\epsilon=0} = \int_s^t d\phi_{u,t}(\phi_{s,u}(y)).\delta v_u(\phi_{s,u}(y))\, du$$

and

$$\begin{aligned}\frac{\partial}{\partial\epsilon}d\phi^\epsilon_{s,t}(y)\big|_{\epsilon=0} = \int_s^t & \left[d^2\phi_{u,t}(\phi_{s,u}(y))d\phi_{s,u}(y)\right]\delta v_u(\phi_{s,u}(y)) \\ & + d\phi_{u,t}(\phi_{s,u}(y))d\delta v_u(\phi_{s,u}(y))d\phi_{s,u}(y)\, du\,.\end{aligned}$$

4.4.1 Differentiability of the current representation

A first step consists in studying the directional derivative of the current

$$\mu_v(\omega) = \int_0^1 \left[\int_{Y_t} \iota_{h_t - v_t}\phi^*_{t,1}\omega\right] dt$$

with respect to the vector field v. Let be $v, \delta v \in L_V^2$ and consider $v_t^\epsilon = v_t + \epsilon \delta v_t$ where $\epsilon \in [0,1]$ and $\phi_{s,t}^\epsilon$ its flow. From the linearity of the interior product, we have

$$\mu_{v^\epsilon}(\omega) = \int_0^1 \left[\int_{Y_t} \iota_{h_t - v_t^\epsilon} \phi_{t,1}^{\epsilon,*} \omega \right] dt \tag{4.53}$$

$$= \int_0^1 \left[\int_{Y_t} \iota_{h_t - v_t} \phi_{t,1}^{\epsilon,*} \omega \right] dt - \epsilon \int_0^1 \left[\int_{Y_t} \iota_{\delta v_t} \phi_{t,1}^{\epsilon,*} \omega \right] dt \,. \tag{4.54}$$

We will address the derivation with respect to ϵ of these two terms separately and we start with the first one that we denote:

$$g(\epsilon) = \int_0^1 \left[\int_{Y_t} \iota_{h_t - v_t} \phi_{t,1}^{\epsilon,*} \omega \right] dt \,.$$

In order to rewrite g, let us introduce some notation. The variables are grouped in pairs:

$$\begin{aligned} \nu_s^\epsilon(y) &= (v_s^\epsilon(y), dv_s^\epsilon(y)) \,, \\ \varphi_s^\epsilon(y) &= (\phi_{s,1}^\epsilon(y), d\phi_{s,1}^\epsilon(y)) \,, \\ \delta\nu_s(y) &= \frac{\partial}{\partial \epsilon} \nu_s^\epsilon(y) \big|_{\epsilon=0} \,, \\ \delta\varphi_s(y) &= \frac{\partial}{\partial \epsilon} \varphi_s^\epsilon(y) \big|_{\epsilon=0} \,. \end{aligned}$$

Hence, $\delta\nu_s(y) = (\delta v_s(y), d\delta v_s(y))$ and it results from Proposition 4.3 that for any $s \in [0,1]$, for any $y \in \mathbb{R}^d$, $\delta\varphi_s(y) \in \mathbb{R}^d \times \mathcal{L}(\mathbb{R}^d)$ is given by

$$\delta\varphi_s(y) = \int_s^1 A_t^s(y) \cdot \delta\nu_t(\phi_{s,t}(y)) dt \,, \tag{4.55}$$

where $(t,y) \mapsto A_t^s(y)$ belongs to $\mathcal{C}([0,1] \times \mathbb{R}^d, \mathcal{L}(\mathbb{R}^d \times \mathcal{L}(\mathbb{R}^d)))$.

Given $\omega \in W$, define $f_\omega : (\mathbb{R}^d \times \mathcal{L}(\mathbb{R}^d)) \to (\Lambda^k \mathbb{R}^d)^*$ such that $f_\omega(\varphi_t^\epsilon(y)) = (\phi_{t,1}^{\epsilon,*}\omega)_y$. This is to say that for any k-vector $\xi_1 \wedge \cdots \wedge \xi_k \in \Lambda^k \mathbb{R}^d$,

$$f_\omega(\varphi_t^\epsilon(y))(\xi_1 \wedge \cdots \wedge \xi_k) = \omega(\phi_{t,1}^\epsilon(y)) \left(d\phi_{t,1}^\epsilon(y)\xi_1 \wedge \cdots \wedge d\phi_{t,1}^\epsilon(y)\xi_k \right) \,.$$

We can easily check that f_ω is $\mathcal{C}^1$. At last, we get

$$g(\epsilon) \doteq \int_0^1 \left[\int_{Y_t} \iota_{h_t - v_t} f_\omega(\varphi_s^\epsilon) \right] dt \,.$$

Let us show now that g is derivable in 0 and let us explicit this derivative.

Lemma 4.1. *Consider the application*

$$g(\epsilon) \doteq \int_0^1 \left[\int_{Y_s} \iota_{h_s - v_s} (f \circ \varphi_s^\epsilon) \right] ds \,. \tag{4.56}$$

Then g is derivable and there exists $t \mapsto \mathcal{J}^a_t$ an application in $\mathcal{C}([0,1],V^*)$ such that

$$g'(0) = \int_0^1 \mathcal{J}^a_s(\delta v_s) ds\,. \tag{4.57}$$

Proof. Denote $K = \bigcup_{s\in[0,1]} Y_s$, i.e. $K = q_0(X)$ and since $q_0 \in \mathcal{C}(X,\mathbb{R}^d)$ and X is compact, K is bounded. We apply the Leibniz's rule to derive under the integral sign so that we get

$$\begin{aligned}
g'(0) &= \int_0^1 \left[\int_{Y_s} \iota_{h_s - v_s}(d_\varphi f(\varphi_s)\cdot \delta\varphi_s)\right] ds \\
&= \int_0^1 \left[\int_{Y_s} \iota_{h_s - v_s} d_\varphi f(\varphi_s) \int_s^1 A^s_t \cdot (\delta\nu_t \circ \phi_{s,t})\, dt\right] ds \\
&= \int_0^1 \left[\int_{Y_s} \int_s^1 \iota_{h_s - v_s}\big(A^s_t(y)^* d_\varphi f(\varphi_s)\big)\cdot (\delta\nu_t \circ \phi_{s,t})\, dt\right] ds\,,
\end{aligned}$$

where $A^s_t(y)^*$ denotes the adjoint operator of $A^s_t(y) \in \mathcal{L}(\mathbb{R}^d, \mathcal{L}(\mathbb{R}^d))$. For any $y \in Y_s$, the integrand $\iota_{h_s-v_s}\big(A^s_t(y)^*\, d_\varphi f(\varphi_s(y))\cdot(\delta\nu_t(\phi_{s,t}(y)))\big)$ belongs to $(\Lambda^k\mathbb{R}^d)^*$ and we want to bound its norm independently of y to guarantee its integrability. This will come from the (H^V_1) conditions that gives a spatial control of the elements of V and their differential.

For any $y \in Y_s$, the application $A^s_t(y)^*\, d_\varphi f(\varphi_s(y))$ belongs to $\mathcal{L}\big(\mathbb{R}^d \times \mathcal{L}(\mathbb{R}^d), (\Lambda^k\mathbb{R}^d)^*\big)$ and can be identified to an element of $(\Lambda^k\mathbb{R}^d)^* \otimes (\mathbb{R}^d \times \mathcal{L}(\mathbb{R}^d))^*$. Moreover, for any $\zeta \in (\Lambda^k\mathbb{R}^d)^* \otimes (\mathbb{R}^d \times \mathcal{L}(\mathbb{R}^d))^*$, consider $l^\zeta_y : V \to (\Lambda^k\mathbb{R}^d)^*$ by

$$l^\zeta_y(u) = \zeta\big(u(y), du(y)\big).$$

Then l^ζ_y is linear and under the (H^V_1) conditions, there exists $c_V \in V$, such that for any $u \in V$, for any $y \in K$, if $\mu = (u, du)$, then

$$\begin{aligned}
|l^\zeta_y(u)|_{(\Lambda^k\mathbb{R}^d)^*} &= |\zeta(\mu(y))|_{(\Lambda^k\mathbb{R}^d)^*} \\
&\le |\zeta|_{(\Lambda^k\mathbb{R}^d)^*\otimes(\mathbb{R}^d\times\mathcal{L}(\mathbb{R}^d))^*} |\mu(y)|_{\mathbb{R}^d\times\mathcal{L}(\mathbb{R}^d)} \\
&\le c_V |u|_V \sup_{y\in K}(1+|y|_{\mathbb{R}^d})|\zeta|_{(\Lambda^k\mathbb{R}^d)^*\otimes(\mathbb{R}^d\times\mathcal{L}(\mathbb{R}^d))^*}\,.
\end{aligned}$$

Hence, l^ζ_y belongs to $(\Lambda^k\mathbb{R}^d)^* \otimes V^*$ and

$$|l^\zeta_y|_{(\Lambda^k\mathbb{R}^d)^*\otimes V^*} \le c_V \sup_{y\in K}(1+|y|_{\mathbb{R}^d})|\zeta|_{(\Lambda^k\mathbb{R}^d)^*\otimes(\mathbb{R}^d\times\mathcal{L}(\mathbb{R}^d))^*}\,.$$

We can therefore apply Fubini's theorem to get that for any $u \in V$

$$\mathcal{J}^a_t(u) \doteq \int_0^t \left(\int_{Y_s} \iota_{h_s-v_s}\left(l^{(A^s_t)^* d_\varphi f(\varphi_s)}_{\phi_{s,1}}(u)\right)\right) ds\,. \tag{4.58}$$

Finally, since $t \to A^s_t(y)$ is continuous, we deduce easily that $t \mapsto \mathcal{J}^a_t$ is continuous. $\square$

To study the second term of μ^ϵ in equation (4.54), we introduce the next lemma.

Lemma 4.2. *Define for a given $\omega \in \mathcal{C}^1_0(\mathbb{R}^d, (\Lambda^k\mathbb{R}^d)^*)$ the function $t \mapsto \mathcal{J}^b_t$ such that for* *any* $u \in V$

$$\mathcal{J}_t^b(u) = \int_{Y_t} \iota_u(\omega)\,. \tag{4.59}$$

Then $\mathcal{J}^b$ *is a continuous function defined from* $[0,1]$ *to* V^*.

Proof. For any $t \in [0,1]$, $\mathcal{J}_t^b$ is linear on V and with the (H_1^V) conditions, there exists $c > 0$ such that for any $u \in V$,

$$\begin{aligned} |\mathcal{J}_t^b(u)| &\leq \int_{Y_t} |u(y)|_{\mathbb{R}^d} |\omega(y)|_\infty d\mathcal{H}^{k-1}(y) \\ &\leq c \sup_{y \in K}(1 + |y|_{\mathbb{R}^d})\ vol(Y_t)|\omega|_\infty |u|_V\,. \end{aligned}$$

Thus, $\mathcal{J}_t^b \in V^*$. Moreover, we can show that $t \to \mathcal{J}_t^b$ is derivable (and in particular continuous). From the spatial regularity of any $u \in V$, we deduce that $\omega^u \doteq \iota_u(\omega) \in \mathcal{C}^1(\mathbb{R}^d, (\Lambda^{k-1}\mathbb{R}^d)^*)$. Now, under the (H^{q_0}) conditions, we can pull backward the integrand of $\mathcal{J}^b$:

$$\mathcal{J}_t^b(u) = \int_{\{t\}\times B} q_0^* \omega^u\,.$$

Therefore, if $\frac{\partial}{\partial t}$ is the vector field on X defined at any point $(t, x_B) \in [0,1] \times B$ by $(1, 0_{T_{x_B}B})$, then $\frac{\partial}{\partial t}$ generates a flow ψ_t on X satisfying $\psi_t(s, x_B) = (s+t, x_B)$. Thus, $\alpha \doteq q_0^* \omega^u \in \mathcal{C}^1(X, \Lambda^{k-1}T^*X)$ is a (k-1)-form on X and it results from the Cartan's formula and the Stokes' theorem that

$$\frac{d}{dt}\mathcal{J}_t^b(u) = \frac{d}{dt}\int_{\{t\}\times B} \alpha = \int_{\{t\}\times B} \iota_{\frac{\partial}{\partial t}} d\alpha + \int_{\{t\}\times \partial B} \iota_{\frac{\partial}{\partial t}} \alpha\,. \tag{4.60}$$

□

4.4.2 Continuity of the minimizers

Finally, we can conclude that all solutions are continuous and the next theorem recalls all assumptions.

Theorem 4.4. *Consider* $X = [0,1] \times B$ *where* B *is a compact oriented manifold with corners and* τ *the projection on the first coordinate of* X. *Assume that* $q_0 \in \mathcal{C}^\infty(X, \mathbb{R}^d)$. *Under the* (H^{q_0}) *and* (H_1^V) *conditions, if* $v^* \in L^2([0,1], V)$ *minimizes the energy defined by*

$$E(v) = \frac{1}{2}\int_0^1 |v|_V^2 dt + \frac{\lambda}{2}|\mu_v - \mu_{\text{tar}}|_{W^*}^2\,,$$

then v^* *belongs to* $\mathcal{C}([0,1], V)$.

More precisely, for any $(v, \delta v)$ *in* $L_V^2 \times L_V^2$, *the application* $\epsilon \mapsto g(\epsilon) \doteq E(v + \epsilon\delta v)$ *is derivable at* 0 *and we have*

$$\begin{aligned} g'(0) &= \int_0^1 \langle v_t, \delta v_t\rangle dt + \lambda \int_0^1 \left[\int_{Y_t} \iota_{h_t - v_t}(\frac{\partial \phi_{t,1}^* \omega}{\partial v}.\delta v)\right] dt - \lambda \int_0^1 \left[\int_{Y_t} \iota_{\delta v_t}\phi_{t,1}^*\omega\right] dt \\ &= \int_0^1 L_V v_t(\delta v_t) + \mathcal{J}_t^a(\delta v_t) - \mathcal{J}_t^b(\delta v_t)\, dt\,, \end{aligned}$$

where K_V and $L_V = K_V^{-1}$ are the isomorphisms between V and V^*, $\omega = K_W(\mu_v - \mu_{tar})$, $\mathcal{J}^a, \mathcal{J}^b \in \mathcal{C}([0,1], V^*)$ are defined by equations (4.58) and (4.59) and h_t is the unique vector field on Y_t defined for almost any $t \in [0,1]$ and any $x \in B_t$ by $h_t(q_0(x)) = \frac{\partial q_0}{\partial t}(x)$.

Proof. We have

$$\frac{\partial}{\partial \epsilon}\frac{1}{2}|\mu_v - \mu_{\mathrm{tar}}|^2_{W^*}\big|_{\epsilon=0} = \frac{\partial}{\partial \epsilon}\mu_{v^\epsilon}(\omega)\big|_{\epsilon=0} .$$

The expression of $\mu_{v^\epsilon}(\omega)$ is given by equation (4.54) and its derivative with respect to ϵ is given above in Section 4.4.1.

At last, if v^* minimizes E then $L_V v_t^* = \mathcal{J}_t^b - \mathcal{J}_t^a$ for almost every $t \in [0,1]$. Since $\mathcal{J}^a$ and $\mathcal{J}^b$ are continuous, $t \mapsto v_t^* = K_V(\mathcal{J}_t^b - \mathcal{J}_t^a)$ is continuous at any $t \in [0,1]$. □

Remark 4.4. *One can easily generalize this theorem with a cost function on L_V^2 of the type $C(v) = \frac{1}{2}\int_0^1 C(v_t, t)dt$. More precisely, assume that there exists $\ell \in \mathcal{C}([0,1], V^*)$ such that for any $t \in [0,1]$, $\frac{\partial C}{\partial v}(v,t) = \ell_t(v)$ and ℓ_t is invertible. If $v^* \in L^2([0,1], V)$ minimizes the energy*

$$E(v) = \frac{1}{2}\int_0^1 C(v_t, t)dt + \frac{\lambda}{2}|\mu_v - \mu_{\mathrm{tar}}|^2_{W^*} ,$$

then for any $t \in [0,1]$

$$v_t^* = \ell_t^{-1}\big(K_V(\mathcal{J}_t^b - \mathcal{J}_t^a)\big) .$$

It will follow that $v^* \in \mathcal{C}([0,1], V)$.

Remark 4.5. *Note that $\mathcal{J}^b - \mathcal{J}^a$ can be identified with the momentum map $\mathcal{J}$. See Chapter 3.*

Remark 4.6. *Note that $\mathcal{J}_0^b$ is always null. Moreover, if $\mathcal{H}^{k-1}(Y_t)$ is null, then $\mathcal{J}_t^a$ is also null. In the case of the horn, Y_0 represents the tip of the horn. It is thus reduced to a point, so that we retrieve the fact that v_0^* is necessary null. See Chapter 3.*

5 Continuous pointwise expression of the momentum

The continuity of the global minimizers of the energy allows to explicit the momentum. This is the key point to explicit then the momentum map with a general coordinate space X (i.e. non discrete) and therefore to explicit an optimal vector field. This result cannot be directly prove with the varifolds and the growth dynamic since it also implies the continuity of the momentum map and thus of all global minimizers of the energy (see Chapter 3).

We saw in Chapter 3 that in order to explicit the gradient of the energy

$$E(q_0, v) = \int_0^1 C(v_t, t)\, dt + \mathcal{A}(v) , \tag{4.61}$$

one could use in the discrete model (i.e. for $X = (\mathbb{R}^d)^k$) the fact that there exists a final momentum $p_1 \in L^\infty(X, \mathbb{R}^d)) = (\mathbb{R}^d)^k$ such that

$$\mathcal{A}'(v; \delta v) = \langle p_1, \delta q_1 \rangle_{(\mathbb{R}^d)^k} .$$

The aim of this section is to show in the general case of a compact manifold X, the existence of an equivalent pointwise momentum variable p_1 acting on δq_1, and to give its expression.

5.1 A lemma

Let X be a smooth orientable compact manifold of dimension k (possibly with corners) and let $M = \mathbb{R} \times X$ be the cylinder generated by X so that M is again a smooth orientable manifold (possibly with corners). Let us introduce for any $\epsilon \in \mathbb{R}$ the submanifold $M_\epsilon = \{\epsilon\} \times X$ of M. The tangent space at a point (ϵ, x) is identified with $\mathbb{R} \times T_x X$ and $\frac{\partial}{\partial \epsilon}$ denotes the vector field defined at any point (ϵ, x) by $(1, 0_{T_x X})$.

Lemma 5.1. *Let $f : M \to N$ be a $\mathcal{C}^1$ mapping from M to a smooth manifold N and ω be a $\mathcal{C}^1$ k-form on N. Consider for $\epsilon \in \mathbb{R}$*

$$g(\epsilon) \doteq \int_{M_\epsilon} f^*\omega \,,$$

where $f^*\omega$ denotes the pull-back of ω by f. Then we have:

1. *The function g belongs to $\mathcal{C}^1(\mathbb{R}, \mathbb{R})$ and*
$$g'(\epsilon) = \int_{M_\epsilon} \iota_{\frac{\partial}{\partial \epsilon}} f^* d\omega + \int_{\partial M_\epsilon} \iota_{\frac{\partial}{\partial \epsilon}} f^*\omega \,. \tag{4.62}$$

2. *There exist two functions $a : X \to T^*N$ and $b : X \to T^*N$ such that for any $x \in X$, $a(x)$ and $b(x)$ belong to $T^*_{f_0(x)}N$ and*
$$g'(0) = \int_X a(x)\,(\delta f(x))\, d\mathcal{H}^k(x) + \int_{\partial X} b(x)\,(\delta f(x))\, d\mathcal{H}^{k-1}(x) \,, \tag{4.63}$$
where $f_0 = f \circ j_0$, $\delta f = \frac{\partial}{\partial \epsilon} f \circ j_{\epsilon|_{\epsilon=0}}$ and $j_\epsilon : X \to M_\epsilon$ is the trivial embedding given by $j_\epsilon(x) = (\epsilon, x)$. Moreover, a and b only depend on f_0 and ω.

Proof. $\frac{\partial}{\partial \epsilon}$ is a smooth vector field generating a flow ψ_t on M that satisfies $\psi_t(\epsilon, x) = (\epsilon + t, x)$. If $\alpha \doteq f^*\omega$, α is a $\mathcal{C}^1$ k-form on M and $g(\epsilon + h) \doteq \int_{M_\epsilon} \psi_h^*(\alpha)$ so that we get from the Cartan formula

$$g'(\epsilon) = \int_{M_\epsilon} \pounds_{\frac{\partial}{\partial \epsilon}} \alpha = \int_{M_\epsilon} \iota_{\frac{\partial}{\partial \epsilon}} d\alpha + \int_{\partial M_\epsilon} \iota_{\frac{\partial}{\partial \epsilon}} \alpha \,. \tag{4.64}$$

Since $\alpha = f^*\omega$ and $d\alpha = d(f^*\omega) = f^*(d\omega)$, we retrieve the equation (4.62). Now if $f_\epsilon \doteq f \circ j_\epsilon$, then

$$\begin{aligned} g'(0) &= \int_{j_0(X)} \iota_{\frac{\partial}{\partial \epsilon}} f^* d\omega + \int_{j_0(\partial X)} \iota_{\frac{\partial}{\partial \epsilon}} f^*\omega \\ &= \int_X j_0^* \left(\iota_{\frac{\partial}{\partial \epsilon}} f^* d\omega \right) + \int_{\partial X} j_0^* \left(\iota_{\frac{\partial}{\partial \epsilon}} f^*\omega \right) \,. \end{aligned} \tag{4.65}$$

We can explicit these two terms. Consider a coordinate chart (U, φ), then the first term of the right-hand side of (4.65) can be rewritten

$$\int_U d\omega(f_0(x)) \left(\frac{\partial f}{\partial \epsilon}(0,x) \wedge \bigwedge_{i=1}^{k} \frac{\partial f}{\partial x_i}(0,x) \right) dx_1 \cdots dx_k \,.$$

Consider now a coordinate chart $(\partial U, \varphi)$ from an open set ∂U of ∂X, then the second term of the right-hand side of (4.65) can be rewritten

$$\int_{\partial U} \omega(f_0(x)) \left(\frac{\partial f}{\partial \epsilon}(0,x) \wedge \bigwedge_{i=1}^{k-1} \frac{\partial f}{\partial x_i}(0,x) \right) dx_1 \cdots dx_{k-1} \,.$$

Finally, since ω and f are of class $\mathcal{C}^1$, the integrands of these two terms are both continuous linear forms applied to $\delta f(x) = \frac{\partial f}{\partial \epsilon}(0,x)$ and they only depend on f_0 and ω. $\square$

5.2 Application

We will apply this lemma in a general situation. The shape $q_1 : X \to \mathbb{R}^d$ generated by a vector field $v \in L^2_V([0,1], V)$ is given by an operator Φ where X is a compact submanifold with corners. We will although assume that Φ need to be restricted to continuous vector field to ensure the regularity of q_1. Yet, we do not specify that v generates q_1 with the growth dynamic. We consider a space of currents $W \hookrightarrow \mathcal{C}^1_0(\mathbb{R}^d, \Lambda^k\mathbb{R}^d)$. The current generated by v is denoted μ_v.

Theorem 5.1. *Consider*

$$\Phi : L^2([0,1], V) \to \mathcal{C}(X, \mathbb{R}^d)$$

such that

1. *For any $v \in \mathcal{C}([0,1], V)$, $\Phi(v) \in \mathcal{C}^1(X, \mathbb{R}^d)$ and $\partial_x \Phi(v)$ is continuous with respect to v.*
2. *Φ is Gateaux-derivable and for any $\delta v \in L^2_V$, $v \mapsto \Phi'(v; \delta v)$ is continuous.*

If v and δv belong to $\mathcal{C}([0,1], V)$ and if $W \hookrightarrow \mathcal{C}^1_0(\mathbb{R}^d, \Lambda^k\mathbb{R}^d)$, then there exists $p_1^X \in \mathcal{C}(X, \mathbb{R}^n)$ and $p_1^{\partial X} \in \mathcal{C}(\partial X, \mathbb{R}^d)$ such that

$$\left.\frac{\partial}{\partial \epsilon}\right|_{\epsilon=0} |\mu_{v^\epsilon} - \mu_{tar}|^2_{W^*} = \int_X \langle p_1^X(x), \delta q_1(x) \rangle_{\mathbb{R}^n} d\mathcal{H}^k(x) + \int_{\partial X} \langle p_1^{\partial X}(x), \delta q_1(x) \rangle_{\mathbb{R}^n} d\mathcal{H}^{k-1}(x) \,.$$

Proof. Let be v and δv in $\mathcal{C}([0,1], V)$ and denote for any $\epsilon \in \mathbb{R}$, $v^\epsilon = v + \epsilon \delta v$, $q_1^\epsilon = \Phi(v^\epsilon)$, $\delta q_1^\epsilon = \Phi'(v^\epsilon; \delta v)$. Consider $f : \mathbb{R} \times X \to \mathbb{R}^d$, defined by $f(\epsilon, x) = q_1^\epsilon(x)$ and let us show that f is of class $\mathcal{C}^1$. We have for any $\epsilon \in \mathbb{R}$, $q_1^\epsilon \in \mathcal{C}^1(X, \mathbb{R}^d)$ and $\delta q_1^\epsilon \in \mathcal{C}(X, \mathbb{R}^d)$. Moreover, since dq_1 and δq_1 are continuous with respect to v, dq_1^ϵ and δq_1^ϵ are continuous with respect to ϵ.

Now, we just have to notice that

$$\partial_\epsilon f(\epsilon, x) = \delta q_1^\epsilon(x)\,,$$
$$\partial_x f(\epsilon, x) = dq_1^\epsilon(x)\,.$$

Since these partial derivatives are continuous, it follows that f is of class $\mathcal{C}^1$.

Finally, we have

$$\mu_{v^\epsilon}(\omega) = \int_X (q_1^\epsilon)^* \omega = \int_{M_\epsilon} f^* \omega\,.$$

Hence, if we apply Lemma 5.1 to $f(\epsilon, x) = q_1^\epsilon(x)$ so that $\frac{\partial f}{\partial \epsilon} \circ j_0 = \delta q_1$, we get

$$\begin{aligned}
\frac{\partial}{\partial \epsilon}\bigg|_{\epsilon=0} |\mu_{v^\epsilon} - \mu_{tar}|^2_{W^*} &= \frac{\partial}{\partial \epsilon}\bigg|_{\epsilon=0} \mu_{v^\epsilon}(\omega) \\
&= \int_X d\omega_{q_1(x)} \left(\delta q_1(x) \wedge \bigwedge_{i=1}^{d} dq_1(x) \cdot T_i^X(x) \right) d\mathcal{H}^k(x) \\
&\quad + \int_{\partial X} \omega_{q_1(x)} \left(\delta q_1(x) \wedge \bigwedge_{i=1}^{d-1} dq_1(x) \cdot T_i^{\partial X}(x) \right) d\mathcal{H}^{k-1}(x)\,,
\end{aligned}$$

where $(q_1, \delta q_1) = (q_1^\epsilon, \delta q_1^\epsilon)$ for $\epsilon = 0$, $\omega = K_W(\mu_v - \mu_{tar}) \in W$ and $(T_i^X)_i$ is an orthonormal basis of $T_x X$, the tangent space at $x \in X$ and $(T_i^{\partial X})_i$ is an orthonormal basis of $T_x \partial X$, the tangent space at $x \in \partial X$.

For any $x \in X$ or any $x \in \partial X$, these two integrands are linear with respect to $\delta q_1(x)$. There exist thus for any $x \in X$, a unique vector $p_1^X(x) \in \mathbb{R}^d$ and likewise for any $x \in \partial X$, a unique vector $p_1^{\partial X} \in \mathbb{R}^d$ such that we get the final result. Moreover, since q_1 and ω are of class $\mathcal{C}^1$, p_1^X and $p_1^{\partial X}$ are continuous. □

Remark 5.1. *Note that with the usual regular conditions on V, this theorem can be applied to the classic dynamic as the growth dynamic.*

6 Conclusion

We examined in this chapter the existence and regularity of global minimizers v to the optimization problem discussed in the previous chapter when the infinitesimal action ξ reproduces the growth dynamic. These questions lie on the choice of the data attachment term. We exhibited two counterexamples for the varifold representation. These situations highlighted the lack of spatial regularity of a shape generated by a discontinuous time-varying vector field $t \mapsto v_t$. This issue is well addressed by the current representation that has a regularization effect of the shapes. We proved indeed, with a data attachment term built on a current representation, the existence of global minimizers as well as their continuity.

We detailed in this chapter the foliated structure induced by the birth tag τ on the coordinate space X when the creation process is regular meaning that the amount of newly created points at each time, i.e. the level sets of τ, evolves smoothly. We justified the canonical description of the biological coordinate system (X, τ) via a direct product $X = [0,1] \times X_0$ where τ is identified with the projection on the first coordinate. An important consequence of this rewriting is the ability to overcome the reparameterizations in time of the scenarios generated by the biological coordinate system (see Chapter 2).

In the last section, we established a pointwise expression of the final momentum p_1. This expression plays a key role to describe the solutions of the optimization problem. The study of the growth dynamic achieved in Chapter 3 and the calibration of the optimization problem by new cost functions are based on this pointwise expression that allows to exploit the previous decomposition of the biological coordinate system.

Chapter 5

Numerical Study of the Growth Model

Contents

1 Introduction

From the point of view of one to one correspondences between homologous points, a growth process can be described by the nonlinear combination of two different processes: a deformation process when a living organism is deforming through time and an expansion process when the growth results from the creation of new material. The observation of the shape without more information does not allow to distinguish these two processes. The development of a horn is thus a interesting case study. We consider indeed a population of horn sharing a basic common pattern defined as follows. The base of the horn plays the role of an active area where new leaves are gradually created pushing outwards the rest of the horn. The horn is assumed to be rigid and is thus only subjected to rotations and translations due to the physical constraints (see figure 5.1). This example allows to isolate the creation process from the general deformation and reduce to its minimum any kind of distortions of the shape due to other biological phenomena.

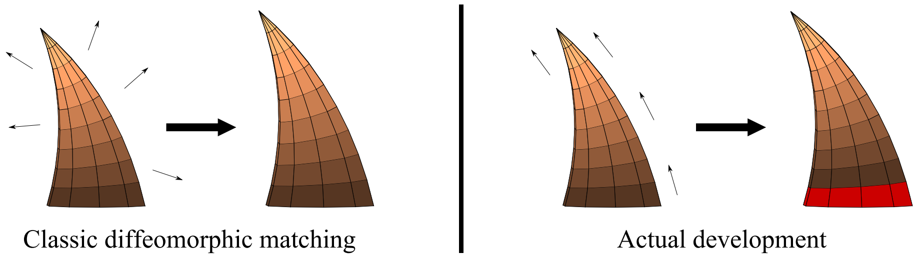

Figure 5.1 – A classic diffeomorphic matching would stretch the small horn to the large one and would thus not reflect the actual development of the horn. Instead, we would like to see an embedding of the small horn inside the target and additionally creation of new material at the base.

The aim is, given few observations at different times of a horn, to reconstruct its continuous development from its youngest state to its oldest one. We will see that our model can actually produce a path modeling the complete deployment of a horn from only one observation. If we imagine the horn at its birth as reduced to a single point, we can construct an optimal continuous path from this point to a nontrivial shape matching the given observation. *In fine*, the complete evolution is encoded in a forecast initial position and its momentum (q_0, p_0), providing the support to a statistical analysis.

In order to model the evolution of a shape during a growth process, we developed in Chapter 2 the concept of *growth mapped evolution* (GME). A GME is given as a path of shapes $[0,1] \ni t \mapsto S_t$ and a flow of mappings $(\phi_{s,t})_{s \leq t}$ such that for any pair $s \leq t \in [0,1]$, the flow deforms the older shape S_s into the younger one S_t: $\phi_{s,t}(S_s) \subset S_t$. The shape S_t is thus made of the image of S_s at time t and of a set of new points created in the time interval $]s,t]$. When $\phi_{s,t}(S_s) = S_t$ for any s, t, the shape evolves through a pure deformation process and we retrieve the standard dynamic through the flow. On the contrary, in the absence of global deformation, $\phi_{s,t} = \mathrm{Id}$ for any s, t so that the shape evolves by pure expansion and we have $S_s \subset S_t$. This last type of scenario plays a central role and such GMEs are called centered. Following D'Arcy Thompson's ideas, these GMEs represent the biological coordinate system of a set of homologous scenarios.

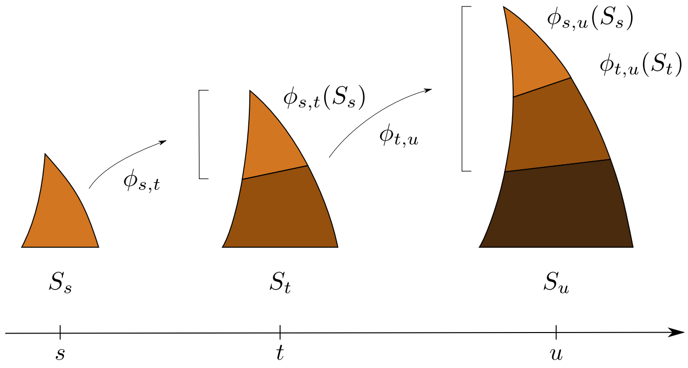

Figure 5.2 – Sequence of three discrete times to illustrate the development of a horn.

1.1 Biological coordinate system

A **biological coordinate system** is a pair (X, τ) where X is a space called the coordinate space and $\tau : X \to [0,1]$ the birth tag on X. It induces a set of shapes

$$X_t \doteq \{x \in X \,|\, \tau(x) \leq t\}\,, \tag{5.1}$$

of the so called active points of the coordinate space X at time t. In this chapter, the biological coordinate system is fixed to

$$\begin{cases} X \doteq [0,1] \times \mathbb{S}^1\,, \\ \tau(x) \doteq t \quad \text{ for any } x = (t, x_0) \in X\,. \end{cases} \tag{5.2}$$

When X is a discrete set, it will be defined by $X = \{0, t_1, \ldots, t_{n-1}, 1\} \times X_0$ where $0 < t_1 < \ldots < t_{n-1} < 1$ and X_0 a finite subset of $\mathbb{S}^1$. A biological coordinate system can be itself identified to the growth scenario of a shape. The sequence of nested shapes X_t, here given by $X_t = [0,t] \times \mathbb{S}^1$, forms a canonical scenario that describes the growth pattern of a population of related shapes. Figure 5.3 displays this scenario in our situation. At time 0, the shape is a circle. It growths into a cylinder under a pure expansion process by the progressive adjunction of identical circles. These circles are given by the sets of points

$$X_{\{t\}} \doteq \{x \in X \,|\, \tau(x) = t\} = \{t\} \times \mathbb{S}^1\,.$$

Any shape X_t is a connected disjoint reunion of some of these sets called the **leaves** of the shape.

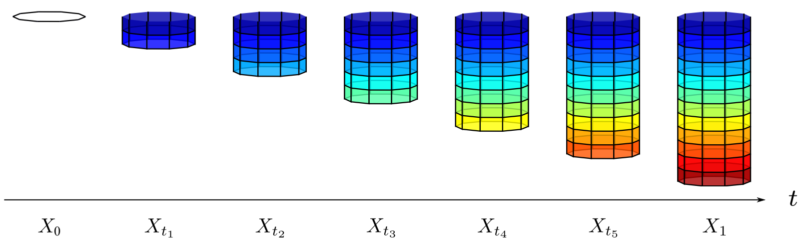

Figure 5.3 – Trivial scenario of the biological coordinate system.

A general scenario $(t \mapsto S_t)_{t\in[0,1]}$ is modeled on the biological coordinate space by a sequence of spatial mappings $t \mapsto (q_t : X \to \mathbb{R}^d)$. The shape S_t is given by the image $q_t(X_t)$ of the active points of X. Depending on the injectivity of the mappings $(q_t)_t$, the generated scenario follows the same expansion process of the biological coordinate system. At each time $t \in]0,1]$, a new leaf $q_t(X_{\{t\}})$ appears whose points have no biological correspondence with the points of the older shapes $S_s, s < t$.

Figure 5.4 illustrates two such types of scenario built on the coordinate system (X, τ). The only difference between these two types is the behavior of the spatial mapping on the first leaf $X_{\{0\}}$. For the first scenario, the spatial mapping is an embedding at all time. For the second one, q_t is an embedding of all leaves but the first one and $q_t(X_{\{0\}})$ is reduced to a point.

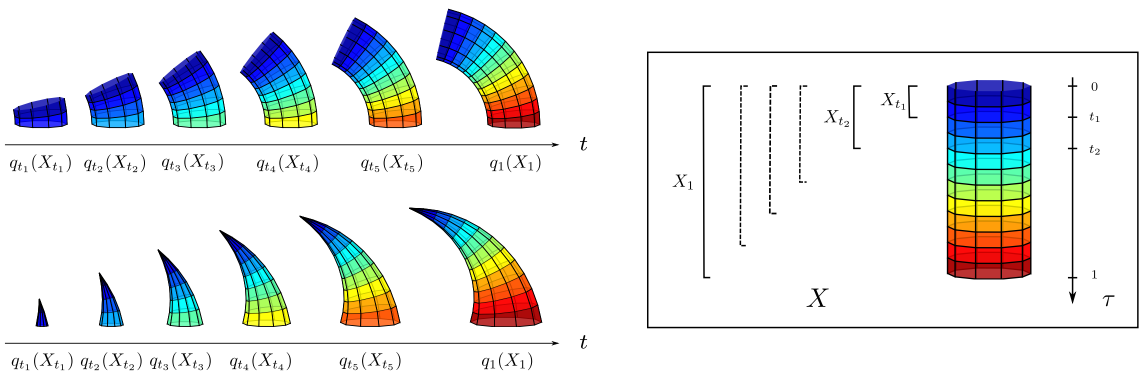

Figure 5.4 – Two examples of scenarios built on the biological coordinate system (X, τ).

In these two examples, the last leaf is always included in the horizontal plane. The **birth place function** introduced in Chapter 2 allows to express this constraint. The birth place function $\tilde{q} : X \to \mathbb{R}^d$ of a scenario associated to a mapping q is defined by

$$\tilde{q}(x) = q_{\tau(x)}(x) = \phi^{-1}_{\tau(x),1}(q_1(x))\,.$$

It can be seen as the pull backward through the flow of each leaf $q_1(X_{\{t\}})$ of the final shape to its initial position $q_t(X_{\{t\}})$ at time $t = \tau(x)$ when it appeared. The evolution of this leaf can then be completely retrieved by the flow $(\phi_{s,t})_{s\le t}$ of the scenario: for any $x \in X$ and any $t \in [\tau(x), 1]$

$$q_t(x) = \phi_{\tau(x),t}(q_{\tau(x)}(x)) = \phi_{\tau(x),t}(\tilde{q}(x))\,. \tag{5.3}$$

To extend the mappings $q_t : X_t \to \mathbb{R}^d$ into homologous mappings on X, we then say that

$$q_t(x) = \begin{cases} \phi_{\tau(x),t}(\tilde{q}(x)) & \text{if } \tau(x) \le t\,, \\ \tilde{q}(x) & \text{otherwise.} \end{cases} \tag{5.4}$$

Hence, we have

$$q_0 = \tilde{q}. \tag{5.5}$$

This mapping q_0 is called the initial condition and the planar constraint can then easily be written as a constraint on the image of q_0.

Remark 1.1. *The birth place function can be highly non injective. For example as we will see in Section 6.4 with the tube, all the new leaves can appear at the same place. The flow of a scenario is able to separate two different leaves. However, if two points of the same leaf $X_{\{t\}}$ appear at the same position, they will never be separated.*

1.2 Reconstitution of a growth scenario

In this chapter, we will study surfaces embedded in $\mathbb{R}^3$ whose scenario is consistent with the biological coordinate system previously defined. Assume that a target scenario is given by $(S_i^{\text{tar}})_i$ a collection of shapes at a finite number of intermediate times $(t_i)_i \subset [0,1]$ (with $\max\{t_i, i\} = 1$). The aim is to retrieve its complete development from its creation at time 0 to its final age at time 1. In practice, it leads to generate a scenario $(t \mapsto S_t)_{t\in[0,1]}$ such that $S_{t_i} \approx S_i^{\text{tar}}$.

We developed in Chapter 3 a generative model based on an **initial position** $q_0 : X \to \mathbb{R}^d$ and the **growth dynamic**

$$\dot{q}_t = \mathbb{1}_{\tau\leq t} v_t \circ q_t \,,$$

where v is a time-varying vector field on $\mathbb{R}^d$ ($v \in L^2([0,1], V)$).

An inexact registration between two scenarios consists then in minimizing an energy that penalizes on one side the deformation with a **cost function** C and on the other side the discrepancy between the two scenarios at the different times t_i with a **data attachment term** $\mathcal{A}$ of the type

$$\mathcal{A}(q_0, v) = \sum_{i=0}^{n} d(S_{t_i}^v, S_i^{\text{tar}})^2 \,.$$

Remark 1.2. *Note as we saw in Chapter 4, that in some critical cases where the shape is folding on itself, the current or the varifold μ^S modeling the form $S_t^v = \{q_t(x) \,|\, x \in X_t\}$ can be different from the one μ^v defined to represent the mapping $q_t : X_t \to \mathbb{R}^d$.*

The energy to minimize can thus be written

$$E(q_0, v) = \int_0^1 C(v_t, t)\, dt + \mathcal{A}(q_0, v) \,.$$

In all our experiments we will present different tools to specify this general model presented in Chapter 3. As we saw in this chapter, an optimal solution $v^* \in L_V^2$ must then satisfy at all time

$$\nabla_v C(v_t^*, t) - K^V \mathcal{J}(q_t, p_t, t) = 0 \,, \tag{5.6}$$

where $K^V : V^* \to V$ is the canonical isomorphism and $\mathcal{J}$ is the momentum map whose expression will be recalled in equations 5.10 and 5.11.

1.3 Deformation spaces

The deformations involved in the model are determined by the choice of the space of vector fields V. This space is usually a Reproducing Kernel Hilbert Space (RKHS) and the representations of the data rely thus on the choice of the kernel.

The choice to study animal horns intended to avoid the ill-posed distinction between diffeomorphic and intrinsic changes. For example, one can think to the question of how to balance the emergence of new matter and the stretching of a shape. In order to exclude this issue, the numerical applications will be mainly performed with affine transformations. These transformations respect the idea that once a portion of the horn has appeared, it behaves as a solid. It is not deformed, only displaced.

Rigid deformations

The group of rotations and translations is the semi-direct product $\mathbb{R}^d \rtimes SO_d(\mathbb{R})$, for which $V = \mathbb{A}_d \times \mathbb{R}^d$, where $\mathbb{A}_d$ is the space of skew-symmetric matrices. The space V is then naturally equipped with a set of norms with a parameter $\alpha \in \mathbb{R}_+^*$ defined for any $v = (A, N) \in \mathbb{A}_d \times \mathbb{R}^d$ by

$$|v|_{V,\alpha}^2 \doteq \alpha \, tr(A^T A) + |N|_{\mathbb{R}^d}^2 \,. \tag{5.7}$$

The rotations are applied to the horn from the center of its base.

Remark 1.3. *In practice, we will work in $\mathbb{R}^3$ and actually only use vertical translations. The space V is then reduced to $V = \mathbb{A}_3 \times \mathbb{R}(0,0,1)$. We will therefore project at every time the optimal translation on the vertical axis.*

The numerical experiments to retrieve the development of an animal horn will mainly be achieved with this space of vector fields.

Reproducing kernel Hilbert space with scalar Gaussian kernel (RKHS)

The case study of horns with rigid deformations is a first step to initiate the study of growth models. Yet, the presented model also works with non rigid deformations. In order to pave the way for more general applications, we will present in the end few experiments with a RKHS with a scalar Gaussian kernel:

$$\begin{array}{rccc} k_V : & \mathbb{R}^d \times \mathbb{R}^d & \longrightarrow & \mathbb{R} \\ & (x,y) & \longmapsto & \exp\left(-\frac{|x-y|^2}{2\sigma^2}\right) \,. \end{array} \tag{5.8}$$

2 Cost functions

2.1 Inadequacy of the classic cost function

An important novelty appears with the growth dynamic. When there is no creation on a small interval $I \subset [0,1]$, we retrieve the classic LDDMM case and the norm of the vector field is constant on I. Otherwise, when there is appearance of new points, this norm should increase. More explicitly, we have in the discrete setup when V is a RKHS with a kernel noted k_V

$$K^V \mathcal{J}(q,p,t) = \sum_{\substack{x \in X \\ \tau(x) \leq t}} k_V(q(x), \cdot) p(x) \tag{5.9}$$

$$= \sum_{\substack{x \in X \\ \tau(x) \leq t}} \exp\left(-\frac{|q(x) - \cdot|^2}{2\sigma_V^2}\right) p(x) \,. \tag{5.10}$$

In the case of rotations and translations, where V is the direct product $\mathrm{Skew}_d \times \mathbb{R}^d$ equipped with the usual norm, this equation becomes

$$K^V \mathcal{J}(q,p,t) = \left(\mathrm{proj}_{\mathrm{Skew}_d} \left(\sum_{\substack{x \in X \\ \tau(x) \leq t}} p(x) q(x)^T \right), \sum_{\substack{x \in X \\ \tau(x) \leq t}} p(x) \right) . \tag{5.11}$$

We call $X_t = \{x \in X, \tau(x) \leq t\}$ the support of $K^V \mathcal{J}(q,p,t)$. The sequence of the supports at times t_i is increasing

$$X_{t_i} \subset X_{t_{i+1}}$$

and therefore, the norm of $K^V \mathcal{J}$ should in general be increasing.

2.1.1 Infinitesimal action of a deformation and growth

This property of the vector field seems prima facie appreciable. Indeed, since the shape is growing, the energy required to deform it should also be increasing. However, we have to distinguish the groups of diffeomorphisms built with global deformations (especially rigid deformations) from the groups built with local deformations (like RKHS whose kernel has a local support) (see Figure 5.5).

The infinitesimal action of a deformation through the growth dynamic can be interpreted in two main parts. At a time t, the local action on the last leaf appeared will define with the initial position the amount of creation of matter at time $t+\delta t$. Anywhere else the action defines the evolution of the old part of the shape through the standard dynamic. With local deformations, these two parts are more or less independent. But, with rigid deformations, these two parts are inseparable.

In the case of the horn, the weight of the rotations and translations is directly linked to the amount of creation of new matter on the base of the horn (see Figure 5.6). A natural approach to reproduce real observations is to consider that this amount of creation is rather constant with respect to time than linear. This is thus in contradiction with the model.

In Figure 5.7, we illustrate the kind of results we can get so far. The model is not able to create efficiently the sharp tip of the horn. This inadequacy induces a considerable slowdown of the convergence of the gradient descent.

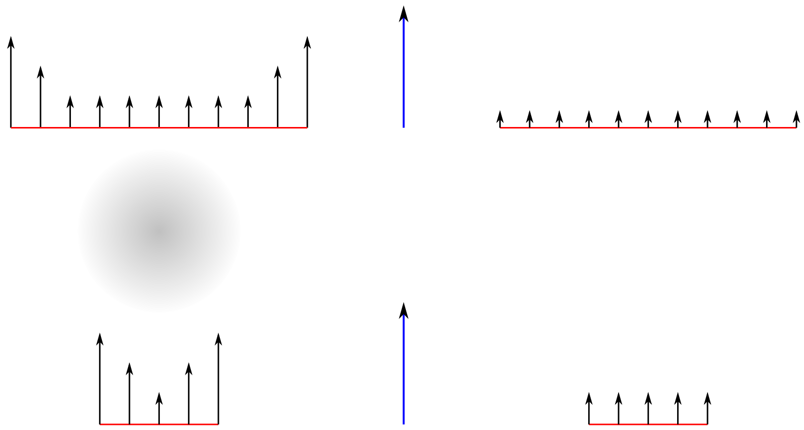

Figure 5.5 – Translation of two segments with a Gaussian kernel (left column) and with the group $\mathbb{R}^2$ of translations in the plan (right column). In all cases, the global translation is given by the two identical blue arrows. The blob in the left column illustrates the scale of the kernel. With a Gaussian kernel, the translation of the segment is given by the sum of the momenta through a convolution with the kernel with respect to their position (see equation 5.10). Otherwise, the translation is the sum of all momenta independently of their position (see equation 5.11). In the first case, the norm of the deformation depends on the size of the segment (see explicit equation 5.28). Conversely, with the Euclidean norm on $\mathbb{R}^2$, the norm of the deformation is the norm of the translation and does not depend on the size of the segment.

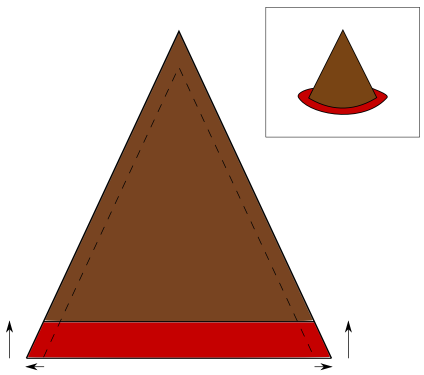

Figure 5.6 – Example of development with the growth dynamic when the deformations are reduced to vertical translations. The vertical expansion of horn is equivalent to the global deformation. Note yet that if we want to quantify the complete amount of expansion, we also have to consider the horizontal component due to the birth position of points to appear. On the top right corner is displayed a top view of the younger horn with the points to appear at their birth position.

2.1.2 Additional property of the rotations and translations Group

The balance between the rotations and the translations in our growth model depends of course on the norm defined on $V = \mathbb{A}_d \times \mathbb{R}^d$ but also on the scale of the shape. We give a heuristic figure (see Figure 5.8) to explain this property. Regarding the optimal matching for a horn, the model tends to favor the translations to deploy the horn at the beginning then to favor the rotations toward the end of the development. Figure 5.9 illustrates this phenomenon: we display after a basic matching with the classic cost function the norms of the two components of the optimal vector field respectively associated to the rotations and the translations. The natural development of a horn requires yet to avoid this behavior. We will see with the adaptive norm how to fix this balance.

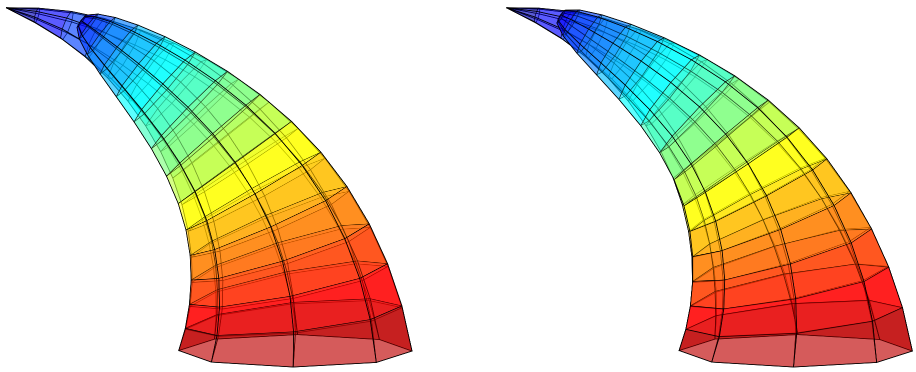

Figure 5.7 – Result of a matching with the *classic cost function*. On the left after 20k iterations, on the right after 200k iterations (i.e. 1day of runtime).

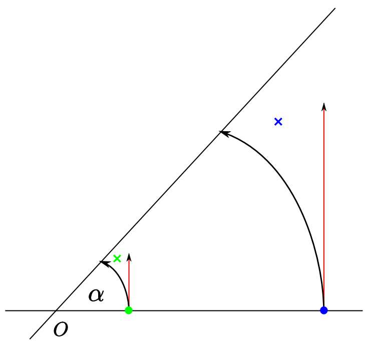

Figure 5.8 – Comparaison of rotation and translation displacements. Consider two matchings of the green point to the green cross and of the blue point to the blue cross. In both cases, we give one rotation and one translation leading to an approximate match. For both green and blue matchings, we use the same rotation of angle α. Yet the second translation is three times more expensive than the first one.

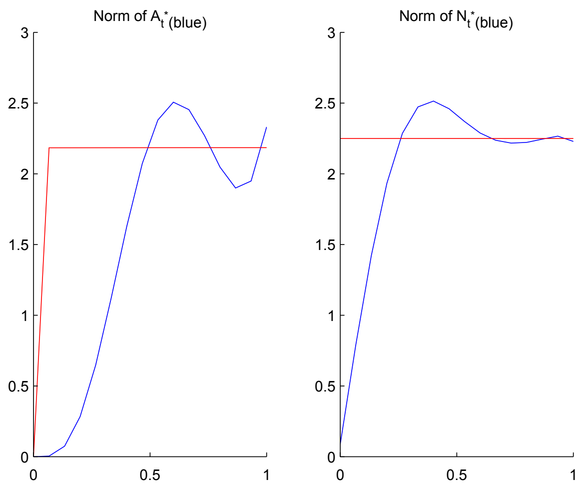

Figure 5.9 – Comparison of the norms of the deformations between the solution (in blue) and the target (in red) for the experiment displayed in Figure 5.7 (on the right). We display separately the norms of the skew-symmetric matrices and the norms of the translations over the time interval $[0, 1]$.

2.1.3 Alternatives and conclusion

The previous observations show that the current theoretical solution is not adapted to model the development of a horn. One can then either change the cost function or the data attachment term in the energy. The addition of intermediate times of the development to favor the convergence of the solution toward the actual development is not enough to modify the global behavior of the solution. Note yet that it does improve the results of some numerical experiments and it will be exploited (see Section 3.3, 6.3 and 7.2). The choice of varifolds over currents also helps to avoid the cancellation of the tip of the horn. At last, an additional landmark on the tips of the horns to match can force the convergence. In order to balance the fact that the support of the vector field is increasing it would yet request to apply a strong weight on the contribution of the tip so that the vector field would primarily be build on this single point. This possibility does not seem reasonable.

In conclusion, one has to change the cost function. In the following sections, we will present different cost functions and explicit the gradient of the energy in each case. We will apply the theorem showed in Chapter 3. An interesting aspect of these new models is that the new cost functions do not require much more computational time in contrast to the addition of intermediate times (that also requires more data).

2.2 Adaptive norm: rotations and translations

2.2.1 Aim

For any time-variant vector field $v = L^2([0,1],V)$, the classic cost function leads in the expression of the energy to the global regularization term

$$\mathcal{R}(v) = \frac{1}{2}\int_0^1 |v_t|_V^2 \, dt \, .$$

The deformation is thus uniformly penalized over time. The idea of the adapted norm is simple. It involves a time-dependent weight to create a time-variant penalization as follows

$$\forall\, v = L^2([0,1],V), \quad \mathcal{R}_\nu(v) \doteq \frac{1}{2}\int_0^1 \nu_t |v_t|_V^2 \, dt \, , \tag{5.12}$$

where ν belongs to $\mathcal{C}^\infty([0,1],\mathbb{R}_+^*)$. The initial growth model tends to generate optimal vector fields with an increasing norm. Since we would rather like to have a norm more or less constant, this weighting function should increase the penalization over time. Hence, ν will be an increasing function of the time. In Chapter 3, we showed that with a discrete coordinate space X this function does not need to tends to 0 at time 0^+. In our experiments, ν will be almost linear with a special care of time 0.

The space of vector fields is now fixed to $V = \mathbb{A}_d \times \mathbb{R}^d$. For any $v \in \mathrm{L}^2([0,1],V)$, we note its canonical decomposition $v = (A,N)$ and at each time $t \in [0,1]$,

$$v_t = (A_t, N_t) \in \mathbb{A}_d \times \mathbb{R}^d \, .$$

As explained previously around the Figure 5.8 and 5.9, applied to the horn developments, this space brings another issue of balance between the rotations and the translations. We recall that V is equipped with the norm $|v|_{V,\alpha}^2 = \alpha\,|A|^2 + |N|^2$ where α is a strictly positive constant. We apply the same concept of weighted penalization to handle this issue. The constant α is replaced by another scalar function that we will still denote $\alpha \in \mathcal{C}^\infty([0,1],\mathbb{R}_+^*)$ to create a penalization on the skew-symmetric matrix increasing over time. *In fine*, we get

$$\forall\, v = L^2([0,1],V), \quad \mathcal{R}_{\nu,\alpha}(v) \doteq \frac{1}{2}\int_0^1 \nu_t |v_t|^2_{V,\alpha_t}\, dt = \frac{1}{2}\int_0^1 \nu_t \left(\alpha_t |A_t|^2_{\mathbb{A}_d} + |N|^2_{\mathbb{R}^d}\right)\, dt\,. \tag{5.13}$$

As for ν, since the size of the horn is increasing, the function α should also be increasing. The problem of time 0 is yet a bit more complicated even with the discrete setup. Indeed, let us recall that at any time t, the optimal vector field is built as an integration of contributions of any point of the actual shape at time t. At time 0, the shape is reduced to a single point. This single point allows in the discrete configuration to generate a non zero initial vector field. However, if this point is located at the center of the ambient space, the model cannot generate an initial rotational impulse. Consider the expression of the momentum map given by equation 5.11. Let us note its canonical decomposition $K^V\mathcal{J} = (K^A\mathcal{J}, K^N\mathcal{J})$. Then the first component applied to a solution (q,p) at time 0 is

$$K^A\mathcal{J}(q_0,p_0,0) = \mathrm{proj}_{\mathbb{A}_d}\left(\sum_{\substack{x\in X\\ \tau(x)=0}} p_0(x)q_0(x)^T\right)$$

At the beginning, the horn is reduced to its tip. We assume this tip to be in the center of the base (see Figure 5.16 for an example of initial position) which is the point 0 of $\mathbb{R}^d$. We have thus for any $x \in X$ such that $\tau(x) = 0$, $q_0(x) = 0$ and consequently

$$K^A\mathcal{J}(q_0,p_0,0) = 0\,.$$

In summary, if we note the optimal vector field $v^* = (A^*, N^*)$, at the beginning of the development, we can have $v_0^* \neq 0$ but we will always have $A_0^* = 0$.

We end this section with some notations. The time-variant parameter α implies to change the norm on V over time. Each norm $|\cdot|_{V,\alpha_t}$ induces a specific isomorphism $K^V_{\alpha_t} : V^* \to V$. For any $l \in V^*$, $K^V_{\alpha_t}(l)$ is defined as the unique element of V such that for any $v \in V$,

$$l(v) = \langle K^V_{\alpha_t}(l), v\rangle_{V,\alpha_t}\,.$$

Throughout the next sections, we will hence use the notation K^V_α when α is a constant and $K^V_{\alpha_t}$ otherwise. Likewise, we will note K^A_α or $K^A_{\alpha_t}$ these isomorphims composed with the projection on the first component and simply K^N the composition with the second component since this last one does not depend on the parameter α.

2.2.2 New cost function and energy

In order to retrieve the regularization term defined by equation 5.13, we define a new cost function given for any $v \in V$ and any $t \in [0,1]$ by

$$C_{\nu,\alpha}(v,t) \doteq \frac{\nu_t}{2}|v|^2_{V,\alpha_t}\,. \tag{5.14}$$

This cost function is smooth and for any $(v,t) \in V \times [0,1]$ and any $\delta v \in V$, if $v = (A, N)$ we have

$$\frac{\partial C}{\partial v}(v,t) \cdot \delta v = \langle \nu_t v, \delta v \rangle_{V,\alpha_t} .$$

Consequently, we have as expected

$$E(q_0, v) = \int_0^1 C(v_t, t)\, dt + \mathcal{A}(q_1) = \frac{1}{2}|v|^2_{L^2_V,\nu,\alpha} + \mathcal{A}(q_0, v) .$$

At last, since we have

$$\begin{aligned}\nabla_v E(q_0, v)_t &= \frac{\partial C}{\partial v}(v_t, t) - \mathcal{J}(q_t, p_t, t) \\ &= \nu_t v_t - K^V_{\alpha_t} \mathcal{J}(q_t, p_t, t) ,\end{aligned}$$

any local minimizer $v^* \in V$ of E must satisfy at any time $t \in [0,1]$

$$v^*_t = v^*(q_t, p_t, t) = \frac{1}{\nu_t} K^V_{\alpha_t} \mathcal{J}(q_t, p_t, t) .$$

2.3 Constrained norm: general situation

2.3.1 Aim

Another solution is to consider the classic energy

$$E(q_0, v) = \int_0^1 \frac{\nu}{2}|v_t|^2_V\, dt + \mathcal{A}(q_0, v)$$

and minimize it under the constraint that for any $t \in [0,1]$,

$$|v_t|^2_V = c_t ,$$

where ν is a constant and $c : [0,1] \to \mathbb{R}^+$ is a smooth known function. Note that this constraint requires some additional information on the target. However, numerical experiments show that one does not need a precise estimation of c_t.

2.3.2 New cost function and energy

For this purpose, we apply the augmented Lagrangian method. This method is detailed for example in [32] and was also recently used in [5]. The constraint is turn into an additive penalization term in the energy. For this purpose, we define a new cost function given for any $v \in V$ and any $t \in [0,1]$ by

$$C_{\lambda,\gamma}(v,t) \doteq \frac{\nu}{2}|v|^2_V - \frac{\lambda_t}{2}(|v|^2_V - c_t) + \frac{\gamma}{2}(|v|^2_V - c_t)^2 . \tag{5.15}$$

The method consists alternately in minimizing the energy and updating the parameters

λ and γ. Assume that we obtained an optimal control v^n of the function

$$E^n(q_0, v) = \int_0^1 C_{\lambda^n,\gamma^n}(v,t)\, dt + \mathcal{A}(q_0, v)\,,$$

then λ is updated according to

$$\lambda_t^{n+1} = \lambda_t^n - \frac{\gamma^n}{2}(\left|v_t^{n+1}\right|_V^2 - c_t)$$

and we choose $\gamma^{n+1} \in]\gamma^n, +\infty[$ with many possible variants (but it is not required to increase γ toward $+\infty$).

This cost function is smooth and for any $(v,t) \in V \times [0,1]$ and any $\delta v \in V$, we have

$$\nabla_v C(v,t) = \big(\nu - \lambda_t + 2\gamma(|v|^2 - c_t)\big)v\,.$$

With the notation $\partial_v E(q_0, v) \cdot \delta v = \int_0^1 < (\nabla_v E)_t, \delta v_t >_V \; dt$, it follows that

$$(\nabla_v E)_t = \nu v_t - \lambda_t v_t + 2\gamma(|v_t|^2 - c_t)v_t - K^V \mathcal{J}(q_t, p_t, t)\,.$$

Consequently, any local minimizer $v \in V$ of E can be written at any time $t \in [0,1]$

$$v_t = n_t K^V \mathcal{J}_t\,,$$

where n_t satisfies

$$\big(\nu + 2\gamma(n_t^2 \left|K^V \mathcal{J}_t\right|^2 - c_t) - \lambda_t\big)n_t - 1 = 0\,.$$

Since this expression can have multiple solutions in $\mathbb{R}$, we look for the one that maximize the Hamiltonian (see Chapter 3).

Proposition 2.1. *With the cost function defined by equation 5.15, the maximum of the Hamiltonian*

$$v \mapsto H(q,p,v,t) = (\mathcal{J}(q,p,t)\,|\,v) - C(v,t)$$

is given by

$$v_t = n_t K^V \mathcal{J}_t\,,$$

where n_t is the largest root of the polynomial

$$R(X) = 2\gamma \left|K^V \mathcal{J}_t\right|^2 X^3 + (\nu - \lambda_t - 2\gamma c_t)X - 1\,.$$

Proof.

$$
\begin{aligned}
H_r(q,p,t) &= \max_{v\in V}\ (\mathcal{J}(q,p,t)\,|\,v) - C(v,t)\\
&= \max_{v\in V}\ (\mathcal{J}_t\,|\,v) - \frac{\nu}{2}\,|v|_V^2 + \frac{\lambda_t}{2}(|v|_V^2 - c_t) - \frac{\gamma}{2}(|v|_V^2 - c_t)^2\\
&= \max_{n_t\in\mathbb{R}} n_t|K^V\mathcal{J}_t|_V^2 - \frac{\nu}{2}n_t^2\left|K^V\mathcal{J}_t\right|^2 + \frac{\lambda_t}{2}(n_t^2\left|K^V\mathcal{J}_t\right|^2 - c_t) - \frac{\gamma}{2}(n_t^2\left|K^V\mathcal{J}_t\right|^2 - c_t)^2\\
&= \max_{X\in\mathbb{R}} -\frac{\gamma}{2}\left|K^V\mathcal{J}_t\right|^4 X^4 - (\frac{\nu}{2} - \frac{\lambda_t}{2} - \gamma c_t)\left|K^V\mathcal{J}_t\right|^2 X^2 + |K^V\mathcal{J}_t|_V^2 X - \frac{\gamma c_t^2}{2} - \frac{\lambda_t c_t}{2}\\
&= \max_{X\in\mathbb{R}} -\frac{\gamma}{2}\left|K^V\mathcal{J}_t\right|^2 X^4 - (\frac{\nu}{2} - \frac{\lambda_t}{2} - \gamma c_t)X^2 + X\,.
\end{aligned}
$$

The right hand side of this last expression is the sum of a pair polynomial and an increasing affine function. Therefore, its maximum is reached at the largest zero of its derivative. The derivative of this polynomial is the polynomial $-R$ introduced above. $\square$

2.4 Constrained norm: rotations and translations

In the specific case of the group of rotations and translations, a general constraint as introduced above will not solve the issue of balance previously presented between the rotations and the translation. We will thus refine the constraint as follows.

2.4.1 Aim

We consider the space $V = \mathbb{A}_d \times \mathbb{R}^d$. For any $v \in \mathbb{L}^2([0,1], V)$, we note $v = (A, N)$ its canonical decomposition and at each time $t \in [0,1]$,

$$v_t = (A_t, N_t) \in \mathbb{A}_d \times \mathbb{R}^d\,.$$

We recall then that V is equipped with the norm $|v|_{V,\alpha}^2 = \alpha\,|A|^2 + |N|^2$. We want to minimize the energy

$$E(q_0, v) = \frac{\nu}{2}\int_0^1 |v_t|_{V,\alpha}^2\,dt + \mathcal{A}(q_0, v)\,,$$

under the constraint that for any $t \in [0,1]$,

$$\begin{cases} |A_t|_{\mathbb{A}_d}^2 = c_t^A\,,\\ |N_t|_{\mathbb{R}^d}^2 = c_t^N\,. \end{cases} \tag{5.16}$$

where c^A and c^N are smooth known functions.

2.4.2 New cost function and energy

The augmented Lagrangian method leads then to introduce the new cost function

$$
\begin{aligned}
C_{\lambda,\gamma}(v,t) \doteq \; & \frac{\nu}{2}\,|v_t|^2_{V,\alpha} \\
& - \frac{\lambda^A_t}{2}(|A_t|^2_{\mathbb{A}_d} - c^A_t) + \frac{\gamma^A}{2}(|A_t|^2_{\mathbb{A}_d} - c^A_t)^2 \\
& - \frac{\lambda^N_t}{2}(|N_t|^2_{\mathbb{R}^d} - c^N_t) + \frac{\gamma^N}{2}(|N_t|^2_{\mathbb{R}^d} - c^N_t)^2
\end{aligned}
$$

and to minimize the new energy

$$
E(q_0, v) = \int_0^1 C_{\lambda,\gamma}(v_t, t)\, dt + \mathcal{A}(q_0, v)\,.
$$

2.4.3 Gradient of the cost function

We have

$$
\begin{aligned}
\nabla_v C(v_t, t) = \; & \nu v_t \\
& - \lambda^A_t \left(\frac{1}{\alpha}A_t, 0\right) + 2\gamma^A(|A_t|^2 - c^A_t)\left(\frac{1}{\alpha}A_t, 0\right) \\
& - \lambda^N_t \big(0, N_t\big) + 2\gamma^N(|N_t|^2 - c^N_t)\big(0, N_t\big)\,.
\end{aligned}
$$

With the notation $K^V_\alpha \mathcal{J}_t = (K^A_\alpha \mathcal{J}_t, K^N \mathcal{J}_t)$, the gradient of the energy

$$
(\nabla_v E)_t = \nabla_v C(v_t, t) - K^V_\alpha \mathcal{J}_t
$$

admits two components with respect to the spaces $\mathbb{A}_d$ and $\mathbb{R}^d$. It can be rewritten $(\nabla_v E)_t = (\nabla_A E)_t + (\nabla_N E)_t$ where

$$
\begin{aligned}
(\nabla_A E)_t &= \nu A_t - \frac{\lambda^A_t}{\alpha} A_t + 2\frac{\gamma^A}{\alpha}(|A_t|^2 - c^A_t) A_t - K^A_\alpha \mathcal{J}_t\,, \\
(\nabla_N E)_t &= \nu N_t - \lambda^N_t N_t + 2\gamma^N(|N_t|^2 - c^N_t) N_t - K^N \mathcal{J}_t\,.
\end{aligned}
$$

2.4.4 Expression of a minimizer

A zero of this gradient is thus written

$$
v^*_t = (a_t K^A_\alpha \mathcal{J}_t, n_t K^N \mathcal{J}_t)\,,
$$

where a_t and n_t are respectively the largest root of the polynomials:

$$\begin{aligned} R^A(X) &= \nu X - \frac{\lambda_t^A}{\alpha} X + 2\frac{\gamma^A}{\alpha}\left(X^2 \left|K_\alpha^A \mathcal{J}_t\right|^2 - c_t^A\right) X - 1 \\ &= 2\frac{\gamma^A}{\alpha}\left|K_\alpha^A \mathcal{J}_t\right|^2 X^3 + \left(\nu - \frac{\lambda_t^A}{\alpha} - 2\frac{\gamma^A}{\alpha} c_t^A\right) X - 1 \end{aligned}$$

$$R^N(X) = 2\gamma^N \left|K^N \mathcal{J}_t\right|^2 X^3 + (\nu - \lambda_t^N - 2\gamma^N c_t^N) X - 1\,.$$

2.5 Combined cost functions in the rotations and translations case

At last, since the adapted norm and the constrained norm are two complementary tools, it seems natural to combined them. We exploited it in the case of rotations and translations. With the same notations as before, we summarize here this new setup. Note that with the right choice of parameters, we can always retrieve either the adapted norm setup or the constrained norm setup.

2.5.1 Energy

$$\begin{aligned} E(q_0, v) &= \int_0^1 C(v_t, t)\, dt + \mathcal{A}(q_0, v) \\ &= \frac{\nu_t}{2}\int_0^1 |v_t|^2_{V,\alpha_t}\, dt \\ &\quad - \frac{\lambda_t^A}{2}\int_0^1 (|A_t|^2_{\mathbb{A}_d} - c_t^A)\, dt + \frac{\gamma^A}{2}\int_0^1 (|A_t|^2_{\mathbb{A}_d} - c_t^A)^2\, dt \\ &\quad - \frac{\lambda_t^N}{2}\int_0^1 (|N_t|^2_{\mathbb{R}^d} - c_t^N)\, dt + \frac{\gamma^N}{2}\int_0^1 (|N_t|^2_{\mathbb{R}^d} - c_t^N)^2\, dt \\ &\quad + \mathcal{A}(q_0, v)\,. \end{aligned}$$

2.5.2 Gradient of the cost function

$$\begin{aligned} \nabla_v C(v_t, t) = \nu_t v_t & \\ &- \lambda_t^A \left(\frac{1}{\alpha_t} A_t, 0\right) + 2\gamma^A(|A_t|^2 - c_t^A)\left(\frac{1}{\alpha_t} A_t, 0\right) \\ &- \lambda_t^N \big(0, N_t\big) + 2\gamma^N(|N_t|^2 - c_t^N)\big(0, N_t\big)\,. \end{aligned}$$

2.5.3 Expression of a minimizer

With the notation $K_\alpha^V \mathcal{J}_t = (K_{\alpha_t}^A \mathcal{J}_t, K^N \mathcal{J}_t)$, we have

$$v_t^* = (a_t K_{\alpha_t}^A \mathcal{J}_t, n_t K^N \mathcal{J}_t)\,,$$

where a_t and n_t are respectively the largest root of the polynomials:

$$\begin{aligned} R^A(X) &= \nu_t X - \frac{\lambda_t^A}{\alpha_t} X + 2\frac{\gamma^A}{\alpha_t}\left(X^2 \left|K^A_{\alpha_t}\mathcal{J}_t\right|^2 - c_t^A\right) X - 1 \\ &= 2\frac{\gamma^A}{\alpha_t}\left|K^A_{\alpha_t}\mathcal{J}_t\right|^2 X^3 + \left(\nu_t - \frac{\lambda_t^A}{\alpha_t} - 2\frac{\gamma^A}{\alpha_t}c_t^A\right) X - 1\,. \end{aligned}$$

$$R^N(X) = 2\gamma^N \left|K^N \mathcal{J}_t\right|^2 X^3 + (\nu_t - \lambda_t^N - 2\gamma^N c_t^N)X - 1\,.$$

3 Data attachment term

3.1 RKHS of currents and varifolds

We recalled in Chapter 1 how to identify smooth shapes to linear forms on some spaces of test functions independently of the parameterization of these shapes. Reproducing Kernel Hilbert Spaces (RKHSs) allow then to compute very efficiently distances between these shapes. We give here a computational approach. We will focus here on discrete surfaces embedding in $\mathbb{R}^3$. More details on currents and varifolds can be found in [28, 26, 15].

Locally, a surface S can be encoded by a position and a unit normal vector, i.e. a pair $(x, \overrightarrow{N_x}) \in \mathbb{R}^3 \times \mathbb{S}^2$. A test function is then a function $\omega : \mathbb{R}^3 \times \mathbb{S}^2 \to \mathbb{R}$ and the pair $(x, \overrightarrow{N_x})$ is associated to the Dirac $\delta_x^{\overrightarrow{N_x}}$ defined by $\delta_x^{\overrightarrow{N_x}}(\omega) = \omega(x, \overrightarrow{N_x})$. Figure 5.10 introduces with triangles how we will model triangulated surfaces.

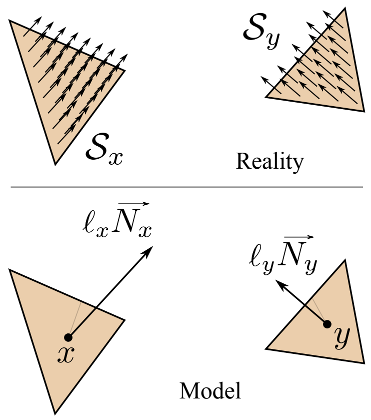

Figure 5.10 – Modeling of a triangle. A triangle is approximated by the position of its center x, its normal unit vector $\overrightarrow{N_x}$ and its area ℓ_x that can also be coded as the length of its normal vector $(\ell_x\overrightarrow{N_x})$. The first triangle is approximated by $\ell_x\delta_x^{\overrightarrow{N_x}}$.

A small triangle is approximated by a linear form of the type $\mu_x = \ell_x\delta_x^{\overrightarrow{N_x}}$. Given a space of test functions W, this representative $\mu_x : W \to \mathbb{R}$ is applied to any $\omega \in W$ by

$$\mu_x(\omega) = \ell_x\omega(x, \overrightarrow{N_x})\,.$$

The union of two triangles is then represented by a sum $\mu_x + \mu_y$. More generally, a triangulated surfaces can be approximated by a finite sum

$$S \approx \mu = \sum_x \ell_x\delta_x^{\overrightarrow{N_x}} \tag{5.17}$$

and we have

$$\mu(\omega) = \sum_x \ell_x \omega(x, \overrightarrow{N_x}) \,. \tag{5.18}$$

The construction of metrics via RKHSs becomes from there rather simple in practice and can be induced by the choice of two real positive kernels on the ambient space $E = \mathbb{R}^n$ and on the set of tangential data $\mathcal{T}$ (general situation). These two kernels generate the RKHS W, i.e. the set of test functions. A kernel k_E measures the distance between the positions of two infinitesimal shapes and a kernel k_T measures the distance between their respective tangential data (here, a unit normal vector with eventually the orientation).

We can now explicit a scalar product between two shapes represented in W' by two sums of Diracs as in equation (5.18). Thanks to the RKHS properties, we have

$$\langle \delta_x^{\overrightarrow{N_x}}, \delta_y^{\overrightarrow{N_y}} \rangle_{W'} = \delta_x^{\overrightarrow{N_x}} \left(k_E(\cdot, y) k_T(\cdot, \overrightarrow{N_y}) \right) = k_E(x,y) k_T(\overrightarrow{N_x}, \overrightarrow{N_y}) \,. \tag{5.19}$$

The scalar product between two shapes $S \approx \mu_S = \sum_x \ell_x \delta_x^{\overrightarrow{N_x}}$ and $S' \approx \mu_{S'} = \sum_y \ell_y \delta_y^{\overrightarrow{N_y}}$ is then deduced by linearity:

$$\langle \mu_S, \mu_{S'} \rangle_{W'} = \sum_x \sum_y \ell_x \ell_y k_E(x,y) k_T(\overrightarrow{N_x}, \overrightarrow{N_y}) \,. \tag{5.20}$$

Finally, we return now to the definition of a data attachment term to compare a target shape to a deformed source shape. Once we have fixed a RKHS W, we denote $\mu^{\mathrm{tar}} \in W'$ the representative of the target shape and $\mu^v \in W'$ the representative of the final state of the solution generated by a vector field $v \in L^2([0,1], V)$. The data attachment term is then given by

$$\mathcal{A}(q_0, v) = \frac{1}{2} \left| \mu^v - \mu^{\mathrm{tar}} \right|_{W'}^2 \,. \tag{5.21}$$

Note that this brief overview is common to currents and varifolds. We can now present three examples W_C, W_V and W_{OV} of RKHSs whose dual embeds respectively currents, non-oriented varifolds or oriented varifolds. The only differences between these RKHSs lie in the choice of the kernels.

1. When k_T is the usual scalar product on $\mathbb{R}^3$, the dual of generated RKHS embeds currents and we have for example with a Gaussian kernel k_E:

$$\langle \delta_x^{\overrightarrow{N_x}}, \delta_y^{\overrightarrow{N_y}} \rangle_{W_C'} = \exp\left(-\frac{|x-y|_{\mathbb{R}^3}^2}{2\sigma^2} \right) \langle \overrightarrow{N_x}, \overrightarrow{N_y} \rangle_{\mathbb{R}^3} \,.$$

2. In the case of non-oriented varifolds, a trick as suggested in [15] is to define $\mathcal{T}$ as the set of oriented tangent spaces and then to symmetrize a kernel k_T with respect

to the orientation. We get for example with two Gaussian kernels:

$$\langle \delta_x^{\overrightarrow{N_x}}, \delta_y^{\overrightarrow{N_y}} \rangle_{W_V'} = \exp\left(-\frac{|x-y|^2_{\mathbb{R}^3}}{2\sigma^2}\right)\left(\frac{1}{2}\exp\left(-\frac{|N_x - N_y|^2_{\mathbb{R}^3}}{2\sigma_N^2}\right) + \frac{1}{2}\exp\left(-\frac{|N_x + N_y|^2_{\mathbb{R}^3}}{2\sigma_N^2}\right)\right).$$

3. The advantage of varifolds in our situation is their non linearity with respect to the tangent space that enables them to model sharp tails as the tip of horns (see Chapter 1). Since shapes like horns are easily oriented, there is no reason to call for non-oriented varifolds. In our experiments, we used a Gaussian kernel for k_E and a little more complex kernel for k_T:

$$\langle \delta_x^{\overrightarrow{N_x}}, \delta_y^{\overrightarrow{N_y}} \rangle_{W_{OV}'} \doteq \exp\left(-\frac{|x-y|^2_{\mathbb{R}^3}}{2\sigma^2}\right)\exp\left(-\frac{|\overrightarrow{N_x} - \overrightarrow{N_y}|^2_{\mathbb{R}^3}}{2\sigma_N^2}\right)\langle \overrightarrow{N_x}, \overrightarrow{N_y} \rangle_{\mathbb{R}^3}. \quad (5.22)$$

The choice of the additional euclidean scalar product to the kernel k_T actually facilitates the computation but moreover when σ_N tends to $+\infty$ it retrieves the scalar product of W_C' on currents. Figure 5.11 illustrates the differences on the gradient of the attachment term for a small and a large σ_N.

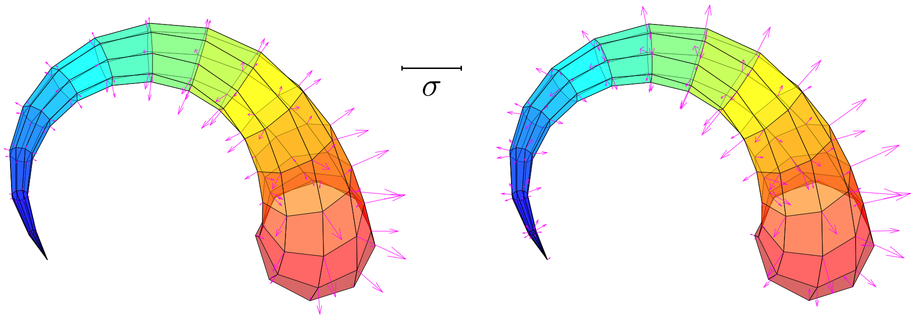

Figure 5.11 – Opposite gradient of the attachment term built with the metric given by equation 5.22. Current model on the left ($\sigma_N = 999$), oriented varifold model on the right ($\sigma_N = 1$). Note how the distribution of the gradient on the tip of the horn is more important with the oriented varifold norm. In both case the scale σ of the spatial kernel is equal to the radius of the base of the horn.

We also computed the energy of the introductory experiment with the classic cost function (see Figure 5.7) with the scalar product defined by equation 5.22 with $\sigma_N = 99999$ and $\sigma_N = 1$. Let us recall that the energy is the sum of the cost function C and the attachment term $\mathcal{A}$.

$\sigma_N = 99999$			
Iterations	C	$\mathcal{A}$	Energy
20k	0.3423	2.7009	3.0433
200k	0.3695	0.5407	0.9102

$\sigma_N = 1$			
Iterations	C	$\mathcal{A}$	Energy
20k	0.3423	10.6736	11.0160
200k	0.3695	2.4765	2.8459

We can see that the norm on oriented varifolds ($\sigma_N = 1$) amplifies significantly the difference between the two steps of the gradient descent.

Figure 5.12 illustrates the role played by the orientation of shapes. Note yet that if one might not know the true orientation and generate it randomly, the matching could then

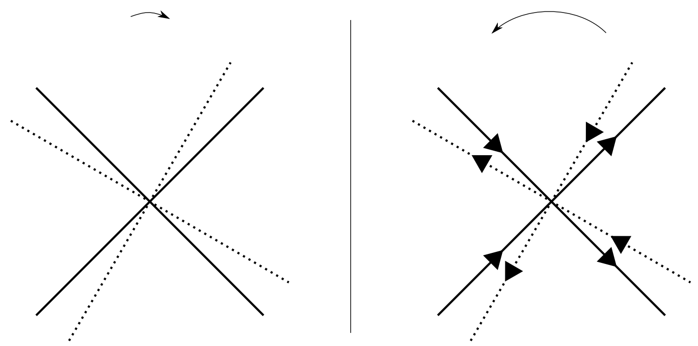

Figure 5.12 – Two matchings by rotation of two crosses. In both case, the doted cross is the source, the other one is the target. On the left side, the lines are not oriented. They should thus be modeled by varifolds and the natural deformation would be a rotation clockwise. On the right side, the lines are oriented. They could thus be modeled by currents or non oriented varifolds and the natural deformation would be a rotation anticlockwise.

be irrelevant and misled. This situation is typical in the case of matching of fiber bundles (see for example [20] on white matter fiber). The orientation on horns can prevent some local minimums. Figure 5.13 displays a case where the boundary of the two horns meet with a wrong correspondence. This situation could be a local minimum of the energy.

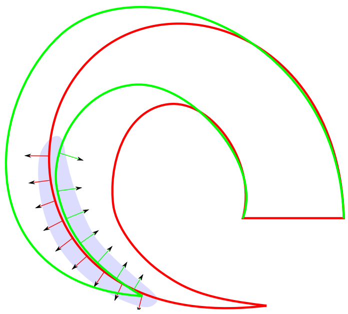

Figure 5.13 – Without orientation the attachment term could not distinguish the two boundaries in the grey area. The separation of these two parts would thus partially increase the energy and could lead to a local minimum.

3.2 Additional landmark

For the specific case of the horn, we add a penalization on the tip of the horns. This tip is the point image by q of the first leaf $X_{\{0\}}$. Consider any $\hat{x} \in X_{\{0\}}$, the new attachment term can then be defined by

$$\mathcal{A}(q_0, v) = \frac{c^{\text{head}}}{2} d(q_1(\hat{x}), \hat{y}^{\text{tar}}) + \frac{c^{\text{data}}}{2} \left|\mu^v - \mu^{\text{tar}}\right|^2_{W'} ,$$

where $\hat{y}^{\text{tar}}$ is the tip of the target horn and d could be simply defined for any $u_1, u_2 \in \mathbb{R}^d$ as the L^2 distance between u_1 and u_2

$$d(u_1, u_2) = \left|u_1 - u_2\right|^2 .$$

However, we preferred to localize the influence of this attachment term through a Gaussian blob

$$d(u_1, u_2) = 1 - \exp\left(-\frac{|u_1 - u_2|^2}{\sigma_{\text{head}}}\right).$$

It allows to delay the influence of this term. Indeed, since the horns might have a high curvature, the gradient descent does naturally not lead the tip of the horn straightforward to its landmark target and force this behavior might actually be a brake. Hence, with this last distance, as long as the tip $q_1(\hat{x})$ is far away from the tip of the target, we stand in a flat area of d.

Without this additional landmark, the tips of both horns have no particular reason to be matched together. This single landmark gives a strong input toward the natural structure of the temporal foliation (see Figure 5.15). Note that the group of rotations and translations is yet rigid enough to avoid the behavior displayed in the figure. Nevertheless, this additional attachment term leads the last step of the gradient descent to a better visual result because at some point, we fall below the scale of details of the general attachment term (current or varifold type).

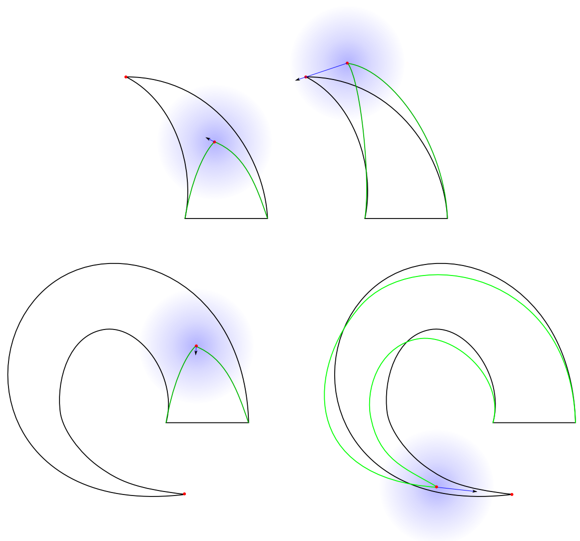

Figure 5.14 – Illustration of the contribution of the Gaussian-L^2 landmark on the tip of the horns (pointed in red). On each row, we display two steps of a gradient descent. The black horn is the target, the green horn is the solution (in progress) at its final state. The blue blob represents the Gaussian blob window of the landmark attachment term. On the second example (on the bottom), the matching of the two landmarks is counterproductive at the beginning of the gradient descent. The Gaussian filter remedies this inconvenience.

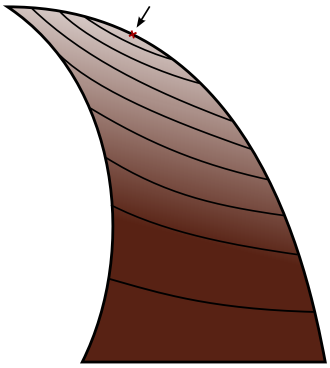

Figure 5.15 – Reconstituted example of a *perfect* geometric match of the final shape to its target without landmark correspondence. The algorithm fails yet to retrieve a coherent scenario to model the growth of the horn as highlighted by the temporal stratification of the generated shape. The arrow points the flat tip of the generated horn. Note however that this situation is very unlikely with the group of rotations and translations, especially when the translations of V are reduced to vertical translations.

3.3 Intermediate times in the input data

Since we want to retrieve an evolution and not only perform a matching to the final state, the intermediate states should have an important role in this model. The rigidity of the rotations and translations can allow to bypass them in some case : for example with simple horns (i.e. with regular growth and low curvature). We will see otherwise and with a Gaussian kernel their influence on the trajectory.

Let $v \in L^2([0,1], V)$ be a vector field that generates a scenario $t \mapsto S^v_t$. Assume that a target scenario is given by a collection $(S^{\text{tar}}_i)_i$ of shapes at a finite number of intermediate times $(t_i)_i \subset [0,1]$ (with $\max\{t_i, i\} = 1$). Given a distance d on shapes, the discrepancy between the two scenarios can be estimated at the different times t_i by an attachment term $\mathcal{A}$ of the form

$$\mathcal{A}(q_0, v) = \sum_{i=1}^{n} d(S^v_{t_i}, S^{\text{tar}}_i)\,.$$

Let us recall that the shape $S^v_{t_i}$ is given by the image $q_{t_i}(X_i)$ of the set

$$X_i = \{x \in X \,|\, \tau(x) \leq t_i\}$$

of active points of the coordinate space X at time t_i. If the shapes are modeled by currents or varifolds in a RKHS W' and these are respectively denoted $\mu^v_i \in W'$ for the solution generated by v and $\mu^{\text{tar}}_i \in W'$ and for the target, the attachment term can be

$$\mathcal{A}(q_0, v) = \sum_{i=1}^{n} \frac{c^{\text{data}}_i}{2} \left|\mu^v_i - \mu^{\text{tar}}_i\right|^2_{W'}\,,$$

where a set of real positive coefficients $(c^{\text{data}}_i)_i$ can be added to weight the terms.

Once again, we can add the Gaussian-L^2 distance on landmarks d_L on each pair of tips of the horns. With the previous notations, the final attachment term is given by

$$\mathcal{A}(q_0, v) = \sum_{i=1}^{n} \frac{c^{\text{head}}}{2} d_L(q_{t_i}(\hat{x}), \hat{y}_i^{\text{tar}}) + \frac{c_i^{\text{data}}}{2} \left|\mu_i^v - \mu_i^{\text{tar}}\right|_{W'}^2 .$$

4 Presentation of the algorithms and code

The code used is entirely performed with Matlab. We recall briefly the classic gradient descent on the vector field.

Algorithm 5 Gradient descent on v

1 - Initialize $v^0 \in L_V^2$ at zero.
Then for any $n \in \mathbb{N}$, given q_0 and v^n,
2 - Compute q^n the solution generated by $v^n \in L_V^2$.
3 - Compute $p_1^n = -d\mathcal{A}(q_1^n)$ and integrate it backward to construct $t \mapsto p_t^n$ over $[0, 1]$.
4 - Compute the gradient at v^n: $t \mapsto \delta v_t^n = \nabla_v C(v_t^n) - K_V \mathcal{J}_f(q_t^n, p_t^n)$.
5 - Update the vector field by $v^{n+1} = v^n + \epsilon \delta v^n$ for a small $\epsilon > 0$.

However, all the experiments are actually achieved with the *Gradient descent on the momentum (Shooting)*. It results from the transformation of the initial problem of matching to an optimization problem of the initial momentum p_0. The new energy to minimize is of the type

$$E(q_0, p_0) = \int_0^1 C(v^*(q_t, p_t, t), t)\, dt + \mathcal{A}(q_0, v)\,, \tag{5.23}$$

where (q, p) is generated by the reduced Hamiltonian system. We will modulate this problem with the new cost functions presented in Section 2. The gradient of this energy requires to introduce the auxiliary variable $(\mathcal{Q}, \mathcal{P})$ of (q, p) presented hereafter. The gradient has then a particularly simple expression:

$$\langle \nabla E(q_0, p_0), (\delta q_0, \delta q_0) \rangle = -\langle \mathcal{Q}_0, \delta q_0 \rangle - \langle \mathcal{P}_0, \delta p_0 \rangle\,. \tag{5.24}$$

The code for the gradient descent in this situation is given in Algorithm 2. We present

Algorithm 6 Gradient descent on the momentum (Shooting)

1 - Initialize: $q_0 = \textbf{init}(\mathcal{S}^{\text{tar}})$ and $p_0 = 0$.
2 - Integrate forward: $(q_1, p_1) = \textbf{compute.forward}(q_0, p_0)$.
3 - Compute the co-variables: $\mathcal{Q}_1 = \textbf{gradient.attachment.term}(q_1, \mathcal{S}^{\text{tar}})$, $\mathcal{P}_1 = 0$.
4 - Integrate backward: $(\mathcal{Q}_0, \mathcal{P}_0) = \textbf{compute.backward}(q, p, \mathcal{Q}_1, \mathcal{P}_1)$.
5 - Update the parameters: $(q_0, p_0) = \textbf{update}(q_0, p_0)$.

here the steps 2 to 5 of the algorithm. The initialization will be discussed further below in Section 5. To simplify, we will only assume that the target is given at the final time. In practice, $\mathcal{A}$ only depends on the target $\mathcal{S}^{\text{tar}}$ and on the final shape q_1 generated by the forward equations.

4.1 Compute forward

The function **compute.forward** performs a integration forward with a Runge Kutta method (RK2). It requires to compute the derivatives

$$(\dot{q}_t, \dot{p}_t) = \textbf{compute.qpdot}(q_t, p_t, t)\,,$$

given by the system

$$\begin{cases} \dot{q}_t &= \mathbb{1}_{\tau \leq t} v^*(q_t, p_t, t)(q_t)\,, \\ \dot{p}_t &= -\mathbb{1}_{\tau \leq t} \big(dv^*(q_t, p_t, t)(q_t)\big)^* \cdot p_t\,. \end{cases} \tag{5.25}$$

The optimal vector field $v^*(q, p, t)$ must satisfies the equation

$$\nabla_v C(v_t, t) - K^V \mathcal{J}(q_t, p_t, t) = 0\,.$$

In all situations, this vector field is built on the momentum map $K^V \mathcal{J}$ up to some projections and weighting. We will explicit it in each case after a brief description of the momentum map.

4.1.1 Momentum map

For a RKHS with a kernel k_V, we have

$$K^V \mathcal{J}(q, p, t) = \sum_{x \in X, \tau(x) \leq t} k_V(\cdot, q(x)) p(x)$$

and thus for any $u, \delta u \in \mathbb{R}^d$

$$dK^V \mathcal{J}(q, p, t)(u) \cdot \delta u = \sum_{x \in X, \tau(x) \leq t} \big(\partial_1 k_V(u, q(x)) \delta u\big) p(x)\,.$$

When k_V is a scalar Gaussian kernel, we will always use the classic cost function so that

$$v_t^* = K^V \mathcal{J}(q_t, p_t, t)\,.$$

At any time $t \in [0, 1]$, we need thus to compute for any $x \in X$ such that $\tau(x) \leq t$

$$\begin{aligned} \dot{q}_t(x) &= \sum_{x' \in X, \tau(x') \leq t} k_V(q_t(x), q_t(x')) p_t(x') \\ &= \sum_{x' \in X, \tau(x') \leq t} \exp\left(-\frac{|q_t(x) - q_t(x')|^2}{2\sigma_V^2}\right) p_t(x') \end{aligned}$$

and

$$\dot{p}_t(x) = \sum_{x' \in X, \tau(x') \leq t} -\frac{1}{2\sigma_V^2} \exp\left(-\frac{|q_t(x) - q_t(x')|^2}{2\sigma_V^2}\right) (p_t(x')^T p_t(x))(q_t(x) - q_t(x'))\,.$$

When the kernel generates the direct product of antisymmetric matrices and translations on $\mathbb{R}^d$, i.e. $V = \mathbb{A}_d \times \mathbb{R}^d$, we have

$$\begin{aligned} K^V \mathcal{J}(q,p,t) &= \big(K^A_\alpha \mathcal{J}(q,p,t), K^N \mathcal{J}(q,p,t)\big) \\ &= \left(\frac{1}{\alpha}\mathrm{proj}_{\mathbb{A}_d}\left(\sum_{x\in X,\tau(x)\le t} p(x)q(x)^T\right), \sum_{x\in X,\tau(x)\le t} p(x)\right) \end{aligned}$$

and for any $u \in \mathbb{R}^d$

$$dK^V\mathcal{J}(q,p,t)(u) = K^A_\alpha \mathcal{J}(q,p,t)\,.$$

Hence, if $v^* = (A^*, N^*)$, the forward equations are given by

$$\begin{cases} \dot{q}_t &= \mathbb{1}_{\tau\le t} A^*_t q_t + N^*_t\,, \\ \dot{p}_t &= \mathbb{1}_{\tau\le t} A^*_t p_t\,. \end{cases} \tag{5.26}$$

From these equations, we can now describe each specific setup. Hereafter, we will mark the cost function with subscripts to indicate the main parameters. Note however than for the constrained norm, the cost functions depend on the two constants ν and α.

4.1.2 Adaptive norm

The cost function is given by

$$C_{\alpha,\nu}(v,t) = \frac{\nu_t}{2}|v|^2_{V,\alpha_t}\,.$$

The optimal vector field is given by

$$v^*(q,p,t) = \frac{1}{\nu_t} K^V_{\alpha_t}\mathcal{J}(q_t,p_t,t)\,.$$

4.1.3 Constrained norm: general situation

The cost function is given by

$$C_{\lambda,\gamma}(v,t) = \frac{\nu}{2}|v|^2_{V,\alpha} - \frac{\lambda_t}{2}(|v|^2_V - c_t) + \frac{\gamma}{2}(|v|^2_V - c_t)^2\,.$$

The optimal vector field is given by

$$v^*(q,p,t) = n_t K^V_\alpha \mathcal{J}(q,p,t)\,,$$

where $n_t = n(q,p,t)$ is the largest root of the polynomial:

$$R(X) = 2\gamma\left|K^V_\alpha \mathcal{J}_t\right|^2 X^3 + (\nu - \lambda_t - 2\gamma c_t)X - 1\,.$$

4.1.4 Constrained norm: rotations and translations

The cost function is given by

$$\begin{aligned}C_{\lambda,\gamma}(v,t) = &\frac{\nu}{2}|v|^2_{V,\alpha}\\ &-\frac{\lambda_t^A}{2}(|A|^2_{\mathbb{A}_d}-c_t^A)+\frac{\gamma^A}{2}(|A|^2_{\mathbb{A}_d}-c_t^A)^2\\ &-\frac{\lambda_t^N}{2}(|N|^2_{\mathbb{R}^d}-c_t^N)+\frac{\gamma^N}{2}(|N_t|^2_{\mathbb{R}^d}-c_t^N)^2\,.\end{aligned}$$

The optimal vector field is given by

$$v^*(q,p,t)=(A_t^*,N_t^*)=(a_tK_\alpha^A\mathcal{J}_t,n_tK^N\mathcal{J}_t)\,,$$

where a_t and n_t are respectively the largest root of the polynomials:

$$R^A(X)=2\frac{\gamma^A}{\alpha}\left|K_\alpha^A\mathcal{J}_t\right|^2X^3+\left(\nu-\frac{\lambda_t^A}{\alpha}-2\frac{\gamma^A}{\alpha}c_t^A\right)X-1\,,$$

$$R^N(X)=2\gamma^N\left|K^N\mathcal{J}_t\right|^2X^3+(\nu-\lambda_t^N-2\gamma^Nc_t^N)X-1\,.$$

4.1.5 Combined cost functions in the rotations and translations case

The cost function is given by

$$\begin{aligned}C_{\alpha,\nu,\lambda,\gamma}(v,t) = &\frac{\nu_t}{2}|v|^2_{V,\alpha_t}\\ &-\frac{\lambda_t^A}{2}(|A|^2_{\mathbb{A}_d}-c_t^A)+\frac{\gamma^A}{2}(|A|^2_{\mathbb{A}_d}-c_t^A)^2\\ &-\frac{\lambda_t^N}{2}(|N|^2_{\mathbb{R}^d}-c_t^N)+\frac{\gamma^N}{2}(|N_t|^2_{\mathbb{R}^d}-c_t^N)^2\,.\end{aligned}$$

The optimal vector field is again given by

$$v^*(q,p,t)=(A_t^*,N_t^*)=(a_tK_{\alpha_t}^A\mathcal{J}_t,n_tK^N\mathcal{J}_t)\,,$$

where a_t and n_t are respectively the largest root of almost the same polynomials R^A and R^N defined above where however the constants α and ν depends now on time:

$$R^A(X)=2\frac{\gamma^A}{\alpha_t}\left|K_{\alpha_t}^A\mathcal{J}_t\right|^2X^3+\left(\nu_t-\frac{\lambda_t^A}{\alpha_t}-2\frac{\gamma^A}{\alpha_t}c_t^A\right)X-1\,,$$

$$R^N(X)=2\gamma^N\left|K^N\mathcal{J}_t\right|^2X^3+(\nu_t-\lambda_t^N-2\gamma^Nc_t^N)X-1\,.$$

Note that when the parameters λ and γ are null, we retrieve the coefficient of the adapted norm setup : $a_t=n_t=\frac{1}{\nu_t}$.

4.2 Compute backward

The function **compute.backward** performs a integration backward of a covariable (or dual variable) (Q, P) with a Runge Kutta method (RK2). Let us recall the definition of these covariables (see Chapter3 for the details). For any trajectory $y = (q, p) \in \mathcal{C}([0, 1], B \times B^*)$, the covariable (Q, P) associated to (q, p) is initialized at time $t = 1$ by

$$\mathcal{Q}_1 = -d\mathcal{A}(q_1) \text{ and } \mathcal{P}_1 = 0 .$$

They then satisfy the system

$$\begin{cases} \dot{\mathcal{Q}}_t &= \partial_q C(v^*(q_t, p_t, t), t) - \partial_p \partial_q H_r(q_t, p_t, t) \cdot \mathcal{Q}_t + \partial_q^2 H_r(q_t, p_t, t) \cdot \mathcal{P}_t \,, \\ \dot{\mathcal{P}}_t &= \partial_p C(v^*(q_t, p_t, t), t) - \partial_p^2 H_r(q_t, p_t, t) \cdot \mathcal{Q}_t + \partial_q \partial_p H_r(q_t, p_t, t) \cdot \mathcal{P}_t \,. \end{cases} \tag{5.27}$$

The second derivatives of the Hamiltonian are computed by finite difference (see [5]). Note that in the case of rotations and translations, these derivatives have yet an expression simple enough to be used.

We explicit now the gradient of the cost function for a general RKHS V or for rotations and translations. The optimal time-varying vector field at any time t, v_t^* depends only on $y_t = (q_t, p_t)$ and t. We replaced then the notation $C(v_t^*, t)$ by $C(y_t, t)$.

4.2.1 General RKHS

With the classic cost function, we have

$$\begin{aligned} C(y_t, t) &= \frac{1}{2} |v^*(y_t, t)|_V^2 \\ &= \frac{1}{2} \sum_{\substack{x \in X \\ \tau(x) \leq t}} \sum_{\substack{x' \in X \\ \tau(x') \leq t}} p(x')^T k_V(q(x'), q(x)) p(x) \,. \end{aligned} \tag{5.28}$$

Since $H_r(y_t, t) = \frac{1}{2} |v^*(y_t, t)|_V^2 = C(y_t, t)$, we have as with the standard dynamic

$$\nabla_q C(y_t, t) = -\dot{p}_t \,, \tag{5.29}$$

$$\nabla_p C(y_t, t) = \dot{q}_t \,. \tag{5.30}$$

4.2.2 Rotations and translations

In the case of rotations and translations, the constrained norm setup generates for any $t \in [0, 1]$ the coefficients a and n that depend on $y_t = (q_t, p_t)$. The gradient of the cost function becomes thus slightly more complicated since we have to compute the derivatives of these two coefficients with respect to y_t. With the combined cost function, we recall that v^* is the solution at all time $t \in [0, 1]$ of

$$\partial_v C(v_t^*, t) = \mathcal{J}(q_t, p_t, t) \,.$$

If we rewrite $C(\cdot,t)$ as a function of y_t, $C(y_t,t) \doteq C(v^*(y_t,t),t)$, we have then

$$\begin{aligned}
\partial_y C(y_t,t)\cdot\delta y &= \partial_v C(v_t^*,t)\circ\partial_y v_t^*\cdot\delta y_t\\
&= \mathcal{J}(y_t,t)\circ\partial_y v^*(y_t,t)\cdot\delta y_t\\
&= \partial_y\left(\mathcal{J}(y_t',t)\,|\,v^*(y_t,t)\right)_{|y'=y}\cdot\delta y_t\\
&= \partial_y\left(a_t\langle K_{\alpha_t}^A\mathcal{J}_t',K_{\alpha_t}^A\mathcal{J}_t\rangle+n_t\langle K^N\mathcal{J}_t',K^N\mathcal{J}_t\rangle\right)_{|y'=y}\cdot\delta y_t\\
&= \partial_y a_t\cdot\delta y_t|K_{\alpha_t}^A\mathcal{J}_t|^2+\partial_y n_t\cdot\delta y_t|K^N\mathcal{J}_t|^2+(\partial_y\mathcal{J}_t\cdot\delta y_t\,|\,v_t^*)\\
&= \partial_y a_t\cdot\delta y_t|K_{\alpha_t}^A\mathcal{J}_t|^2+\partial_y n_t\cdot\delta y_t|K^N\mathcal{J}_t|^2+(\delta p_t\,|\,\xi_{q_t,t}(v_t^*))+(\partial_q\xi_{q_t,t}(v_t^*)^*\cdot p_t\,|\,\delta q_t)\\
&= \partial_y a_t\cdot\delta y_t|K_{\alpha_t}^A\mathcal{J}_t|^2+\partial_y n_t\cdot\delta y_t|K^N\mathcal{J}_t|^2+(\delta p_t\,|\,\dot q_t)+(-\dot p_t\,|\,\delta q_t)\ .
\end{aligned}$$

The variables a and n are roots of the polynomials R^A and R^N. Consider R^A as a functional of the variables (y,t,a) and assume that a is a simple root then on a small neighborhood of (y,t), there exists a unique root $a(y,t)$ of $X\mapsto R^A(y,t,X)$ and we have thus locally $R^A(y,t,a(y,t))=0$. We denote $a_t=a(y,t)$ and derive this expression.

$$\begin{aligned}
\partial_y a(y,t)\cdot\delta y &= -\frac{\partial_y R^A(y,t,a(y,t))\cdot\delta y}{\partial_a R^A(y,t,a(y,t))}\\
&= -\frac{4\frac{\gamma^A}{\alpha}a_t^3}{6\frac{\gamma^A}{\alpha}\left|K_\alpha^A\mathcal{J}_t\right|^2a_t^2+(\nu-\frac{\lambda_t^A}{\alpha}-2\frac{\gamma^A}{\alpha}c_t^A)}\left(\partial_y\mathcal{J}_t\cdot\delta y\,|\,K_\alpha^A\mathcal{J}_t\right)\\
&= -\frac{4\frac{\gamma^A}{\alpha}a_t^3}{6\frac{\gamma^A}{\alpha}\left|K_\alpha^A\mathcal{J}_t\right|^2a_t^2+(\nu-\frac{\lambda_t^A}{\alpha}-2\frac{\gamma^A}{\alpha}c_t^A)}\frac{1}{\alpha}\left(\langle\delta p,\mathbb{1}_{\tau\le t}A\cdot q\rangle_B-\langle\mathbb{1}_{\tau\le t}A\cdot p,\delta q\rangle_B\right).
\end{aligned}$$

Likewise,

$$\begin{aligned}
\partial_y n(y,t)\cdot\delta y &= -\frac{\partial_y R^N(y,t,n(y,t))\cdot\delta y}{\partial_n R^N(y,t,n(y,t))}\\
&= -\frac{4\gamma^N n_t^3}{6\gamma^N\left|K^N\mathcal{J}_t\right|^2n_t^2+(\nu-\lambda_t^N-2\gamma^N c_t^N)}\left(\partial_y\mathcal{J}_t\cdot\delta y\,|\,K^N\mathcal{J}_t\right)\\
&= -\frac{4\gamma^N n_t^3}{6\gamma^N\left|K^N\mathcal{J}_t\right|^2n_t^2+(\nu-\lambda_t^N-2\gamma^N c_t^N)}\langle\delta p,\mathbb{1}_{\tau\le t}N\rangle_B\,.
\end{aligned}$$

4.3 Update

The update is simply given by

$$\begin{cases} q_0 &= q_0+\mu_q\mathcal{Q}_0\,,\\ p_0 &= p_0+\mu_p\mathcal{P}_0\,. \end{cases} \tag{5.31}$$

The step size (μ_q,μ_p) of the gradient descent is slightly increased after each successful step and decreased when the energy increases.

In some case, especially when we want to interpolate intermediates times, the gradient $\mathcal{P}_0$ is smoothed before the update. This is achieved by a convolution with a Gaussian with respect to space ($q_0(x) \in X$) and time ($\tau(x) \in [0,1]$) as follows:

$$\mathrm{Smooth}\,\mathcal{P}_0 = \sum_{x' \in X} \exp\left(-\frac{|q_0(x) - q_0(x')|^2}{2\sigma_p^2}\right) \exp\left(-\frac{|\tau(x) - \tau(x')|^2}{2\sigma_\tau^2}\right) \mathcal{P}_0(x')\,.$$

We could have smooth $\mathcal{P}_0$ with respect to spatial localization in the coordinate space ($x \in X$). The choice of using q_0 brings the geometry of the shape in the ambient space. However, since the shape has not been deployed yet, the addition of the time correlation is then important since q_0 can be strongly not injective (see the example of the tube).

5 Numerical experiments: general settings

5.1 Model

The meshes all have the same structure : $3 \times l \times L$ points. We will indeed only consider horns or tubes. This means that the shape at time 0 is reduce to one leaf of l points in $\mathbb{R}^3$. For the horns, this leaf is merged to a single point to model the end of the tip. Otherwise, this leaf is a curve that will form the first boundary of the shape. Then, the $L-1$ other leaves of l new points of $\mathbb{R}^3$ will gradually appear during the development. The leaves always appear at regular time intervals. For example if $L = 2k+1$, at half time the shape is formed by the $k+1$ first leaves.

The time discretization of the interval $[0,1]$ used for the integration steps (forward and backward) is equal to the image of τ. Which means that $L = T$. Refine this discretization did not seem to improve significantly the results in the following examples. However, in Section 7, to display the norm of the optimal vector field obtained, we compute the associated trajectory one more time at the end of the algorithm with a finer discretization to show that between the appearance of two successive leaves, the dynamic is classic (no creation from a discrete point of view) and the norm is thus constant.

For most experiences displayed below, we will give the runtime of the algorithm. Since the decision to stop the gradient descent can be quite subjective, we will give the average time for 100 iterations then the full time associated to the results as they are displayed.

5.2 Initial position

Once the number of leaves and the number of points of the meshes are fixed, the first step to create a scenario is to generate its initial position. Let us recall that the initial position can be seen as the pull backward through the flow of each leaf $q_1(X_{\{t\}})$ of the final shape to its position $q_t(X_{\{t\}})$ at time t when it appeared.

In order to generate a horn target, we define the form of the last leaf that will be the base of the target at its final state and compute a linear reduction of this leaf toward the center that will be the tip of the horn at its birth. To initialize the algorithm, the initial position q_0 is defined likewise via the base of the target. We compute a linear reduction of the base (closed polyline) to generate the L initial leaves.

In Section 6.4, we will see that the initial position of a tube is very different. Since every leaves of the tube have a similar shape, their pull backward at their initial position

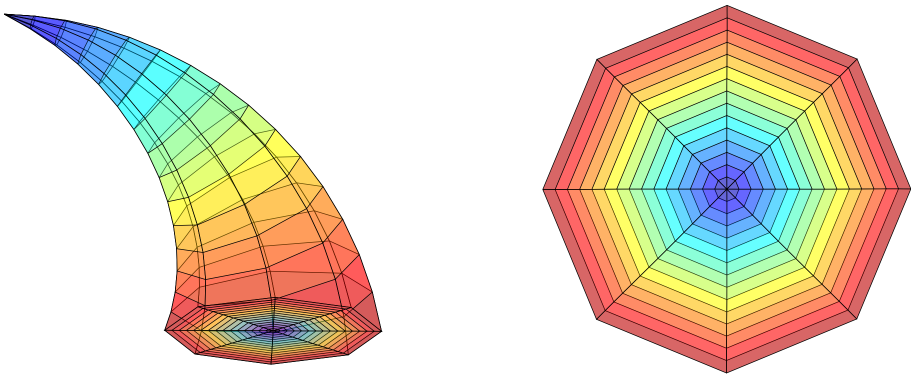

Figure 5.16 – Generation of the initial position from the base of the target.

leads to a superimposition in the plan embedding the creation process (as for the horns) of circular curves eventually completely identical.

5.3 Target simulation

All our experiments are achieved with simulated target shapes. These targets are simulated with the generative model implied by the growth dynamic. We create a flat initial position as presented above on the right side of Figure 5.16, a deformation and we compute the target's growth scenario. All our targets are generated by rotations and translations (i.e. we generate a deformation from $V = \mathbb{A}_d \times \mathbb{R}^d$). We will note hereafter $v^{\text{tar}} = (A^{\text{tar}}, N^{\text{tar}})$ the vector field that generates the target.

To be more accurate, we only use vertical translations. Since we also always work in $\mathbb{R}^3$, it leads to

$$V = \mathbb{A}_3 \times \mathbb{R}(0, 0, 1)\,.$$

In all our experiments, the meshes of the target and the solutions have the same number of points. This implies that for both shapes the new leaves appear at the same time. The alignment of the leaves when the shapes are displayed one over the other allows then to visually measure the correlation of the evolution of each pair of leaves. Since this alignment can be disturbingly perfect, we add a slight noise to the target. The scale of this noise is not significant with respect to the scale of the attachment term on the shape. It will just allow to clear any doubt when the matching of the leaves with the target are visually perfect. The comparisons between the results and the target (final shape, development, deformation) will then be done with the initial data but the algorithm runs with these noisy targets (see Figure 5.17).

5.4 Parameters of the data attachment term

We refer to Section 3 for the notations. The scale with respect to the position is given by

$$\sigma = r\,,$$

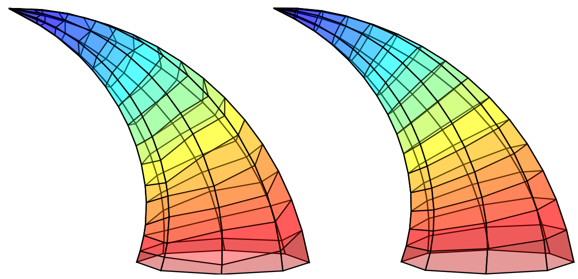

Figure 5.17 – Example of a target (on the right) and its noisy version used in the algorithm. In case of intermediate times, we will apply this noise to every input shape.

where r is the radius of the base of the horn. The scale of the kernel that compares the unit normal vector does not depend on the shape and is either fixed to

$$\sigma_N = 1$$

or

$$\sigma_N >> 1$$

to retrieve a current attachment term.

In case of multiple intermediate times of the growth scenario of the target, we have to choose the weights of the different terms induced by these input in the attachment term. These weight are given by

$$\mathcal{A}(q_0, v) = \sum_{i=1}^{n} \frac{c^{\text{head}}}{2} d(q_{t_i}(\hat{x}), \hat{y}_{\text{tar}(i)}) + \frac{c_i^{\text{data}}}{2} \left|\mu_i^v - \mu_i^{\text{tar}}\right|^2 .$$

We tried few possibilities to define c^{data} as a decreasing coefficient with respect to time. It appeared that choosing c^{data} constant gave better results.

5.5 Parameters of the cost function

A general expression of the cost function embedding every cases described previously is given by

$$\begin{aligned} C_{\alpha,\nu,\lambda,\gamma}(v,t) = &\frac{\nu_t}{2}|v|^2_{V,\alpha_t} \\ &- \frac{\lambda_t^A}{2}(|A|^2_{\mathbb{A}_d} - c_t^A) + \frac{\gamma^A}{2}(|A|^2_{\mathbb{A}_d} - c_t^A)^2 \\ &- \frac{\lambda_t^N}{2}(|N|^2_{\mathbb{R}^d} - c_t^N) + \frac{\gamma^N}{2}(|N_t|^2_{\mathbb{R}^d} - c_t^N)^2 . \end{aligned}$$

The adapted norm setup corresponds to the case $\lambda \equiv \gamma \equiv 0$ and the constrained norm setup corresponds to the case α and ν constant. For this last setup, we always use the exact norm of the vector field that generates the target (i.e. $c^A = |A^{\text{tar}}|^2$ and $c^N = |N^{\text{tar}}|^2$ with the notations introduced above).

Besides the global relative weight of all these parameters, we need to choose for the adapted norm parameters α and ν their evolution in time. We tried on a basic horn (as in the first example we will see) few possibilities (linear, $t \mapsto ln(1+t)$, $t \mapsto \sqrt{t}$) and a linear function of the time seemed to be the best solution. We use thus the increasing sequence $r_1, \ldots, r_L$ of the radius of the L leaves of q_0 to initiate α and ν. *In fine*, we just have to adjust two constants to weight these two sequences. At this point however, we have $\alpha(0) = \nu(0) = 0$. To obtain two strictly positive coefficients, we replace the radius $r_1 = 0$ associated to the tip of the horn by $r_1 = \frac{1}{1+l} r_2$ (since there is a ratio of 1 point against $1 + l$ points between the two first leaves).

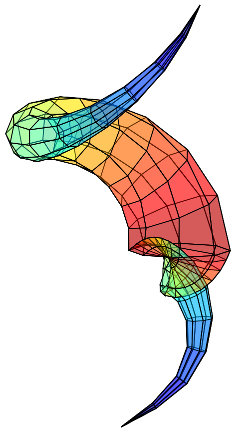

Figure 5.18 – Solution after 1 iteration of gradient descent with too high constraints (on the top, the target, on the bottom, the solution).

Remark 5.1 (Soft Constraint : Initialization)**.** *When the horn is long and curved as in Section 6.3, the coefficients λ and γ must be chosen really small (note that they will increase during the gradient descent) otherwise quite unpleasant behaviors can be produced during the first steps of the gradient descent. Indeed, the constraints will strongly increase the weight of the rotation and the horn will rotated around its base. The energy will decrease compared to the flat disc that is the shape at the beginning but then there is no chance to recover a shape close to a horn (see Figure 5.18).*

Remark 5.2 (Soft Constraint : Update)**.** *Besides a soft initialization of the constraints, we also keep these constraints relatively soft through the update as described in the recall of the augmented Lagrangian method (in Section 2.3). The main reason is to show that we do not need a strong constraint to obtain good results and therefore if we do not have the initial information, we could still proceed to the constrained gradient descent with a rough estimation of the norm. Moreover, we will see with the rotations that this constraint can be tricky because the algorithm does not equally treat every axes of rotation.*

Remark 5.3 (Balance of the Parameters between the Cost Function and the Attachment Term)**.** *We observed that with the constrained norm, the global weight of the cost function in the energy is much less important than with a classic cost function. With the Gaussian kernel, we choose the coefficient of the cost function such that at the steady-state the cost function and the attachment term have the same order of magnitude.*

6 Numerical experiments: rotations and translations

We present in this section four examples of matchings with the deformation group of rotations and translations. For all the experiments, the aim is to retrieve the complete development of the shape over time. The faithful recovering of the development will be evaluated by visual comparison of the shapes, of the norm of the vector fields or of the laddering of the leaves. The different cost functions previously introduced will be fully exploited and compared throughout these examples. We recall that the *constrained norm setup* applies a constraint on the norm of the optimal vector field, the *adapted norm setup* changes the weight on this norm over time to favor the growth at the beginning of the development and the *combined setup* mixes this two tools.

For Examples 1, 2 and 4, the only input data is the final state of the target. For Example 3, the horn being more complex, we also consider some intermediate times of the development of the target. In Example 4, the horns are exchanged for tubes: besides the exploration of other types of shapes, it will highlight the complexity of horns with their singularity at the top. At last, the optimization of the initial position will be explored in Example 5.

6.1 Example 1 - Cost functions competition

For this first example, we consider a simple horn with a low curvature and a regular growth pattern. This means that the norm of the vector field used to generate the target is constant (see the red curves in Figure 5.20).

From a shape point of view, we can say from Figure 5.19 that the development is very well recovered. The perfect alignment of the horizontal leaves between the solution and the target at the final state reflects by itself the quality of the matching on the whole development. In all experiments, the target and the solution have willingly the same number of leaves in order to observe this alignment (see Section 5.3).

The transverse curves however seem to slightly diverge at the top of the horns. This indicates that the deformation associated to the solution is not exactly the one used to generate the target. This difference will be deepened hereafter.

Regarding the norm of the vector fields, let us note $|A^*|$ and $|N^*|$ the norms of the skew-symmetric matrices and the norm of the translations for a solution and likewise $|A^{\text{tar}}|$ and $|N^{\text{tar}}|$ the respective norms associated the target, all defined on the time interval $[0, 1]$ of the development of the horns. Figure 5.20 compares for each setup these norms for the solution (in blue) and for the target (in red). As a first observation, $|N^*|$ is no longer null at time 0 and although $|A^*|$ is always null at time 0 (as explained in Section 2.2), it jumps immediately for $t > 0$ towards $|A^{\text{tar}}|$. These behaviors are thus quite different from those observed with the classic function in Figure 5.9. Moreover, the norms with the *contrained norm setup* are not perfectly recovered because we chose to apply a soft constraint as explained in Remark 5.2. They are even softer in the combined setup but as we can observe it is enough to force the jump of $|A^*|$ at $t = 0^+$.

An interesting property of the group of rotations and translations is that the momenta can only be rotated over time. Hence, their norms remain constant and the initial momentum allows to visualize how the vector field v^* is built. The initial momentum with the *adapted norm* displayed in Figure 5.21 is homogeneous. This implies that all the points

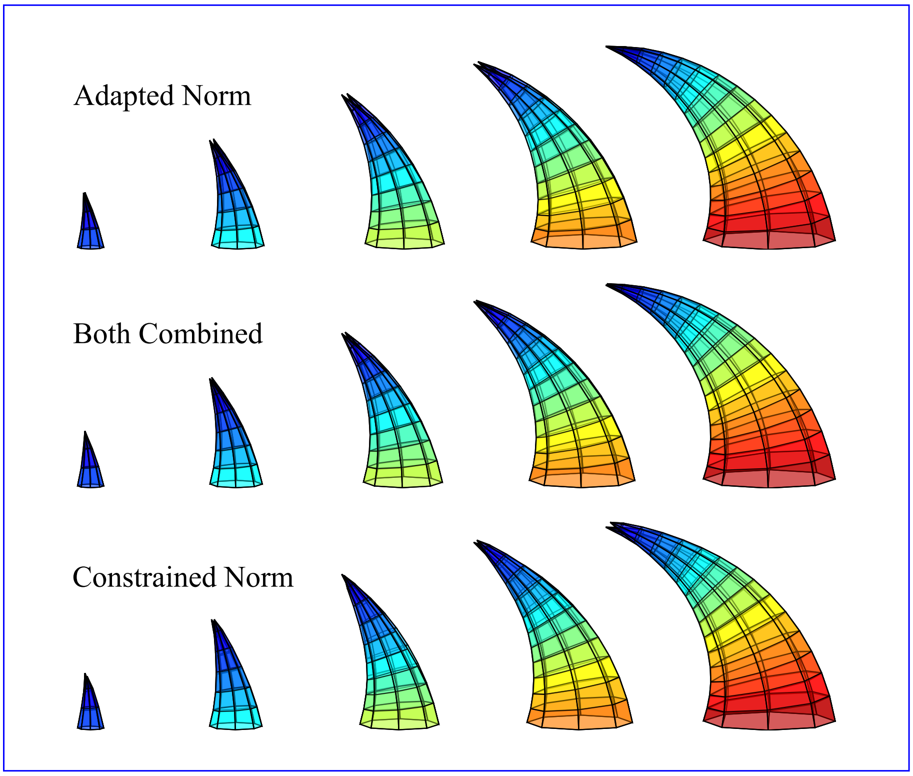

Figure 5.19 – We display on each row the development of the solution overlayed with the target's development. These three experiments have been computed in 30 minutes for the adapted norm setup and 1 hour for the two other setups. The time required for 100 iterations of the gradient descent lies in all cases around 30sec.

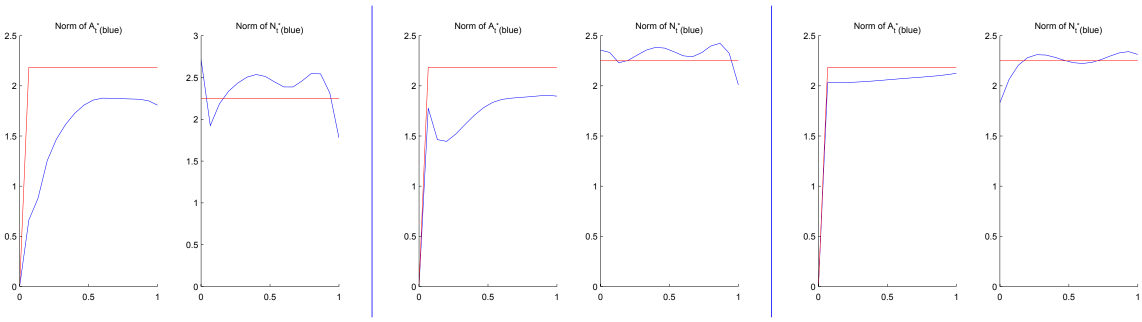

Figure 5.20 – Comparison of the norms of the deformations between the solution (in blue) and the target (in red). From left to right, with the *adapted norm setup*, the *combined setup*, and the *constrained norm setup*. We display separately in each case the norms of the skew-symmetric matrices and the norms of the translations over the time interval $[0, 1]$.

contribute to v^* with equal importance. On the contrary, with the *constrained norm* the initial momentum is concentrated around the first leaves. This initial momentum looks similar to the one obtained with the *classic cost function* (see Figure 5.22). The constraints seem thus to generate the same solution but to accelerate the convergence of the gradient descent when the adapted norm setup tends to create a different solution. The

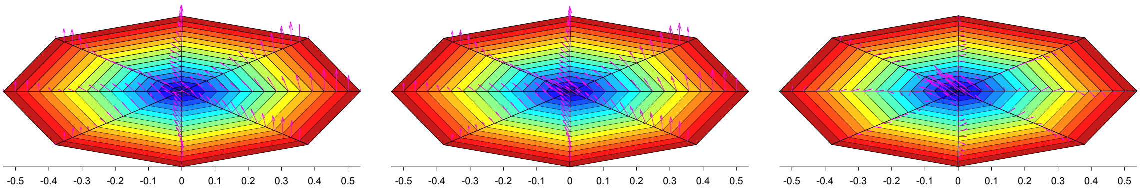

Figure 5.21 – Initial momentum p_0 on the initial position q_0. From left to right, with the *adapted norm setup*, the *combined setup*, and the *constrained norm setup*. Note how the initial momentum p_0 is concentrated on the first points around the tip in the case of the constrained norm. We take here the opportunity to remind that with the shooting method on the initial momentum, the initial momentum and position encode the whole development of the shape.

main difference between these two momenta is the orientation around the tip of the horn. In Figure 5.22, the momentum is mainly directed upwards in the middle. This can be explained by the balance issue between the rotations and the translations as discussed in Section 2.1 (see Figure 5.8): the model favors the translations over the rotations at the beginning of the development.

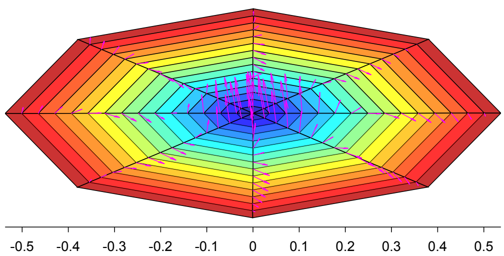

Figure 5.22 – Initial momentum with the classic cost function. The final state of the horn is displayed in Figure 5.7 (result after 200k iterations).

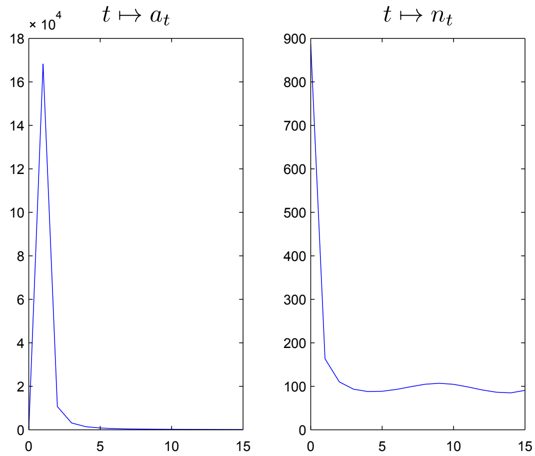

Figure 5.23 – Coefficients in the equation of the optimal vector field $v^* = (a_t K_\alpha^A \mathcal{J}_t, n_t K^N \mathcal{J}_t)$ obtained with the *constrained norm setup* (see Section 2.4).

6.1.1 Horizontal rotation

Figure 5.20 reveals that the skew-symmetric matrix is always underestimated by the algorithm. We tried to adjust the weight between A and N but the problem lies elsewhere. As noticed previously and as it can be observed again on Figure 5.24, the vertical lines on the horns slightly diverge on their way from the base to the top. These lines highlight how the horn turns on itself during its development and ends twisted (the emerging part of the shape is rotated but the future points remains static at their initial position which creates the twist effect).

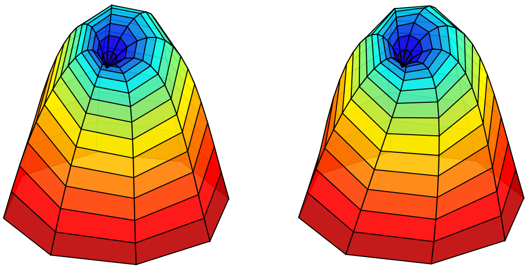

Figure 5.24 – Comparison of the horizontal rotations through the vertical lines between the solution in the *combined setup* (on the left) and the target (on the right).

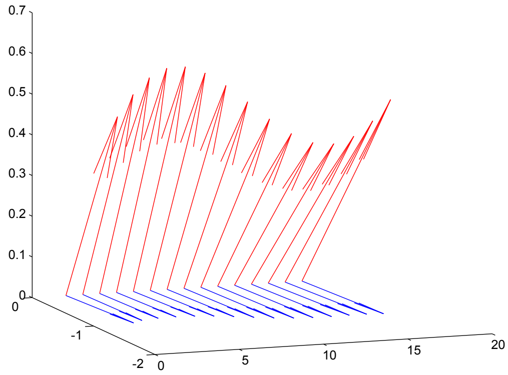

Figure 5.25 – To complete Figure 5.24, we display here $t \mapsto \omega_t$ the angular velocity vector of the solution in the *combined setup* (in blue) and the target (in red) (equivalent to A^* and A^{tar}).

This type of deformation leaves the horn almost invariant unless under a high curvature (or for example completely invariant for a regular cone). Hence, as confirmed by Figure 5.25, the algorithm ignores the vertical component of the angular velocity vector equivalent to the skew-symmetric matrix. In Example 6.3 the horn will have a higher curvature that will enforce the algorithm to retrieve this horizontal rotation.

Remark 6.1. *Let us recall that to apply a constraint on the norm, we always use the exact norm of the vector field that generates the target (i.e.* $c^A = |A^{\mathrm{tar}}|^2$ *and* $c^N = |N^{\mathrm{tar}}|^2$ *with the notations of Section 2.4). This choice can thus lead to a bad setting of these parameters. A strong constraint that takes into account a large horizontal rotation can be in conflict with an optimal solution. We tried on this example to apply a strong constraint. The algorithm does not retrieve the horizontal rotation but twists in a wrong direction the tip of the horn to compensate for the lack of rotation. Moreover, we also ran the algorithm under a soft constraint with different values of* c^A *and* c^N *with success on this example. This shows a large flexibility of the* constrained norm setup.

6.1.2 Additional landmark on the tip of the horn

Figure 5.26 displays the result of the matching with the adapted norm but without landmarks on the tip of the horns. We can observe that the tip of the horn has been turned inside. At the beginning of the gradient descent, the tip of the horn is outside. At some point, the generated horn becomes close to the target but bigger. We can assume that the momentum of the tip of the horn is used to recalibrate the deformation. The momentum on this particular point is used more than the others because the position of the tip of the horn barely change the shape at the scale of the global attachment term.

On the bottom of the figure, we can observe that all the initial localized momenta are directed upward except the one of the tip. After the end of the algorithm, we computed one more time the covariable $\mathcal{P}_0$ and looked at the tip point. Although the gradient $\mathcal{Q}_1$ of the attachment term displayed on the right side of the figure tends to push the tip outside

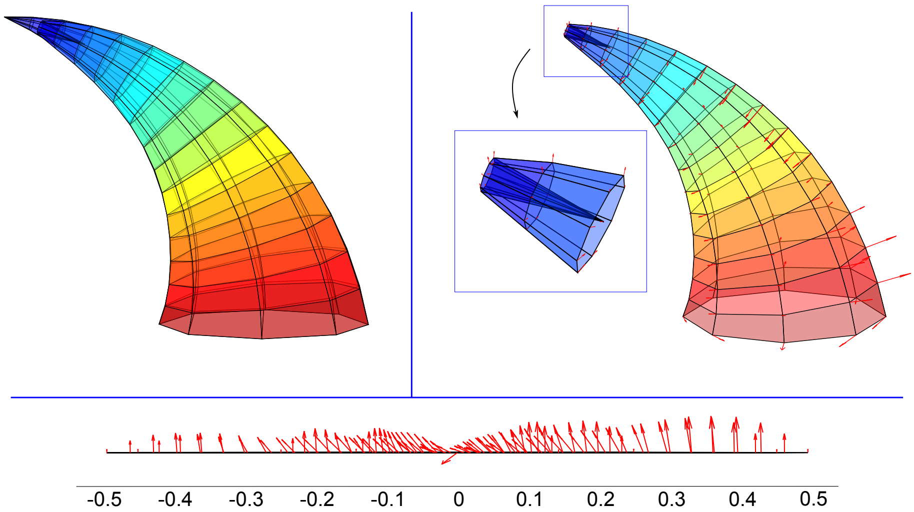

Figure 5.26 – Matching without landmarks on the tip of the horns. On the left, the overlay of the solution and the target at time 1. On the right, the solution at time 1 with the gradient $\mathcal{Q}_1$ of the attachment term. On the bottom, the initial momentum p_0 on the initial position q_0.

the horn (it requires a strong zoom on the figure to observe it), the vertical component of $\mathcal{P}_0$ at the tip point was still negative.

Remark 6.2. *This problem of the tip illustrates well an important property of the model. When the localized momenta of the last leaves determines only the evolution of their area of the shape, the momenta of the first leaves plays a role on the evolution of the whole shape. The dependence of these last momenta to the whole shape is accentuated in the case of the horn since the relative size of their local area tends to* 0*. We will see another situation with the example of a tube in Section 6.4.*

Remark 6.3. *At last, a natural question is to consider a basic setup with the classic cost function and this additional landmark on the tip of the horn. A strong weight on this landmark accelerates indeed the convergence of the algorithm and offers a non null initial vector field (which allows to create the tip of the horn instead of a flat top). However, this setup accentuates the concentration of the momentum on the tip of the horn as commented before. The momentum tends to a Dirac on the landmark. An optimal vector field would thus be built on a* punctual momentum. *This solution could be enough for simple horns but becomes quickly inadequate for more complex horns.*

6.2 Example 2 - Non constant growth

Now that the model is optimized to favor vector field with a constant norm, an interesting question is to test its flexibility. Indeed, if we think to the applications in medical imaging, one would like to be able to detect abnormal growth. The vector field v^{tar} used to generate the target in this example has a non constant norm. The parameters of the constraint takes into account this variation since we fixed as before for any $t \in [0,1]$, $c_t^A = |A_t^{\text{tar}}|^2$ and $c_t^N = |N_t^{\text{tar}}|^2$. Surprisingly, the *adapted norm setup*, that should promote a constant growth, achieved a better matching than the *constrained norm setup*.

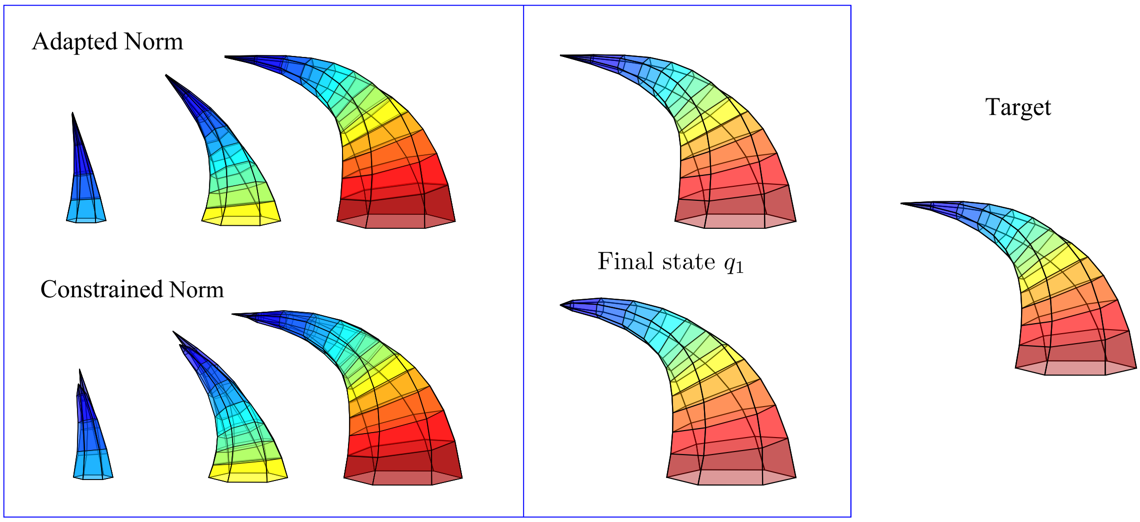

Figure 5.27 – We display on each row the development of the solution overlayed with the target's development, then the final state q_1 in each case and the target. Note that besides the issue on the tip of the horn for the constrained norm setup, the horizontal rotation is slightly better recovered with the adapted norm setup.

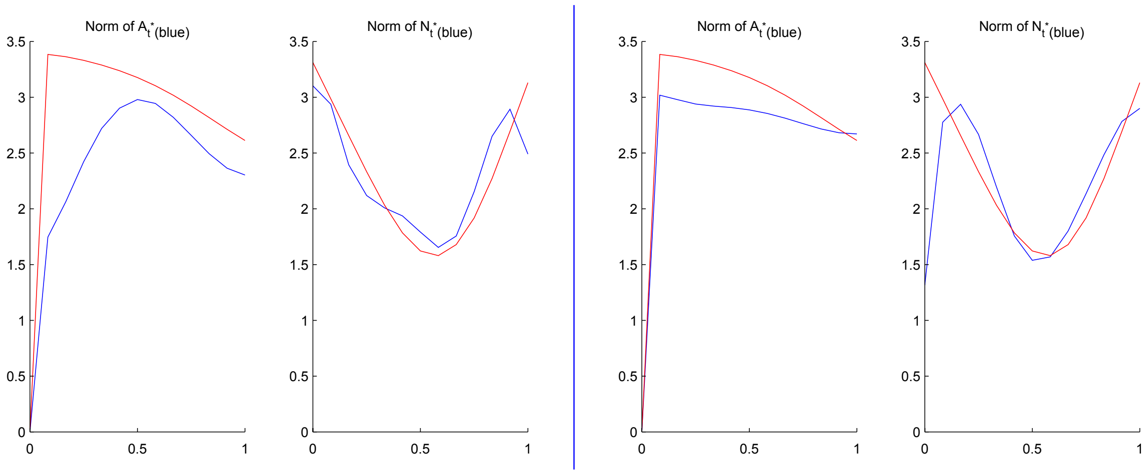

Figure 5.28 – Comparison of the deformations between the solution (in blue) and the target (in red). On the left, with the adapted norm setup. On the right, with the constrained norm setup. We display separately in each case the norms of the skew-symmetric matrices and the norms of the translations over the time interval $[0, 1]$.

For this example, we only performed three updates of the Lagrangian coefficients. The constraint seem strong enough to retrieve the global behavior of the development. We tried several settings of parameters without resolving the issue at the tip of the horn for the constrained norm setup. Note that as for the first example with the classic cost function, the horn is globally recovered with the first step of the gradient descent, then the energy continues to decrease very slowly (see Figure 5.30). It would be interesting to deepen this problem and find a way to accelerate the convergence.

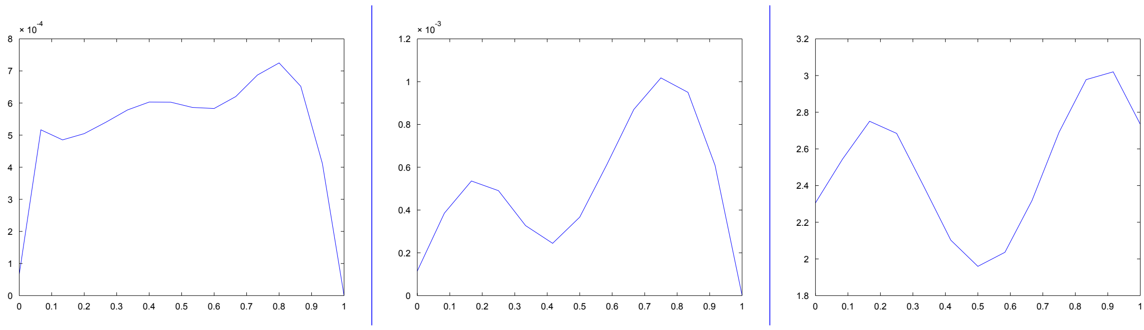

Figure 5.29 – Observation of the norm of the mean initial momentum p_0 on each leaf with the adapted norm setup: $t_i \mapsto |\text{mean}\{p_0(x) \,|\, \tau(x) = t_i\}|_{\mathbb{R}^3}$. On the left, for the previous Example 1 where the expected norm of v^* is constant, in the middle, for this Example 2. On the right, norm of the optimal vector field v^* for Example 2. The addition of a new leaf of initial momenta at each time of creation t_i explains the ability of the model to highlight delay in the growth.

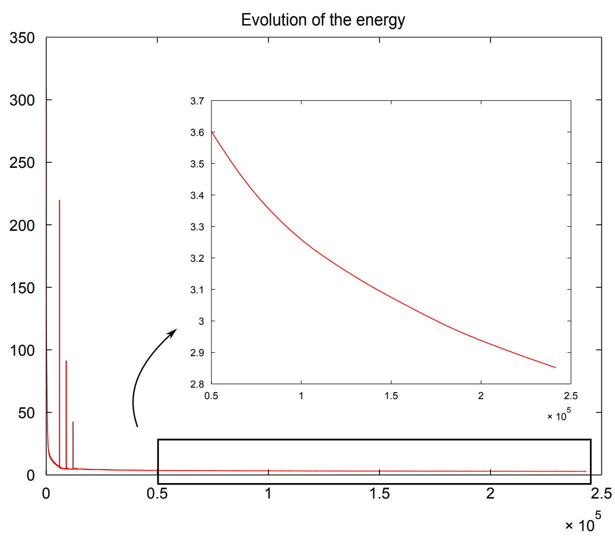

Figure 5.30 – Evolution of the energy during the gradient descent with the constrained norm setup. We cut the 50 first iterations. The three pikes at the beginning correspond to the update of the Lagrangian parameters. Time for 100 iterations : 27.5 sec (250k iterations : 18 hours). Comparison with the adapted norm setup : time for 100 iterations : 21 sec (25k iterations : 1,5 hour). (size of the mesh in both cases : $3 \times 6 \times 13$).

6.3 Example 3 - Intermediate times

We saw with the previous examples than in a case of a short horn, the final state is enough to retrieve very well the growth dynamic of the horn during its complete development. In the next example, we generate a much longer horn with a higher curvature. We will here compare the result of the matching with and without intermediate times. Four intermediate times of the horn are added to the input data (see Section 5.4 for the expression of the data attachment term). In both situations, we will use the combined norms setup. The results are displayed in Figure 5.31 to 5.33.

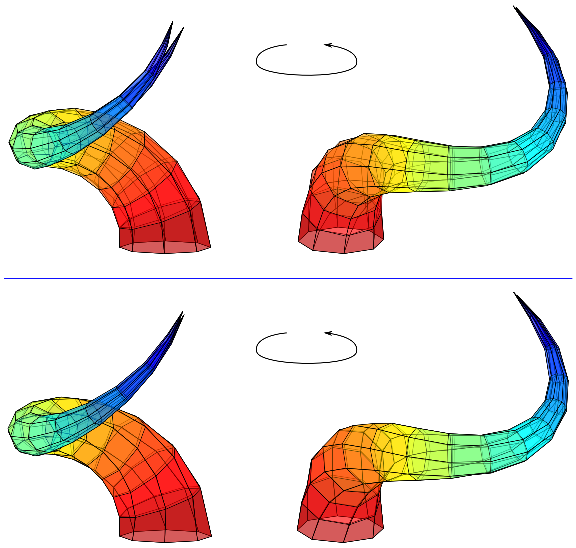

Figure 5.31 – Display of the final state q_1 of the solution overlayed with the target from two points of view. On the top row, without intermediate times. On the bottom row, with intermediate times. The matching of the final shape is better with intermediate times. Moreover, we can also already see here that the horizontal rotations are better recovered with the intermediate times. Indeed, if we look closely, we can see the longitudinal lines diverging on the first row. This difference will striking on the complete development (see Figure 5.32).

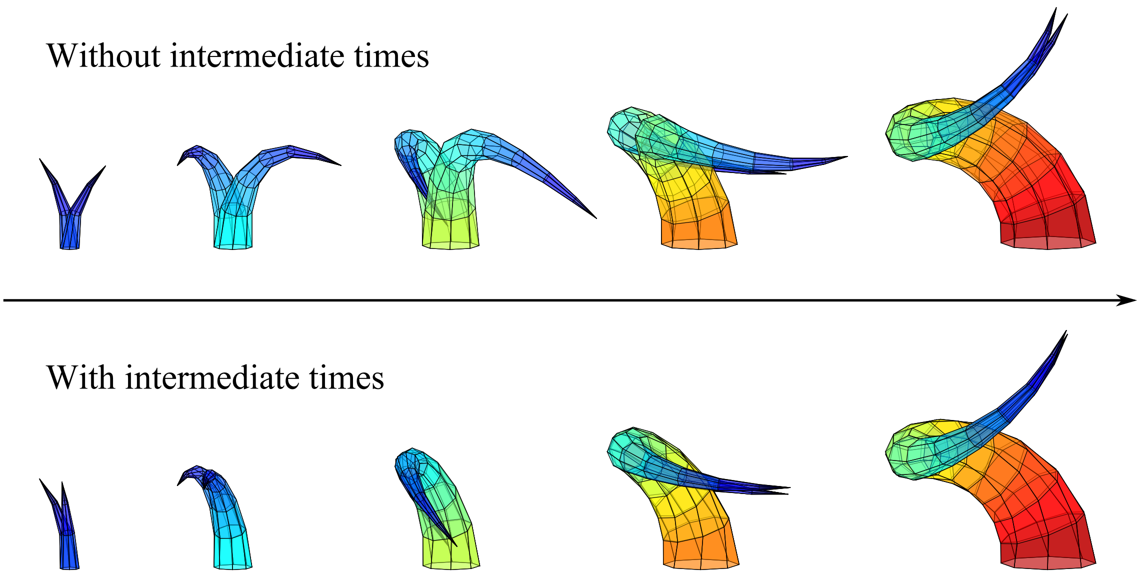

Figure 5.32 – We display on each row the development of the solution overlayed with the target's development. On the top row, without intermediate times. On the bottom row, with intermediate times. The growth dynamic of the development is significantly better retrieved with the intermediate times. Note that with intermediate times, the average time for 100 iterations is 72 sec (110k iterations : 22 hours) and without intermediate times, the average time for 100 iterations is 40 sec (230k iterations : 25 hours).

We see on this example that the horizontal rotation that might leave the final shape invariant has a deep impact on the growth scenario of the horn's development. Without the additional information of few intermediate times, the model does not retrieve this component of the deformation. Figure 5.33 gives a finer analysis of the situation.

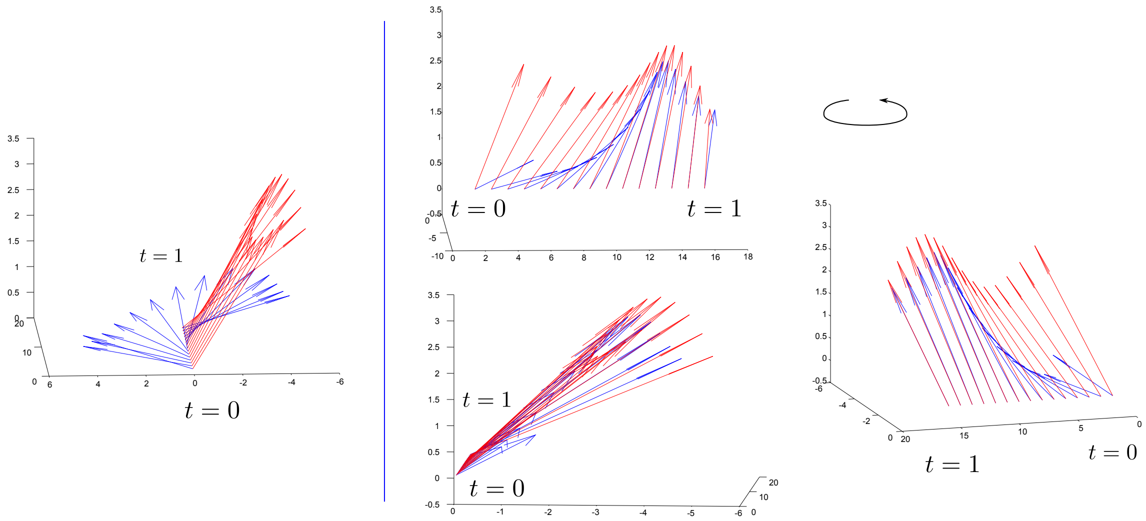

Figure 5.33 – We display here the angular velocity vector $t \mapsto \omega_t$ associated to the skew-symmetric matrices of the solution A^* (in blue) and of the target A^{tar} (in red). On the left side, for the solution without intermediate times. On the right side, for the solution with intermediate times through three different points of view of the same figure. Note that the target has a vector ω more or less constant over time, evolving as a small wave. In the first case, we can observe an important change of the solution at the end. The rotation on itself of the horn is adjusted only at the end of its development. This explains the differences at the beginning of the development on the first row of Figure 5.32.

Remark 6.4. *On this example, the Lagrangian parameters have been updated in both cases about 50 times. The constraint needed yet to be treated carefully. Indeed, when the norms converge faster than the shapes, the gradient descent tends to end prematurely.*

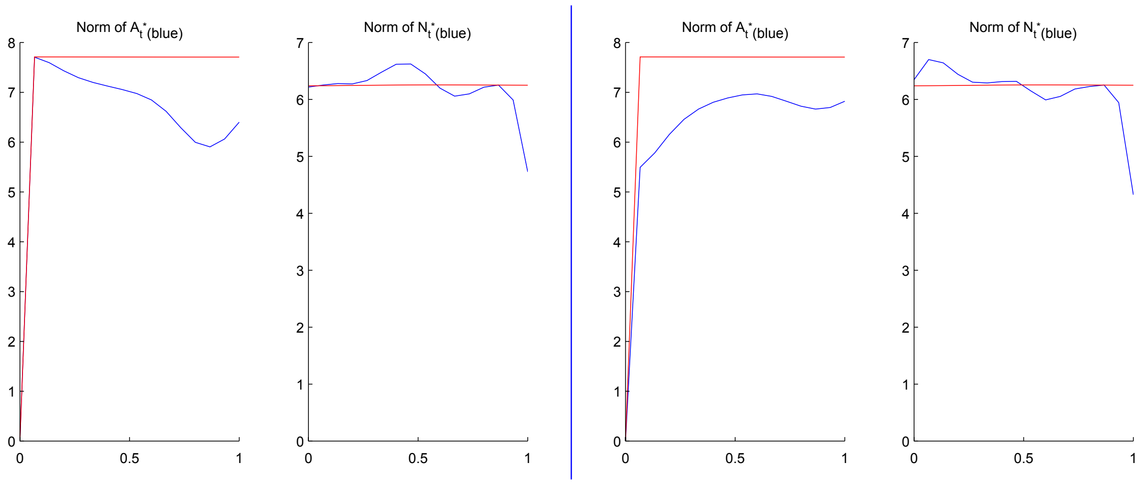

Figure 5.34 – Comparison of the deformations between the solution (in blue) and the target (in red). On the left, without intermediate times. On the right, with intermediate times. We display separately in each case the norms of the skew-symmetric matrices and the norms of the translations over the time interval $[0, 1]$.

6.4 Example 4 - Boundary effect

The attachment term built with metrics on currents and varifolds grants an important role to the boundary of the shapes. The Cartan's formula shows that the optimal vector field is given as an integral operator on two domains, the shape and its boundary, with their respective volume form. The dependence of these two terms in the discretization of the shapes with respect to the number of points has been studied for example in [16]. Here, we give a new example of shapes : tubes. The coordinate space remains $X = [0, 1] \times \mathbb{S}^1$ and the birth tag is the projection of the first coordinate. Yet, the image of the first leaf is now a close curve. This changes completely the form of the initial position. Instead of a disc as for the horns, the initial leaves could be here all superimposed into one single curve. We display in Figure 5.37 the initial momentum on the initial position.

We will see that the existence of a boundary attenuates slightly the issues discussed in Section 2.1 but does not solve them. At the initial time 0, the shape is not anymore reduced to a point but to a curve. This implies that $v_0^* \neq 0$ even before the discretization of the shape.

In this specific example, the attachment term is reduced to the *oriented varifold norm*. No landmark is added on the initial boundary.

In the three experiments displayed in Figure 5.35, the final state of the target is always perfectly recovered. However, from left to right the laddering of the leaves becomes more regular. With the *classic cost function*, the development of the tube strongly accelerates over time as the thickness of the slices increases from the top to the bottom. On the contrary, with the *constrained norm setup* the thickness of the slices is almost constant. These observations are corroborated by norms of the vector fields displayed in Figure 5.36. In the last setup, these norms for the target and the solution are almost perfectly equal. We took indeed the opportunity on this example to strengthen the constraint in the *constrained norm setup* (mainly by the number of update of the Lagrangian parameters

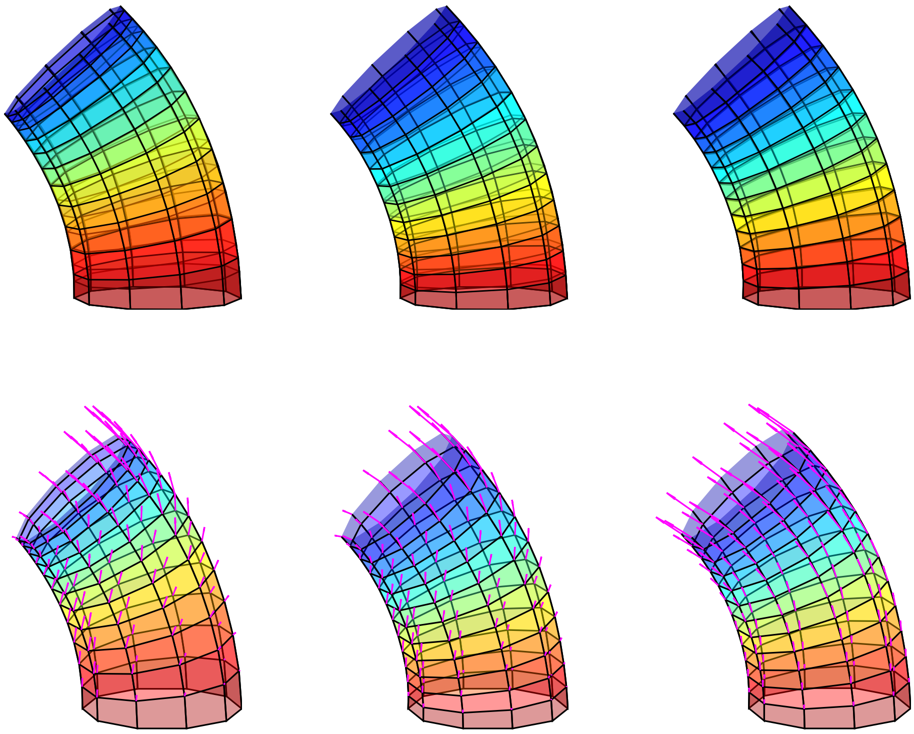

Figure 5.35 – We display on the top row the solution overlayed with the target at time 1. On the second row, we display the momentum of the solution at time 1. From left to right, the results are produced with the *classic cost function*, the *adapted norm setup* and the *constrained norm setup*.

: 12 against 3 for the two first examples). The evolution of the energy for this setup is displayed in Figure 5.38.

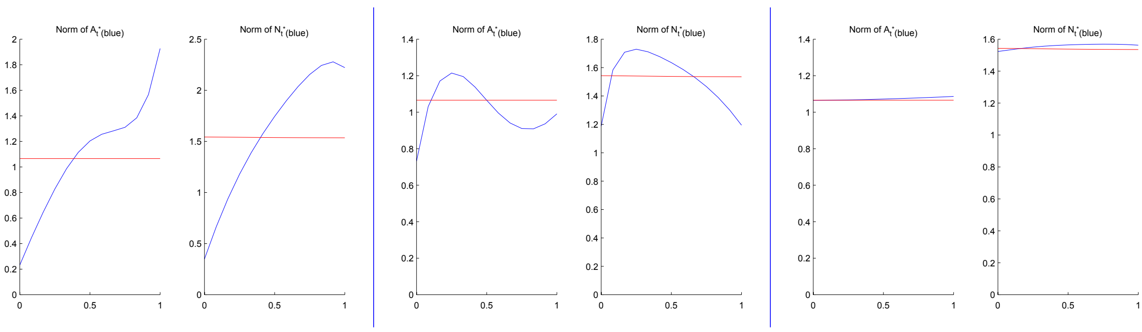

Figure 5.36 – Comparison of the deformations between the solution (in blue) and the target (in red). From left to right, with the *classic cost function*, with the *adapted norm setup* and the *constrained norm setup*. We display separately in each case the norms of the skew-symmetric matrices and the norms of the translations over the time interval $[0, 1]$. Note that for shapes with boundary like these tubes and unlike horns, $|A^*|$ is no longer null at time 0. In every setup, the runtime for 100 iterations is 32 sec. In the two first cases, the algorithm had roughly converged after 8min (1500 iterations). We let the algorithm run a bit longer for the constrained norm setup, as an example, with 7000 iterations (i.e. 30min).

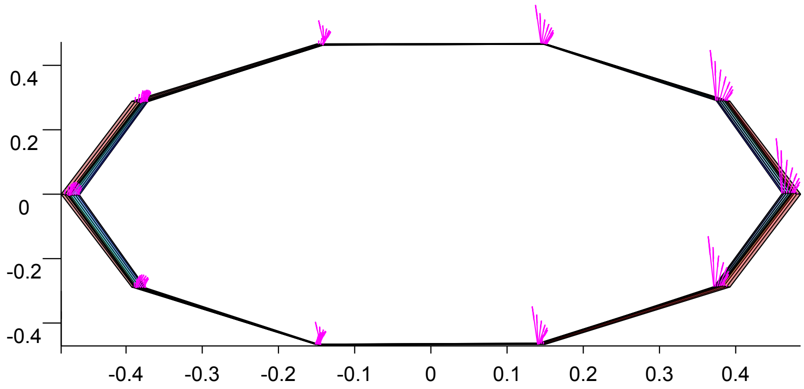

Figure 5.37 – Initial momentum p_0 on the initial position q_0.

This example also allows to illustrate the possibility for the initial position $q_0 : X \to \mathbb{R}^d$ to be highly non injective. If the creation process occurs at a specific fixed area independent of the time, each leaf appears at the same position of the other ones. Hence the set $\{q_0(X_{\{t\}}), t \in [0,1]\}$ of all initial position of the leaves would be reduced here to one close curve.

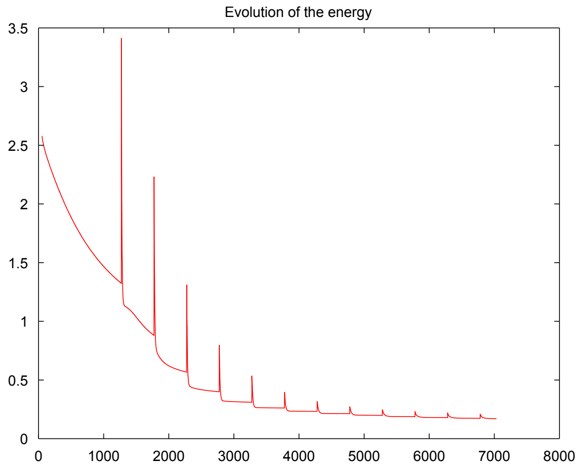

Figure 5.38 – Evolution of the energy during the gradient descent with the *constrained norm setup*. The peaks correspond to the updates of the Lagrangian coefficients. These updates are achieved at a minimal interval of 500 iterations and below a given threshold for the slope of the energy curve. We cut the 50 first iterations.

Remark 6.5. *We can observe on this example that the runtimes of the algorithm is shorter than for the horns. The time for 100 iterations is equivalent, but the algorithm converges much faster. This is due to the difficulty to match the peak of horns. The main part of the horn is retrieved quickly but then the most part of the gradient descent is dedicated to the peaks.*

Remark 6.6. *On this experiment, the initial position is exactly the one used to generate the target. We will see in the next example that we could have proceed without this input. Without the initial position of the target, we could have compute a interpolation, similar to that described in Section 5.2, from the base of the target to the projection of its top boundary in the initial plan.*

6.5 Example 5 - Optimization of the initial position

To finish the numerical experiments with the group of rotations and translations, we generate a target with a disturbance of the positions of the initial leaves. Figure 5.39 displays the initial position of the target. Unlike before, the arrangement of the leaves is no longer regular. The external curve that models the base is close to a circle but the next curves are then gradually deformed into ellipses. This behavior can hardly be estimated from the final state of the target. Hence, the initial position q_0 is initialized here as before: as a linear reduction of the base (last leaf) of the target (see Section 5.2).

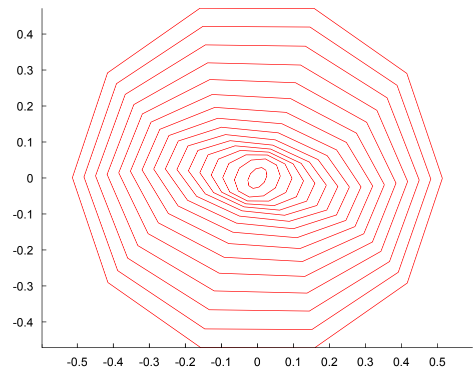

Figure 5.39 – Initial position of the target.

The algorithm is applied with the *combined norms setup*. The constraint on the norm is rather high to compensate the freedom induced by the relaxation of the initial position.

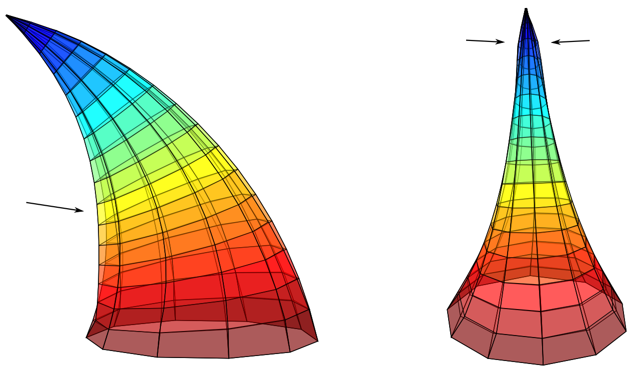

Figure 5.40 – Display of the final state q_1 of the solution overlayed with the target from two points of view. The black arrows point the few areas where the matching is non optimum. Figure 5.24 displayed a similar front view of the horn and highlights how, here, the horn strongly tapers from the base to the top.

During the gradient descent, q_0 is updated by the equation

$$q_0 = q_0 + \mu_q \mathcal{Q}_0 \,.$$

Yet, q_0 is then projected in the horizontal plane. The optimization of q_0 in this example is rather successful. We can observe in Figure 5.41 how the leaves have been transformed from circles (in cyan) to ellipses (in blue) and perform a close match to the initial position of the target (in red) after this optimization. The gradient Q_0 has been smooth as described for $\mathcal{P}_0$ in Section 4.3 and cancel on the boundary. The balance between the optimization of p_0 and q_0 has yet not been deepen. Note that one or few additional intermediate times would be a strong input in this typical situation. One could for example expect to resolve the issue pointed by the arrow on the left in Figure 5.40. Indeed, the initialization of

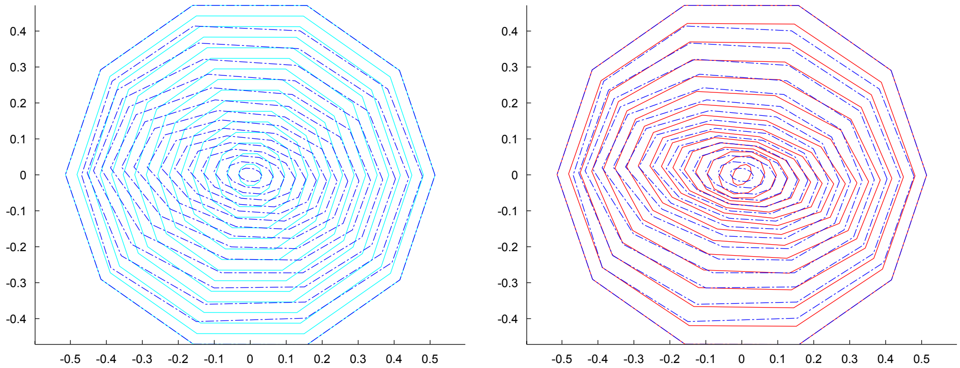

Figure 5.41 – Deformation of the initial position q_0. On the left, the initial positions of the solution at the first step of the algorithm (in cyan) and at the end of the algorithm (blue dash line). On the right, comparison of the optimized initial position of the solution (blue dash line) with the initial position of the target (in red).

the initial position would be more accurate with the simple input of the bases of the intermediate times (i.e. a distribution of few leaves of the initial position of the target that we could interpolate).

7 Numerical experiments: RKHS with a Gaussian kernel

To retrieve the rigidity of the rotations and translations, we used a large scale for the Gaussian kernel of V (see Figure 5.54). In the two following example, a landmark on the tip of the shape was added to estimate the data attachment term.

7.1 Example 1 - The cone

The cone is the first example we tested with simply translations. Its construction is almost perfectly retrieved after few iterations (with the adapted norm as the constrained norm). A Gaussian kernel produces a result a bit less regular as displayed in Figure 5.42. Five intermediate times are used to ensure the regularity of the development.

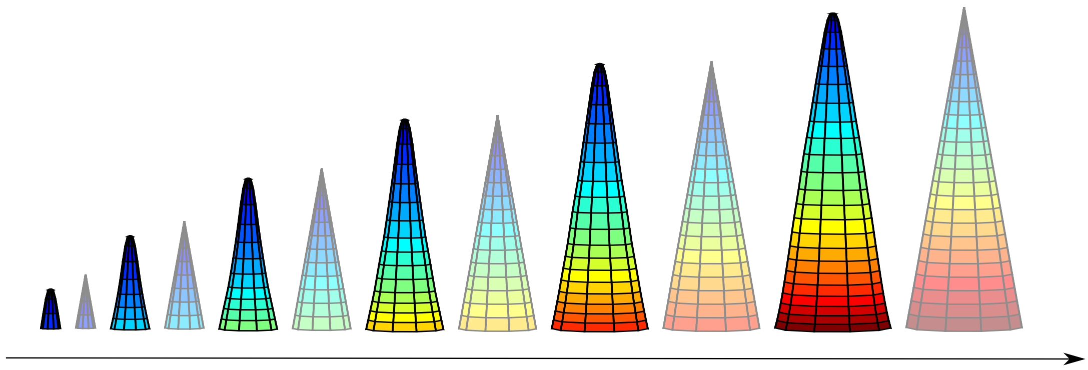

Figure 5.42 – Development of a cone. The faded evolution is the target. These five intermediate states of the target have been used to estimate the data attachment term during the gradient descent.

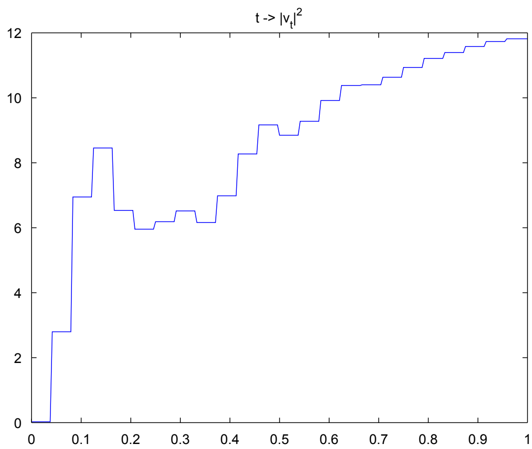

Figure 5.43 – Square norm of the vector field. The time subdivision is refined by a factor of 5. Between the birth of two leaves, the **growth dynamic** is reduced to the **standard dynamic** and the norm of the vector field is constant.

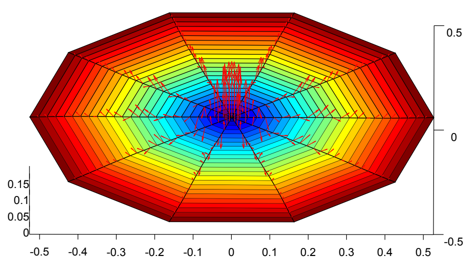

Figure 5.44 – Initial momenta p_0 on the initial position q_0. The arrangement of the momentum (concentrated around the tip) is strongly linked to the scale of the kernel. Here, we have : $\sigma_V = 0.9$

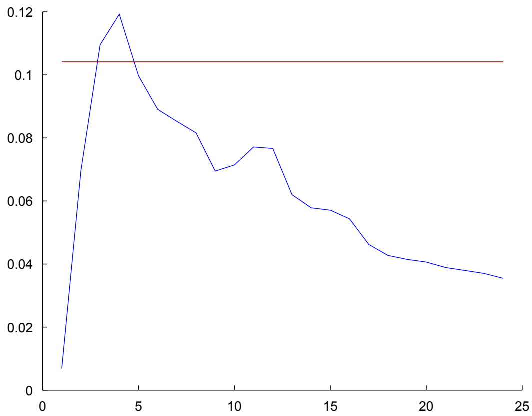

Figure 5.45 – Partial information on the amount of creation at the base of the cone measured by the thickness of every new slice. In blue for the solution, in red for the target.

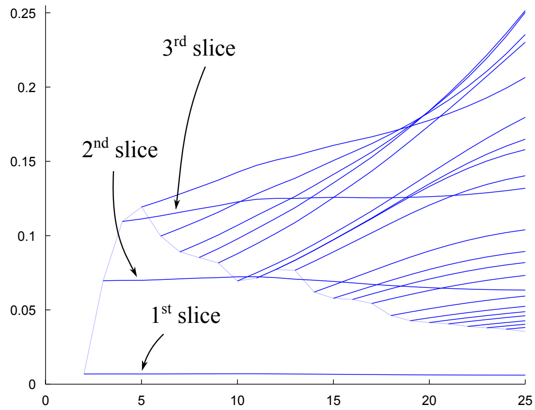

Figure 5.46 – Evolution of the thickness of each slice of the cone over time. The first slice is the part of the cone between the two first leaves and its thickness is displayed by the first curve (the longest one).

As discussed in Section 2.1.1, the growth process is more complex to exhibit with non rigid deformations like here. A constant amount of creation at the base of the horn is no longer linked to a constant norm of the vector field as before. The norm of the vector field also depends on the size of the shape and the scale of the kernel. We can observe on Figure 5.42 that the growth retrieved by the algorithm seems too strong during the beginning of the development then too slow. Indeed, on the last three states displayed, the leaves are farther apart on the top of the cone then they become closer. However, the growth is not anymore reduced to the creation process on the base since we can also observe that the thickness between two leaves tends to increase slightly over time.

To deepen these observations, we display on Figure 5.45 the thickness between the last two leaves appeared at each appearance of a new leaf. It measures thus the amount of *pure creation* over time at the base of the cone (we only measure the thickness here but we could then estimate the mass). The growth of the target is perfectly regular (red constant curve). For the solution, besides a difficulty at the first times, this quantity decreases strongly. However, the algorithm compensates this lack of creation by stretching the cone afterwards. Indeed, Figure 5.46 displayed the thickness of each slice (part of the cone between two leaves) of the cone over time. The thickness of the 3 first slices are rather constant but the next slices continue to grow during all the evolution of the shape.

The start of each horizontal lines corresponds to its thickness at the appearance of the second leaf that delimits its boundary. Hence, connecting the beginning of each line with the faded curve restores the blue curve of Figure 5.45.

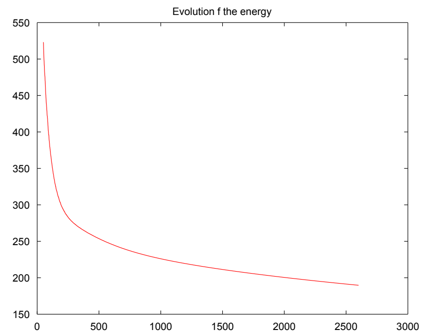

Figure 5.47 – Evolution of the energy during the gradient descent. Time for 100 iterations : 4min. Global runtime : 1h45 (size of the mesh : $3 \times 10 \times 25$).

7.2 Example 2 - Basic horn

We take the opportunity on this last example to observe the impact of intermediate times. The orientation of the leaves are much better retrieved with the intermediate times. Yet, the global curvature of the horn struggles to emerge in this last setup (see also Figure 5.49 and 5.50). Moreover, the two red slices are smaller than expected while the blue, the cyan and the green slices have been gradually spread during the development. On the other hand, the thickness of the slices without intermediate times are globally more regular. At last, we observe for the cone as for the basic horn, a tendency to see the thickness of the layers increase from the bottom to the top. Moreover, this thickness increases during the development of the shape illustrating that the growth process can also results from deformations as soon as we leave the rigid setting.

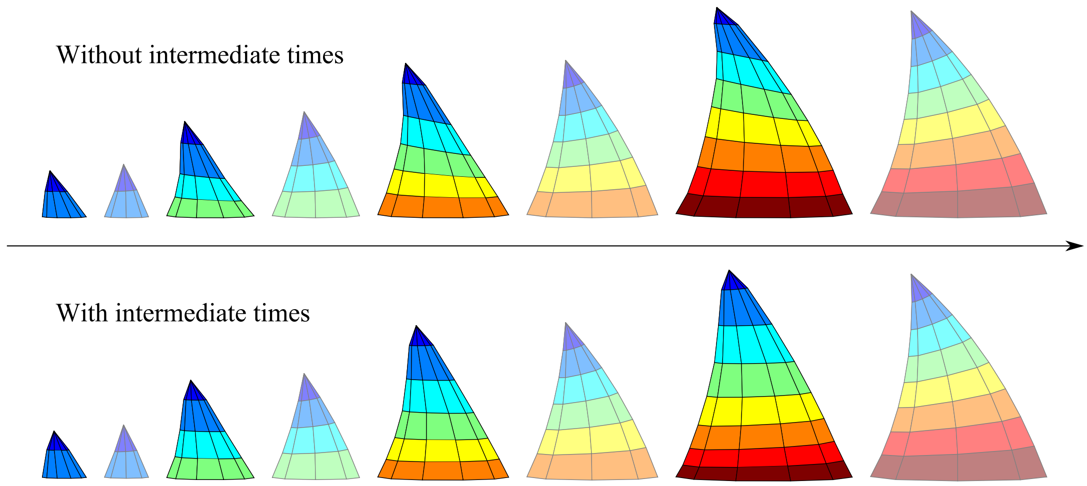

Figure 5.48 – Development of the horn with and without intermediate times. The faded evolution is the target. On the first row, the matching only included the final state of the target. On the second row, all the intermediate states displayed have been used in the gradient descent.

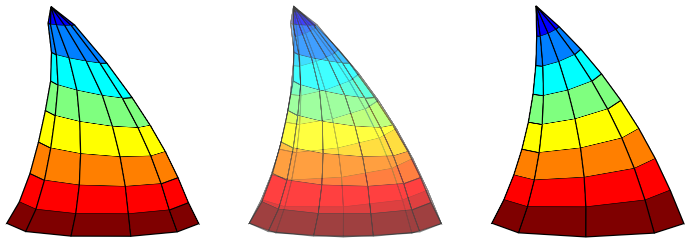

Figure 5.49 – Final state of the horn without intermediate times. On the left, the result at time 1. On the right, the target. In the middle, the overlay of both.

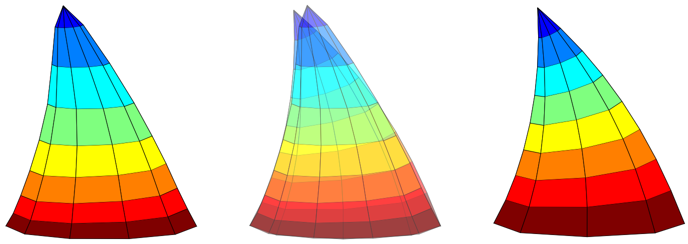

Figure 5.50 – Final state of the horn with intermediate times. On the left, the result at time 1. On the right, the target. In the middle, the overlay of both.

Figure 5.51 displays the initial momenta p_0 on the initial position q_0. In both cases, the momenta have been smoothed during their optimization as described in Section 4.3. It led to a significant improvement especially with intermediate input. This operation did not seem necessary with the group of rotations and translations (see previous Example 3).

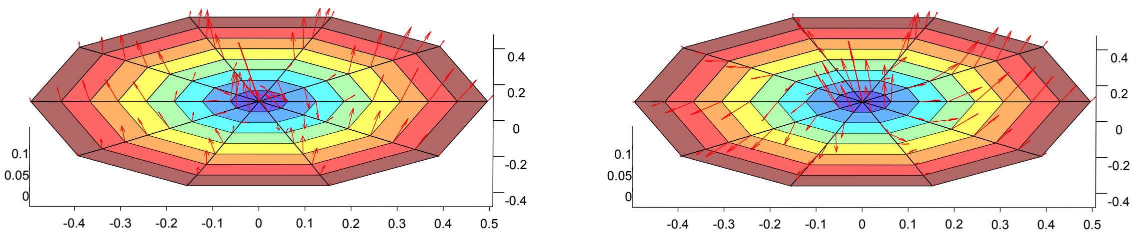

Figure 5.51 – Initial momenta p_0 on the initial position q_0. On the left, without intermediate times. On the right, with intermediate times. Note that although the gradient of the momentum is smoothed with a significant impact in the result, the optimal initial momentum is in the end not very smooth.

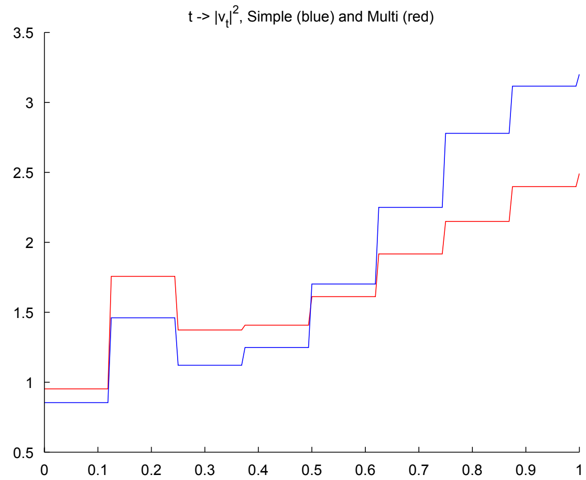

Figure 5.52 – Square norm of the vector field. Blue curve for the solution without intermediate times, red curve for the solution with intermediate times.

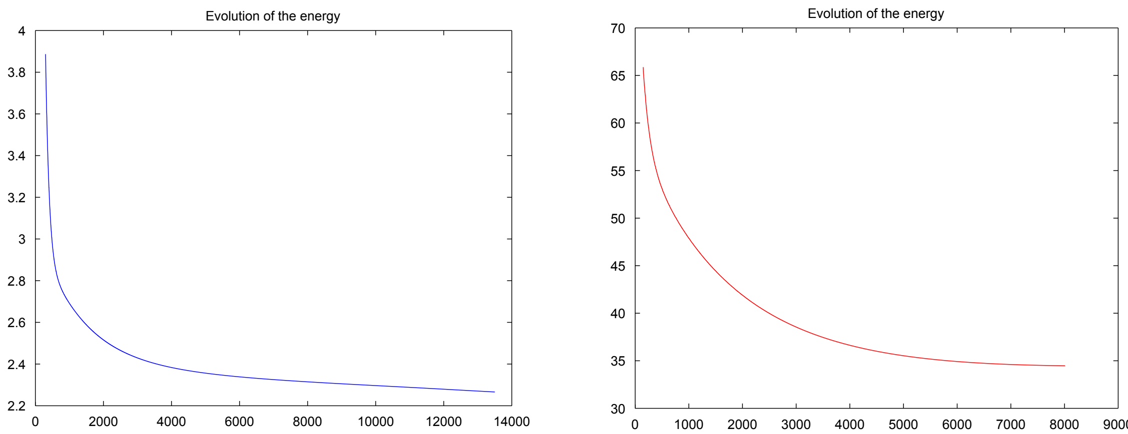

Figure 5.53 – Evolution of the energy during the gradient descent. On the left, without intermediate times. Time for 100 iterations : 23sec (size of the mesh : $3 \times 10 \times 9$). On the right, with intermediate times. Time for 100 iterations : 40sec (size of the mesh : $3 \times 10 \times 9$, 4 intermediate and final times). Global runtime for both experiments : 50mn.

7.2.1 Scale of the deformation

Let us recall that the Gaussian kernel is given by

$$\begin{array}{rccc} k_V : & \mathbb{R}^d \times \mathbb{R}^d & \longrightarrow & \mathbb{R} \\ & (x, y) & \longmapsto & \exp\left(-\frac{|x-y|^2}{2\sigma^2}\right) \end{array} \tag{5.32}$$

and that the optimal vector field v^* is given at time t as the sum of the contribution of every active point $x \in X, \tau(x) \leq t$ via their current position and momentum:

$$v_t^* = \sum_{x \in X, \tau(x) \leq t} k_V(\cdot, q_t(x)) p_t(x)\,.$$

Figure 5.54 highlights the scale of the deformations used in these two experiments. We display on the same horn two vector fields with different scales σ_V, generated by the same Dirac momentum (arbitrary chosen) attached to the tip of the horn. Note that for the smallest scale, the acceleration of the norm of the optimal vector field is stronger than for the largest scale (see the global slopes on Figure 5.52). Despite this acceleration, the flexibility of the smallest scale seems to favor a more regular creation process as discussed above regarding the thickness of the layers.

Figure 5.54 – The vector fields displayed on each horn are both generated by a Dirac momentum on the tip of the horn. It can be seen for a general momentum as the contribution of one active point to the optimal vector field. Each picture illustrates one scale. The scale on the left is $\sigma_V = 0.5$ as used without the intermediate times and on the right, $\sigma_V = 0.7$ as used with the intermediate times.

8 Conclusion

We examined in this chapter the algorithm to optimize the initial momentum p_0 and applied it to illustrate the matching problem detailed in Chapter 3. We modulated this problem with new cost functions corresponding either to a time-varying weighting of the penalization on the flow (*adapted norm setup*) or to the addition of a constraint on the norm of the vector field (*constrained norm setup*). We applied a new data attachment term using the representation of surfaces by oriented varifolds. It was joined with a local landmark attachment term to refine the result at small scale around the landmark.

This thesis was motivated by the need for new models to faithfully reproduce a biological phenomenon. It raises the issue to integrate additional prior information into the traditional framework proposed by the LDDMM methods. In the case of growth scenarios, the aim is to model the creation process but also to quantify it. The validation of the numerical experiments focused specifically on the latter criterion. The different cost functions were compared regarding the goal to retrieve the norm of the vector field used to generate the target. The flexibility of the model was tested in order to evaluate its ability to identify abnormal behavior such as growth delay. In contrast to the classic LDDMM, building the momentum map with the growth dynamic through a gradual influx of new initial momenta gives this flexibility and eliminates the need of reparametrizations in time to detect such anomalies.

The model integrated without difficulty the addition of input data at known intermediate times to reconstruct a scenario by interpolation. It can improve the results of an experiment that could have approached the limits of the model by the high sharpness and curvature of the studied horn. We also experimented the optimization of the initial position q_0 and investigated the initial boundary effect. Since the model should not be limited to affine deformations, the chapter is concluded with some experiments with a Gaussian kernel RKHS to model vector fields.

At last, as in the classic LDDMM framework, each scenario is completely characterized by the low dimensional variables initial position q_0 and initial momentum p_0, paving the way to a statistical analysis of the scenarios' population.

Bibliography

[1] P. A. Absil, R. Mahony, and R. Sepulchre. Riemannian geometry of grassmann manifolds with a view on algorithmic computation. *Acta Appl. Math.*, 80:199–220, 2004.

[2] J. Ashburner and K.J. Friston. Diffeomorphic registration using geodesic shooting and Gauss-Newton optimisation. *Neuroimage*, 55(3-3):954-967, 2011.

[3] W. Allard. On the first variation of a varifold. *Annals of mathematics*, 95(3), 1972.

[4] F. Almgren. *Plateau's Problem: An Invitation to Varifold Geometry.* Student Mathematical Library, 1966.

[5] S. Arguillère, E. Trélat A. Trouvé and L. Younes. Shape Deformation Analysis From the Optimal Control Viewpoint. *Journal de Mathématiques Pures et Appliquées*, Volume 104, Issue 1, July 2015, Pages 139-178.

[6] S. Arguillère. The abstract setting for shape deformation analysis and lddmm methods. In *Geometric Science of Information*, pages 159–167. Springer, 2015.

[7] S. Arguillère. The general setting for shape analysis. *arXiv preprint arXiv:1504.01767*, 2015.

[8] V. Arsigny, O. Commowick, X. Pennec and N. Ayache. A log-euclidean framework for statistics on diffeomorphisms. *International Conference on Medical Image Computing and Computer-Assisted Intervention*, Springer Berlin Heidelberg, 924-931, 2006.

[9] B. Avants and J. C. Gee. Geodesic estimation for large deformation anatomical shape averaging and interpolation. *Neuroimage*, 23:S139-S150, 2004.

[10] M.F. Beg, M.I. Miller, A. Trouvé and L. Younes. Computing large deformation metric mappings via geodesic flows of diffeomorphisms. *International journal of computer vision*, 61 (2), 139-157, 2005.

[11] M. Bauer, M. Bruveris, P. Harms, and P. W. Michor. Geodesic distance for right invariant sobolev metrics of fractional order on the diffeomorphism group. *Annals of Global Analysis and Geometry*, 44(1):5-21, 2013.

[12] M. Bauer, P. Harms, and P. W. Michor. Sobolev metrics on shape space of surfaces. *Journal of Geometric Mechanics*, 3(4):389-438, 2011.

[13] A. Borel and J.-P. Serre. Corners and arithmetic groups (with an appendix, *Arrondissement des variétés à coins*, by A. Douady and L. Hérault). *Commentarii Mathematici Helvetici 48*, 436-491, 1973.

[14] H. Brézis. *Analyse fonctionnelle - Théorie et applications.* Dunod, 2005.

[15] N. Charon and A. Trouvé. The Varifold Representation of Non-oriented Shapes for Diffeomorphic Rregistration. *SIAM journal on Imaging Sciences*, 6:2547–2580, 2013.

[16] B. Charlier, N. Charon and A. Trouvé. The fshape framework for the variability analysis of functional shapes. *Foundations of Computational Mathematics*, Springer, 2015.

[17] Deformetrica's software. Toward a comprehensive framework for the spatiotemporal statistical analysis of longitudinal shape data. *http://www.deformetrica.org/*.

[18] S. Durrleman, M. Prastawa, N. Charon, J. R. Korenberg, S. Joshi, G. Gerig and A. Trouvé. Morphometry of anatomical shape complexes with dense deformations and sparse parameters. *Neuroimage.* 2014 Nov 1;101:35-49. doi: 10.1016/j.neuroimage.2014.06.043. Epub 2014 Jun 26.

[19] S. Durrleman, X. Pennec, A. Trouvé, J. Braga, G. Gerig, and N. Ayache. Toward a comprehensive framework for the spatiotemporal statistical analysis of longitudinal shape data. *Int. Journal of Computer Vision*, 103(1):22–59, 2013.

[20] S. Durrleman, P. Fillard, X. Pennec, A. Trouvé, and N. Ayache. Registration, atlas estimation and variability analysis of white matter fiber bundles modeled as currents. *NeuroImage*, 2010.

[21] S. Durrleman, X. Pennec, A. Trouvé, and N. Ayache. A forward model to build unbiased atlases from curves and surfaces. *Proc. of the International Workshop on the Mathematical Foundations of Computational Anatomy*, 2008.

[22] S. Durrleman, X. Pennec, A. Trouvé, N. Ayache, and J. Braga. Comparison of the endocast growth of chimpanzees and bonobos via temporal regression and spatiotemporal registration, *1st workshop on Spatiotemporal Image Analysis for Longitudinal and Time-Series Image Data*, Beijing, Septembre 2010.

[23] H. Federer. *Geometric measure theory.* Springer, 1969.

[24] G. Reeb. *Sur certaines propriétés topologiques des variétés feuilletées.* Hermann, 1952.

[25] P. T. Fletcher. Geodesic regression and the theory of least squares on riemannian manifolds. *International journal of computer vision*, 105(2):171–185, 2013.

[26] J. Glaunès. *Transport par difféomorphismes de points, de mesures et de courants pour la comparaison de formes et l'anatomie numérique.* PhD thesis, 2005.

[27] J. Glaunès, A. Trouvé, and L. Younes. Diffeomorphic matching of distributions: A new approach for unlabelled point-sets and sub-manifolds matching. *IEEE Computer Society Conference on Computer Vision and Pattern Recognition*, 2:712–718, 2004.

[28] M. Vaillant and J. Glaunes. Surface matching via currents. *Proceedings of Information Processing in Medical Imaging (IPMI), Lecture Notes in Computer Science*, 3565(381-392), 2006.

[29] U. Grenander. General pattern theory: A mathematical study of regular structures. *Clarendon Press Oxford*, 1993.

[30] U. Grenander and M. I. Miller. Computational anatomy: an emerging discipline. *Quarterly of Applied Mathematics - Special issue on current and future challenges in the applications of mathematics*, Volume LVI Issue 4, 617-694, 1998.

[31] U. Grenander, A. Srivastava, and S. Saini. *Characterization of biological growth using iterated diffeomorphisms.* 3rd IEEE International Symposium on Biomedical Imaging: Nano to Macro, 2006.

[32] K. Ito and K. Kunisch. Lagrange Multiplier Approach to Variational Problems and Applications. volume 15 of*Advances in Design and Control*, Society for Industrial and Applied Mathematics (SIAM), Philadelphia, PA, 2008.

[33] S.C. Joshi and M.I. Miller. Landmark matching via large deformation diffeomorphisms. *IEEE Transcript Image Processing*, 9(8):1357-1370, 2000.

[34] F. Labourie. Geométrie différentielle. 2013. Available at *http://math.unice.fr/ labourie/preprints/pdf/geomdiff.pdf.*

[35] J.M. Lee. Introduction to Smooth Manifolds (Second Edition). *Springer*, 2016.

[36] J.E. Marsden and T.S. Ratiu Introduction to Mechanics and Symmetry - A Basic Exposition of Classical Mechanical Systems (Second Edition). *Springer-Verlag*, Volume 17 of Texts in Applied Mathematics, 1999.

[37] P.W. Michor and D. Mumford. An overview of the Riemannian metrics on spaces of curves using the Hamiltonian approach. *Appl. Comput. Harmon. Anal.*, 23(1):74-113, 2007.

[38] M.I. Miller and L. Younes. Group Actions, Homeomorphisms, and Matching: A General Framework. *International Journal of Computer Vision*, January 2001, Volume 41, Issue 1, pp 61-84.

[39] M. I. Miller, A. Trouvé, and L. Younes. On the metrics and euler-lagrange equations of computational anatomy. *Annual Review of Biomedical Engineering*, 4:375-405, 2002.

[40] M. I. Miller, A. Trouvé, and L. Younes. Geodesic shooting for computational anatomy. *Journal of Mathematical Imaging and Vision*, 24(2):209-228, 2006.

[41] X. Tang, D. Holland, A.M. Dale, L. Younes and M.I. Miller Shape abnormalities of subcortical and ventricular structures in mild cognitive impairment and Alzheimer's disease: detecting, quantifying, and predicting. *Human brain mapping*, 35 (8), 3701-3725.

[42] M. Niethammer, Y. Huang, and F.-X. Vialard. Geodesic Regression for Image Time-Series. *Medical Image Computing and Computer-Assisted Intervention*, 14(Pt 2):655–662, 2011.

[43] L. S. Pontryagin, V. G. Boltyanskii, R. V. Gamkrelidze, and E. F. Mishchenko. The mathematical theory of optimal processes. Translated by D. E. Brown. *A Pergamon Press Book. The Macmillan Co.*, New York, 1964.

[44] A. Qiu, L. Younes, M. I. Miller, and J. G. Csernansky. Parallel transport in diffeomorphisms distinguishes the time-dependent pattern of hippocampal surface deformation due to healthy aging and the dementia of the alzheimer's type. *NeuroImage*, 40(1):68–76, 2008.

[45] W. Rudin. *Analyse réelle et complexe.* Dunod, 3rd ed., 2009.

[46] S. Schwabik and Y. Guoju. *Topics in Banach Space Integration.* World Scientific, 2005.

[47] D. Thompson. *On Growth and Form.* Dover reprint of 1942 2nd ed.(1st ed., 1917), 1992.

[48] M.I. Miller, A. Trouvé and L. Younes. Hamiltonian Systems and Optimal Control in Computational Anatomy: 100 Years Since D'Arcy Thompson. *Annual Review of Biomedical Engineering*, Vol. 17, 447-509, 2015.

[49] E. Trélat. *Contrôle optimal : théorie et applications.* Vuibert, Collection *Mathématiques Concrètes*, 2nd ed., 2008.

[50] A. Trouvé. Action de groupe de dimension infinie et reconnaissance de formes. *C R Acad Sci Paris Sér I Math*, 321(8):1031–1034, 1995.

[51] A. Trouvé and F.-X. Vialard. Shape Splines and Stochastic Shape Evolutions: A Second Order Point of View. *Quarterly of Applied Mathematics*, page 26, 2010.

[52] A. Trouvé and L. Younes. Local Geometry of Deformable Templates. *SIAM Journal on Mathematical Analysis*, 37(1):17, Nov. 2005.

[53] F.-X. Vialard, L. Risser, D. Rueckert, and C. Cotter. 3d image registration via geodesic shooting using and efficient adjoint calculation. *Journal International Journal of Computer Vision*, 97(2):229–241, April 2012.

[54] L. Younes. *Computable elastic distances between shapes.* SIAM Journal on Applied Mathematics 58 (2), 565-586, 1998.

[55] L. Younes. *Shapes and Diffeomorphisms*, volume 171. Series: Applied Mathematical Sciences, 2010.

[56] M.I. Miller, L. Younes, J.T. Ratnanather, T. Brown, H. Trinh, D.S. Lee, D. Tward, P.B. Mahon, S. Mori, M. Albert, BIOCARD Research Team. Amygdalar atrophy in symptomatic Alzheimer's disease based on diffeomorphometry: the BIOCARD cohort. *Neurobiology of aging*, Vol. 36, S3-S10, 2015.